

# Plasma Proteomics for Biomarker Discovery to Predict Progression of Initially Asymptomatic Moderate- Severe Aortic Stenosis

Submitted for the Doctor of Philosophy

Daniel Chu Siong CHAN  
2020

## **Abstract**

# **Plasma Proteomics for Biomarker Discovery to Predict Progression of Initially Asymptomatic Moderate-Severe Aortic Stenosis**

Daniel Chu Siong CHAN

The optimal timing of aortic valve replacement in asymptomatic moderate-severe aortic stenosis (AS) is challenging. Robust markers predicting symptom onset or aortic valve related events in these patients are urgently needed. Plasma proteomics offers an opportunity to identify novel biomarkers in these patients. Two sample preparation workflows for mass spectrometry were developed and compared – a) Immunodepletion + Protein prefractionation on a reversed phased C18 column and b) extracellular vesicle pulldown followed by calcium silicate hydrate pulldown. The extracellular vesicle and calcium silicate hydrate pulldown method was more reproducible with >1500 protein identifications. This method was used for biomarker discovery in 92 propensity-matched event vs no-event samples, using one dimensional liquid-chromatography-linked tandem mass spectrometry with ion mobility specific collision energies for proteomic analysis. Samples were recruitment plasma samples from the PRIMID-AS study, a prospective observational multicentre study of asymptomatic moderate-severe AS patients with extensive phenotyping with electrocardiography, echocardiography, bicycle exercise testing and multiparametric cardiac magnetic resonance testing with T1 mapping, late gadolinium enhancement and stress first pass perfusion imaging. The primary endpoint was valve replacement for spontaneous AS-related symptoms or cardiovascular death or unplanned cardiovascular hospitalisation. 49 proteins were found to be differentially expressed, which may represent novel associated pathways such as fatty acid oxidation, inflammation, cell death/apoptosis/autophagy, arrhythmogenesis, neural remodelling and lysosomal survival. Of these, 17 were selected for verification using <sup>18</sup>O-isotope-labelled-pooled internal standards as the reference. Apolipoprotein D (APOD) emerged as a strong predictor of the primary endpoint, independent to exercise testing, sex, peak velocity, mean gradient and N-terminal-pro-brain natriuretic peptide. Addition of APOD to baseline characteristics resulted in a net reclassification improvement of 50-78%, particularly in moderate AS. Important correlates of APOD were tetranectin and body mass index. This biomarker could be used to optimally time aortic valve replacement in this group of patients.

## Acknowledgements

I want to thank everyone who has helped me through the work required to complete this thesis. Specific mentions are PQ and Jodie, excellent colleagues who taught me mass spectrometry and laboratory science and helping me troubleshoot when experiments don't go well. Dr Thong my postdoctoral colleague who kept me entertained and was an immense help for sample preparation in large studies. Ben, Richie and Sanjay my PhD colleagues who helped me with knowledge where it was lacking and helping with writing scripts and little programmes that make life much easier.

I wish to thank the British Heart Foundation for funding my research. I am ever indebted to Professor Don Jones who helped immensely with the understanding of mass spectrometry, and the science of proteomics, Professor Gerry McCann for supporting me from the outset in grant applications, providing the opportunity to develop this project around proteomic analysis of the PRIMID-AS samples and continuing to support me in building my academic career. I also wish to thank Dr Anvesha Singh, co-principal-investigator for the PRIMID-AS study for sharing her data to allow meaningful interpretation of my data. Thanks also to Sue Mackness, research nurse who was helpful when I needed to source data from the case-report forms.

A sincere and heartfelt thanks to Professor Leong Ng for supervising my PhD, and providing me with all the glorious insight into chemistry, predictive statistics and modelling; for being patient with me when things don't go well and supporting me in my pursuit for academia.

Last but not least, I wish to thank my family, in particular my wife Felicia, and children Aidan and Matthew for putting up with me through thick and thin and providing me with love and support.

Daniel

04/02/2020

## List of Abbreviations Used

ADAMTS1	A disintegrin and metalloproteinase with thrombospondin motifs 1 protein	eGFR	estimated glomerular filtration rate - (mL/min/1.73m <sup>2</sup> )
AGC	automatic gain control	ELISA	enzyme-linked immunosorbent assays
AHA	American Heart Association	ESC	European Society of Cardiology
AS	Aortic stenosis	ESI	electrospray ionisation
AUC	area under the curve	ETT	exercise tolerance testing (in PRIMID-AS refers to symptom-limited bicycle exercise testing)
AV	aortic valve	EV	extracellular vesicle
AVA	aortic valve area	FA	formic acid
AVR	Aortic valve replacement	FAO	fatty acid oxidation
AV-Vmax	peak velocity across the aortic valve	FDA	Food and Drug administration body
BCA	bicinchoninic acid assay	FDR	false discovery rate
BMI	Body mass index	FFA	free fatty acids
BNP	brain natriuretic peptide	GDF-15	growth differentiation factor - 15
BP	blood pressure	GO	gene ontology
BSA	body surface area, using the Mosteller formula ( $\sqrt{[\text{height}(\text{cm}) \times \text{weight}(\text{kg})/3600]}$ units: m <sup>2</sup> )	HCD	higher energy collision induced dissociation
CABG	coronary artery bypass grafting	HF	heart failure
CID	collision induced dissociation	HPLC	high performance liquid chromatography
CMR	cardiac magnetic resonance	HsTNI	high sensitivity troponin I (units: pg/mL)
CSH	calcium silicate hydrate	IAA	iodoacetamide
CT	computed tomography	ICAM1	Intercellular adhesion molecule 1
DDA	data-dependent acquisition mode	IEX	ion exchange chromatography
DIA	data independent acquisition	IgA	Immunoglobulin alpha
DTT	dithiothreitol	IgG	immunoglobulin gamma
ECM	extracellular matrix	IL1- $\beta$	interleukin 1 beta
ECV	extracellular volume fraction	IL-8	Interleukin 8
EDTA	Ethylenediaminetetraacetic acid	IMS	ion mobility separation
EF	ejection fraction	LC	liquid chromatography

LGE	late gadolinium enhancement	NTproBNP	N terminal of pro-brain natriuretic peptide (units: pmol/L)
LPL	lipoprotein lipase	NYHA	New York Heart Association functional classification of symptoms
LV	left ventricle/ventricular	PPV	positive predictive value
LVEDV	left ventricular end diastolic volume	PRIMID-AS	Prognostic Importance of Microvascular Dysfunction in asymptomatic patients with AS study; Clinicaltrials.gov no. NCT01658345
LVEDVI	LVEDV indexed to BSA	PRM	parallel reaction monitoring
LVESV	left ventricular end systolic volume	PSM	peptide sequence match
LVESVI	LVESV indexed to BSA	RANK	Receptor activator of nuclear factor $\kappa$ B
LVH	left ventricular hypertrophy	RANKL	Receptor activator of nuclear factor $\kappa$ B ligand
LVM	left ventricular mass	ROC	receiver operating characteristic
LVMi	left ventricular mass indexed to body surface area	RPLC	reversed phase liquid chromatography
LXR/RXR	Liver X receptor/Retinoid X Receptor	Runx2	Runt-related transcription factor 2
MAC	membrane attack complex	SDS-PAGE	sodium dodecyl sulfate based polyacrylamide-based discontinuous gel electrophoresis
MALDI	matrix-assisted laser desorption ionisation	suPAR	soluble urokinase plasminogen activator receptor
MARS	multiple affinity removal system	SV	stroke volume
MI	myocardial infarction	SVI	stroke volume index
MMP	matrix metalloproteinase	TAVI	transcatheter aortic valve implantation
MPG	mean pressure gradient (of the aortic valve)	TAVR	transcatheter aortic valve replacement
MPR	myocardial perfusion reserve	TCEP	tris (2-carboxyethyl) phosphine
MRM	multiple reaction monitoring	TFA	trifluoroacetic acid
MRproADM	Mid regional pro adrenomedullin	TGF- $\beta$ 1	transforming growth factor - beta 1
MS	mass spectrometry/mass spectrometer	TNF $\alpha$	tumour necrosis factor alpha
MS/MS	tandem mass spectrometry	TOF	time of flight
MS2	product ion scan	TWIMS	triwave ion mobility separation
NGAL	neutrophil gelatinase-associated lipocalin	UPLC	ultra performance liquid chromatography
NOTCH1	Notch homolog 1, translocation-associated	VCAM1	vascular cell adhesion molecule 1
NPV	negative predictive value	VEGF	vascular endothelial growth factor
OPA	O-phthalaldehyde	VLDL	very low density lipoprotein

## Table of contents

Chapter 1	Introduction.....	16
1.1	Epidemiology of aortic stenosis (AS) .....	16
1.2	Pathophysiology of AS .....	17
1.2.1	Asymptomatic AS .....	17
1.2.2	The development of symptomatic AS.....	21
1.3	Current management of asymptomatic AS .....	27
1.4	The argument for more biomarkers .....	30
1.5	Current state of the art for biomarkers of prognosis in AS .....	34
1.6	Plasma Proteomics to identify Biomarkers .....	37
1.6.1	Proteomics.....	37
1.6.2	Plasma .....	39
1.6.3	Mass Spectrometry.....	53
1.6.4	Data Analysis .....	57
1.6.5	Verification and Validation.....	60
1.6.6	Rationale .....	61
1.7	Hypotheses.....	61
1.8	Overall Experimental Design.....	62
Chapter 2	Method Development.....	64
2.1	Introduction.....	64
2.2	Methods and Materials.....	65
2.2.1	Pre-analytical Aspects.....	65
2.2.2	Denaturation Methods.....	65
2.2.3	Reduction Methods .....	66
2.2.4	Alkylation Methods.....	66
2.2.5	Digestion Methods .....	67
2.2.6	Protein/Peptide Assays.....	67
2.2.7	Desalting Methods .....	68
2.2.8	Immunodepletion of plasma proteins with a MARS-Human 14 Column.....	70
2.2.9	Protein fractionation.....	71
2.2.10	Combined immunodepletion and protein fractionation workflow .....	72
2.2.11	Extracellular vesicle pulldown .....	72
2.2.12	Enrichment with calcium silicate hydrate (CSH).....	74
2.2.13	Tandem EV pulldown + CSH enrichment workflow.....	74
2.2.14	Nanoparticle Tracking Analysis.....	75
2.2.15	Mass Spectrometry analysis.....	75
2.2.16	Data Analysis .....	77
2.2.17	Experiments performed.....	79

2.3	Results.....	86
2.3.1	Urea vs. ADC for denaturation .....	86
2.3.2	DTT vs. TCEP for reduction.....	86
2.3.3	Denaturation before protein fractionation vs. denaturation+reduction+alkylation before protein fractionation .....	87
2.3.4	Guanidine vs. urea in denaturation+reduction+alkylation first workflow .....	88
2.3.5	Proteins found in each fraction in qualitative analysis.....	89
2.3.6	Non-acetate-based EV pulldown vs acetate-based EV pulldown method .....	89
2.3.7	Optimal conditions for EV pulldown using acetate-based method.....	90
2.3.8	Nanoparticle Tracking Analysis.....	90
2.3.9	Comparing calcium silicate hydrate on precleared plasma vs. precleared plasma which has had EVs removed.....	92
2.3.10	Effect of denaturant on calcium silicate hydrate preparation.....	93
2.3.11	Immunodepletion .....	93
2.3.12	Prefractionation on mRP-C18 column.....	94
2.3.13	Reproducibility of quantification for immunodepletion and protein fractionation workflow .....	96
2.3.14	EV Pulldown.....	97
2.3.15	CSH Enrichment .....	101
2.3.16	Do both methods explore mutually exclusive proteomes?.....	101
2.3.17	Reproducibility of quantification of EV & CSH pulldown workflow .....	101
2.4	Discussion.....	102
2.4.1	Method development.....	102
2.4.2	Immunodepletion Method.....	103
2.4.3	Fractionation with the mRP-C18 column .....	103
2.4.4	Reproducibility of the immunodepletion and protein fractionation workflow .....	104
2.4.5	EV-pull down method.....	105
2.4.6	CSH enrichment.....	107
2.4.7	Reproducibility of the EV+CSH workflow.....	108
2.4.8	Challenges and Limitations.....	108
2.5	Conclusion .....	109
Chapter 3	Biomarker Discovery .....	110
3.1	Introduction.....	110
3.2	Aims and Objectives .....	110
3.3	Methods.....	111
3.3.1	Patients.....	111
3.3.2	Sample selection for biomarker discovery.....	113
3.3.3	Sample preparation .....	114
3.4	Results.....	120
3.4.1	Balance of cases vs controls.....	120

3.4.2	General mass spectrometric findings .....	123
3.4.3	Results from Progenesis QI.....	126
3.4.4	Baseline and prognostic variables for patients in the PRIMID-AS study .....	139
3.5	Discussion .....	139
3.5.1	Literature Review of the Potential Candidates.....	141
3.5.2	Group1: Neuronal axon guidance .....	142
3.5.3	Group2: Negative Regulation of Smooth Muscle Cell Proliferation .....	144
3.5.4	Group3: Complement and coagulation cascade/ Innate Immune response.....	147
3.5.5	Group4a: Lipid Metabolism and Transport + Glucose Metabolism .....	156
3.5.6	Group 4b: Ion Transport, Oxidative Stress, Inflammation.....	166
3.5.7	Group 5: Oxidative stress and other proteins .....	169
3.5.8	Remaining Proteins .....	172
3.5.9	Summary of probable mechanisms representing progression of AS .....	177
3.6	Limitations .....	180
3.7	Conclusion .....	181
Chapter 4	Verification .....	183
4.1	Introduction.....	183
4.2	Hypotheses.....	188
4.3	Methods.....	188
4.3.1	Patient selection .....	188
4.3.2	Sample Preparation .....	189
4.3.3	Heavy Labelling.....	189
4.3.4	Experimental design.....	190
4.3.5	Parallel Reaction Monitoring .....	191
4.3.6	Data analysis and target peptide selection .....	192
4.3.7	Assessment of assay performance.....	193
4.3.8	Statistical Analysis.....	193
4.4	Definitions.....	194
4.4.1	Severe AS.....	194
4.4.2	Positive Exercise Test .....	195
4.4.3	Outcomes .....	195
4.5	Results.....	195
4.5.1	Assay Performance .....	195
4.5.2	Baseline Characteristics of patients .....	214
4.5.3	Prognostic baseline characteristics to outcome on cox regression.....	216
4.5.4	Fine-Grey Univariate association of baseline characteristics for significant variables on univariate analysis .....	218
4.5.5	Analysis of Kaplan-Meier curves of important risk factors .....	219
4.5.6	Baseline Model .....	220
4.5.7	Baseline values of targeted peptides/proteins grouped by AS Severity .....	222



4.5.8	Univariate Association of targeted peptides/proteins to composite outcome .....	222
4.5.9	Multivariable analysis .....	222
4.5.10	Subgroup Analyses .....	228
4.5.11	Risk Stratification in moderate AS .....	229
4.5.12	Prognostic variables in the Moderate AS group .....	232
4.5.13	Prognostic variables in the Severe AS Group .....	233
4.5.14	Net reclassification improvement analysis.....	233
4.5.15	Negative and positive predictive values.....	235
4.5.16	Correlates and Determinants of APOD.....	240
4.5.17	Other Notable correlations .....	243
4.6	Discussion .....	247
4.6.1	Parallel Reaction Monitoring (PRM) .....	248
4.6.2	Differences between severe and moderate AS .....	250
4.6.3	Prognostic markers of the endpoint.....	252
4.6.4	APOD was independently prognostic of the endpoint.....	253
4.6.5	APOD is a novel marker of cardiovascular risk.....	254
4.6.6	APOD may be more prognostic in males.....	255
4.6.7	APOD function .....	256
4.6.8	Relationship of APOD with peak VO2 .....	257
4.6.9	Correlates of APOD .....	257
4.6.10	Limitations .....	259
4.7	Conclusion .....	262
Chapter 5	Summary and Future Work.....	263
5.1	Summary .....	263
5.2	Context.....	264
5.3	Future Work.....	267
Chapter 6	Appendix.....	269
6.1	Tables summarising current state-of-the-art of prognostic biomarkers in aortic stenosis ..	269
6.2	Larger network diagram(s) for proteins in the discovery study .....	269
6.3	Protein lists (digital copy) .....	269
Chapter 7	References.....	307

## Table of Tables

Table 1-1: Differences between recommendations from different societies.....	28
Table 1-2: Arguments for and against the use of plasma or serum for biomarker discovery .....	41
Table 2-1: Gradient for mobile phases on NanoAcquity UPLC for peptide separation .....	76
Table 2-2: Gradient for separation on the Ultimate 3000 .....	77
Table 3-1: Average values between NoEvents and Events used for propensity matching .....	123
Table 3-2: Proteins that were differentially expressed between Events and No Events .....	129
Table 3-3: Differentially expressed proteins in CSH experiment.....	133
Table 3-4: Proteins/Genes and their associated terms/functions/pathways .....	138
Table 3-5: List of genes that did not have a pathway associated on ClueGO.....	142
Table 4-1: Coefficients of variation in percentage of measured ratios .....	197
Table 4-2: Percentage coefficient of variation of light and heavy sum areas in 4 replicates. ....	203
Table 4-3:Scatterplots comparing PRM assay results with EV and CSH protein abundances.....	209
Table 4-4: Scatterplots comparing PRM assay results with EV and CSH protein abundances.....	210
Table 4-5: Scatterplots comparing PRM assay results with EV and CSH protein abundances.....	211
Table 4-6: Scatterplots comparing PRM assay results with EV and CSH protein abundances.....	212
Table 4-7:Scatterplots comparing PRM assay results with EV and CSH protein abundances.....	213
Table 4-8: Baseline characteristics of patients grouped by AS severity .....	215
Table 4-9: Comparison between discovery cohort and whole cohort for verification.....	216
Table 4-10: Univariate associations with the composite endpoint.....	217
Table 4-11: Developing a compact model reflecting baseline risk.....	221
Table 4-12: Comparison between mean levels of peptides measured in moderate and severe AS ....	223
Table 4-13: Prognostic independence of APOD against baseline variables .....	227
Table 4-14: All variables interacting with AS severity.....	229
Table 4-15: Prognostic variables in moderate AS .....	232
Table 4-16: Prognostic variables in severe AS .....	233
Table 4-17: Continuous net reclassification improvement analysis .....	234

Table 4-18: Negative and positive predictive values for dichotomised variables.....	236
Table 4-21: Spearman correlations for proteins to APOD.....	240
Table 4-22: Spearman correlations for clinical variables to APOD.....	241
Table 4-23: Correlates of APOD .....	242
Table 4-24: Protein correlates of APOD.....	243
Table 4-25: All correlates .....	244

## Table of Figures

Figure 1-1: Number of aortic valve replacements in the past decade in UK .....	16
Figure 1-2: Central Figure - what is the optimal timing for AVR .....	33
Figure 1-3: Complexity of the plasma proteome. ....	42
Figure 2-1 Schematic of immunodepletion with a MARS-Human 14 column .....	70
Figure 2-2 Typical chromatogram of a MARS-Hu-14 depletion. ....	71
Figure 2-3: Schematic illustrating differences in BigDiluteCold, NoDiluteNoCold and DiluteCold.....	82
Figure 2-4: Comparing denaturant on number of proteins identified .....	86
Figure 2-5: Comparing DTT vs. TCEP on number of proteins identified .....	86
Figure 2-6: Two chromatograms of protein separation on the MRP-C18 column of immunodepleted plasma that has been denatured with urea before separation .....	87
Figure 2-7: Two chromatograms of protein separation on the mRP-C18 column of immunodepleted plasma that has been denatured with urea, reduced with DTT and alkylated with IAA first before separation .....	87
Figure 2-8: Two chromatograms of protein separation on the mRP-C18 column of immunodepleted plasma that has been denatured with guanidine, reduced with DTT and alkylated with IAA first before separation.....	88
Figure 2-9: Time points where fractions were collected .....	89
Figure 2-10: Differences in numbers of protein groups identified with the no-acetate vs. acetate EV pulldown methods .....	90
Figure 2-11: Number of proteins and CVs of protein quantification amounts .....	90
Figure 2-12: Distribution of particle sizes isolated in EV pulldown method .....	91
Figure 2-13: CSH on precleared plasma and EV-free plasma identify similar numbers of proteins and are reproducible methods .....	92

Figure 2-14: Effect of denaturant on CSH preparation.....	93
Figure 2-15: Eight depletion chromatograms .....	94
Figure 2-16: Reproducible protein amounts in low abundant fraction from MARS14-Hu column.....	94
Figure 2-17: Chromatograms of 8 fractionations.....	95
Figure 2-18: Variation in peptide amounts within each fraction over 8 separations .....	96
Figure 2-19: Low number of proteins with a quantification CV <0.2 in all fractions. ....	97
Figure 2-20: Venn Diagram showing overlap between proteins within each fraction .....	97
Figure 2-21: Molecular function of proteins identified in the EV pulldown method.....	98
Figure 2-22: Cellular component localisation of proteins identified .....	99
Figure 2-23: Pathway Analysis of functions of proteins from EV pulldown method .....	100
Figure 2-24: Overlap of proteins seen in EV and CSH pulldown .....	101
Figure 2-25: Variability in quantification of proteins in EV and CSH methods .....	102
Figure 3-1: Schematic of sample preparation for biomarker discovery .....	115
Figure 3-2: Distribution of propensity scores between matched cases and controls .....	121
Figure 3-3: Distribution of propensity scores before and after matching between groups....	122
Figure 3-4: Variation in Protein Hits over course of EV-study by injection order.....	124
Figure 3-5: Sum Top3 Peptide Intensities over course of EV-study by injection order.....	125
Figure 3-6: Variation in Protein Hits over course of CSH-study by injection order .....	125
Figure 3-7: Sum Top3 Peptide Intensities over course of CSH-study by injection order .....	126
Figure 3-8: Principal component plot of EV experiment revealing clusters of experimental data.....	127
Figure 3-9: Cluster assignment in EV-study for statistical adjustment .....	128
Figure 3-10: Boxplots showing differences in abundance between Events and NoEvents for proteins that were differentially expressed in the EV experiments .....	130

Figure 3-11: Principal component plot for CSH Experiment .....	131
Figure 3-12: Cluster assignment for the CSH Experiment .....	132
Figure 3-13: Boxplots showing differences in abundance of proteins between Event/NoEvent in the CSH experiment.....	134
Figure 3-14: Principal component plots from EV experiment stratified by recruitment site	135
Figure 3-15: Other principal component plots from EV experiment stratified by recruitment site .....	135
Figure 3-16: Principal component plot for CSH experiment stratified by recruitment site...	136
Figure 3-17: Other principal component plot for CSH Experiment stratified by recruitment site .....	136
Figure 3-18: Histogram showing distribution of the magnitude of differences of abundances between significantly different proteins in Events vs NoEvents .....	140
Figure 3-19: Hypothetical interaction between MASPs, Factor 13 and protein S.....	152
Figure 3-20: Schematic showing relationship between tetranectin, plasminogen, fibrin and their modulators .....	154
Figure 3-21: Hypothetical schematic showing probable relationship between APOC3, GPLD1, APOD, Lipoprotein Lipase and fatty acid oxidation in the cardiomyocyte.....	158
Figure 3-22: Schematic indicating large number of binding sites for Thrombospondin 1 giving it a multitude of potential functions.....	161
Figure 3-23: Proposed ion transport mechanisms affected which imply an arrhythmogenic aetiology for symptom development .....	169
Figure 3-24: Network diagram highlighting links and potential functions of differentially expressed proteins in asymptomatic AS .....	182
Figure 4-1: Cartoon of a triple quadrupole single reaction/multiple reaction monitoring experiment.....	185

Figure 4-2: Cartoon illustrating a parallel reaction monitoring experiment .....	186
Figure 4-3: Patient flow diagram .....	189
Figure 4-4: Calibration curves of targeted peptides.....	198
Figure 4-5: Sum areas of selected MTVTDQVNCPK (surrogate for APOD) .....	200
Figure 4-6: Sum areas of heavy and light MTVTDQVNCPK (APOD surrogate) .....	201
Figure 4-7: Ratio of light to heavy MTVTDQVNCPK (APOD surrogate) .....	202
Figure 4-9: Measured light to heavy ratio in a heavy standard made up in water, injected over several days at 8°C .....	205
Figure 4-10: Fluctuation of retention times for a typical peptide over course of study.....	206
Figure 4-11: Systematic change in absolute ion intensities due to chromatographic column changes did not affect light:heavy ratio measurements .....	207
Figure 4-12: Analysis of Kaplan-meier curves of important prognosticators in aortic stenosis. .....	219
Figure 4-13: Box/Dotplots for significantly different peptides .....	224
Figure 4-14: Cumulative incidence of competing events dichotomized by APOD median..	225
Figure 4-15: Cumulative incidence plot of competing events for APOD dichotomized by optimal thresholds .....	226
Figure 4-16: Forest plot of hazard ratios for APOD in different subgroups.....	228
Figure 4-17: APOD levels were higher in males with events but not different between females with or without events .....	228
Figure 4-18: Receiver operating characteristic curves for mean pressure gradient and APOD in the moderate AS group .....	230
Figure 4-19: Cumulative Incidence curves for mean pressure gradient and APOD dichotomised by optimal cut-offs .....	231
Figure 4-20: Net Reclassification Improvement Analysis.....	235

Figure 4-21: Kaplan-meier curves illustrating differences between event-free probabilities stratified by the number of positive risk factors. ....	238
Figure 4-22: Receiver operating characteristic curve of the 5-point risk-score.....	239
Figure 4-23: Tetranectin and BMI may explain more than 2/3 of the attributable variance of APOD.....	244
Figure 4-24: Scatterplot matrix showing correlation between apolipoproteins C3, C2, D and H, afamin and serum amyloid a4 .....	245
Figure 4-25: Scatterplot matrix showing correlations between factor 13B, plasminogen and tetranectin.....	246
Figure 6-1: Whole network diagram.....	287
Figure 6-2: Top-left of network diagram in Figure 3-24 .....	288
Figure 6-3: Top-right of network diagram in Figure 3-24.....	289
Figure 6-4: Middle of network diagram in Figure 3-24.....	290
Figure 6-5: Bottom of network diagram in Figure 3-24 .....	291



## Chapter 1 Introduction

### 1.1 Epidemiology of aortic stenosis (AS)

Calcific AS is increasing in frequency. Aortic valve replacement (AVR) operations in the US have doubled in the past decade, and are likely to double further in the next 20 years (Nkomo et al., 2006). In the United Kingdom, between 2006 and 2015, the number of isolated first-time AVRs has indeed nearly doubled (Figure 1-1) and continues to rise (source: UK National Adult Cardiac Surgery Audit, accessed from the Blue Book Online, Society of Cardiothoracic Surgery in Great Britain and Ireland, <http://bluebook.scts.org>).

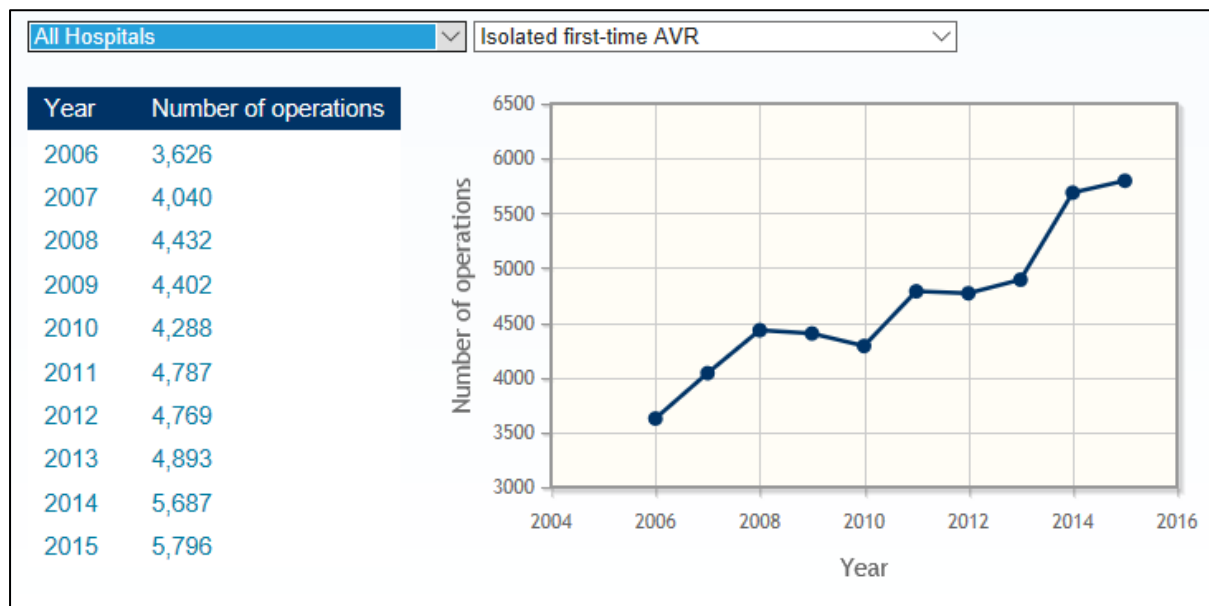


**Figure 1-1: Number of Isolated first-time aortic valve replacements in the past decade in UK (source: UK National Adult Cardiac Surgery Audit, accessed from the Blue Book Online, Society of Cardiothoracic Surgery in Great Britain and Ireland, <http://bluebook.scts.org>)**

AS is the most common valvular disease requiring surgery (Iung et al., 2003). The Cardiovascular Health Study (Supino et al., 2006) which looked at 5201 individuals above the age of 65 found 26% to have aortic sclerosis where the aortic valve (AV) is thickened with associated calcification but without any significant obstruction to blood flow. In comparison, 2% of the entire sample aged > 65 had AS. The prevalence of AS in this

particular group varies between age groups; 1.3% in the 65-75 age group, 2.4% in the 75-85 group and 4% in the >85 age group. Although not officially measured, one can extrapolate from population statistics that AS affects ~308000 individuals in the UK. The rate of progression of AS to surgery, symptom development or endpoints like heart failure (HF) or sudden death is determined by AV obstructive severity and the response of the myocardium to obstruction (Pellikka et al., 2005, Cioffi et al., 2011).

Other causes of AS include congenital AS, which is usually unicommissural, but is unlikely to go unnoticed before adulthood, due to the very high prevalence of symptoms and risk of sudden death. The other rare cause of AS is rheumatic heart disease occurring as a result of a prior Group-A-Streptococcus infection. In this circumstance, AS is unlikely to occur in isolation, without affecting the mitral valve, and is extremely rare in a developed country due to effective treatment of streptococcal infections since the advent of antibiotics early in the last century (Roberts, 1970).

## **1.2 Pathophysiology of AS**

### **1.2.1 Asymptomatic AS**

#### **1.2.1.1 Valvular narrowing**

The AV is a tricuspid valve positioned just beyond the orifice of the left ventricular outflow tract (LVOT) at the outlet of the heart. The cusps are thin, mobile and appose at a central point in a 'Mercedes-Benz' appearance, and are supported in a ring by their attachment to the aortic annulus. As such, the mechanical stress applied by systemic BP after the systolic phase of the cardiac cycle has ejected its contents into the aorta, is evenly distributed between the three cusps, throughout diastole (Thubrikar et al., 1986).

In calcific AS, the leaflets progressively become fibrosed, thickened and then finally calcified, with the resultant effect of reduced mobility and increased stiffness, leading to progressive orifice narrowing. Whilst historically, this process has been thought to be due to 'wear and tear', increasingly there is evidence that various pathways and pathologies are involved, including biochemical, humoral and genetic pathways, which ultimately will determine the rate of progression and symptom development.

AS is characterised by obstructed blood flow due to a reduction in effective orifice size of the AV. With degenerative AS, there is often corresponding calcification on the AV, with stiffening of the AV leaflets. In contrast, in rheumatic AS, there is classically commissural fusion along the edges of the cusps, resulting in a reduced effective orifice area, but with valvular tips that remain mobile.

#### **1.2.1.2 Factors that initiate disease**

The development of AS has many similarities to the development of atherosclerosis. The process begins with endothelial injury, which in AS is probably caused by mechanical stress. As in atherosclerosis, disease localises to areas of increased mechanical stress and reduced shear stress. Two coronary arteries perfuse the heart, the left and the right, and these usually arise from the cusps of the left and right aortic sinuses respectively. As a result of the increased shear stress in these areas in supplying blood flow to the myocardium, they are relatively spared from development of AV lesions. Conversely the non-coronary cusp, which has relatively lower shear stress, but a relatively similar mechanical stress to the other two cusps, is more likely to develop AV lesions. Furthermore, mechanical stress is highest where the AV cusps arise from the aortic wall, as they are the sites of maximum flexion. Correspondingly, 50% of the lesions in AS are seen in this location (Otto et al., 1994). Evidence that mechanical stress is an important initiating and driving factor of AS comes

from bicuspid AVs. Bicuspid valves inherently undergo more stress than tricuspid valves as the mechanical stress on the valve is spread across two points of maximal flexion compared to three. As a result, bicuspid valves almost universally anticipate the requirement for AVR by approximately 2 decades (Pachulski and Chan, 1993).

#### **1.2.1.2.1 The role of inflammation**

Endothelial injury and disruption allows lipid penetration into the valvular endothelium, which then accumulate as foci of intense inflammation (O'Brien et al., 1996, Olsson et al., 1999). These highly cytotoxic lipids are likely to stimulate and mediate the inflammatory processes and subsequent valvular calcification (Parhami et al., 1997) similar to atherosclerosis. Evidence that there is intense inflammatory activity includes localisation of adhesion molecules at sites of valvular lesions (Ghaisas et al., 2000). These molecules facilitate endothelial infiltration by macrophages and T-cells which release inflammatory cytokines such as TGF- $\beta$ 1, TNF $\alpha$  and IL1- $\beta$  (Jian et al., 2003, Kaden et al., 2003). The cytokines in turn drive progressive fibrosis of the valve. In addition, circulating C-reactive protein (Galante et al., 2001) is elevated in AS and valves with AS are 'hotter' than normal valves in-vivo (Toutouzas et al., 2008). Macrophage uptake of 18-fluorodeoxyglucose, widely used to measure macrophagic activity in atherosclerosis (Fayad et al., 2011), is elevated in valvular AS (Dweck et al., 2012a).

At the tissue level, there is evidence of neovascularisation and micro-haemorrhages, focussed around calcific lesions with intense inflammation, with associated increase in T-cell density. There is associated upregulation of ICAM1 and VCAM1 in these new-vessels, confirming that these neo-vessels are the likely entry point for macrophages into the valve. There is inflammatory haemorrhage in 78% of severe AS valves which is associated accelerated disease progression (Akahori et al., 2011). Progression of vascular atherosclerosis often leads

to formation of a thin fibrous cap which could subsequently rupture and cause thrombosis with resultant vascular occlusion. In contrast, in AS, due to the location of the disease in the aorta and mobility of the AV, continuous inflammation results instead in accumulated fibrosis and remodelling of the extracellular matrix, leading to thickening and stiffening of the valvular cusps. Valvular media contains fibroblast-like cells and vimentin, some of which differentiate into myofibroblasts thought to be responsible for accelerated valvular fibrosis (Liu et al., 2007). Additionally, angiotensin converting enzyme (ACE) is likely to play a key role in mediating fibrosis. ACE generates angiotensin II locally in valvular lesions and are likely to activate angiotensin receptors which have been identified on valvular myofibroblasts (O'Brien et al., 2002).

#### **1.2.1.3 The importance of calcification**

Calcification seems to be an important event in AS, and can easily be quantified on computed tomography (CT). Extent of calcification correlates well with AS severity (Cowell et al., 2003), progression of disease (Davies et al., 1991) and development of symptoms and significant events (Rosenhek et al., 2000). The process appears to be driven by myofibroblasts which differentiate into osteoblasts through a coordinated signalling process involving Wnt3-crp5-b-catenin, RANK/RANKL and Runx2-NOTCH1 (Caira et al., 2006, Kaden et al., 2004a, Garg et al., 2005). These osteoblasts which make bone, along with associated calcification factors such as sialoprotein, osteopontin and bone morphogenic-2 (Rajamannan et al., 2003, O'Brien et al., 1995, Mohler et al., 2001, Kaden et al., 2004b) leads to further remodelling and calcification, producing lamellar bone and microfractures (Mohler et al., 2001) characteristic of late stage severe disease.

Why only  $\frac{1}{6}$  of AV calcification accelerates to cause haemodynamic obstruction and stenosis is unclear (Cosmi et al., 2002). AV calcification is associated with a lower bone mineral

density, advanced age and hypertension (Aksoy et al., 2005). There is an association between AV calcification and the presence of the B-allele of the *BsmI* polymorphism of the Vitamin-D receptor. This polymorphism, is also associated with reduced bone mineral mass in homozygotes (Ortlepp et al., 2001). Calcium homeostasis has also been implicated (Urena et al., 1999) because patients with end-stage renal failure on haemodialysis with a higher vitamin-D and higher calcium-phosphorus product are more likely to develop calcific AS. This is thought to be driven by hyperparathyroidism. However, not all individuals with AV calcification have any of these predisposing factors.

## **1.2.2 The development of symptomatic AS**

### **1.2.2.1 Development of symptoms**

Symptomatic AS carries an extremely poor prognosis, with a mortality of approximately 25% per year. The classical triad of AS symptoms are exertional angina, exertional syncope and exertional dyspnoea. The average survival with symptom development is 5, 3 and 2 years with the onset of angina, exertional syncope and dyspnoea or other HF symptoms respectively (Ross and Braunwald, 1968).

However, asymptomatic AS carries an excellent outlook. It is often difficult to predict when an asymptomatic individual will develop symptoms, but the point at which symptoms occur especially with the presence of severe AS would prompt urgent surgical referral for AVR.

### **1.2.2.2 Angina**

Angina occurs when there is a mismatch between oxygen demand and oxygen supply in the myocardial tissue bed. Myocardial tissue is unique from other tissue beds in that it only obtains its blood supply in diastole, with highly optimal oxygen extraction. A normal individual has a coronary blood flow reserve of 500-800% of the resting blood supply. This

reserve can then supply adequate oxygen to satisfy an increased myocardial demand during exercise. In the presence of left ventricular hypertrophy (LVH), there is both an increased myocardial tissue mass and therefore corresponding resting demand, as well as exertional demand, with resultant reduction in coronary blood flow reserve of 50-75% of the resting supply. Furthermore, this is compounded potentially by the reduction in capillary supply in hypertrophied myocardium (Breisch et al., 1984), leading to anginal symptoms.

#### **1.2.2.3 Dyspnoea or HF symptoms**

LVH also leads to impaired diastolic function. The diastolic phase in the cardiac cycle comprises both an active phase and passive phase. The myocardium actively relaxes before the ventricle fills passively from the left atrium. In LVH, the active phase takes longer, due to the increased mass. The diastolic time is fixed and therefore, passive filling of the ventricle is delayed and has to be completed in a shorter period of time (Zile and Brutsaert, 2002).

Chronic LVH also increases wall stiffness resulting in high ventricular filling pressures.

Collectively this impairs diastolic filling and progression leads to reduced capacity of the left atrium to 'absorb' the increased pressures, leads to back pressure on the pulmonary venous circulation resulting in pulmonary congestion and dyspnoea (Hess et al., 1984).

#### **1.2.2.4 Syncope**

The mechanism of AS causing syncope is not certain. Exercise causes a requisite drop in total peripheral resistance. In normal individuals this is accompanied by an increase in SV which maintains blood pressure (BP) and end organ perfusion. In AS the SV may not increase sufficiently due to the obstruction and the resultant BP mismatch is thought to lead to exertional syncope (Schwartz et al., 1969). A 20 mmHg drop in BP during exercise testing in severe AS carries a IIa recommendation for AVR (Nishimura et al., 2014) although there is conflicting evidence regarding the usefulness of hypotension to predicting outcome (Das et

al., 2005). The alternative theory is that the extremely high intracardiac pressures during exercise to increase cardiac output causes a reflex vasodepressor response mediated by baroreceptors within the heart, leading to a drop in BP causing syncope (Richards et al., 1984). The remaining theory is that a combination of a substrate for ventricular arrhythmias and adrenergic drive may cause an arrhythmia that causes syncope.

#### **1.2.2.5 The response of the myocardium**

Left ventricular hypertrophy (LVH) seems to be central in the development of symptoms and progression to HF. Its development is quite well described.

The normal effective AV outlet is approximately 3cm<sup>2</sup> in size. A 50% reduction in orifice area from normal has a minimal effect on the pressure gradient (Carabello and Paulus, 2009). However a continued worsening of the obstruction will lead to an increase in pressure overload. As the pressure gradient across the narrowed AV gradually increases, the pressure the left ventricle has to generate to overcome the afterload increases, inducing the left ventricle to compensate.

The compensatory mechanism is described by the Laplace equation (Grossman et al., 1975) which describes that

$$\text{wall stress} = \frac{\text{pressure} \times \text{radius}}{2 \times \text{wall thickness}}$$

Wall stress is equal to afterload, and this is determined by the pressure gradient divided by double the wall thickness. Therefore, in the presence of an increasing pressure gradient, a corresponding increase in wall thickness will allow minimal change to the afterload.

Cardiac output is determined by the product of stroke volume (SV) and heart rate. SV is determined by the preload, cardiac contractility and afterload. Starling's law of the heart



describes the relationship between all three (see (Katz, 2002) and references therein). An increase in preload and cardiac contractility or/and a reduction in afterload leads to increased SV. Conversely, an increase in afterload but without a corresponding rise in contractility or preload will lead to reduced cardiac output.

LVH is commonly seen in AS and has long been thought to be beneficial in AS to maintain cardiac output. However LVH has been linked to HF (Levy et al., 1990) and is a marker of poor prognosis in other cardiovascular conditions with hypertrophic features, e.g. hypertrophic cardiomyopathy (Spirito et al., 2000) and hypertension (Schillaci et al., 2000).

The LVH response in AS is highly heterogeneous (Cioffi et al., 2011) which has prognostic implications. Inappropriately high LV mass, defined by Cioffi and colleagues as an indexed LV Mass (LVMI)  $>110\%$  predicted, was associated with a lower midwall stress-corrected fractional shortening (a marker of subclinical depression of LV function), with an associated increase in event rates (AVR, death, HF, non-fatal MI and development of symptoms). This may explain the poor correlation between severity of AS and symptom onset (Salcedo et al., 1989, Gunther and Grossman, 1979). More recent CMR studies confirm that there is no correlation between peak AV velocity (AS severity) and indexed LVMI (Dweck et al., 2012b). In fact, the degree of LVH appears to be affected by other risk factors, such as age (Salcedo et al., 1989), being male, obesity (Lavie et al., 2009), polymorphisms on the ACEI/D gene (Orlowska-Baranowska et al., 2004), coexistent hypertension (Rieck et al., 2010) and arterial stiffness (Briand et al., 2005, Hachicha et al., 2009).

#### **1.2.2.6 Progression to HF**

After a sustained period of compensated hypertrophy, the LV eventually becomes unable to maintain a forward flow through the AV against the increased afterload. The heart then

transitions into a state of failure, which is associated with development of symptoms, adverse events and poor prognosis.

This change is marked at a cellular level by two processes (Hein et al., 2003) where there is an excess of myocardial myocyte apoptosis without commensurate myocyte regeneration, resulting in a 5-10% loss of myocytes annually (Bishopric et al., 2001). The rate of loss is thought to be affected by the level of afterload (Cheng et al., 1995, Leri et al., 1998) but also seems to involve angiotensin II (Gonzalez et al., 2002, Schluter and Wenzel, 2008) whereby its local release in the myocardium is mediated by stretch, and its blockade in hypertension with angiotensin receptor blockers appears to reduce the rate of myocyte apoptosis. The lack of coronary blood flow reserve and reduced myocardial microperfusion may also worsen cardiomyocyte apoptosis (Galiuto et al., 2006). The use of renin-angiotensin blockers in severe AS and preserved LV ejection fraction was recently shown to be associated with a lower LV mass index and lower incidence of concentric hypertrophy (Goh et al., 2017). A prospective pilot randomized controlled trial showed that ramipril use was associated with a progressive reduction in LV mass in asymptomatic patients with moderate severe AS, with trending improvement in myocardial physiology (preserved tissue systolic velocity) and slower progression of the AS (slower reduction in valve area) when compared to placebo, although there was no difference in major adverse cardiovascular events or AVR (Bull et al., 2015).

Fibrosis is an obligatory process in myocardial hypertrophy (Anderson et al., 1979, Krayenbuehl et al., 1989) and seems to be focussed in areas of apoptosis (Bing et al., 1997) in a process akin to scarring in response to an injury. There is myofibroblastic infiltration and secretion of extracellular matrix proteins such as collagen I & III (Weber, 2004), a process which can be seen on cardiac magnetic resonance (CMR) with late gadolinium enhancement (LGE) as midwall fibrosis. This finding is associated with an 8-fold increased risk of

mortality (Dweck et al., 2011) and is promising as a predictor of adverse outcome in asymptomatic AS. Whilst AVR improves the poor prognosis associated with mid-wall fibrosis by 4 times, the adverse prognosis does not return to normal despite AVR, where the mortality rate in patients with midwall fibrosis who underwent AVR was 53.8 per 1000 patient years vs. 13.7 per 1000 patient years in the No fibrosis group (Dweck et al., 2012b). Although patients with AVR had regression of LV mass and extracellular volume (interstitial reversible fibrosis), there was no reduction in LGE/fibrosis up to 2 years after AVR (Everett et al., 2018). In asymptomatic patients who did not have AVR, fibrosis burden increased by an average of 78%. This suggests that by the time fibrosis has developed to a detectable level on CMR, it is already too late for AVR to have its maximal prognostic benefit.

Possible reasons for the irreversible risk despite a mechanical relief from the obstruction with AVR include the possibility of residual systolic and diastolic abnormalities after AVR (Hein et al., 2003, Martos et al., 2007, Gonzalez et al., 2003) and arrhythmic tendencies (Nazarian, 2011) as seen in other conditions associated with myocardial fibrosis (Assomull et al., 2006) although work in this area is lacking.

Given the appalling prognosis of symptomatic AS and presence of mid-wall fibrosis in AS, timing of AVR should be *before* development of symptoms and LGE on CMR. In practice, this may be difficult to achieve, based on the current evidence.

### **1.3 Current management of asymptomatic AS**

Although AVR techniques have improved substantially over the years, surgical (or more recently, percutaneous) AVR has remained the only effective method for mechanically relieving the obstruction caused by progressive AS. This treatment is particularly urgent when symptoms develop, with an incremental mortality risk of 2% for each month that the patient is waiting for surgery from symptom presentation (Lund et al., 1996).

International guidelines agree that AVR is indicated in symptomatic severe AS (Baumgartner et al., 2017a, Nishimura et al., 2014). Furthermore, asymptomatic severe AS in the presence of impaired LV ejection fraction (<50%) also receives a Class I recommendation, albeit with a lower level of evidence (B in American guidelines and C in European guidelines). This is because of the extraordinary improvement in symptoms following AVR and that in the absence of any other cause of LV dysfunction, the dysfunction is likely to make substantial improvement after reducing the pressure overload, and justifies the surgical risk. Surgical risk in healthy individuals without evidence of frailty or other risky conditions is low, at <1.5% risk of mortality in centres of excellence (Nishimura et al., 2014). AVR is also indicated in asymptomatic severe AS patients who develop symptoms (of dizziness, angina or dyspnoea) on an exercise test, which still receives a Class I indication in both European and American guidelines, although the recommendation weakens to IIa, Level C (European) or IIa Level B (American) for a fall in BP below the baseline during an exercise test (without developing symptoms), based on weak evidence (Das et al., 2005). The guidelines differ on their recommendations for rapid progression of AS (Table 1-1).

	AHA 2014 (Nishimura et al., 2014)	Recommendations	ESC 2017 (Baumgartner et al., 2017)	Recommendations
Symptomatic Severe AS	AVR indicated	Class I LOE A	AVR indicated	Class I LOE A
Asymptomatic Severe AS + LVEF <50%	AVR indicated	Class I LOE B	AVR indicated	Class I LOE C
Asymptomatic Severe AS + symptoms on Exercise testing	AVR indicated	Class I LOE B	AVR indicated	Class I LOE B
Asymptomatic severe AS + no symptoms on ETT + fall in BP below baseline	AVR should be considered	Class IIa LOE B	AVR should be considered	Class IIa LOE C
Asymptomatic severe AS + rapid progression of AS + low surgical risk + either AV-Vmax > 5.5m/s or severe calcification and AV-Vmax increase by >0.3m/s/year or 3x age & sex corrected BNP without other explanation or Severe unexplained pulmonary hypertension			AVR should be considered	Class IIa LOE C
Asymptomatic severe AS and low surgical risk + AV-Vmax > 5m/s	AVR should be considered	Class IIa LOE C		
Asymptomatic severe AS and low surgical risk + AV-Vmax increase by >0.3 m/s/year	AVR may be considered	Class IIb LOE C		

**Table 1-1: Differences between recommendations from different societies; AHA: American Heart Association, ESC: European Society of Cardiology, AS: AS, AVR: Aortic Valve Replacement, LOE: Level of Evidence, ETT: Exercise testing, BP: Blood pressure, AV-Vmax: peak velocity across aortic valve, BNP: Brain natriuretic peptide. Classes of recommendation: I – action recommended/indicated, IIa – action should be considered, IIb – action may be considered; Levels of Evidence: A – supported by multiple randomized trials and confirmatory evidence on metaanalyses, B – supported by a single randomized control trial or multiple non-randomized trials, C-expert consensus where robust evidence is lacking**

There is a lack of robust predictors of prognosis in AS to influence clinical decisions thus requiring clinicians to monitor patient-reported symptoms very closely and referring for surgery as soon as symptoms develop. Whilst this constitutes excellent follow-up from the patient's perspective, the wide variations in rate of progression of moderate asymptomatic AS requires that patients with moderate AS (AV-Vmax 3-3.9m/s) to be followed up (and receive repeat imaging) every 1-2 years, and patients with severe AS (AV-Vmax >4m/s) to be followed up and re-imaged every 6-12 months.

Asymptomatic AS carries an excellent prognosis. Even with conservatively-managed asymptomatic severe AS (AV-Vmax>4m/s or AVA<1cm<sup>2</sup>) the incidence of sudden death ranges from 0.4%/yr (Rosenhek et al., 2000) to 4.8%/yr if these patients were strictly not operated on (Amato et al., 2001). In a series of 116 asymptomatic patients with very severe AS (AV-Vmax>5ms), the risk of sudden death is only 0.3%/yr (Rosenhek et al., 2010). The average risk of sudden death with asymptomatic AS is, therefore, <1% as long as patients remain truly asymptomatic.

Exercise testing is currently used to determine if asymptomatic individuals with Severe AS are truly asymptomatic. One series showed that its positive predictive value in predicting spontaneous AS symptoms at 1 year is 57% but the negative predictive value is 84% and is most specific in those aged <70yrs (Das et al., 2005). In contrast, another series, which studied the negative predictive value of exercise testing, found that of 73% participants with mod-severe AS and a normal exercise test, 50% went on to have an event (AVR or CV death) during a follow up period of 20±14 months, suggesting that the negative predictive value of exercise testing is potentially only valid within a limited time-frame (Marechaux et al., 2010), or that exercise testing, while better than nothing, was not a very good positive predictor or events in asymptomatic AS.

54.3% of AVR is performed in those aged >70 (Lung et al., 2003) in keeping with the fact that degenerative AS is most prevalent in the elderly (>70). Symptom determination in this group can be especially problematic and is further compounded by the diminishing accuracy of exercise testing. Especially in patients with limited mobility, self-reported symptoms may not be forthcoming, and objective assessment may be challenging (Manning, 2013). Event-free survival in asymptomatic severe AS patients aged >70 years declined steeply from 73% at 1 year to 16% at 4 years in this age group, with no difference between patients aged below 80 or above 80 years, with the event-free survival of patients age <70 years being significantly better (Zilberszac et al., 2017). Importantly, 43% of patients aged >70 years who became symptomatic abruptly developed severe symptoms as their first symptom, despite close 6 monthly follow-up, which was associated with worse long term survival (Piérard et al., 2014).

#### **1.4 The argument for more biomarkers**

Whilst there is a clear signal of poorer outcome if fibrosis (by LGE) has developed, there is no definitive clinical data to support early AVR in asymptomatic AS at present, although randomized controlled trials for early AVR vs current guideline-based approaches are ongoing (EVoLVeD, AVATAR (Banovic et al., 2016) and EARLY TAVR; ClinicalTrials.gov NCT03094143, NCT02436655, NCT03042104). Early AVR for asymptomatic severe AS could be performed in patients who are chronologically younger and potentially fitter for surgery, reducing the surgical risk. They are also less likely to have developed the later irreversible damage from fibrosis which is associated with poor prognosis. Furthermore, much of the early fibrosis, identified by increased extracellular volume fraction (ECV) could be reversible with relief of pressure overload (Everett et al., 2018), before the onset of replacement fibrosis (Figure 1-2).

However, AVR is not risk-free. There is a small but significant risk of surgery, currently estimated at ~2.7% in Europe (Iung et al., 2003) but ~1.5% in America (Nishimura et al., 2014) in a healthy patient without concurrent coronary disease. Isolated AVR surgical mortality in the UK between 2010 and 2015 has been on a downward trend (1.84% to 1.55%), despite an increase in the proportion of higher-risk patients, based on the EuroScore (bluebook.scts.org). If concurrent CABG is being considered, the risk increases to 4.3% in Europe (Iung et al., 2003) or 3.22% in the UK in 2015 (bluebook.scts.org). There are also other risks to consider, e.g. prosthetic valve infective endocarditis, thrombosis with mechanical prostheses, associated risks of anticoagulation, and in the case of a bioprosthesis, valvular deterioration, necessitating eventual repeat surgery to replace the valve. These cumulative risks are estimated at about 1% per year (Thai and Gore, 2000).

A recent large multicentre registry of 3815 consecutive patients with severe AS ( $AV\text{-}V_{\max} > 4\text{m/s}$ ) found 1808 to be asymptomatic. Of these, 291 patients had an early AVR strategy, and 1517 had a watchful waiting strategy. These patients were propensity-matched, but differences remain, namely younger age and more severe AS in the early AVR group, which found less incidences of death (15.4% vs. 26.4%) or HF hospitalisation (3.8% vs. 19.9%) in the early AVR group vs. the watchful waiting group during a 5-year follow up period (Taniguchi et al., 2015). Whilst conclusions cannot be drawn from this registry, namely because the choice of early AVR vs. conservative strategy was made by the patient's physicians (likely biased), it does suggest that in low-surgical-risk patients, early AVR could safely be considered, and may be beneficial. In the Euro Heart Survey, 20% of AS interventions were classed as 'over-use' of the intervention, suggesting their surgeons/cardiologists believe that AVR should be performed early (Iung et al., 2003).



However, until results of randomized controlled trials to determine the optimal timing of AVR in patients with asymptomatic moderate to severe AS are forthcoming, clinicians lack the evidence to support any recommendation other than waiting for symptoms to develop. Until then, more robust predictors of outcome are needed in the form of biomarkers (Figure 1-2). Ideally, these will be identified from a cohort of patients and investigators blinded to the results of the test under evaluation, thus not biasing the results.

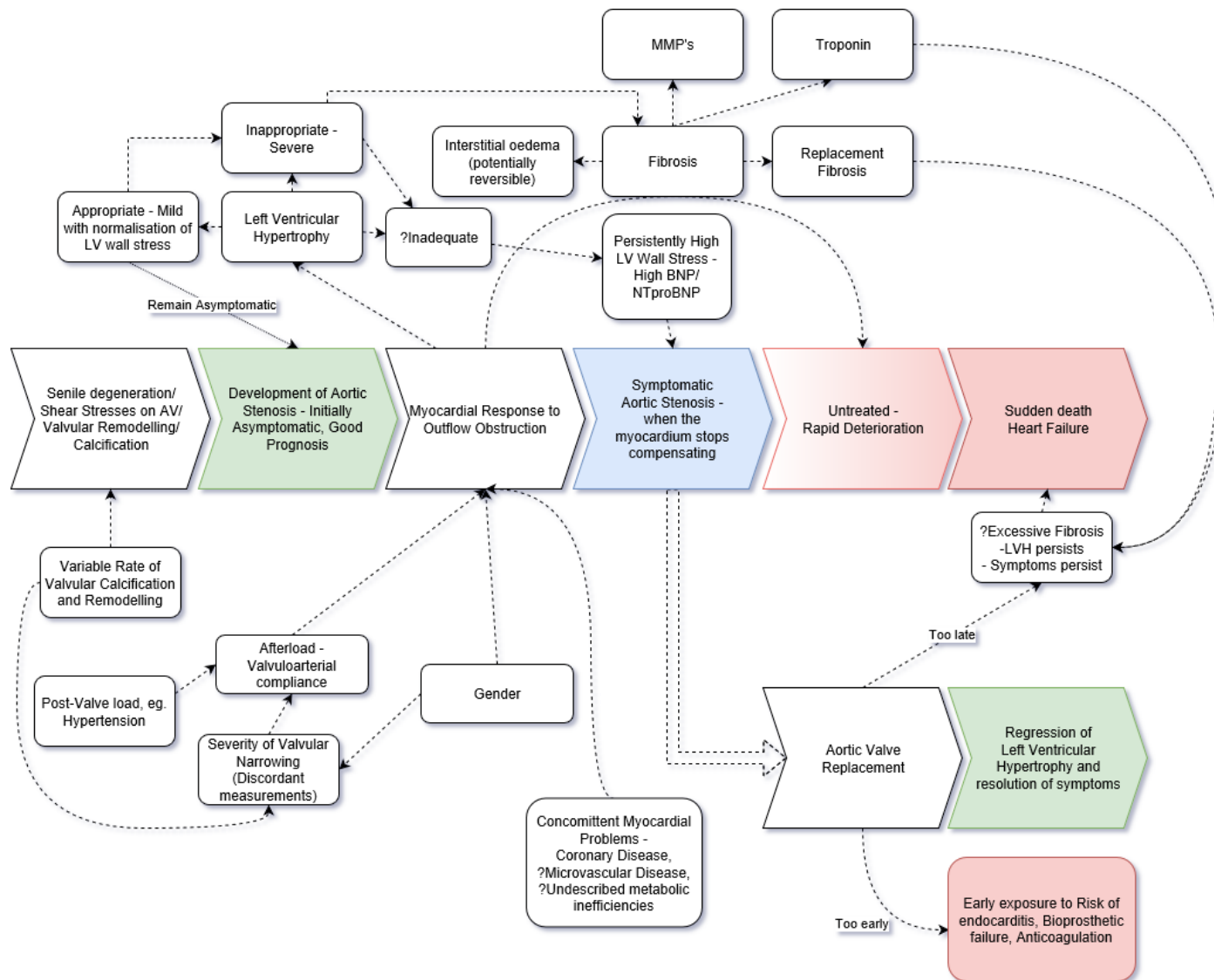


Figure 1-2: Central Figure - what is the optimal timing for AVR - should it be before onset of replacement fibrosis, troponin & BNP elevation, and symptoms? LV: left ventricle, BNP: brain natriuretic peptide, MMP: matrix metalloproteinase, AV: aortic valve

## **1.5 Current state of the art for biomarkers of prognosis in AS**

A systematic literature search in Pubmed for the terms “biomarkers” and “aortic stenosis” and “prognosis” identified 124 articles which were not classed as reviews. Of these, a systematic perusal of the titles and abstracts only identified 53 publications in English related to blood biomarkers whether directly or indirectly. All these publications are summarised in tables in the appendix.

Most of the work in this area focused on the natriuretic peptides which are markers of neurohormonal activation, with 9 publications on BNP (Sato et al., 2019, Goodman et al., 2016, Henri et al., 2016, Ben-Dor et al., 2013, Mannacio et al., 2013, Katz et al., 2012, Iwahashi et al., 2011, Kefer et al., 2010, Lancellotti et al., 2010) and 10 publications on NTproBNP (Kaneko et al., 2019, Mizutani et al., 2017, Mizutani et al., 2018, Nguyen et al., 2017, Farré et al., 2014, Boer et al., 2013, Elhmidi et al., 2013, Weber et al., 2006, Bergler-Klein et al., 2004). Cardiac troponin, a marker of myocardial injury has 7 publications on the subject (Kohler et al., 2016, Koskinas et al., 2016, Chin et al., 2014, Chorianopoulos et al., 2014, Frank et al., 2013, Saito et al., 2013, Rosjo et al., 2011). Unsurprisingly, both natriuretic peptides and troponin feature in 5 multi-marker analyses (Ferrer-Sistach et al., 2019, Dahou et al., 2018, Auensen et al., 2017, Lindman et al., 2015, Solberg et al., 2012).

The populations in which these studies were performed, ranged from moderate to severe AS, with or without AVR. Most outcome studies however were performed in patients with severe AS undergoing AVR, particular TAVI, and should be interpreted appropriately as this particular group of patients are by definition very high surgical risk. In this high risk group, both natriuretic peptides and troponin were mostly independently associated with increased short and longer term mortality, although the findings were not completely uniform; 6/7 studies found natriuretic peptides to be associated with mortality. Of the 4 studies in TAVI

testing troponin, 1 of the studies found that troponin was a better predictor of mortality compared to NTproBNP.

Other markers associated with mortality in this population were anaemia, GDF-15 & MRproADM (marker of cardiovascular stress) (Lindman et al., 2015), as well as acute kidney injury post-TAVI, and there were a few markers which predicted this injury (NGAL, Cystatin C and anaemia) (Elmariah et al., 2016, Arai et al., 2015, Johansson et al., 2014, Kidher et al., 2014).

Quite interestingly NTproBNP and MRproADM (Csordas et al., 2015, Lopez-Otero et al., 2013) were compared with the logistic Euroscore II, commonly used to evaluate perioperative surgical risk, and both were found to be superior to the score in the TAVI population. Being aware of the high risk only helps inform the decision-making for the patient; in this high-risk group it is not clear how the mortality risk can be lowered. One study found that natriuretic peptides predicted mortality in conservatively treated severe AS, but not patients with AVR (Weber et al., 2006), implying that surgery in these patients with higher natriuretic peptide levels probably does alter the risk of mortality, but these findings have not been described elsewhere.

Other biomarkers have been described; cardiac myosin-binding protein C has a similar prognostic association as troponin (Anand et al., 2018). 5-adenosyl-homocysteine was associated with acute kidney injury after TAVI (Elmariah et al., 2016); Fibulin-1 was associated with diastolic dysfunction/restrictive filling in severe AS (Dahl et al., 2012); Galectin-3, a marker of fibrosis, was found not to be associated with AV-related events (Arangalage et al., 2016), although this population included mild AS (NTproBNP in the same population associated with AV-related events, but not independent of AS severity (Nguyen et al., 2017)). Sheer stress is considered important in severe AS, and high molecular weight

von-willebrand-factor could be used to differentiate true-severe AS from pseudo-severe AS in low-flow low gradient AS (Kellermair et al., 2018). Microparticles released from platelets were elevated in severe AS undergoing TAVI, with the surgery lowering the amount of circulating microparticles, suggesting improvement in sheer forces (Jung et al., 2017). A number of microRNA's have been associated with left ventricular hypertrophy as well as mortality (Chen et al., 2014, Rosjo et al., 2014, Garcia et al., 2013). Finally, lipoprotein(a) and soluble urokinase plasminogen activator receptor (suPAR), both associated with increased cardiovascular risk (from ischaemic heart disease), were associated with coronary artery disease and ischaemic events respectively, in AS patients, highlighting the contribution of concomittent coronary disease to prognosis (Hodges et al., 2016, Ljungberg et al., 2017). Of note, one study mentions that elevated troponin post-TAVI in patients with complex coronary disease was associated with significant mortality post-TAVI (Koskinas et al., 2016).

Multi-marker risk stratification strategies have been explored (Ferrer-Sistach et al., 2019, Dahou et al., 2018, Auensen et al., 2017, Lindman et al., 2015, Solberg et al., 2012, Kapelouzou et al., 2015, Parenica et al., 2012, Elmariah et al., 2016). Of the 7 publications looking at multiple markers, 6 looked at long term adverse outcomes. One was done in asymptomatic severe AS, another was done in low-flow-low-gradient AS. One study in asymptomatic severe AS found that when troponin was compared directly with NTproBNP in the same proportional hazards model, NTproBNP was classed as not having an independent prognostic effect (Ferrer-Sistach et al., 2019). Conversely, in a separate population of patients referred for AVR, troponin was not retained in a parsimonous model to predict mortality (Lindman et al., 2015). Yet another study finds both (as well as diabetes), together to be strongly predictive of mortality in patients with severe AS referred from valve replacement (Solberg et al., 2012).

In summary, the current biomarker landscape in terms of prognosis in AS has been very focused on natriuretic peptides and troponin. Overall, high levels of troponin or natriuretic peptides were associated with higher risk of adverse events, even when asymptomatic, but not necessarily when mild AS patients were included in the studies. Some more novel biomarkers have been found in single studies to be potentially important and deserve additional work, implying a need to focus on other pathways associated with progression of AS. Multi-marker studies have the potential of measuring multiple pathways at once and hence can better describe the overall risk, but studies evaluating multiple markers so far have not suggested additional importance of other markers when compared directly with natriuretic peptides or troponin. More of these studies are therefore urgently required.

## **1.6 Plasma Proteomics to identify Biomarkers**

### **1.6.1 Proteomics**

Proteomics refers to the study of proteomes and their functions. The term proteomics was coined in 1995, wherein it was defined as the "large-scale characterisations of the entire protein complement of a cell line, tissue or organism" (Anderson and Anderson, 1996, Wasinger et al., 1995). An inclusive view of proteomics involves identifying protein-protein interactions, protein modifications, and protein localisation, etc. The proteome changes in response to alterations in gene expression or environmental pressure. The effect can be observed in alteration in protein expression at various levels, such as the level of the organism, tissue or cellular level. As a result, proteomics is a natural vehicle for clinical biomarker discovery.

The profiling of proteins, whether by quantitative or qualitative means in clinical tissue samples, or bodily fluids such as plasma, urine or cerebrospinal fluid is termed clinical proteomics (Banks and Selby, 2003). In its simplest form, an experiment comparing the

proteomic profile between a diseased patient group and a healthy patient group which is otherwise controlled helps identify the differences in protein expression associated with the disease, and can help identify potential biomarkers of disease.

#### **1.6.1.1 Bottom-up proteomics**

Bottom-up proteomics involves identifying proteins from its constituent peptides, so as to provide as complete a view of the proteome as possible, then looking for changes in protein expression levels in two or more groups with a different phenotype. This typically is a three-step approach, which comprises 1) sample preparation 2) sample analysis and 3) data analysis. There are many established protocols with regard to this, with no clearly superior method. State-of-the-art mass spectrometric (MS) technology has enabled the large-scale identification of unknown masses with considerable accuracy and sensitivity, and paired with large libraries of known spectra and sequences for proteins, has substantially improved the rate at which proteins can be identified.

All steps involved in identifying the proteome and quantitating its constituents affect both the identifications and the quantities measured. As such a robust workflow with high reproducibility is required in order to enable meaningful conclusions about any MS experiment.

A typical bottom-up proteomics experiment involves the digestion of proteins with the enzyme trypsin to create tryptic peptides. Trypsin is a highly specific enzyme, cleaving the protein at the C-terminal end of lysine or arginine residues, except when either of these residues is flanked by proline. This simplifies the deduction of the identifications of the peptides, especially with comprehensive sequence libraries. These peptides are then separated by online liquid chromatography coupled to a mass spectrometer, which detects these peptides as masses, and reports them in the form of mass/charge ( $m/z$ ) ratios. The resultant

m/z results are passed on to a bioinformatics platform for data analysis which identifies the masses, by matching the generated spectra from these masses against databases of known peptides/proteins as well as quantifying the amount of these masses by some measure of ion intensity. Differentially expressed proteins in samples and controls are then verified as biomarkers through other methods such as enzyme-linked immunoassays to determine if the biomarker is truly associated with the disease, ideally in a prospective cohort or blinded verification cohort.

### **1.6.2 Plasma**

Plasma is a suitable medium to identify biomarkers. Obtaining samples is minimally invasive, quite acceptable to patients and after extraction can be stored at -80°C indefinitely for future analysis. Given that plasma is the circulating medium in mammals after separation of the cellular component, it lends itself to being a carrier of all the differentially expressed proteins in the organism (Anderson and Anderson, 2002) that have either been secreted by tissues, or leaked by tissues in response to either a change in expression or/and environmental insult, e.g. in the case of troponin which is leaked after myocyte necrosis into plasma. Finally, biomarkers discovered in plasma could easily be translated into clinical practice.

#### **1.6.2.1 Plasma vs. Serum**

The decision between using plasma vs. serum for biomarker discovery is a pragmatic one. The difference between the two media is that plasma has an anti-coagulant additive added to it at the time of sampling, so that clotting factors are not activated. This means that all the clotting factors are still present to be assayed, and there is potentially reduced post-sampling protease activity. The cells are separated from the plasma by centrifugation, and taken off gently avoiding the buffy coat after centrifugation. Serum on the other hand, is what is



obtained after venepuncture, after allowing the sample to clot naturally. The clear fluid would be free of clotting proteins.

There are arguments for and against the use of either plasma or serum in biomarker discovery (Table 1-2), but the decision is generally a pragmatic one. For example, levels in plasma cannot be directly compared to levels in serum, therefore if a research group has a tradition of using plasma for all their studies to date, will continue using it for the future, should there ever be a need to compare individual levels between studies. Our research group has abundant experience using plasma in clinical studies for biomarker discovery and therefore this was the medium used in this study.

	Plasma	Serum
Clotting Proteins	Present in abundance, No activation of proteases during clotting which may fragment other proteins	Absent (therefore improving access to lower abundance proteins)
Non-specific protein loss	Not affected	Non-specific protein losses within blood clot which may not be completely predictable
Sampling considerations	Requires fixed additive (EDTA) to blood ratio. Ideally should be fully processed within a narrow but fixed time window (1 hour), due to potential for cellular lysis, secretion of platelet activation products.	Blood allowed to clot between 30-60 minutes in a designated serum isolation collection tube. <30 minutes clotting may result in cellular components being present. >60 minutes clotting may result in cellular lysis.
Cellular component	Separated by centrifugation, not present if buffy coat not disturbed	Separated by clotting, lower risk of presence if clotting time adhered to

Table 1-2: Arguments for and against the use of plasma or serum for biomarker discovery

### 1.6.2.2 Challenges with plasma proteomics

Translating novel biomarkers identified from plasma to clinical use, has been slow (Anderson, 2010). This is, in part, due to plasma's extreme complexity. 99% of proteins in plasma are made up of highly abundant plasma proteins. The top 7 of these are albumin, IgG, alpha-1-antitrypsin, IgA, transferrin, haptoglobin, and fibrinogen. There are other proteins as well in plasma; these have been termed moderately abundant and low abundance proteins. Whilst the abundant proteins play an important role in plasma, either as carrier proteins or as acute phase reactants, identifying novel biomarkers requires us to look past the bulk of plasma proteins into the low abundance proteins where changes in expression are more likely to be disease-specific and potentially more sensitive.

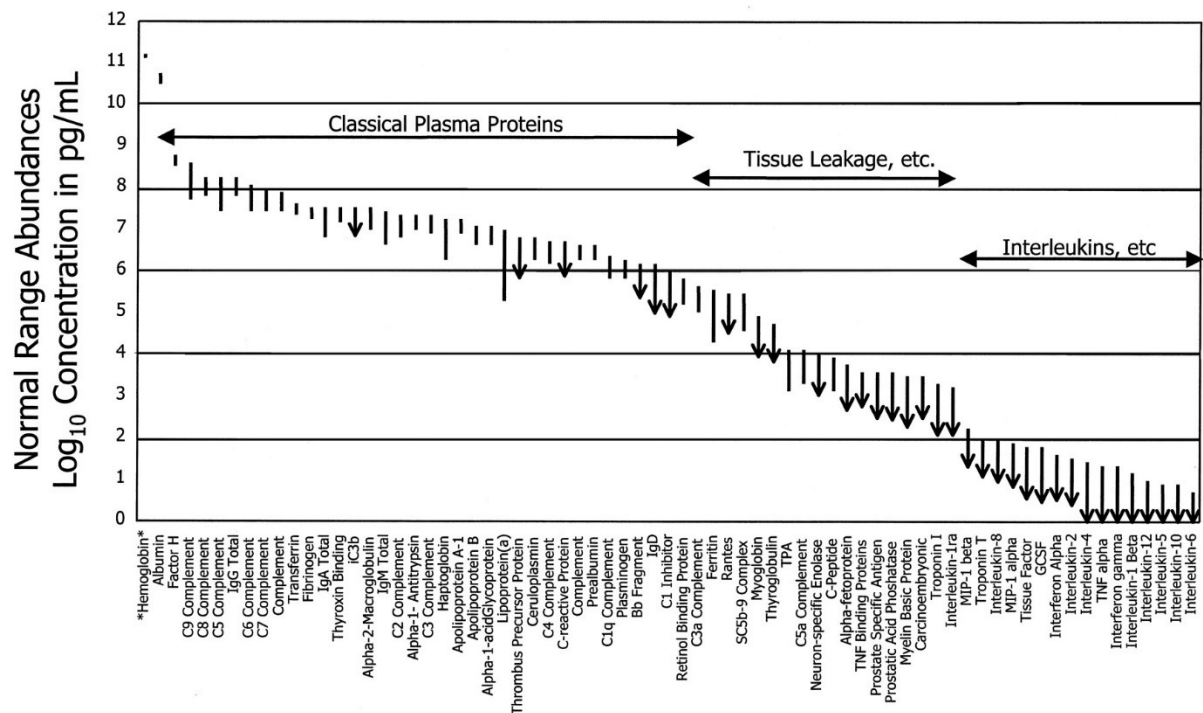


**Figure 1-3: Complexity of the plasma proteome. 70 analytes in plasma occupying an abundance range spanning 12 orders of magnitude. Permissions obtained, original published in (Anderson and Anderson, 2002).**

Plasma proteins span approximately 12 orders of magnitude (Anderson and Anderson, 2002)(i.e.  $10^{12}$ ) in abundance (Figure 1-3). For example, there is approximately  $10^6$  times more albumin than prostate specific antigen in plasma. Unfortunately, current technology for MS quantitation is limited to between 4-5 orders of magnitude (Anderson and Anderson, 2002), which means that using unbiased mass spectrometric analysis (i.e. without targeting/filtering a specific molecule), the discovery/quantification of lower abundance proteins will be masked by high abundance proteins if the range of abundances in the sample exceeds this dynamic range. Extending this by combining fractionation methods or 2 dimensional electrophoresis increases this dynamic range by up to 100x, but is still short of the 12 orders desired.

### 1.6.2.3 Overcoming the challenges of plasma proteomics

The field has seen significant advancements in mass spectrometric technology, as well as bioinformatics methods. Fractionation of samples into fewer complex fractions have been

used increasingly to attempt to address the high dynamic range of plasma. The focus shifted first on increasing the numbers of identifications, then later towards improving the quality of these identifications, resulting in an overall drop in numbers.

#### **1.6.2.3.1 Immunodepletion**

One of the most popular methods of improving the detection of the low abundance proteins is by immunodepletion. This method involves binding the high abundance proteins to immobilised antibodies on a stationary phase, such as a silica mount, and allowing the low abundant One of the most popular methods of improving the detection of the low abundance proteins is by immunodepletion. This method involves binding the high abundance proteins to immobilised antibodies on a stationary phase, such as a silica mount, and allowing the low abundant proteins to flow through. Many chromatographic columns have been designed for this purpose, with good results. Examples of these include ProteoPrep, Seppro and MARS-14. The Multiple Affinity Removal System (MARS) – developed by Agilent, combines polyclonal antibodies targeting the top 14 high abundant proteins, which are albumin, haptoglobin, transferrin, IgG, IgA, alpha-1-antitrypsin, alpha-2-macroglobulin, alpha-1-acid glycoprotein, apolipoprotein-A1, apolipoprotein-AII, complement C3, IgM, transthyretin and fibrinogen (Echan et al., 2005, Pieper et al., 2003). It is highly reproducible chromatographically and retains its affinity for these proteins over 200 runs. Immunodepletion improves identification of proteins in plasma by 25% (Tu et al., 2010). Despite this, only 5-6% of the total protein identifications in plasma that has been immunodepleted are low-abundance proteins, and 90% of the proteins identified were the top-50-most-abundant proteins in plasma. Most commercially-available depletion columns perform similarly well, removing >98% of targeted proteins and ~95% of the total protein (Beer et al., 2017). More extensive depletion (tandem IgY 14 and SuperMix immunoaffinity depletion) of high abundance (Top 14) and medium abundance proteins (additional 60

proteins) using avian polyclonal IgY-antibodies effectively captured 99% of the total protein (Shi et al., 2012). Extensive depletion in this way consistently identified 3-6x more low abundant proteins than other depletion methods. Authors reported that whilst the MARS14 column identified ~200 protein groups by 2 or more peptides and ~50 protein groups by 1 unique peptide on a Q Exactive Plus instrument in a 4-hour run, the IgY14/Supermix tandem depletion identified ~680 protein groups by 2 or more peptides and ~120 protein groups by 1 unique peptide on the same instrument (Beer et al., 2017). The downside to this methodology is cost – a tandem IgY14/SuperMix depletion system costs ~£16000 for a set of columns that are good for 100 injections – at ~£160/sample. The MARS14 column costs £3000 and is good for 200 injections at ~£15/sample. An additional concern about extensive immunodepletion is the loss of non-targeted proteins of interest, due to non-specific binding either to the column, the antibody or to the targeted proteins on the column eg. albumin (Gundry et al., 2007). Finally, non-targeted protein losses may vary from run-to-run, which may confound the interpretation of protein quantification.

#### **1.6.2.3.2 Fractionation**

##### **1.6.2.3.2.1 Protein fractionation**

Pairing depletion with a fractionation step could hypothetically reduce the complexity of plasma, and improve the ability to detect low abundance proteins. Plasma proteins could be fractionated based on their various properties in a liquid phase through the use of liquid chromatography. Hypothetically, quantification of proteins resolved to their own fraction should be more representative than if compared to quantification of proteins which have been digested, then their peptides fractionated in one dimension, concatenated, then quantified post-hoc during mass spectrometric analysis.

Proteins typically have a tertiary structure in aqueous media where the hydrophobic residues are sequestered at the core and charged polar residues are on the surface.

Chromatographic modalities that can separate proteins based on different properties may therefore reduce the complexity of plasma. Proteins of high abundance could be isolated in discrete fractions, reducing masking of low abundance proteins from other fractions.

Ion exchange chromatography (IEX) leverages the attractive charges on the charged residues on the surface of proteins to the stationary phase of the opposite charge. It has been used with success as part of a 3-dimensional separation in shotgun-proteomics, more than doubling the number of protein identifications (Zhang et al., 2012, Hood et al., 2005). The mild nature of the conditions typically used in ion exchange chromatography do not denature proteins, but highly hydrophilic proteins (eg. Membrane and structural proteins) need to be solubilized first with organic solvents or solubilizing agents to be used with IEX. Elution in IEX involves a gradient of increasing salt concentration. Often however, very high salt concentrations are required making these method incompatible with mass spectrometry. Changing the pH of the mobile phase could also be used to change the net-charge of the proteins, thus reducing the salt concentration required for elution.

Hydrophobic interaction chromatography is another method that starts with a high concentration of a salt which reduces the water available to hydrate proteins, at which point the proteins will adsorb onto a modestly hydrophobic surface. As a reducing salt concentration gradient is run, adsorbed proteins are resolvated and elute in the order of their increase in hydrophobicity of their tertiary structure, not dissimilar to reversed-phase chromatography, although the stationary phase is much less hydrophobic and the mobile phase not denaturing. This separation method can be very useful not only to map peptides but also allow detailed post-translational modification analysis of single proteins as well as study protein complexes and interactions (Rackiewicz et al., 2017).

Size exclusion chromatography on the other hand uses hydrophilic stationary phases with defined pore-sizes and is non-denaturing. Paired with 2D-peptide fractionation, size exclusion chromatography is successful in improving protein identifications in liver tissue lysate (Zhang et al., 2007), as well as mammary epithelial cell lysate (Jacobs et al., 2004).

Although reversed phase liquid chromatography (RPLC) is the most widely used high performance liquid chromatography (HPLC) method, these applications tend to be for peptides and not proteins. The reason it tends to be unsuitable is because the stationary phases tend to be very hydrophobic and cause proteins to denature. Further denaturation occurs with the use of organic solvents featuring extreme pH's all leading to the loss of their protein's tertiary structure. Denaturation of large proteins potentially would lead to exposure of very large numbers of hydrophobic residues resulting in simultaneous interactions with the stationary phase, which would make protein elution much more difficult and lead to very wide protein peaks or no elution at all. Despite this, the macroporous high recovery reversed-phased silica mounted c18 column (mRP-C18) appeared to have very promising results with good protein recovery and good protein resolution as long as optimal column conditions were adhered to, leading to identifications of low abundant proteins when paired with immunodepletion (Martosella et al., 2005).

The preferred conditions for their fractionation involved maintaining a high column temperature (80°C) and utilising a binary gradient with water and 0.1% trifluoroacetic acid (TFA) as the aqueous buffer and acetonitrile and 0.08%TFA as the organic buffer. The shallowest part of the gradient of increasing organic composition was between 30-55% organic. The gradient length was 54 minutes. The maximal protein loading capacity was reported to be between 400-500 µg before apparent overloading. This has since been revised by the manufacturer to 380 µg. Finally, the method does not suffer from carry over, if the sample has been immunodepleted of the top-6 abundant proteins first. The group confirms

that using the preferred conditions, 98% protein recovery could be expected, in contrast to lower recoveries from other C8 columns also investigated for protein fractionation.

Martosella tested a variety of temperatures and found that 80°C significantly improved separation resolution. Peak widening was noted at 40°C and 26°C for most peaks. Martosella found that temperature was by far the most important factor in separation efficiency. Other conditions were tested too, varying from no acid to higher concentrations of TFA in the mobile phases, and two different denaturants – guanidine and urea. There were minimal differences between the separations with the two denaturants, although urea was preferred. Martosella went on to lyophilise the fractions, reconstitute in 8M urea in an Ammonium bicarbonate buffer, digest with Lys-C followed by Trypsin, without a reduction or alkylation step.

This was modified in a subsequent protocol (Zolotarjova et al., 2008) to include a Trifluoroethanol (TFE)-based denaturation step (Ru et al., 2006) where 50% TFE was used, followed by reduction and alkylation with DTT and IAA respectively. By combining immunodepletion, protein fractionation with the mRP-C18 and two dimensional (2D) online LC/MS/MS, they were able to identify several low abundant proteins in multiple fractions, with a high number of peptides identifying these proteins, although they combined protein fractionation with 2D online peptide separation LC/MS/MS, which is not a high throughput method.

A few other groups have done some additional work on the mRP-C18 column, giving rise to some variation in protocols (Adachi et al., 2006, Malen et al., 2008, Ye and Li, 2014, Blankley et al., 2013), but they all retain the TFA as the acid modifier, acetonitrile as the organic solvent of choice and the column temperature of 80°C in their protocols. The only



real variation is the gradient steepness and the time of the entire duration of the separation, as well as the time from which fractions are collected.

#### **1.6.2.3.2.2 Peptide level fractionation**

Peptide level fractionation involves digestion of proteins with a specific protease, typically trypsin, then fractionating using a chromatographic mode. Typically examples are strong anionic/cationic exchange or high pH RPLC, coupled with online low pH RPLC for the 2nd dimension during LC prior to MS analysis. This method is very successful and reproducible, due to the stability and predictable properties of individual peptides, whether hydrophobicity, polarity or pI.

A recent state of art review summarised 20 studies illustrating the fractionation methods that the proteomic community has reported, and whilst not exhaustive, is representative of the heterogeneity of methods used and described, the results obtained with variable levels of success (Pernemalm and Lehtiö, 2014). However, authors cited difficulty in comparing studies or methods; samples were depleted using different methods, different combinations of fractionation steps, and different combinations of LC/MS/MS equipment. These all made assigning any alleged improvement to any particular part of the workflow difficult.

Furthermore, the authors also commented that “the number of replicates, number of fractions and amount of loaded sample heavily affects the results”. What is clear is that individual steps (including immunodepletion) can be considered ‘fractionation’ steps and whilst some fractionation steps increase the number of protein identifications dramatically (eg. From Top-12 depletion to Top-12 depletion + Supremix depletion resulting in a doubling of protein groups (Qian et al., 2008)), other fractionation steps have a less profound impact (Cao et al., 2012), e.g. increasing the number of fractions from 20 to 40 in SDS-PAGE only increased identifications by 32% (i.e. 1.6% more identifications per additional fraction) or increasing

the number of fractions from 20 to 40 in peptide-high-pH RPLC fractionation only increased identifications by 40% (i.e. 2% more identifications per additional fraction).

#### **1.6.2.3.2.3 Challenges with fractionation**

The overarching issue with multi-dimensional fractionation is the loss in throughput. The increase in protein identifications is not commensurate with the increase in analytical time. The second concern is that the incremental number of steps for sample preparation could result in significant sample losses and introduce factors which confound quantification and affect reproducibility.

#### **1.6.2.3.3 Enrichment**

Enrichment of low abundance proteins could also improve their detection. An example is the Proteominer technology, which was recently compared with top-20 immunodepletion (Hakimi et al., 2014). Although improving identification of low abundant species in plasma, quantitation may be affected due to saturation of the enrichment mechanism, resulting in skewed protein quantitation results.

Alternative to the commercial systems for enrichment, other methods also enrich for certain subproteomes, e.g. phosphoproteomes with metal-ion affinity chromatography (Yue and Hummon, 2013).

##### **1.6.2.3.3.1 Calcium Silicate Hydrate (CSH) Enrichment**

Our research group had been working on enriching for proteins associated with high density lipoprotein, long implicated with a protective role in a variety of cardiovascular conditions. Enrichment of plasma lipoproteins with a CSH matrix is both cheap and easy to perform. It was originally developed to study plasma lipoproteins separated by non-centrifugal methods (Gordon et al., 2010), but in fact our research group has found it useful for single-shot plasma

proteomics (Emmens et al., 2018), even if the focus of the proteome it exposes is that of the high-density lipoproteome because it is highly relevant to the field being studied.

#### **1.6.2.3.3.2 Extracellular vesicle (EV) enrichment**

Most cells release exosomes (50-150 nm diameter), which are produced by inward budding and scission of the endosomal membrane containing intraluminal vesicles, which fuse with the plasma membrane, and contain intracellular proteins. Microvesicles however, are released by shedding of plasma membranes and are 100nm to 1µm in diameter. Current methods do not obtain pure exosomes, and instead provide a mixture of exosomes, microvesicles and other EVs like apoptotic bodies or even low density lipoproteins (Kowal et al., 2016, Sódar et al., 2016). However, EVs are associated with cardiovascular disease (Davidson et al., 2017) with potential for novel biomarker discovery, if a satisfactory method to enrich for associated proteins exist.

Ideal methods needed to be cheap and reproducible, and did not require large quantities of sample (due to limited availability). One study demonstrated a simple workflow for isolating microparticles, by a sequence of washing platelet-poor-plasma after centrifugation at 18890g at room temperature for 30 minutes, removing the supernatant each time (Østergaard et al., 2012). Methods such as size-exclusion chromatography followed by ultracentrifugation (Smalley et al., 2007) were considered, but would have been too cumbersome for larger sample sets. The pellet after centrifugation contains platelet fragments, microparticles and a plethora of vesicles of different origins, including lipoproteins and protein complexes as well as plasma proteins (György et al., 2011).

Another group identified a simple method of salting-out exosomes from biological fluids based on the expression of the negatively-charged phospholipid phosphatidylserine on exosomes, by precipitation from solution by neutralizing the surface charge with acetate

(Brownlee et al., 2014). Authors demonstrated that titration of samples with 0.1M acetate to pH 4.75 resulted in rapid precipitation of virtually all exosomes in the sample, which could be resolubilized in an acetate-free buffer at neutral pH, with exosomes that had the same properties as exosomes isolated by ultracentrifugation. Although this “salting-out” method does selectively precipitate exosomes, it also non-selectively co-precipitates some non-exosomal proteins, which authors identified as alpha-2-macroglobulin as well as fibrinogen. These two promising methods were worthwhile to be compared with an immunodepletion + protein fractionation workflow to see which was better for biomarker discovery.

#### **1.6.2.3.4 Digestion, Denaturation, Reduction & Alkylation**

Trypsin is a highly specific enzyme cleaving peptide bonds on the C-terminal of lysine or arginine, but not if either are flanked by proline. Tryptic efficacy is dependent on temperature, duration of digestion, pH, and protein characteristics. Whilst optimal temperature, duration of digestion and pH are well described for trypsin, improving protein digestion is less well described. Typically protein will benefit from denaturation, which unfolds proteins so that its lysine and arginine residues are exposed. Subsequently, proteins should be reduced which breaks covalent disulphide bridges between cysteine residues on different parts of the amino acid chain, which may potentially conceal further lysine and arginine residues within. The reduced residues should then be alkylated to prevent reformation of their disulphide bonds, and the resultant protein should now be an unfolded polypeptide chain ready for optimal tryptic digestion.

Common methods for denaturation include introduction of chaotropic agents (urea, guanidine), surfactants/detergents (SDS, sodium deoxycholate), solvents (methanol, acetonitrile, TFE) or using heat. Other less known and evaluated methods includes denaturation with acid (Wu et al., 2011). Similarly there are a variety of methods for

reduction of proteins, but the best known are DTT, tris (2-carboxyethyl) phosphine (TCEP) and mercaptoethanol. Two classical methods for alkylation are IAA and iodoacetate. The choice of any of these agents depends a lot on the conditions of the buffer that the plasma proteins are in, effectiveness and time considerations, as well as ease of use. One study compared 14 combinations of heat, solvent, chaotropics and surfactants and their effects on tryptic digestion efficiencies on plasma protein and found that the best denaturant, in terms of a combination of efficacy and reproducibility was SDS, followed closely by deoxycholate (Proc et al., 2010). SDS however causes significant ion suppression even in small quantities, which causes significant ion suppression in our research labs, whilst deoxycholate could easily be fully removed prior to analysis.

Reduction methods using DTT and TCEP are comparable in efficacy but TCEP appeared more robust in terms of stability of its reduction but also its wide active pH range (1.5-8) (Han and Han, 1994). In aqueous solution, its reduction reaction is irreversible and complete. It is unreactive with IAA, obviating the need to remove it before alkylation (Getz et al., 1999). TCEP however is acidic if just diluted in water, and therefore should be neutralised first, or used in an alkaline buffer (e.g. if using with deoxycholate).

Alkylation is performed with IAA, a thiol-compound which irreversibly reacts with available thiol groups on cysteine exposed by reduction of sulphydryl reducing agents (Smythe, 1936). Iodoacetate, its acid derivative, reacts slower. Alkylation prevents the reformation of the disulphide bonds that have been reduced to allow time for trypsin to digest any lysine or arginine residues on the chain that may have been hidden by the folded protein. IAA reactions occur well at room temperature but need to be performed in the dark and takes 20-30 minutes to complete. Its reaction can then be quenched by addition of excess DTT or inactivated by light.

Tryptic digestion is most efficient at pH 8-9, at 37°C and completeness of digestion varies by time from protein to protein (Proc et al., 2010). It is sensitive to the presence of chaotropes/solvents/surfactants/iodoacetamide in variable quantities; therefore these need to be factored into the workflow decision making process to ensure preserved efficacy. Trypsin concentrations used vary from 1:100 to 1:25 enzyme:substrate (w:w) ratio. The higher concentrations of trypsin may cause trypsin autodigestion when it has run out of substrate; and its proteolytic fragments may then cause signal suppression in the same way high abundant peptides do.

After tryptic digestion which is typically allowed to continue for 16 hours for convenience, the sample is acidified to denature trypsin and prevent autolysis, to a pH of <2. The sample is then desalted by solid phase extraction, e.g. with C18 columns, C18 cartridges or C18 Zip Tips.

### **1.6.3 Mass Spectrometry**

Mass spectrometry is the analysis of charged ions, under vacuum with a resultant spectrum readout that allows significant information to be arrived at about the ionised molecule (including mass, isotopic profile, structural information and elemental composition).

Modern MS of biological samples utilises equipment which are modular and customisable to almost any requirement. Each setup has its pros and cons and ultimately the cost element becomes the limiting factor in what technology is available to the researcher.

Two different types of MS setups were used in the biomarker discovery and verification workflow.

### 1.6.3.1 Q-exactive Platform

The ThermoFisher-Scientific Q-Exactive hybrid-quadrupole Orbitrap is a benchtop analyser which combines a quadrupole with an orbitrap analyser, coupled with ultra-high performance liquid chromatography.

In principle, the sample is first desalted then separated by low pH RPLC on a C18 column. The eluting analytes/peptides become ionised/protonated by electrospray ionisation (ESI), which occurs at atmospheric pressure. ESI is a soft ionisation technique, leading to minimal fragmentation of the analyte. A high differential voltage applied across the ESI needle causes protonation of the molecules, through the formation of a Taylor cone. The positive charges that accumulate on the molecule/analyte continue to repel each other until two things occur; the analyte loses enough solvent to enter the gas phase and it gains one or more protons, permitting travel in the direction of the voltage gradient into the mass spectrometer.

Unlike other atmospheric pressure ionisation techniques such as matrix-assisted laser desorption ionisation (MALDI), ESI allows formation of multiply-charged macromolecules, which effectively increases the detector's effective mass range on many platforms and has revolutionised MS-analysis of biomolecules.

Charged molecules are carried into the MS where filtering and focussing occurs. In the case of the Q-exactive, the first stage is focusing with the S-Lens, followed by transfer through the hexapole. Here, additional neutral ions are removed from the analyte path, reducing background noise. Charged molecules are directed electrically by the hyperbolic quadrupole mass filter and collected in the C-Trap. A packet of charged molecules are then sent into the Orbitrap™ mass analyser for the full-MS scan, providing the MS1/precursor ion value in the form of  $m/z$ , and with corresponding ion intensities, allowing quantitation of that particular ion.

Most MSs perform MS in tandem (known as tandem MS/MS) where the second analysis involves fragmentation of the precursor ions into their constituents (usually by collision induced dissociation (CID) or in the case of the Q-exactive, higher-energy collision-induced dissociation (HCD)), resulting in a spectra of fragment ions. In data-dependent acquisition (DDA) mode, precursor-ions (e.g. top-10 abundant) are selected by the quadrupole for fragmentation in the collision cell. These fragments are then passed into the orbitrap mass analyser for detection (Makarov, 2000).

The ion current of the orbiting ions are then translated by a fourier-transform-algorithm to constituent  $m/z$ s of the fragments. This allows detection of several molecules instantaneously, with very high mass accuracy. The fragment ion  $m/z$ s are then used *in-silico* to reconstruct the most accurate identification of the precursor masses, increasing the confidence of the identification of the peptide being analysed.

DDA results in good quality spectra from which confident identifications can be made, with small data file sizes, lower computational overheads and storage costs for analysis. However, while the detector is fragmenting selected ions, unselected ions are not detected and are lost. Because peak picking is somewhat stochastic by nature, the result is that when comparing quantities between groups, there are missing data arising from ions that have not been fragmented. A promising computational method to reduce missing data from DDA acquisitions has recently emerged (Zhang et al., 2016a) which may be able to work around this problem.

#### **1.6.3.2 Synapt-G2 & G2-S**

The alternative approach is for data independent acquisition (DIA). DIA can be utilised on a Waters Synapt-G2 or G2S, a quadrupole-time-of-flight (TOF) platform. Like the QExactive



platform, the system is coupled to a NanoAcquity UPLC, which separates the peptides by RPLC. The samples are also ionised by ESI.

Uncharged ions are filtered by the Z-spray, where an electrical charge is applied in tangent to the flow of ions from the electrospray so that only charged ions get into the mass spectrometer. There is subsequently a Step-wave, a series of RF modulators, which apply another tangential voltage on the ions that have made it into the mass spectrometer so that further neutral ions can be removed; it is this add-on that differentiates a Synapt G2-S from a G2.

Ions then pass through a quadrupole where there is the opportunity to focus only certain types of ions (e.g., within a certain  $m/z$  range) then transferring into a trap. The detector cycles between detecting all precursor ions (no fragmentation) and detecting all fragments (fragmentation occurs in a collision cell just after the trap). CID occurs by electrically accelerating the ions into neutral gas molecules.

In the case of  $MS^E$ , these ions are then transferred into the TOF detector, and all fragment ions are detected in a continuous stream, separated by the time-of-flight of the ions to reach the detector. The size of the ion current on reaching the detector reflects the abundance of the ion allowing quantitation. An additional level of separation could occur before fragmentation, called “TriWave-Ion-Mobility-Separation” or TWIMS. This technology involves a counter-flow of neutral gas applied in the IMS cells, allowing separation of precursor (or fragment) ions both by their physical shape and size and thus improving resolution. Isobaric precursor ions with the same  $m/z$ s will then separate by ‘drift-time’, in an ion-chromatogram fashion, adding a layer of separation. The application of ramped voltages to fragment everything after IMS is called High definition  $MS^E$  (HDMS<sup>E</sup>). More recently the use of drift-time specific collision energies in the transfer cell adds an additional level of specificity with improved

signal to noise ratios, leading to increased identification of proteins in the sample (Distler et al., 2014). Data are generated in a continuous stream, and because everything is fragmented, the data files generated are much bigger (14 GB vs. 1 GB for Q-Exactive) and require a lot more computational resources to analyse. The benefit of a DIA (data independent acquisition) method like this is the ability to return to the same data file in the future and interrogate it again for other experiments *in-silico*.

#### **1.6.4 Data Analysis**

The subsequent step in the plasma proteomics workflow is the analysis of data that has been generated from mass spectrometry. This field is an area of intense research and has improved substantially over the past decade.

In principle, the sample that has been prepared for ‘bottom-up’ proteomics should only contain peptides. With appropriate clean-up, background chemical noise can be reduced to a minimum, such that most of the charged particles that enter the MS are peptides. The MS generates data containing accurate precursor  $m/z$ s and these are paired with fragment  $m/z$  values together with retention times. Theoretically, unique peptides will have a unique retention time, and therefore, only a limited number of peptides of different identities will co-elute at the same time. This can be optimised by adjusting the elution gradient and conditions for the elution. The longer the gradient or ‘run-time’ the better the theoretical resolution between peptide peaks.

These limited numbers of peptides that co-elute are more likely to have different  $m/z$  and should be able to be differentiated. Furthermore, peptides that are co-eluting are then further fragmented, and these fragment ions will then provide accurate  $m/z$ ’s that theoretically will add up accurately to the precursor ion values. However, in practice, assigning one peptide to one MS/MS spectrum is challenging even with complex algorithms (Michalski et al., 2011),

largely due to chimeric spectra due from co-fragmented peptides which makes up a large proportion of these spectra.

The processing software takes a database file (fasta file) containing all known protein amino acid sequences for a particular organism and digests the proteins *in-silico*. This is highly specific if trypsin is used. The theoretical tryptic-digested peptides with their theoretical molecular weights can then be compared to the list of m/zs generated by MS. This is made even more accurate by comparing the fragment-ion-spectra with the theoretical fragment ion spectra, and an accurate match can be made of the precursor mass. In order to reduce false positives, a decoy database of peptides is also generated from the theoretical tryptic peptide digest database, typically with a reverse-sequence of amino acids. These will therefore have the same precursor mass, but will have different fragmentation sites and therefore spectra.

Statistical algorithms are used to reduce the false discovery rate (FDR) while matching spectra to a pre-specified threshold, typically set at 1%. This means that of all the peptide sequence matches (PSMs) that have a particular probability, <1% of these PSMs were false positives. These calculations arise from the deductions made in the presence of the decoy database.

Despite this robust method of identifying unknown masses, however, it is not unusual for >60% of the charged masses detected by MS to be unidentified by the usual means. Post-translational modifications, genetic mutations, unknown chemical modifications and post-digestion degradations all contribute to unidentified masses. These is only partially mitigated by predicting potential post-translational modifications, chemical modifications and degradations.

There are a lot of data obtained from identified spectra. These peptides infer the presence of proteins. Whilst the presence of many peptides can be explained by multiple proteins, a

substantial number are unique to one protein (i.e. the presence of the peptide identification can only be explained by one protein in the database). If the confidence of the peptide identification is high, and the peptide is unique, the protein it came from can be inferred by that peptide alone (also known as one-hit wonders). However, because a PSM may be incorrect (a false positive), regardless of its uniqueness, there is no robust method to otherwise validate it. Most incorrect protein assignments only have one peptide inferring their presence. There is a lot of debate surrounding this issue (Gupta and Pevzner, 2009, Serang and Noble, 2012, Claassen et al., 2012, Reiter et al., 2009). The current consensus is that at least 2 peptides are required to confidently infer the presence of a protein in an untargeted experiment.

The protein inference problem has been comprehensively reviewed, e.g. (Nesvizhskii and Aebersold, 2005). Firstly, peptide coverage for abundant proteins is high, but researchers tend to be interested in low abundant proteins which have low coverage. High peptide coverage results in high confidence, and the converse is true for low peptide coverage. Secondly, unique peptides can be surrogates for protein quantitation but, many peptides are degenerate (i.e. could originate from multiple different proteins). Deciding what proteins are present in a sample containing both unique peptides and degenerate peptides can be performed using the Occam's Razor approach (Nesvizhskii et al., 2003). Multiple methods to assign probabilities of individual PSM assignments being correct (not occurring by chance) are available, such as the empirical modelling method, PeptideProphet (Keller et al., 2002) and the semi-supervised learning method, Percolator (Kall et al., 2007) with extensive similarities. The Waters Synapt systems have data processed in Protein Lynx Global Server (PLGS) which employ an ion accounting system with similar checks and tests to provide confidence that a particular peptide exists within a protein (Li et al., 2009).

Inferred proteins can be quantified based upon the abundances of their constituent peptides, which has a linear relationship with the ion intensity of the peptides. Increased accuracy of abundances can be obtained by utilising both information on fragment ion intensity and precursor ion intensity. Spiking a standard protein (e.g. alcohol dehydrogenase from *Saccharomyces cerevisiae*) into the analyte provides a reference to which molar amounts of individual protein species can be inferred from the ion intensities, allowing absolute label-free quantitation of proteins in the sample. The Top3 method of quantification (Silva et al., 2006) has been recently shown to be the best correlated to protein abundances throughout the quantification range in the absence of labelled standards (Ahrné et al., 2013).

### **1.6.5 Verification and Validation**

Robust statistical modelling is performed to identify the best candidates found through this workflow to be validated as putative biomarkers. These could be verified in the unadulterated sample used for bottom-up proteomics, with immunoassays. Increasingly however, there is a trend towards using multiple-reaction monitoring (MRM) methods or parallel-reaction monitoring (PRM) methods to validate putative biomarkers. These methods use spiked-in isobaric peptide (or protein) standards, which are of known concentration and have a known retention time. The spiked-in peptide signal is then compared against the native signal, and a ratio obtained, which can then be used to calculate the absolute quantity of the peptide. The experiments have high sensitivity and are predominantly not affected by ion-suppression from highly abundant peptides. Traps in the MS can be set-up to select only masses of interest, within a known retention time, and can monitor multiple masses in the same experiment. The MRM experiments can easily be scaled, and antibodies do not need to be raised to the peptide/proteins of interest. Developing multiplexed immunoassays are very challenging and often the manufacturer determines which peptide to make antibodies to (Anderson and Anderson, 2002). In contrast, with MRM/PRMs the researcher can decide

which masses to monitor, as long as heavy peptides can be synthesised to mimic the peptide of interest.

If these conditions can be satisfied, then randomized controlled trials utilising these biomarker candidates could then be considered to see if a change in clinical decision making based on these biomarker candidates results in an improvement in a patient's outcome.

In practice however, this type of biomarker pipeline typically takes several years to complete, and often fails at the validation stage, suggesting that mass spectrometry proteomics-based biomarker discovery workflows still need further improvements at various stages.

### **1.6.6 Rationale**

The identification of suitable biomarkers that can identify patients with initially asymptomatic moderate-severe AS who will benefit from early AVR would be of immense clinical benefit. Biomarkers reflecting the complex process of LV remodelling progressing to decompensation are of particular interest. In addition, the use of multiple markers may allow the safe identification of patients who are not at risk of complications in the short term, allowing less frequent review with important health care savings.

## **1.7 Hypotheses**

In this project I aim to test the following hypotheses in patients with asymptomatic moderate severe AS.

- 1) Plasma proteomics will uncover more accurate biomarkers that predict prognosis independent of existing risk stratification methods.
- 2) Plasma proteomics will help us recognize novel pathways that are involved in progression of asymptomatic moderate-severe AS.

In order to test the above hypotheses, the following objectives will be met.

- 1) Develop a method for sample preparation which is reproducible, with high throughput which can be used for biomarker discovery.
  - a. Develop and test a workflow utilising MARS-14 immunodepletion as the first step in improving identification of low abundance plasma proteins and protein level fractionation of the sample with the mRP-C18 column prior to digestion.
  - b. Develop and test a workflow 'EV pulldown' and CSH-enrichment in tandem, as two 'fractions' as a sample preparation method for high-throughput plasma proteomics.
  - c. Compare both workflows and selecting the best method of the two for biomarker discovery.
- 2) Utilise the selected workflow for biomarker discovery, by comparing the proteomic profile of propensity matched patients who reached an endpoint (cases) vs patients who did not reach an endpoint (controls), to identify a short list of proteins to call candidate biomarkers.
  - a. Utilise label-free quantitation to determine up- and down-regulated proteins in both groups.
  - b. Complete quantitation and statistical modelling with Progenesis QI.
  - c. Perform gene ontology analysis to understand the interactions between proteins and pathways
  - a. Create a shortlist of proteins for validation with a PRM method
- 3) Develop and test a PRM method for multiplexed-analysis of shortlisted proteins.
- 4) Validate shortlisted proteins in full study cohort, with the PRM method.

## 1.8 Overall Experimental Design

Plasma samples were from patients recruited into the PRIMID-AS study. Recruitment samples were used. The 'Prognostic Importance of Microvascular Dysfunction in

asymptomatic patients with AS' study (PRIMID-AS) study was a prospective, observational, multi-centre study of asymptomatic moderate to severe AS in the UK, comparing myocardial perfusion reserve (MPR) with exercise testing (Singh et al., 2013, Singh et al., 2017b).

Briefly, inclusion criteria were  $\geq 2$  of: AVA  $< 1.5\text{cm}^2$ , peak gradient  $> 36\text{mmHg}$  or MPG  $> 25\text{mmHg}$ , and willingness to accept AVR if symptoms develop. Exclusion criteria were: previous coronary artery bypass grafting or valve surgery, absolute contraindications to CMR testing or adenosine, other severe valve disease, EF  $\leq 40\%$ , recent myocardial infarction ( $< 6$  months) and planned surgery. All participants provided written informed consent including for biomarker discovery. The study had National Research Ethics Service approval (Unique Ethics identification number: 11/EM/0410) and complied with the Declaration of Helsinki.

All clinical, imaging, electrocardiographic, exercise testing, outcome, natriuretic peptide and troponin data relevant to the PRIMID-AS study were collected as part of the PRIMID-AS study, which ran between 2012 to 2015 (Principal Investigator: Gerry McCann, Co-Principal Investigator: Anvesha Singh, NCT01658345). My involvement was restricted to proteomic biomarker discovery and data analysis relating to proteomic data, including associations with phenotypic data from the PRIMID-AS study.

Method development was performed on a single healthy volunteer's samples. Both the biomarker discovery step and verification step were performed in patient samples. Biomarker discovery was performed on propensity-matched samples (46 cases and 46 controls) whilst the verification step was performed on all the patient samples (168 samples) although the additional samples were all controls. Further details are given in Chapter 3.



## **Chapter 2 Method Development**

### **2.1 Introduction**

A key starting point in proteomics is having a reproducible sample preparation method that yields a high number of targetable proteins. Incremental steps in sample preparation increases variability. Additional steps to improve reproducibility (e.g. with heavy-labelling using isobaric tags) may result in significantly higher cost and time required for sample preparation, data acquisition and analysis. To mitigate this, samples often need to be pooled in order to simplify sample preparation, resulting in loss of individual patient level data.

In this section, 2 methods were developed and compared to see which allowed a satisfactory compromise in throughput and results. The end-point to be compared was protein numbers and reproducibility of quantification of each protein.

The first method was immunodepletion followed by protein fractionation by RPLC before reduction, alkylation and digestion. Inspired by earlier techniques which combined multidimensional fractionation of proteins before LCMS/MS (Beer et al., 2011, Tang et al., 2011), I wanted to develop a similar method involving protein fractionation without gel electrophoresis to increase throughput.

The second method was fractionation by enrichment of proteins using CSH, a cheaply available matrix with an affinity for hydrophobic proteins, enriching for lipoprotein-associated protein and enrichment for EVs. Lipoproteins are intrinsically linked with cardiovascular disease, justifying the focus on this subproteome, even if this method may not include analysis of other plasma proteins which were not “selected-for”. EVs may provide an extended view of low abundance proteins in plasma.

One of the two methods would then be used for discovery of biomarkers in the next section.

## **2.2 Methods and Materials**

### **2.2.1 Pre-analytical Aspects**

All blood samples for method development were sourced from one healthy volunteer who provided written informed consent. Blood samples were obtained by venepuncture from the brachial fossa of the healthy volunteer. 50 mL of blood was drawn into pre-chilled EDTA-containing tubes (final EDTA to blood concentration 1.5 mg/mL). Tubes were turned-over 8-10 times and then stored at 4°C and centrifuged at 1300g (in a centrifuge with a swinging bucket rotor) at room temperature within 4 hours of venepuncture for 15 minutes. Plasma was aliquoted into 1 mL aliquots with disposable pipettes carefully avoiding the cell layer and buffy coat, then stored at -80°C.

### **2.2.2 Denaturation Methods**

#### **2.2.2.1 Urea Denaturation**

Urea was purchased from Sigma. 6M urea was used for denaturation (Urea:Water (w/w) ratio of 0.495). Solid urea of known mass was added to a known volume of water/solute containing the plasma proteins, and allowed to denature at room temperature for 30 minutes, before any further steps are performed.

#### **2.2.2.2 Guanidine Denaturation**

Guanidine was purchased from Sigma. 6M guanidine was used for denaturation (guanidine:water (w/w) ratio of 1.009). Denaturation was allowed to occur at 65°C for 30 minutes, before any further steps are performed.

### **2.2.2.3 Deoxycholate Denaturation**

Deoxycholic acid was purchased from Sigma. A 2% solution of ammonium deoxycholate (ADC) was made by first dissolving 0.8 g deoxycholic acid in 40 mL of water. 320  $\mu$ L of 25 M ammonium hydroxide (Sigma) was then added to the solution, and titrated to a pH of 8. An equal volume of this solution was added to the solution containing proteins needing denaturation, so that the denaturation occurred at a concentration of 1% ADC. Denaturation was allowed to occur at 65°C (in a convection oven) for 30 minutes unless otherwise specified. The overall ADC concentration was diluted further to 0.5% before digestion if performed directly after.

### **2.2.3 Reduction Methods**

#### **2.2.3.1 Dithiothreitol (DTT) Reduction**

DTT was purchased from Sigma. A 1 M stock solution of DTT was made then diluted in a pH 7-8 solution containing the proteins requiring reduction to a final concentration of 10 mM. The reaction was allowed to take place at 65°C for 30 minutes.

#### **2.2.3.2 Tris(2-carboxyethyl)phosphine reduction (TCEP)**

TCEP was purchased from Sigma. A 1 M stock solution of TCEP was prepared (pH 2). This was diluted to a final concentration of 10mM in the solution containing the proteins requiring reduction. The reaction was allowed to take place at room temperature for 10 minutes.

### **2.2.4 Alkylation Methods**

#### **2.2.4.1 Iodoacetamide alkylation (IAA)**

IAA was purchased from Sigma. A 500 mM stock solution of IAA was made and diluted to a final concentration of 20 mM in the solution (pH 7-8) containing proteins requiring

alkylation. Alkylation was allowed to take place at room temperature in the dark for 30 minutes. After this period, the solution was exposed to light to inactivate IAA before digestion.

## **2.2.5 Digestion Methods**

### **2.2.5.1 Trypsin digestion**

Acetylated-trypsin from bovine pancreas (catalog no: T6763) was sourced from Sigma. Solid trypsin was dissolved in a 1 mM solution of hydrochloric acid to a final concentration of 1mg/mL. Trypsin was then used at a ratio of 1:25 (trypsin:protein ratio) in a solution at pH 7.8, in a 37°C incubator over a 16 hour period. After the digestion period, the solution was acidified to 1% formic acid (FA) to stop further digestion.

## **2.2.6 Protein/Peptide Assays**

### **2.2.6.1 Bicinchoninic Acid Protein Assay**

Bicinchoninic acid and other materials for the assay were purchased from Sigma. The bicinchoninic acid (BCA) assay gives an estimation of the amount of protein in a sample and is based on the method first published by Smith (Smith et al., 1985). The BCA assay working solution was made by added 50  $\mu$ L of C with 1.25 mL of B and 1.35 mL of A. A is 0.8 g of anhydrous sodium bicarbonate and 0.16 g of tartaric acid was added to 10 mL of water, and titrated with sodium hydroxide to pH 11.25. B was 1 g of BCA dissolved in 25 mL of water. C was 0.4 g of copper sulphate dissolved in 10 mL of water. In a clear plate, serial dilutions of protein standard of known mass (bovine serum albumin) were added to form a standard curve. 1-5  $\mu$ L of protein-containing solution was pipetted into individual wells on the same plate. Each well was then made up to 100  $\mu$ L with water, and 100  $\mu$ L of the working solution

then added to each well. The reaction was allowed to take place in a 65°C oven for 20 minutes. The plate was read at an absorbance wavelength of 562 nm.

### **2.2.6.2 O-phthalaldehyde Peptide Assay**

O-phthalaldehyde (OPA), dimethylformamide (DMF), boric acid, Brij®S100 and potassium hydroxide were purchased from Sigma. The working solution of OPA was made by adding 10 µL of A for every 1 mL of B. A was 8 mg of OPA in 100 µL of dimethylformamide (DMF). B was 100 mM boric acid with Brij®S100 added at a concentration of 1mg/mL, titrated to a pH of 10 with potassium hydroxide. 2 µL of mercaptoethanol was then added to this mix just before peptide assay. OPA reacts with primary amines in the presence of reduced sulfhydryl groups producing a fluorescent product with an emission wavelength of 455 nm with excitation at 340 nm (Goodno et al., 1981). Unlike the BCA assay, it is not affected by detergents and reducing conditions, but is affected by the presence of other contaminating primary amines in the solution. To perform the assay, serial dilutions of a known protein or peptide standard was used for calibration. On the same plates, samples containing the protein/peptides of interest were placed in individual wells. Each well was made up to 50 µL with water. 100 µL of working solution was added to each well and the plate read in a Glowmax Fluorometer (ThermoFisher) at emission 455 nm and excitation 340 nm.

### **2.2.7 Desalting Methods**

#### **2.2.7.1 Empore-C18 SD cartridge desalting method**

Empore-C18 SD cartridges (1 mL capacity) were purchased from 3M. Desalting was done on a vacuum manifold with a maximum negative pressure of 15mmHg. First, the cartridge was preconditioned with 1 mL of methanol (Sigma). The cartridge was then washed with 3 mL of

0.1% FA. The solution containing peptides to be desalted were then pipetted into the cartridge. After the solution had flowed through, the membrane was washed with 3 mL of 0.1% FA. The peptides were eluted into a new vessel with 60% acetonitrile (Fisher Scientific HPLC grade) in 0.1% FA followed by 80% acetonitrile in 0.1%FA. These eluted peptides were then dried in a Speedvac (ThermoFisher Scientific) for 2 hours followed by lyophilisation overnight in a freeze dryer.

## 2.2.8 Immunodepletion of plasma proteins with a MARS-Human 14 Column

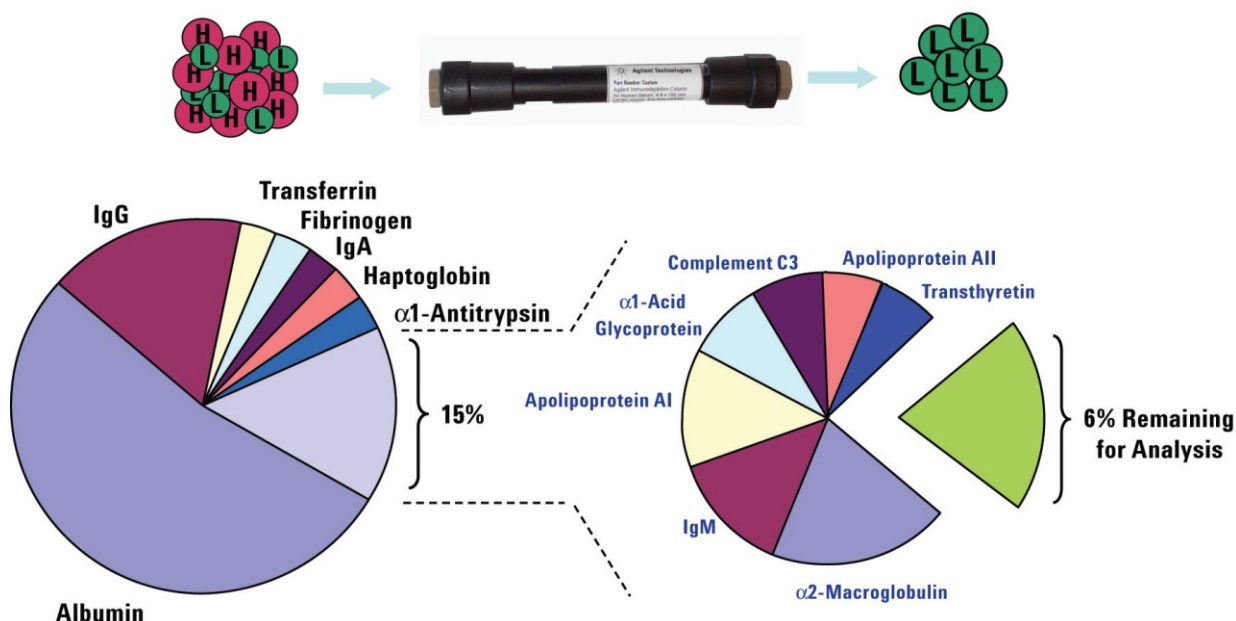


**Figure 2-1** Schematic of immunodepletion with a MARS-Human 14 column from Agilent. Top – Plasma containing high (H) abundant proteins and Low (L) abundant proteins are passed through the column. The top-14 High abundant proteins are bound to immobilised antibodies to these proteins within the column. The unbound proteins that ‘flow-through’ are (L) low abundant proteins, which can be further analysed. 94% of protein mass is removed, making up the top-14 fraction, leaving 6% behind for further analysis. (Source: Agilent (Mrozinski et al., 2008))

Immunodepletion was performed using a 4.6 x 100 mm Multiple Affinity Removal System – Human 14 column (MARS-Human 14) from Agilent according manufacturer’s instructions. Briefly, 40 µL of human plasma was diluted in 120 µL of Buffer A (proprietary solution from Agilent) a pH-neutral salt-containing buffer and filtered through a 0.22 µm spin filter (SpinX filter, Co-star) at 14000g for 1 minute. This sample was then placed in a Waters Alliance 2765 separations module (HPLC) with an integrated autosampler. The sample was kept at 4°C in the autosampler. 160 µL of the dilute sample was injected into the MARS Human-14 column, after equilibration with Buffer A at an initial rate of 0.13 mL/min with the column maintained at room temperature (~23°C). The flow-through was detected with a UV detector set at 280 nm to detect proteins. A characteristic chromatogram is shown in (Figure 2-2). The low abundant fraction was collected and saved. After the flow-through fraction had been collected, the flow-rate of the HPLC was increased to 1 mL/min to flush any excess unbound proteins out. The mobile phase was then switched to Buffer B at 1 mL/min for 5 minutes.

This urea-containing low-pH buffer denatured the antibodies in the column and released bound proteins, which were seen as a spike in the chromatogram. After flushing, the column was regenerated with Buffer A for 5 minutes at 1 mL/min then equilibrated at 0.13 mL/min. The full depletion run was completed in 35 minutes. Used under optimal conditions, manufacturers state that the column could tolerate 200 injections without deterioration. Whilst the manufacturers claim that 40  $\mu$ L is the plasma loading capacity for the column, Blankley found that the optimal injection for good high abundant protein depletion was in fact 25  $\mu$ L of plasma (Blankley et al., 2013).

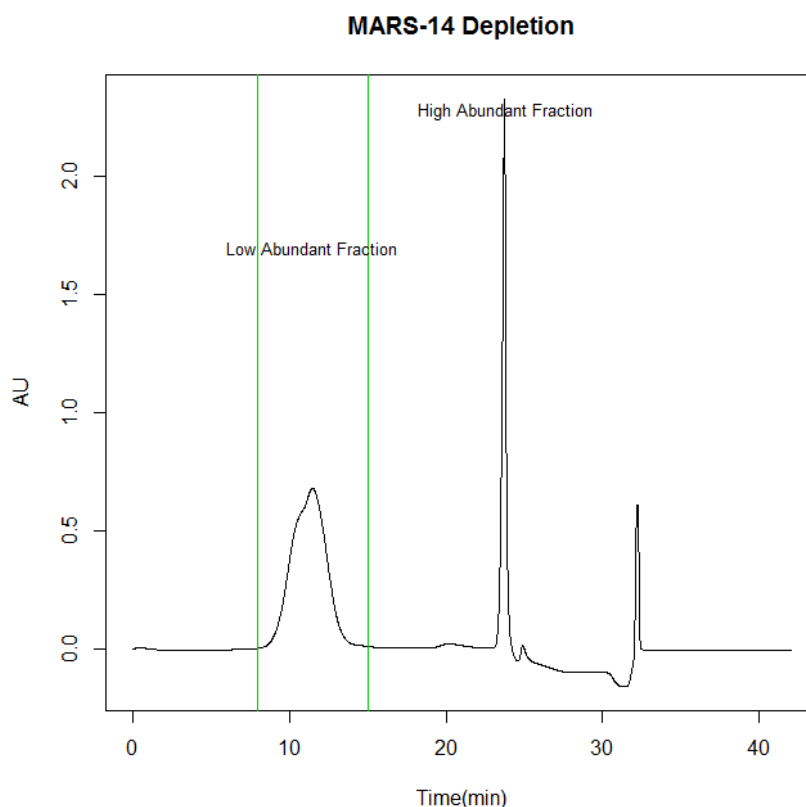


**Figure 2-2 Typical chromatogram of a MARS-Hu-14 depletion of human plasma. Low and High abundance fractions are marked. The low abundant fraction is collected for analysis.**

### **2.2.9 Protein fractionation**

A 4.5x50 mm mRP-C18 Hi Recovery column (Agilent) was used for fractionation. HPLC-grade acetonitrile, TFA, FA and water were purchased from Fisher Scientific. Buffer A for fractionation was water with 0.1% TFA acid (v/v); Buffer B is acetonitrile with 0.08% TFA



(v/v). The flow rate through the column was set at 0.75 mL/minute. The gradient used for fractionation was 10% Buffer B for 3 minutes, then 30-70% B over 2 minutes, 70-100% B over 1 minute and held at 100% B for a further 2 minutes before decreasing back to 10% B over 2 minutes to reequilibrate the column. 6 Fractions were collected between 4.8 and 10 minutes. Because the first and last fraction contained minimal protein, these two fractions were combined into one fraction. The operating temperature of the column was 80°C (Martosella et al., 2005).

#### **2.2.10 Combined immunodepletion and protein fractionation workflow**

First, 40-120 µL of plasma was immunodepleted. The low abundant fraction was assayed using the BCA assay. This was then denatured, reduced with DTT and alkylated with IAA, then acidified with acetic acid (from Sigma) to 1% prior to fractionation. This workflow allowed the sample to be cleaned up during the fractionation step. Fractionation was performed on the mRP-C18 column, and 5 fractions were collected. These were then dried in the SpeedVac, then lyophilised. The following day, the sample was re-suspended in water. A protein assay was performed with the OPA assay, using albumin as standard. This sample was then digested with trypsin overnight then desalted and lyophilized again overnight. After resuspension in 0.1% FA, a peptide assay was performed, and 0.25 µg was injected for MS/MS.

#### **2.2.11 Extracellular vesicle pulldown**

##### **2.2.11.1 EV pulldown with acetate**

This method was adapted from Brownlee's work (Brownlee et al., 2014). 200 µL of frozen plasma samples were thawed at room temperature, vortexed, then pre-cleared by centrifugation at 3000g for 10 minutes to remove residual cellular debris. The 'debris-free' supernatant was carefully transferred into 1M ammonium acetate (ammonium hydroxide

titrated to pH 4.75 with acetic acid, both sourced from Sigma) to a final concentration of 100 mM ammonium acetate. The extracellular vesicles (EV) were allowed to precipitate on ice for 45 minutes. The solution was diluted further with 1.2 mL of additional 100 mM ammonium acetate at room temperature, before centrifugation in a benchtop centrifuge (Eppendorf) at 20000g for 30 minutes at room temperature. The EV-free supernatant was drawn off, then the pellet washed twice by replacing additional 100 mM ammonium acetate, followed by brief vigorous mixing and repeat centrifugation at 20000g for 30 minutes. In total, 3 rounds of centrifugation and washing were completed. After the final centrifugation step, the ammonium acetate supernatant was removed. The sample was denatured with ADC and reduced with DTT as described in sections 2.2.2.3 and 2.2.3.1. The sample was alkylated with IAA. It was then diluted (doubled in volume) with 50 mM ammonium bicarbonate (Sigma) then digested overnight with 1 µg of trypsin. Following digestion, trypsin was denatured with FA, to a final concentration of 1% v/v. The samples were centrifuged further for 10 minutes at 20000g to remove the precipitated ADC. The supernatant was desalted as described in section 2.2.7.1, evaporated in the SpeedVac and lyophilized overnight. Lyophilised samples were suspended in 0.1% formic acid, a peptide assay performed and 1 µg peptide injected for MS/MS.

#### **2.2.11.2 EV pulldown without acetate**

This method was based on (Østergaard et al., 2012). 1 mL of debris-free-plasma (i.e. 1500g centrifugation after venepuncture for 15 minutes, plasma separated, then further 3000g centrifugation for 10 minutes, then platelet-poor supernatant retrieved) was centrifuged at room temperature for 30 minutes at 18890g. 950 µL of supernatant was removed, and replaced with 950 µL ammonium bicarbonate 50 mM. This was further centrifuged at 18890g for 30 minutes. In total, these series of washes was performed 3 times. The EVs were pelleted

at the bottom of the centrifugation tube. These were then denatured, reduced, alkylated, digested, desalted then lyophilised and reconstituted in 0.1% formic acid before MS analysis, as in section 2.2.11.1.

### **2.2.12 Enrichment with calcium silicate hydrate (CSH)**

CSH (trade name: LRA™- Lipid Removal Agent, sourced from Supelco, Bellefonte, Pennsylvania, USA) was prepared in a 100 mg/mL suspension in 50 mM ammonium bicarbonate. This was subjected to three successions of washes involving centrifugation at 3000g for 10 minutes, then replacing the supernatant and resuspending with an equal volume of 50 mM ammonium bicarbonate, with a final concentration of 100 mg/mL of CSH. Plasma was contacted with CSH in a 50:100 (v/v) ratio and allowed to bind for 1 hour, in a tumbler. After binding, the unbound plasma proteins were washed off with 3 repeated steps of centrifugation at 14000g for 10 minutes, removal of the supernatant and re-suspending in 50 mM ammonium bicarbonate. After the final wash, the sample was denatured with ADC and reduced with DTT at 65°C for 30 minutes as described in sections 2.2.2.3 and 2.2.3.1. The proteins were then alkylated with IAA, then the volume doubled with 50 mM ammonium bicarbonate, followed by digestion with 80 µg trypsin overnight (trypsin:protein ratio of 1:25). The sample was then acidified and centrifuged. The supernatant was desalted, dried and lyophilized then reconstituted the following day like the EV samples.

### **2.2.13 Tandem EV pulldown + CSH enrichment workflow**

Both the EV and CSH workflows were compatible, so sample preparation workflows were combined into two parallel workflows with the same starting material to maximize use of plasma samples. The overall workflow was to start by performing an EV pulldown with 200 µL plasma. After the EVs were pelleted, 350 µL of the supernatant (equivalent to 50 µL plasma i.e. 350 µL/1400 µL total volume × 200 µL starting volume of plasma) were

contacted with CSH as described in the previous section, then both ‘fractions’ were prepared in parallel as described for separate MS analysis.

#### **2.2.14 Nanoparticle Tracking Analysis**

For additional confirmation about the size of the particles that have precipitated from the EV pulldown method, nanoparticle tracking analysis was performed on the Nanosight NS500 nanoparticle tracking device (Malvern Instruments, Malvern, United Kingdom). The device tracks the light scatter from particles, which is directly proportional to the size of the particles and therefore can reveal the distribution of sizes of particles within a field of view.

Nanoparticle tracking analysis was performed using camera sensitivity of 14. Three video acquisitions were performed over 60 seconds, at 25°C, with a delay/settling time of 10 seconds and advancing between each field of view. The device was primed with 500 µL of sample driven by Millipore water. Analysis was then performed in a batch at the end of the video capture, where the particle detection threshold was set to 6. Samples were analysed in triplicate.

#### **2.2.15 Mass Spectrometry analysis**

##### **2.2.15.1 Waters Synapt G2 + Nanoacquity UPLC**

The sample (peptide mix/protein digest) was spiked with a peptide standard digest (alcohol dehydrogenase (ADH) from yeast/*Saccharomyces cerevisiae*; Uniprot Accession No. P00330) so that there was 50 fmol of this standard per injection in 0.1% FA. This was then sampled from the sample manager maintained at 8°C. The sample was first further desalted in the nanoACQUITY UPLC Symmetry C18 Trap column at a 0.3 µl/min. The sample was then pushed onto a nanoACQUITY UPLC 1.8µm HSS T3 75 µm × 150 mm C18 column for peptide separation, using an elution gradient defined by %A and %B, where A was 0.1% formic acid and B was 100% acetonitrile (v/v) + 0.1% FA (Table 2-1). The gradient was 65

minutes long and data was acquired throughout. The sample eluting from the column was ionized using electrospray and analysed in the Waters Synapt G2 mass spectrometer using HDMS<sup>E</sup>. The TOF analyser cycles between precursor and product ion analysis every 0.5 s. The product ions are then pushed into the TOF analyser in the same way as precursor ions, and data is acquired both as intensity (surrogate for abundance) as well as  $m/z$  using DIA.

Time(min)	Flow( $\mu\text{L}/\text{min}$ )	%B
<b>Initial</b>	0.3	3
<b>20.0</b>	0.3	14
<b>30.0</b>	0.3	20
<b>40.0</b>	0.3	25
<b>51.0</b>	0.3	31
<b>52.0</b>	0.3	31
<b>52.1</b>	0.3	31
<b>52.2</b>	0.3	31
<b>53.0</b>	0.3	35
<b>53.1</b>	0.3	35
<b>54.0</b>	0.3	37
<b>55.0</b>	0.3	42
<b>63.0</b>	0.3	69
<b>65.0</b>	0.3	3

**Table 2-1: Gradient for mobile phases on NanoAcquity UPLC for peptide separation; %B refers to percent buffer B (100% acetonitrile + 0.1% formic acid)**

#### 2.2.15.2 Thermo QExactive + Dionex UPLC

The sample was reconstituted the same way (section 2.2.15.1). This was then sampled from the autosampler at 4-5°C. The sample was first desalted on a cartridge-based trap-column, using a 300  $\mu\text{m}$  x 5 mm C18 PepMap (5  $\mu\text{m}$ , 100Å) and separated using Easy-Spray pepMap C18 column (75  $\mu\text{m}$  x 50 cm) at a flow rate of 0.3  $\mu\text{L}/\text{min}$  on a Ultimate 3000 RSLC nano HPLC system (Dionex/ThermoFisher Scientific, Bremen, Germany), using an elution gradient defined by %A and %B, where mobile phase A was 0.1% FA and B was 80% acetonitrile/20% water (v/v) + 0.1% FA (Table 2-2). The column was operated at a constant temperature of 45°C. The nanoHPLC system was coupled to a Q-Exactive mass spectrometer (ThermoScientific, Bremen, Germany). The Q-Exactive was operated in DDA top10 mode.

Full scans (precursor ions) were acquired at a resolution of 70000 at 200-2000m/z, with an automatic gain control or target ion value (AGC) of  $10^6$  with a maximum fill time of 50 ms. MS<sup>2</sup> scans (product ion scans) were acquired at a resolution of 17500, with an AGC of  $10^5$  with a maximum fill time of 100 ms. The dynamic exclusion time for the Top10 algorithm was set at 30s, to increase dynamic range.

Notably, whilst the number of protein identifications between platforms are not directly comparable, reproducibility of quantification was internally controlled. The immunodepletion + prefractionation workflows were tested on the Synapt-G2 platform, whilst the EV + CSH workflows were tested on the Q-Exactive platform. This was necessary because of the limited availability of mass spectrometric platforms due to other on-going studies at the time.

Time (mins)	%B	Flow rate ( $\mu$ L/min)
Initial	3	0.3
10	10	0.3
47	50	0.3
56	90	0.3
82	3	0.3

**Table 2-2: Gradient for separation on the Ultimate 3000; %B refers to percent buffer B which was 80% acetonitrile/20%water + 0.1%formic acid**

## 2.2.16 Data Analysis

Data files from the Waters platform were exported from Mass Lynx version 4.1 and processed on Protein Lynx Global Server (PLGS) version 3.0.2. These files were processed using the threshold settings – high energy 350, low energy 50 and intensity 500. A fixed carbamidomethylation on cysteine (i.e. alkylation) modification was used. In addition, variable modifications with methionine oxidation and deamidation of asparagine and phosphorylation on STY were also used to allow for variable chemical modifications. One missed cleavage was allowed. Finally, for protein inference, the inclusion rules used were 2 peptides per protein, 5 fragments per protein and 2 fragments per peptide were used. The

samples were processed at 1% FDR to improve confidence about protein inference.

Quantification of the protein is inferred from the sum of the top 3 abundant precursor ions for the protein (Top3 or Hi3 quantification). Protein amounts were normalized to alcohol dehydrogenase protein amounts.

Data files from the Q-exactive platform were processed in Proteome Discoverer 2.1. Peptide spectrum searches were performed using the SequestHT engine within Proteome Discoverer against the human database from Uniprot (downloaded November 2013), allowing for 2 missed cleavages, with a minimum peptide length of 6 and maximum of 144. Precursor mass tolerances was set at 10ppm and a fragment mass tolerance of 0.02 Da, and only precursor masses between 350 and 5000 Da were allowed. A fixed carbamidomethylation on cysteine was used, and up to 3 variable modifications were allowed, which were methionine oxidation, deamidation of asparagine, phosphorylation on STY and acetylation of the protein N-terminus. Peptides were validated with Percolator against a decoy database. Only high confidence peptides were retained and a minimum of two peptides required for protein inference. Proteins were validated using FidoCT, and quantified using the Top3 abundant combination of unique and razor peptides, using strict parsimony (non-unique peptides can only be used to make up quantification values for one protein only). All analyses were filtered using a 1% FDR. Protein amounts were normalized on alcohol dehydrogenase amounts, by specifying in Proteome Discoverer that protein amounts should be normalised to alcohol dehydrogenase protein amounts.

Protein lists were exported into Microsoft Excel for evaluation. Where reproducibility was assessed, the coefficient of variation (CV), the ratio of standard deviation to the mean was calculated. A CV of  $<0.2$  was considered acceptable for reproducibility.

## **2.2.17 Experiments performed**

### **2.2.17.1 Comparing urea vs. ADC for denaturation**

Urea was compared with ADC to see which was ‘better’ at denaturation. For this experiment – the workflow of urea denaturation + DTT reduction + IAA alkylation was compared with ADC denaturation + DTT reduction + IAA alkylation. The experiment was performed on undepleted plasma and digested with trypsin as described in section 2.2.5.1, lyophilised and desalted as described in section 2.2.7.1. The samples were analysed on the QExactive. The principal comparative factor was the number of protein groups. Samples were prepared in triplicate.

### **2.2.17.2 Comparing DTT vs. TCEP reduction**

Next, DTT reduction was compared with TCEP reduction using ADC denaturation and IAA alkylation. The samples were prepared otherwise in the same way as section 2.2.17.1.

### **2.2.17.3 Comparing denaturation only vs. denaturation + reduction + alkylation before protein fractionation**

Denaturation with urea before protein fractionation on the mRP-C18 column (as performed by original authors (Martosella et al., 2005)) was compared with denaturation with urea + reduction with DTT + alkylation with IAA before protein fractionation on the mRP-C18 column to see if there was an appreciable effect on separations. The rationale was to save time after fractionation to avoid having multiple extra steps after the fractionation step before the sample could be digested. The comparison was the qualitative appearance of the chromatograms to see which was better (narrower peaks, reproducible retention times).

Plasma was immunodepleted as in section 2.2.8. Four immunodepletions were performed of the same plasma sample. Two were assigned to the denaturation-first workflow, and two



were assigned to the denaturation+reduction+alkylation-first workflow. For the denaturation-first workflow, the low abundant fraction was denatured with urea before separation on the mRP-C18 column. For the other workflow, the low abundant fraction was denatured with urea, then reduced with DTT and alkylated with IAA before separation on the column as described before. Chromatograms were recorded. No fractions were collected in this particular experiment.

#### **2.2.17.4 Comparing guanidine+DTT+IAA vs. urea +DTT+IAA before fractionation**

Due to concerns that urea use would affect the extent of carbamylation of lysine residues which could might impair the efficacy of trypsin digestion (Kollipara and Zahedi, 2013), guanidine for denaturation was also compared with urea, by substituting urea for guanidine as described in section 2.2.2.2, in the denaturation/reduction/alkylation before fractionation workflow and comparing the separation chromatograms. Two sample preparation replicates were performed.

#### **2.2.17.5 Evaluation of whether fractionation isolates proteins into individual fractions**

Using the immunodepletion + guanidine/DTT/IAA-first + mRP-C18 fractionation workflow to separate the sample into 6 fractions, and combining the first and last (fractions 1 and 6) into one fraction for analysis, mass spectrometric analysis was performed to assess whether fractionation isolates proteins into individual fractions. The fractions were collected between 4.8-6.8 mins, 6.8-7.3 mins, 7.3-7.8 mins, 7.8-8.3 mins, 8.3-8.8 mins and 8.8-10 mins and labelled as fraction 1 to 6 respectively. Whilst there was no comparator, the measure of interest was number of proteins identified, and how many by percentage of these were found within one, two or more fractions. After fractionation, samples were dried in a vacuum to remove volatile acids and the acetonitrile, then lyophilised overnight. Proteins were

suspended in water, a protein assay performed, and then digested with trypsin as described in section 2.2.5.1. After desalting, the samples were analysed on the QExactive.

#### **2.2.17.6 Comparing a non-acetate-based EV-pulldown method vs an acetate-based EV-pulldown method**

Given that two simple centrifugation based methods for EV pulldown have been described, these were compared as an initial strategy to see if there was any difference between the two. Samples were prepared from a single healthy volunteer. Plasma samples were pre-cleared by centrifugation at 3000g for 10 minutes to remove cellular debris. These samples were then prepared according to section 2.2.11.1 and section 2.2.11.2 for an acetate-based vs. a non-acetate-based EV pulldown method respectively. The main difference between the two was a) the use of acetate to precipitate the EVs and b) the non-acetate based method started with 1 mL of plasma, whilst the acetate based method started with 200  $\mu$ L. Samples were analysed singly as this was an exploratory test.

#### **2.2.17.7 Optimised conditions for EV-pulldown with the acetate-based method**

It was not clear if all the steps for EV-pulldown were strictly necessary. The original method described that the ideal pH was 4.5, and that at least 3 washes were required as a minimum to significantly reduce plasma protein content (Brownlee et al., 2014). I aimed to establish whether dilution of plasma was necessary for the initial centrifugation step, whether the acetate-based precipitation needed to occur at 4°C and whether the dilution volume needed to be large or whether a smaller volume was sufficient (to simplify pipetting). Therefore, 3 conditions were tested, named BigDiluteCold, NodiluteNoCold and DiluteCold (Figure 2-3). Endpoints were number of proteins identified and reproducibility of quantification. Samples were prepared in duplicates.

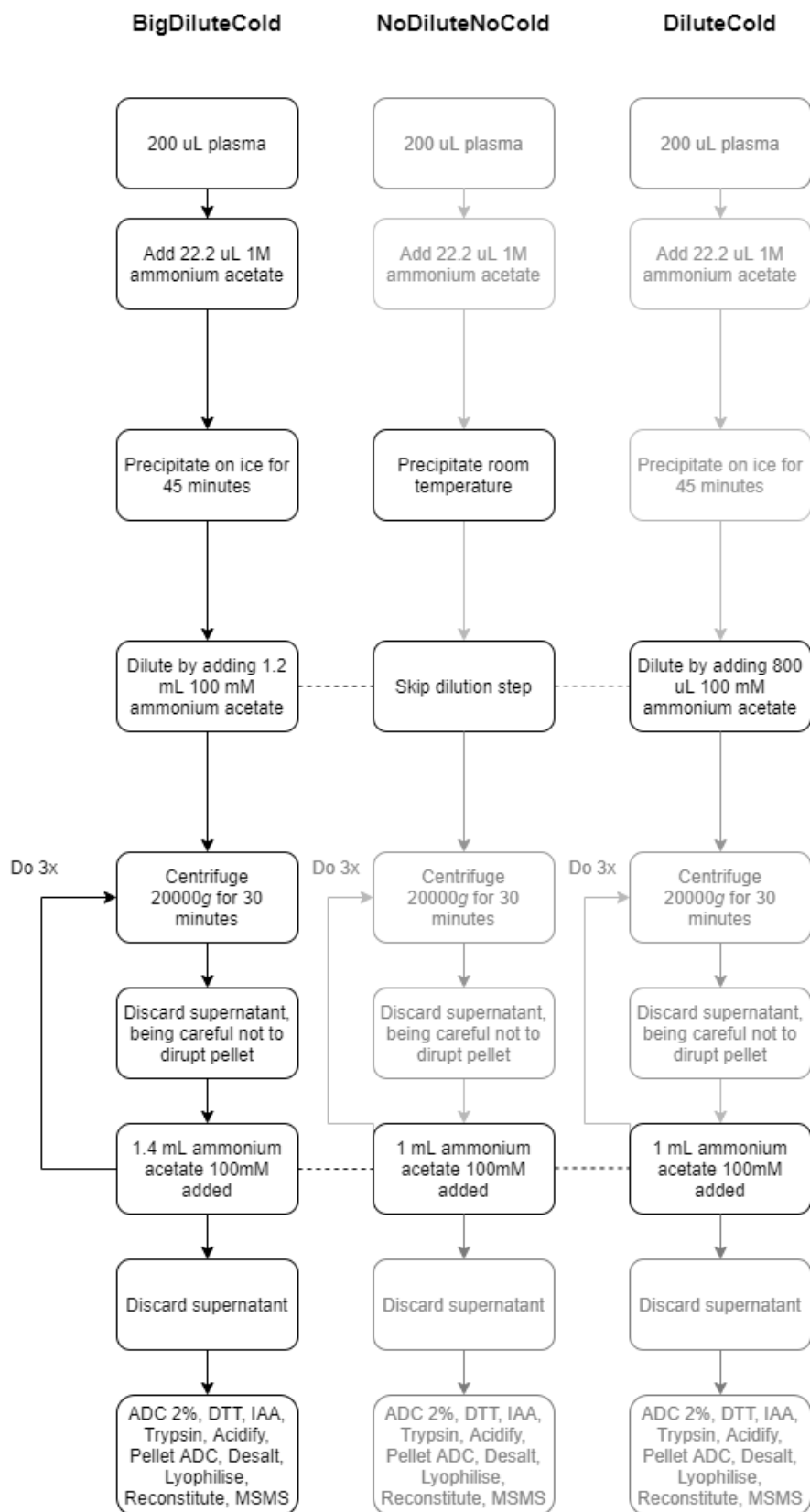


**Figure 2-3: Schematic illustrating differences in BigDiluteCold, NoDiluteNoCold and DiluteCold, all greyed out steps were not changed, black steps were where there were key differences; ADC: ammonium deoxycholate, DTT: dithiotreitol, IAA – iodoacetamide, MSMS: tandem mass spectrometry analysis**

### **2.2.17.8 Nanoparticle tracking analysis**

For additional confirmation about the size of the particles that have precipitated from the EV pulldown method, nanoparticle tracking analysis was performed as described in section 2.2.14. Samples were prepared using a slightly modified protocol to reduce the hypothetical risk of vesicular damage during sequential centrifugation. First, 22.2  $\mu$ L ammonium acetate was added to 200  $\mu$ L pre-cleared plasma. EVs were allowed to precipitate on ice for 45 minutes. This suspension was further diluted with 100 mM ammonium acetate, followed by a single 20000g centrifugation step for 30 minutes. The supernatant was drawn off and the pellet was suspended in 100  $\mu$ L of phosphate buffer solution (PBS). Two dilutions of the suspension were made (1:50 and 1:100) in 1 mL of PBS. Nanoparticle tracking analysis was then performed as described in section 2.2.14.

### **2.2.17.9 CSH enrichment in precleared plasma vs. precleared+EV-removed plasma**

The CSH method was initially used directly on plasma that had not been either pre-cleared (i.e. cellular debris removed) nor had its EVs removed/precipitated. In order to ascertain how much and what proteins were removed by first precipitating the EVs, an experiment comparing the two was performed. Specifically, in one arm, “CSH\_plasma”, 25  $\mu$ L defrosted pre-cleared plasma (i.e. centrifugation at 3000g for 10 minutes keeping only the supernatant) was contacted with 100  $\mu$ L of the CSH slurry as described in section 2.2.12. In the other arm, “CSH\_EV-free” was prepared as follows. First, 200  $\mu$ L plasma was pre-cleared of cellular debris by centrifugation at 3000g for 10 minutes. The supernatant was transferred to a clean tube, 22.2  $\mu$ L 1 M ammonium acetate was added and EVs allowed to precipitate on ice for 45 minutes. 1.2 mL of 100mM ammonium acetate was added, then this was centrifuged at 20000g for 30 minutes. 350  $\mu$ L of the EV-free supernatant (equivalent to 50  $\mu$ L plasma) was then contacted with 100  $\mu$ L of CSH slurry, with subsequent steps the same as for the

“CSH\_plasma” arm. Samples were prepared in duplicate and analysed on the QExactive. The number of proteins and quantification CVs were compared.

#### **2.2.17.10 Comparing urea, heat and ADC as denaturants in calcium silicate hydrate preparation**

In order to ascertain whether the denaturation methods with 6M urea, heat and ADC 2% (ADC) affected protein identification and reproducibility of protein quantification, an experiment was performed to compare the three methods. Precleared-EV-free plasma was used for this experiment. 350  $\mu$ L of the pre-cleared-EV-free plasma was contacted with 100  $\mu$ L CSH slurry as described in 2.2.12 and tumbled for 1 hour to bind. The solutions were then sequentially centrifuged and washed with ammonium bicarbonate 50mM 3x as described. For the urea arm, 200  $\mu$ L 6M urea was added and allowed to react for 30 minutes at room temperature. For the heat arm, 200  $\mu$ L of ammonium bicarbonate 50mM was added and the solution heated in a heating block at 65°C for 30 minutes. For the ADC arm, 200  $\mu$ L 2% ADC was added. For the no-denaturant arm, 200  $\mu$ L of ammonium bicarbonate 50 mM was added. After denaturation, samples were reduced with DTT, diluted further with 200  $\mu$ L ammonium bicarbonate 50mM, and digested with trypsin overnight. The next day, all samples were acidified to 1% FA (final concentration). The sample containing ADC was centrifuged at 14000g for 10 minutes to pellet the ADC, retaining the supernatant. All samples were then desalted, lyophilised and underwent MS analysis in the same way on the Synapt-G2S. Samples for each condition were prepared in triplicate. The measure compared was the number of protein identifications and CVs of protein quantification amounts.

#### **2.2.17.11      Evaluating reproducibility**

The immunodepletion and protein prefractionation reproducibility experiment was performed on a plasma samples derived from a healthy volunteer. 8 technical replicates were performed to evaluate reproducibility. Each fraction was analysed separately, and in a random order to reduce systematic error.

The EV and CSH reproducibility experiment samples were prepared from plasma samples from the same healthy volunteer. 8 technical replicates was performed to evaluate reproducibility.

In order to ascertain MS variation in quantification, after the 8 replicates had been prepared through their respective processes (EV and CSH) a small volume (50  $\mu$ L) of each of the 8 replicates were pooled to form a quality control sample (QC for both the EV and CSH pathways) which was injected between every 5 injections of the technical replicates. Each sample was injected in duplicate. The order of the samples being analysed was randomized from the sample preparation in order to mitigate the potential for systematic error.

## 2.3 Results

### 2.3.1 Urea vs. ADC for denaturation

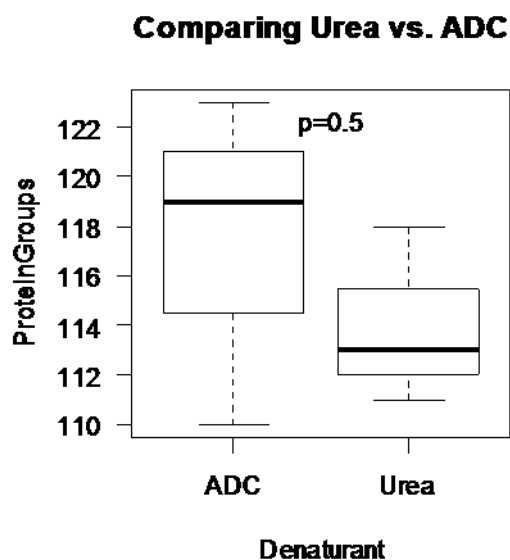


Figure 2-4: Comparing denaturant on number of proteins identified; ADC=ammonium deoxycholate

There were potentially more proteins identified with ADC, although the difference was not significant (Figure 2-4). One might also infer that urea gave more consistent results although again the difference was not significant.

### 2.3.2 DTT vs. TCEP for reduction

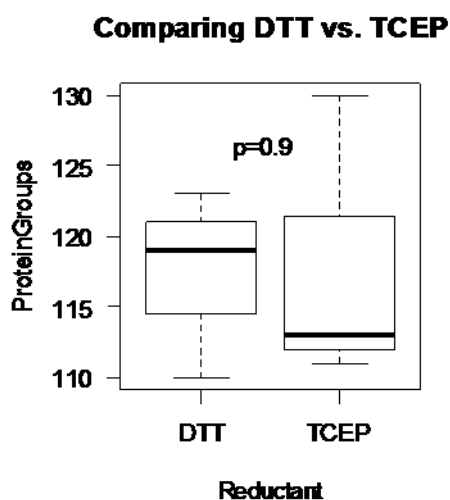


Figure 2-5: Comparing DTT vs. TCEP on number of proteins identified; DTT= Dithiothreitol, TCEP= Tris(2-carboxyethyl)phosphine

There was no significant difference between the number of proteins identified with either reduction method (Figure 2-5). One might infer that DTT gave more consistent results although again the difference was not significant.

### 2.3.3 Denaturation before protein fractionation vs. denaturation+reduction+alkylation before protein fractionation

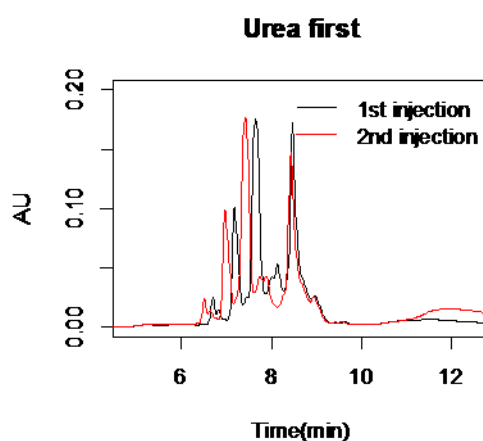


Figure 2-6: Two chromatograms of protein separation on the MRP-C18 column of immunodepleted plasma that has been denatured with urea before separation

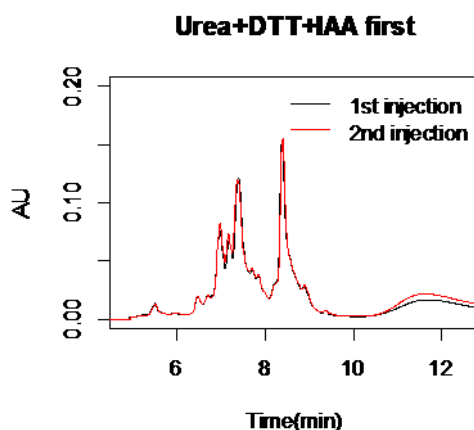


Figure 2-7: Two chromatograms of protein separation on the mRP-C18 column of immunodepleted plasma that has been denatured with urea, reduced with DTT and alkylated with IAA first before separation

Qualitatively, both denaturation first vs. denaturation+reduction+alkylation first result in similar chromatograms (Figure 2-6 & Figure 2-7). However, there was variability in the retention times with the denaturation first chromatogram. As the peak widths appeared quite



similar, I concluded that using the denaturation+reduction+alkylation first workflow was the more pragmatic option.

#### 2.3.4 Guanidine vs. urea in denaturation+reduction+alkylation first workflow

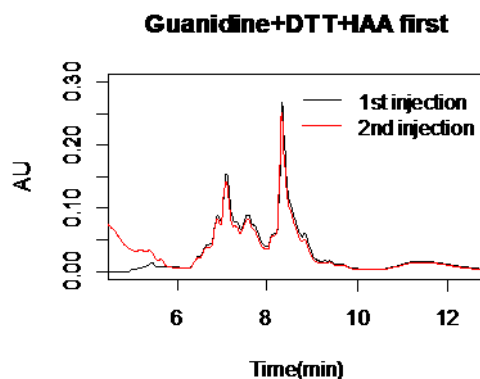
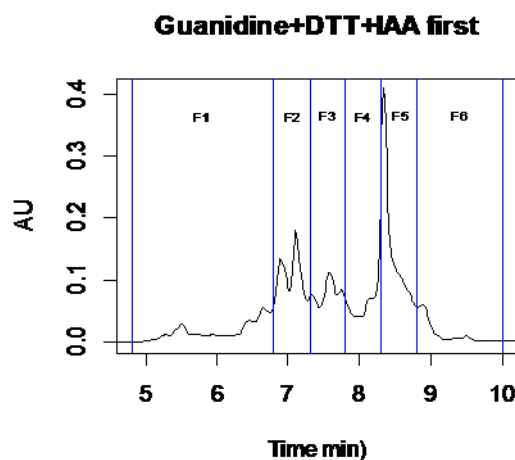


Figure 2-8: Two chromatograms of protein separation on the mRP-C18 column of immunodepleted plasma that has been denatured with guanidine, reduced with DTT and alkylated with IAA first before separation

Using guanidine instead of urea did not appear to affect the protein separations significantly (Figure 2-7 vs. Figure 2-8), although there was some peak broadening with guanidine especially around 7-8 minutes of the chromatogram. I was sufficiently concerned about excessive carbamylation due to urea that I concluded the guanidine workflow was an acceptable alternative for separations and because the mRP-C18 column would desalt the sample anyway, there should not be any detriment to using guanidine for the workflow.

### 2.3.5 Proteins found in each fraction in qualitative analysis



**Figure 2-9: Time points where fractions were collected. F1 and F6 were combined for downstream analysis**

In a single run with 5 analysed fractions (i.e. Fractions 2,3,4,5 and 1+6), 227 proteins were identified (1% peptide and protein FDR, minimum 2 peptides per protein). The protein list is available in the Appendix for review. Of these, 31%, 13%, 13%, 26% and 17% of these proteins were seen in 5, 4, 3, 2 and 1 fractions respectively. This implied that this method was only partially successful in reducing the complexity of the sample, especially when using this short gradient for fractionation and using small numbers of fractions.

### 2.3.6 Non-acetate-based EV pulldown vs acetate-based EV pulldown method

Both the non-acetate-based and acetate-based EV pulldown methods yielded a similar number of protein groups (219 and 220 protein groups respectively). Whilst there was a sizable overlap in proteins identified between the two methods (61%), one might have expected a larger overlap than was seen, given that they both isolate EV populations from plasma (Figure 2-10). However, given that the no-acetate method did not yield a superior number of protein identifications but required much more plasma to start with, the acetate-based method was preferred for further development.

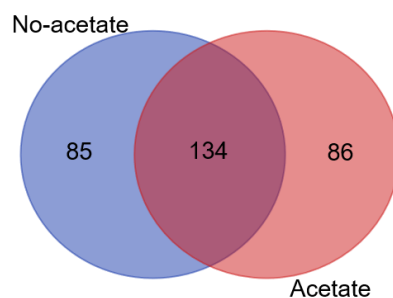


Figure 2-10: Differences in numbers of protein groups identified with the no-acetate vs. acetate EV pulldown methods

### 2.3.7 Optimal conditions for EV pulldown using acetate-based method

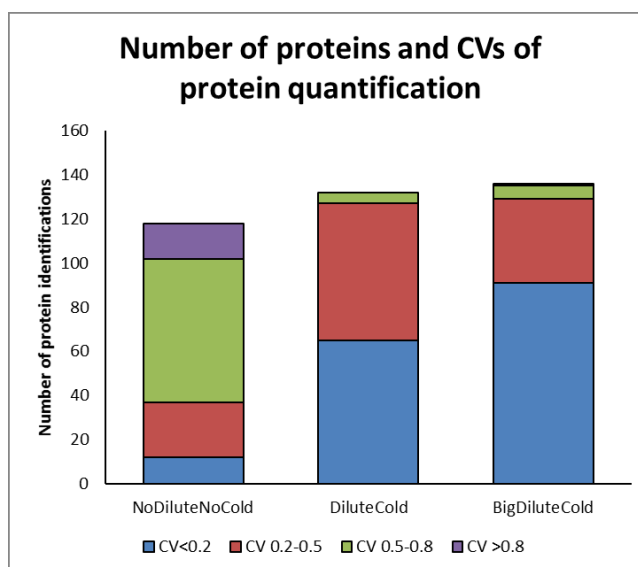


Figure 2-11: Number of proteins and CVs of protein quantification amounts. Y-axis – protein identifications, colours indicate CVs of quantification amounts; CV: coefficient of variation; Interpret as the taller the column and the larger the contribution of the blue column, the better

It was clear that a large volume of dilution, with precipitation on ice (BigDiluteCold) were necessary steps to ensure a good and consistent result in the EV pulldown method (Figure 2-11). These steps could therefore not be skipped to speed-up sample preparation.

Interestingly the numbers of proteins here were much lower than from the prior experiment reported in section 2.3.6. The reason may be that for CVs to be calculated, at least two amounts (in a duplicate) needed to be available, thus proteins that were only identified once were excluded from the number of identifications.

### 2.3.8 Nanoparticle Tracking Analysis

Nanoparticle tracking analysis demonstrated that the predominant species from the EV pulldown method measured between 90-100nm (Figure 2-12). In addition to the predominant

peak at 90-100nm, there was also a much smaller less dominant peak at ~300nm which represented microparticles. The area under the curve (an indication of the number of particles) inferred that the particle yield from 200  $\mu$ L of plasma was  $7-9 \times 10^9$  particles. This translated, after digestion and desalting, to ~30ug of peptide, which was substantially more than the typical 2ug extracted using a non-acetate based centrifugation method from 1mL of plasma (Østergaard et al., 2012).

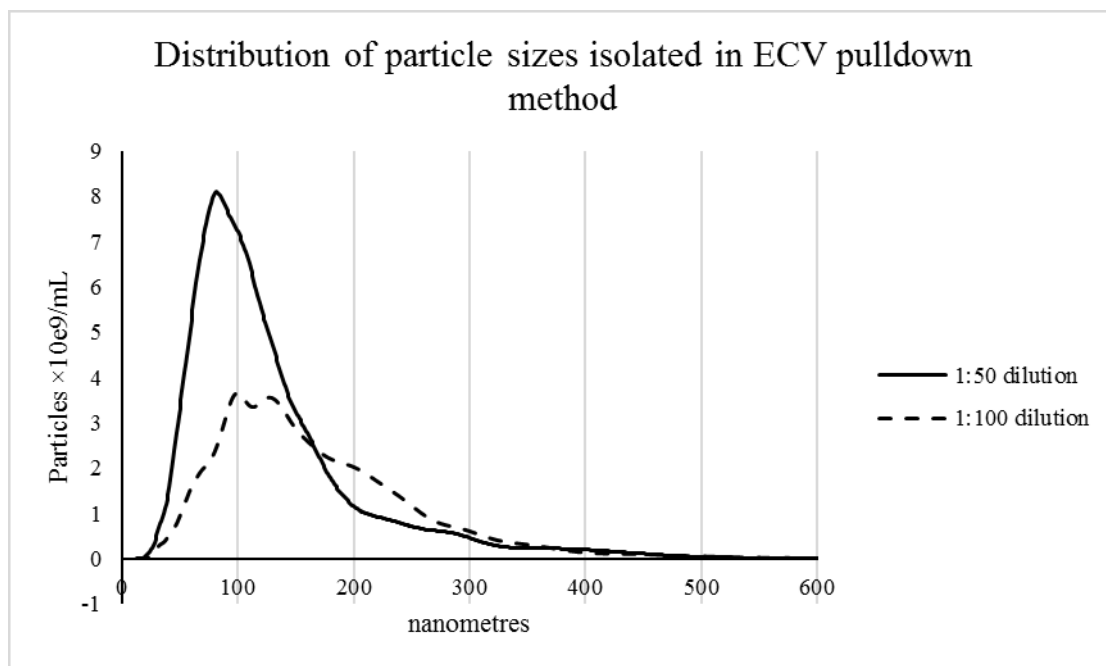


Figure 2-12: Distribution of particle sizes isolated in EV pulldown method

### 2.3.9 Comparing calcium silicate hydrate on precleared plasma vs. precleared plasma which has had EVs removed

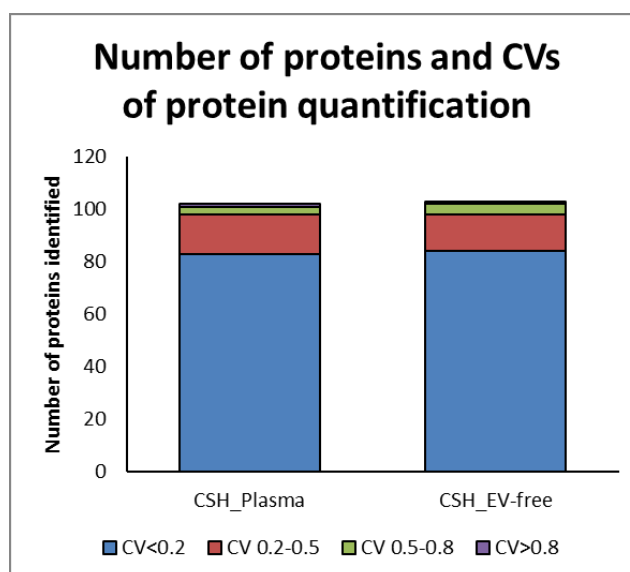


Figure 2-13: CSH on precleared plasma and EV-free plasma identify similar numbers of proteins and are reproducible methods

The numbers of proteins and the CVs for quantification were very similar in EV-free precleared plasma as it was for pre-cleared plasma (Figure 2-13). The proteins identified were compared with the proteins from EVs (the “BigDiluteCold” experiment reported in the prior section); the table for this comparison can be seen in the Appendix. Whilst there was considerable overlap between the three lists, the proteins that were enriched-for by the EV-pulldown method represented mainly intracellular proteins or transmembrane proteins, whilst the proteins enriched-for by the CSH method were mainly plasma proteins. The proteins which were common to both, were apolipoproteins and some abundant proteins. This comparison here implied that using EV-pulldown followed by CSH-enrichment in tandem on the same sample was complementary and reproducible for quantification, especially as plasma samples were scarce.

### 2.3.10 Effect of denaturant on calcium silicate hydrate preparation

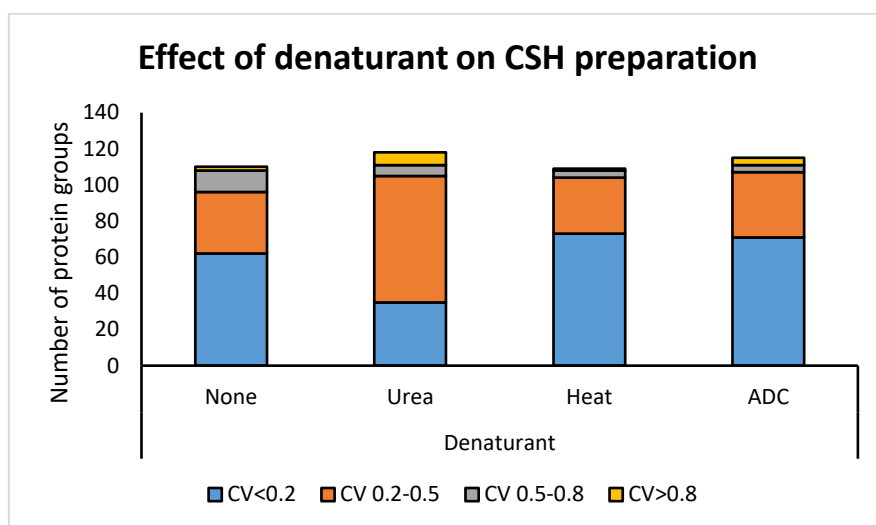


Figure 2-14: Effect of denaturant on CSH preparation; CSH: calcium silicate hydrate; ADC: ammonium deoxycholate; CV: coefficient of variation; Interpret as the taller the bar and the larger the blue bars the better

When considering which denaturation method was better in the CSH preparation, urea appeared to yield slightly more proteins but had less reproducible quantification (Figure 2-14). Heat and ADC were comparable. For pragmatic reasons (the heating block used to apply heat was limited to 30 samples at a time and the lab only had one heating block), ADC was chosen as the denaturant for both EV-pulldown and CSH-enrichment.

### 2.3.11 Immunodepletion

The manufacturer's recommended method used for immunodepletion was very reproducible (Figure 2-15). Chromatograms overlaid on top of each other show that the abundances and amount eluted/trapped by the column remained the same between runs.

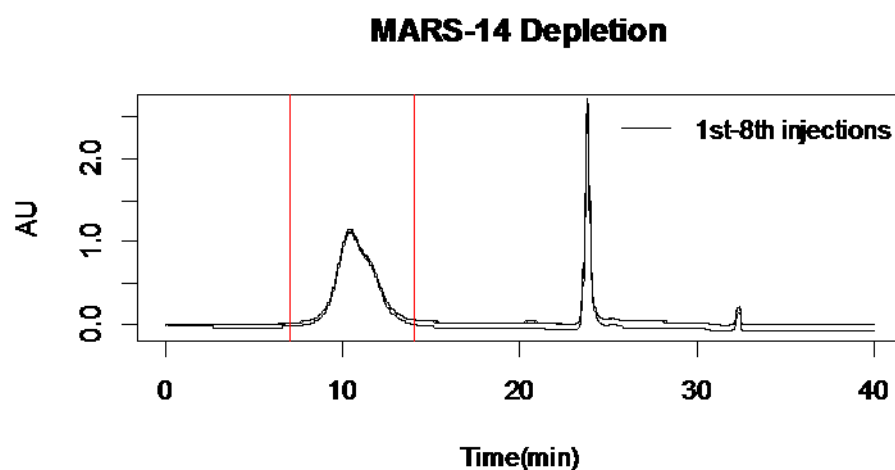


Figure 2-15: Eight depletion chromatograms which were very similar, lower abundant fraction between red lines were collected.

Likewise the protein amounts eluted in the low abundant fraction were also very similar (Figure 2-16), with a CV of 0.1.

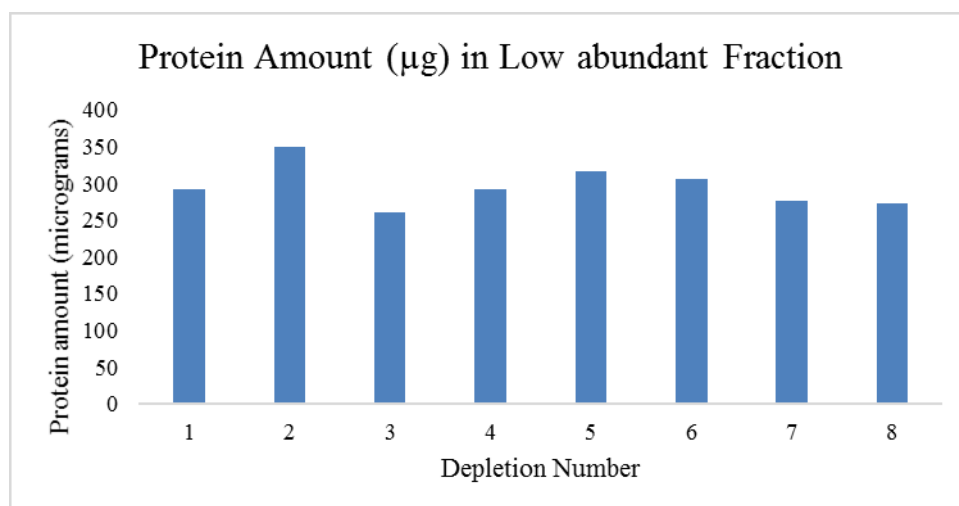
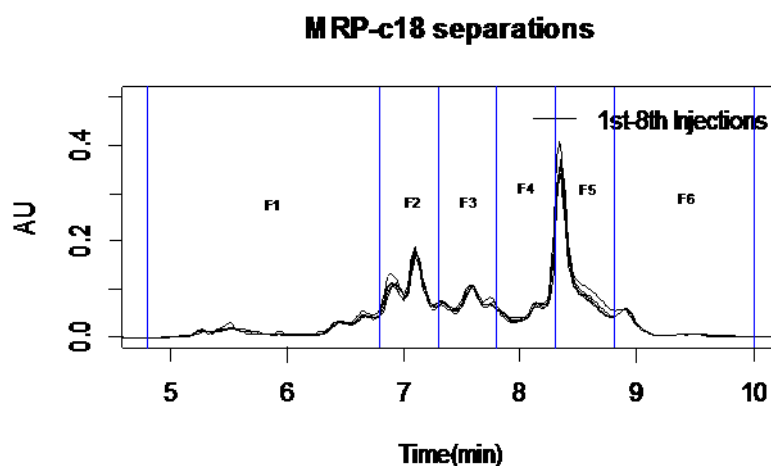


Figure 2-16: Reproducible protein amounts in low abundant fraction from MARS14-Hu column

### 2.3.12 Prefractionation on mRP-C18 column

Chromatograms of the fractionation on the mRP-C18 column were very reproducible; 250  $\mu\text{g}$  of each depletion was fractionated (Figure 2-17).



**Figure 2-17: Chromatograms of 8 fractionations, vertical lines correspond to collection points for each fraction. F1 and F6 were combined for downstream analysis.**

Protein assay of each fraction was not meaningful due to fairly low abundances of proteins in each fraction. After digestion, desalting and lyophilisation, peptide abundances were confirmed to be very low, with an average of 81% loss (compared to post-depletion protein assay). The peptide amounts in each fraction were consistent over 8 injections, with the most peptides in fraction 4 & 5, corresponding with the elution peak during separation (Figure 2-17 & Figure 2-18).



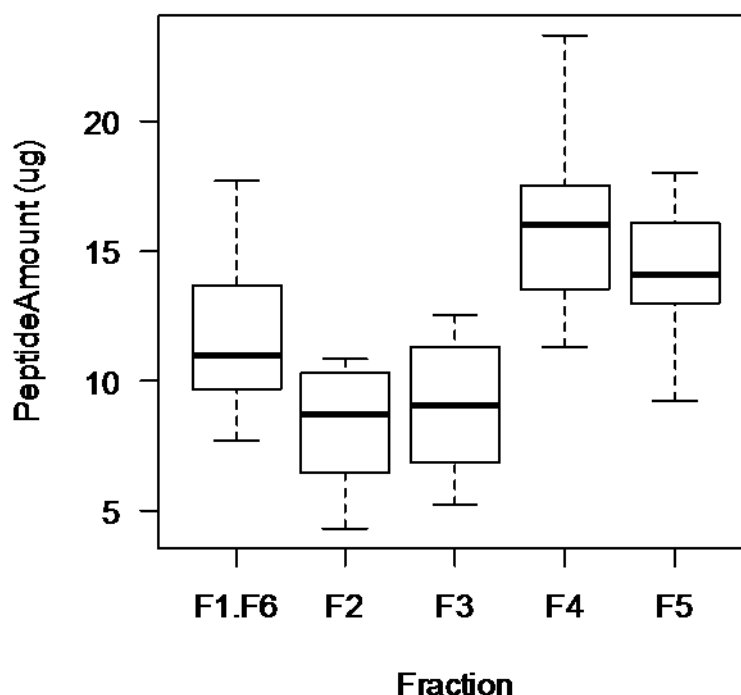
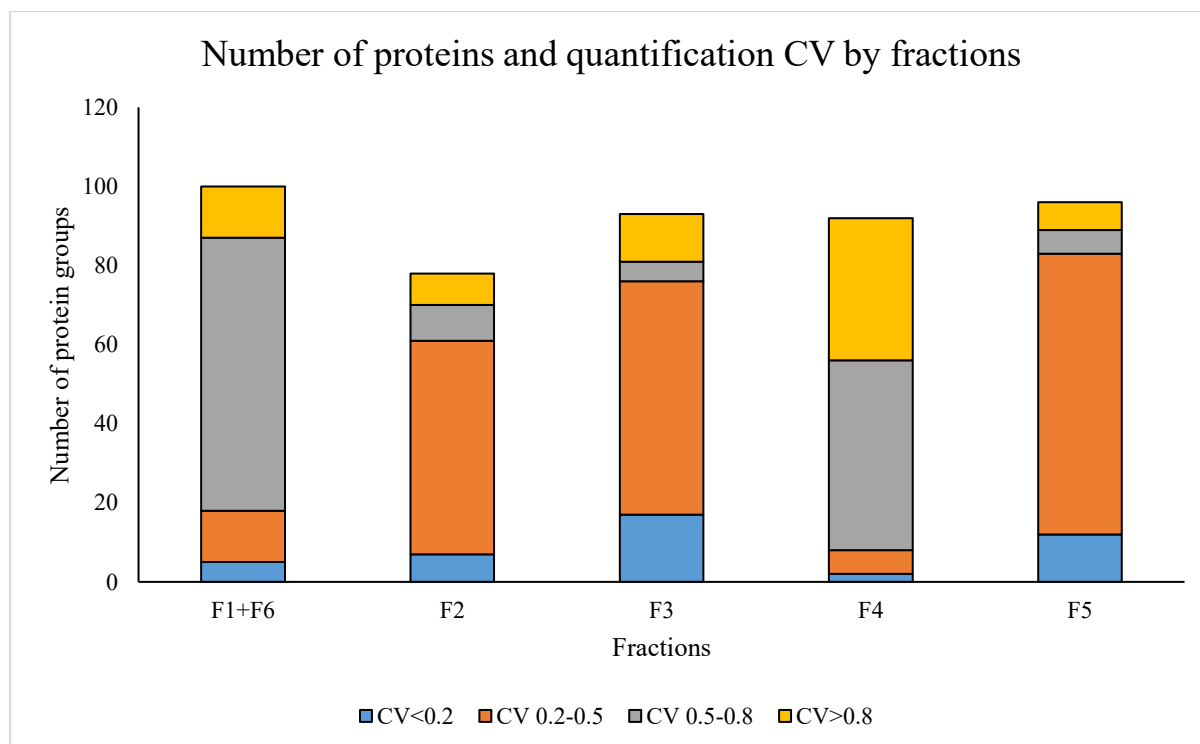


Figure 2-18: Variation in peptide amounts within each fraction over 8 separations

### 2.3.13 Reproducibility of quantification for immunodepletion and protein fractionation workflow

After MS analysis, on the Waters Synapt-G2 platform, all protein list results were collated and summarized to demonstrate both the number of proteins found in each fraction and the variability in quantification for each protein. Over the 8 replicates (40 separate injections), 218 unique proteins were detected. 61 proteins were found in all 5 fractions (Figure 2-20). Protein identifications ranged from 135-163 (mean 148) per sample after combining all 5 fractions. Reproducibility assessment was performed on individual fractions to minimize the error from combining amounts from 5 fractions. Reproducibility was poor with this method (Figure 2-19). Overall, this workflow resulted in excessive protein losses during sample preparation and had poor reproducibility.



**Figure 2-19:** Low number of proteins with a quantification CV < 0.2 in all fractions, colours refer to CV (coefficient of variation) as indicated in legend; the larger the blue bars are, the more reproducible the quantification of proteins within the fraction, lower CVs better.

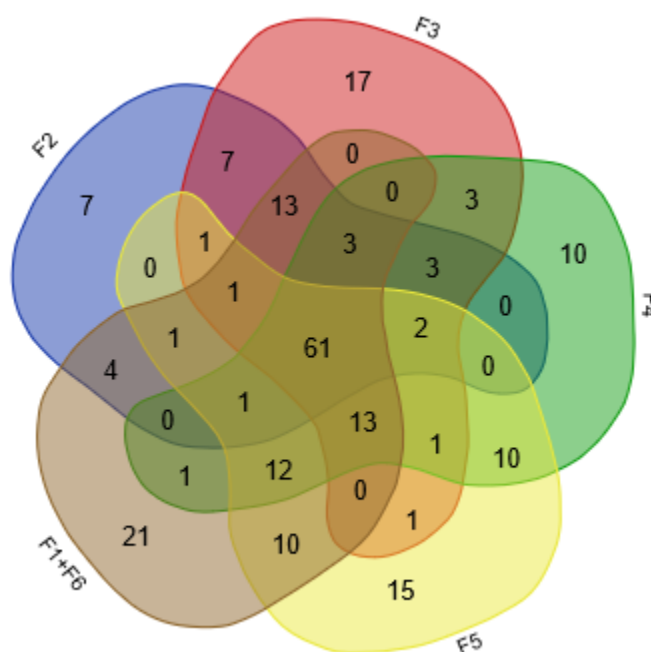


**Figure 2-20:** Venn Diagram showing overlap between proteins within each fraction

### 2.3.14 EV Pulldown

The number of single run protein groups from the EV pull-down method averaged at  $213 \pm 2$  protein groups.

The 213 proteins that appeared in all of the injections had Gene Ontology analysis (with PantherDB – pantherdb.com) to evaluate the protein classes and pathways in which these proteins participated. When considered by molecular function, 107 functions were identified. Approximately 2/3 of the proteins participated in binding and catalytic activity (Figure 2-21).

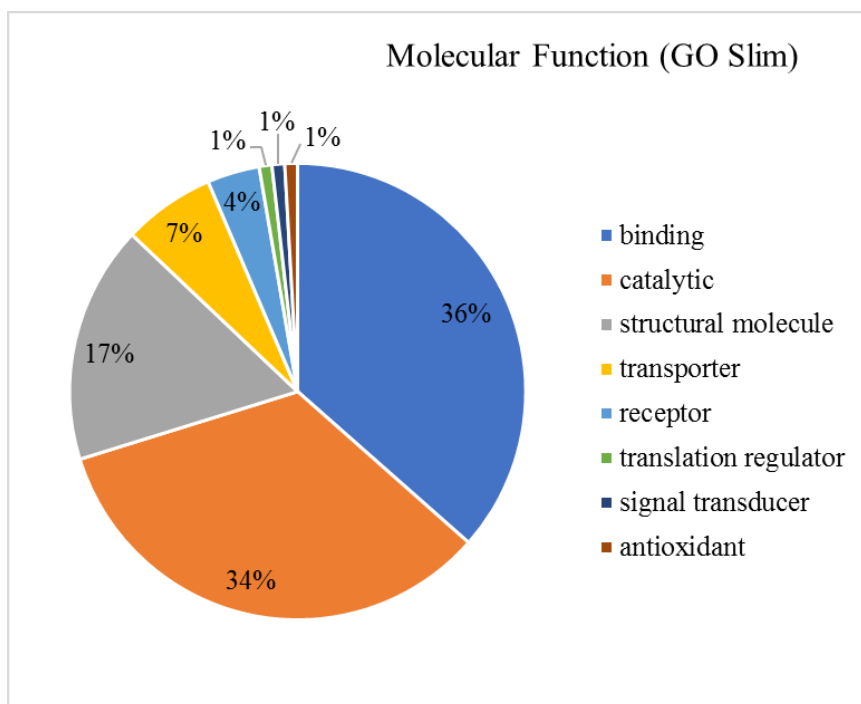


**Figure 2-21: Molecular function of proteins identified in 100% of injections from the EV pulldown method; In total 86.6% of proteins had functions in binding, catalytic activity as well as structural molecules.**

Less than half the proteins with a gene ontology function identified could be mapped to cellular or intracellular components, with a significant proportion (almost 50%) which could be plasma proteins or extracellular proteins (Figure 2-22).

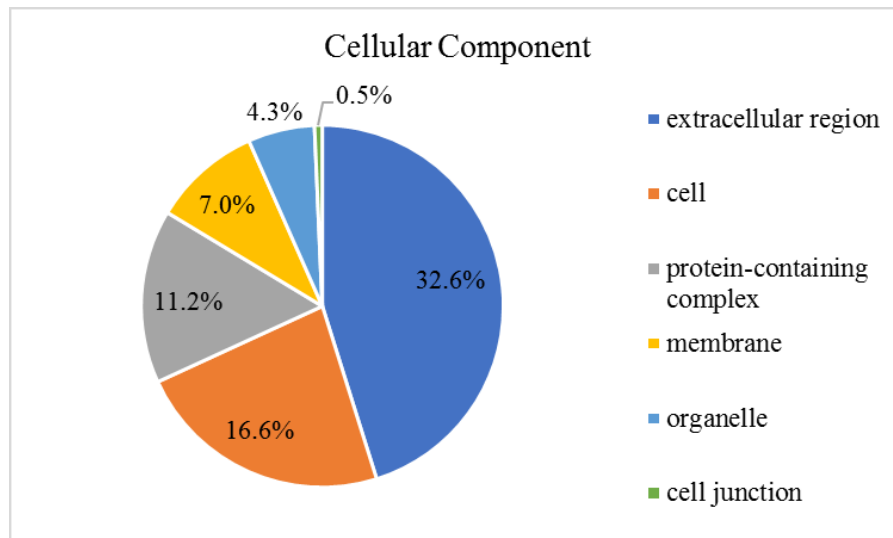
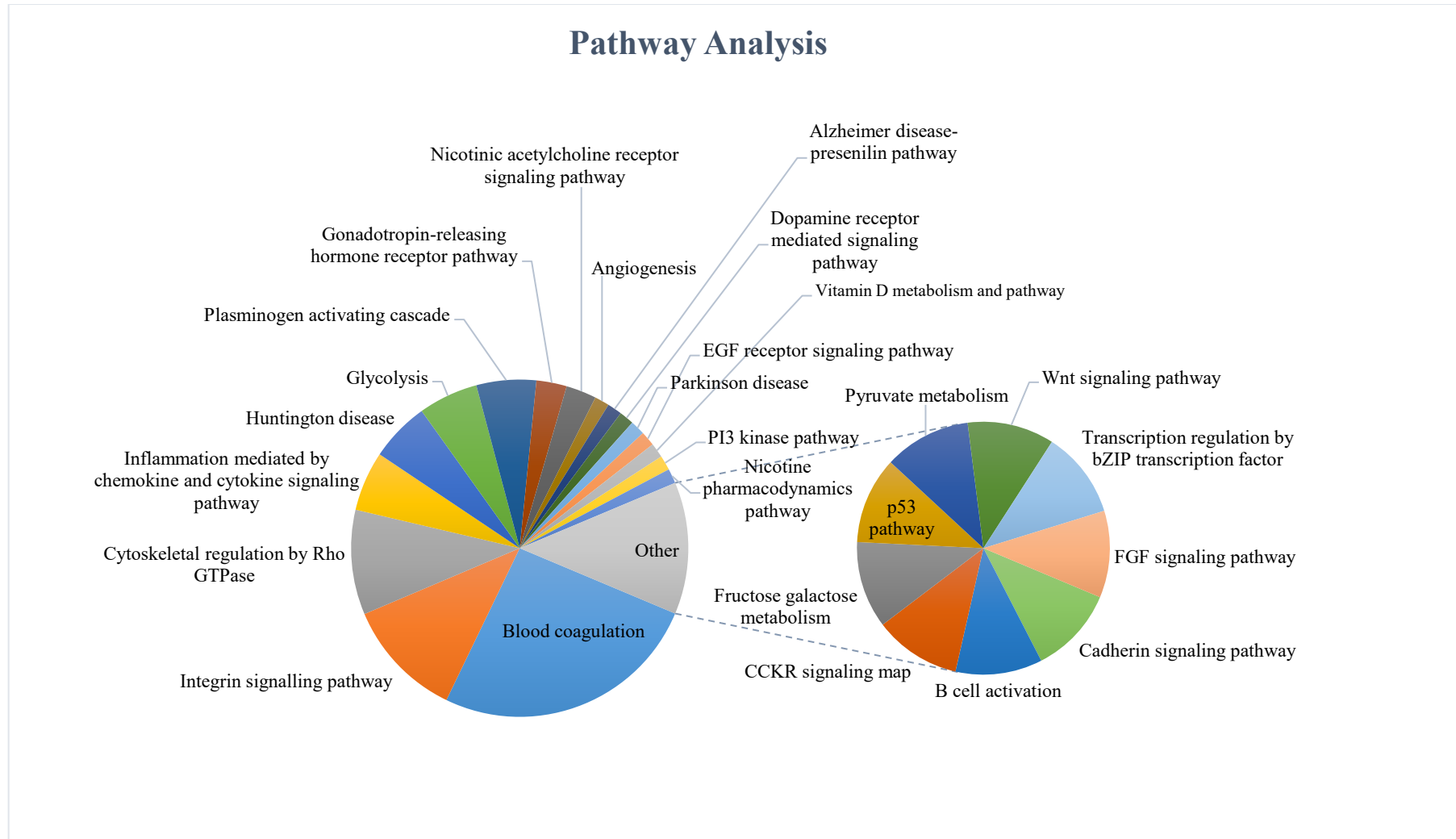


Figure 2-22: Cellular component localisation of proteins identified

Finally, pathways were available for 55% of the proteins in the list (Figure 2-23). Major pathways involved (52.8% of proteins) were blood coagulation, integrin signalling, cytoskeletal regulation by RhoGTPase and inflammation mediated by chemo- and cytokines.



**Figure 2-23: Pathway Analysis of functions of proteins isolated from EV pulldown method; pathways suggest proteins pulled-down participate in intracellular machinery**

### 2.3.15 CSH Enrichment

The average number of protein groups identified by CSH enrichment were  $224 \pm 1.9$ . The total number of unique hits was 247, of which 213 were detected in all 8 injections (86.2%).

Proteins enriched-for by the CSH method, were primarily plasma proteins, in particular if considering only proteins that were detected in all 8 injections. However, there was a preponderance for apolipoproteins, due to the affinity of the method for phospholipids.

### 2.3.16 Do both methods explore mutually exclusive proteomes?

A comparison between proteins seen in the EV and CSH workflows was made (Figure 2-24). Unsurprisingly, there was significant overlap between proteins seen in both workflows, due to the nature of the CSH method, but reassuringly there were proteins unique each of the two methods implying that both methods were complementary.

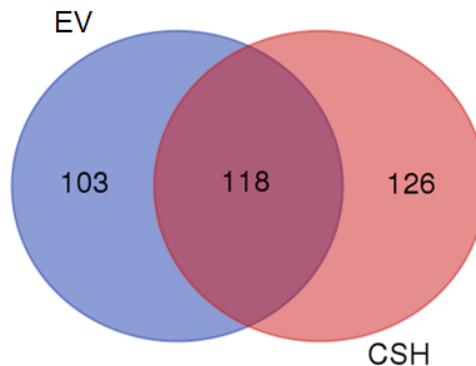
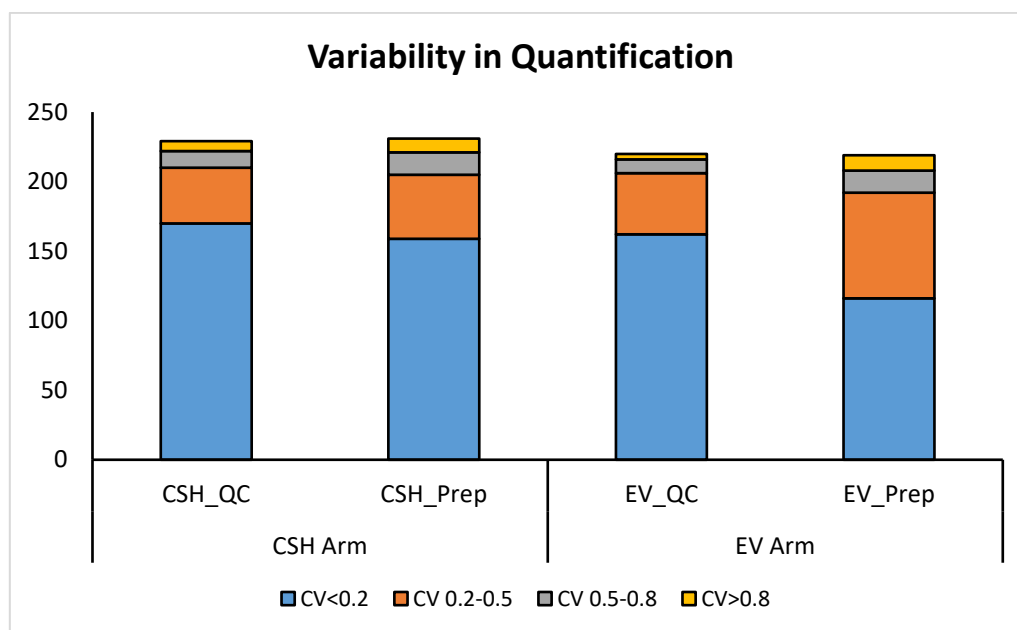


Figure 2-24: Overlap of unique proteins seen in EV and CSH pulldown; diagram confirms that both methods are complementary

### 2.3.17 Reproducibility of quantification of EV & CSH pulldown workflow

A workflow combining both EV and CSH pulldown for analysis resulted in more reproducible quantification of proteins within the samples for the same number of replicates (Figure 2-25). There were more proteins with a CV  $< 0.2$  in the CSH method compared to the EV method, but both EV and CSH methods had far more proteins with low variation compared to the immunodepletion + prefractionation workflow. Additionally the figure also

demonstrated that there was variation inherent to the mass spectrometer (machine variability) which, although it was reassuringly low, was not absent. The fact that the CSH method had reproducibility similar to machine variability suggests there was minimal technical variation in the preparation technique, making it highly suitable for quantitative label-free shotgun proteomics.



**Figure 2-25: Variability in quantification of proteins in EV and CSH preparation methods, as part of the same workflow; the QC stacked bars represent the variability of the mass spectrometer, all injections for the QC samples were from the same sample vial in the autosampler, whilst each replicate for EV\_Prep and CSH\_Prep were separate sample replicates, reflecting the variability in the sample preparation method, but also the contribution of machine variability**

## 2.4 Discussion

### 2.4.1 Method development

Several methods for denaturation were used in sample preparation in these experiments. All appeared comparable in reproducibility (heat, urea, ADC and guanidine) although urea may have had a slightly lower reproducibility with protein quantification. Similar findings were found by others (Proc et al., 2010). Guanidine was eventually used in the immunodepletion and fractionation protocol because the mRP-C18 column would facilitate clean-up in one step (ie. fractionation + sample clean-up). ADC was used for denaturation in the EV+CSH

workflow because there was no simple but efficient way to remove guanidine, whereas deoxycholate did not have this problem. ADC was incompatible with acid pH's, which was the working pH of the mRP-C18 column. Guanidine also severely impairs trypsin digestion (Scheerlinck et al., 2015); mandating a clean-up step; hence it was not used for the EV+CSH workflow. Urea was avoided due to risk of in-vitro carbamylation and also appeared to have reduced protein quantification reproducibility.

The acetate-based method for EV pulldown was selected due to its non-inferiority as a method to the non-acetate based method, and because it needed less plasma to start with. It was clear that precipitation of the EVs on ice was important, as well as a large dilution volume prior to sequential centrifugation and washes, for good protein identification numbers and for good protein quantification reproducibility.

#### **2.4.2 Immunodepletion Method**

In these experiments I found that the immunodepletion method on its own reproducibly yielded a similar amount of protein in the low abundant fraction, with good reproducibility of retention times. Each depletion with subsequent fractionation into 5 fractions, resulted in identification of an average of 148 proteins. These findings were lower than what others have been able to achieve (Tu et al., 2010, Smith et al., 2011). This could be due to sample losses from the workflow, but could also reflect the use of an older MS platform which is less sensitive and shorter LC times (e.g. 75 minute gradient used vs 4 hr gradient in Smith *et al.*).

#### **2.4.3 Fractionation with the mRP-C18 column**

Inspiration for the use of reversed phased HPLC prefractionation of immunodepleted plasma proteins to improve mass spectrometry identification of lower abundant proteins was obtained from the work of others (Martosella et al., 2005). The elution gradient in Martosella's work was modified because the original 50 fractions was impractical, and hence



a more achievable 10 minute gradient was used (Blankley et al., 2013), with adjustment of the timings of fraction collection to coincide with the peaks where possible.

Other methods of reducing complexity of plasma have been described, such as the popular MudPIT method (multi-dimensional protein identification technique) which involves ion exchange separation of tryptic peptide fragments either discontinuously or continuously prior to reversed phase liquid chromatography and online MS/MS detection (Washburn et al., 2001). The caveat to any significant fractionation step however is the required time for analysis, e.g. a single sample fractionated into 15 fractions over 60 minutes then separated for 75 minutes and injected on MS/MS takes  $60 + 15 \times 75 = 1185$  minutes for sample analysis alone. Paired with the time taken to process the MS/MS data file (2-3 hours per data file = 2250 minutes per sample), and one can see how any workflow utilizing this number of fractions could quickly become impractical, if individual sample level information was required.

#### **2.4.4 Reproducibility of the immunodepletion and protein fractionation workflow**

Although initially showing promise with reproducible chromatograms and acceptable lengths of protein lists, the actual quantification of proteins, which was the target of the method, was unsatisfactory. The low reproducibility of measured values of proteins from injection to injection within the same fraction in spite of collecting fractions from the same peaks in the chromatograms was a significant hindrance to the use of this workflow for any inferential work. Possible reasons for the poor reproducibility may be the adjustment of injection amounts from each fraction on the mass spectrometer based on peptide assay values, or sample losses during the workflow. It was therefore necessary to reduce the fractionation steps, to keep all the proteins in the sample together for analysis.

### **2.4.5 EV-pull down method**

The EV-pull down method was not only simple in execution but also a reproducible method for quantification purposes. Whilst there were appreciably more proteins identified in both the EV+CSH workflows, both separately and combined, their main attraction is the high reproducibility in only 2 fractions.

A position statement by the International Society of Extracellular Vesicles (ISEV) gives steps to characterise extracellular vesicles (Théry et al., 2018). Two major criteria need to be fulfilled, which are that proteins in the sample need to belong to 2 or more categories as set out in their position statement, and that the size of the particles need to be confirmed by 2 different but complementary technologies (electron microscopy and single particle analysers). Briefly, category 1 proteins are transmembrane proteins or GPI-anchored proteins localised to cellular membranes which confirm presence of a lipid bilayer structure specific to EVs, which could be tissue specific or not; category 2 proteins are intracellular proteins which could be cytosolic; category 3 proteins are a list of 'negative controls' demonstrating purity of preparation – presence of these extracellular proteins which include plasma proteins, proteins typical of plasma protein complexes and apolipoproteins suggest that the preparation is not that of pure EVs, and category 4 or 5 proteins which are suggestive of EVs with specific functions.

The EV-pulldown experiment identified integrins (integrin beta-6, ADAMTS1), transmembrane proteins (category 1 proteins) which are non-tissue specific. Additionally, heat shock proteins (HSPA1A) and cytoskeletal proteins (Tubulin alpha-4A) could also be demonstrated, both of which belong to the cytosolic protein group (category 2 proteins). Mitochondrial proteins were also identified (pyruvate carboxylase, acetyl-coenzyme A synthetase-like and leucine rich PPR motif protein) which confirms that the method also

isolates proteins from intracellular compartments (category 4 proteins). Finally some other secreted proteins associated with recovered EV's (category 5 proteins) were also identified – transforming growth factor beta 1, fibronectin, galectin-3 binding proteins and CD5 antigen-like protein. Importantly however, plasma proteins were also present, typical examples found were – apolipoproteins (A IV, A V, CII, CIII, D, E and M), albumin and there were also proteins associated with protein aggregates (eg. ubiquitin 40S - a ribosomal protein). This means that this EV-pulldown method does not isolate pure EVs but also includes lipoproteins and protein complexes – both of which may masquerade as EVs on electron microscopy or particle tracking analysis.

#### **2.4.5.1 Nanoparticle Tracking Analysis**

Nanoparticle tracking analysis was performed as a confirmatory step to demonstrate that the particles isolated using the EV-pulldown method were in the exosome - microvesicle size-range. Nanoparticle tracking works on the principle of Brownian motion where the velocity of motion of any particle is directly proportional to its mass and energy. The energy available to each mass in a body of fluid is fixed if the temperature is fixed, therefore the activity of the particle is directly proportional to its mass. Nanoparticle tracking utilises a laser aimed at a sample; its light is scattered by the particles within the sample. The scatter is 'tracked' by a sensor, which ascertains the mobility of the particles. The device tracks up to 5000 particles at any one time, which allows the ascertainment of a distribution of particle sizes within a field of view of a sample. The EV-pulldown pellet when resuspended had particles with the modal size in the 90-100 nm range, confirming that these particles precipitated by the acetate method were of the exosome size-range, and that a 200  $\mu$ L sample provided plenty of particles for analysis. Electron microscopy assessment of the particles could not be performed due to cost and technical reasons, and would have helped confirm the size of the particles. It

must be noted however, exosomes were claimed to be enriched (and confirmed on electron microscopy and particle tracking analysis) by authors who first described this method (Brownlee et al., 2014).

#### **2.4.6 CSH enrichment**

The CSH enrichment method has been used with success in our laboratories for a number of years for proteomic profiling of plasma (Bhandari et al., 2015, Emmens et al., 2018). The original method was described in 2010 and was developed to simplify the proteomic characterization of human plasma lipoprotein populations to avoid the process of ultracentrifugation (Gordon et al., 2010). The matrix selectively adsorbs phospholipids in an irreversible fashion, and along with it their associated proteins.

In the original method (and the updated method (Heink et al., 2015)), plasma was first separated by size with gel filtration, then the lipoproteins selected with the CSH resin, then digested with trypsin, before subsequent reduction and alkylation. The only modification in the workflow presented in my experiments, was the use of ADC as the denaturant – as a mass spectrometry compatible surfactant alternative to sodium dodecyl sulphate, as well as performing reduction and alkylation before digestion. The reason for doing this is that in principle, the surface area for the CSH resin is thought to be saturated with hydrophobic particles. The binding is thought to be irreversible, so bound particles/proteins have to be “digested off” the resin by trypsin. Reduction and alkylation was performed before digestion to ensure that adequate access to the trypsin binding sites in the folded proteins was given, to improve recovery of the proteins in the sample.

I have not used CSH to only isolate lipoprotein species; instead the aim was to reduce the complexity of plasma. It was no surprise that the protein species identified in the CSH-

enrichment method included those described as associated with high and low density lipoproteins (Heink et al., 2015, Gordon et al., 2010).

The degree of overlap of proteins seen between EV and CSH proteins was not surprising. Membrane associated proteins are typically highly hydrophobic and given that vesicles were encapsulated in a lipid-bilayer, one could speculate that in plasma samples that have not been cleared of exosomes, that these particles would preferentially associate with CSH, although their concentrations, in comparison with lipoproteins, are probably lower and would therefore be less likely to be detected as part of the CSH workflow alone.

#### **2.4.7 Reproducibility of the EV+CSH workflow**

Comparing the immunodepletion+fractionation workflow with the EV+CSH workflows, the latter had significantly better reproducibility for label-free shotgun proteomic analysis. Whilst the CVs for technical replicates was not as low as e.g. immunoassays, the variance seen in the protein quantification was sufficiently low for hypothesis generation and unmasking of pathways that may be over- or under-expressed in a certain condition. Working with two fractions instead of 5 was also substantially more pragmatic.

#### **2.4.8 Challenges and Limitations**

There were significant limitations in interpreting this work. I did not compare whether immunodepletion alone vs. enrichment with CSH or EV pulldown alone were better/sufficient for biomarker discovery. The experience of others in this field (Smith et al., 2011) suggest that immunodepletion on its own is reproducible, and therefore by inference, the source of the technical variation in the immunodepletion + protein fractionation workflow was likely to have been from the fractionation aspect. Comparing two different workflows on different mass spectrometric platforms was an important limitation in itself; it is difficult to attribute the difference in reproducibility directly to one aspect of the workflow. However,

time and machine-availability constraints prevented these experiments from being performed in a fully controlled fashion, and should therefore be interpreted with healthy skepticism. The method development was only performed on plasma from a single healthy volunteer. As such, other sources of pre-analytical variation e.g. different individuals, sampling issues, different operators, and different geographical sites were not tested. This may have important implications in particular to EV-pulldown, as patient/disease samples were likely to be very different samples.

## **2.5 Conclusion**

The current immunodepletion + fractionation workflow developed cannot work for biomarker discovery, due to its poor reproducibility. The EV + CSH workflow was found to be suitable for biomarker discovery, due to its low variance and was sufficiently pragmatic. The method was felt to be suitable for plasma-proteomic-profiling, with the caveat that the method may select for hydrophobic proteins, lipoprotein or phospholipid-associated-proteins. This could be viewed as a strength; EVs are formed of membrane phospholipid bilayers and carry molecular messengers to distant sites and could be a rich source of novel biomarkers.

## **Chapter 3 Biomarker Discovery**

### **3.1 Introduction**

In this section, the EV+CSH workflow was applied for discovery of novel biomarkers in AS. Samples from the PRIMID-AS study (Singh et al., 2013) were used. The primary outcome of the PRIMID-AS study was a composite of: spontaneous symptom development necessitating referral for AVR, or death/hospitalisation for AV-related events (syncope, chest pain, breathlessness or HF). Recruitment plasma samples were available. The study and general methods was introduced in section 1.8.

Existing risk-stratification methods are satisfactory, but have poor specificity or sensitivity in identifying patients who are likely to spontaneously develop symptoms or events in asymptomatic moderate-severe AS. Early AVR in well-selected individuals is associated with low perioperative risk (1%), but difficult to justify in the absence of symptoms because of the low risk of sudden death without surgery if asymptomatic (<1%) due to low excess benefit. Early identification of patients likely to develop spontaneous symptoms or events could improve the optimal timing of surgery, especially with long elective waiting times, where the risk continues to increase after symptoms develop (Carabello, 2013).

This discovery step therefore aimed to generate specific targets that would be suitable for verification.

### **3.2 Aims and Objectives**

The aim was to utilise the EV+CSH workflow to ‘discover’ biomarker candidates which would then be used to generate specific hypotheses with respect to the endpoints in the PRIMID-AS study.

Therefore, the objectives were:-

- 1) To discover candidate biomarkers that are differentially expressed in plasma between patients that reached the primary-endpoint (AVR for symptomatic AS, unplanned hospitalisations for syncope, chest pain or HF or cardiovascular death) and those that did not reach the primary endpoint, by the end of the study in initially asymptomatic patients with moderate-severe AS,
- 2) To interpret the biological meaning of these findings, and generate hypotheses about which candidate biomarkers should be verified using other techniques.

### **3.3 Methods**

#### **3.3.1 Patients**

Plasma samples were from patients recruited into the PRIMID-AS study. Recruitment samples were used.

The PRIMID-AS study was a prospective, observational, multi-centre study of asymptomatic moderate to severe AS in the UK, comparing myocardial perfusion reserve (MPR) with exercise testing (Singh et al., 2013, Singh et al., 2017b). Briefly, inclusion criteria were  $\geq 2$  of: AVA  $< 1.5\text{cm}^2$ , peak gradient  $> 36\text{mmHg}$  or MPG  $> 25\text{mmHg}$ , and willingness to accept AVR if symptoms develop. Exclusion criteria were: previous CABG or valve surgery, absolute contraindications to CMR testing or adenosine, other severe valve disease, EF  $\leq 40\%$ , recent myocardial infarction ( $< 6$  months) and planned surgery. All participants provided written informed consent. The study had National Research Ethics Service approval (Unique ethics identification number: 11/EM/0410) and complied with the Declaration of Helsinki.



### **3.3.1.1.1 Investigations**

All patients underwent 12-lead electrocardiography, transthoracic echocardiography, CT-Calcium scoring, symptom-limited bicycle exercise testing (ETT), venous blood sampling for biomarker analysis and 3T multi-parametric CMR at baseline (including stress and rest first-pass perfusion imaging, pre- and post-contrast T1 mapping and late gadolinium enhancement (LGE)). A positive ETT was defined as ‘any AS symptom on ETT or fall in BP below baseline during exercise’ (Baumgartner et al., 2017a). A positive ETT was not used to define ‘spontaneous AS symptoms’. CMR image analysis was undertaken at the core lab by a single blinded observer (Anvesha Singh), as previously described (Singh et al., 2013, Singh et al., 2017b). Multi-detector CT images through the AV were acquired in the diastolic phase of the cardiac cycle, using sequential acquisitions of 3mm slices in full inspiration. AV-calcium score was calculated using the Agatston method (Agatston et al., 1990) and reported in Agatston units.

### **3.3.1.1.2 Biomarker Analysis**

Blood samples were obtained by venepuncture from brachial fossae of recumbent patients at the time of recruitment, after informed consent. Equipment for blood sampling was provided by the study sponsor and all recruitment sites received appropriate training for sample handling protocols, to reduce pre-analytical variation.

In brief, up to 50 mL blood was drawn into pre-chilled EDTA-containing tubes. Tubes were turned-over 8-10 times and then stored at 4°C and centrifuged at 1300g (in a centrifuge with a swinging bucket rotor) on-site at room temperature within 4 hours of venepuncture for 15 minutes. Plasma was aliquoted into 1 mL aliquots with disposable pipettes carefully avoiding the cell layer and buffy coat, then stored at -80°C on site and transferred in a batch at the end of the study to the biobank at University of Leicester using an approved cold-chain courier.

Plasma was defrosted only once prior to analysis. Biomarker analysis was performed in a batch at the end of the study. N-Terminal pro-brain natriuretic peptide (NTproBNP) was analysed using our in-house non-competitive immunoassay (Khan et al., 2008). HsTNI was analysed using the ARCHITECT *STAT* high-sensitivity assay (Abbott Laboratories, Abbott Park, IL, USA) by colleagues in University of Edinburgh (Dr Marc Dweck and Dr Russell Everitt).

### **3.3.1.1.3 Follow-up and endpoints**

Patients had a minimum follow-up of 12 months or until reaching the primary endpoint. The primary endpoint was a composite of AVR for spontaneous symptoms or unplanned hospitalisation with HF, chest pain, syncope or any cardiovascular death. Management decisions were left to the patients' attending physicians, who were blinded to all investigations other than echocardiography. Endpoints were adjudicated by 2 independent cardiologists.

### **3.3.2 Sample selection for biomarker discovery**

Out of 174 patients recruited for the PRIMID-AS study, 168 had sufficient recruitment plasma samples for analysis, of which 46 reached the primary outcome. As such, to maximise biomarker candidate discovery, patients with the 46 endpoints (Event Group) were matched with 46 patients without end-points (NoEvent Group). Matching was performed in R (version 3.3.1, R-project.org) by propensity matching with the 'MatchIt' package, instead of direct matching because patients could not be matched directly on more than just age and sex. Other variables such as presence/absence of arrhythmia, body mass index (BMI), presence/absence of hypercholesterolaemia, systolic and diastolic blood pressure (SBP/DBP), presence/absence of diabetes (DM), left ventricular ejection fraction (LVEF), NYHA class, AV-Vmax, sex, smoking status, and weight may all affect the likelihood of reaching the primary endpoint.

After calculating a propensity score for an individual based on the independent variables to the outcome measure using a logistic regression model, the function then matches the controls with the cases using the nearest neighbour approach (Ho et al., 2011).

### **3.3.3 Sample preparation**

#### **3.3.3.1 Materials and methods**

All materials sourced as described in chapter 2. In this experiment, a ‘DTT Premix’ stock was prepared to simplify denaturation and reduction. It was a 20 mL mixture of 10 mL ADC 2%, 9.8 mL of ammonium bicarbonate 50 mM and 200  $\mu$ L 1M DTT. This yielded a mixture with pH 7.8, 1% ADC and 10 mM DTT. A CSH slurry was prepared as described in section 2.2.12.

#### **3.3.3.2 General preparation**

Aliquots from the study were randomized in pairs in sample preparation order using the function ‘sample’ in R. They were prepared in 5 batches of (3 $\times$ 18 and 2 $\times$ 19 samples). The batches were prepared sequentially after randomization. Within each batch, 11.2  $\mu$ L (if from batch of 18) or 10.6  $\mu$ L (if from batch of 19) of each sample was pooled to create a quality control sample. Each of these was prepared the same way as the samples. When the samples were ready for MS analysis, a quality control (QC) peptide sample was established by pooling the 5 QC samples to form one common pool to be used throughout the study. One pooled QC was prepared for the EV samples and another was prepared for the CSH samples. The following methods were used to prepare the samples for proteomic analyses. A simplified schematic of the workflow used can be seen in Figure 3-1.

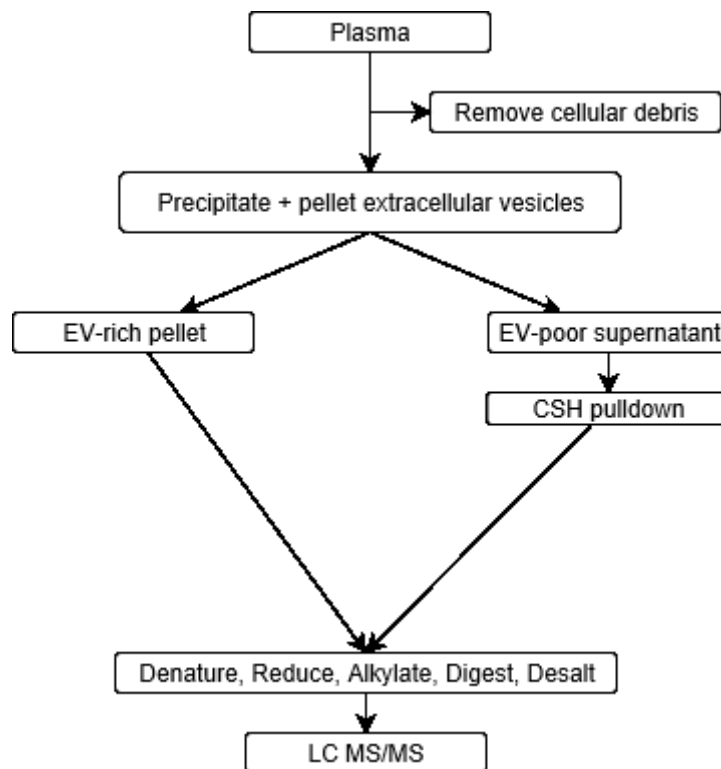


Figure 3-1: Schematic of sample preparation for biomarker discovery; EV: Extracellular vesicles; CSH: calcium silicate hydrate; LC MS/MS: Tandem mass spectrometry

### 3.3.3.3 EV sample preparation

Each batch of aliquots was defrosted at room temperature for 2 hours before preparation on the day of the experiment. 200  $\mu\text{L}$  of sample was then centrifuged at 3000g for 10 minutes to remove cellular debris. The supernatant was transferred to a clean tube. 22.2  $\mu\text{L}$  of 1 M ammonium acetate (pH 4.75) was added, mixed thoroughly then placed on ice for 45 minutes. The sample was then diluted with 1200  $\mu\text{L}$  100 mM 37°C ammonium acetate, to reduce its viscosity, then centrifuged at 20000g for 30 minutes. The supernatant was removed for parallel processing with CSH-enrichment. The EV-pellet was further cleaned through a process of repeated washing with 500  $\mu\text{L}$  of 100 mM ammonium acetate, mixing thoroughly, then centrifugation at 20000g for a further 30 minutes and discarding the supernatant. In total, the washing process was performed 3 times. After the final wash step, the EV-pellet was denatured and reduced with 100  $\mu\text{L}$  of DTT premix for 30 minutes at 65°C. 4  $\mu\text{L}$  of 0.5 M iodoacetamide (IAA) was added (final concentration 20mM), and allowed to alkylate for 30

minutes in the dark at room temperature. 100  $\mu$ L of 50mM ammonium bicarbonate was added (diluting ADC to final concentration 0.5%), followed by 1 $\mu$ g of trypsin for digestion overnight in a 37°C incubator.

The following day, samples were acidified with FA to a final concentration of 1%, mixed thoroughly then centrifuged at 14000g for 3 minutes. The supernatant was then desalted, dried in a SpeedVac for 1 hr 30 minutes, and lyophilised in a freeze-dryer overnight as previously described (section 2.2.7).

#### **3.3.3.4 CSH sample preparation**

350  $\mu$ L of EV-poor plasma (from section 3.3.3.3) was allowed to bind to 100  $\mu$ L of CSH for 1-hour by gentle tumbling. Unbound plasma proteins were washed off by 3 cycles of centrifugation at 14000g for 10 minutes, discarding the supernatant, adding 1 mL of 50mM ammonium bicarbonate then mixing thoroughly. After the final wash cycle, the supernatant was discarded. The sample was denatured and reduced with 300  $\mu$ L DTT Premix for 30 minutes at 65°C. This was followed by alkylation with 12  $\mu$ L of 1M IAA for 30 minutes at room temperature in the dark. 300  $\mu$ L 50mM ammonium bicarbonate was added, then 80  $\mu$ g of trypsin (trypsin:protein ratio of 1:25) to digest at 37°C overnight. The samples were then desalted, dried and lyophilised overnight like the EV-samples.

#### **3.3.3.5 Sample preparation for MS analysis**

Lyophilised samples were suspended in fixed volumes of 0.1% FA (30  $\mu$ L for EV samples and 50  $\mu$ L for CSH samples). The OPA peptide assay was used to determine approximate amounts of peptide in each sample. The concentrations were adjusted with 0.1% FA so that all samples had the same concentration (600 ng) of peptide. Each sample was then prepared by adding an equal volume of 100 fmol of a standard protein digest (alcohol dehydrogenase

from *Saccharomyces cerevisiae*, Uniprot: P00330) to an equal volume of sample, then 1 µl of the sample was injected, containing 300 ng peptide and 50 fmol ADH per-injection on column.

### **3.3.3.6 MS Analysis**

Samples were analysed on a Waters Synapt-G2S Mass Spectrometer (Waters, Manchester, UK), coupled to a NanoAcquity Ultra Performance Liquid Chromatography (UPLC) (Waters, Manchester, UK) as previously described (section 2.2.15.1).

#### **3.3.3.6.1 Scheduling**

To begin, QC samples were injected in triplicate. The data were analysed and an average number of protein ‘hits’ for the QC samples were taken as a benchmark, whereby subsequent QC injections were not to deviate from the benchmark by more than 10% of the initial value. Samples were analysed in singles, with a blank injection after each sample, and a QC injection after every 5 samples. A further triplicate injection of QC samples was performed at the end of the study.

#### **3.3.3.6.2 Data analysis**

Raw data generated from the mass spectrometer were analysed on Progenesis QI for Proteomics version 3.0 (Nonlinear Dynamics, Newcastle upon Tyne, UK). Apex3D processing used 130 as the low energy (LE) threshold and 25 for the high energy (HE) threshold. For ion accounting, the reference proteome library was searched twice. The library used was the ‘reviewed’ human .FASTA database from Uniprot (downloaded 18 November 2013, with 39673 sequences including isoforms). Criteria used in the first round of database searching was 1 fragment per peptide, 3 fragments per protein and 1 peptide per protein, at 4% FDR. After the first library search, the library was searched again using 2 fragments per

peptide, 5 fragments per protein and 2 peptides per protein, at 1% FDR. In addition, carbamidomethylation on Cysteine was used as a static modification and methionine oxidation, deamidation of asparagine, and phosphorylation of serine, threonine and tyrosine were used as variable modifications. 2 missed cleavages were allowed. Progenesis QI was allowed to select its reference chromatogram, to which other chromatograms were aligned. Quantification by Progenesis Qi was performed by creating an aggregate chromatogram (run) containing all the features in the experiment, then comparing these features to the features present in each sample, improving the signal-to-noise ratio. Finally, Progenesis Qi also normalised all features (or peaks), adjusting the intensity of peaks based on the assumption that most of the peptides/proteins in the sample do not change between samples (<http://www.nonlinear.com/progenesis/qi/v2.3/faq/how-normalisation-works.aspx>). As a result, the average total intensities for all peptides/features in all samples should be similar.

For data generation monitoring during the experiment, raw files were analysed with Protein Lynx Global Server version 3.0.2 (Waters, Manchester, UK), using thresholds of 130-LE, 25-HE, 500-intensity, and 2 fragments per peptide, 5 fragments per protein and 2 peptides per protein (or more). The number of protein ‘hits’ was recorded and at the end of the study, samples that had protein ‘hits’ that were more than 2 standard deviations from the average number of hits were repeated. Where samples were re-analysed, if the repeated sample’s results ‘hits’ was closer to the study average, then the repeated sample’s results were used for analysis, otherwise, the first attempt’s results were used.

After Progenesis QI analysis, result files were generated, including a ‘protein output file’, where in this study a Hi10 quantification method was used (i.e. protein quantified on up to the sum of the top 10 most intense unique peptides for the protein). The use of a Hi10 quantification method was based on our observation that often a large number of peptides in a protein did not correlate with each other, hence utilising a larger number of peptides to infer a

protein amount was potentially better. In addition, a Peptide Output file was also generated, allowing close scrutiny to be applied to the proteins seen.

### **3.3.3.7 Result Analysis**

The baseline summary characteristics used for matching after propensity matching was tested with a student's t-test for parametric data and chi-squared test for categorical data. Normality was tested with the Shapiro-wilk test and with Q-Q plots. P-value < 0.05 was taken as statistically significant. For results generated from Progenesis QI, first the data was pre-processed to remove some of the lower confidence peptides and proteins. First, all non-unique peptides were removed. Second, only peptides with 8-25 amino acid residues were retained. Third, peptides that contained phosphoryl-STY, de-amidation-N and methionine-oxidation were excluded. Fourth, all peptides with missed cleavages were excluded. Finally, the list of remaining peptides were used to ascertain which proteins to focus on, because verification/validation was to be performed with suitable surrogate peptides that have previously been observed.

Having discarded the unsuitable peptides, the remaining proteins were used for further analysis. A Mann-Whitney U test was used to determine if the proteins were significantly up or downregulated in the NoEvents Group vs the Events Group. Where a correlation test was performed, a 2-tailed Spearman test for correlation was performed, and reported as (rho, p-value).

Both the EV and CSH protein lists were analysed, and the differentially up and downregulated proteins combined into a single list to be evaluated for pathway analysis.

Pathway analysis was performed with Cytoscape (version 3.5.1) (Shannon et al., 2003) with the ClueGO (version 2.3.4) (Bindea et al., 2009) and CluePedia (version 1.3.4) plugins, using the method described in a tutorial by Trindade et. Al (Trindade et al., 2018). Specific settings



used were searches performed in GlueGo:Functions mode, grouping by prespecified 'Clusters'. Ontology/Pathways used were GO Biological Processes and WikiPathways, using 'all available evidence' for annotation. Network specificity was set between 'Medium' and 'Detailed', with GO Tree Interval set as 5 to 11, GO Term/Pathway Selection was based on a criteria of a minimum of 2 Genes OR 5% Genes within the term OR was 60% specific to the GO Term. The GO Term/Pathway Network Connectivity considered a kappa score of 0.4 to qualify for a link. After annotation, results were exported as a spreadsheet. Biological 'meaning' for the results was further supplemented by literature review on each biomarker candidate.

### **3.4 Results**

One hundred seventy four patients were recruited and followed up for an average of  $369 \pm 156$  days (range 181-791). 168 had sufficient recruitment plasma samples for analysis, of which 46 reached the primary outcome. These comprised 40 AVRs for spontaneous symptoms, 1 cardiovascular death & 5 unplanned hospitalisations (1 chest pain, 2 dyspnoea, 1 HF, 1 syncope)). The time delay from blood sampling to event was variable, ranging from 5-677 days with a median of 242 days.

#### **3.4.1 Balance of cases vs controls**

168 patients were evaluated for matching, using the MatchIt algorithm. Figure 3-2 visually displays the distribution of propensity scores of the matched "Event" units and matched 'No Event' units. Although better matched, the groups were not completely balanced (Figure 3-3). Baseline characteristics of the two matched groups can be seen in Table 3-1.

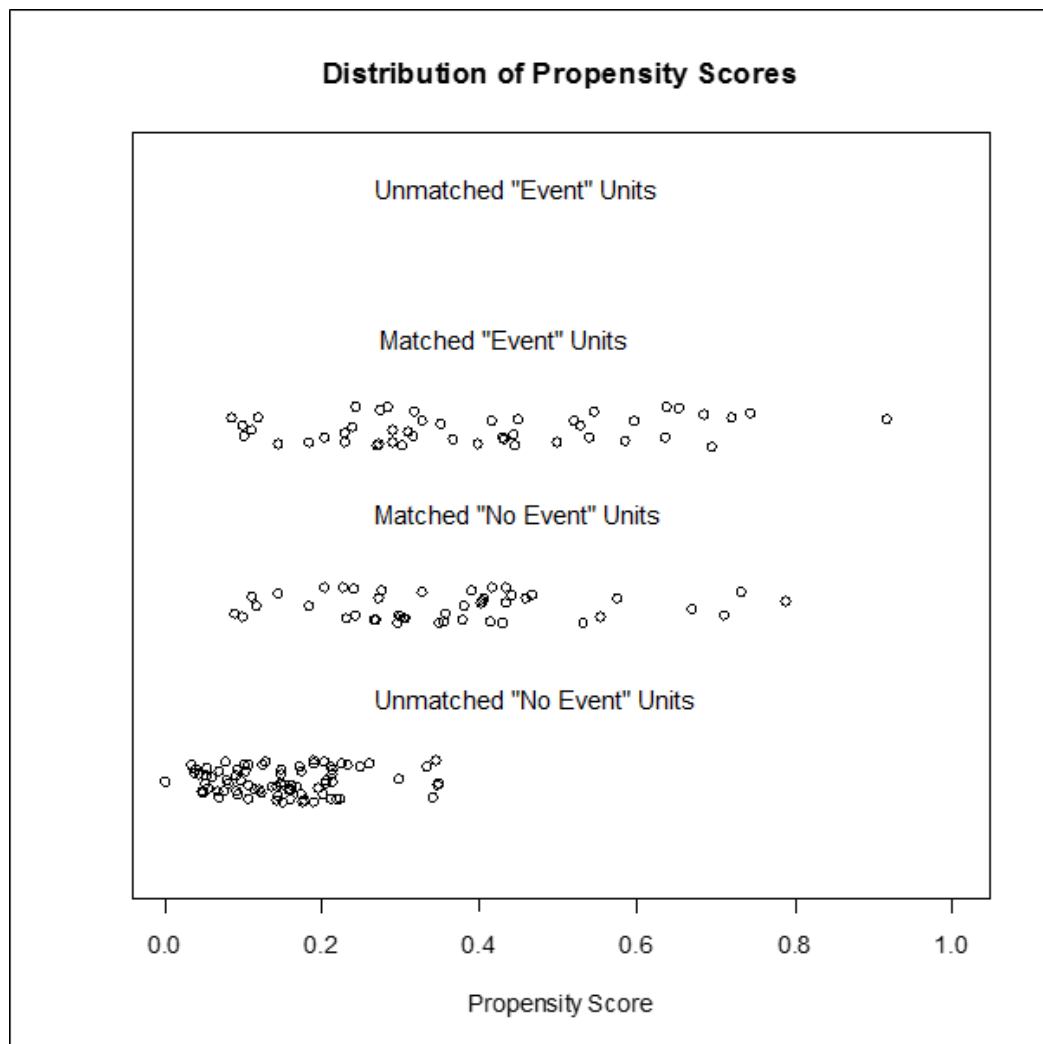
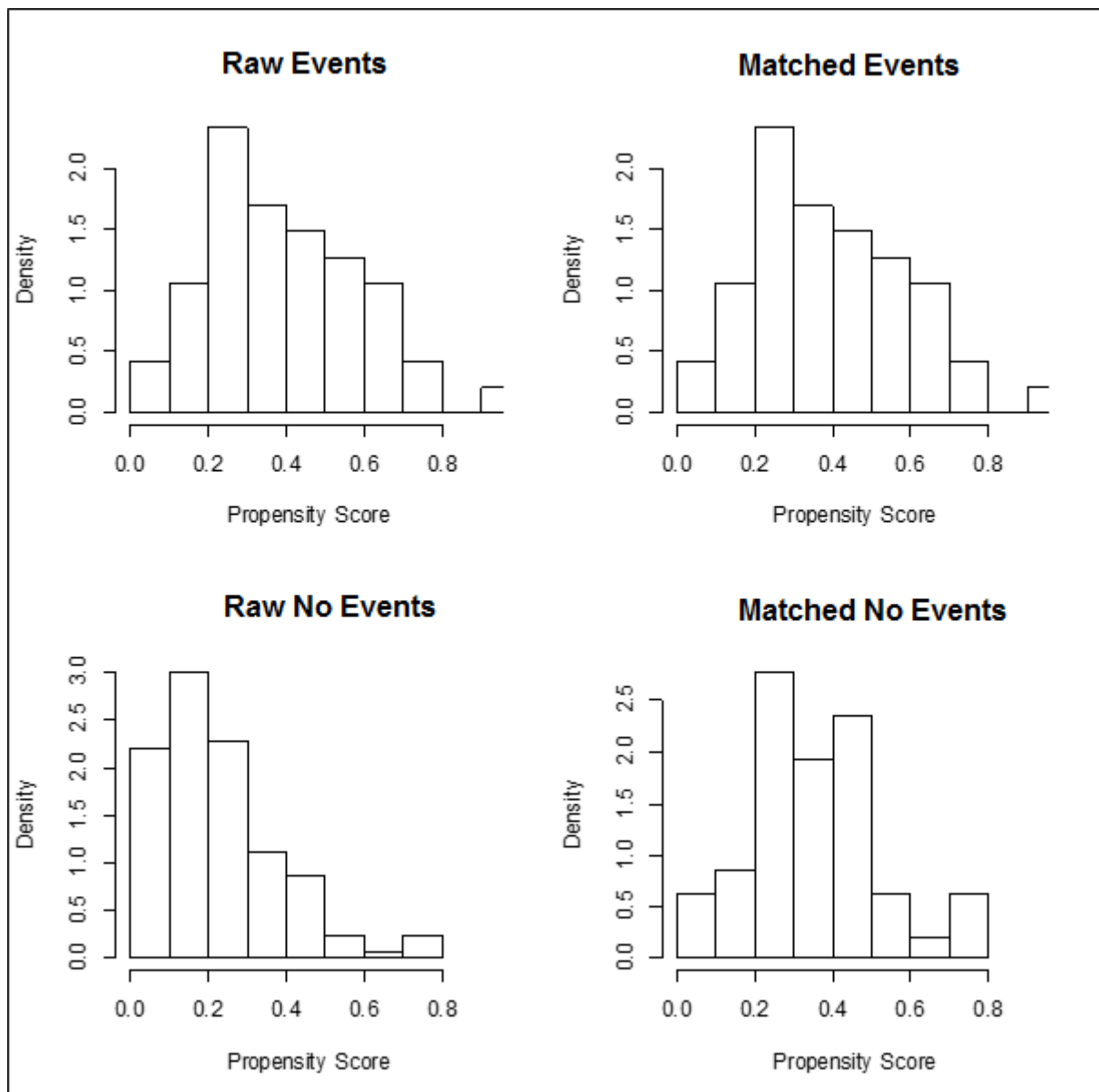


Figure 3-2: Distribution of propensity scores between matched Events and NoEvents patients



**Figure 3-3: Distribution of propensity scores before and after matching between groups; Note: no difference between Raw and Matched Events because all events were used in discovery.**

Both groups had a similar distribution for matched features (Table 3-1). There a similar number of co-morbidities, sex-split, NYHA class, AV-Vmax, BMI, LV function and blood pressure.

Factor	Group	NoEvents N=46	Events N=46	p.value
Arrhythmia (%)	Yes	3 ( 6.5)	4 ( 8.7)	1
	No	43 (93.5)	42 (91.3)	
Cholesterol (%)	Yes	19 (41.3)	21 (45.7)	0.642
	No	24 (52.2)	20 (43.5)	
	Unknown	3 ( 6.5)	5 (10.9)	
Diabetes (%)	Yes	4 ( 8.7)	7 (15.2)	0.522
	No	42 (91.3)	39 (84.8)	
Hypertension (%)	Yes	26 (56.5)	24 (52.2)	0.834
	No	20 (43.5)	22 (47.8)	
NYHA (%)	I	45 (97.8)	45 (97.8)	1
	II	1 ( 2.2)	1 ( 2.2)	
Sex (%)	Male	31 (67.4)	28 (60.9)	0.664
	Female	15 (32.6)	18 (39.1)	
Smoker (%)	Yes	5 (10.9)	4 ( 8.7)	0.621
	No	26 (56.5)	22 (47.8)	
	Past	15 (32.6)	20 (43.5)	
Age		68.54 (12.00)	68.62 (11.66)	0.976
Peak Velocity (m/s)		3.96 (0.55)	4.15 (0.61)	0.139
BMI		27.23 (3.81)	27.35 (3.88)	0.883
Systolic BP		146.29 (21.30)	146.80 (22.82)	0.912
Diastolic BP		76.03 (10.23)	75.52 (10.74)	0.816
LV Ejection Fraction		57.06 (5.40)	57.45 (4.61)	0.708
Weight (kg)		78.48 (13.82)	77.72 (12.53)	0.784

**Table 3-1: Average values between NoEvents and Events used for propensity matching; NYHA: New York Heart Association Class, I – mild limitation in activity, II – moderate limitation in activity; BMI: body mass index; BP: blood pressure; LV: left ventricle**

### 3.4.2 General mass spectrometric findings

In the EV-study, there were two ‘events’ beyond the control of the course of the experiment that occurred. Specifically, there were two electrospray-emitter occlusions that necessitated an ‘emitter rebuild’ involving a process of (re)building a clean emitter block, with a new silica emitter tip, confirming ideal positioning against a reference sample (Glu-Fib peptide), then performing a ‘lock-spray and calibration setup’ with Glu-Fib. This was followed by running of a HeLa standard digest, which was required to give >2000 hits to be assured of sufficient machine sensitivity. In both cases, the experiment was suspended for 4 days for these steps to be accomplished. Utilising the protein hits from the samples as a guide, there was no apparent detriment to the number of hits (protein identifications) in each sample.

Figure 3-4 shows how the QC sample's hits remained fairly constant throughout the study, with more variability in the actual experimental samples as expected. Additionally, there was a slight drift downwards in the number of identifications from the beginning to the end of the study, although in absolute terms there was only an average drop of 5 protein identifications comparing the beginning vs. the end of the study in the QC samples.

When plotting the sum Top3 matched peptide intensities for all proteins identified in each sample (as a surrogate for the total amount of sample), the variability in the total signal intensity is reassuringly stable, particularly in the QC samples, although there were some outliers in the actual samples (Figure 3-5).

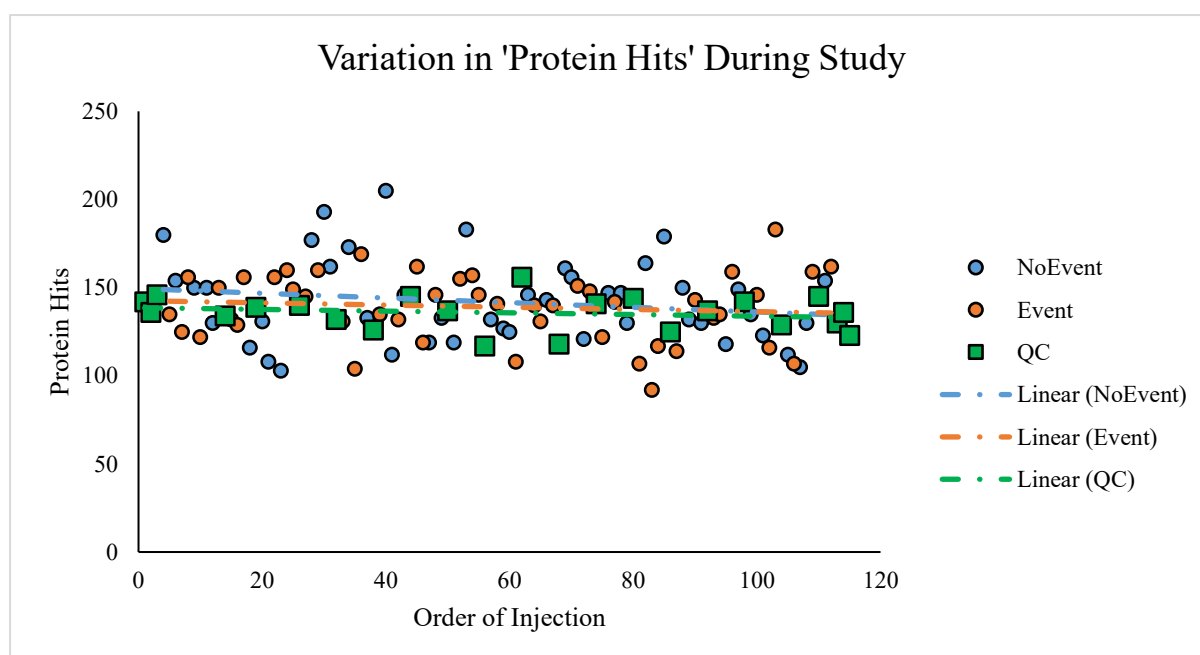


Figure 3-4: Variation in protein hits over course of EV-study by injection order

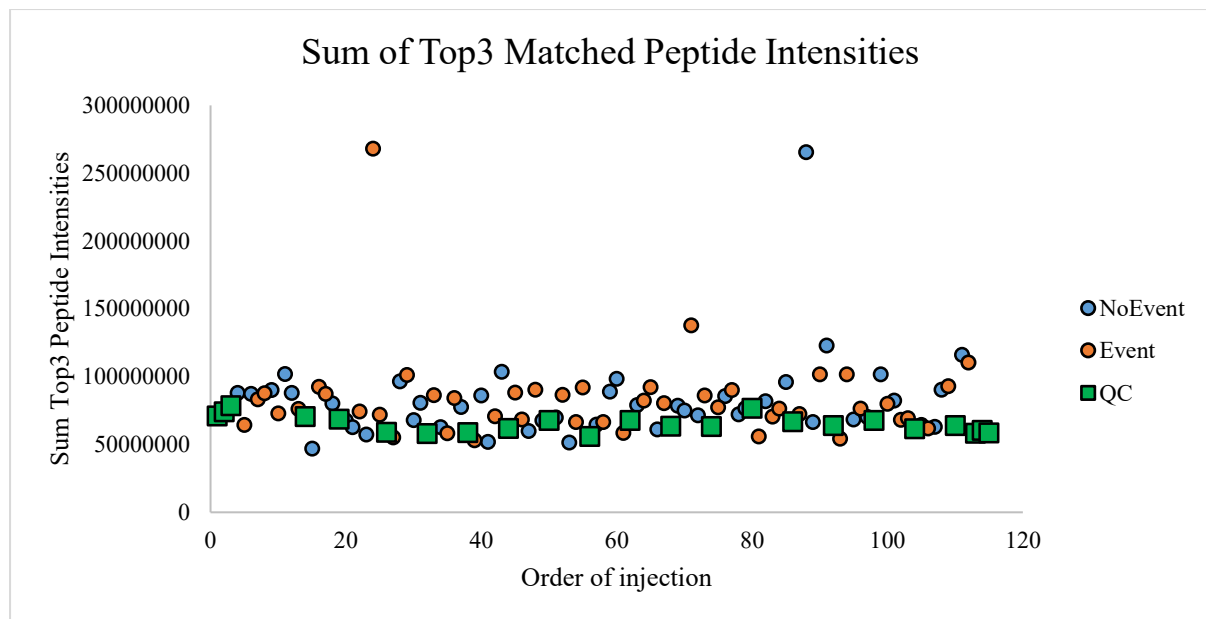


Figure 3-5: Sum Top3 Peptide Intensities over course of EV-study by injection order

The number of hits correlated with total intensity (Spearman's  $\rho = 0.403-0.42$ ,  $p < 0.001$ ), even in the presence of outliers.

Similar findings were seen with CSH part of the study (Figure 3-6 & Figure 3-7).

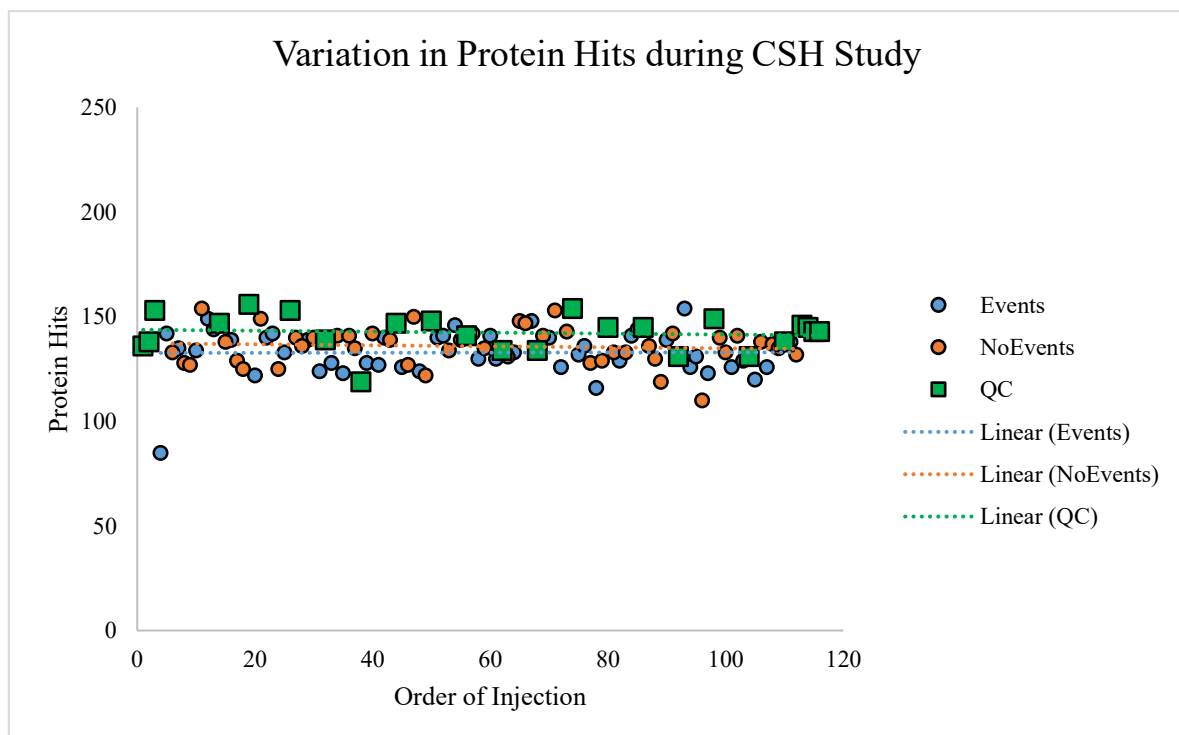


Figure 3-6: Protein hits during the CSH study by injection order

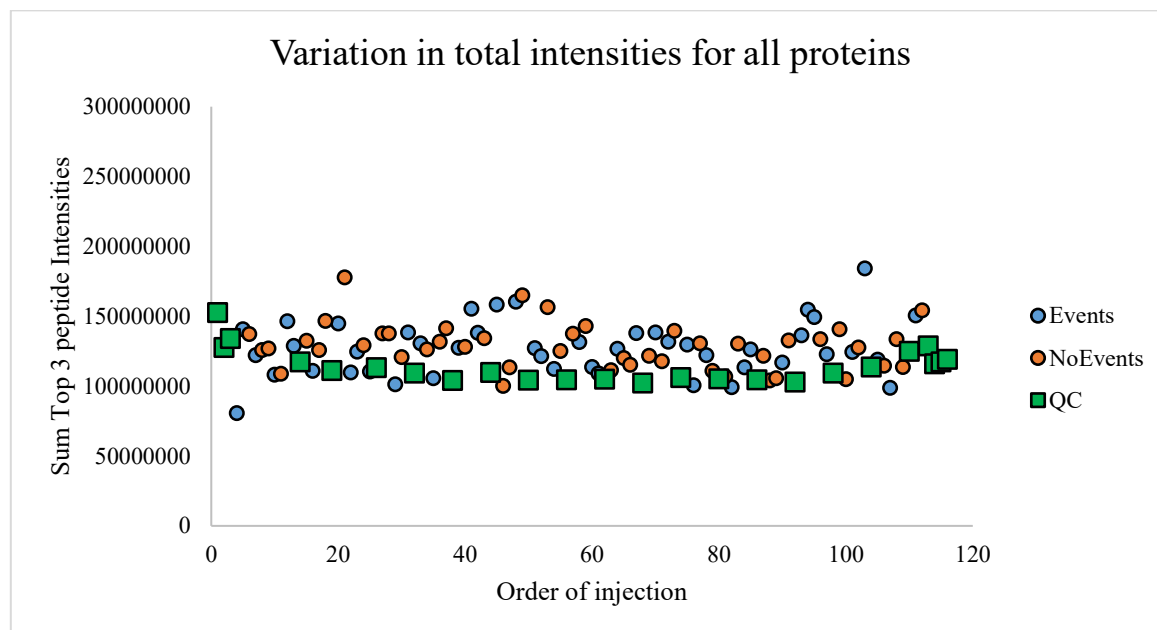


Figure 3-7: Sum Top3 Peptide Intensities over course of CSH-study by injection order

Interestingly, with the CSH samples, there was no correlation between hits and intensity, even when outliers were removed.

In total, three samples were repeated as they had protein hits just outside the 2-standard-deviation-from-the-mean-rule specified, but the repeats did not bring the sample results any closer to the mean and therefore the initial samples results were used.

### 3.4.3 Results from Progenesis QI

#### 3.4.3.1 EV Results

Using the protein lists of quantification and identification results from Progenesis QI, the EV experiment identified 1415 protein groups ("hits") with quantification and an additional 1405 protein groups without quantification. Only quantified proteins were used for analysis.

There was nearly a 7-fold increase in the number of protein identifications compared to the reproducibility study (section 2.3.17) which could be due to a number of factors such as more samples being analysed, more injections being analysed (the QC samples were also

analysed), the use of patient samples which may have more proteins in illness, the use of a different MS platform (Synapt-G2S) and the way the data were analysed with the use of Progenesis QI for proteomics, which quantifies features first before identification, with significantly improved signal-to-noise ratio and resultant identifications.

When the EV protein results were used to generate a principal component plot, to visualise unsupervised patterns in the underlying data, 3 ‘clusters’ could be seen (Figure 3-8).

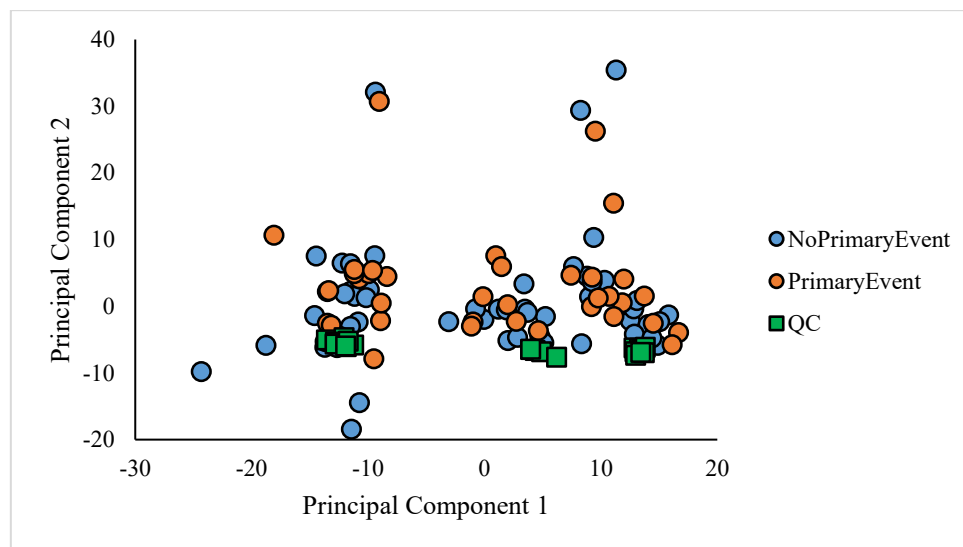


**Figure 3-8: Principal component plot of EV experiment revealing clusters of experimental data**

These ‘clusters’ corresponded to periods during which the experiment ran continuously, with separation coinciding with periods when the experiment had to be suspended for essential maintenance (i.e. emitter-tip blockages). These systematic errors introduced into the data were not overtly detectable on the number of ‘hits’ or total peptide intensities during the study, but nevertheless affected the quality of the data.



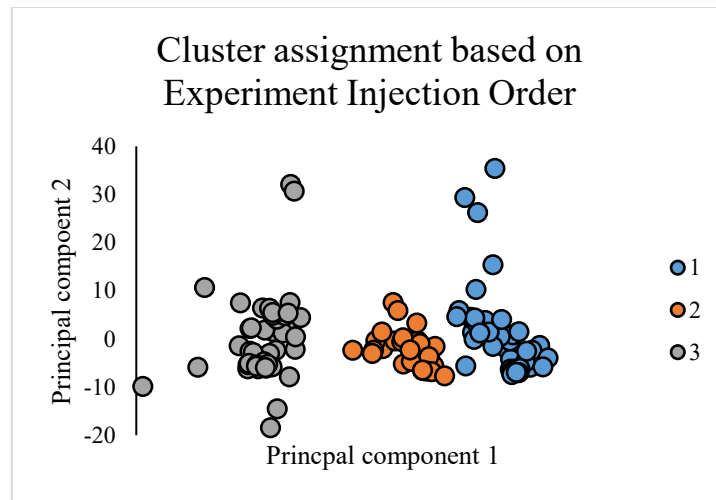


Figure 3-9: Cluster assignment in EV-study for statistical adjustment

In order to mitigate this effect, to determine which proteins were differentially expressed/regulated in the patients with/without Primary Events, each cluster was assigned a value, such that the cluster class could be ‘adjusted for’ in a logistic regression model (Figure 3-9). In addition, Mann-Whitney-U statistics were also calculated between the Primary Event and NoPrimary Event groups to identify any additional potential biomarker targets that may have been spuriously excluded.

After selecting only proteins with targetable peptides (section 3.3.3.7), only 742 proteins remained to be statistically evaluated. Of these, 25 were significantly different in abundance between the Events/NoEvents groups, after adjustment in a logistic regression model. Further testing with Mann Whitney U statistics identified 3 further proteins which were significantly different, although there were a number of ‘cluster adjusted’ protein results which were not significant on non-parametric statistics. Table 3-2 and Figure 3-10 summarise the 28 different proteins groups in the EV experiment by Primary Event.

Uniprot	Protein Group	Gene	% Diff	p-MWU	p-log	Higher In
P07996	Thrombospondin-1	THBS1	22%	0.035	0.036	No Event
Q9UKZ4	Teneurin-1	TENM1	22%	0.096	0.042	No Event
P35442	Thrombospondin-2	THBS2	18%	0.035	0.03	No Event
Q2UY09	Collagen alpha-1(XXVIII) chain	COL28A1	18%	0.015	0.02	No Event
P05160	Coagulation factor XIII B chain	F13B	16%	0.138	0.041	No Event
P46100	Transcriptional regulator ATRX	ATRX	16%	0.104	0.021	No Event
P35542	Serum amyloid A-4 protein	SAA4	15%	0.04	0.034	No Event
A0AVI2	Fer-1-like protein 5	FER1L5	15%	0.027	0.036	No Event
Q86VF7	Nebulin-related-anchoring protein	NRAP	15%	0.069	0.044	No Event
P80108	Phosphatidylinositol-glycan-specific phospholipase D	GPLD1	14%	0.005	0.009	No Event
Q04756	Hepatocyte growth factor activator	HGFAC	14%	0.091	0.044	No Event
P10909	Clusterin	CLU	13%	0.138	0.049	No Event
P31749	RAC-alpha serine/threonine-protein kinase	AKT1	11%	0.053	0.04	No Event
Q12805	EGF-containing fibulin-like extracellular matrix protein 1	EFEMP1	11%	0.08	0.031	No Event
Q9NR12	PDZ and LIM domain protein 7	PDLIM7	10%	0.042	0.114	No Event
Q00187	Isoform 2 of Mannan-binding lectin serine protease 2	MASP2	4%	0.027	0.041	No Event
Q6ZS30	Neurobeachin-like protein 1	NBEAL1	1%	0.123	0.04	Event
P51790	H(+)/Cl(-) exchange transporter 3	CLCN3	3%	0.045	0.135	Event
P14770	Platelet glycoprotein IX	GP9	5%	0.031	0.486	Event
A6H8Y1	Transcription factor TFIIIB component B'' homolog	BDP1	6%	0.076	0.03	Event
Q13418	Integrin-linked protein kinase	ILK	7%	0.047	0.047	Event
Q7Z3B4	Nucleoporin p54	NUP54	7%	0.041	0.034	Event
Q6ZNE9	RUN and FYVE domain-containing protein 4	RUFY4	10%	0.024	0.021	Event
Q8IUC4	Rhopilin-2	RHPN2	18%	0.13	0.033	Event
P01009	Alpha-1-antitrypsin	SERPINA1	25%	0.007	0.006	Event
Q8IYS0	GRAM domain-containing protein 1C	GRAMD1C	29%	0.036	0.025	Event
Q5JSJ4	Protein DDX26B	DDX26B	30%	0.011	0.01	Event
Q06609	DNA repair protein RAD51 homolog 1	RAD51	62%	0.109	0.04	Event

**Table 3-2: Proteins that were differentially expressed between Events and No Events, p-MWU: p values from Mann Whitney test, p-log: p-values from logistic regression after adjusting for clusters; %Diff: %Difference is a ratio of the medians of proteins in Events vs NoEvents expressed as a percentage**

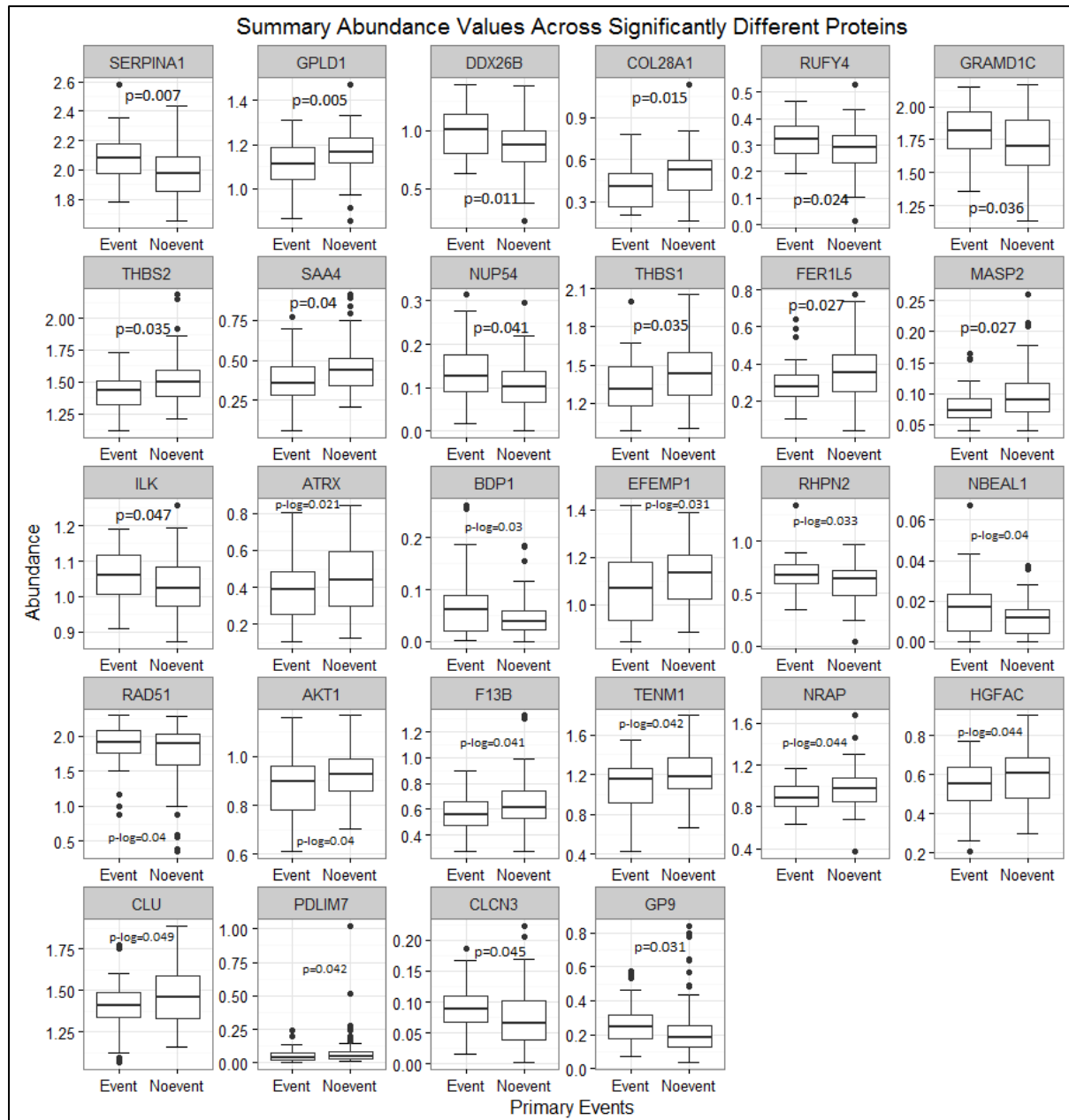


**Figure 3-10: Boxplots showing differences in abundance between Events and NoEvents for proteins that were differentially expressed in the EV experiments**

### 3.4.3.2 CSH Results

The CSH experiment identified and quantified 1175 proteins, and an additional 433 proteins which could not be quantified by Progenesis QI. This increase in proteins identified mirrored the increment seen in the EV experiment, likely for the same reasons. After filtering the peptides as described in the methods section, there were 768 quantifiable proteins in the

protein list. Figure 3-11 shows the principal component plot for the first and second principal component, to demonstrate any underlying patterns in the data.

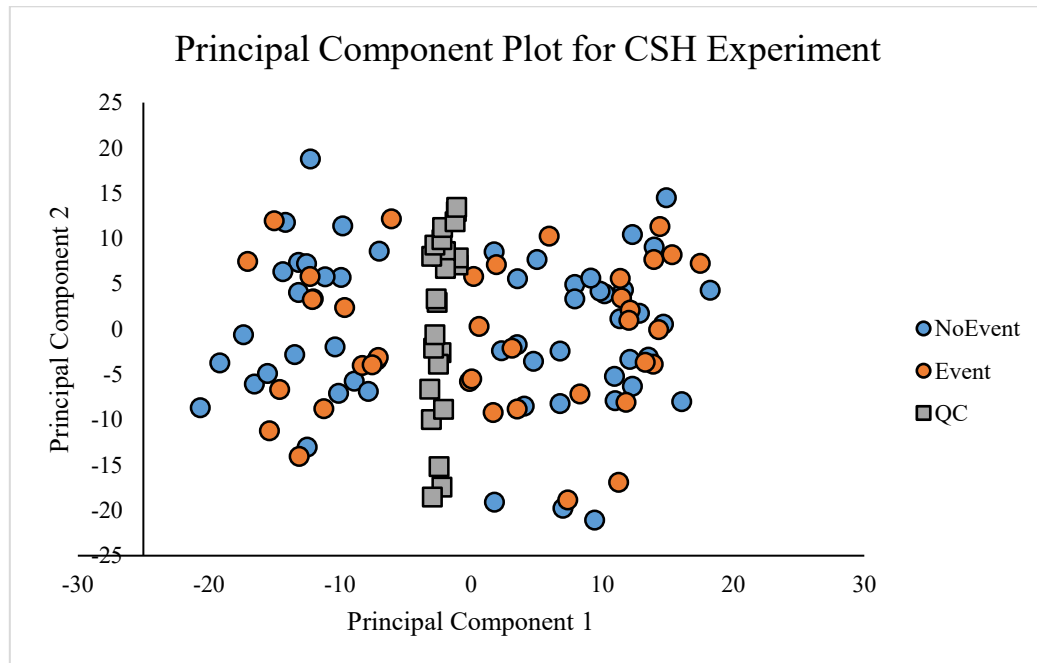
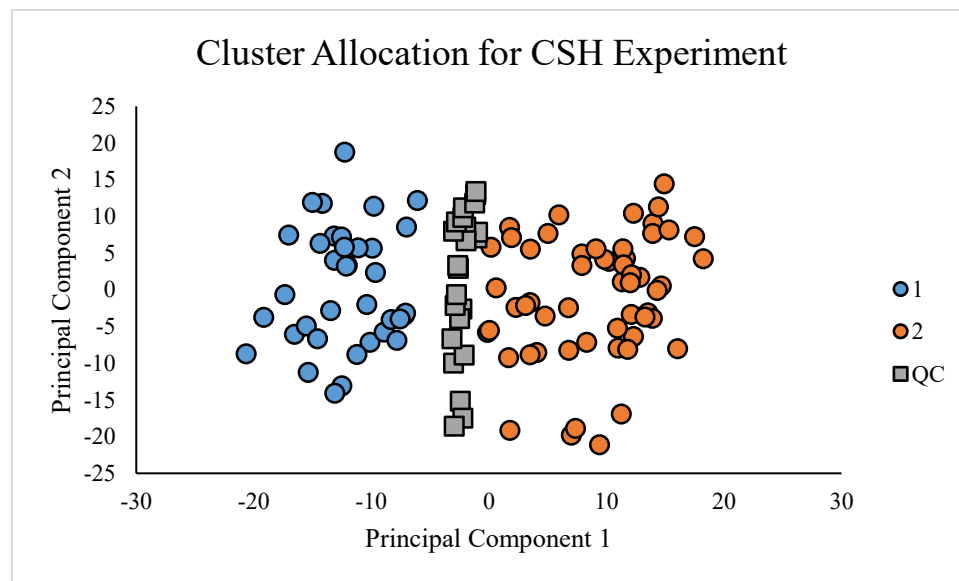


Figure 3-11: Principal component plot for CSH Experiment showing a less obvious clustering of data into two groups

The plot confirmed that there were no overt disruptions during the experiment being conducted on the mass spectrometer, because the QCs cluster together as a single group with minor drift in principal component 2. There were two ‘clusters’ however, along principal component 1 in the samples prepared, which may be due to sample preparation batch differences, but the distribution of NoEvents and Events within each cluster appear similar and unbiased. For the sake of completeness, clusters were assigned values, just as in the EV experiment, and ‘adjusted for’ in a logistic regression model (Figure 3-12). Table 3-3 and Figure 3-13 summarise the differentially expressed protein groups in the Event vs No Event groups. There were 35 protein groups in the CSH experiment that were found to be differentially expressed. Protein C5orf42, IgVII-BUT and LINC00324 were subsequently

left-out from further evaluation due to lack of available literature and would be difficult to interpret, leaving 32 proteins to be considered as potential candidates.



**Figure 3-12: Cluster assignment for the CSH Experiment**

Uniprot	Protein Group	Gene	% Diff	p-MWU	p-log	Higher In
P02656	Apolipoprotein C-III	APOC3	19%	0.017	0.016	No Event
O94915	Protein furry homolog-like	FRYL	19%	0.022	0.022	No Event
P49321	Nuclear autoantigenic sperm protein	NASP	14%	0.072	0.029	No Event
P01767	*Ig heavy chain V-III region BUT	IgVII.BUT	12%	0.023	0.019	No Event
P48740	Mannan-binding lectin serine protease 1	MASP1	11%	0.046	0.039	No Event
P30043	Flavin reductase (NADPH)	BLVRB	9%	0.121	0.047	No Event
Q9H799	*Uncharacterized protein C5orf42	C5orf42	8%	0.02	0.083	No Event
P02765	Alpha-2-HS-glycoprotein	AHSG	8%	0.106	0.043	No Event
P43652	Afamin	AFM	7%	0.008	0.017	No Event
Q15413	Ryanodine receptor 3	RYS3	6%	0.049	0.044	No Event
Q8N7Z5	Putative ankyrin repeat domain-containing protein 31	ANKRD31	6%	0.01	0.021	No Event
Q5T8P6	RNA-binding protein 26	RBM26	5%	0.029	0.02	No Event
P02760	Protein AMBP	AMBP	5%	0.037	0.044	No Event
P02749	Beta-2-glycoprotein 1	APOH	5%	0.028	0.192	No Event
Q7Z7A4	PX domain-containing protein kinase-like protein	PXK	3%	0.032	0.185	No Event
Q92830	Histone acetyltransferase KAT2A	KAT2A	2%	0.127	0.025	Event
O75051	Plexin-A2	PLXNA2	4%	0.054	0.047	Event
Q8NAT9	*Putative uncharacterized protein encoded by LINC00324	LINC00324	6%	0.085	0.05	Event
A8MW92	PHD finger protein 20-like protein 1	PHF20L1	7%	0.029	0.066	Event
Q8IWN7	Retinitis pigmentosa 1-like 1 protein	RP1L1	7%	0.022	0.027	Event
P18074	TFIIH basal transcription factor complex helicase XPD subunit	ERCC2	7%	0.08	0.025	Event
Q9HCM2	Plexin-A4	PLXNA4	7%	0.01	0.012	Event
Q9NWX6	Probable tRNA(His) guanylyltransferase	THG1L	7%	0.039	0.075	Event
Q7Z7A1	Centriolin	CNTRL	7%	0.036	0.05	Event
P78417	Glutathione S-transferase omega-1	GSTO1	8%	0.012	0.005	Event
Q9H3G5	Probable serine carboxypeptidase CPVL	CPVL	8%	0.003	0.005	Event
P05090	Apolipoprotein D	APOD	8%	0.064	0.018	Event
Q92619	Minor histocompatibility protein HA-1	HMHA1	8%	0.037	0.052	Event
Q92614	Unconventional myosin-XVIIIa	MYO18A	8%	0.018	0.03	Event
Q8NB59	Synaptotagmin-14	SYT14	10%	0.015	0.063	Event
P05452	Tetranectin	CLEC3B	10%	0.104	0.026	Event
Q09428	ATP-binding cassette sub-family C member 8	ABCC8	11%	0.007	0.064	Event
Q6IQ55	Tau-tubulin kinase 2	TBK2	11%	0.153	0.048	Event
Q9BZ29	Isoform 4 of Dedicator of cytokinesis protein 9	DOCK9	11%	0.027	0.068	Event
P01009	Alpha-1-antitrypsin	SERPINA1	12%	0.07	0.023	Event

**Table 3-3: Differentially expressed proteins in CSH experiment between Events and NoEvents; p-MWU: p values from Mann Whitney test, p-log: p-values from logistic regression after adjusting for clusters; %Diff: %Difference is a ratio of the medians of proteins in Events vs NoEvents expressed as a percentage**

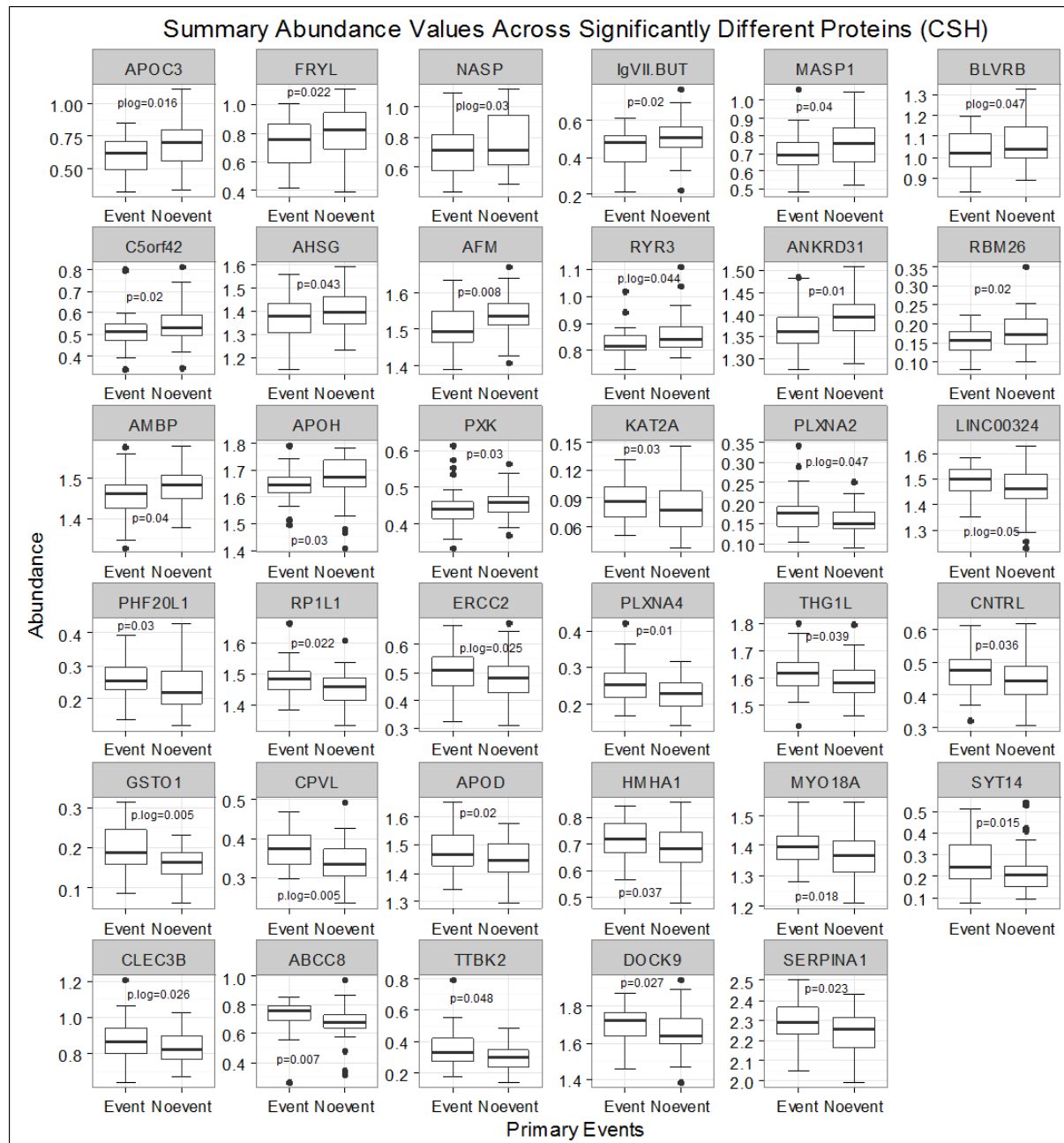
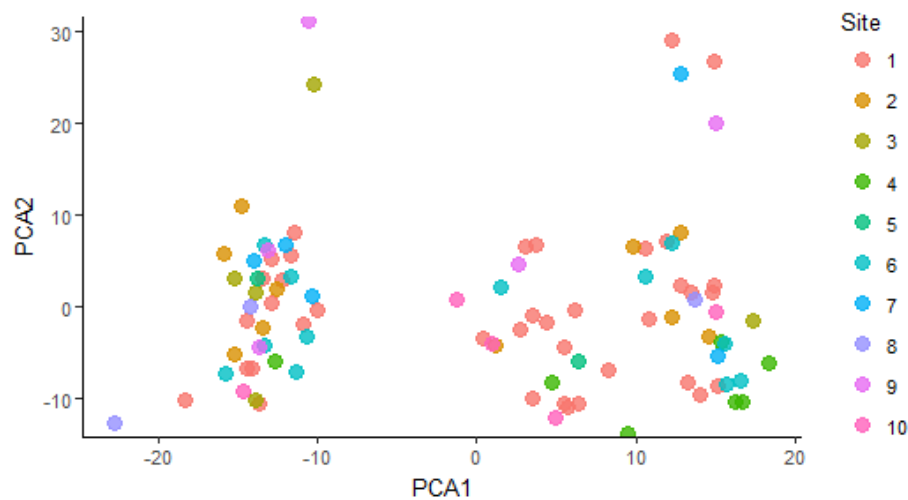


Figure 3-13: Boxplots showing differences in abundance of proteins between Event/NoEvent in the CSH experiment.

### 3.4.3.3 Pre-analytical Considerations

In this multisite study (10 UK sites), an important variable which may have contributed to pre-analytical variation is the sample-handling-practices of personnel at different sites. Whilst all personnel received appropriate training, the facilities used are different, and may have contributed to pre-analytical variation. To qualitatively assess this, samples from different sites were marked on a principal component plot to see if there were patterns suggestive of

bias by recruitment site. There was no apparent contribution by recruitment site to the clustering of the data (Figure 3-14 & Figure 3-15).



**Figure 3-14: Principal component plots from EV experiment stratified by recruitment site; colours correspond to recruitment sites**

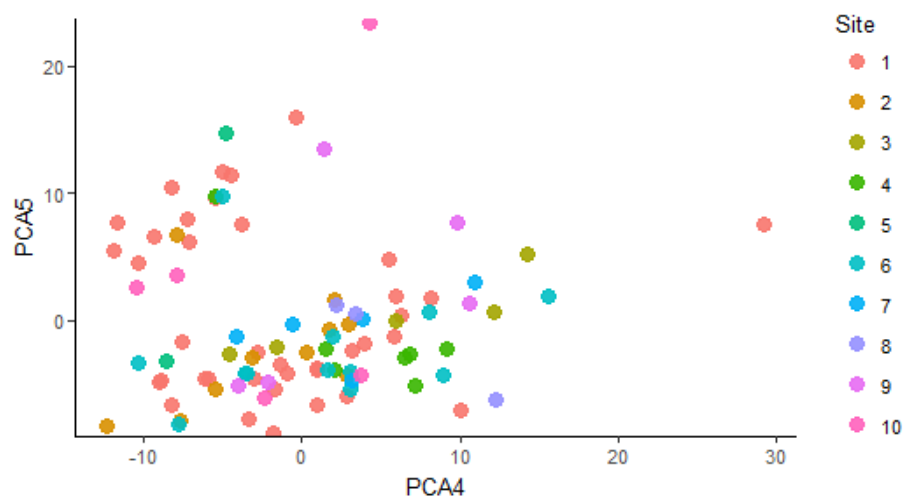


**Figure 3-15: Other principal component plots from EV experiment stratified by recruitment site; colours correspond to recruitment sites**

The same test was applied to the CSH experiment to evaluate this (Figure 3-16 & Figure 3-17). Again there was no bias towards recruitment site(s) which may have contributed to this clustering of data. It is unlikely that pre-analytical factors explain the clustering of the data. More likely, analytical factors were the cause (e.g. preparing samples in two batches and emitter tip blockages).



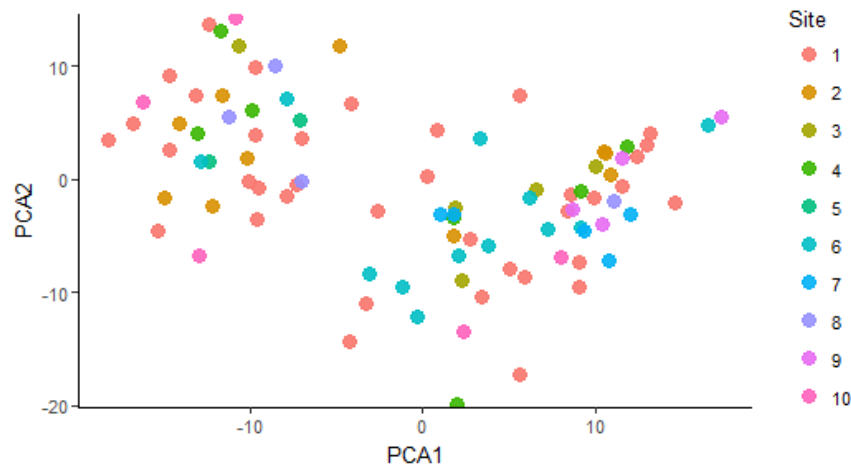


Figure 3-16: Principal component plot for CSH experiment stratified by recruitment site; colour: recruitment site

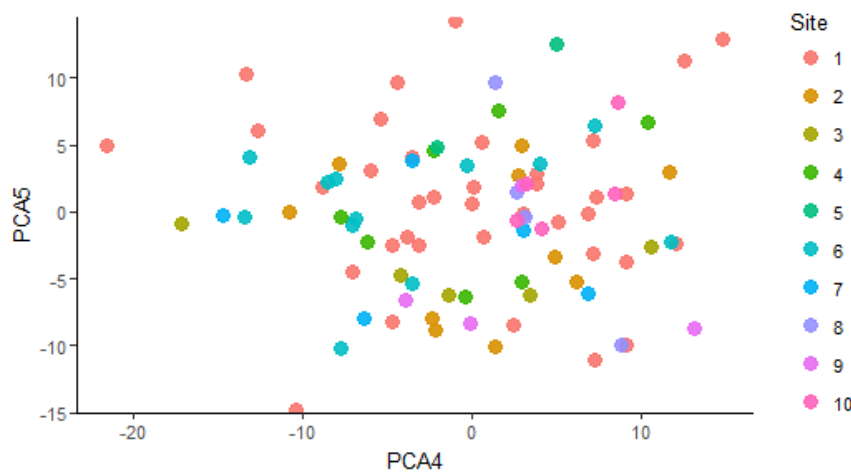


Figure 3-17: Other principal component plot for CSH Experiment stratified by recruitment site; colour: recruitment site

### 3.4.3.4 Gene Ontology Analysis

In total, there were 29 proteins that were upregulated in NoEvents, compared to 30 proteins that were upregulated in Events to be evaluated for biological plausibility, so that an assessment could be made about the likelihood of usefulness as a biomarker.

Gene Ontology and Pathway analyses were performed in Cytoscape and ClueGO to ascertain if there were differentiated pathways between Events vs NoEvents groups. Out of 29 Genes/Proteins uploaded in the NoEvents Cluster, 1 was not functionally annotated in either

Ontology selected. On the other hand, out of 30 Genes/Proteins uploaded in the Events Cluster, 4 were not functionally annotated.

After applying the criteria described earlier (section 3.3.3.7) (for an acceptable balance between pathway specificity and sensitivity) only 22 Genes out of the 59 Genes (37.29%) were associated to representative Terms and Pathways. After 3 iterations of grouping of the terms and pathways, there were 5 main groups of pathways which were relevant, with 50% overlap between the groups. This information was more readable as a table, after removing redundancies, particularly in the largest group (Table 3-4).

Group No.	Genes	Associated terms/functions/pathway	Cluster
Group1	<i>ATRX</i>	DNA replication-independent nucleosome assembly	No Events
	<i>NASP</i>		
Group2	<i>MASP1</i>	Complement and coagulation cascades	No Events
	<i>MASP2</i>		
	<i>SERPINA1</i>		
	<i>F13B</i>		
	<i>CLU</i>		
Group3	<i>PLXNA2</i>	Neuronal axon guidance	Events
	<i>PLXNA4</i>		
Group4	<i>AKT1</i>	Porphyrin	No Events
	<i>APOH</i>	anion transport	
	<i>AMBP</i>	cholesterol reverse transport	
	<i>APOC3</i>	HDL clearance	
	<i>CLU</i>	fatty acid metabolism	
	<i>THBS1</i>	lipid catabolism and transport	
	<i>BLVRB</i>	lipoprotein lipase	
	<i>GPLD1</i>	long-chain fatty acid transport	
	<i>RYR3</i>	triglyceride metabolism	
	<i>CLEC3B</i>	glucose metabolism	
	<i>KAT2A</i>	mitochondrial cytochrome c	
		myelin	
		coagulation	
		fibrinolysis	
		plasminogen	
		haemostasis	
		JNK cascade	
		Heme	
		endothelial proliferation and migration	
		fibroblast	
Group5	<i>APOD</i>	Negative regulation of smooth muscle cell proliferation	Events
	<i>ERCC2</i>		
	<i>ILK</i>		

Table 3-4: Proteins/Genes and their associated terms/functions/pathways and their grouping into Events or NoEvents

The large number of proteins/genes and functions in Group4 highlight how individual genes/proteins have multiple functions and intersect with other pathways. Some themes remain, however, for example: 1) catabolism of lipids/fatty acids/glucose for energy, associations with aerobic (mitochondrial) energy generation, and utilisation of lipids as an energy source. 2) Coagulation/ haemostasis/ platelet activation balanced with anti-

coagulation/ fibrinolysis although fibrinolysis could be associated also with cellular migration, such as in 3) fibroblast/ endothelial proliferation and migration.

#### **3.4.4 Baseline and prognostic variables for patients in the PRIMID-AS study**

The baseline characteristics of patients from the PRIMID-AS study and baseline prognostic characteristics will be described in detail later (sections 4.5.2 and 4.5.3). In brief, the principal variables which were associated with AS severity were a) echocardiographic measures of stenosis severity:- the AV-Vmax, MPG, the AVA (the lower the valve area, the worse the stenosis), b) troponin levels, c) severity of AV calcification and d) level of LV remodelling (measured by LVMI and eccentricity of remodelling).

Characteristics associated with the primary outcome were measures of AS severity, AV calcification, natriuretic peptide levels, haemoglobin levels (lower levels higher risk), renal function (measured by estimated glomerular filtration rate (eGFR) – where lower values translated to higher risk), sex (females associated with high risk) and a positive ETT.

### **3.5 Discussion**

An important observation from the data was that the difference in medians between groups, expressed as a percentage difference in median abundance (arbitrary units), were quite small, with the largest difference of ~60% (outlier), but with most of the percentage difference centred around 8% (Figure 3-18). This highlighted that the differences in proteomic profiles between these two very similar phenotypes (Events vs NoEvents) were small and challenging.

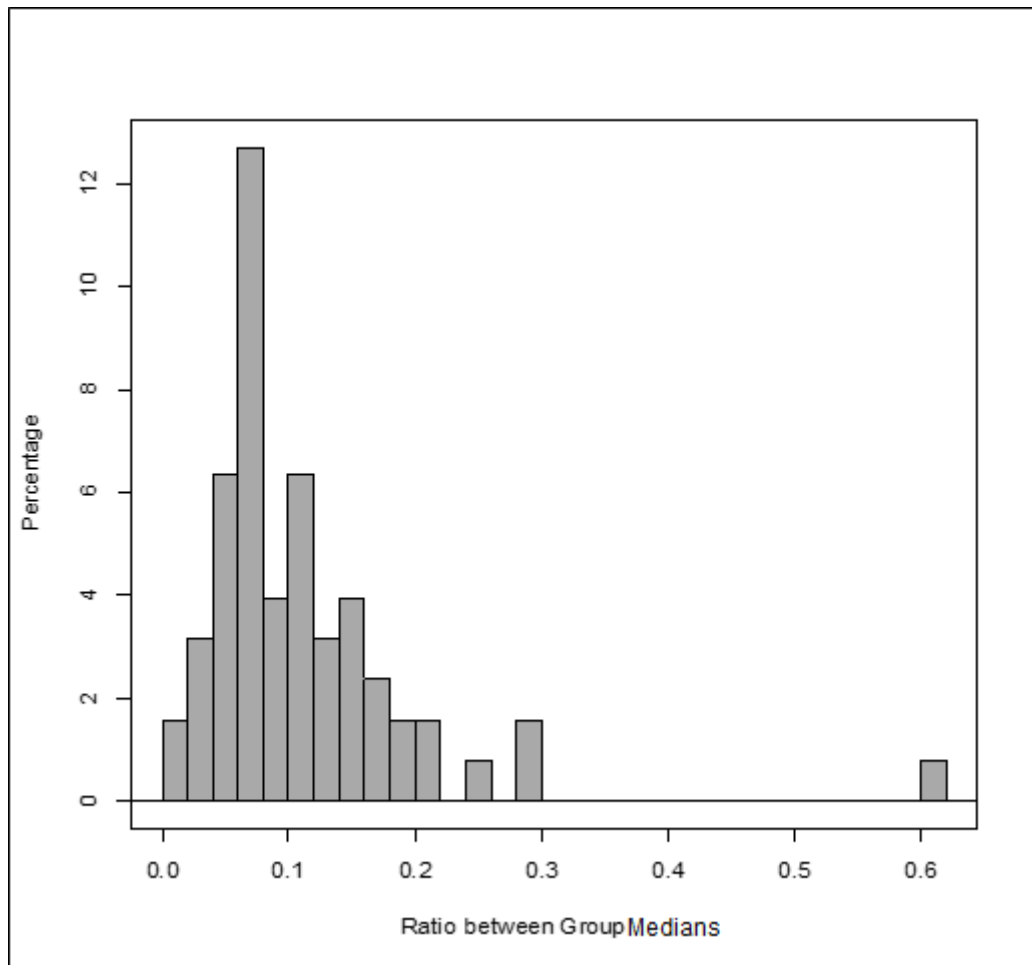


**Figure 3-18: Histogram showing distribution of the magnitude of differences of abundances between significantly different proteins in Events vs NoEvents**

### **3.5.1 Literature Review of the Potential Candidates**

The use of Gene Ontology/Pathway Analysis to understand relationships between genes/proteins in the lists was helpful in so far as it highlighted the potential relationships between the genes/proteins. However the limitations were that not all genes/proteins could be ‘grouped’ and therefore displayed on the network analysis, based on the filtration rules. Furthermore, because ontologies and pathways are constantly being updated, the findings for these bioinformatics tools are only as good as the databases that they draw information on, and it is more likely that a ‘weak link’ is a ‘novel’ marker, compared to the stronger well known links between protein and function.

Out of the 59 genes/proteins, 35 genes/proteins were not assigned a group and therefore not given/annotated with a pathway or ontology, mainly because 2 genes per pathway was required to select a pathway to be considered for network analysis (Table 3-5).

Event	NoEvent
<i>NBEAL1</i>	<i>TENM1</i>
<i>*CLCN3</i>	<i>*THBS2</i>
<i>GP9</i>	<i>COL28A1</i>
<i>BDP1</i>	<i>*SAA4</i>
<i>NUP54</i>	<i>FERIL5</i>
<i>RUFY4</i>	<i>NRAP</i>
<i>RHPN2</i>	<i>HGFAC</i>
<i>GRAMD1C</i>	<i>EFEMP1</i>
<i>DDX26B</i>	<i>PDLIM7</i>
<i>RAD51</i>	<i>FRYL</i>
<i>PHF20L1</i>	<i>AHSG</i>
<i>RP1L1</i>	<i>*AFM</i>
<i>THG1L</i>	<i>ANKRD31</i>
<i>CNTRL</i>	<i>RBM26</i>
<i>GSTO1</i>	<i>PXK</i>
<i>CPVL</i>	
<i>HMHA1</i>	
<i>MYO18A</i>	
<i>SYT14</i>	
<i>*ABCC8</i>	
<i>TTBK2</i>	
<i>DOCK9</i>	

**Table 3-5: List of genes that did not have a pathway associated on ClueGO, \*indicates gene may be related to some of the earlier described pathways from literature review**

The absence of a pathway map does not imply absence of information on these proteins, merely that they did not fulfil the specificity settings or clustering settings used to combine the other results at the time of analysis. The interactome is incomplete, but continues to improve with time, such that future analysis of the same data may improve the pathway and interaction mapping. In the first instance, focus was placed on pathways with larger numbers of members; increased group membership lends confidence to the relevant pathway being dysregulated.

### 3.5.2 Group1: Neuronal axon guidance

#### PLXNA2 & PLXNA4

Both plexin A2 and A4 were more abundant in patients with events compared to no events.

Plexins A2 and A4 are semaphorin receptors which associate with neuropilins. Plexin A4 is

necessary for actin tubule formation, and may play a crucial role in  $\beta$ -fibroblast-growth-factor-induced angiogenic sprouting of blood vessels. It complexes with vascular-endothelial growth-factor-receptor-2 (VEGFR2) and modulates VEGF signalling (Kigel et al., 2011). Both participate in axonal repulsion; necessary to guide nerve growth (Suto et al., 2003, Suto et al., 2005).

Semaphorins are known for their role as repulsive axon guidance factors (Kolodkin et al., 1993) regulators of angiogenesis (Tamagnone, 2012), of immune response (Kumanogoh and Kikutani, 2013) and of tumour progression (Sakurai et al., 2012). All class 3-secreted semaphorins bind to one of two neuropilin receptors (NRP1 & 2) except for Semaphorin-3E (Gu et al., 2005). Neuropilins contain short intracellular domains, limiting signal transduction ability, but they associate with members of the class-A plexin receptor subfamily, to transduce class-3 semaphorin signals. These plexins also function as binding receptors or signal transduction receptors for other membrane-anchored members of the class 4, 5 and 6 semaphorin subfamilies (Gu and Giraudo, 2013), which do not require NRP for receptor binding. Plexins have weak sequence similarity to GTPase-activating proteins and therefore also activate the small GTPase R-Ras (Oinuma et al., 2004).

The relative excess in plexin A2 and A4 in patients with events suggests that there was increased neuronal/axonal remodelling in this group, alluding to a potential mechanism of symptom development. Alternatively, plexin A4's ability to modulate VEGF activity may be relevant in progression from compensated hypertrophy to HF (Kigel et al., 2011, Oka et al., 2014).



### 3.5.3 Group2: Negative Regulation of Smooth Muscle Cell Proliferation

ERCC2, ILK, APOD

ERCC2 refers to excision repair cross-complementation group 2 protein. It is also known as xeroderma pigmentosum D protein (XPD), and is a protein involved in transcription-coupled nucleotide excision repair. Gene defects in this gene have been associated with the cancer-prone xeroderma pigmentosum complementation group D, photosensitive

trichothiodystrophy and Cockayne syndrome. (Entrez Gene ID: 2068, updated 3 Dec 2017).

This protein participates in nucleotide excision repair and is employed in unwinding the DNA double helix after damage is initially recognized. The types of damages repaired are bulky chemical adducts, UV-induced pyrimidine dimers and oxidative damage(Andressoo et al., 2006).

ILK refers to integrin-linked protein kinase which regulates integrin-mediated signal transduction (Hannigan et al., 1996, Delcommenne et al., 1998) and may act as a mediator of integrin signalling. It has been associated with several cellular functions including migration, proliferation and adhesion. In animals, ILKs have been linked to the pinch-parvin complex (IPP complex) which controls muscle development. ILK in mammals may lack catalytic activity (doesn't function as a kinase) but supports scaffolding protein functions in focal adhesions. The IPP complex couples integrins to the actin cytoskeleton (Legate et al., 2006).

It also phosphorylates integrin cytoplasmic domains and downstream signaling proteins, regulating integrin-mediated events. Zebrafish studies suggest that integrin-linked kinase has a stretch-sensing function in cardiomyocytes (Bendig et al., 2006). The ability of ILK to induce bidirectional integrin signalling infers the possibility that ILK regulates the hearts response to mechanical stress. Mutations in *ilk* have been associated with dilated cardiomyopathy (DCM) showing defects in endothelial cells and cardiomyocytes in models

(Knoll et al., 2007). Mice with targeted *Ilk*-deletion in heart muscle developed spontaneous HF with DCM and fibrosis. There was also associated reduction of phosphorylation of focal adhesion kinase (FAK) and protein kinase B (Akt)(White et al., 2006), associated participants in ILK's downstream signalling. Whilst deletion of *Fak*, *Akt1*, *Pinch1* and  $\beta$ 1-integrin all do not result in the same phenotype as *Ilk* deletion; DCM ensues in the former, after biomechanical stress such as aortic constriction.

In a model of cardiac specific *Ilk*-KO, deep sequence analysis of gene expression identified osteopontin as the single most upregulated transcript (47 fold different)(Dai et al., 2014), which has in other studies been implicated in development and progression of HF(Behnes et al., 2013), and shown to play a key role in development in pressure-overload HF, with potential therapeutic implications(Li et al., 2017). Furthermore, ILK was found to be elevated in human cardiac hypertrophy (Lu et al., 2006) and also induced cardiac hypertrophy in transgenic mice.

In AS patients, ILK was higher in abundance in patients with events. This could represent increased compensatory increase in integrin-crosslinking, reflecting excessive biomechanical stress, as a survival mechanism to prevent lethal HF. Downstream signalling may then increase expression of atrial natriuretic factor and VEGF, augmenting cardiac force by increasing the heart's calcium transients (Bendig et al., 2006).

### **3.5.3.1 Apolipoprotein D (APOD)**

APOD is a 29kDa protein belonging to the lipocalin superfamily of glycoproteins (Rassart et al., 2000), predominantly associated with high density lipoprotein (HDL), which has been implicated in governing stress response (Pascua-Maestro et al., 2017), lipid metabolism (Perdomo et al., 2010) and aging (Muffat and Walker, 2010).

In adult blood vessels, APOD is expressed at high levels in atherosclerotic lesions (Sarjeant et al., 2003), inhibiting platelet derived growth factor–BB (PDGF-BB)-induced smooth muscle cell proliferation through inhibition of extracellular signal-regulated kinase 1/2 (ERK1/2). Both PDGF-BB and APOD were shown to work together to mediate vascular smooth muscle cell (VSMC) migration (Leung et al., 2004). When endothelial cells were co-cultured with VSMC's and fibroblasts, APOD expression decreased in the VSMCs and fibroblasts, causing an increase in cell adhesion and focal contacts, without affecting stress fiber formation (Pajaniappan et al., 2011) involving NOTCH3 signalling. Taken together, APOD inhibits VSMC proliferation, and endothelial cells modify the signalling, resulting in improved binding of VSMCs to the vascular basement membrane.

APOD expression is thought to be beneficial for cell survival in neuronal cells (Muffat and Walker, 2010, Ganfornina et al., 2008), and has been found to extend lifespan and improve stress resistance in *Drosophila* (Muffat et al., 2008). The mechanism for this may be through preservation of lysosomal functional integrity (Pascua-Maestro et al., 2017). In addition, APOD has been reported to be protective in a mouse model of ischaemia/reperfusion with coronary ligation, with reduced infarct size. In contrast a deficiency of APOD was associated with increased infarct size (Tsukamoto et al., 2013), a finding that the authors concluded was likely to be due to its anti-oxidant properties.

*APOD* variants have been associated with the incidence of obesity and hyperinsulinemia and type II diabetes mellitus, with mutations linked to elevated plasma triglycerides and reduced HDL-cholesterol levels (Vijayaraghavan et al., 1994, Baker et al., 1994, Desai et al., 2002). In mice with altered lipid metabolism, APOD increased triglyceride catabolism through lipoprotein lipase, leading to reduced plasma triglyceride levels (Perdomo et al., 2010).

Literature is limited on APOD in HF, but protein levels and mRNA expression levels of *APOD* have been found elevated in patients with HF (Wei et al., 2008). Its association with HF makes APOD an attractive biomarker to be studied further in AS, because the myocardial response to pressure overload is thought to be the primary reason for the variability in rate of progression from asymptomatic to symptomatic AS, as well as the variability in prognosis, as reviewed in Chapter 1. Metabolic perturbations in myocardial energetics have been well described, highlighted by depressed fatty-acid oxidation (FAO) and increased reliance on glucose utilization as hallmarks of a failing myocardium (Wende et al., 2017). Indeed, an increase in APOD which may increase triglyceride catabolism through lipoprotein lipase activity, would increase the substrate availability for FAO, but may not remedy the situation due to the inherent repressed capacity for utilising increased fatty acids.

### **3.5.4 Group3: Complement and coagulation cascade/ Innate Immune response**

#### **3.5.4.1 Mannan-binding-lectin serine proteases 1 & 2 (MASP 1 & 2)**

The complement system is a complementary immune pathway best known for its functions in identifying and assisting the immune system in the event of a bacterial or foreign organism invasion. It comprises three pathways, the classical, the alternative and the lectin pathway.

The classical pathway involves an antigen-antibody reaction that initiates a cascade of complement activation, leading to formation of a membrane attack complex (MAC).

Byproducts of this pathway's activation are C5a, C3a and C2b.

The alternative pathway is activated by bacterial lipopolysaccharide, cobra venom factor and yeast cell walls. Circulating C3 undergoes spontaneous hydrolysis to form C3b in the presence of these factors. C3b activates factor B, exposing its active site to be activated/cleaved by factor D, producing FBa and FBb. FBb binds C3b forming C3bBb

which is a C3 convertase. Subsequent effects are similar to the classical pathway with the final common pathway.

The lectin pathway is activated by recognition of mannose and glucose binding sites on foreign-bodies like *Neisseria* species. These sites are recognized by a mannan-binding lectin (MBL) protein, which are associated with mannan-binding-lectin serine proteases (MASP). Specifically, upon binding to the receptors of the pattern recognition motifs of MBL, MASP1 auto-activates, allowing activation of C2 to C2a and 2b. MASP1's auto activation activates MASP2, a requisite process for further downstream activation of the lectin system (Heja et al., 2012). MASP2 cleaves C4 to become C4a and C4b, as well as co-activating C2. Binding of C2a and 4b forms a C2a4b complex which is a C3 convertase, and further downstream effects share the final common pathway as the alternative and classical pathways. In addition to activating MASP2, MASP1 also drives alternative pathway activation by converting factor D and factor B to their active forms, facilitating formation for C3 convertase (Takahashi et al., 2010).

These three pathways allow amplification of the immune response to foreign invasion. Neither the lectin nor alternative pathways require adaptive immune responses, because their pattern recognition sites are genome-encoded and are therefore more 'innate' than the classical pathway. Products of complement system activation are the MAC, which cause cell lysis in the area that the complement system is activated. Additionally, C3b activate neutrophils, macrophages and monocytes to induce phagocytosis. C5a facilitates chemotaxis and C3a, 4a and 5a all activate mast cells resulting in histamine and serotonin release, which potentiate natural defence mechanisms. C2b also increases vascular permeability.

In addition to being important in infection, the lectin-pathway is also activated in ischaemia-reperfusion injury. MASP2 deficient mice had significantly reduced neurological deficits and

histopathological damage after transient ischaemia and reperfusion, compared to wild-type mice, but MASP1 deficient mice were not protected. Factor B-deficient mice were also protected against neurological damage in this context (Orsini et al., 2016). MASP2 deficient mice also demonstrated reduced C3 deposition on at-risk tissue, reflecting reduced complement system activation.

In the PRIMID-AS cohort, MASPs 1 and 2 were lower in patients with events. This could simply reflect increased peripheral consumption, because they need to localise to their site of action.

#### **3.5.4.2 Factor 13B (F13B)**

Factor 13 is a transglutaminase tetramer composed of two active/catalytic subunits, factor F13A, and two inactive/inhibitory subunits, F13B. The 'a' subunit is synthesized in bone marrow, but the 'b' subunit is synthesized in the liver and therefore, the tetramer formation must occur in the circulation where they circulate complexed with fibrinogen. The 'b' subunit is a glycoprotein consisting of 10 sushi domains. The complexing of the 'b' and 'a' subunits is necessary to prevent the 'a' unit from being slowly spontaneously activated (Mary et al., 1988). The 'b' subunit protects the 'a' subunit from proteolysis and prolongs its half-life. Factor 13, and approximately 50% of the F13B in circulation was unbound and available for binding (Yorifuji et al., 1988). Although it was unclear why the 'b' subunit was in excess in the circulation, it was possible that the excess 'b' was necessary to reduce the risk of any 'a' subunits spontaneously activating. On the other hand, 99% of circulating factor 13A is complexed as a tetramer with only 1% present as homodimers.

Single nucleotide polymorphisms associated with lower F13B levels increased the risk of embolic strokes (Hanscombe et al., 2015). Conversely, some other *F13B* polymorphisms

(also associated with reduced factor 13 levels) were associated with reduced risk of coronary artery disease and history of myocardial infarction (Mezei et al., 2015).

Along with other coagulation proteins and their inhibitors, factor 13 is increased in AS valves predominantly in macrophages and myofibroblasts around calcified areas. Associated impairment of fibrinolysis was associated with increased severity of the valve disease (Natorska and Undas, 2015). Factor 13 predominantly co-localised with alternative-pathway activated macrophages, and plasma factor 13 activity was found to be positively correlated to valvular fibrin production, macrophagic infiltration of the AV and valve gradient (Kapusta et al., 2012). In disseminated intravascular coagulation, F13B levels were lower by ~37% relative to normal pooled controls (Sugimura et al., 1996). This difference was similar, but less profound than the lower levels seen with F13A levels, which was ~44% lower.

In PRIMID-AS patients with no events had higher F13B levels. One possible explanation is that continuous activation of the coagulation system (peripheral consumption) in more advanced AS leads to lowered measurable levels of F13B, although the magnitude of change is probably much smaller if compared to disseminated intravascular coagulation. Persistent coagulation may lead to higher subclinical thromboembolic events and account for the presyncopal episodes that AS patients describe.

MASP1 and MASP2 also activate the coagulation system. Ex-vivo, MASP1 activates fibrinogen to fibrin by converting prothrombin to thrombin, activating factor 13 to factor 13A and thrombin activatable fibrinolysis inhibitor (TAFI) leading to cross-linked fibrin (more stable) (Hess et al., 2012). Additionally, MASP2 has also been shown to participate in the coagulation cascade in vitro. Both MASP1 and 2 are thought to be activated by platelets and fibrin formation (Kozarcanin et al., 2016), and both lead to further fibrin formation. Likewise, both MASP1 and MASP2 are lower in patients with events.

One might therefore hypothesize that in patients with events, with lower MASP1, MASP2 and F13B, there was excessive coagulation and complement system activation with consumption in circulating factors (Figure 3-19).



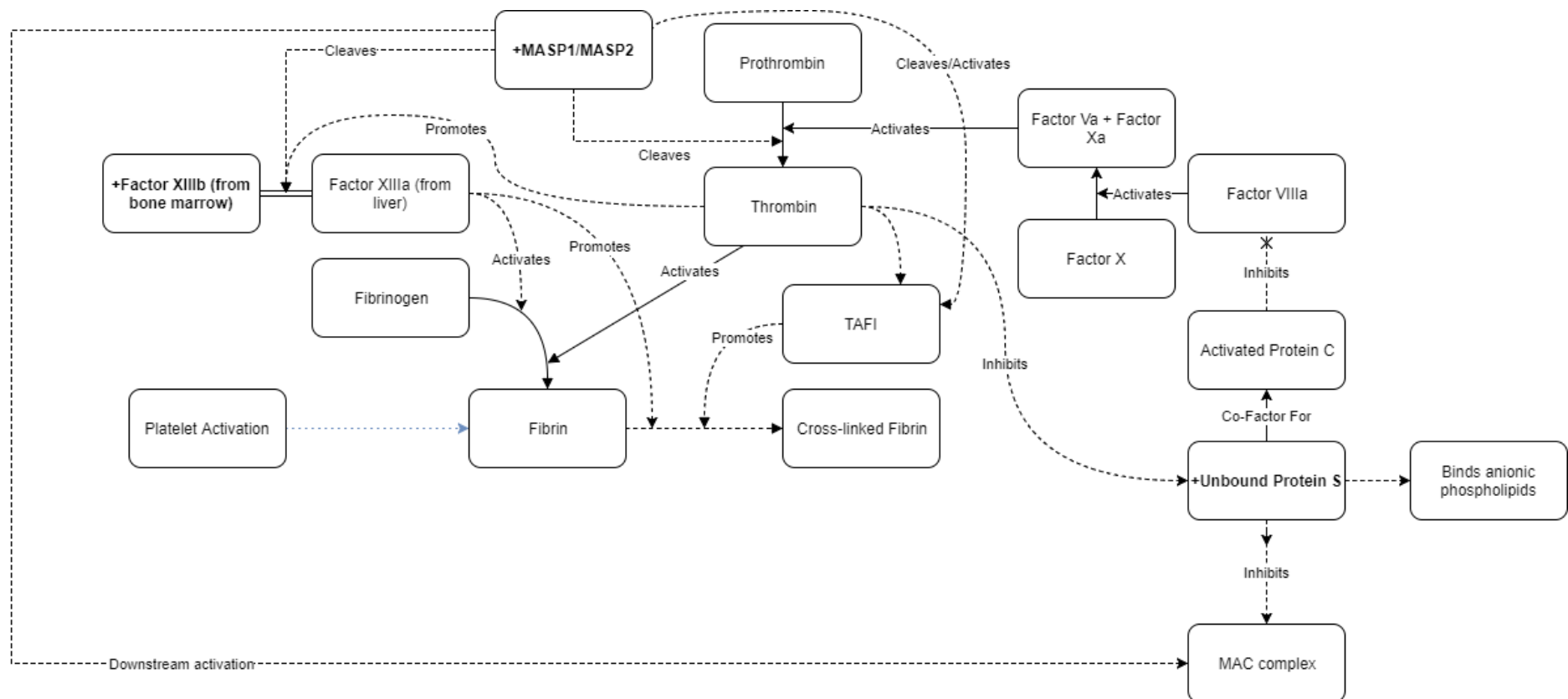


**Figure 3-19: Hypothetical interaction between MASPs, Factor 13 and protein S; TAFI: thrombin activatable fibrinolysis inhibitor; MAC: membrane attack complex**

#### **3.5.4.3 Tetranectin (gene: *CLEC3B*, protein: TETN)**

Tetranectin is a C-type lectin plasma protein occurring in the mammalian musculoskeletal system (Xu et al., 2001), a good marker for muscle fibre damage resulting from eccentric exercise (Kalhovde *et al*, unpublished data but referenced in (Wernbom et al., 2012)). Eccentric exercise resulted in increased tetranectin staining of muscle fibres involved in the exercise, which the authors speculated was due to increased sarcolemmal permeability to tetranectin. Its presence in muscle damage was not coincidental; it appeared to participate in wound repair. Mice lacking tetranectin (*Clec3b* KO mice) demonstrated delayed wound healing, taking 50% longer to demonstrate complete re-epithelialization (Iba et al., 2009) and demonstrating delayed fracture healing in bone (Iba et al., 2013). Its role in wound repair is unclear, although its ability to activate plasminogen by a tissue type plasminogen activator is thought to be important. Tetranectin is closely associated with myogenesis during embryonic development, and skeletal muscle regeneration. Although developing muscles during gestation demonstrate intense tetranectin staining at myotendinous and myofascial junctions, this staining is absent in stable adult muscle. However, after exposure to an insult or toxic damage, myoblasts, myotubes and the stumps of damaged myofibers exhibited intense tetranectin staining (Wewer et al., 1998). In stable coronary artery disease, serum tetranectin was found to be significantly lower, compared to healthy controls (Chen et al., 2015). In colorectal cancer, higher tetranectin levels were found to be associated with better prognosis (Hogdall et al., 2002). Interestingly, urokinase plasminogen activator (uPA) was also linked, with higher levels of uPA associated with poorer prognosis. Recently, soluble urokinase plasminogen activator receptor (suPAR) was associated with ischaemic cardiovascular events in asymptomatic AS, although the association was less strong for AV-related events (Hodges et al., 2016).

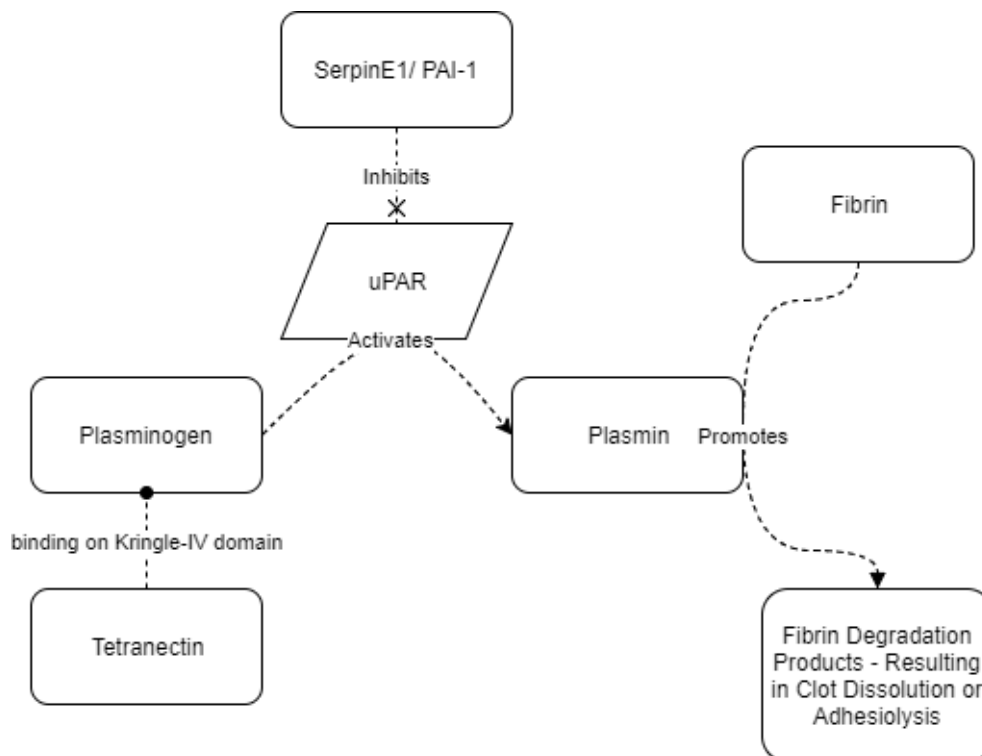


**Figure 3-20: Schematic showing relationship between tetranectin, plasminogen, fibrin and their modulators: uPAR: urokinase plasminogen activator receptor, SerpinE1/PAI-1: plasminogen activator inhibitor-1**

Elevated tetranectin levels in AS patients with events may reflect the remodelling process. If suPAR is associated with AV-related events in AS then the net effect of increased suPAR would be increased fibrinolysis/remodelling. This would be congruent with the increased tetranectin levels we have seen in the PRIMID-AS cohort with events.

#### 3.5.4.4 Alpha-1-Antitrypsin (gene - *SERPINA1*, protein -A1AT)

Alpha-1-antitrypsin is a ubiquitous enzyme present in high abundance in plasma. Its link to disease is best seen in deficient individuals, as a cause for accelerated lung disease (Lieberman, 1976), especially in the presence of smoking. These individuals also are at risk of early hepatic cirrhosis (Teckman and Lindblad, 2006). A1AT is well known as an enzyme that neutralises the effects of proteolytic enzymes and is seen as a regulator of excessive and potentially harmful proteolytic activity (Lieberman, 1976). Specifically, in A1AT deficiency, individuals have increased neutrophil elastase activity participating in alveolar remodelling in the presence of toxic stimuli. Unchecked in deficient individuals, this is associated with early

lung fibrosis and bronchiectasis with destruction of lung architecture. A1AT is also an acute phase reactant with a four-fold increase in plasma abundances in the presence of sepsis or myocardial infarction probably because high levels are required to neutralise proteolytic enzymes (by covalent binding) in healing and remodelling (de Serres and Blanco, 2014).

Its links to heart disease are less obvious. Individuals with severe A1AT-deficiency had a lower risk of death from ischaemic heart disease, but with a higher risk of death from respiratory disease, hepatic disease, diverticulitis and pulmonary embolism, compared to the age and sex matched Swedish population (Tanash et al., 2016).

Mice subjected to short-term aortocaval shunt-induced *volume* overload developed eccentric hypertrophy with preserved ejection fraction. Proteomic studies on their ventricular tissues revealed a lower levels of A1AT, which authors suggested was associated with higher elastin degradation and contributing to early dilatation (Mohamed et al., 2016). There are no previous studies to date investigating A1AT in a pressure overload model.

A1AT was found to be upregulated in stenotic AVs, a hot bed of inflammatory activity, when compared to controls, reiterating its ubiquity in inflammation (Martin-Rojas et al., 2012).

In PRIMID-AS, patients who had events had higher circulating levels of A1AT. This may indicate increased inflammatory activity in these patients. Alternatively, patients without events may have had lower circulating levels of A1AT reflecting higher elastin degradation earlier in the adaptive remodelling process.

#### **3.5.4.5 Apolipoprotein L1 (APOL1)**

Apolipoprotein L1 was not significantly different between Events and NoEvents in PRIMID-AS ( $p=0.06$ , only 4% difference). However, the trend was to being higher in those without events. Similar to MASPs 1&2, B2GP1, Clusterin and Protein S, it participates in innate

immunity. It forms pores on lysosomal membranes of trypanosomes causing influx of chloride, swelling of lysosome and lysis of the trypanosome (Perez-Morga et al., 2005).

There is an association with kidney disease if there is a variant form of APOL1, but with resistance against trypanosomes (Cuypers et al., 2016). This variant form is associated with increased risk of focal segmental glomerular sclerosis (FSGS) and hypertensive end-stage kidney disease. There is otherwise little known about its intracellular function. Recombinant *APOL1* conferred chloride and potassium permeability (Bruno et al., 2017). APOL1 was considered a potential target due to similarities in function as MASPs, clusterin and protein S.

### **3.5.5 Group4a: Lipid Metabolism and Transport + Glucose Metabolism**

#### **3.5.5.1 APOC3/APOC2/PHLD axis**

The myocardium derives between 60-70% of its energy from oxidation of long-chain free fatty acids, and the balance from glycolysis or glycogenolysis (van der Vusse et al., 1992, Bing et al., 1954). Although more energy dense than glucose, fatty acid oxidation (FAO) requires more oxygen, and is therefore less flexible. Increased energy requirements when oxygen supply is limited results in preferential glucose metabolism. This is seen in cardiac hypertrophy, with the shift being proportional to the extent of hypertrophy (Neglia et al., 2007, Otsuka et al., 2002, de las Fuentes et al., 2003). Circulating triglycerides, transported by VLDLs are converted to free fatty acids (FFAs) by lipoprotein lipase (LPL) bound to cardiomyocytes and endothelial cells. In the presence of excessive FFA and glucose, luminal/endothelial LPLs are auto-inhibited to avoid lipid overload.

In hypertrophic hearts of patients undergoing AVR (Heather et al., 2011), fatty acid translocase (FAT) or CD36, the predominant fatty acid transporter across the cell membrane, was found to inversely correlate with levels of glucose transporters, GLUT1 and GLUT4. FAT was found to be lower in hypertrophic cardiac cells (from biopsies), compared to

control, and with associated decreases in the plasma levels of fatty acid binding proteins. Conversely, GLUT4 was associated with increasing LV mass. Increasing fatty acid utilisation is however, beneficial at early stages of pressure overload (Sung et al., 2017).

APOC3 is a well-known inhibitor of LPL, resulting in increased plasma triglyceride levels. APOC2 is a co-factor of LPL, which facilitates its activity (Jong et al., 1999). APOC3 and APOC2 are both produced predominantly in the liver and bound to both LDLs and HDLs in the circulation, where they can act on their receptors. Their primary receptors, LPLs, are found in intestinal cells and on peripheral sites, tasked with the transport of lipids from the intestinal lumen, into the circulation, then into peripheral tissues for storage (adipose tissue) or catabolism (e.g. cardiomyocytes). *Cd36*-null mice were found to have increased APOC3 levels, a finding that correlated with plasma levels of triacylglycerol (Drover et al., 2005). APOC2 was also affected similarly, although the difference was not significant (between WT and *Cd36*-null mice).

Increasing mitochondrial FAO was associated with up-regulation of the LPL and VLDL receptor, but with concomitant down-regulation of APOC3 (Lindquist et al., 2017). Authors concluded that the resultant observed plasma triglyceride clearance seen was likely to be due to the associated APOC3 downregulation.

One could extrapolate that the lower APOC3 seen in patients in AS with events reflected increased mitochondrial FAO. There would be an associated increase in LPL activity and lower plasma triglyceride levels.

APOC3-dependent inhibition of LPL is potentiated if LPL is bound to glycosylphosphatidylinositol-anchored high density lipoprotein-binding protein (GPIHBP1), which is the predominant form of LPL (Larsson et al., 2017). This anchor allows APOC3 to act mainly on surfaces on which LPL is bound, whilst being less active on free-LPL. This

anchor can be hydrolysed by glycosylphosphatidylinositol-specific phospholipase D1 (gene: *GPLD1*, protein: PHLD), releasing LPL from the cell surfaces. More recently GPIHBP1 has been found to be requisite for trans-endothelial cell LPL transport, to replace LPL on endothelial surfaces that may have been lost into the circulation (Fong et al., 2016). Whether the reduction in PHLD in patients with events reflects a reduction in LPL release into the circulation, or a reduction in GPI-anchored LPL being marginalised into the plasma endothelium, is unclear.

APOC3, APOC2 and *GPLD1* likely reflect maladaptive energy states in pressure overload (Figure 3-21). APOD is also upregulated in those with events, and is inversely correlated with APOC3 and APOC2. This is due to its opposing effect on LPL. Overall, lower APOC3 and APOC2 levels but higher APOD levels in patients with events probably reflect increased mitochondrial FAO to preserve myocardial energetics (Abdurrachim et al., 2015).

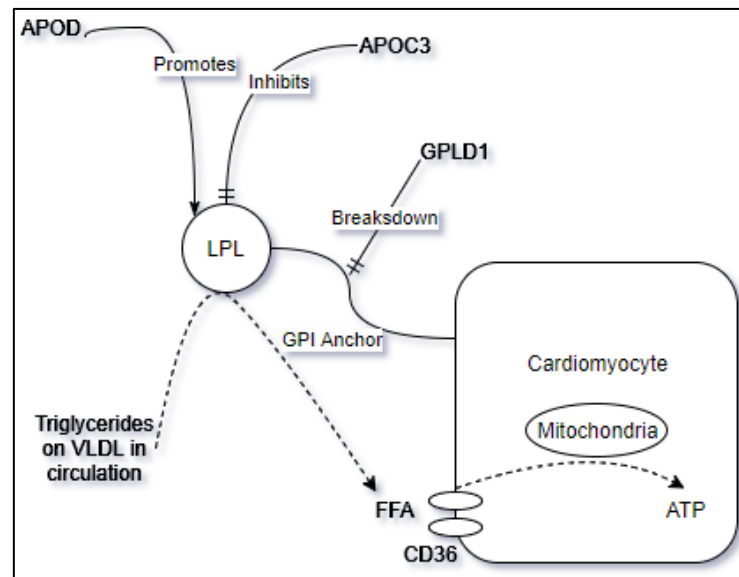


Figure 3-21: Hypothetical schematic showing probable relationship between APOC3, *GPLD1*, APOD, Lipoprotein Lipase and fatty acid oxidation in the cardiomyocyte

### 3.5.5.2 Histone acetyltransferase (KAT2A)

Histone acetyltransferases (HATs) acetylate conserved lysine residues on histone proteins by transferring an acetyl group from acetyl-CoA to form e-N-acetyl-lysine (Roth et al., 2001). In

this way, genes bound to the histone proteins can be turned on or off (i.e. it is a transcription regulator). Generally, histone acetylation increases gene expression (as opposed to down-regulation). In addition, HATs also acetylate non-histone proteins, such as nuclear receptors and other transcription factors to facilitate gene expression.

HAT's subcellular localization classifies them. Type-A HATs are located in the nucleus and are involved in the regulation of gene expression through acetylation of nucleosomal histones in the context of chromatin. KAT2A is also known as GCN5. These HATs require co-activators to function to increase transcription. Their increased levels in PRIMD-AS patients with events suggest that there was increased remodelling/turnover/protein expression in these patients, compared to those without events.

### **3.5.5.3 RAC-alpha serine/threonine-protein kinase (AKT1)**

AKT1 is one of three highly homologous serine/threonine kinases known collectively as protein kinase B or Akt (PKB/Akt) (Nicholson and Anderson, 2002). The two other members are AKT2 and AKT3 respectively. PKB/Akt is activated in cells exposed to multiple stimuli including hormones, growth factors and extracellular matrix components.

The activation occurs downstream of phosphoinositide 3-kinase, then results in the translocation of PKB/Akt to the plasma membrane, where it is phosphorylated and activated by other kinases. PKB/Akt regulates many of the proteins involved in cellular survival and senescence. AKT1 can inhibit apoptosis by phosphorylating and inactivating the apoptotic machinery. AKT1 signalling is necessary for normal growth, with AKT1- knockout mice exhibiting 20% lower body and organ sizes compared to their wild-type littermates throughout their lifespan (Cho et al., 2001).

Although the adult heart largely does not regenerate, minute amounts of pluripotent cardiac stem cells remain, allowing a low-level of cellular turnover. Whilst physiological ventricular



hypertrophy occurs in response to exercise, pathological hypertrophy occurs due to pressure overload. In *Akt1*-knockout mice, AKT1 was demonstrated to be necessary for physiological cardiac hypertrophy, and regulating pathological cardiac hypertrophy (DeBosch et al., 2006). Compared to wild-type mice, these *Akt1*-KO mice lacked a cardiac hypertrophic response both to exercise and insulin-like growth factor stimulation. However, *Akt1*-KO mice demonstrated an exaggerated hypertrophic response to endothelin-1 and transverse aortic constriction, which corrected when wild-type *Akt1* was introduced by adenoviral transduction. AKT1 levels may therefore reflect the myocardium's counter-regulatory hypertrophic response to pressure overload.

In PRIMID-AS, AKT1 was found to be higher in patients without events which may reflect the protective effect of AKT1 in these individuals. AKT1 could be higher initially, in the early stages of pressure-overload, by participating in hypertrophy induction to compensate for the increased myocardial wall stress. Chronic pressure overload may then lead to AKT1 levels falling as cardiomyocytes die and replacement fibrosis sets in.

#### **3.5.5.4 Thrombospondin 1 and 2 (gene: THBS1, THBS2; protein: TSP1, TSP2)**

The extracellular matrix (ECM) is a complex meshwork of structural proteins (e.g. collagen 1 & 3), proteoglycans, glucosaminoglycans and a basement membrane. This meshwork maintains tissue structure and strength. Matricellular proteins are non-structural proteins present in low abundances within normal ECM, but are expressed at increased levels following tissue injury or when undergoing pathological change.

Thrombospondin 1 (TSP1) was first discovered in ECM. It was also demonstrated to be a major component of  $\alpha$ -granules in platelets, released upon platelet activation (Baenziger et al., 1971). TSP1 is calcium-binding multifunctional protein which regulates cellular adhesion

and migration, cellular proliferation, apoptosis and cytoskeletal organisation (Chen et al., 2000, Jiménez et al., 2000).

TSP1 has multiple domains which can interact with an array of specific cellular receptors (Figure 3-22) (Krishna and Golledge, 2013). As such this may result in conflicting and opposing effects of TSP1 in various cells types. TSP1 is a ligand for CD36, proteoglycans, several integrins and CD47/integrin-associated protein. The N-terminal has a heparin-binding domain which binds heparin sulphate proteoglycans, whilst in the thrombospondin-sequence-repeat-1 (TSR-1) domain, which contains the sequence CSVTCG binds CD36. The RGD sequence in TSR-3 binds a variety of integrin-B receptors, and the C-terminal cell-binding domain binds CD47. TSP-1 also interacts with fibronectin, fibrinogen and other components of the fibrinolytic system such as plasminogen, urokinase and its inhibitor plasminogen activator inhibitor (PAI-1) as well as to cathepsin G and elastase.

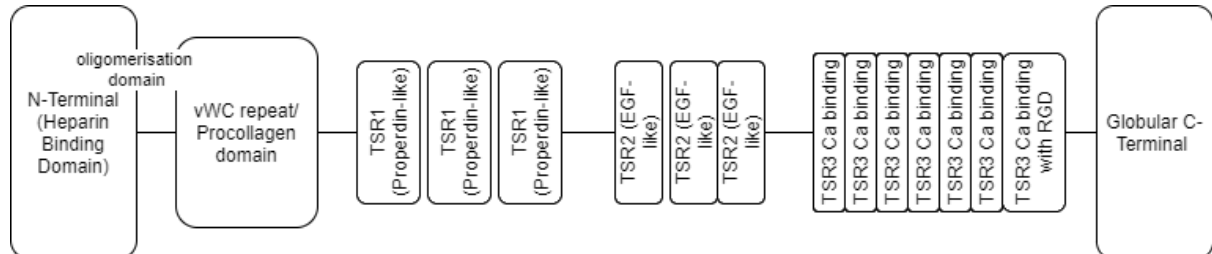


**Figure 3-22: Schematic indicating large number of binding sites for Thrombospondin 1 giving it a multitude of potential functions (source: (Krishna and Golledge, 2013))**

It is not surprising that many downstream effects have been attributed to TSP1 signalling, given the array of TSP1's targets. Some effects are somewhat contradictory with each other (e.g. parts of TSP1 promote angiogenesis, whilst others inhibit it).

TSP1's TSR1 region is its signature section, which interacts with CD36 on cell membranes. As well as being a fatty acid translocase as described before, this receptor is also a scavenger molecule, whose interaction with TSP1 is responsible for most of the anti-angiogenic and inflammatory effects (Dawson et al., 1997, Yamauchi et al., 2002). The C-terminal G domain which is involved in platelet aggregation, also enables adhesion of endothelial cells through

the CD36 receptor (Bonnefoy et al., 2008). Interaction with CD47, a component of the  $\beta$ 3-integrin complex expressed on T-cells and polymorphs, gives TSP1 a role in immune tolerance (Grimbert et al., 2006). Its binding to CD47 inhibits IL-2 release, which may help regulate the immune system in infection (Avicé et al., 2000).

In addition, part of the TSP1 TSR1 region activates latent transforming growth factor-beta (TGF- $\beta$ ). Binding of TSP1 to the latency-associated peptide which is initially bound to mature TGF- $\beta$  as a small latency complex releases the TGF- $\beta$ , allowing it in turn to activate its own ligands which then has downstream effects (Jones et al., 2009). In the vasculature, it is protective, being anti-atherogenic and a plaque-stabilizing factor (Moura et al., 2007). In pressure-overloaded hearts, it promotes matrix preservation and prevents ventricular dilatation, by regulating fibroblast phenotype (Xia et al., 2011). TSP1 is markedly upregulated in the interstitial space following transverse aortic constriction. In *Thbs1*-disrupted mice, the pressure-overloaded heart demonstrated excessive infiltration of dysfunctional fibroblasts (ie. did not deposit collagen) and failed to differentiate appropriately into myofibroblasts. In addition, there was associated defective TGF- $\beta$ /SMAD2 signalling, and increased MMP 3 and 9 activity. *Thbs1* disrupted mice had more extensive sarcomeric loss and sarcolemmal disruption, earlier hypertrophy and more severe late dilatation in response to pressure-overload. TSP1 deposition is therefore integral to the reparative process that ensues in pressure overload, although not all its effects on fibroblasts and fibroblast protein expression is TGF- $\beta$  dependent (Sweetwyne et al., 2010, Motegi et al., 2008).

Increased TSP2 production is not only highly expressed in hypertensive hearts (Kimura et al., 2016) but also is a risk-factor for developing HF (Schroen et al., 2004). In renin-overexpressing rats, *Thbs2* was only overexpressed (in cardiac biopsy specimens) in rats that went on to develop HF. In humans, TSP2 was increased in human hypertrophied hearts with

decreased ejection fraction. *Thbs2*-KO rats were more likely to have fatal cardiac rupture with angiotensin II, with HF in the surviving mice but not the wild type. Angiotensin II also increased MMP2 and MMP9 activity more in these mice compared to wild-type mice, alluding to the protective role of TSP2 in hypertrophied hearts.

Both TSP1 and 2 are anti-inflammatory (Kirk and Cingolani, 2016). TSP1's effect is direct via the anti-inflammatory effect of TGF- $\beta$ . In wound healing, TSP2 seems to peak later in repair process compared to TSP1 (Agah et al., 2002), so must modulate different aspects of inflammatory response, but both *Thbs1* and *Thbs2*-knockout mice took twice as long to reduce oxazolone-induced inflammation (Lamy et al., 2007).

In PRIMID-AS, TSP1 and TSP2 were higher in patients with events which is in keeping with their protective role in pressure overload.

### **3.5.5.5 Beta-2-glycoprotein 1 (APOH)**

Beta-2-glycoprotein, best known in the literature as the antigen to which anti-cardiolipin antibodies form in anti-phospholipid syndrome (APS), does not have any other role in heart disease to date.

Its physiological function has not been convincingly elucidated. APOH is both evolutionarily conserved and abundant in human circulation (de Groot and Meijers, 2011). It scavenges lipopolysaccharide (LPS), suggesting that it is important in host defence against bacteria. It also has an affinity to anionic phospholipids, which is a 1000-fold stronger when it has formed a homodimer (Willems et al., 1996). It is also involved in the clearance of microparticles, as well as removing protein and cellular waste. In rats, there is evidence that APOH facilitates triglyceride metabolism (Wurm et al., 1982) (potentially through potentiation of LPL activity (Nakaya et al., 1980)). In addition, APOH binds to oxidized LDL

(oxLDL), inhibiting the uptake of oxLDL into macrophages (Hasunuma et al., 1997), a step implicated in atherogenesis. Lipoprotein(a), another well-known atherogenic factor, has also been shown to complex with APOH (Kochl et al., 1997), and complexed APOH-LP(a) was associated with increased severity and outcome in ischaemic stroke, as well as coronary artery disease (Wang et al., 2012). In these circumstances, APOH binding to oxLDL or LP(a) was likely to mitigate oxLDL's harmful effects, instead of potentiating it, because the presence of APOH actually downregulated CD36, IL1b and IL-6, in macrophages, having an anti-atherogenic effect (Wang et al., 2016).

Another physiological function of APOH is likely to be in innate immunity. In response to injury, exposure of neoepitopes occur. This is seen in experimental ischaemia-reperfusion injury (Zhang et al., 2016b). Neoepitope exposure induced a response triggered by natural antibodies (natural IgM) recognizing the foreign markers and activating the complement system. Phosphatidylserine is also exposed during endothelial injury. APOH undergoes conformational change when activated. Its domain 5 binds exposed phosphatidyl serine, leaving its domain 1 free to bind antibodies. A physiological example of this process is LPS from *Streptococcus pyogenes* binding to APOH's domain V (Agar et al., 2011). Domain 1 then presents an antibody-binding region to facilitate phagocytosis of the whole structure. Recombinant domain 5 was able to prevent ischaemia-reperfusion injury, by preventing endogenous APOH from binding to neoepitopes and mediating IgM activity.

In PRIMID-AS, APOH is lower in patients with events, which may reflect excess tissue injury in these patients. It also infers that *lower* circulating APOH levels reflect *increased* inflammation/immune activation.

### 3.5.5.6 Clusterin (CLU)

Clusterin localises to different subcellular compartments. There are 3 isoforms of significance. There is a nuclear isoform, cytosolic isoform and a secreted isoform (Koltai, 2014). Whilst the nuclear isoform promotes apoptosis, secreted and cytosolic isoforms (produced during cellular stress) are anti-apoptotic (Koltai, 2014, Sansanwal et al., 2015).

Clusterin chaperones golgi proteins, facilitating the folding of secreted proteins in an ATP-independent way (Lin et al., 2014). It is ubiquitous, and participates in several processes including lipid transport, membrane recycling, cell adhesion, apoptosis and complement-mediated cell lysis. Overproduction of the secretory clusterin protects cells from cellular stress-induced apoptosis e.g. chemotherapy, radiotherapy and androgen/estrogen depletion (Koltai, 2014).

Cardiac cells treated with clusterin reversed the increased apoptotic signalling seen when challenged with hydrogen peroxide (Jun et al., 2011), a protection that appears to be mediated through the triggering of AKT (see section 3.5.5.3) and glycogen-synthase kinase 3-beta (GSK3b). AKT phosphorylates GSK3b inhibiting its kinase activity, preventing the opening of mitochondrial permeability transition pore (mPTP) (Juhaszova et al., 2009). This prevents the release of cytochrome-C from mitochondria, blocking a cascade of events leading to apoptosis. However, GSK-3b can be phosphorylated on its tyrosine residue by an incompletely known mechanism, activating its kinase activity. This form of GSK-3b then activates BAX protein (proapoptotic) which promotes the degradation of antiapoptotic proteins, such as BCL-2 (Beurel and Jope, 2006). In neonate rat ventricular cells, clusterin prevented angiotensin-II induced apoptosis (Ma et al., 2015). Angiotensin-II activation of the AT1-receptor-phosphorylated p38-MAPK and PI3K/AKT pathway activates nuclear factor kappa-B (NFkB) and nicotinamide adenine dinucleotide phosphate (NADPH) oxidase,

leading to apoptosis. In clusterin overexpression, activation of PI3K/AKT and p38 MAPK was inhibited, leading to reduction in NFkB, NADPH oxidase and Akt activation, preventing apoptosis.

Clusterin levels were higher in patients with recovered heart function after heart transplantation, compared to those who did not recover, suggesting that higher clusterin levels, which may have reflected increased anti-apoptotic signalling, was one of the markers of cardiac recovery (Hollander et al., 2014).

Clusterin also inhibits the complement system. In myocardial infarction, clusterin deposited around areas of infarction, co-localizing with components of the MAC (Vakeva et al., 1993), and was thought to prevent this complex from causing membrane lysis, although the protection could also be complement independent (Krijnen et al., 2005).

In PRIMID-AS, clusterin was higher in patients with no-events. This suggests that clusterin has a protective (potentially due to its antiapoptotic function) role in these patients.

### **3.5.6 Group 4b: Ion Transport, Oxidative Stress, Inflammation**

#### **3.5.6.1 H/CL exchange transporter 3 - CLCN3**

Myocardial ischaemia is usually accompanied by shortening or progressively prolonged QT intervals and action potential duration (APD), which may cause arrhythmias and sudden cardiac death (Antzelevitch, 2007, Anumonwo and Pandit, 2015). Inhibition of repolarizing outward potassium ( $K^+$ ) currents due to hypoxia, oxidative stress and metabolic blockade in conditions of ischaemia are a major mechanism for the prolongation of APD, effective refractory period (ERP) and QT interval (Carmeliet, 1999). Furthermore, myocardial ischaemia leads to energy depletion and intracellular acidification, resulting in a fall in ATP/ADP ratio and increase in cellular swelling, triggering regulatory volume decrease

(RVD) (Bozeat et al., 2011). This mechanism controls cell size and volume through a wide array of signalling cascades, which include activation of ion channels by releasing potassium, chloride and water from the intracellular compartment of swollen cells to restore cell volume and function.

Cardiac myocytes contain CLCN3-related-volume sensitive outwardly-rectifying channels which play an important role in RVD during cellular damage in myocardial ischaemia and reperfusion, which are an important mechanism of ischaemia pre-conditioning. In addition, these channels also reduced APD and ERP in ischaemia, reducing life-threatening arrhythmias (Yu et al., 2016).

In PRIMID-AS, patients with events had higher levels of CLCN3. This may be a compensatory increase implying that there was more cellular damage in patients with events. Higher levels of CLCN3 in this group also allows one to speculate that undesirable arrhythmias were indeed a potential mechanism of AS-related syncope.

### **3.5.6.2 ATP binding cassette sub family C member 8 (ABCC8)**

ABCC8 or sulphonylurea-receptor-1 (SUR1) modulate ATP-sensitive potassium channels (KATP) and modulate insulin release. KATP channels are multimers of four pore-forming Kir6.1 or 6.2 (KCNJ8 or KCNJ11) subunits and four sulfonylurea receptors (SUR1 or SUR2) subunits (Nichols, 2006).

These channels are highly expressed in various tissues. In cardiomyocytes, they coupled electrical and metabolic signals at the cell surface during adaptation to stress (Zingman et al., 2002) causing hyperpolarisation and preventing additional  $\text{Ca}^{2+}$  entry when energy levels were exhausted. In the mouse heart, SUR1 and Kir6.2 subunits were thought to be specific for atrial channels (Flagg et al., 2008), compared to SUR2 and Kir6.1 subunits which were



predominant in the ventricle. Additionally, the SUR1 and Kir6.2 subunits also formed the pancreatic KATP complex necessary for insulin secretion which can be targeted by sulfonylureas to increase insulin secretion. More recently, SUR1 has been demonstrated to localise to ventricular myocytes as well (Arakel et al., 2014). However, SUR1 KATP channels were co-localised to atrial surface membrane, but were predominantly *intracellular* in ventricular myocytes. In response to beta adrenergic stimulation, SUR1-KATP channels translocate to T-tubule membranes at the cell surface, decreasing APD and inhibiting additional  $\text{Ca}^{2+}$  influx.

In PRIMID-AS patients, SUR1-KATP was higher in patients with events. This could be explained by a compensatory increase in SUR1-KATP in response to increased myocardial stress from injury/ischaemia/pressure overload and associated sympathetic drive, to reduce APD.

### **3.5.6.3 Ryanodine receptor-3 (RYR3)**

Ryanodine receptor-3 is expressed in various tissues, but with a slightly higher preponderance in the brain. Ryanodine receptor-2 is found primarily in the heart, and ryanodine receptor 1 is expressed primarily in skeletal muscle. Ryanodine receptors mediate calcium release from the sarcoplasmic endoplasmic reticulum. In skeletal muscle this occurs when there is coupling of RYR1 to the voltage-dependent L-type calcium channel, whilst in cardiac muscle, this primarily occurs through calcium-induced calcium release (Parkinson and Mier, 1983). Recently, RYR3 channels were found to localise to the cell periphery in Purkinje cells, whilst RYR2 channels were found throughout the cells. Furthermore, *Ryr3* gene expressions were 100 times higher in Purkinje fibres compared to myocardial cells. This layer (where RYR3 localise) of calcium channels were more sensitive to  $\text{Ca}^{2+}$  than RYR2 in the endoplasmic reticulum of Purkinje fibres, which authors suggested would limit

spontaneous  $\text{Ca}^{2+}$  release from the endoplasmic reticulum, stabilising the electrical function of Purkinje fibres (Daniels et al., 2017).

In PRIMID-AS patients, RYR3 was found to be lower in patients with events. As the other two channels (ABCC8 & CLCN3) appear to have protective roles, lower RYR3 may be the driver for electrical instability.

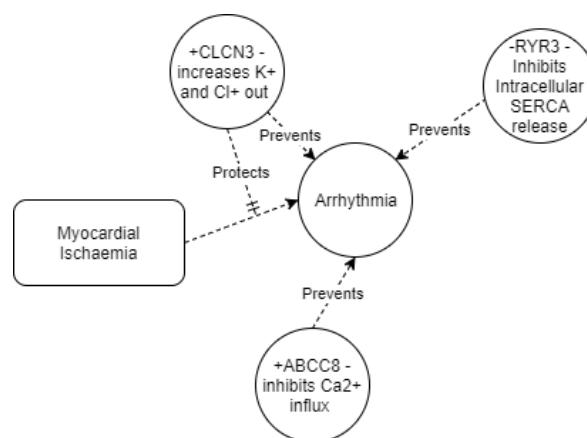


**Figure 3-23: Proposed ion transport mechanisms affected which imply an arrhythmogenic aetiology for symptom development; CLCN3: H/CL exchange transporter3; ABCC8: sulphonyl urea receptor 1; RYR3: ryanodine receptor 3; SERCA: sarco/endoplasmic reticulum calcium ATPase**

### 3.5.7 Group 5: Oxidative stress and other proteins

#### 3.5.7.1 Serum Amyloid A4 (SAA4)

Serum amyloid A4 is a constitutively expressed apolipoprotein found associated with HDL in plasma (Steel et al., 1993) (Yamada et al., 1996a). Its actual function has not yet been elucidated. Present to a lesser degree in LDL, it co-localizes with apolipoprotein B in atherosclerotic lesions. SAA4 and SAA1 loaded onto LDL improved binding to fibroblasts and macrophages, although degradation was also increased in both cells. oxLDL binding was also enhanced with SAA1 and SAA4, although degradation of oxidized LDL was only enhanced by SAA1, but these bindings were reduced in the presence of HDL. Therefore it was thought that HDL impedes lipid uptake from cells from LDL by removal of

SAA4(Yamada et al., 1997). SAA4 also goes up with inflammation (Yamada et al., 2001, Zhang et al., 2005). Higher levels were associated with dementia (Murphy et al., 2009) and hypertriglyceridemia(Yamada et al., 1996b). In fact, patients with rheumatoid arthritis had levels similar to post-renal transplant surgery patients (Kumon et al., 1997), implying similar levels of inflammation in the two conditions.

In PRIMID-AS patients, SAA4 was higher in patients without events. One might infer that these patients had higher low-level inflammation than those with events. However, as SAA4 has previously been shown to be higher in hypertriglyceridaemia (Yamada et al., 1996b), and APOC3 causes hypertriglyceridemia, SAA4 levels in this cohort more likely reflected circulating triglyceride levels.

### **3.5.7.2 Afamin (AFAM)**

Afamin is an abundant Vitamin E-binding glycoprotein of the albumin family (Voegelé et al., 2002). Its functions are largely unclear, and is partly attributed to the lack of understanding of its molecular function. Vitamin-E transport in plasma is mostly performed by circulating lipoproteins, but afamin levels correlate with vitamin-E levels in other fluids like cerebrospinal fluid (CSF) and ovarian fluid, inferring that afamin may take over vitamin-E transport in compartments unsuitable for lipoproteins (Jerkovic et al., 2005). There is an association between afamin and ovarian carcinoma (Melmer et al., 2013). Transgenic mice overproducing afamin had increased body weight, circulating lipids and blood glucose (Kronenberg et al., 2014). Epidemiological studies also confirm an association of afamin with all aspects of the metabolic syndrome (Dieplinger and Dieplinger, 2015).

In PRIMID-AS, afamin was higher in patients without events, and may reflect circulating lipoprotein levels.

### **3.5.7.3 Hemopexin (HEMO)**

Hemopexin is a scavenger for heme. When hemoglobin is released in haemolysis, free heme generates reactive oxygen species (ROS) in cardiomyocytes. This is seen in hemolytic conditions, e.g. beta thalassaemia. Heme-driven ROS affect calcium homeostasis impairing systolic function (Ingoglia et al., 2017, Sag et al., 2011, Kohler et al., 2014). AS-related intravascular haemolysis is not well reported, but has been identified in patients with valvular prostheses. A recent study found that 20/30 AS patients demonstrated evidence of increased erythropoiesis, with a lower erythrocyte and haemoglobin compared to control subjects (Sugiura et al., 2016). This is indirect evidence that intravascular haemolysis occurs in moderate-severe AS. There is also prior *in-vitro* evidence of chronic haemolysis causing chronic heme loading in cardiomyocytes (particularly in *Hpx*-KO mice), with associated systolic dysfunction and reduced contractility. Hemopexin is synthesized in the liver, and binds an equimolar amount of heme with high affinity. Complexed heme:hemopexin is taken up in the liver where heme is catabolized by heme-oxygenases (Tolosano et al., 2010).

In PRIMID-AS, patients without events had higher hemopexin levels, although this was not statistically significant. Given that lower haemoglobin levels were associated with events, hemopexin had to be considered as a potential biomarker given the potential importance of intravascular haemolysis leading to symptom development (Schaer et al., 2013).

### **3.5.7.4 Protein AMBP**

Protein AMBP is a precursor protein giving rise to two different secreted proteins after endopeptidase cleavage. One product, alpha-1-microglobulin (A1M), is a small globular plasma heme-binding anti-oxidant glycoprotein belonging to the lipocalin family (Allhorn et al., 2002), with additional immune regulatory properties (Logdberg and Akerstrom, 1981). The other product is bikunin, a Kunitz-type proteinase inhibitor of the inter-alpha-inhibitor

family(Salier et al., 1996), and is also a structural component of extracellular matrix (Chen et al., 1992). The reason for co-synthesis of these two proteins is not understood.

A1M is thought to be an extravascular tissue housekeeping and cleaning protein (Akerstrom and Gram, 2014). It binds to apoptosis-induced cells on the mitochondrial-complex-1-subunit NDUFAB1, inhibiting mitochondrial swelling and reversing deranged mitochondrial ATP production when exposed to heme and ROS. Other functions include free radical scavenging. Due to its small size (26KDa), it is freely filtered in the kidneys, and taken up in the proximal tubule through endocytosis, where it is catabolised, along with heme and other reactive oxygen species.

*AMBP* gene expression is upregulated secondary to oxidative stress in pre-eclampsia. This is thought to be caused by extracellular haemoglobin. In a starved-pregnant-ewe model, the starvation induced haemolysis and release of haemoglobin, heme and free radicals. Treatment of these ewes with A1M prevented the pathological effects (increased bilirubin, damage to placenta and kidneys with increased glomerular permeability (Wester-Rosenlof et al., 2014)), protection which was not seen in the placebo arm.

In PRIMID-AS, protein AMBP levels may reflect excessive oxidative stress. Lower AMBP levels in patients with events may reflect excess consumption in this group.

### **3.5.8 Remaining Proteins**

The remaining proteins that were differentially expressed between in the Events vs. No Events groups are briefly described in the following tables for two reasons; 1) They have not been associated with the other proteins in pathway analyses 2) Explaining their relevance in symptom/event development in AS was difficult, and for pragmatic reasons were not be prioritised for targeting in a verification study.

Protein	UniprotID	Gene	Higher In	Found In	Summary of Function	KeyWord 1	KeyWord 2
Teneurin-1	Q9UKZ4	<i>TENMI</i>	NoEvents	EV	Neural development, regulates neuroplasticity, mediates reorganisation of actin and tubulin cytoskeleton, increasing dendritic arborisation (Young and Leamey, 2009)	Neural development	
Protein furry homolog-like	O94915	<i>FRYL</i>	NoEvents	CSH	Maintains integrity of polarized cell extensions during morphogenesis in nerves (Hayette et al., 2005)	Neural development	
Collagen alpha-1(XXVIII) chain	Q2UY09	<i>COL28A1</i>	NoEvents	EV	May act as a cell binding protein ( <a href="https://www.uniprot.org/uniprot/Q2UY09">https://www.uniprot.org/uniprot/Q2UY09</a> )	Cell-Matrix Adhesion	
Transcriptional regulator ATRX	P46100	<i>ATRX</i>	NoEvents	EV	Involved in transcriptional regulation and chromatin remodelling. May be involved in telomere maintenance (Episkopou et al., 2014, Lovejoy et al., 2012).	DNA transcription	
Fer-1-like protein 5	A0AVI2	<i>FER1L5</i>	NoEvents	EV	Role in myoblast fusion. Probably mediator of endocytic recycling for membrane trafficking events during myotube formation (Posey et al., 2011, Redpath et al., 2016).	Muscle formation	
Nebulin-related-anchoring protein	Q86VF7	<i>NRAP</i>	NoEvents	EV	May be involved in anchoring the terminal actin filaments in the myofibril to the membrane and in transmitting tension from the myofibrils to the extracellular matrix ( <a href="https://www.uniprot.org/uniprot/Q86VF7">https://www.uniprot.org/uniprot/Q86VF7</a> ). Overexpression in mice leads to RV dysfunction. Early upregulation in mice in DCM (Lu et al., 2011).	Muscle formation	
Nuclear autoantigenic sperm protein	P49321	<i>NASP</i>	NoEvents	CSH	DNA replication, cell cycle progression and cell proliferation ( <a href="https://www.uniprot.org/uniprot/P49321">https://www.uniprot.org/uniprot/P49321</a> )	Cell Replication	
Hepatocyte growth factor activator	Q04756	<i>HGFAC</i>	NoEvents	EV	Activates hepatocyte growth factor by dimerizing it, which in turn acts as a growth factor for a broad spectrum of tissues and cell types ( <a href="https://www.uniprot.org/uniprot/P14210">https://www.uniprot.org/uniprot/P14210</a> )	Growth Factor	
EGF-containing fibulin-like extracellular matrix protein 1	Q12805	<i>EFEMP1</i>	NoEvents	EV	May play role in cell adhesion and migration (Hu et al., 2009)	Cell-Matrix Adhesion	

Protein	UniprotID	Gene	Higher In	Found In	Summary of Function	KeyWord 1	KeyWord 2
PDZ and LIM domain protein 7	Q9NR12	<i>PDLIM7</i>	NoEvents	EV	ENIGMA. May function as a scaffold on which the coordinated assembly of proteins can occur. Necessary for bone formation (positive regulation of osteoblast differentiation (Liu et al., 2002)).	Protein Assembly	
Flavin reductase (NADPH)	P30043	<i>BLVRB</i>	NoEvents	CSH	A broad specificity oxidoreductase which reduces a variety of flavins. In liver it reduces biliverdin to bilirubin and is involved in heme catabolism (Cunningham et al., 2000).	Pro-oxidant	
Alpha-2-HS-glycoprotein (alias: Fetuin-A)	P02765	<i>AHSG</i>	NoEvents	CSH	N-linked glycoprotein, needed to effect cytoprotective activity of some drugs. Promotes endocytosis, has opsonic properties and influences mineral phase of bone. Lower levels associated with higher mortality risk in CAD (Chen et al., 2017). Lower levels of AHSG predicts death in sepsis, but is negatively correlated to adiponectin (Karampela et al., 2017). Promoter of insulin resistance (Hennige et al., 2008).	Insulin Resistance	
RNA-binding protein 26	Q5T8P6	<i>RBM26</i>	NoEvents	CSH	Probably binds RNA	DNA transcription	
PX domain-containing protein kinase-like protein	Q7Z7A4	<i>PXK</i>	NoEvents	CSH	Modulates brain sodium-potassium-ATPase, may participate in electrical excitability and synaptic transmission (Mao et al., 2005).	Neural signalling	
Neurobeachin-like protein 1	Q6ZS30	<i>NBEAL1</i>	Events	EV	Highest in ovary. May be located in cell lysosome, and may facilitate vesicle trafficking (Chen et al., 2004).	Neural signalling	Lysosome
Platelet glycoprotein IX	P14770	<i>GP9</i>	Events	EV	Part of the platelet 1b-ix-v complex which transduces extracellular signals into the platelet for platelet activation. VWF is a ligand for this receptor (Feghhi et al., 2016).	Pro-coagulant	
Transcription factor TFIIIB component B" homolog	A6H8Y1	<i>BDP1</i>	Events	EV	Activates RNA polymerase III transcription (Schramm et al., 2000)	Protein Assembly	
PHD finger protein 20-like protein 1	A8MW92	<i>PHF20L1</i>	Events	CSH	Zinc finger protein. Function not known.	Oncogene	

Protein	UniprotID	Gene	Higher In	Found In	Summary of Function	KeyWord 1	KeyWord 2
Retinitis pigmentosa 1-like 1 protein	Q8IWN7	<i>RP1L1</i>	Events	CSH	Required for the differentiation of photoreceptor cells (Bowne et al., 2003). Retina specific.	DNA transcription	
Probable tRNA(His) guanylyltransferase	Q9NWX6	<i>THG1L</i>	Events	CSH	Adds GMP to end of tRNA. Necessary for tRNA recognition and fidelity of protein synthesis (Hyde et al., 2010).	Protein Assembly	
Nucleoporin p54	Q7Z3B4	<i>NUP54</i>	Events	EV	Component of nuclear pore complex for trafficking across nuclear membrane (Buss and Stewart, 1995).	Nuclear-Cytosolic trafficking	
Centriolin	Q7Z7A1	<i>CNTRL</i>	Events	CSH	Involved in cell cycle progression and cytokinesis (Gromley et al., 2003).	Cell Replication	
Glutathione S-transferase omega-1	P78417	<i>GSTO1</i>	Events	CSH	This protein glutathionylates thiol-containing proteins, protecting them from oxidation from ROS, and acts as a redox switch (Paul et al., 2015).	Anti-oxidant	Autophagy, Cellular Survival
Probable serine carboxypeptidase vitellogenic-like CPVL	Q9H3G5	<i>CPVL</i>	Events	CSH	May be involved in digestion of phagocytosed particles in lysosome, participating in inflammatory protease cascade, and trimming of peptides for antigen presentation (Harris et al., 2006) (and <a href="https://www.uniprot.org/uniprot/Q9H3G5">https://www.uniprot.org/uniprot/Q9H3G5</a> )	Lysosome Function	
Minor histocompatibility protein HA-1	Q92619	<i>HMHA1</i>	Events	CSH	Contains a GTPase activator for the Rho-type GTPases (RhoGAP) domain that would be able to negatively regulate the actin cytoskeleton as well as cell spreading (de Kreuk et al., 2013).	Cell Adhesion/migration	
Unconventional myosin-XVIIIa	Q92614	<i>MYO18A</i>	Events	CSH	May link Golgi membranes to cytoskeleton and participate in the tensile force required for vesicle budding from the Golgi (Buschman and Field, 2017).	Vesicular budding	
Synaptotagmin-14	Q8NB59	<i>SYT14</i>	Events	CSH	Calcium independent trafficking and exocytosis of secretory vesicles in non-neuronal tissue ( <a href="https://www.uniprot.org/uniprot/Q8NB59">https://www.uniprot.org/uniprot/Q8NB59</a> )	Vesicular budding	
RUN and FYVE domain-containing protein 4	Q6ZNE9	<i>RUFY4</i>	Events	EV	Integral to autophagy. Dendritic cell differentiation + IL4 = Autophagy (via mTORC1 and RUFY4 induction), promoting LC3 degradation and lysosome tethering (Terawaki et al., 2015).	Lysosome Function	Autophagy



Protein	UniprotID	Gene	Higher In	Found In	Summary of Function	KeyWord 1	KeyWord 2
Tau-tubulin kinase 2	Q6IQ55	<i>TTBK2</i>	Events	CSH	Key regulator of ciliogenesis. Stabilizes microtubules (centrioles) (Goetz et al., 2012). Heterozygous mutations on this gene causes spinocerebellar ataxia (Bouskila et al., 2011).	Initiating Ciliogenesis	
Isoform 4 of Dedicator of cytokinesis protein 9 (aka Zizimin-1)	Q9BZ29	<i>DOCK9</i>	Events	CSH	Guanine nucleotide-exchange factor that activates CDC42, exchanging GDP for free GTP. Overexpression increased filopodia activity in fibroblasts (Meller et al., 2002).	Cellular adhesion, migration	
Rhopilin-2	Q8IUC4	<i>RHPN2</i>	Events	EV	Binds GTP-RhoA. In Rho pathway to limit stress fibre formation (Peck et al., 2002).	Cellular Adhesion, migration	
GRAM domain-containing protein 1C	Q8IYS0	<i>GRAMD1C</i>	Events	EV	Unknown		
Protein DDX26B	Q5JSJ4	<i>DDX26B</i>	Events	EV	Integrator Complex 6 Subunit-like. Has a vWF-A domain. Otherwise function unknown.		
DNA repair protein RAD51 homolog 1	Q06609	<i>RAD51</i>	Events	EV	Important role in homologous strand exchange (Inano et al., 2017). Regulates mitochondrial DNA copy number under conditions of oxidative stress (Wang et al., 2015).	DNA Repair	

### **3.5.9 Summary of probable mechanisms representing progression of AS**

Overall, the proteins found to be higher and lower in PRIMID-AS patients having an event or no-event appear to represent some broad themes and potential mechanisms and may explain progression from asymptomatic to symptomatic AS (Figure 3-24).

#### **3.5.9.1.1 Neural Remodelling**

PLXN2, PLXN4, NBEAL1, FRYL, TENM

Higher levels of plexin-A2, plexin-A4 and neurobeachin-like-protein-1 but lower levels of protein furry homolog and teneurin were associated with symptom development in AS.

Eventual onset of anginal symptoms for some of these individuals may reflect a culmination of increased nerve growth.

#### **3.5.9.1.2 Altered lipid metabolism**

APOC3, APOC2, APOD, GPLD1, AHSG, AFM, SAA4

There was decreased APOC3 and APOC2, but increased APOD. There was reduced GPLD1 as well, which reflect reduced release of LPL from endothelial cell surfaces or increased stability of the GPI-bound LPL during its translocation to the cell surface. The net effect may be to increase fatty acid availability to cells. Initial pressure overload probably causes a mismatch between myocardial energy supply and demand, which may be compensated by a short-term increased reliance on glycolysis to maintain cardiac output. Chronic reliance on this may lead to compensatory increase in fatty acid supply, but with unsuccessful increase in fatty acid oxidation, leading to decompensation.

#### **3.5.9.1.3 Myocardial/Fibroblast Remodelling**

COL28A1, FER1L5, NRAP, TTBK2, DOCK9, RHPN2, HMHA1, CNTRL, EFEMP1, HGFAC, THBS1 & 2, ILK

The process of remodelling likely involves reorganisation of tissue architecture to normalise LV wall stresses due to pressure overload. This may involve increases in cellular migration, intracellular cytoskeletal strengthening, focal adhesion points, cellular proliferation and replacement fibrosis. This may result in reduced tissue elasticity and contractility, with diastolic dysfunction, which may lead to breathlessness.

#### **3.5.9.1.4 Cell Death/Apoptosis/Autophagy**

RUFY4, CPVL, GSTO, APOD, CLU, AKT1, MYO18A and SYT14

Increased oxidative stresses on cardiomyocytes and fibroblasts may lead to increased signalling for cell death. RUFY4, CPVL and GSTO all probably participate in lysosome function and APOD may play a key role in preventing lysosome failure. The balance between pro-apoptotic signalling and anti-apoptotic signalling determine cellular survival. Increased MYO18A and SYT14 may represent increased apoptosis giving rise to apoptotic bodies.

#### **3.5.9.1.5 Innate Immunity, Complement Cascade and Coagulation Cascade Activation**

MASP1, MASP2, APOH, C3, C4B, F13B, Protein S, GP9, CLEC3B, APOL1

Circulating components of the innate immunity, complement cascade and coagulation cascades are probably consumed from the peripheral circulation, in patients at higher risk of spontaneous symptom development. Using the innate immunity hypothesis, neoepitopes exposed because of tissue damage bind MASPs and APOH, as well as activate platelets and coagulation factors because of interacting pathways. Constitutively expressed proteins in these pathways may measure lower in those who go on to have an event, due to peripheral

consumption, but inducible proteins may increase in expression in response tissue/cellular injury.

#### **3.5.9.1.6 Arrhythmogenesis**

CLCN3, RYR3, ABCC8, PXX

AS-related syncopal episodes may occur because of undetected arrhythmias, given that several proteins associated with ion-transport may be dysregulated leading to prolonged action potential duration and effective refractory period in myocardial cells. Altered abundances of these proteins could be compensatory mechanisms for survival in response to persistent pressure overload.

#### **3.5.9.1.7 Heme Catabolism**

AMBP, HEMO, BLVRB

There was an association with intravascular haemolysis and AS severity. This may lead to excessive free haemoglobin being released into the circulation. There is probably a corresponding reduction in proteins that bind free heme, reflecting the peripheral consumption of these factors, with an increase in downstream activities that recycle heme. These markers therefore may be a surrogate for intravascular haemolysis.

#### **3.5.9.1.8 DNA transcription Activity/ Protein Assembly**

KAT2A, NASP, ATRX, RBM26, BDP1, NUP54, THG1L, RAD51, ERCC2, PDLIM7

Reflecting the increased in inter- and intracellular signalling occurring when cells are under stress, there was an increase in proteins associated with DNA transcription activity and

proteins associated with protein assembly, as well as proteins associated with DNA repair and correction.

#### **3.5.9.1.9 Inflammation**

A1AT

A1AT was higher in patients who developed events, suggesting that there was a relatively higher level of inflammation in these patients. Higher A1AT levels may simply reflect the compensatory mechanism to overall increased proteolytic activity to prevent collateral damage.

### **3.6 Limitations**

There were several limitations to the interpretation of the results presented in this chapter.

Firstly it must be acknowledged that this experimental design compared two ‘groups’ of patients who were indistinguishable except for their risk of developing the composite endpoint. As such the risk was time-dependent, and therefore arguably, putative biomarkers identified would represent a continuum of risk. These biomarker levels which in this study were only sampled at one time point would have been likely to change, given that the disease by definition was expected to progress; although whether the levels were going to go up or down may be different in each individual. Many diseases demonstrate time-dependent change (Höglund et al., 2012) and plasma biomarkers can show marked individual variability when measured over time (Silkoff et al., 2016, Razavi et al., 2016). This is therefore an inherent limitation of a cross-sectional sampling of plasma samples.

Due to the small number samples in this discovery study, compared to the large number of variables, as well as the similarity in the phenotype being evaluated, it was not surprising that when a Benjamini-Hochberg FDR adjustment was performed, no candidates were

‘significantly different’ between the two groups being evaluated, even when the false discovery rate was set at 80%. Therefore, the list of candidates presented were of unadjusted p-values with >80% probability of a false discovery. Finally, the much of the discussion regarding pathophysiology/mechanisms are speculative; and can only be hypothesis generating.

### **3.7 Conclusion**

In summary, I utilised the EV + CSH workflow to perform label-free proteomic profiling on patients with asymptomatic moderate-severe AS comparing those that reached an endpoint vs those that did not, to discover potential biomarkers that identify patients that are at higher risk of progressing to symptom development or unplanned hospital admissions or cardiovascular death. Presence of symptoms continues to be a key determinant in prognosis and for indicating AVR, and symptom development may well be a protective mechanism in these patients.

Although the clinical phenotype between those at risk and those not at lower risk was very similar, this chapter demonstrates that there were proteomic phenotypic differences between the two groups and highlights potential pathophysiological pathways involved in progression of asymptomatic moderate-severe AS. These pathways may be associated with remodelling, which include cellular apoptosis, inflammation, immunity activation, response to oxidative stress, neural remodelling, as well as altered lipid metabolism, although at this stage, the true contribution of each protein/pathway is only be speculative, but worthy of further study.

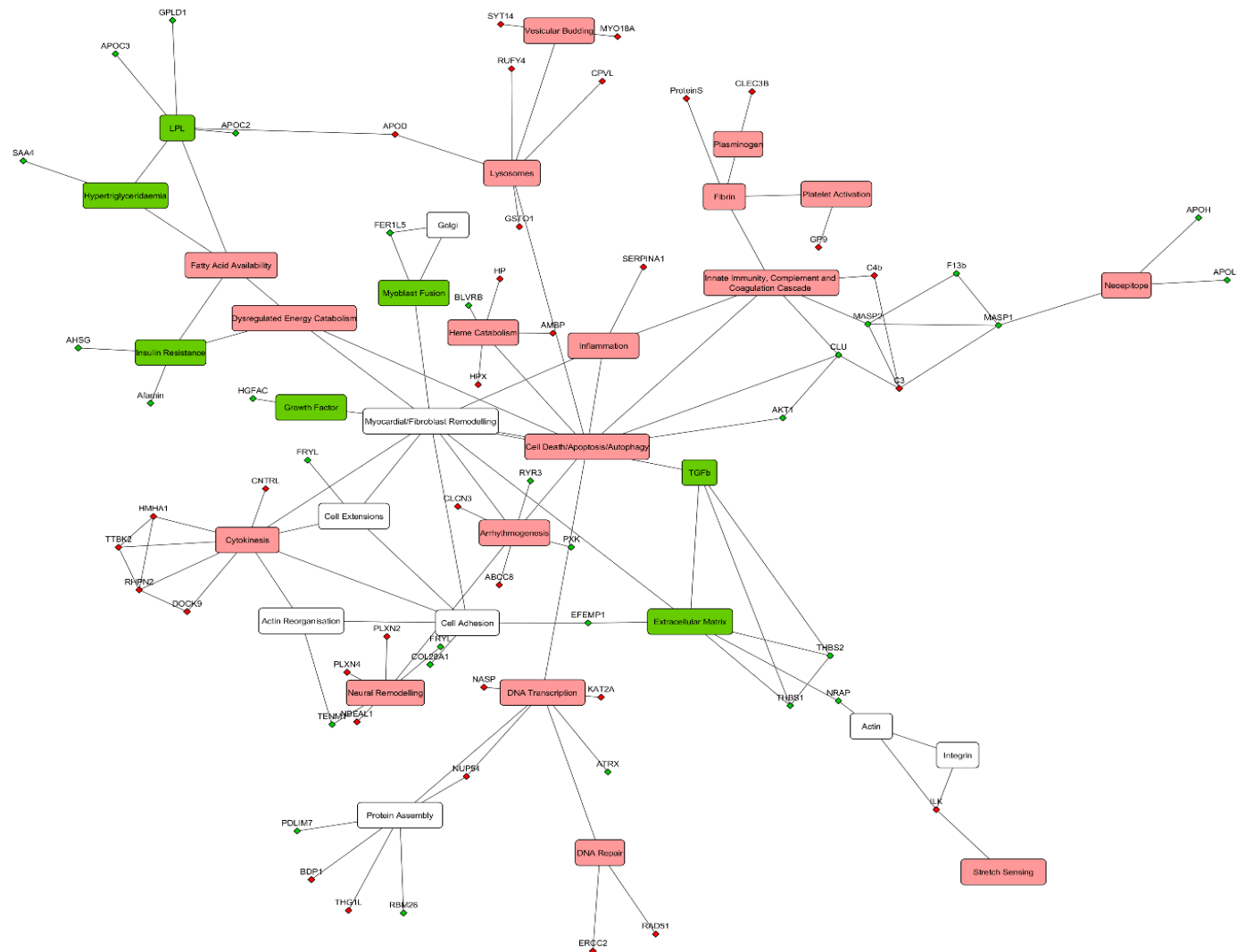


Figure 3-24: Network diagram highlighting links and potential functions of differentially expressed proteins in asymptomatic AS, red indicates higher in patients who develop events, green indicates lower in patients who develop events; larger copy in appendix

## Chapter 4 Verification

### 4.1 Introduction

Having identified potential biomarkers using label-free plasma proteomics and extensive literature database mining, were subjected to a verification process. Verification involves utilising a different method to acquire the data on the same samples. This step would check that the initial results found were not chance findings, because random error in it would be distinct from the original study. This step would lend confidence in the targets found, such that these targets could be considered biomarker candidates.

In the previous chapter, 59 proteins were discussed that were potential biomarkers, based on the p-values for differential expression. However, due to the low number of ‘events’ or cases, there was inadequate power to choose a set of p-values with a FDR between 1-5%. Using the Benjamini-Hochberg method to identify the q-value threshold, below which a population of p-values were considered significant, in both the EV and the CSH lists, no protein was ‘significant’ unless the FDR was set at >80%. As such, it is assumed that the probability of false positives in the 59-protein set was >80%.

Antibody-based assays have traditionally been used to confirm the findings on mass spectrometry. It is the gold standard methodology for determining analyte amounts, due to its robustness and ease of development, specificity and sensitivity. Furthermore, once the assay has been developed, the actual testing on the whole sample set can be completed rapidly.

Antibody-based assays can be performed as enzyme-linked immunosorbent assays (ELISA), or western blots. The higher throughput method is an ELISA, which is a plate-based method. With proteins, one would raise an antibody to the protein, with one antibody immobilised on the plate, and the other (on a separate epitope on the protein) being biotinylated so that it can



be conjugated to a light sensitive molecule, which can be leveraged to produce a highly specific signal to represent abundance of a particular analyte. Western blotting leverages antibody binding to the analyte in the sample, then depending on gel electrophoresis, which will allow the standard and antibody complex to travel a specific distance, which can then be the template to which samples and antibody complexes can be compared. The density of the bands seen is semi quantitative.

These antibody-based assays allow one analyte to be measured at a time. Therefore, if a panel of analytes were to be analysed, multiple assays need to be performed. The antibodies are often raised to recombinant protein or purified protein. There is little control over the epitope to which the antibody forms, although with recombinant peptide sequences, these have improved in specificity. Researchers are often limited by the peptides/proteins that manufacturers have produced, because the time taken to reproducibly manufacture an antibody can take 6 or more months.

More recently an alternative method has emerged. Targeted MS techniques leverage the specificity of tandem MS/MS, retention times and similarity of mass spectra to measure eluting peptides. Proteotypic peptides are usually targeted because there is no ambiguity about inferences to their protein of origin. However, the price for this specificity includes the need to decide on whether to measure post-translational modifications, chemical modifications and other modifications.

Targeted MS/MS work are divided into single reaction monitoring (SRM), MRM and PRM. In SRM, a peptide is ionised and filtered by a quadrupole (Figure 4-1). Peptides not fulfilling the precursor ion mass/charge criteria will be filtered-out. Following the first filter (often called Q1), the ion is fragmented using an optimised collision energy. Due to the predictable nature of fragmentation, a specific fragment ion can then be selected in the second

quadrupole (often called Q3) and detected by an ion detector, with the intensity of the signal being proportional to the abundance of the fragment. The transition (Q1/Q3) selectivity confirms the peptide being eluted. This specificity can be increased by selecting additional transitions for the same peptide, and co-eluting transitions increase the confidence that a targeted peptide was present.

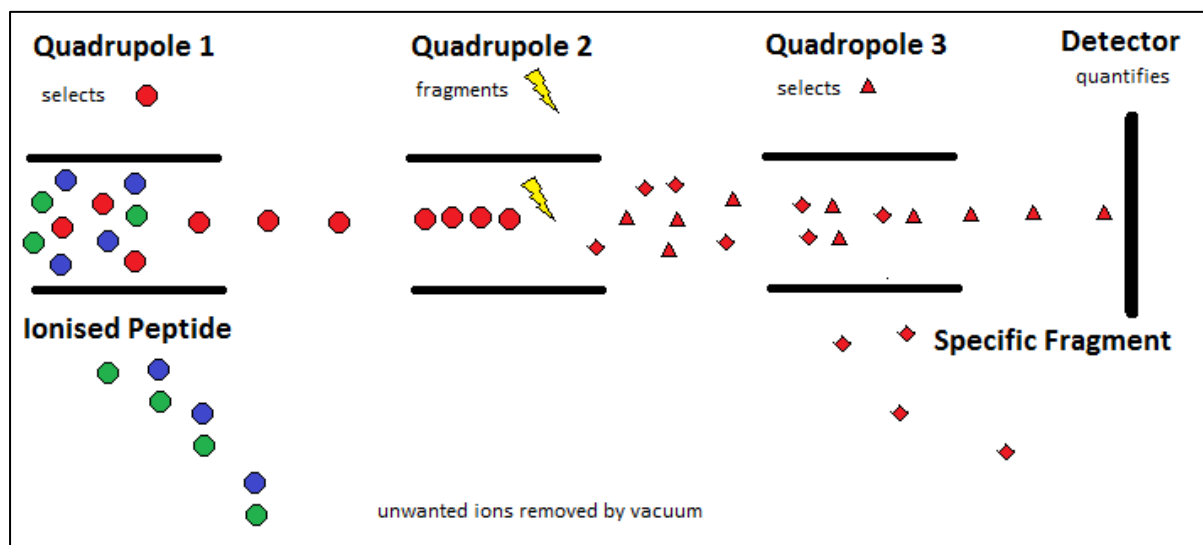


Figure 4-1: Cartoon of a triple quadrupole single reaction/multiple reaction monitoring experiment

With MRM, multiple transitions are monitored sequentially. Due to the fast scan times ( $\sim 0.2\text{ms}$ ) in these mass spectrometers (no need to measure mass, just detect them) the duty cycle for each ion transition monitored is very low, which allows sequential detection of several ions over a chromatographic run.

Although theoretical transitions can be predicted with tools such as SRMCollider (Röst et al., 2012), databases such as SRMAtlas (Kusebauch et al., 2016) or more recently MRMAssayDB (Bhowmick et al., 2018), add experimental data for various MS platforms, allowing researchers to select/design ideal targeted assays for MRMs, serving as a good starting point when the intended target(s) are known, reducing the number of experimental cycles necessary.

However, in the absence of prior experimental data, a reasonable starting point would be with a pure peptide (synthetic standard), followed by a computational consideration of the ideal transitions, and experimental optimisation to identify the ‘best’ fragment to allow maximal sensitivity, as well as the ‘best’ collision energy to give the ‘best’ fragment. These steps are especially necessary if different platforms were used for discovery and targeted methods, because of differences in collision methods and fragmentation patterns.

With PRM, a peptide is ionised and filtered by a quadrupole (Figure 4-2). The targeted peptide ion is then fragmented in the collision cell, then a full scan of the fragments is performed in the orbitrap analyser (or TOF detector), providing information on mass and intensity for each fragment. In this way, all fragment ions of the isolated precursor mass are detected in one scan cycle (approximately 20Hz or 50ms). The benefit of PRM is the acquisition of full scans of all fragment ions, increasing specificity of the molecule being monitored, without pre-selecting transitions. The fragment ions are then used to quantify the peptide.

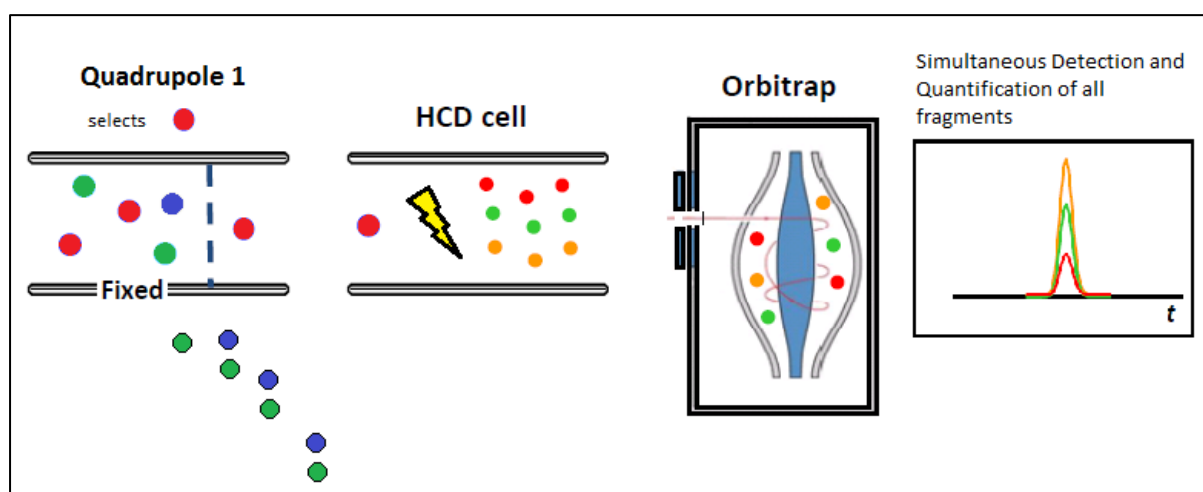


Figure 4-2: Cartoon illustrating a parallel reaction monitoring experiment. Fragments are detected simultaneously and quantified after the experiment.

Targeted methods work best with labelled standards. However, labelled synthetic peptides can be expensive and can take a while to manufacture. I wished to leverage the presence of existing peptides in the samples for quantification by heavy oxygen labelling. The process of

labelling peptides with heavy oxygen has previously been described (Kim et al., 2011, Yao et al., 2001). In principle,  $^{16}\text{O}$  on the C-terminal of the peptides are exchanged for  $^{18}\text{O}$ , giving the heavy-labelled peptides a mass difference of 4 Daltons compared to the endogenous (light) peptides. The catalyst for this process is trypsin, because of its activity on the C-terminal with a lysine or arginine residue. The process leverages the molar excess of  $^{18}\text{O}$ , swapping the  $^{16}\text{O}$  on the C-terminus with the heavy labels. There are two oxygens on the C-terminal; full-labelling results in a 4 Da mass difference.

Only y-series fragments (from the C-Terminal) will reflect the mass difference, whereas b-series fragments (from the N-terminal) will not. This is not typically an issue because the Thermo QExactive mass spectrometers preferentially detect y-ions. When targeting peptides, the m/z of doubly charged light:heavy peptides will be 2 Da apart, and 1 Da apart if triply charged. Therefore, this heavy-labelling method is better suited for a high-resolution accurate mass (HRAM) mass spectrometer, which is better at differentiating much smaller mass differences.

One of the perceived problems with  $^{18}\text{O}$  labelling is instability of the heavy label, largely due to back-exchange of  $^{18}\text{O}$  to  $^{16}\text{O}$  (Patwardhan et al., 2006). This instability is probably due to the presence of residual active trypsin in the samples. It is therefore imperative that trypsin is either removed (by immobilisation (Sevinsky et al., 2007)) or completely denatured, both in the heavy samples and light samples. Others have reported stable  $^{18}\text{O}$  labels for up to two weeks at 4°C (Petritis et al., 2009).

Due to time constraints and lack of *a-priori* experience in this facility in creating and optimizing methodology for PRM and using heavy oxygen labelled-standards made from pooled QC samples, a pragmatic approach was taken to select targets for method development. Only 17 proteins were targeted and were selected for their easily detectable and

quantifiable peptides. Time to optimize sensitivity was not required. Hemopexin was also targeted although the p-value for difference was 0.06, because it was easily seen and the hypothesis was sound.

## **4.2 Hypotheses**

The hypotheses being tested in the verification phase were as follows: -

- 1) Alpha-1-antitrypsin, Apolipoprotein C3, Apolipoprotein C2, Apolipoprotein D, Beta-2-glycoprotein 1, Complement C3, Hemopexin, Serum Amyloid A4, Tetranectin, GPLD1, Afamin, Apolipoprotein L1, Thrombospondin 1, Factor 13B, Protein S, Plasminogen and Protein AMBP are associated with spontaneous symptom development or death/hospitalisation of AV-related events in initially asymptomatic moderate severe aortic stenosis.
- 2) The above markers are independent markers of endpoints, even when adjusted for AS severity, sex and positive ETT.
- 3) The values acquired in the verification phase correlate significantly with values derived from the discovery study.

## **4.3 Methods**

### **4.3.1 Patient selection**

Recruitment plasma samples from patients from PRIMID-AS were used. Unlike the discovery study (46 case vs 46 matched controls), all available recruitment samples (n=168) were used for the verification study (Figure 4-3). Bicycle exercise testing results, Cardiac MRI results – including T1 Mapping, Late Gadolinium Enhancement and Stress results were also available. Definitions used in the study have been highlighted below. Except for

proteomic data, all the other data from the PRIMID-AS study were collected by others directly involved in the study as described in section 3.3.1.

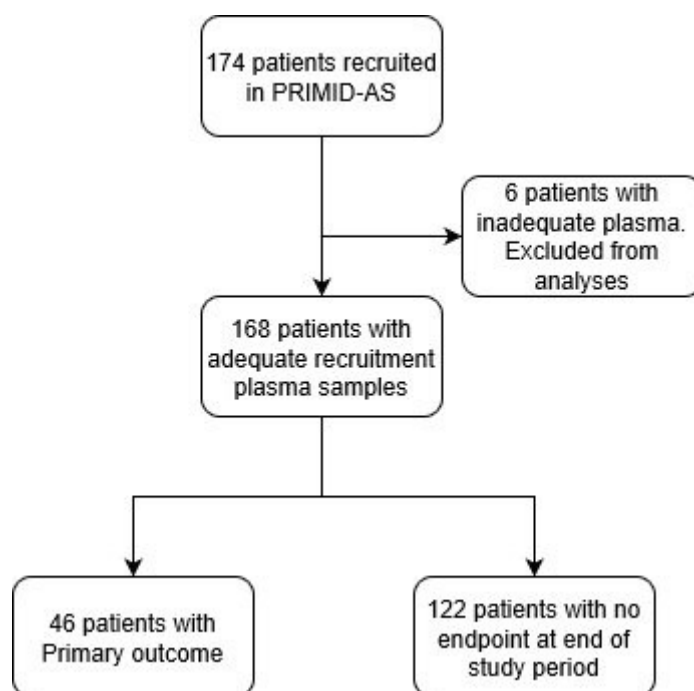


Figure 4-3: Patient flow diagram

#### 4.3.2 Sample Preparation

Samples were prepared with CSH (see section 2.2.12). Plasma was contacted directly to washed-CSH, forgoing the EV pulldown step. The reason for this was pragmatic; the EV-pulldown step was the most time-consuming aspect, and there were a sufficient number of CSH-discovered targets to pursue. The remaining steps were unchanged. Lyophilised peptides were resuspended in variable volumes of water so that they all had the same concentrations. These were stored at  $-80^{\circ}\text{C}$  until MS analysis.

#### 4.3.3 Heavy Labelling

A standard was created by pooling 35  $\mu\text{L}$  of peptide from each patient sample. This pool was then labelled and spiked into the samples at a fixed ratio. First, the volume of the pool was reduced so that it could fit in a single reaction Eppendorf (1.5 mL). There were initially 6 Eppendorfs of standard, containing a total of 5.88 mg of standard. These were lyophilised. 40

$\mu\text{g}$  of trypsin was prepared in 300  $\mu\text{L}$  50 mM ammonium bicarbonate, containing 10 mM calcium chloride, then lyophilised. When all substrates were lyophilised, 300  $\mu\text{L}$  of heavy water ( $^{18}\text{O}$  water 97% pure, Sigma) was combined with all the standards and trypsin mixture, and allowed to label overnight at 37°C. After labelling, trypsin was denatured by heating for 20 minutes in a water-bath with a temperature set between 90°C and 100°C. Individual patient peptide samples were also subjected to this denaturation step. The 300  $\mu\text{L}$  of standard was then acidified to 5% FA and made up to 5.88 mL with normal water (concentration - 1  $\mu\text{g}/\mu\text{L}$ ), and equally split across 90 aliquots. The estimated amount of standard in each aliquot was 65  $\mu\text{g}$  peptide (5.88mg/90 aliquots). 90 aliquots were made, so that there was enough standard for future experiments, as these standards cannot be reproduced. These were then lyophilised to remove any excess water in the samples and stored at -80°C until they were used.

#### **4.3.4 Experimental design**

The sample analysis order was randomised using the ‘sample’ function in R. Batches of eight samples were prepared at a time. Heavy standards were made up on the day that they were run on LCMS, by re-suspending the standards in 65  $\mu\text{L}$  0.1% formic acid (1  $\mu\text{g}/\mu\text{L}$ ). The samples were defrosted from -80°C and prepared by spiking in 12.5  $\mu\text{L}$  of heavy standard into 25  $\mu\text{L}$  of sample (also 1  $\mu\text{g}/\mu\text{L}$ ) resulting in a ratio of 1 part heavy to 2 parts light, using the same calibrated pipette each time. The whole volume was further diluted with 37.5  $\mu\text{L}$  6% acetonitrile in 0.1% formic acid (final peptide concentration 0.5  $\mu\text{g}/\mu\text{L}$ ). Samples were run in duplicates, with a blank injection between every sample. Every 5 samples, a standard containing only the heavy made up on the day was run to assess the stability of the heavy peptides. Later in the study, as it became clear that the peptides were stable for more >1 day, a vial of heavy-labelled-standard was left (sufficient for 28 injections) at the autosampler temperature (8°C) and injected daily to assess the longevity of the labelled-standards when

left at autosampler temperature. A DDA of 0.5  $\mu\text{g}$  of standard HeLA digest was performed every week to ascertain that the mass spectrometer was performing as expected, i.e. the number of protein identifications remained within 10% of the initial value. When the number of protein identifications deviated by more than 10%, the experiment was paused, and a series of maintenance steps undertaken until the number of protein identification for a HeLa injection returned to the benchmarked figure.

#### **4.3.5 Parallel Reaction Monitoring**

The samples were separated on an Ultimate 3000 RSLC nanoHPLC system (Dionex/ThermoFisher Scientific, Bremen, Germany). Samples were loaded onto a cartridge-based trap column, using a 300  $\mu\text{m}$  x 5 mm C18 PepMap (5  $\mu\text{m}$ , 100A) and then separated using the Easy-Spray pepMap C18 column (75  $\mu\text{m}$  x 50 cm) with a gradient from 3-10% B in 0.2 mins, 10-15% B in 5.8 mins, 15-51.2% B in 34 mins, 51.2-90% B in 4 mins, holding at 90% B for 3.5 mins then 90-3% B in 1 min and equilibrating at 3% B for 35.5mins, where mobile phase A was 0.1% FA in water and mobile phase B was 80%/20% acetonitrile/water in 0.1% FA. Flow rate was set at 0.3  $\mu\text{L}/\text{min}$ . The column was operated at a constant temperature of 45  $^{\circ}\text{C}$ .

The nanoHPLC system was coupled to a Q-Exactive mass spectrometer. To create the initial spectral library, data was acquired in DDA top 10 mode; full-MS scans were acquired at a resolution of 70,000 at 200  $m/z$ , scanning from 50 $m/z$  to 2000 $m/z$ , with an AGC of  $1e^6$  and a maximum fill time of 50 ms.  $\text{MS}^2$  scans were acquired at a resolution of 17,500, with an AGC target of  $1e^5$ , and a maximum fill time of 100 ms. The dynamic exclusion was set at 30s.



For parallel reaction monitoring, acquisition was performed over 70 minutes, with a resolution of 35000 at 200 m/z and an AGC of  $3e^6$  with the maximum fill time set at 110 ms. The isolation window was set at 1.8 m/z with data acquisition performed in centroid mode.

#### **4.3.6 Data analysis and target peptide selection**

The raw DDA data was processed in Proteome Discoverer 2.1 (PD). The peptide search within PD was performed using the SequestHT algorithm, using a precursor mass tolerance of 10 ppm, 0 missed cleavages, and searched against the UniProt human .FASTA file (as in section 3.3.3.6.2). When searching, carbamidomethylation of cysteine was set as a static modification, and methionine oxidation as a variable modification. Analyses were filtered using a 1% false discovery rate.

The library search file (.msf) was then imported into Skyline.ms ver 3.2 (Bereman et al., 2012). In Skyline, the peptide lists were filtered for peptides 8-25 residues in length, 1<sup>st</sup> 25 residues from N-terminal of protein excluded, no missed cleavages and unique peptides were selected based on the uniqueness by gene. Proteins were selected from the hypothesis lists, but filtered peptides were selected for targeting based on three criteria; 1) an interference free chromatographic profile, 2) intensity (higher intensity better) and 3) retention time on the chromatogram, where no more than 3 targeted peptides (i.e. 3 pairs of light/heavy precursors) would elute at any one time. The higher intensity charge state of the peptide was chosen (2 or 3) if there was an option.

The inclusion list and their scheduled monitoring times were exported from Skyline and imported as a global isolation list in the MS Method on the QExactive mass spectrometer in Xcalibur. The default normalised collision energy (NCE=27) was used. For each precursor, the scheduled monitoring period was set as a 2-minute window from the precursor's retention

time. The chromatographic peak width was set as 12 s (Full Width Half Maximum).

Acquisition was then performed as described in the parallel reaction monitoring section.

Chromatographic retention times varied with ambient temperature, and with column changes.

Therefore, if any of the peaks were truncated during an acquisition, a new scheduling window was set (predicted and exported by skyline) and re-imported into the MS Method for each subsequent run.

Raw files were then imported into skyline for quantification of the peptides based on their fragment ions. Because of the variability of intensities between runs, all quantities were normalised to heavy peptides. The light/heavy ratio for each peptide was then used for data analysis as a surrogate for amount because the actual amount of heavy peptide was not known.

#### **4.3.7 Assessment of assay performance**

To ascertain PRM assay performance, calibration curves were plotted to evaluate linearity of dose response. Dilution series were performed with the heavy standard as the numerator ( $1\mu\text{g}/\mu\text{L}$ ) and light sample – from a single volunteer (final sample concentration of  $1\mu\text{g}/\mu\text{L}$ ) as the spiked in ‘standard’. Three dilutions were made, so that the expected heavy:light ratio was 1:1, 1:25 and 1:250. Heavy:light ratios were then measured using the PRM method described earlier in triplicate. CVs were calculated for these concentrations from the triplicate injections to assess repeatability. An undiluted heavy sample was also measured as the fourth data point in the calibration curve.

#### **4.3.8 Statistical Analysis**

Light/heavy ratio data was acquired in duplicate for each peptide. The final value used was the mean of the duplicates. Parametric data was summarised and presented as mean $\pm$ standard

deviation. Non-parametric data was presented as median [1<sup>st</sup> Quartile – 3<sup>rd</sup> Quartile]. Where appropriate non-parametric data was log-transformed for modelling purposes. Hazard ratios were calculated in a cox proportional hazards model, to ascertain independence of effect on the hazard. Subgroup analyses were performed to assess heterogeneity of effect across various subgroups. If there was heterogeneity of effect, an interaction term was added to the cox model to determine the significance of the interaction. Kaplan-Meier curves were plotted to demonstrate difference in event-free survival dichotomized by risk. Where appropriate, the Grey test for cumulative incidence of competing events was performed, and Fine-Grey proportional hazards regression performed for competing events. The log-rank test was used to calculate the statistical significance of the difference in survival curves. The non-parametric Spearman correlation test was used to determine correlations between variables of interest, and results were expressed as rho, p-value where rho was the correlation coefficient. Receiver operating curves (ROC) were generated using the ‘pROC’ package in R plotting sensitivity against 1-specificity. Derivation of optimal thresholds was done by selecting the value of the variable being dichotomised at which the sum total specificity and sensitivity was maximal. Comparing the difference in prognostic accuracy between two models was performed by comparing the area under the curve (AUC) of the ROC using the De Long test. Net reclassification improvement analysis was performed using the method originally described (Pencina et al., 2008, Pencina et al., 2011) using the package ‘PredictABEL’ in R (Kundu et al., 2011).

## **4.4 Definitions**

### **4.4.1 Severe AS**

Severe AS refers to definitions in the updated 2017 ESC Guidelines for valvular heart disease (Baumgartner et al., 2017a). Severe AS was defined as  $MPG \geq 40$  mmHg or  $AV-V_{max} \geq 4$

m/s. In cases where  $AVA \leq 1 \text{ cm}^2$  but  $MPG < 40 \text{ mmHg}$  and  $AV-V_{\max} < 4 \text{ m/s}$ , then all cases with Stroke Volume Index (SVI - stroke volume/BSA)  $< 35 \text{ ml/min}$  and  $LVEF \geq 50\%$  and AV Calcium score  $\geq 2000$  in men and  $\geq 1200$  in women were classified as severe AS. All other cases were classified as moderate AS.

#### **4.4.2 Positive Exercise Test**

An incremental bicycle test was carried out as defined by the study protocol as previously described (Singh et al., 2013). The exercise test was considered ‘positive’ if the patients became symptomatic at any point during the exercise test or had a drop in blood pressure below baseline. All other results were considered ‘negative’. Exercise test results were not made available to the patient’s attending physician and therefore did not trigger for referral for AVR.

#### **4.4.3 Outcomes**

##### **4.4.3.1 Primary Outcome**

The primary outcome measure of the study was a composite of spontaneous symptoms necessitating referral for AVR or death/hospitalisation for AV-related events (syncope, breathlessness, and HF or chest pain).

### **4.5 Results**

#### **4.5.1 Assay Performance**

##### **4.5.1.1 Dynamic Response**

Dynamic response was assessed using the heavy:light ratio in triplicate. A positive control was also analysed (heavy only, no light), but not in triplicate. The expected ratio of heavy to light for this was arbitrarily set at 333 (inverse of light:heavy ratio in the heavy stock of

approximately 0.003. Coefficient of variation (%CV) generally increased as concentrations of heavy (the numerator) decreased. Despite this, the correlation between the measured ratio and the expected ratio for the technical replicates remained excellent for all peptides and the calibration curves appeared linear across the higher range of concentrations tested (Table 4-1 and Figure 4-4). The absolute value of the expected ratios and measured ratios were slightly discrepant, probably because the 'light' was made from a single person's sample, whilst the 'heavy' was made from a pooled sample. Because the light:heavy ratio of the peptides for the main experiment was expected to range from 0.1 (10x more heavy than light) to 10 (10x more light than spiked-in heavy) all the peptides selected for study were retained as their %CV was likely to remain <10%. Additionally, the injections were performed in duplicate, and the mean for each duplicate was used to mitigate the variability at lower concentrations.

Peptide Sequence	Uniprot	Protein Name	CV*			Average Measured Ratio			R <sup>2</sup>
			1	0.04	0.004	1	0.04	0.004	
MTVTDQVNC PK	P05090	APOD	2%	2%	2%	1.5	0.08	0.015	1
VTEPISAESGEQVER	O14791	APOL1	1%	4%	0%	1.2	0.06	0.017	1
DALSSVQESQVAQQAR	P02656	APOC3	2%	7%	10%	1.3	0.05	0.015	1
GWVTDGFSSLK	P02656	APOC3	2%	3%	1%	0.5	0.02	0.004	1
DTEEDFHVDQVTTVK	P01009	A1AT	1%	2%	14%	2.5	0.1	0.018	1
TIVTTLQDSIR	P07996	TSP1	1%	3%	21%	2.3	0.12	0.062	1
IAPQLSTEELVSLGEK	P43652	AFAM	2%	2%	17%	1.2	0.06	0.014	1
EALQGVGDMGR	P35542	SAA4	5%	3%	3%	0.9	0.04	0.008	0.999
TLLLVGSPTWK	P80108	PHLD	1%	67%	42%	1.5	0.04	0.005	1
LYDYCDVPQCAAPSFDCGKPQVEPK	P00747	PLMN	3%	4%	6%	2.1	0.11	0.034	1
TVMVNIENPEGIPVK	P01024	CO3	1%	0%	6%	1.5	0.05	0.01	1
IPIEDGSGEVVLSR	P01024	CO3	3%	6%	5%	1.7	0.06	0.013	1
DVDECSLKPSICGTAVCK	P07225	PROS	1%	3%	13%	1.4	0.07	0.021	1
GECQAEGVLFFQGDR	P02790	HEMO	2%	4%	5%	1.4	0.07	0.014	1
DYFMPCPGR	P02790	HEMO	4%	2%	6%	2.4	0.13	0.017	0.999
VVAQGVGIPEDSIFTMADR	P02760	AMBP	0%	1%	29%	2.7	0.11	0.007	1
LDTLAQEVALLK	P05452	TETN	2%	3%	7%	1.6	0.07	0.008	1
ATFGCHDGYSLDGP EEIECTK	P02749	APOH	1%	1%	10%	9	0.39	0.045	1
TYLPAVDEK	P02655	APOC2	8%	4%	6%	1	0.04	0.006	0.997
VLHGDLIDFVCK	P05160	F13B	8%	22%	6%	1.3	0.04	0.006	0.997

Table 4-1: Coefficients of variation in percentage of measured ratios at different concentrations; \* 1, 0.04 and 0.004 were the expected ratios of heavy to light, R2 is the correlation between the average measured ratios and expected ratio

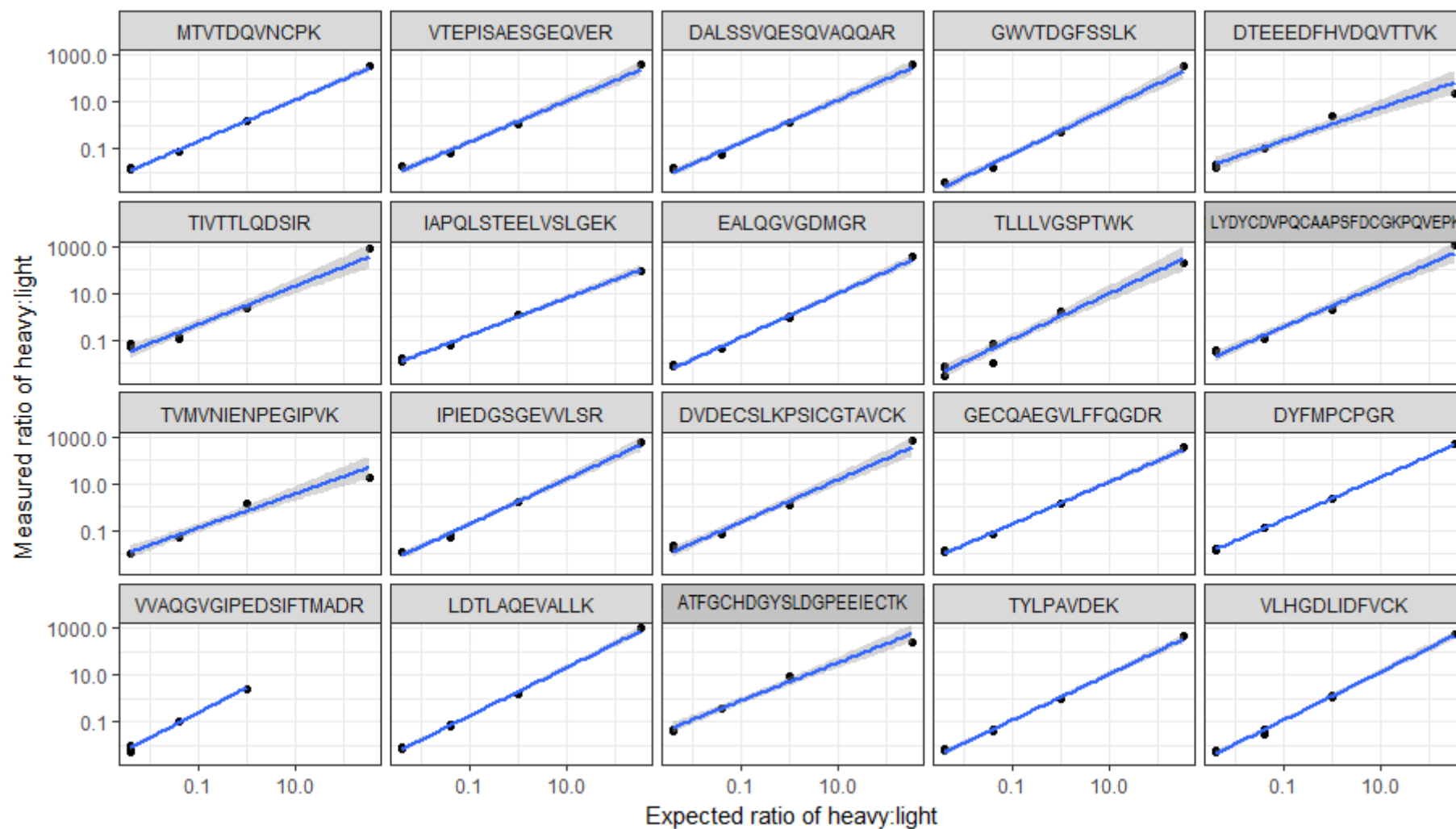


Figure 4-4: Calibration curves of targeted peptides, each dilution performed in triplicate, except for the heavy stock (highest heavy:light ratio). Curves plotted on log<sub>10</sub> scale to accommodate range of ratios.

#### **4.5.1.2 Reproducibility**

The use of heavy labelled standards allowed adjustment for the significant run to run variability observed. Figure 4-5 and Figure 4-6 shows the variability of the sum peak areas of the fragment ions for the MTVTDQVNCpk peptide (surrogate for APOD) in the same sample injected 4 times on the same day but with improvement after normalising to the internal standard (Figure 4-7). This variability improved substantially (up to 20×) by using the ratios of the sum areas of the light peptide fragments to the heavy peptide fragments for all the peptides tested (Table 4-2).



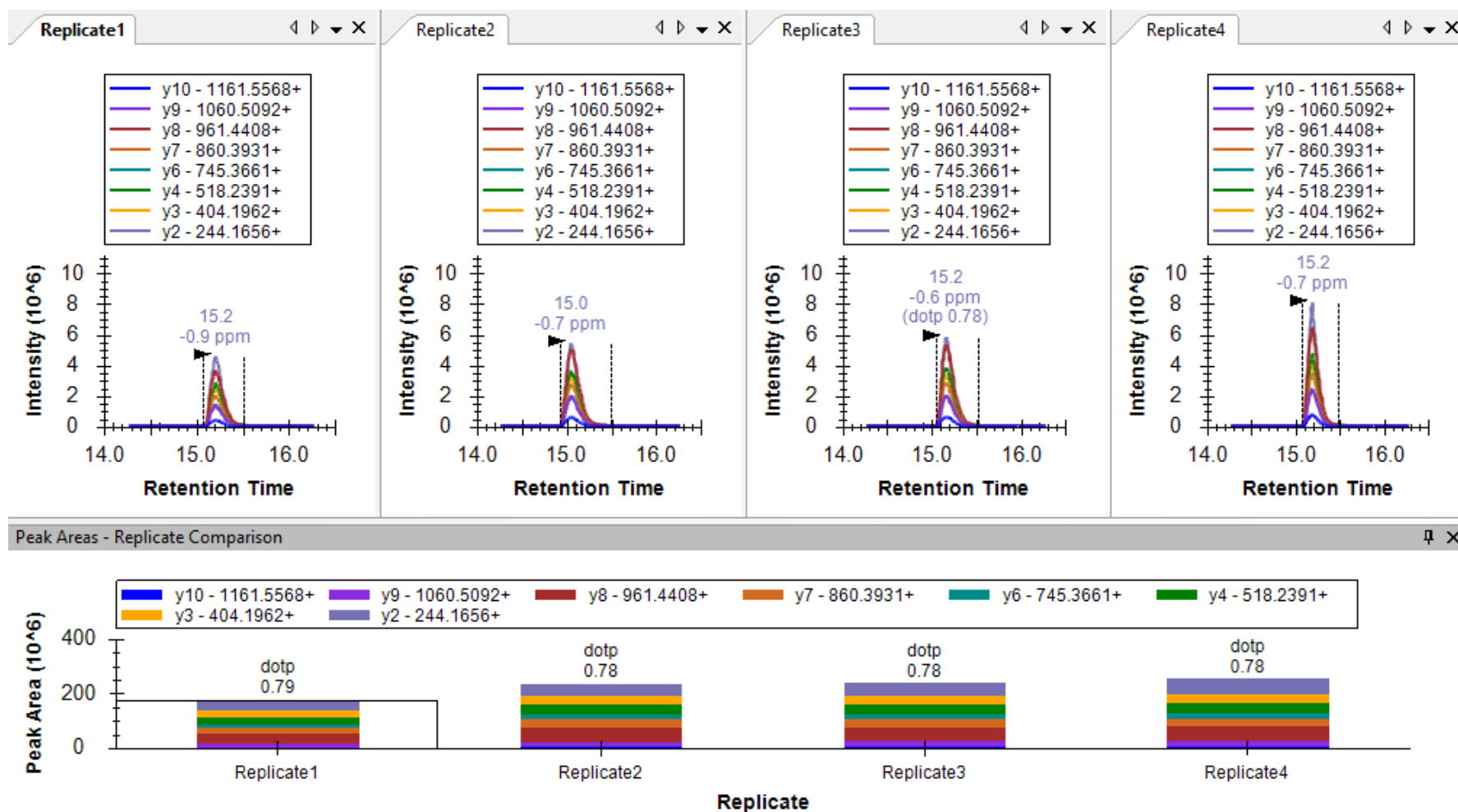


Figure 4-5: Sum areas of selected MTVTDQVNC PK (surrogate for APOD) transitions (Light); colours indicate peak areas and chromatograms of respective y-fragment ions; dotp value indicates confidence of peak belonging to peptide; numbers indicate mass and charge state of ions

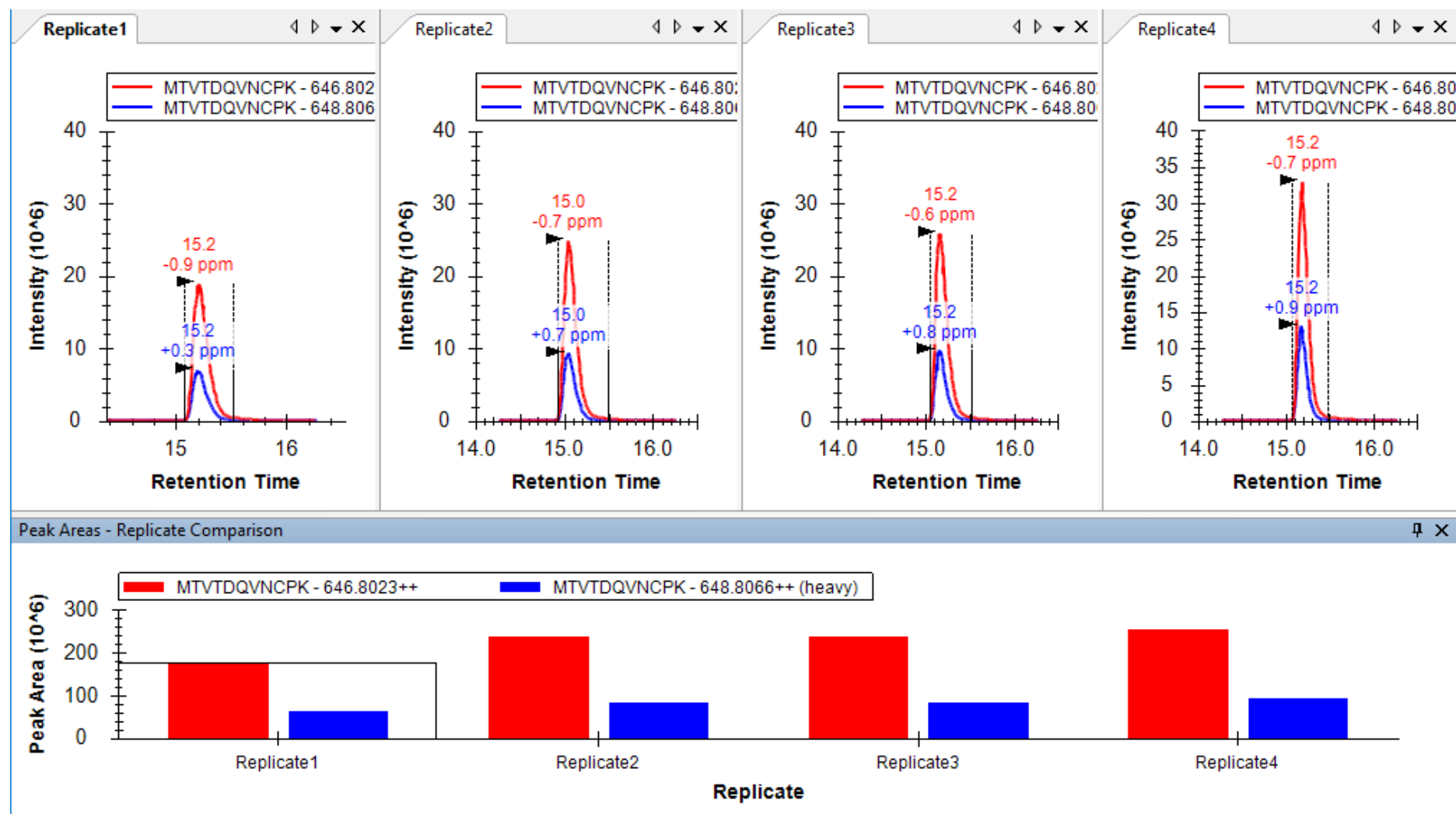


Figure 4-6: Sum areas of heavy and light MTVTDQVNC PK (APOD surrogate) transitions, shown separately in bar graphs at lower part of the screen in this screenshot. Red colour indicates the light peptide and blue colour indicates the heavy peptide.

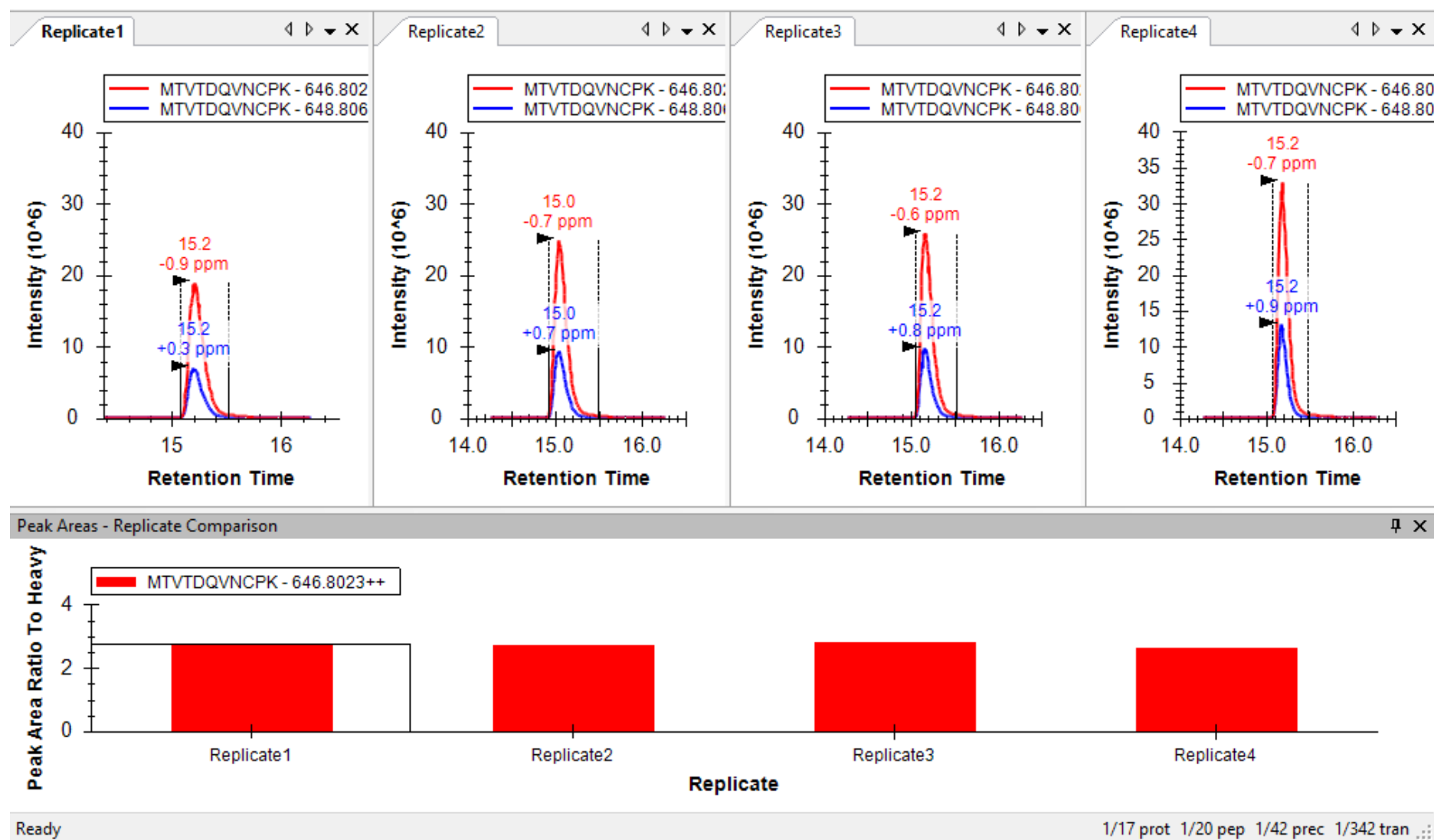


Figure 4-7: Ratio of light to heavy MTVTDQVNCPPK (APOD surrogate), showing that ratio measurements were far more reproducible

Uniprot	Protein	Peptide	%CV light	%CV heavy	%CV ratio
P05090	APOD	MTVTDQVNC PK	15%	16%	2%
O14791	APOL1	VTEPISAESGEQVER	20%	19%	1%
P02656	APOC3	DALSSVQESQVAQQAR	14%	15%	8%
P02656	APOC3	GWVTDGFSSLK	12%	16%	8%
P01009	A1AT	DTEEDFHVDQVTTVK	3%	1%	2%
P07996	TSP1	TIVTTLQDSIR	18%	16%	8%
P43652	AFAM	IAPQLSTEELVSLGEK	17%	18%	2%
P35542	SAA4	EALQGVGDMGR	21%	21%	3%
P80108	PHLD	TLLVGSPTWK	22%	24%	4%
P00747	PLMN	LYDYCDVPQCAAPSFDCGKPQVEPK	11%	10%	3%
P01024	CO3	TVMVNIENPEGIPVK	16%	18%	4%
P01024	CO3	IPIEDGSGEVVLSR	17%	18%	3%
P07225	PROS	DVDECSLKPSICGTAVCK	13%	13%	3%
P02790	HEMO	GECQAEGVLFFQGDR	16%	17%	3%
P02790	HEMO	DYFMPCPGR	13%	16%	4%
P02760	AMBP	VVAQGVGIPEDSIFTMADR	34%	34%	3%
P05452	TETN	LDTLAQEVALLK	26%	28%	3%
P02749	APOH	ATFGCHDGYSLDGPEEIECTK	8%	8%	1%
P02655	APOC2	TYLPAVDEK	10%	10%	2%
P05160	F13B	VLHGDLIDFVCK	3%	9%	8%

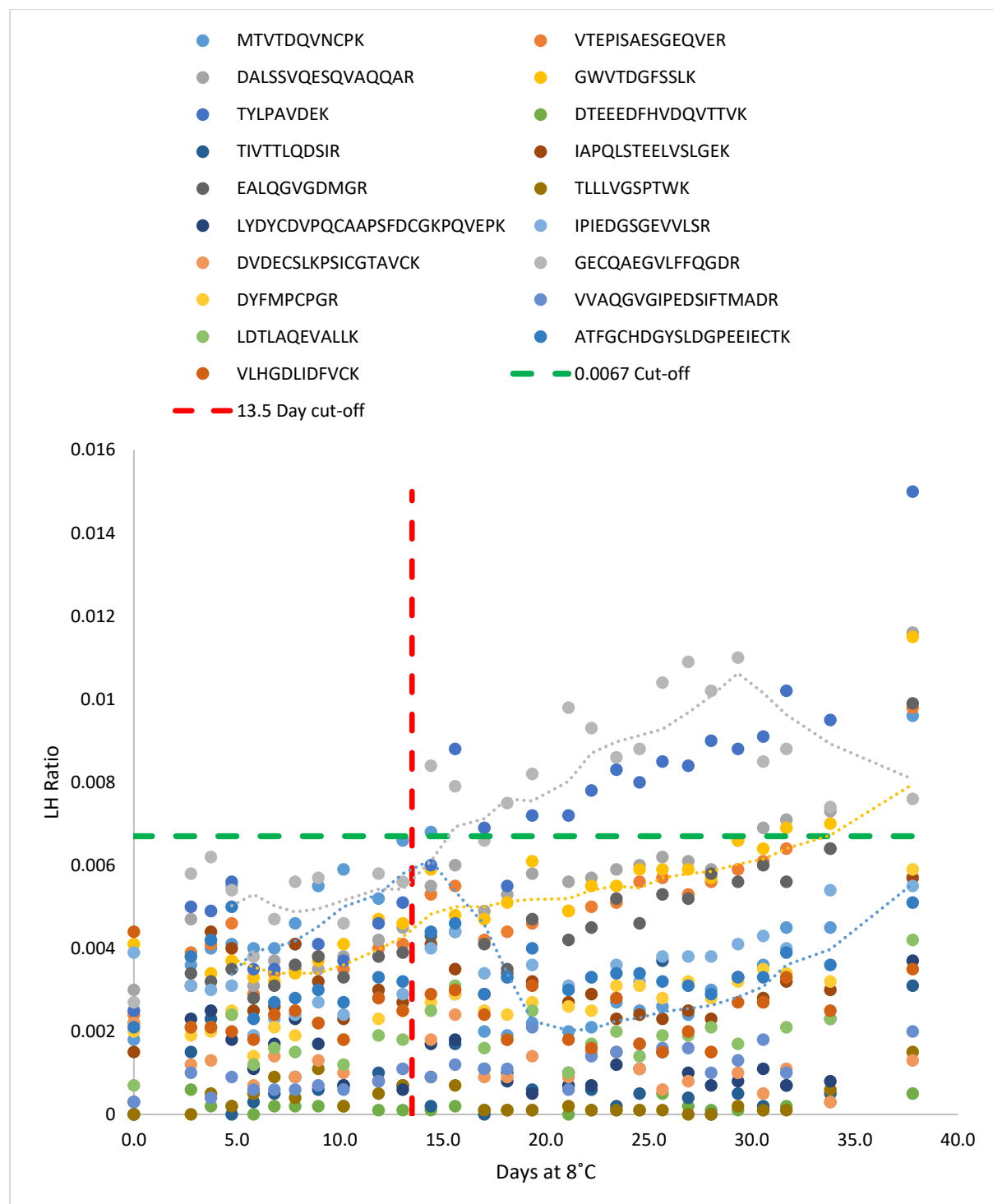
**Table 4-2: Percentage coefficient of variation of light and heavy sum areas in 4 replicates, comparing with the variation of the ratios of each peptide; CV: Coefficient of variation, calculated as standard deviation÷mean expressed in %. CV\_Ratio refers to the CV calculation for the ratios of light to heavy.**

#### 4.5.1.3 Stability of Heavy Labelled Peptides

The  $^{18}\text{O}$ -labelled heavy standards were stable at the temperature of the autosampler ( $8^\circ\text{C}$ ).

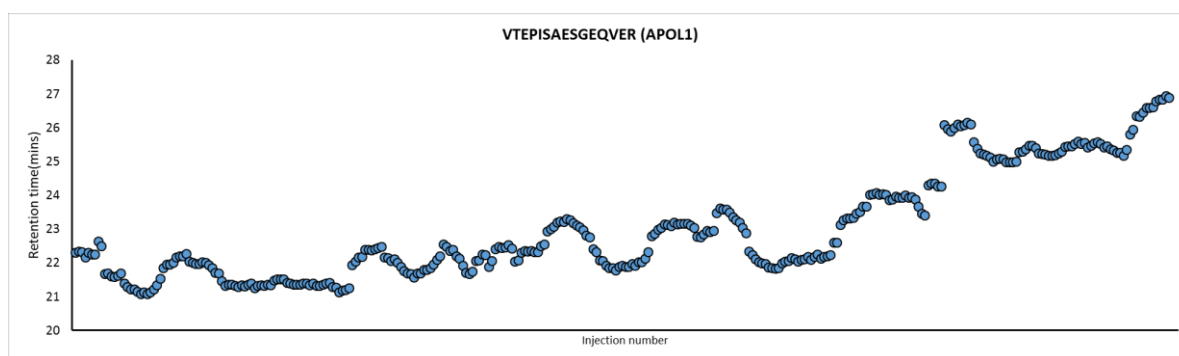
The same heavy standard aliquot made up in normal water, was injected every 8 injections on the mass spectrometer, translating to a median interval of 28.3 hours [range 23.2-95.8]. In nature, the abundance of light:heavy in nature is 99.8:0.2 for  $^{16}\text{O}$ : $^{18}\text{O}$ . The sample was labelled with  $^{18}\text{O}$  water which was 97% pure, therefore the ratio of light:heavy in this heavy standard should not be more than 3:97 (3.1%). A reasonable (arbitrary) cut-off wherein one would consider that the heavy standard was not stable was set at 3% of the initial ratio (within the 3% CV), i.e.  $(\text{light} + \text{error})/(\text{heavy} - \text{error})$  should be within the measurement error of that particular concentration. In practice, as long as the light fraction in the sample was not close to the limit of detection, or substantially less ( $<1/25$ ) than the heavy fraction, minute amounts of back exchange from the heavy to light was unlikely to affect the results significantly.

Figure 4-8 illustrates the ratio of light:heavy in the heavy standard injected over 38 days. If the cut-off of ratio of 0.031 was used, the heavy standard could be considered stable at  $8^\circ\text{C}$  for at least 38 days. However, if a stricter cut-off of 0.0066 ( $\sim 3\times$  the light fraction in a pure heavy sample), the heavy standard could be considered stable in these conditions for 13.5 days. This was not important in this study because a fresh standard was prepared daily and spiked-in with the samples; however, relevant for future applications, this method of heavy labelling would yield stable labels for up to 38 days in these conditions depending on the application (i.e. if the ratio being measured is more than 1:50).



**Figure 4-8:** Measured light to heavy ratio in a heavy standard made up in water, injected over several days at 8°C; back exchange from heavy to light only apparently begins to drift after day 14 for some peptides.

Having established that the assay had acceptable performance, the study was run to completion. Retention times were reasonably stable, but minor daily fluctuations (~4-5 minutes) meant that the 2-minute scheduling windows for each peptide needed manual adjustment after each injection to ensure that the mass spectrometer was monitoring for the right precursor at the right time in each subsequent injection. Of note, large changes in ambient temperature (e.g. freezing winter conditions) meant that retention times could shift by up to 5 minutes per day. It was unclear whether the general drift upwards of retention times was due to ambient temperature or other variables (like device cleanliness) (Figure 4-9).



**Figure 4-9: Fluctuation of retention times for a typical peptide over the course of the study**

The column needed replacing twice during the course of the study, which also resulted in a change in retention times. Columns from different manufacturing batches led to differing absolute ion intensities; however, normalized values (i.e. LH ratios) were unaffected by this variability (Figure 4-10).



**Figure 4-10: Systematic change in absolute ion intensities due to chromatographic column changes did not affect light:heavy ratio measurements**



#### **4.5.1.4 Correlation between Discovery Study Protein abundances vs. Surrogate Peptide abundances**

Light/Heavy ratio results obtained in duplicate were averaged and this value was used as the measured value for the peptide. There was overall acceptable correlation between the protein abundances in the discovery study and the surrogate peptide abundances. In total, 12 discovery proteins had acceptable correlation with their peptide surrogates in the verification study, but 4 proteins did not correlate at all. Tables 4-3 to 4-7 show the correlations between the discovery study and verification study. As expected (given the sample preparation method for the verification study), PRMs mostly correlated well with CSH-workflow protein abundances, but TSP1 correlated much better with EV-workflow protein abundances.

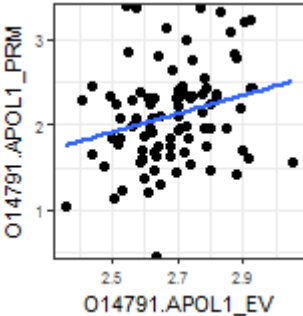
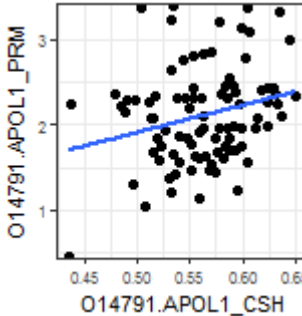
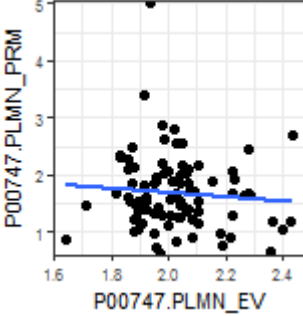
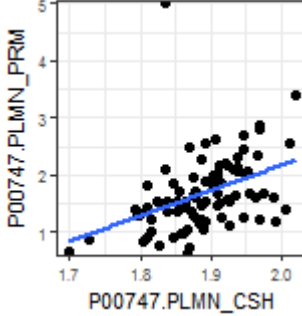
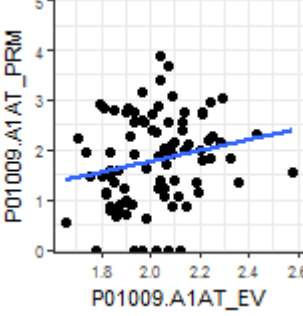
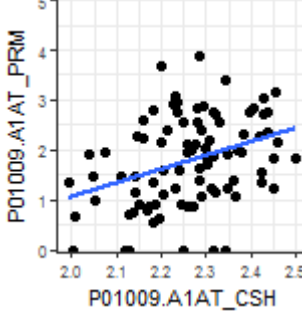
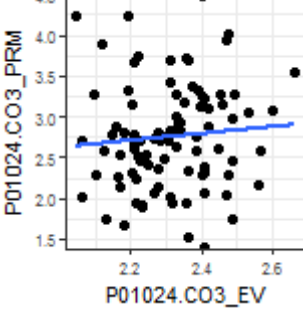
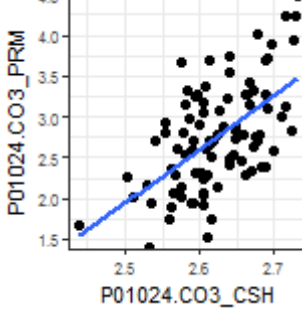
Uniprot	Protein	EV		CSH	
		rho	p	rho	p
O14791	APOL1	0.26	<b>0.012</b>	0.23	<b>0.029</b>
					
P00747	PLMN	-0.07	0.506	0.49	<b>&lt;0.001</b>
					
P01009	A1AT	0.28	<b>0.006</b>	0.36	<b>0.001</b>
					
P01024	CO3	0.11	0.309	0.52	<b>&lt;0.001</b>
					

Table 4-3: Scatterplots comparing PRM assay results with EV and CSH protein abundances (n=92); where two peptides were measured in PRM assays, their abundances were averaged for correlation; PRM: parallel reaction monitoring, EV: extracellular vesicle workflow, CSH: calcium silicate hydrate workflow, rho: Spearmann correlation coefficient, p: p.value- p<0.05 taken as significant

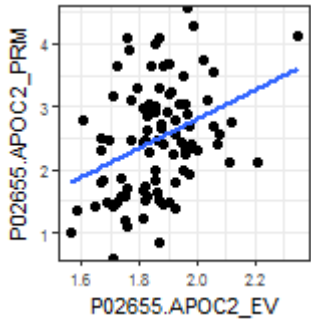
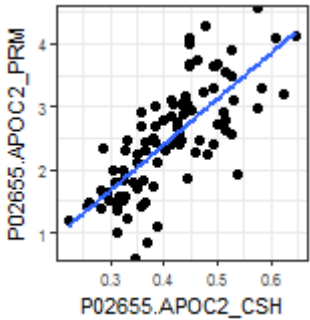
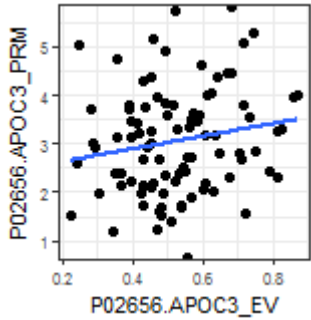
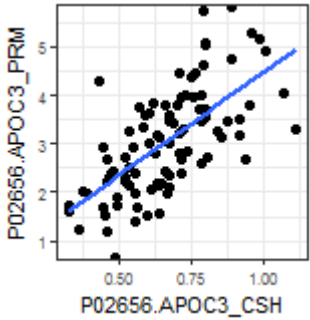
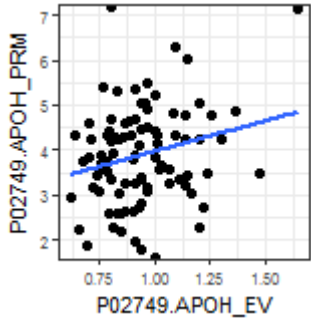
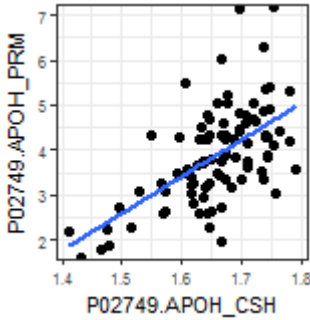
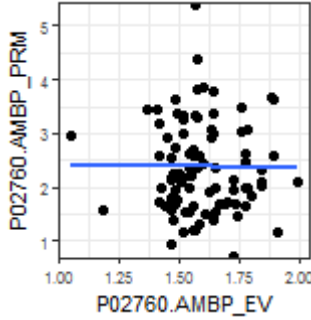
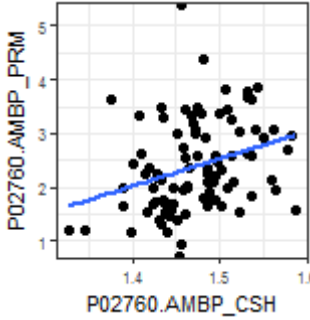
Uniprot	Protein	EV		CSH	
		rho	p	rho	p
P02655	APOC2	0.33	<b>0.001</b>	0.78	<b>&lt;0.001</b>
					
P02656	APOC3	0.18	0.081	0.68	<b>&lt;0.001</b>
					
P02749	APOH	0.16	0.12	0.56	<b>&lt;0.001</b>
					
P02760	AMBP	0.02	0.814	0.35	<b>&lt;0.001</b>
					

Table 4-4: Scatterplots comparing PRM assay results with EV and CSH protein abundances (n=92); where two peptides were measured in PRM assays, their abundances were averaged for correlation; PRM: parallel reaction monitoring, EV: extracellular vesicle workflow, CSH: calcium silicate hydrate workflow, rho: Spearmann correlation coefficient, p: p.value- p<0.05 taken as significant

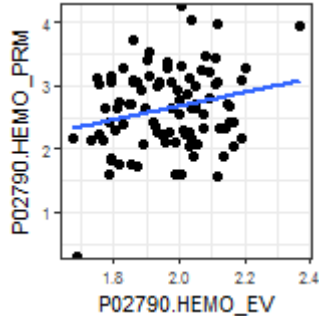
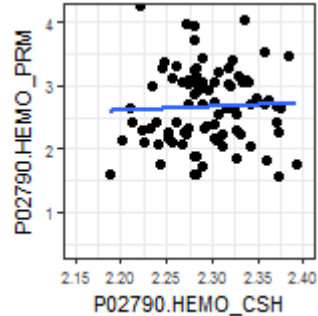
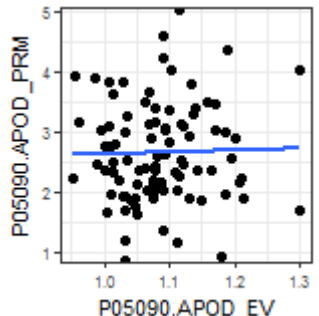
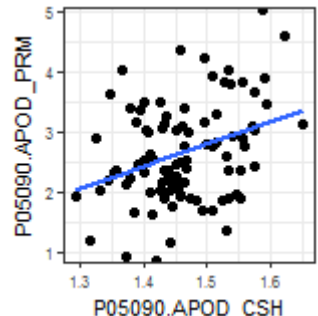
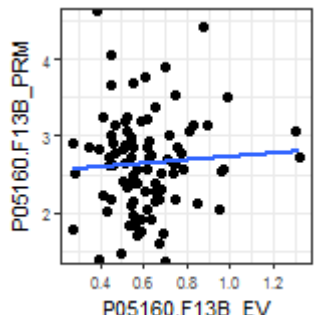
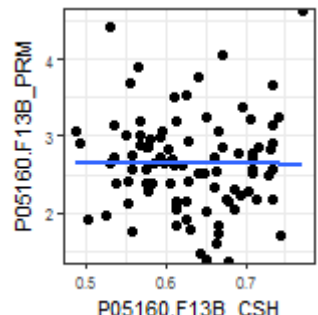
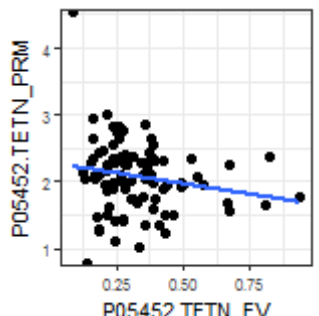
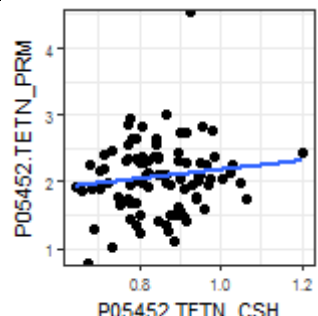
Uniprot	Protein	EV		CSH	
		rho	p	rho	p
P02790	HEMO	0.15	0.163	0.09	0.406
					
P05090	APOD	0.04	0.701	0.27	<b>0.01</b>
					
P05160	F13B	-0.01	0.917	-0.05	0.611
					
P05452	TETN	-0.19	0.073	0.07	0.491
					

Table 4-5: Scatterplots comparing PRM assay results with EV and CSH protein abundances (n=92); where two peptides were measured in PRM assays, their abundances were averaged for correlation; PRM: parallel reaction monitoring, EV: extracellular vesicle workflow, CSH: calcium silicate hydrate workflow, rho: Spearmann correlation coefficient, p: p.value- p<0.05 taken as significant

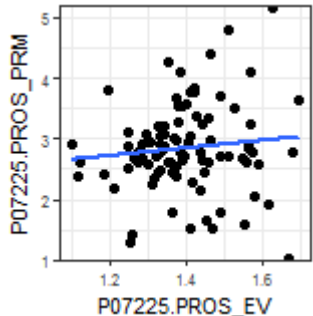
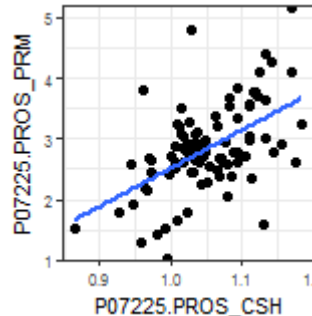
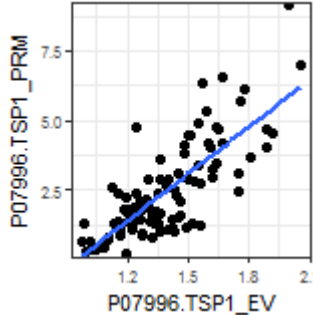
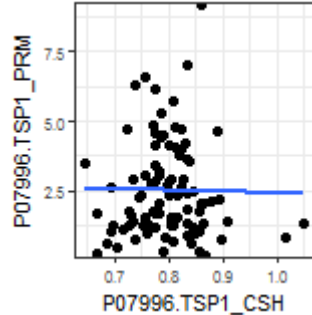
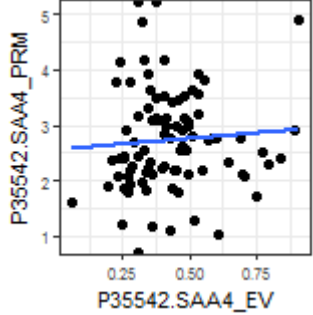
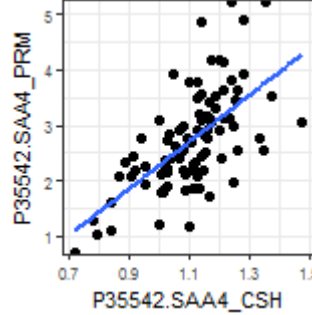
Uniprot	Protein	EV		CSH	
		rho	p	rho	p
P07225	PROS	0.13	0.217	0.47	<0.001
					
P07996	TSP1	0.75	<0.001	-0.03	0.777
					
P35542	SAA4	0.12	0.256	0.65	<0.001
					

Table 4-6: Scatterplots comparing PRM assay results with EV and CSH protein abundances (n=92); where two peptides were measured in PRM assays, their abundances were averaged for correlation; PRM: parallel reaction monitoring, EV: extracellular vesicle workflow, CSH: calcium silicate hydrate workflow, rho: Spearman correlation coefficient, p: p-value- p<0.05 taken as significant

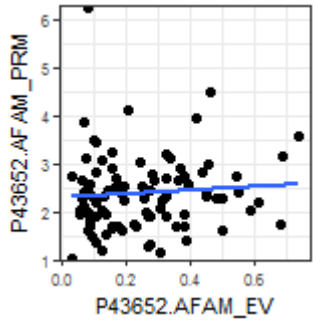
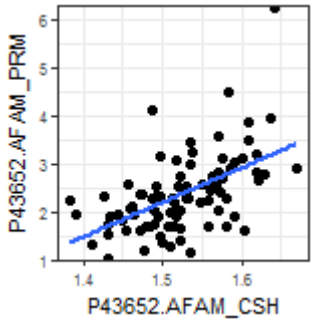
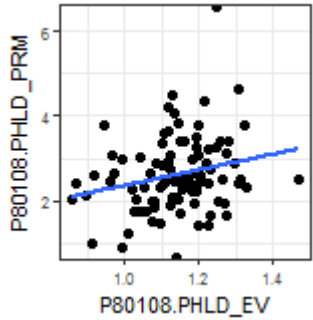
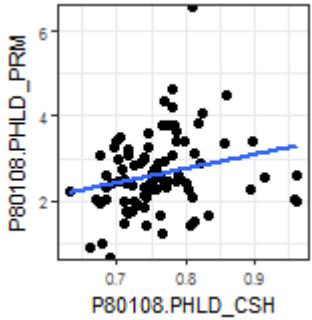
Uniprot	Protein	EV		CSH	
		rho	p	rho	p
P43652	AFAM	0.09	0.372	0.57	<b>&lt;0.001</b>
					
P80108	PHLD	0.22	<b>0.033</b>	0.29	<b>0.005</b>
					

Table 4-7: Scatterplots comparing PRM assay results with EV and CSH protein abundances (n=92); where two peptides were measured in PRM assays, their abundances were averaged for correlation; PRM: parallel reaction monitoring, EV: extracellular vesicle workflow, CSH: calcium silicate hydrate workflow, rho: Spearmann correlation cooefficient, p: p.value- p<0.05 taken as significant

#### **4.5.2 Baseline Characteristics of patients**

168 patients were included in the analyses, with an average follow-up time of  $368.7 \pm 156$  days (range 181-791). Of these, 67 (39.9%) had severe AS, 41 (24.4%) were female and 54 (32.1%) tested positive on exercise testing. During the follow-up period, there were 58 (34.5%) events. Of these only 46 were spontaneous events (primary outcome), the others had asymptomatic (prophylactic) AVR (competing events). There was 1 death and 5 hospitalisations (1 syncope, 1 chest pain, 2 dyspnoea, 1 HF). Competing events were not included in the primary outcome.

As expected, those with severe AS had lower AVAs but higher MPG and AV-Vmax (Table 4-8). The calcium scores and hsTNI was also higher. There was also more remodelling (mass and remodelling) in the severe AS group. Notably markers of fibrosis (LGE and ECV were both similar between the two groups. MPR was lower in the severe AS group, and the event rate in the severe AS group was almost twice as high.

In comparing the discovery cohort and the whole cohort used for verification (Table 4-9); there were 92 patients in the discovery cohort, but 168 patients in the whole cohort. There were proportionally more females, severe AS, positive exercise tests, slightly higher natriuretic peptide levels and endpoints in the discovery cohort compared to the verification cohort. In short, the main difference between the two cohorts is the verification cohort had more moderate AS.

	Moderate AS (n=101)	Severe AS (n=67)	p value
Age	65±14.15	68±12.41	0.197
Female (%)	23 (22.8%)	18 (26.9%)	0.585
Diabetes (%)	12 (11.9%)	12 (17.9%)	0.368
Hypertension (%)	57 (56.4%)	34 (50.7%)	0.528
Haemoglobin (g/dL)	14.32±1.20	14.09±1.26	0.244
eGFR (mL/min/1.72m <sup>2</sup> )	87.65±29.01	87.78±28.66	0.977
BMI (kg/m <sup>2</sup> )	27.99±3.80	27.89±4.66	0.875
Systolic blood pressure (mmHg)	146±21	149±21.2	0.54
Diastolic blood pressure (mmHg)	78±11	77±10.4	0.722
Positive exercise test (%)	33 (32.7%)	21 (31.3%)	1
Stroke volume index (ml/m <sup>2</sup> )	46.98±10.19	51.33±13.18	0.018
Valve area (cm <sup>2</sup> )	1.18±0.28	1.01±0.32	<0.001
Valve area index (cm <sup>2</sup> /m <sup>2</sup> )	0.60±0.13	0.52±0.14	<0.001
Peak velocity (m/s)	3.50±0.25	4.42±0.44	<0.001
Mean pressure gradient (mmHg)	28.11±5.06	46.77±12.05	<0.001
AV Calcium Score (AU)	1601 [1006, 2196]	2956 [1743, 4249]	<0.001
Males Only	1774 [1322, 2604]	3208 [2349, 4502]	<0.001
Females Only	776 [298, 1132]	1829 [1301, 2561]	<0.001
AV Calcium Index	0.84 [0.59, 1.22]	1.58 [1.12, 2.18]	<0.001
Hs Troponin (pg/mL)	5.00 [2.77, 9.27]	7.08 [5.09, 11.18]	0.002
NTproBNP (pmol/L)	54.09 [16.75, 136.04]	67.07 [21.36, 227.11]	0.213
LVEF	56.54±4.54	56.84±5.31	0.697
LVEDVI (mL/m <sup>2</sup> )	86.10±15.79	88.97±20.60	0.309
LVESVI (mL/m <sup>2</sup> )	37.70±9.38	38.80±11.68	0.501
LVMi (g/m <sup>2</sup> )	54.28±11.49	62.61±15.36	<0.001
LVM/LVEDV (g/mL)	0.64±0.10	0.71±0.11	<0.001
Extracellular volume fraction	25.04±2.38	24.66±2.50	0.415
Late gadolinium enhancement (%)	46 (45.5%)	34 (50.7%)	0.531
Myocardial perfusion reserve	2.44±0.69	1.98±0.57	<0.001
Primary Outcome (%)	20 (19.8%)	26 (38.8%)	0.008

**Table 4-8: Baseline characteristics of patients grouped by AS severity; eGFR: estimated glomerular filtration rate, AS: aortic stenosis, AV: aortic valve, AU: arbitrary units, LV: left ventricular, EDVI: end diastolic volume index, ESVI: end systolic volume index, MI: mass index, LVM/LVEDV: ratio of LV mass to LV end diastolic volume**



	Discovery Cohort, n=92	Whole cohort, n=168
Age	68±11	66±13
Female (%)	33 (36.3%)	41 (24.4%)
Diabetes (%)	11 (12.1%)	24 (14.3%)
Hypertension (%)	50 (54.9%)	91 (54.2%)
Haemoglobin (g/dL)	13.9±1.2	14.2±1.2
eGFR (mL/min/1.73m <sup>2</sup> )	82.6±23.3	87.7±28.8
Body mass index (kg/m <sup>2</sup> )	27.3±3.8	27.9±4.2
Systolic blood pressure (mmHg)	147±22	147±21
Diastolic blood pressure (mmHg)	76±10	77±11
Positive ETT (%)	38 (41.8%)	54 (32.1%)
Stroke volume index (mL/m <sup>2</sup> )	50.21±12.60	48.72±11.64
Valve area (cm <sup>2</sup> )	1.05±0.29	1.11±0.31
Valve area index (cm <sup>2</sup> /m <sup>2</sup> )	0.55±0.14	0.57±0.14
Peak velocity (m/s)	4.05±0.59	3.87±0.56
Mean pressure gradient (mmHg)	39.23±13.48	35.55±12.52
Severe AS (%)	46 (50%)	67 (40%)
AV calcium score (AU)	2071 [1278, 2929]	1899 [1206, 3022]
AV calcium index	1.12 [0.8, 1.58]	1.07 [0.69, 1.65]
Hs Troponin (pg/mL)	5.8 [3.4, 11.3]	5.6 [3.3, 10.6]
NTproBNP (pmol/L)	79 [22, 232]	57 [20, 158]
LV ejection fraction	57±5	57±5
LVEDVI (mL/m <sup>2</sup> )	85.45±16.88	87.25±17.86
LVESVI (mL/m <sup>2</sup> )	36.88±10.16	38.14±10.34
LVMi (g/m <sup>2</sup> )	57.15±12.61	57.60±13.75
LVM/LVEDV (g/mL)	0.68±0.12	0.66±0.11
Extracellular volume fraction	25.5±2.5	24.9±2.4
Late gadolinium enhancement (%)	44 (48.4%)	80 (47.6%)
Myocardial perfusion reserve	2.21±0.66	2.25±0.68
Primary outcome (%)	46 (50.5%)	46 (27.4%)

**Table 4-9: Comparison between discovery cohort and whole cohort for verification; eGFR: estimated glomerular filtration rate, AS: aortic stenosis, AV: aortic valve, AU: arbitrary units, LV: left ventricular, EDVI: end diastolic volume index, ESVI: end systolic volume index, MI: mass index, LVM/LVEDV: ratio of LV mass to LV end diastolic volume**

#### 4.5.3 Prognostic baseline characteristics to outcome on cox regression

As expected, higher gradients and lower valve area were strongly associated with the endpoint, and accordingly, being classified as ‘severe AS’ was also strongly associated with the endpoint. High sensitivity troponin I was not associated with the endpoint, whilst higher NTproBNP and a positive exercise test were (Table 4-10). AV Calcium Index, a sex-adjusted

measure of aortic valve calcification, was also associated with the endpoint. Finally, lower myocardial perfusion reserve was also associated with the endpoint. A lower eGFR and haemoglobin were also weakly associated with the endpoint.

	<sup>1</sup> HR (95% CI for HR)	p	<sup>2</sup> HR (95% CI for HR)	p
Age	1 (0.99-1)	0.19	1.02 (0.99-1.04)	0.21
Female	2.1 (1.2-3.8)	0.015	2.22 (1.20-4.13)	0.011
Diabetes	1.1 (0.48-2.4)	0.87	1.07 (0.47-2.47)	0.87
Hypertension	0.86 (0.48-1.5)	0.6	0.87 (0.49-1.55)	0.63
Haemoglobin	0.80 (0.63-1)	0.056	0.78 (0.61-0.99)	0.042
eGFR	0.99 (0.97-1)	0.041	0.99 (0.98-1.00)	0.016
Body mass index (per kg/m <sup>2</sup> )	0.96 (0.89-1)	0.25	0.96 (0.89-1.03)	0.27
Systolic blood pressure	0.98 (0.96-1)	0.26	0.98 (0.95-1.01)	0.19
Diastolic blood pressure	1 (0.99-1)	0.94	1 (0.98-1.01)	0.9
Positive exercise test	2.1 (1.15-3.68)	0.015	2.04 (1.16-3.60)	0.014
Stroke volume index (per ml/m <sup>2</sup> )	0.99 (0.97-1)	0.46	0.99 (0.97-1.02)	0.51
Valve area (per cm <sup>2</sup> )	0.071 (0.022-0.23)	<0.001	0.09 (0.02-0.34)	<0.001
Valve area index (per cm <sup>2</sup> /m <sup>2</sup> )	0.0056 (0.0005-0.063)	<0.001	0.01 (0.00-0.17)	0.001
Peak velocity (per m/s)	3.5 (2.1-5.7)	<0.001	3 (1.82-4.93)	<0.001
Mean pressure gradient (per mmHg)	1.1 (1-1.1)	<0.001	1.05 (1.03-1.07)	<0.001
Severe AS	2.7 (1.5-4.9)	<0.001	2.42 (1.36-4.29)	0.003
AV Calcium Index	1.5 (1.2-2.1)	0.003	1.47 (1.12-1.93)	0.005
Hs Troponin (per pg/mL)	0.99 (0.82-1.2)	0.9	0.97 (0.82-1.16)	0.76
NTproBNP (per pmol/L)	1.2 (1-1.4)	0.011	1.2 (1.04-1.37)	0.012
LV ejection fraction (per percent)	1 (0.95-1.1)	0.71	1.02 (0.96-1.08)	0.55
LVEDVI (per ml/m <sup>2</sup> )	0.99 (0.97-1)	0.29	0.99 (0.97-1.01)	0.22
LVESVI (per ml/m <sup>2</sup> )	0.99 (0.96-1)	0.34	0.98 (0.95-1.01)	0.27
LVMl (per g/m <sup>2</sup> )	1 (0.98-1)	1	1 (0.98-1.02)	0.8
LVM/LVEDV (per g/mL)	5.9 (0.53-66)	0.15	4.49 (0.37-54.89)	0.24
Extracellular volume fraction (per percent)	1.1 (0.97-1.3)	0.12	1.13 (0.98-1.31)	0.085
Late gadolinium enhancement	1.4 (0.76-2.4)	0.31	1.29 (0.73-2.28)	0.39
Myocardial perfusion reserve (per percent)	0.61 (0.39-0.97)	0.039	0.65 (0.42-1.01)	0.056

**Table 4-10: Univariate associations with the composite endpoint; 1Univariate Analysis using cox proportional hazards; 2Univariate Analysis using Fine-Grey proportional hazards for competing events; HR: hazard ratio, CI: confidence interval, eGFR: estimated glomerular filtration rate, AS: aortic stenosis, AV: aortic valve, AU: arbitrary units, LV: left ventricular, EDVI: end diastolic volume index, ESVI: end systolic volume index, MI: mass index, LVM/LVEDV: ratio of LV mass to LV end diastolic volume**

#### **4.5.4 Fine-Grey Univariate association of baseline characteristics for significant variables on univariate analysis**

The analyses of significant univariate associations were repeated with Fine-Grey proportional hazards regression for competing events to confirm whether competing events affected the results (Table 4-10). Largely the results remained unchanged, although for some ‘borderline’ variables, eg. eGFR and Haemoglobin, this change made the variables more ‘significant’, whilst making myocardial perfusion reserve lose its significance.

#### 4.5.5 Analysis of Kaplan-Meier curves of important risk factors

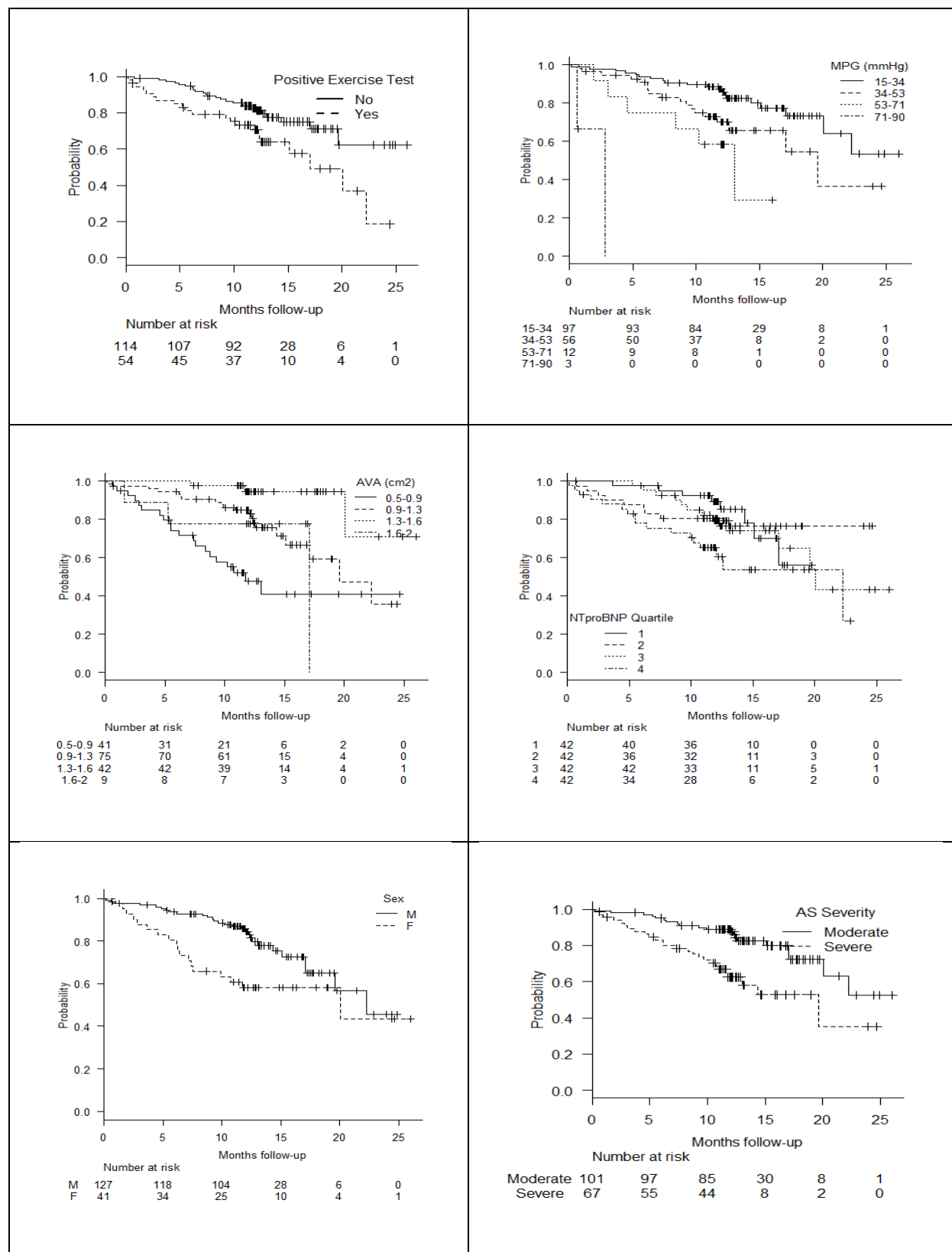


**Figure 4-11: Analysis of Kaplan-meier curves of important prognosticators in aortic stenosis. Curves refer to patients from the PRIMID-AS study. Clockwise from top left: Event-free Kaplan-Meier curves for positive exercise test; ranges of mean pressure gradient (MPG); NTproBNP quartiles; AS severity; sex and aortic valve area ranges. Crosses on curves indicate censoring.**

Kaplan-Meier analyses (Figure 4-11) suggest that the lowest-risk group are those that have a low MPG and high AVA, but with a negative exercise test. However a negative ETT was still associated with a ~ 40% event rate. Being male appeared to be associated with lower risk initially, but later the risk ‘catches up’ with females. Consistently, having severe AS was associated with 2.6x higher risk, compared to moderate AS. In cox models, being female was associated with double the risk (HR 2.04 (1.13-3.7) p 0.02) compared to males, after adjusting for severity.

#### **4.5.6 Baseline Model**

A multivariable model that appropriately reflected the existing risk needed to contain some measure of AS severity, exercise testing and sex (Table 4-11). A stepwise selection approach based on Akaike Information Criterion with a combination of these markers showed that continuous measures of valve area and mean pressure gradients was better compared to the binary “Severe AS” (Model 2 better fit than Model 3), and when present in the same model together (Model 4), stepwise selection resulted in a compact model (Model 2) that excluded the binary “Severe AS” variable.

	Model 1		Model 2		Model 3		Model 4	
	HR (95% CI)	p	HR (95% CI)	p	HR (95% CI)	p	HR (95% CI)	p
Female	1.81 (0.89-3.69)	0.1	-	-	1.86 (1.02-3.41)	0.043	1.44 (0.78-2.64)	0.24
Haemoglobin	1.18 (0.88-1.59)	0.28	-	-	-	-	-	-
eGFR	1.00 (0.98-1.01)	0.81	-	-	-	-	-	-
Positive ETT	2.02 (1.11-3.70)	0.022	1.83 (1.02-3.30)	0.044	1.98 (1.09-3.60)	0.025	1.83 (1.01-3.32)	0.047
AVA	0.18 (0.05-0.69)	0.012	0.16 (0.05-0.59)	0.006	-	-	0.18 (0.05-0.67)	0.011
MPG	1.05 (1.02-1.07)	<0.001	1.04 (1.02-1.07)	<0.001	-	-	1.05 (1.01-1.08)	0.006
NTproBNP	1.13 (0.96-1.33)	0.14	1.12 (0.97-1.28)	0.12	1.14 (0.99-1.31)	0.062	1.12 (0.97-1.28)	0.11
Severe AS	-	-	-	-	2.36 (1.21-4.62)	0.012	0.89 (0.35-2.30)	0.82
AV Calcium Index	-	-	-	-	1.33 (0.95-1.85)	0.097	-	-
Harrell's C	0.772		0.764		0.74		0.773	
R <sup>2</sup>	0.245		0.227		0.162		0.234	

**Table 4-11: Developing a compact model reflecting baseline risk; eGFR: estimated glomerular filtration rate, ETT: exercise tolerance test, AVA: Aortic valve area, MPG: mean pressure gradient, AS: aortic stenosis, AV: aortic valve; A selection of multivariable models:-**

**Model 1:** all significant variables on univariate analyses entered into Cox model;

**Model 2:** compact model from stepwise selection, from Model 1 and Model 4;

**Model 3:** An example of a model that included AV Calcium Index in the absence of MPG or AVA; stepwise regression did not remove any of the variables in the model, but addition of MPG to the model led to removal of both the AV Calcium Index and Severe AS variable;

**Model 4:** Variables entered into model to illustrate that more information was present in AVA and MPG leading to removal of “Severe AS” and sex from the model on stepwise selection (Model 2).

However, as clinicians make many decisions based on established cut-offs, subsequent analyses included one model with “Severe AS” as the variable representing AS-severity, and another containing both MPG and AVA but not Severe AS to achieve this.

#### **4.5.7 Baseline values of targeted peptides/proteins grouped by AS Severity**

The measured values of the targeted peptides were largely similar between moderate AS and severe AS, except for Factor 13B, Apolipoprotein L1 and Protein AMBP, all of which were lower in severe AS than moderate AS (Table 4-12 and Figure 4-12).

#### **4.5.8 Univariate Association of targeted peptides/proteins to composite outcome**

Out of the 20 peptides tested, there was only one which was significantly associated with the endpoint, which was the surrogate for apolipoprotein D (Table 4-12 and Figure 4-13). This was confirmed on Fine Grey proportional hazards regression for competing events, with similar hazard ratios. Higher APOD (dichotomised by its median value) was associated with a higher incidence of the composite endpoint, but not competing events (p 0.51). Cumulative incidence curves illustrate the proportional increase in risk if APOD was  $\geq$  median levels (Figure 4-13). Alternatively, similar results were seen when APOD was dichotomized by its optimal thresholds on a ROC curve (Figure 4-14).

#### **4.5.9 Multivariable analysis**

Adding APOD to the baseline model showed that it remained independently prognostic (Table 4-13). The findings were replicated in Fine-Grey analyses. Substituting Severe AS for MPG and AVA did not reduce the prognostic ability of APOD. In fact, on stepwise selection, NTproBNP was not retained, whilst APOD was, both when using Severe AS or AVA and MPG. These imply that APOD was a stronger prognosticator of the composite endpoint in asymptomatic AS compared to NTproBNP.

UniprotID	Protein	Name	Peptide	Moderate AS (n=101)	Severe AS (n=67)	<sup>§</sup> p value	&HR (95% CI)	&p value
P01009	A1AT	Alpha 1 Antitrypsin	DTEEDFHVDQVTTVK	2.38 (4.48)	2.50 (3.99)	0.86	0.98 (0.89-1.1)	0.69
P43652	AFAM	Afamin	IAPQLSTEELVSLGEK	2.52 (0.76)	2.33 (0.83)	0.134	0.92 (0.63-1.3)	0.66
P02760	AMBP	Protein AMBP	VVAQGVGIPEDSIFTMADR	2.53 (0.90)	2.20 (0.79)	0.017	0.99 (0.71-1.4)	0.97
P02655	APOC2	Apolipoprotein C2	TYLPAVDEK	2.52 (0.88)	2.33 (0.90)	0.178	0.93 (0.67-1.3)	0.65
P02656	APOC3	Apolipoprotein C3	DALSSVQESQVAQQAR	2.73 (1.17)	2.46 (1.03)	0.125	0.95 (0.73-1.2)	0.68
P02656	APOC3	Apolipoprotein C3	GWVTDGFSSLK	3.51 (1.59)	3.24 (1.28)	0.24	0.96 (0.79-1.2)	0.71
P05090	APOD	Apolipoprotein D	MTVTDQVNC PK	2.56 (0.67)	2.51 (0.90)	0.648	1.7 (1.2-2.4)	0.002
P02749	APOH	B2Glycoprotein	ATFGCHDGYSLDGPEEIECTK	3.85 (1.06)	3.79 (1.21)	0.707	0.95 (0.73-1.2)	0.68
O14791	APOL1	Apolipoprotein L1	VTEPISAESGEQVER	2.28 (0.62)	2.08 (0.64)	0.041	0.98 (0.62-1.6)	0.93
P01024	CO3	Complement C3	IPIEDGSGEVLSR	2.47 (0.58)	2.39 (0.64)	0.425	0.85 (0.53-1.4)	0.51
P01024	CO3	Complement C3	TVMVNIENPEGIPVK	3.38 (1.04)	3.25 (1.13)	0.45	0.85 (0.64-1.1)	0.26
P05160	F13B	Factor 13B	VLHGDLDIFVCK	2.67 (0.67)	2.44 (0.65)	0.026	1 (0.68-1.6)	0.84
P02790	HEMO	Hemopexin	DYFMPCPGR	2.74 (1.12)	2.62 (0.90)	0.474	1.2 (0.91-1.5)	0.22
P02790	HEMO	Hemopexin	GECQAEGVLFFQGDR	2.47 (0.57)	2.30 (0.65)	0.07	1.3 (0.78-2.1)	0.34
P80108	PHLD	Phospholipase D	TLLLVGSPTWK	2.76 (0.86)	2.58 (0.92)	0.201	1 (0.72-1.4)	0.99
P00747	PLMN	Plasminogen	LYDYCDVPQCAAPSFDCGKPQVEPK	1.66 (0.65)	1.65 (0.72)	0.976	0.87 (0.56-1.3)	0.52
P07225	PROS	Protein S	DVDECSLKPSICGTAVCK	2.84 (0.76)	2.74 (0.77)	0.383	1.2 (0.84-1.8)	0.27
P35542	SAA4	Serum Amyloid A4	EALQGVGDMGR	2.72 (0.84)	2.49 (0.86)	0.081	1.1 (0.8-1.5)	0.56
P05452	TETN	Tetranectin	LDTLAQEVALLK	2.14 (0.53)	2.09 (0.65)	0.59	1.2 (0.75-1.9)	0.43
P07996	TSP1	Thrombospondin 1	TIVTTLQDSIR	2.73 (1.85)	2.36 (1.84)	0.208	0.91 (0.77-1.1)	0.3

**Table 4-12: Comparison between mean levels of peptides measured in moderate and severe AS, and univariate association with the endpoint; means expressed as mean (standard deviation); <sup>§</sup> refers to p value for differences between group means in Moderate and Severe AS; & refers to hazard ratios (95% confidence interval) and p values for univariate association with the composite endpoint**



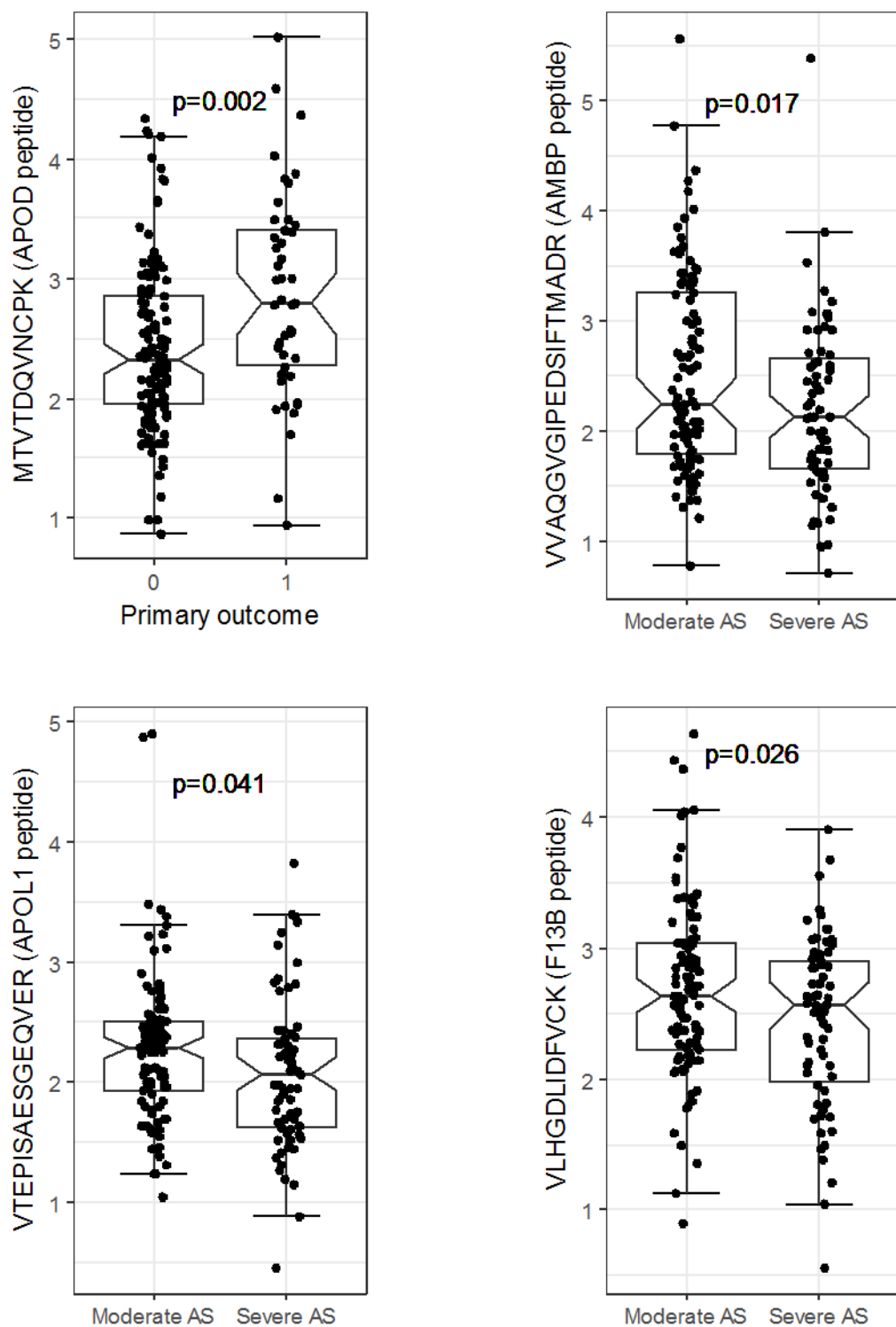


Figure 4-12: Box/Dotplots for significantly different peptides; APOD – apolipoprotein D, APOL1 – apolipoprotein L1, AMBP – protein AMBP, F13B – factor 13B, p-values <0.05 taken as significant

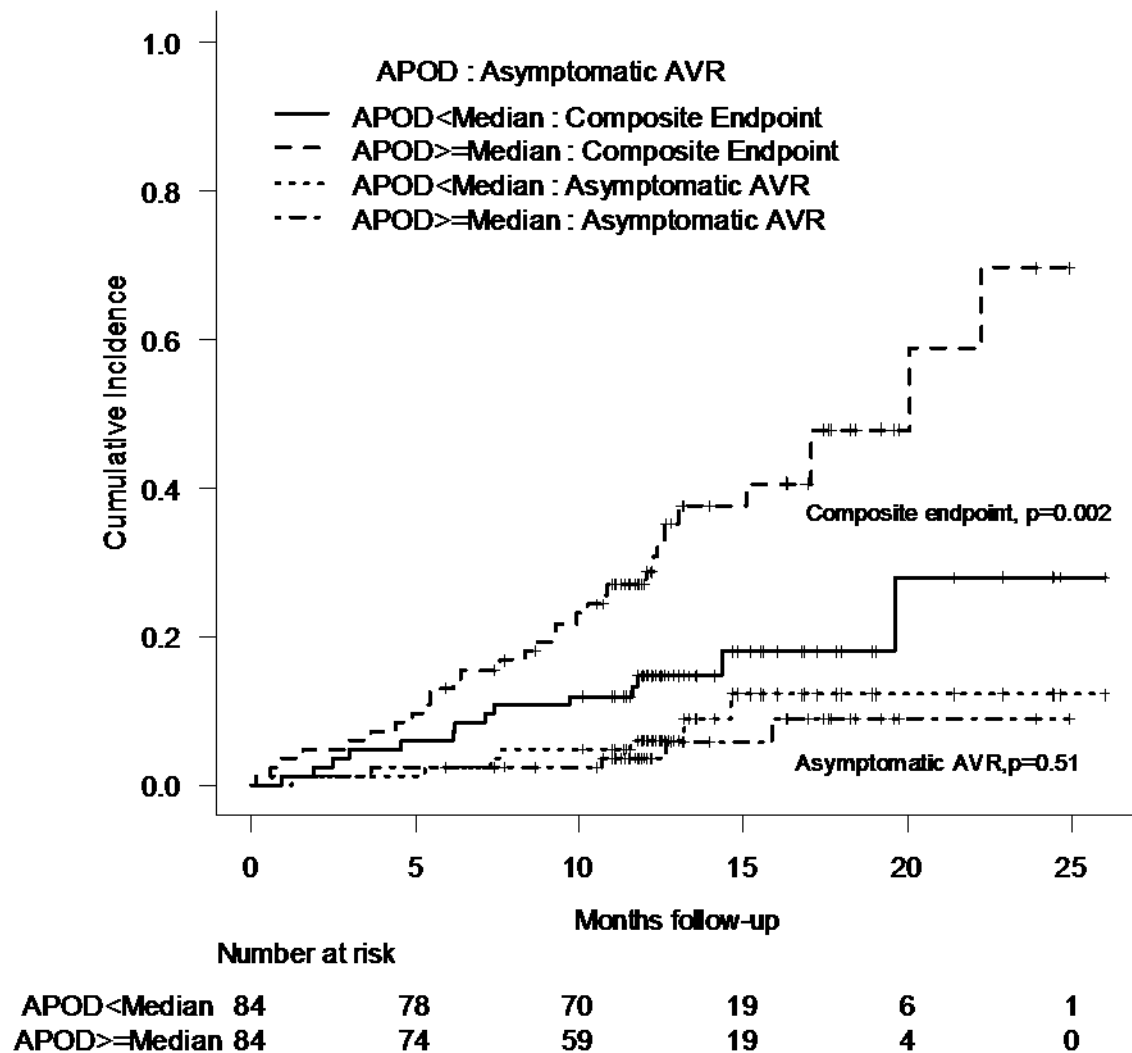


Figure 4-13: Cumulative incidence of competing events dichotomized by APOD median; p.values of difference between time to event for APOD values above and below median; tick-marks indicate censoring

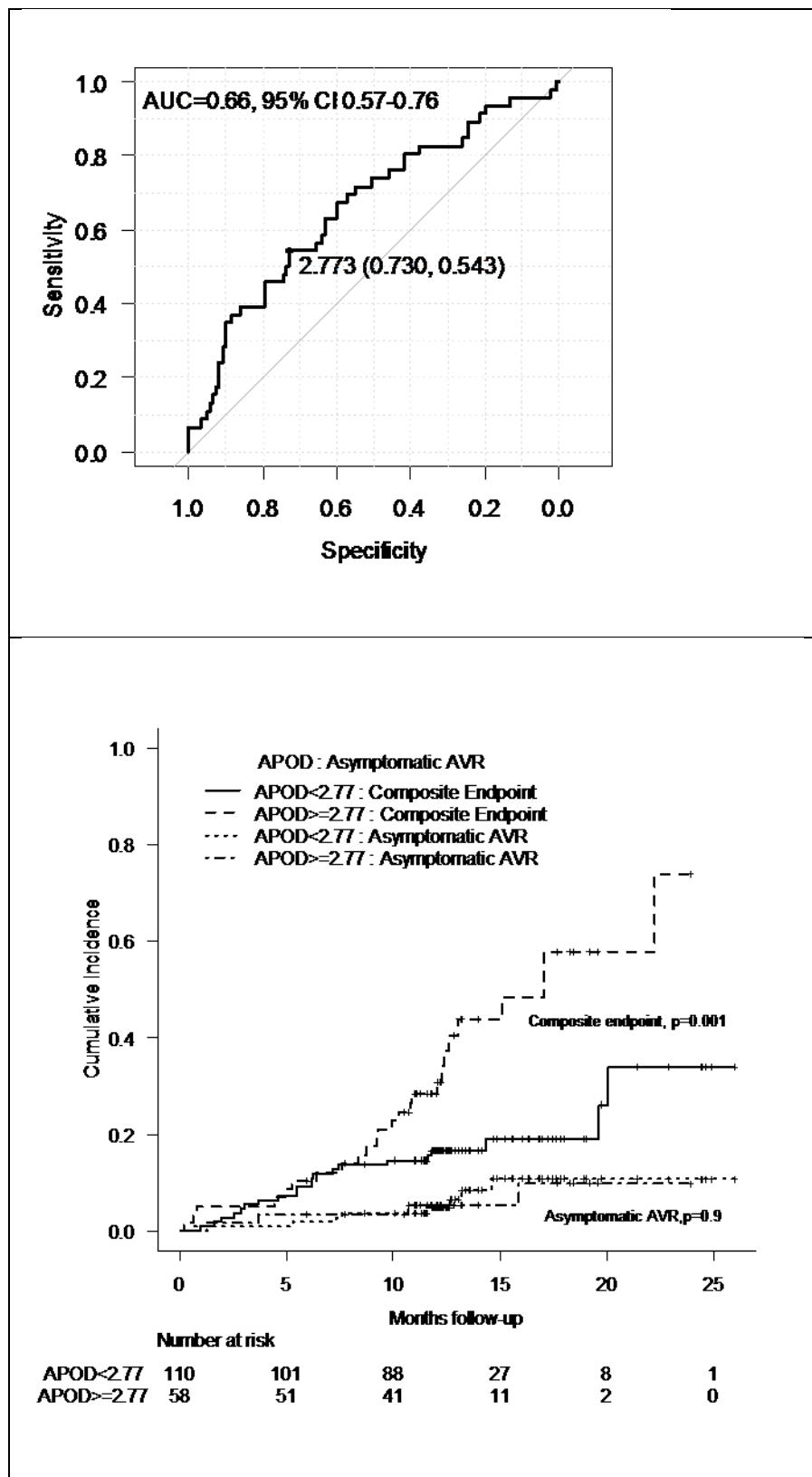


Figure 4-14: Cumulative incidence plot of competing events for APOD dichotomized by optimal thresholds; top box – receiver operating curves to derive optimal thresholds for APOD peptide, AUC = area under the curve, annotated point showing the threshold at which the sum specificity and sensitivity were maximal for the composite endpoint, bottom box – cumulative incidence plot for APOD dichotomized by optimal threshold; p.values of difference between time to event for APOD values above and below thresholds; tick-marks indicate censoring

	Model 1		Model 2		Model 3		Model 4		Model 5	
	Hazard Ratio	p value	Hazard Ratio	p value	Hazard Ratio	p value	Hazard Ratio	p value	Hazard Ratio	p value
Female	2.08 (1.13-3.82)	<b>0.019</b>	2.33 (1.24-4.38)	<b>0.009</b>	1.75 (0.93-3.32)	0.084	1.82 (0.96-3.45)	0.068	2.23 (1.22-4.07)	<b>0.0092</b>
Positive ETT	2.43 (1.30-4.52)	<b>0.0052</b>	2.38 (1.28-4.43)	<b>0.0062</b>	2.12 (1.16-3.87)	<b>0.015</b>	2.22 (1.22-4.03)	<b>0.009</b>	2.62 (1.42-4.83)	<b>0.0021</b>
Severe AS	2.94 (1.59-5.46)	<b>0.0006</b>	2.56 (1.4-4.69)	<b>0.0023</b>	-	-	-	-	3.01 (1.63-5.57)	<b>0.0005</b>
NTproBNP	1.09 (0.94-1.26)	0.25	1.08 (0.94-1.25)	0.26	1.07 (0.92-1.23)	0.39	-	-	-	-
APOD	1.71 (1.22-2.39)	<b>0.0019</b>	1.75 (1.29-2.37)	<b>0.0004</b>	1.51 (1.05-2.17)	<b>0.025</b>	1.60 (1.14-2.25)	<b>0.0073</b>	1.83 (1.33-2.53)	<b>0.0002</b>
AVA	-	-	-	-	0.28 (0.07-1.07)	0.062	0.28 (0.07-1.08)	0.065	-	-
MPG	-	-	-	-	1.04 (1.02-1.07)	<b>0.0002</b>	1.05 (1.02-1.07)	<b>&lt;0.0001</b>	-	-

**Table 4-13: Prognostic independence of APOD against baseline variables, APOD retained in all models on stepwise selection implying it was a strong prognosticator; AVA: aortic valve area, MPG: mean pressure gradient, AS: aortic stenosis, ETT: exercise tolerance test**

**Model 1: Cox model with variables on enter;**

**Model 2: Fine-Grey model with variables on enter,**

**Model 3: Same as Model 1 but with Severe AS substituted with AVA and MPG;**

**Model 4: Forward selection from Model 3;**

**Model 5: Forward selection from Model 1**

#### 4.5.10 Subgroup Analyses

Subgroup analyses revealed that APOD was more prognostic in moderate AS and/or males (Figure 4-15). Tests for heterogeneity were positive with moderate AS but not for sex. APOD was prognostic regardless of whether exercise tests were positive. APOD levels were higher in males who did have an event compared to those that did not, whilst this was not seen in females (Figure 4-16).

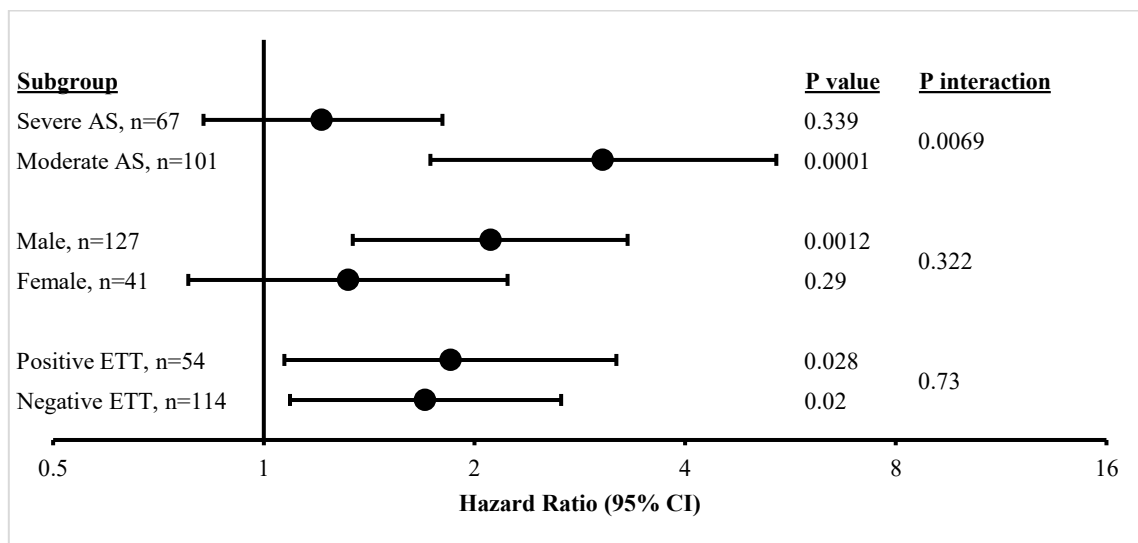


Figure 4-15: Forest plot of hazard ratios for APOD in different subgroups

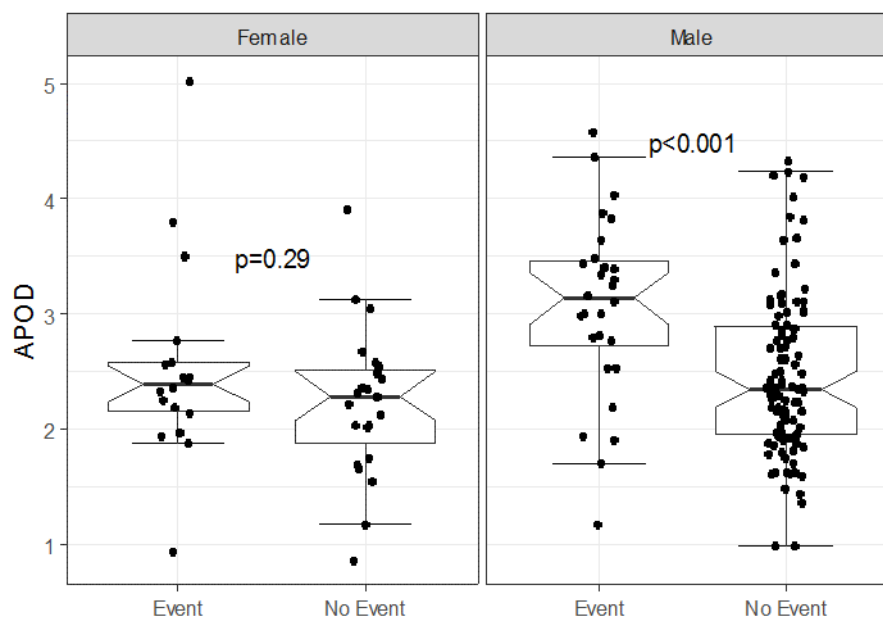


Figure 4-16: APOD levels were higher in males with events but not different between females with or without events

#### 4.5.11 Risk Stratification in moderate AS

Variables that interacted with AS severity (“SevereAS”) were limited to MPG, Stroke Volume Index and APOD (p-interaction 0.001, 0.014 and 0.007 respectively) (Table 4-14). Subgroup analyses based on these variables indicated that MPG was more prognostic in the moderate group, as was APOD, whilst stroke volume index (SVI) was more prognostic in the severe group.

	Moderate AS	Severe AS	p-interaction
Mean pressure gradient	1.27 (1.14-1.42) p<0.01	1.04 (1.01-1.08) p=0.02	0.001
APOD	3.05 (1.73-5.4) p<0.01	1.21 (0.82-1.8) p=0.3	0.007
Stroke volume index	1.02 (0.98-1.07) p=0.33	0.96 (0.92-0.99) p=0.01	0.014

**Table 4-14: All variables interacting with AS severity; Hazard ratios and 95% confidence intervals within subgroups of Moderate and Severe AS**

This suggested that further risk stratification could be performed in the moderate AS subgroup, both with MPG and APOD.

Receiver operating curves were constructed for MPG and APOD in the moderate AS subgroup (Figure 4-17). The AUC for MPG and APOD were 0.79 and 0.8 respectively. The optimal cut-off value for MPG for further risk stratification in the moderate group was 30mmHg. The optimal cut-off value for APOD was 2.77, which was slightly above the median for the moderate group.

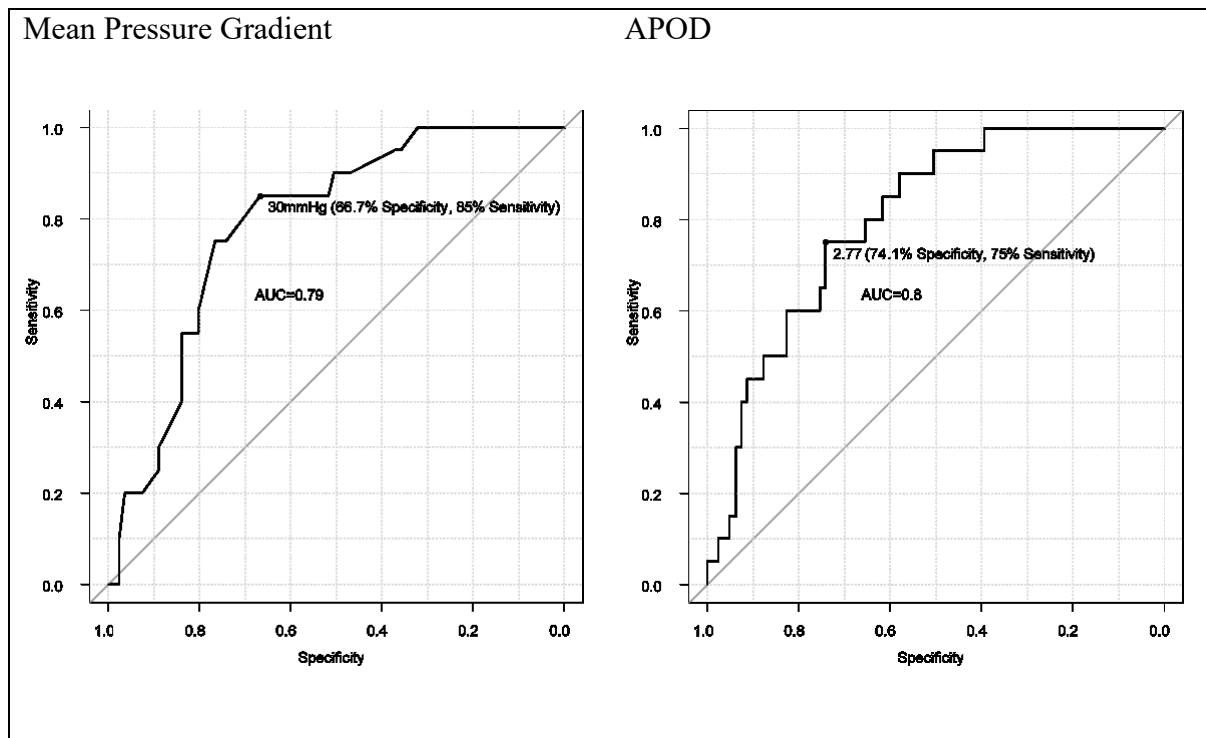


Figure 4-17: Receiver operating characteristic curves for mean pressure gradient and APOD in the moderate AS group, with optimal cut-offs shown; AUC: area under the curve

In the moderate AS group, therefore, the group with MPG  $\geq$  30mmHg had a higher risk of the endpoint. Higher APOD measurements (in this case  $\geq$  2.77) was also associated with substantially higher risk (Figure 4-18).

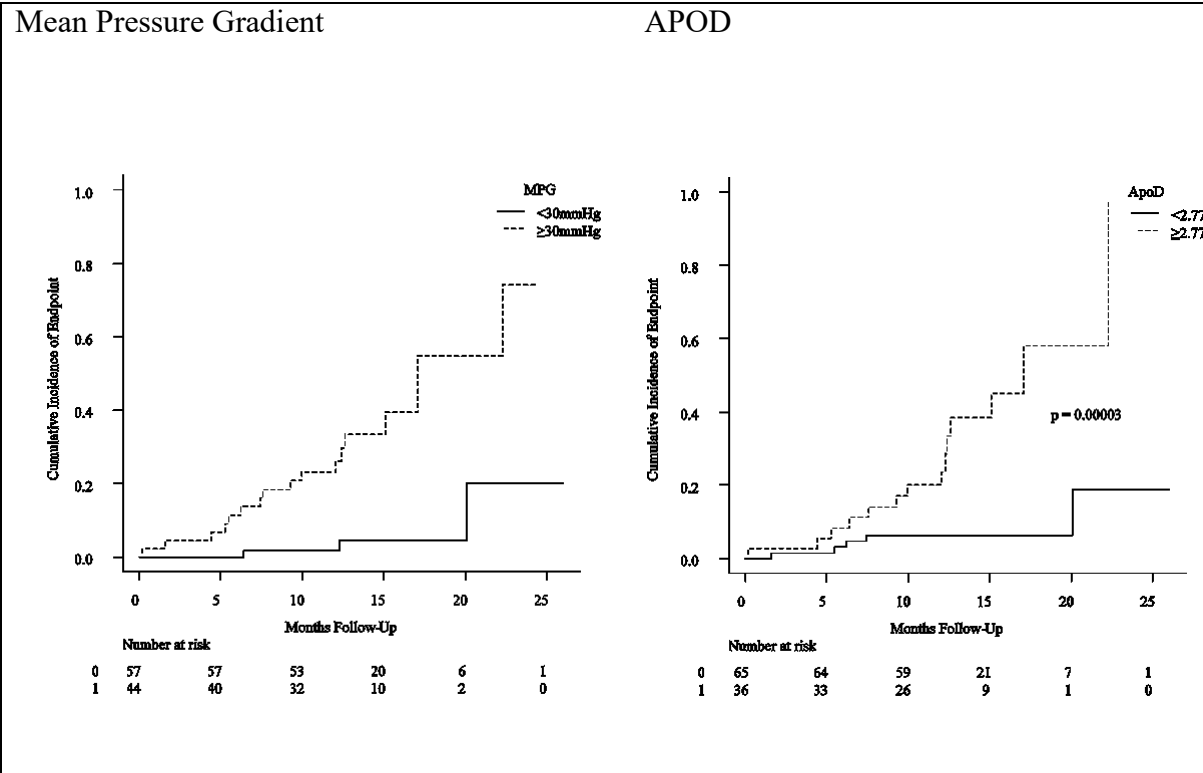


Figure 4-18: Cumulative Incidence curves for mean pressure gradient and APOD dichotomised by optimal cut-offs



#### 4.5.12 Prognostic variables in the Moderate AS group

Other prognosticators of the endpoint in the moderate AS group were considered (Table 4-15). A univariate variable-wide analysis revealed AVA, AV-Vmax, MPG, left atrial minimal volume, a positive exercise test and APOD to be the only prognostic markers in this group. However, a multivariable analysis confirmed MPG and APOD to be the most important independent prognosticators in this group, with the most compact model having a Harrell's C-index of 0.84.

	Univariate		*Multivariable	
	HR (95% CI)	p value	HR (95% CI)	p value
Aortic Valve Area	0.16 (0.03-0.87)	0.034	-	-
Peak Velocity	26 (2.9-230)	0.004	0.01 (0.00-0.90)	0.045
Mean Pressure Gradient	1.3 (1.1-1.4)	<0.001	1.36 (1.15-1.61)	0.0004
Left Atrial minimal volume	1.02 (1.001-1.04)	0.04	1.02 (0.99-1.06)	0.13
Positive Exercise Test	3.13 (1.28-7.68)	0.013	2.59 (0.92-7.28)	0.07
APOD	3 (1.7-5.4)	<0.001	2.85 (1.37-5.95)	0.0051

Table 4-15: Prognostic variables in moderate AS; \*variables stepwise selected showing most compact model

#### 4.5.13 Prognostic variables in the Severe AS Group

For completeness, prognosticators of the endpoint in severe AS were assessed to see if they were different from those in moderate AS (Table 4-16). Sex, LV ejection time, aortic valve area, peak velocity and mean pressure gradient, indexed stroke volume as well as valvulo-arterial impedance were univariate prognosticators. A positive exercise test was not associated with the end-point in this subgroup, although cardiopulmonary exercise test parameters were, specifically peak VO<sub>2</sub> and MaxOxygenPulse (max value of VO<sub>2</sub>/heart rate), on univariate analysis.

However, when put into a multivariable model, only sex, stroke volume index, mean pressure gradient and LV ejection time remained prognostically independent. A stepwise selection led to a compact model containing only these four variables, with a Harrell's C-index of 0.78.

	Univariate		*Multivariable compact model	
	HR (95%CI)	p value	HR (95%CI)	p value
Female	2.4 (1.1-5.3)	0.026	2.18 (0.96-4.94)	0.061
LV Ejection Time (ms)	1.01 (1-1.01)	0.019	1.01 (1.01-1.02)	0.0012
AVA	0.066 (0.011-0.38)	0.0024	-	-
Peak Velocity	3.4 (1.3-8.7)	0.012	-	-
Mean Pressure Gradient	1 (1-1.1)	0.019	1.06 (1.02-1.10)	0.0019
Stroke Volume Index	0.96 (0.92-0.99)	0.011	0.93 (0.90-0.97)	0.00027
Valvulo-arterial impedance	1.5 (1.1-2.1)	0.013	-	-
CPET - Max Oxygen Pulse	0.85 (0.74-0.97)	0.019	-	-
CPET - PeakVO <sub>2</sub>	0.88 (0.8-0.97)	0.0068	-	-

**Table 4-16: Prognostic variables in severe AS; Max Oxygen Pulse is VO<sub>2</sub>/heart rate, \*all variables in table included from outset, stepwise forward/backward selection resulted in the compact model.; AVA-aortic valve area, CPET-cardiopulmonary exercise test, peakVO<sub>2</sub>- maximal oxygen consumption**

#### 4.5.14 Net reclassification improvement analysis

A net reclassification improvement analysis was performed to evaluate if APOD improved the risk stratification over and above baseline risk (Table 4-17 and Figure 4-19). This analysis was performed in all patients – with one baseline model containing sex, exercise testing, “Severe AS” and NTproBNP and another baseline model containing exercise testing, MPG,

AVA and NTproBNP (Table 4-11). This was also performed in moderate AS where baseline risk was defined by peak velocity and MPG (Table 4-15).

Compared to baseline, addition of APOD resulted in a ~50% improvement in classification of risk compared to the baseline model alone. There was both a net increase in up-classifying patients at risk, as well as the converse, resulting in a higher probability of a higher risk score in patients who went on to have an event, and higher probability of a lower risk score in those that did not. There was minimal difference when “Severe-AS” was used instead of a combination of AVA and MPG in the baseline model.

In moderate-AS only, the reclassification was more dramatic, with a 78% net improvement in risk stratification, with 45% net up-classification of risk in those with events, and 33% down-classification of in those who did not go on to have an event, compared to the use of MPG and peak velocity alone.

These confirm that addition of APOD to existing risk stratification strategies could result in better accuracy in determining risk in these patients.

Baseline Model	Continuous Net Reclassification Improvement			
	%Overall	% Events	% No-Events	P value
Sex + AVA + MPG + ETT + NTproBNP	51.2 (17.9-89.3)	23.9 (3.7-53.6)	27.3 (14.2-36.1)	0.012
Sex + Severe AS + ETT + NTproBNP	50.1 (19.1-67.9)	23.9 (4.3-32.6)	26.2 (14.8-39.4)	0.004
Moderate AS Only   MPG + Peak velocity	78.3 (21.2-105)	45 (5.6-59.2)	33.3 (8.4-57.3)	0.0001

**Table 4-17: Continuous net reclassification improvement analysis, comparing baseline model vs baseline model + APOD; AVA – aortic valve area, MPG – mean pressure gradient, ETT – positive exercise test, AS – aortic stenosis**

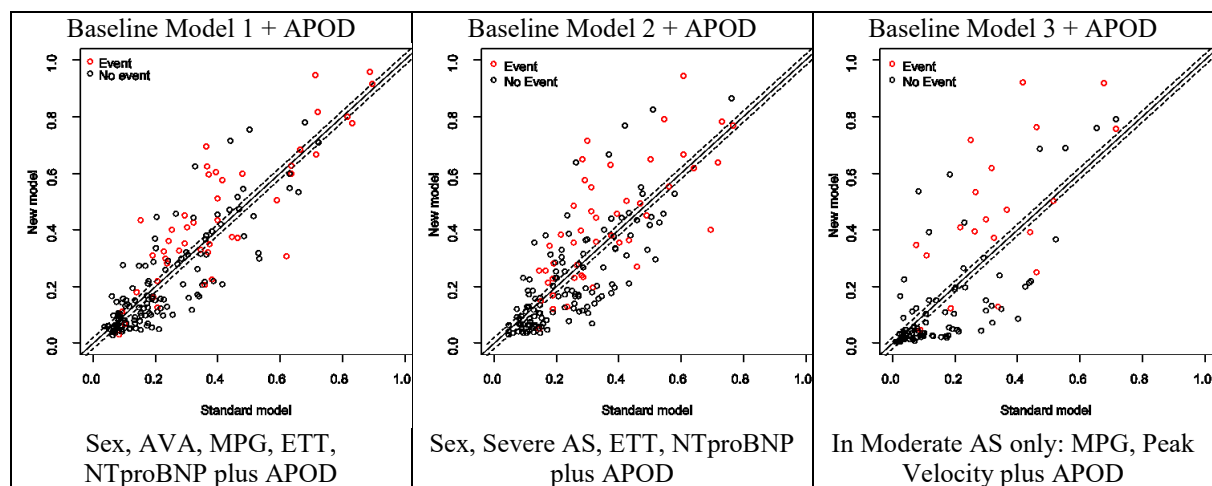


Figure 4-19: Net Reclassification Improvement Analysis; Illustration showing increase in upclassification of patients with events (red) and downclassification of patients without events (black) over the baseline model (diagonal line); AVA – aortic valve area, MPG – mean pressure gradient, ETT – positive exercise test

#### 4.5.15 Negative and positive predictive values

Negative and positive predictive values (NPV and PPV) were also calculated for dichotomised variables for the whole cohort, moderate and severe AS in Table 4-18. When considering both moderate and severe AS together, all variables had a higher NPV than PPV, with MPG < 30mmHg identifying the lowest-risk group of patients. In patients with moderate AS only, both MPG < 30mmHg and APOD < 2.77 had comparable NPVs (>90%). On the other hand, in patients with severe AS only, being female or having a MPG of  $\geq 46$  mmHg was associated with the highest PPV of reaching the composite endpoint.

	Whole Cohort			Moderate AS			Severe AS		
	NPV	PPV	p-value	NPV	PPV	p-value	NPV	PPV	p-value
Severe AS	80%	39%	0.008	x	x	x	x	x	x
Female	78%	44%	0.009	83%	30%	0.231	69%	61%	0.05
Mean pressure gradient	90%	39%	<0.001	93%	44%	<0.001	&72%	&54%	&0.04
Positive ETT	78%	39%	0.027	88%	36%	0.007	63%	43%	0.79
NTproBNP $\geq$ 127.9 pmol/L	80%	43%	0.003	86%	34%	0.027	69%	52%	0.12
APOD $\geq$ 2.77	81%	43%	0.002	92%	42%	<0.001	64%	45%	0.59

**Table 4-18: Negative and positive predictive values for dichotomised variables in the whole PRIMID-AS cohort, moderate and severe AS separately of the composite endpoint; Mean pressure gradient  $\geq$  30mmHg unless specified otherwise; & predictive values for mean pressure gradient  $\geq$  46 mmHg (determined on ROC curve for severe AS only); AS-aortic stenosis, ETT-exercise tolerance test; p-value from Fisher's exact test when constructing two-way tables**

In order to illustrate the additive risk of these variables (risk factors) to reaching the endpoint, each risk factor was given one point, and a simplistic risk score was constructed by addition of all positive risk factors. Kaplan-Meier curves were plotted for each score (Figure 4-20). Severe AS was not used in the risk-score – because of collinearity with MPG. There was one patient with a risk-score of 5, but did not reach an endpoint, which may have been due to early censoring. All patients with a score of 0 did not reach the composite endpoint, whilst progressive increase in the score was associated with incremental risk of reaching the composite endpoint sooner.

A ROC curve was also constructed, which showed that the risk of reaching the composite endpoint increased sharply if three or more risk factors were positive (Figure 4-21).

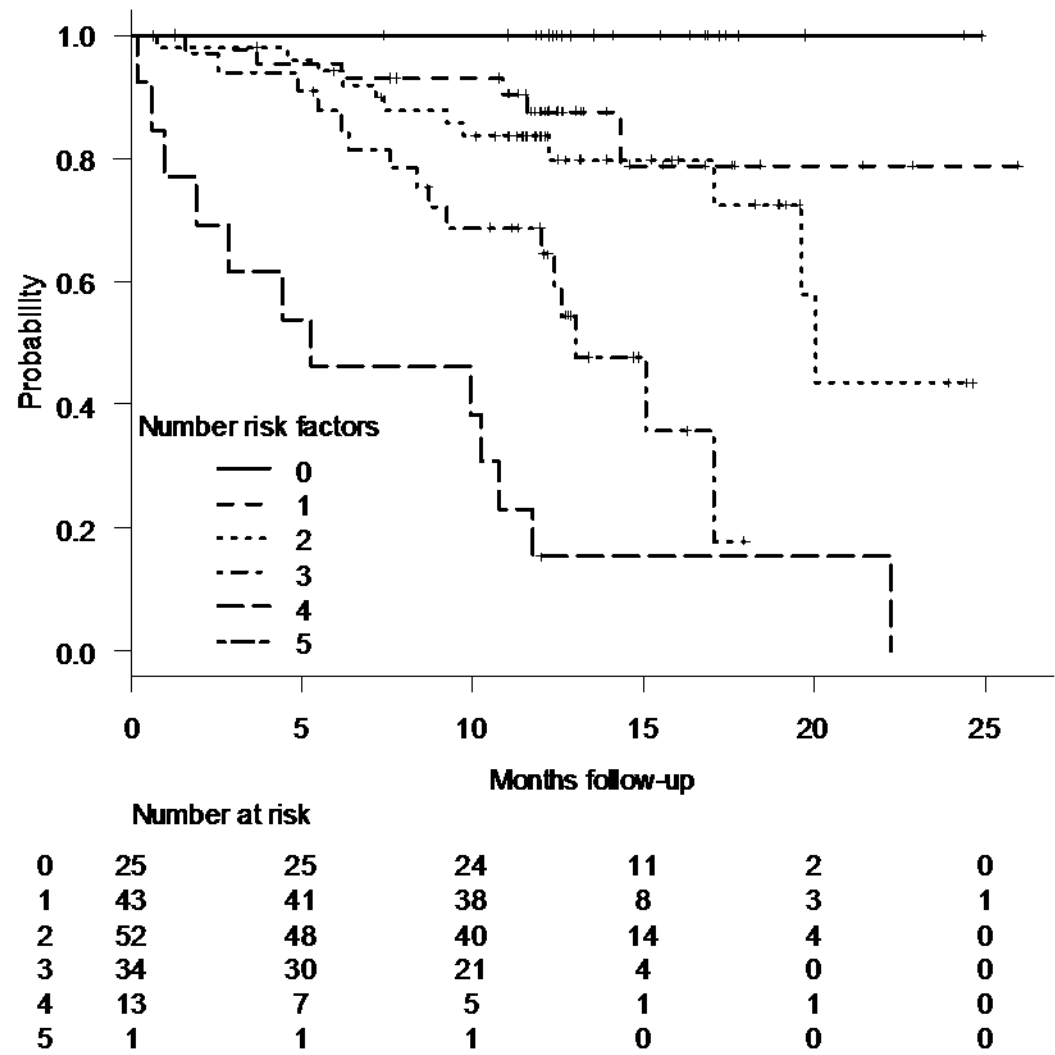


Figure 4-20: Kaplan-meier curves illustrating differences between event-free probabilities stratified by the number of positive risk factors, which were female sex, positive exercise test, mean pressure gradient  $\geq 30\text{mmHg}$ ,  $\text{APOD} \geq 2.77$ ,  $\text{NTproBNP} \geq 127.9 \text{ pmol/L}$ ; post-hoc adjusted p-values which were significant ( $<0.05$ ) were 0 vs 3, 0 vs 4, 1 vs 3, 1 vs 4, 2 vs 3, 2 vs 4 and 3 vs 4. All other score comparisons were not significant.

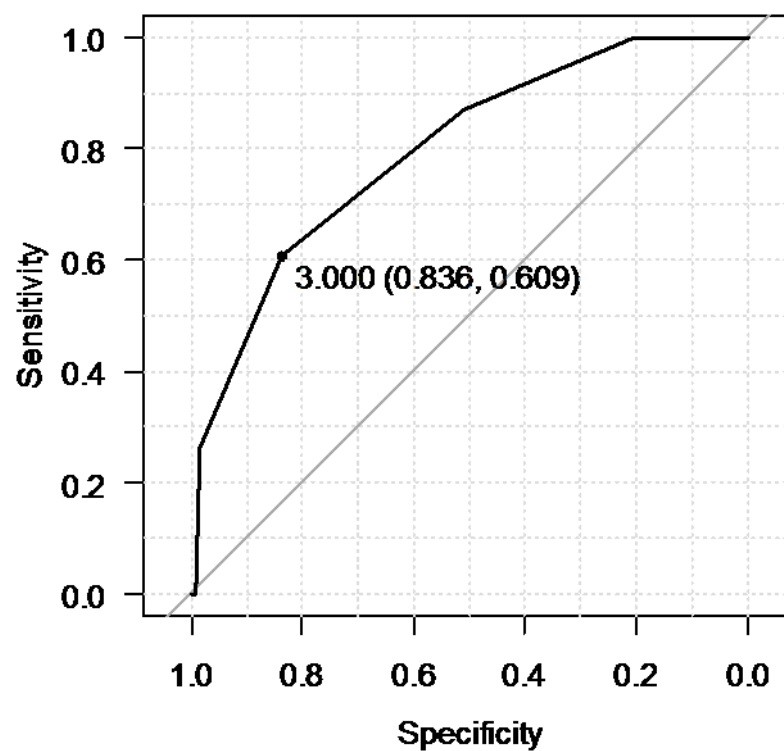


Figure 4-21: Receiver operating characteristic curve of the 5-point risk-score showing that 3 (or more) risk-factors was associated with a steep increase in risk of reaching the endpoint; area under the curve of 0.8 (95% confidence interval 0.73-0.87), the threshold of 3-risk factors has a specificity of 83.6%, sensitivity of 60.9%, negative predictive value of 85% and positive predictive value of 58.3%



#### 4.5.16 Correlates and Determinants of APOD

To ascertain which factors influenced the levels of APOD to deduce its potential roles in AS, correlation with other variables were performed. APOD correlated strongly with several of the other proteins targeted in the study, but in order of correlation, the top four were tetranectin, factor 13b, afamin and phosphatidylinositol-glycan-specific phospholipase D (Table 4-19).

Uniprot Accession	Gene Name	Protein Name	Spearman rho
P05452	TETN	Tetranectin	0.49
P05160	F13B	Factor 13B	0.42
P43652	AFAM	Afamin	0.4
P80108	PHLD	Phosphatidylinositol-glycan-specific phospholipase D	0.37
P02790	HEMO	Hemopexin	0.36
P35542	SAA4	Serum Amyloid A4	0.35
O14791	APOL1	Apolipoprotein L1	0.3
P02760	AMBP	Protein AMBP	0.29
P02655	APOC2	Apolipoprotein C2	0.25
P07225	PROS	Protein S	0.24
P02656	APOC3	Apolipoprotein C3	0.24
P01024	CO3	Complement C3	0.22
P02749	APOH	Beta-2-glycoprotein	0.21

**Table 4-19: Spearman correlations for proteins to APOD. Only significant correlations reported, all with p-value <0.01, ranked with the highest correlation first.**

Correlations with clinical variables were performed as well for the same reasons. These found some interesting patterns – moderate correlation with diastolic blood pressure, diastolic perfusion time (which is RR interval minus LV ejection time), predicted peak VO<sub>2</sub>, RV end diastolic volume index, creatinine, maximal left atrial size index, LV ejection time and NTproBNP, but inversely correlated to heart rate, eGFR and BMI (both the appropriate opposite of RR interval and creatinine respectively) (Table 4-20). The stronger correlations had a lower p-value.

Clinical Variable	Spearman rho
Resting Diastolic Blood Pressure	0.26 <sup>\$</sup>
Resting RR interval	0.26 <sup>\$</sup>
Diastolic Perfusion Time	0.23 <sup>\$</sup>
Predicted PeakVO2	0.22 <sup>\$</sup>
Right ventricular end diastolic volume index	0.21 <sup>\$</sup>
Creatinine	0.20 <sup>\$</sup>
Left ventricular ejection time	0.20 <sup>*</sup>
Peak VO2	0.19 <sup>*</sup>
Global stress myocardial blood flow x LVMI	0.17 <sup>*</sup>
Maximal left atrial size index	0.16 <sup>*</sup>
NTproBNP	0.16 <sup>*</sup>
Weight	-0.19 <sup>*</sup>
Heart rate	-0.24 <sup>\$</sup>
Estimated glomerular filtration rate	-0.25 <sup>\$</sup>
Heart rate on continuous wave doppler	-0.26 <sup>\$</sup>
Body mass index	-0.27 <sup>\$</sup>

**Table 4-20: Spearman correlations for clinical variables to APOD. \$rho value with p-value of correlation <0.01, \*rho value with correlation p-value > 0.01 & < 0.05, LVMI: Left ventricular mass index, Peak VO2: Peak oxygen consumption, RR interval: time between two R waves on ECG at rest.**

The clinical variables in the table were put into a linear regression model to ascertain determinants of the APOD level. Due to aliasing, diastolic perfusion time was excluded. Variance inflation factors were calculated and collinear variables were rationalised. As such, eGFR, weight, heart rate, predicted peakVO2 were excluded (all dependent on weight or heart rate). The remaining variables all had a variance inflation factor of <2. Variables were standardized to a mean of zero and unit standard deviation for linear regression modelling to make more meaningful inferences on the beta estimates.

Both models (Table 4-21) show that these variables could only explain 22% of the variance in the APOD. The major correlates were BMI, NTproBNP, stress myocardial blood flow × left ventricular mass index, diastolic blood pressure and heart rate.

	Model 1		Model 2	
	Beta (95%CI)	p.value	Beta (95% CI)	p.value
BMI	-0.23 (-0.43--0.04)	0.02	-0.28 (-0.43--0.14)	0.00017
NTproBNP	0.24 ( 0.05- 0.44)	0.014	0.24 ( 0.09- 0.38)	0.0013
Stress Myocardial Bloodflow x LVMI	0.16 (-0.03- 0.35)	0.1	0.21 ( 0.06- 0.35)	0.0051
Diastolic BP	0.21 ( 0.03- 0.39)	0.021	0.19 ( 0.05- 0.34)	0.0091
RR interval on ECG	0.14 (-0.06- 0.35)	0.17	0.19 ( 0.05- 0.33)	0.0098
Peak VO2	0.11 (-0.13- 0.34)	0.36	-	-
Creatinine	0.08 (-0.11- 0.27)	0.42	-	-
Maximal Left atrial indexed volume	0.07 (-0.15- 0.29)	0.54	-	-
LV ejection time	0.03 (-0.19- 0.25)	0.77	-	-
Right ventricular end diastolic volume index	0.01 (-0.21- 0.24)	0.89	-	-
Residual Standard Error	0.94		0.89	
Multiple R <sup>2</sup>	0.222		0.224	
Adjusted R <sup>2</sup>	0.153		0.199	
F statistic	3.27 on 10 & 116 degrees of freedom		8.91 on 5 & 154 degrees of freedom	

**Table 4-21: Correlates of APOD. Model 1, all correlating variables excluding collinearity on enter, Model 2: Model 1 stepwise selected based on AIC to produce a compact model. All variables have been standardized to a mean of 0 and standard deviation of 1 for this step.**

The same analyses were performed for the proteins measured (Table 4-22). All the significantly correlated proteins to APOD were entered into a linear regression model to ascertain which were independently correlated to APOD levels, both on ‘enter’ as well as a stepwise selection. Tetranectin, complement C3, serum amyloid A4, phosphatidylinositol-glycan specific phospholipase D, and protein AMBP were all independent correlates, which together explained 41.3% of the variance of APOD.

Protein	Model 1		Model 2	
	Beta (95%CI)	p value	Beta (95%CI)	p value
Tetranectin	0.55 ( 0.35- 0.75)	<0.0001	0.56 ( 0.38- 0.73)	<0.0001
Complement C3	-0.43 (-0.63--0.23)	<0.0001	-0.43 (-0.62--0.25)	<0.0001
Serum Amyloid A4	0.23 ( 0.09- 0.36)	0.001	0.24 ( 0.11- 0.36)	0.0002
Phosphatidylinositol-glycan-specific phospholipase D	0.11 (-0.05- 0.26)	0.19	0.16 ( 0.02- 0.3)	0.024
Protein AMBP	0.09 (-0.05- 0.23)	0.2	0.13 ( 0.01- 0.25)	0.04
Afamin	0.15 (-0.02- 0.31)	0.081	0.14 (-0.02- 0.3)	0.087
Protein S	0.12 (-0.03- 0.27)	0.12	-	-
Factor 13B	0.10 (-0.09- 0.28)	0.3	-	-
Apolipoprotein L1	-0.07 (-0.26- 0.13)	0.49	-	-
Hemopexin	0.06 (-0.14- 0.26)	0.57	-	-
Apolipoprotein C3	-0.03 (-0.13- 0.08)	0.6	-	-
Beta-2-glycoprotein 1	-0.02 (-0.12- 0.09)	0.78	-	-
Residual Standard Error	0.6		0.6	
Multiple R <sup>2</sup>	0.43		0.413	
Adjusted R <sup>2</sup>	0.39		0.391	
F statistic	9.77 on 12 & 155 degrees of freedom		18.9 on 6 & 161 degrees of freedom	

**Table 4-22: Protein correlates of APOD; Model 1: all significantly correlated proteins entered into linear regression model; Model 2: Stepwise selection of Model 1 variables to create a compact model, showing selected proteins. All variables have been standardized to mean of 0 and standard deviation of 1 for this step.**

Finally, the significant clinical variables and proteins were combined in a linear regression model (Table 4-23), and then stepwise selected, leaving tetranectin, BMI, serum amyloid A4, afamin, NTproBNP, and complement C3 as independent correlates of APOD (46.2% attributable variance). In fact, 67% of the attributable variance (Figure 4-22) was explained by tetranectin and BMI alone, implying an important relationship of these two variables to APOD levels.

#### 4.5.17 Other Notable correlations

All the apolipoproteins were highly intercorrelated, and these correlated well with afamin and serum amyloid A4 (Figure 4-23). Plasminogen, tetranectin and factor 13B were highly intercorrelated (Figure 4-24).

	Model 1		Model 2	
	Beta (95%CI)	p.value	Beta (95%CI)	p.value
Tetranectin	0.38 ( 0.23- 0.53)	<0.00001	0.38 ( 0.23- 0.53)	<0.00001
BMI	-0.23 (-0.36--0.09)	0.0012	-0.22 (-0.36--0.09)	0.00098
Serum Amyloid A4	0.28 ( 0.13- 0.42)	0.00024	0.31 ( 0.17- 0.45)	0.00002
Afamin	0.18 ( 0.02- 0.35)	0.029	0.27 ( 0.14- 0.39)	0.00005
NTproBNP	0.16 ( 0.03- 0.29)	0.015	0.16 ( 0.04- 0.28)	0.0099
Complement C3	-0.24 (-0.41--0.06)	0.0093	-0.22 ( -0.4--0.04)	0.014
RR interval on ECG	0.12 (-0.01- 0.24)	0.065	0.12 ( 0- 0.24)	0.054
Stress myocardial blood flow x LVMI	0.09 (-0.03- 0.22)	0.15	0.09 (-0.03- 0.22)	0.15
Diastolic BP	0.09 (-0.04- 0.21)	0.18	-	-
Protein AMBP	0.07 (-0.06- 0.21)	0.29	-	-
Phosphatidyl-inositol glycan specific phospholipase D	0.07 (-0.09- 0.24)	0.37	-	-
Residual Standard Error	0.75		0.75	
Multiple R2	0.475		0.462	
Adjusted R2	0.436		0.433	
F Statistic	12.2 on 11 & 148 degrees of freedom		16.2 on 8 & 151 degrees of freedom	

**Table 4-23: All correlates: combining significant multivariable clinical and protein determinants; Model 1: All variables entered into linear regression model; Model 2: All variables in Model 1 stepwise selected resulting in compact model; All variables have been standardized to mean of 0 and standard deviation of 1 for this step**

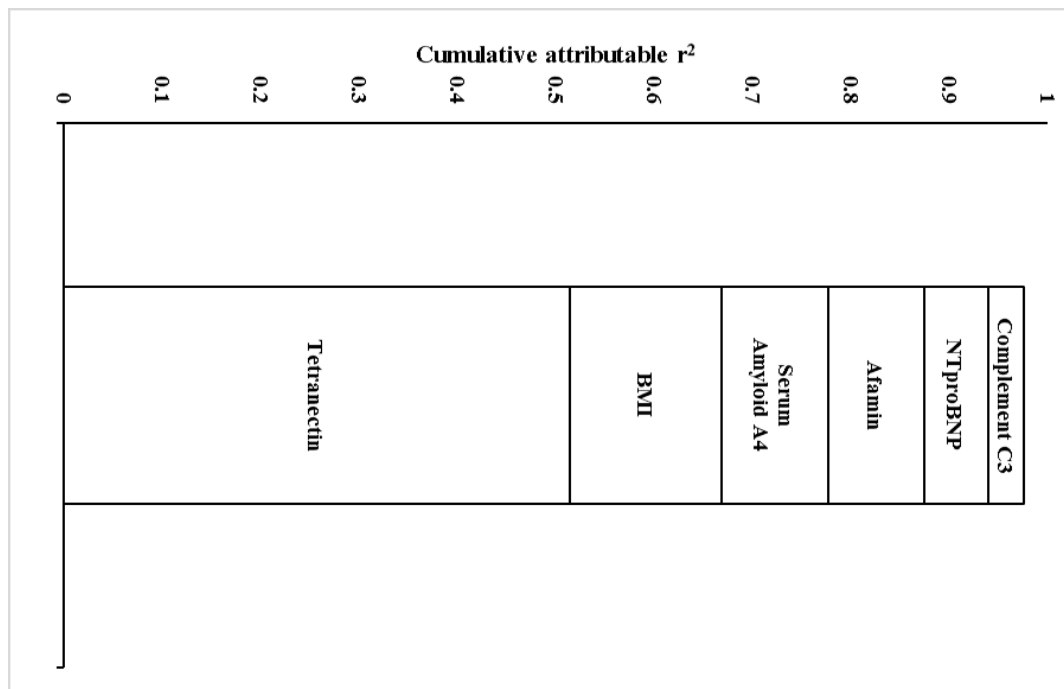


**Figure 4-22: Tetranectin and BMI may explain more than 2/3 of the attributable variance of APOD; presented is percentage of the cumulative multiple r² with the multiple r² in Model 2 of Table 4-23 as denominator.**

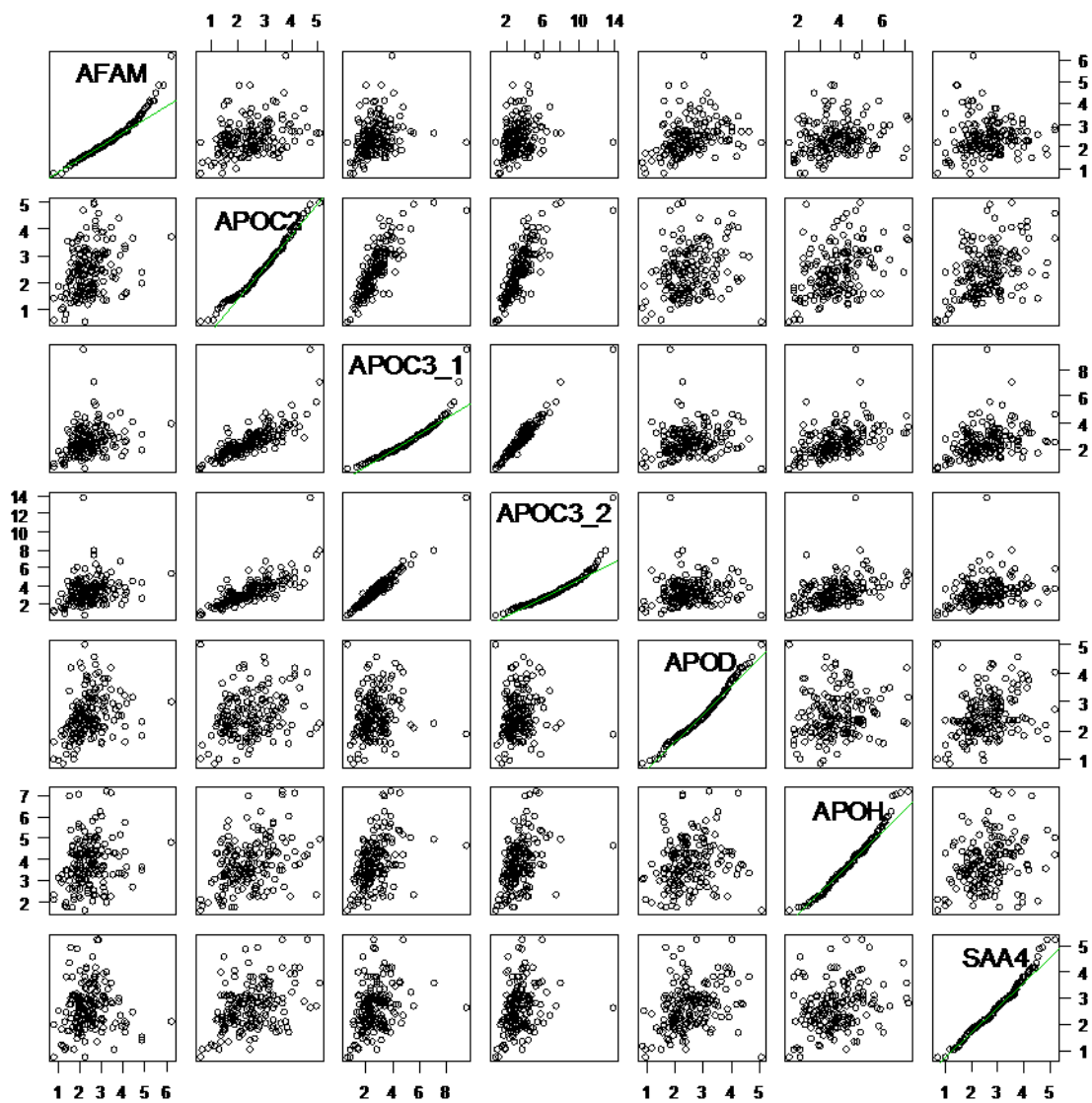


Figure 4-23: Scatterplot matrix showing correlation between apolipoproteins C3, C2, D and H, afamin and serum amyloid a4; APOC3\_1 refers to the DALSSVQESQVAQQAR peptide and APOC3\_2 refers to the GWVTDGFSSLK peptide, both from APOC3

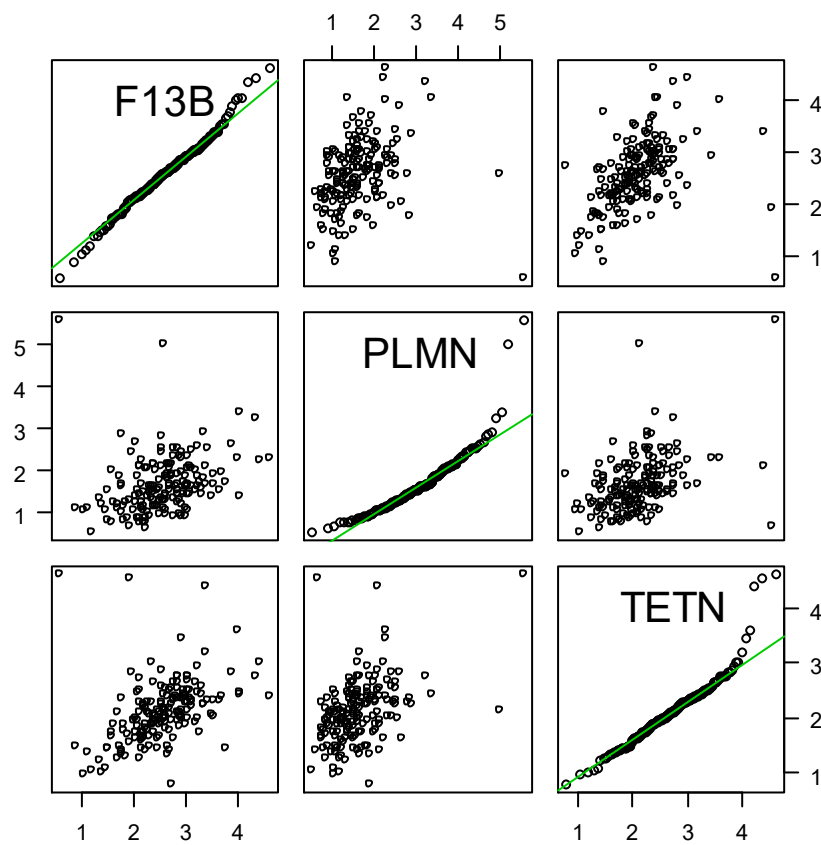


Figure 4-24: Scatterplot matrix showing correlations between factor 13B, plasminogen and tetranectin

## 4.6 Discussion

There were several important findings in this part of the study. Severe and moderate AS were phenotypically different, with more remodelling in severe AS, higher troponin levels and lower myocardial perfusion reserve. Imaging markers of remodelling or fibrosis were not associated with the composite endpoint of spontaneous symptom development or death/hospitalisation of AV-related events.

Instead, variables that were associated were sex (female increased risk), a lower haemoglobin and eGFR, and a higher NTproBNP. Markers of AS-severity were appropriately associated with the composite endpoint, as was AV calcification. A positive exercise test was also a risk factor for the endpoint.

A proteomics approach to 'discover' proteins that were associated with the endpoint (either positively or negatively) was executed and then a labelled-peptide-based approach to measure peptides as surrogates for the proteins being studied was developed. This whole process identified initially 59 proteins associated with the endpoint, but pragmatically only 17 were verified.

I found that phenotypically, proteins associated with AS-severity were not associated with the endpoint. These proteins were factor 13B, apolipoprotein L1 and protein AMBP, all of which were lower in severe AS. Out of the 17 targeted proteins, only apolipoprotein D was significantly associated with the composite endpoint, which was independently prognostic to a baseline model containing sex, MPG, valve area, NTproBNP and exercise testing.

Subgroup analyses showed that APOD was more prognostic in moderate AS and males.

Other variables that interacted with the severe AS classification was MPG and SVI.



Net reclassification improvement analyses showed that APOD improved discrimination between events and non-events by up to 78% in the moderate AS group, but also by up to 50% in all participants in the study, over and above baseline risks. Finally, up to 46% of the variance in APOD could potentially be attributed to tetranectin, BMI, afamin, serum amyloid A4, complement C3 and NTproBNP, implying the importance these variables play in APOD levels.

#### **4.6.1 Parallel Reaction Monitoring (PRM)**

Targeted proteomics is a robust method of rapidly moving from discovery proteomics to verification or validation in a large number of samples. In comparison with immunoassays, mass spectrometric peptide-based methods allow researchers to be specific about which peptide (including modifications) to target to answer their hypothesis. Additionally, targeted mass spectrometric assays allow multiplexed analysis of many peptides in a single analysis. There are various guidelines about targeted proteomics assay design (Holman et al., 2012, Liebler and Zimmerman, 2013, Mani et al., 2012), including more recently, best-practice guidelines as to necessary experiments to reassure others of the reliability of the assays (Carr et al., 2014). These guidelines have translated to the sharing of large-scale databases of assays which provide potential end-users with the necessary information about how suitable a targeted mass-spectrometric assay is for their purposes. One such example is the Clinical Proteomic Tumor Analysis Consortium (CPTAC) Assay Portal (Whiteaker et al., 2014), a repository of well-characterised targeted mass-spectrometric-based assays. Expert consensus is that targeted peptides should be unique, without reactive residues (e.g. methionine or N-terminal glutamine), without N or C-terminal peptides – which are usually susceptible to degradation, without sites of known post-translational modification (unless these are specifically being targeted), should not be susceptible to missed cleavages, and finally should

be easily detectable in an LC-MS experiment. It is also sensible to target at least 2 peptides per protein.

However, whilst it is ideal that these guidelines on peptide selection are adhered to, it is not always possible (Chiva and Sabidó, 2017) but also may not be more accurate than random peptide selection. I tried to exclude all peptides that contained reactive residues (e.g. methionine) but this led to too few visible peptides from a DDA LC-MS experiment being available for targeting. Many of the shortlisted peptides co-eluted at the same time, and therefore needed to be rationalised. For example, if 6 peptides co-eluted within the same time window, but 4 of the proteins had additional surrogate peptides eluting elsewhere in the chromatogram, these 4 peptides would be removed from the shortlist. Despite this, almost all proteins being targeted were left with single unique peptides as surrogates and this had to be accepted as a limitation. Longer gradients were attempted, but due to several issues with columns blocking and poorly-reproducible retention times (not due to changes in gradients), and because time was at a premium, this was not pursued further. A limited attempt was made at assessment of linearity, limits of quantification and repeatability, which suggested that the assay was robust enough for this step of the verification study. However, these steps would not completely satisfy stringent requirements described by others (Carr et al., 2014). For example, the linearity of quantification assessment was made on 4 calibration points, not 6, the experiment assessing repeatability of each concentration was made on a triplicate, not 6 replicates. However, given that the assays appeared to be linear near the middle of the quantification curve, and that the standards were made of a pool of all samples, the concentration of the standard was likely to be near the middle of the linear quantification curve where the results should be sufficiently reliable.

#### **4.6.2 Differences between severe and moderate AS**

Experts generally agree that severe AS should be associated with increased risk (Otto, 2018).

The European guidelines recently made changes to how severe AS should be defined to increase the specificity of the definition (Baumgartner et al., 2017a, Baumgartner et al., 2017b). The principal changes were a) AVAI is no longer used to define severe AS, b) the primary determinant of severe AS is high MPG or high AV-Vmax, c) in the presence of low flow and low AVA ( $SVI < 35 \text{ ml/m}^2$ ), low gradient severe AS with preserved ejection fraction may exist, and should be considered as severe AS, if there are other supporting features. These features may include high AV calcium scores (Clavel et al., 2013, Clavel et al., 2014, Pawade et al., 2018),  $MPG > 30 \text{ mmHg}$  and advanced age, and other features described in (Baumgartner et al., 2017b). In this study, it was observed, as expected, in severe AS, valve area was lower, gradients and valvular calcification were higher.

Appropriately, as valvular stenosis becomes more severe, one should observe a higher rate of progression to spontaneous events, especially when symptomatic (Otto et al., 1997, Otto, 2006). This was seen in this study as well, with severe AS having almost double the event rate to moderate AS. Furthermore, there was notably increased remodelling (hypertrophy as measured by LVMI, and LV mass/volume) in severe AS, which was expected. The myocardium should remodel and increase wall thickness to reduce LV wall stress. Whilst remodelling is adaptive initially, in some cases, this could become maladaptive, resulting in an increased event rate in asymptomatic AS if there is excessive left ventricular remodelling/hypertrophy (Cioffi et al., 2011).

The troponin level was also higher in severe AS. In AS, this has previously been associated with midwall fibrosis (Chin et al., 2016) (as measured by LGE), which correlated with

excessive LVH and strain (Chin et al., 2014), and was associated with increased risk of all-cause mortality which persisted even after AVR.

MPR, previously demonstrated to be a major determinant of aerobic exercise capacity (Steadman et al., 2012), was significantly lower in severe compared to moderate AS. In this cohort, MPR was previously shown to predict symptom onset in initially asymptomatic AS (Singh et al., 2017b), although it was no better than exercise testing in ascertaining this risk.

Interestingly however, out of all the proteins that were targeted in the verification study, only protein AMBP, apolipoprotein L1 and factor 13B were significantly different in values in severe AS; all were lower than in moderate AS.

Protein AMBP is a precursor of alpha-1-microglobulin and bikunin. The function of bikunin is unknown, but alpha-1-microglobulin is a lipocalin that plays a role in extravascular tissue cleaning and housekeeping, reducing oxidative damage of heme and oxygen free radicals by binding these molecules covalently and transferring to the kidneys for extraction and recycling (Akerstrom and Gram, 2014, Allhorn et al., 2002).

APOL1 is a pore-forming molecule that promotes ion-permeability in vesicles, which is the mechanism by which it protects hosts from African trypanosomes (i.e. by forming pores in trypanosome-containing vesicles intracellularly) but some variants are associated with an increased risk of nephropathy (Bruno et al., 2017, Cuypers et al., 2016). Whether lower measured values of APOL1 reflects the presence of APOL1 variants in the individual is unknown.

Factor 13B is the inhibitory component of a tetrameric complex (Factor 13); its role is to inactivate/inhibit factor 13A. Free factor 13A (termed activated factor 13) on the other hand activates and promotes fibrin crosslinking (Mary et al., 1988) promoting coagulation. 50% of

Factor 13B in circulation is unbound (Yorifuji et al., 1988) probably to ensure that inappropriate intravascular coagulation does not occur. The measured factor 13B may actually reflect the unbound form of the protein, instead of the complexed form.

Lower circulating amounts of these three proteins in severe AS may reflect peripheral consumption suggesting increased haemolysis and intravascular coagulation activation.

#### **4.6.3 Prognostic markers of the endpoint**

In PRIMID-AS being female, having more severe AS, higher NTproBNP and positive exercise testing were all strongly associated with the endpoint. These were all as expected from existing literature. The role of sex in asymptomatic AS has previously been explored (Singh et al., 2017a), where key sex-related differences may explain the discrepancy of symptom onset between males and females with asymptomatic moderate severe AS. Females exhibited less LVH and less fibrosis, with lower matrix metalloproteinase 3 and syndecan 4 levels, both of which are markers of remodelling. Earlier symptom onset in females may be related to a higher wall stress and filling pressures in females (due to reduced compensatory hypertrophy in females). Interestingly however, event-free survival curves, although separating early between males and females, converge later during follow-up suggesting that only a subset of females had a higher risk than males, whilst the others had a similar risk.

As expected, severe AS, high NTproBNP and positive exercise testing were associated with a higher risk of the endpoint. However the early separation with subsequent convergence of adjusted survival curves for NTproBNP and AVA later in the course of follow-up suggest that the risk associated with these markers may interact with sex. This has been noted before, wherein females generally had higher NTproBNP levels compared to men, regardless of hormone status (Lam et al., 2011), and that NTproBNP levels were inversely correlated with free testosterone levels. Furthermore, in HF, NTproBNP was differentially prognostic

between sexes, wherein it seemed to be less useful in females for composite events (in hospital death/death after discharge/rehospitalisation) (Kim et al., 2017).

A positive exercise test in this cohort increased the risk of the endpoint. In subgroup analyses, a positive exercise test was associated with the outcome in the moderate AS group, compared to the severe AS group. However, on multivariable analyses, a positive exercise test was not independently prognostic, but this was perhaps due to the presence of APOD in the model (Table 4-15). The specificity of exercise testing in this cohort of patients in predicting symptom onset has previously been reported to be poor, especially in the more elderly patients (Das et al., 2005) where the PPV was 57% in all patients, but 79% in patients aged <70 years with similar sensitivity. In PRIMID-AS, in severe AS, exercise testing had a 35% sensitivity but 71% specificity for anticipating the composite endpoint over the follow-up period. The PPV was low at 43% whilst the NPV was 57%. In the age<70 subgroup with severe AS, exercise testing was even less helpful – with a PPV of 38% but a similar NPV of 56%. The same was true for moderate AS, with a PPV of 36% but the NPV was higher at 88%. It seems therefore that a negative exercise test is more useful than a positive one, in moderate AS at least.

#### **4.6.4 APOD was independently prognostic of the endpoint**

In this study, APOD emerged as a novel biomarker independently prognostic to anticipating the endpoint. Although it added prognostic information to the whole cohort, it was most useful in the moderate AS subgroup. This was independent of sex, AS severity (or valve area and MPG), exercise testing and NTproBNP. Net reclassification improvement analysis confirmed that there is a 78% net improvement in continuous analysis in moderate AS, but a more modest net improvement in the whole group of ~50%. This novel finding implies that APOD could be useful in helping clinicians be more confident about the likelihood for

developing symptoms in the near future and help with optimal timing of AVR especially, and is worthy of further study.

#### **4.6.5 APOD is a novel marker of cardiovascular risk**

APOD has previously been found to be increased in both in the plasma and myocardium in patients with HF when comparing failing hearts for transplantation and non-failing hearts (Wei et al., 2008).

*APOD* overexpression was found to protect against ischaemia reperfusion injury and reduce myocardial infarction in a mouse model. There was a correlation between its ability to reduce injury in a hypoxia/reoxygenation in primary mouse cardiomyocytes, with its antioxidant potency in a standard antioxidant assay (Tsukamoto et al., 2013). This suggested that its protective effect was exerted by its antioxidant effect. Recently, plasma levels of oxidized phospholipid levels on Apo A and B have been found to be linearly related to faster progression of AS severity in mild-moderate AS (Capoulade et al., 2018), highlighting the importance of lipid peroxidation in AS.

APOD, along with other factors in the Liver X Receptor/ Retinoid X Receptor pathway (LXR/RXR), were found to be reduced in a model of chronic-pacing-induced cardiomyopathy. In this model, 6 months of chronic pacing led to increased cellular hypertrophy, myolysis, fibrosis and cellular lipid accumulation, and an increase in inflammatory and apoptosis markers (Lin et al., 2019), suggesting the importance of this pathway in myocardial cytoprotection.

In contrast, in human umbilical vein endothelial cells, used to study endothelial cell function (Park et al., 2006), LXR-agonism with a synthetic agonist resulted in diminished angiogenesis of these cells, via induction (increase) in *APOD*, with resultant reduction in

VEGF, IL-8, MMP-8 & 9 (Lai et al., 2017); which are required in maintenance of compensated myocardial hypertrophy in pressure overload (Oka et al., 2014).

In asymptomatic AS, increasing plasma levels was associated with a higher risk of reaching the endpoint. Higher levels may reflect the increased oxidative stress in those individuals and may reflect incremental LXR/RXR activation, with resultant transition from compensated hypertrophy (with maintained angiogenesis) to HF (with reduced angiogenesis).

#### **4.6.6 APOD may be more prognostic in males**

In subgroup analyses, higher APOD levels were associated with the outcome in males, but not females. This may be due to the lower number of female patients. APOD levels were significantly higher in males who reached the endpoint, compared to males who did not, but this differential pattern was not seen in females. Upregulation of APOD has previously been found to be dependent on dihydrotestosterone. This was observed in androgen insensitivity syndrome, where complete nulling of androgen receptor expression (e.g. phenotypic females but with XY chromosomes) was associated with absence of APOD induction (Appari et al., 2009).

As described earlier, female patients with asymptomatic AS demonstrated a much less aggressive remodelling response to AS (Singh et al., 2017a), yet being female was associated with a higher risk of reaching the endpoint, suggesting that the compensated LV hypertrophy seen in males may delay symptom onset. However, compensated LVH also progresses to HF, with increasing degrees of fibrosis and myocyte degeneration as LV function deteriorates (Hein et al., 2003).

In another animal study with experimental pressure overload and hypertrophy, male mice that developed progressive LVH and remodelling demonstrated improvements in hypertrophy, myocardial fibrosis, LV function and size after treatment with finasteride, a 5- $\alpha$ -reductase



inhibitor, which inhibits testosterone activation (Zwadlo et al., 2015). In the same study, female mice that were treated with finasteride also demonstrated improvements in LV remodelling parameters, similar to male mice. Peripheral conversion of oestrogen to androgens may have been inhibited by finasteride in females, a process that largely occurs in peripheral adipose tissues. Put together, one possible hypothesis is that APOD is a surrogate for testosterone or dihydrotestosterone activity, which in turn may have a causal effect on LV remodelling and its incipient problems.

#### **4.6.7 APOD function**

In the development of HF, one of the first processes that have been observed is a change in energy source from fatty acid oxidation to glucose/carbohydrate metabolism. APOD has previously been shown in rats to be associated with improved triglyceride catabolism, facilitating VLDL-hydrolysis as a fuel source for fatty acid oxidation in cells (Perdomo et al., 2010). Obese rats with enhanced APOD production displayed lower triglyceride levels in their plasma due to improved VLDL hydrolysis, a lipoprotein lipase-dependent activity. Higher APOD levels being associated with the composite endpoint in asymptomatic AS suggests an increased dependence of cardiomyocytes on fatty-acid oxidation as an energy source. APOD may actually reflect the increase in energy requirements and the associated VLDL-hydrolysis to accommodate this. As all of the patients had preserved LV function, the ‘switch’ from fatty acid oxidation to glucose/carbohydrate metabolism has probably not occurred yet.

APOD has also been found to perform a protective function, stabilising the membranes of vulnerable lysosomes in the presence of oxidative stress (Pascua-Maestro et al., 2017). In the presence of paraquat, lipid peroxidation occurs in lysosomal membranes. APOD was found to localise, after endocytosis, to damaged lysosomes. Authors hypothesized that APOD did so to

repair the lysosomal membranes to prevent complete lysis. In addition, they hypothesized that any lysosomes which failed to be repaired were then phagocytosed. Whilst this function was only demonstrated in neurons and astrocytes, it is possible that the same function occurs in other cells that undergo oxidative stress. Lysosomal storage disorders, such as LAMP2 mutations and Fabry's disease, manifest in the cardiovascular system as excessive LVH, implying that lysosome failure may be directly responsible for this phenotype in AS.

#### **4.6.8 Relationship of APOD with peak VO<sub>2</sub>**

Maximal aerobic capacity (peak VO<sub>2</sub>) has previously been shown to be useful in asymptomatic AS (Steadman et al., 2012). In univariate analysis, peak VO<sub>2</sub> was prognostic of the endpoint, particularly in severe AS. Peak VO<sub>2</sub> is dependent on age, sex and weight (Wasserman et al., 1987), which is adjusted-for in predicted-peak-VO<sub>2</sub>. Whilst APOD correlated with both predicted-peak-VO<sub>2</sub> and peak VO<sub>2</sub>, it did not correlate with percent-peak-VO<sub>2</sub> (ratio of actual vs predicted peak VO<sub>2</sub>), which suggests that its association with peak VO<sub>2</sub> was dependent on weight. APOD was inversely correlated with weight (Table 4-20), and the predicted peak VO<sub>2</sub> calculation adjusts for (1/weight), which probably explains the positive correlation between APOD and predicted peakVO<sub>2</sub> or peakVO<sub>2</sub>.

#### **4.6.9 Correlates of APOD**

Multivariable linear regression showed that independent correlates of APOD in this study were tetranectin, BMI, serum amyloid A4, afamin, NTproBNP and complement C3.

However, despite the large number of variables, only 46% of the variance could be attributed to the described variables, of which 2/3 could be explained by tetranectin and BMI.

The function of tetranectin is unclear. It is a C-type lectin plasma protein present in the mammalian musculoskeletal system (Xu et al., 2001, Wernbom et al., 2012) and is thought to be integral to wound and fracture healing (Iba et al., 2013). It also enhances plasminogen

activation, catalysed by tissue plasminogen activator (Clemmensen et al., 1986). Both tetranectin and plasminogen have been found in cancers (Christensen and Clemmensen, 1991, Wewer and Albrechtsen, 1992, De Vries et al., 1996), where together with fibroblastic cells and extracellular matrix probably facilitated migration of tumour cells. Tetranectin, APOD, plasminogen and factor 13B were all highly inter-correlated which may allude to their incidental relationship with each other in the literature suggestive of shared pathways.

Body mass index being a negative correlate of APOD is a novel finding. Plasma APOD has been reported to decrease during normal pregnancy, but the decrement is even greater if there is excessive gestational weight gain (Do Carmo et al., 2009). Authors hypothesized that this was in part due to haemodilution in pregnancy, but also that there may be some role from 17 beta-oestradiol, which inhibited APOD secretion in breast cells (Simard et al., 1990).

Oestrogen levels increase markedly at the end of gestation and may suppress APOD secretion, and plasma levels of APOD were much lower in breast feeding women after delivery, compared to those that did not (Do Carmo et al., 2009). Authors hypothesized that this could potentially be explained by inhibition of oestrogen by prolactin (Wang et al., 1980) which is increased in breastfeeding to maintain lactation.

In this study cohort, although most patients were advanced in age, APOD levels were higher in males who went on to have an event compared to females. In a different study, APOD levels after age and sex adjustment were associated with incident Type II diabetes, but after adjusting for BMI, APOD was no longer significantly associated, whilst other apolipoproteins were (especially APOC3) (Brahimaj et al., 2017). This implied that APOD is associated with BMI, but did not have an independent prognostic effect on incident Type II diabetes. APOD's relationship with BMI is probably linked to testosterone levels, of which there is a known inverse relationship (Eriksson et al., 2017).

Afamin is a highly abundant Vitamin E-binding glycoprotein similar to albumin (Voegelé et al., 2002). Its physiological function is unclear, but is associated with all aspects of the metabolic syndrome (Dieplinger and Dieplinger, 2015), e.g. circulating lipids, glucose and bodyweight. Its correlation with APOD may be generally reflective of circulating lipoprotein levels. Like afamin, serum amyloid A4 is associated with lipid levels, in particular hypertriglyceridaemia (Yamada et al., 1996b, Yamada et al., 1996a), and is also a minor acute phase reactant. Although previously linked to development of dementia (Murphy et al., 2009), levels in this study probably reflect the lipid status.

Complement C3 is an integral substrate for the final part of the complement activation pathway, with both the lectin and alternative pathway culminating in formation of a C3 convertase, which activates complement C3 and results in formation of the membrane attack complex. In an infection, this would result in opsonisation of foreign cells. Conversion of C3 is also a chemoattractant to phagocytes, which is important in remodelling in after tissue injury (Orsini et al., 2016). The correlation between complement C3 levels and APOD may reflect the incremental activation of the complement system in the presence of cellular stress.

NTproBNP also correlated weakly with APOD levels, contributing minimally in linear regression. This was not surprising given that natriuretic peptides have been shown both to be associated with symptom-free survival and perioperative mortality (Bergler-Klein et al., 2004, Farré et al., 2014). However, in this study, APOD appeared to be a better prognosticator of endpoints, especially in moderate AS.

#### **4.6.10 Limitations**

Due to time constraints, it was not possible to optimally select for two surrogate peptides per protein being investigated. Although 2-3 unique peptides were selected for proteins at the assay development phase, it soon became clear that several peptides for different proteins co-

eluted at very similar chromatographic times, with significant overlap between very similar mass/charge ratios to be monitored. This affected the accuracy of quantification/resolution of quantification, such that the number of sampling points across each peak dropped below the acceptable threshold of 12 points. For this reason, a decision was made to rationalise the masses being monitored at co-eluting time points to maximise the number of proteins being measured. Whilst this may theoretically reduce the specificity of the quantification, each peptide that was selected as a surrogate based on its length and uniqueness, which was confirmed in a Uniprot BLAST search to be assured that the peptide sequence did not occur in any other known protein.

Whilst one cannot be certain that the peptide measured is indeed a suitable surrogate for the protein without further experimentation, one can be certain that the same analyte was measured across both the patients with and without events.

The peptide targeted for APOD contained a methionine residue in it. The modified form (methionine oxidation) was not targeted due to the limited analytical space of the PRM assay, but brief early exploratory tests (data not shown) showed that the methionine oxidized form of the peptide only existed in negligible amounts in samples.

Although the stability of the light peptides in the autosampler over several days was not assessed formally, the heavy peptides were (Figure 4-8), and overall would appear to be fairly stable over the short duration in which they were being used as standards.

Run to run differences in absolute quantification seen in these experiments infer that shotgun proteomic experiments, which are typically label-free experiments, should be interpreted with some caution. The fact that most of the targeted peptides correlated well with the proteins 'discovered' in the discovery study was reassuring, but the fact that almost 1/3 did not correlate well has important implications on how one should select biomarker candidates.

This could to some extent be mitigated by using a labelled approach, which could be limited by the number of isotopic labels, but also by increasing the number of samples.

The use of the same cohort of patients (PRIMID-AS patients) but including all patients as the verification cohort only effectively doubled the number of 'controls'. There was an effective increase in proportion of patients with moderate AS in the verification cohort compared to the discovery cohort. This was an important limitation. This step was therefore a verification process and not a validation process; validation should still be performed in different cohorts of patients if the results are to be generalizable.

The event-rate in this study was low. Despite this, after adjusting for the multiple biomarkers investigated in the verification part of the study, APOD was still significantly associated with the endpoint. Identifying more novel markers will require a substantially larger patient cohort if adjusting for multiple testing. The PRIMID cohort was unique in that patients were recruited from multiple centres with extensive phenotyping, physicians were blinded to phenotyping results to avoid referral bias. However, symptom development remains a soft endpoint which is subjective, and the referrer's prejudices about the severity of the stenosis may bias a patient's perception on symptoms.

APOD may reflect high density lipoprotein levels, because the CSH method used to enrich for lower abundance proteins has an increased affinity for hydrophobic proteins, which explains the preponderance of apolipoproteins. However, although Apolipoprotein C3 and C2 were both correlated to APOD, neither of the former were associated with the endpoint, suggesting that APOD levels were affected by other factors in addition to general lipoprotein levels.

## 4.7 Conclusion

In this study, I identified APOD as a novel plasma-based biomarker associated with spontaneous symptom-development or death/hospital admissions due to AS in patients with moderate-severe AS over short-term follow up. It was independently prognostic to sex, AS severity, exercise testing and NTproBNP. It was particularly useful in moderate AS but was also useful across the whole cohort. On the whole, addition of APOD to existing risk-stratification models improved classification substantially, with between 50-78% net improvement in reclassification over baseline. Important correlates of APOD levels in plasma were tetranectin, BMI, afamin, serum amyloid A4, complement C3 and NTproBNP levels, which allude to the molecular function of APOD. Important markers which were not prognostic of the composite endpoint were LGE, ECV and high sensitivity troponin. Utility of APOD as a marker to anticipate events could help with optimal timing of AVR.

## **Chapter 5 Summary and Future Work**

### **5.1 Summary**

In this thesis, I set out to test two hypotheses:-

- 1) That plasma proteomics would discover biomarkers that were better than existing risk stratification strategies in asymptomatic moderate-severe AS, and
- 2) That plasma proteomics would uncover novel pathways involved in the progression of asymptomatic moderate-severe AS.

I explored two sample preparation workflows – immunodepletion + protein fractionation, and EV+CSH pull-down method. I found that for label-free proteomic quantification and protein identification, the latter method identified more proteins and was highly reproducible. I showed that the EV+CSH workflow can prepare samples cheaply and can be ready for MS analysis within 3 days, and can be easily scaled-up to a large clinical study. Combined, these workflows identified and quantified >1500 proteins on a 75 minute gradient, allowing fairly rapid profiling of plasma proteins.

I also explored the protein network pathways arising from differential protein expression patterns which may be important in the progression of asymptomatic moderate-severe AS to either symptomatic AS or an AV-related event. There was a suggestion of increased cell death/apoptotic/autophagy factors, inflammation, ion-channel remodelling, DNA transcription and repair, neuronal remodelling, heme catabolism, coagulation and complement activation, lysosomal protection as well as a probable increase in fatty acid oxidation which may all contribute to progression of this condition.



I selected a number of pragmatic targets to create a multiplexed-PRM assay utilising a heavy-labelled pooled-standard as the internal standard for verification, and discovered the importance of APOD as a strong and independent prognostic predictor of progression of asymptomatic moderate-severe AS during short to medium term follow-up. This marker is novel in the field of cardiovascular science, and particularly in AS. I observed that this marker substantially up-classified patients who went on to have an event and down-classified patients who did not have an event, making it a potentially useful tool in the optimal timing of AVR in patients with asymptomatic moderate-severe AS. I explored potential determinants of APOD and identified tetranectin as a strong correlate, as well as body weight.

In summary, I have tested the hypotheses laid out above; 1) Plasma proteomics does discover biomarkers that are independent to existing strategies and 2) Plasma proteomics has revealed novel pathways that are dysregulated in progression of asymptomatic AS. I did not identify a superior multimarker panel that improved on APOD + baseline characteristics (e.g. having moderate AS with MPG >30mmHg).

## **5.2 Context**

The field of MS-based plasma proteomics is coming of age. The work presented here represents only the tip-of-the-iceberg of what is possible in this field. It is an example of the traditional triangular approach of biomarker discovery – looking for as many potential candidates as possible in a small number of clearly defined phenotypic samples, validating as many candidates as one can afford, in validation cohorts (generally much larger than discovery cohorts) then confirming a few clear-cut single biomarkers for clinical use (Rifai et al., 2006). However, the rate of FDA-approval of new biomarkers has not mirrored the exponential growth of biomarker candidates from proteomic studies (Anderson, 2010), which could be due to the attrition rate at the validation stage.

Experts propose that the reason for this was the (initial) inherent limitation of MS-based plasma proteomics – low throughput analysis (Geyer et al., 2017). Deep proteome discovery required extensive fractionation and depletion steps – often taking several days to weeks from sampling to human interpretable results, at prohibitive costs. In comparison, large scale clinical enzymatic assays can deliver thousands of results per hour at low cost, and whilst immunoassays are more expensive, most of the widely used automated assays available require between 10-30 minutes for analysis.

An alternative paradigm is to utilise high-throughput proteomics to profile the proteome of individuals, and retain all the information to be studied both now and later. This rectangular approach to biomarker discovery, where the discovery and validation cohort of samples are analysed in parallel with shotgun proteomics, but only significantly differentiated proteins within the discovery cohort are tested within the validation cohort, has been proposed as a natural evolution in biomarker analysis that maximizes the multiplexing capability and specificity of MS-proteomics-based methods to personalise medicine (Geyer et al., 2017). In order to obtain the statistical power for this sort of study, very large sample sets need to be analysed (despite the high reproducibility of each measurement) to account for the high number of variables/analytes being identified and measured. This sort of analysis would not only cover most if not all of the known biomarkers in the market, but also several other proteins within a single test, allowing the relative differences between proteins to be measured and interpreted accordingly. The additional benefit of having all these additional data points profiled is that all the data has been banked and future retrospective analysis of different disease/outcomes in the same individuals will be possible, identifying relevant pathways without repeating the tests or performing different tests.

The methods explored in this thesis could be finessed to increase the throughput – due to the high reproducibility the CSH method, and could be extended to a 96-well format for

automated liquid handling robots to automatically prepare each sample for MS analysis.

Recently, one group demonstrated how one could use only 1  $\mu\text{L}$  of plasma from a fingerprick, combined with an accelerated denaturation, reduction, alkylation, digestion and desalting protocol all occurring within a pipette tip; followed by a short LCMSMS run, to quantify 300 proteins. The whole sample preparation process from blood withdrawal, digestion and mass spectrometer only took 3 hours (Geyer et al., 2016), but given the accelerated protocol could profile the proteome of 72 patients per day. They also describe that the addition of a single fractionation step would increase the quantification to 1000 proteins, but with an increased time cost. Many of the accelerated methods could be adopted to the methods in this thesis to increase throughput, which could allow extensive profiling of large biobanks of people/patients, allowing better precision in medicine (Geyer et al., 2017).

Plasma proteomics does not stand alone in this pursuit of precision medicine. Other complementary methods – genomics and metabolomics also help improve on the precision of diagnosis and treatment. Genomics has identified genotypes and single nucleotide polymorphisms with high accuracy which are associated with disease and disease susceptibility. Proteomics is a form of transcriptomic technology – as it is the expressed protein machinery that determines the phenotype. Between genotyping and protein expression there is also RNA sequencing, another form of transcriptomic profiling. On the other hand, metabolomic profiling involves looking at small molecules that are produced whether as by-products of host metabolism or from the microbiota that accompany their hosts – e.g. in the gut. Increasingly these symbiotic organisms are thought to participate in health and disease and add complexity to the multiple interactions which determine phenotype.

Producing data for analysis is the easier aspect of these ‘omics’ technologies, in comparison to interpretation of patterns in the data. This is largely due to gaps in the knowledge base regarding the roles of various proteins/genes/metabolites on disease and health. However,

advancements in machine-learning and ‘deep-learning’ or artificial intelligence may well negate the need to fully understand the biology behind the ‘perturbations’ but allow recognition of the diagnosis and potentially allow prescription of precise therapeutic options for the condition (Beckmann and Lew, 2016). Already these approaches have been applied to improve precision in paediatric cancer diagnosis and treatment (Forrest et al., 2018).

In AS, survival is determined by two factors – the ability to compensate for the pressure overload – without cellular loss, and the risk of AVR. Due to the pressures on the health system, waiting lists are inevitable and methods to identify asymptomatic patients at risk of decompensating could potentially allow early referral for AVR even before symptoms develop. It is this scenario where measuring APOD levels may be most useful in AS.

The counter argument is that given the low risk of AVR, should we not just perform AVR on everyone with moderate-severe AS pre-emptively? Pre-emptive AVR without performing further risk stratification would not only increase the number of patients awaiting AVR on waiting lists, increasing the risk of those who need it urgently, but also unnecessarily exposing patients with low risk of progression to procedural risks and risks of a deteriorating bioprosthetic valve.

### **5.3 Future Work**

This study has generated several new hypotheses that need more work. Having verified that APOD was associated with the endpoint, quantotypic peptides of APOD should be identified. The assay could be optimized with synthetic peptide standards, and a proper optimisation for ultimate sensitivity could be performed and used in an independent validation study. Of the other 59 proteins, the proteins associated with oxidative stress look promising – (GSTO and CPVL) to be evaluated as related biomarkers. Due to their low abundance levels and limited detectability, a peptide heavy standard will need to be created and an optimised workflow to

detect the peptides in the sample may allow these promising proteins to be reliably measured, just like APOD.

APOD has been found in myocardium; however, its molecular role in the endothelium or myocardium in response to AS needs further investigation. It may be that it has an active role or it may be that it is simply a buffer to prevent excessive damage to intracellular lysosomes. Another possibility is that the beneficial effect may have something to do with liver and fat metabolism. Evaluating its molecular function in myocardium could first be done on tissue culture, before it could be evaluated in another species. Other proteins in the LXR/RXR pathway could also be evaluated in AS to extend the understanding and prognosis associated with the disease.

Once more is understood about APOD's role, it could be used to improve selection of patients for randomised control trials of early AVR vs watchful waiting in asymptomatic AS, and may be used to improve the risk stratification in these patients, especially if they are unable to exercise, or where symptom reporting may be considered unreliable.

## **Chapter 6    Appendix**

- 6.1   Tables summarising current state-of-the-art of prognostic biomarkers in aortic stenosis**
- 6.2   Larger network diagram(s) for all differentially expressed proteins in the discovery study**
- 6.3   Protein lists (digital copy – available online)**

## **6.1 Tables for all current prognostic biomarkers in AS**

Rest of page intentionally blank

Class	Source	Biomarker	What it measures	Population	Outcomes	Findings	Comment
BNP	(Sato et al., 2019)	Brain natriuretic peptide	Neurohormonal activation	Severe symptomatic aortic stenosis who underwent transcatheter aortic valve replacement (n=193)	Brain natriuretic peptide levels pre and post valve replacement in subgroups of left ventricular remodelling	Brain natriuretic peptide levels decreased after valve replacement. Eccentric hypertrophy had the highest levels pre valve replacement and the greatest decrease post procedure. Brain natriuretic levels associated with all-cause mortality, and poorer reverse remodelling and poorer exercise tolerance following valve replacement	High BNP levels preoperatively associated with poorer prognosis after valve replacement and associated with eccentric hypertrophy
BNP	(Goodman et al., 2016)	BNP	Neurohormonal activation	Moderate-severe aortic stenosis with preserved ejection fraction (n=531)	mortality	BNP associated with increased mortality (HR 1.16) and provides incremental prognostic information to Left ventricular global longitudinal strain.	Increasing BNP independently associated with increased risk of death
BNP	(Henri et al., 2014)	Serial BNP levels	Change in neurohormonal activation	Asymptomatic aortic stenosis (n=69)	Symptoms, AVR or CV death	Higher rate of change of BNP (>20pg/mL/year) associated with higher risk of endpoint (HR 2.73) after adjustment	Higher rate of change of BNP during follow up associated with higher risk of aortic valve related events



Class	Source	Biomarker	What it measures	Population	Outcomes	Findings	Comment
BNP	(Ben-Dor et al., 2013)	BNP	Neurohormonal activation	Severe AS undergoing TAVI (n=289)	Mortality	BNP level not significantly associated with degree of AS severity or mortality	BNP is not associated with mortality but correlated with ejection fraction and pulmonary pressures
BNP	(Mannacio et al., 2013)	BNP	Neurohormonal activation	Severe aortic stenosis undergoing AVR (n=113)	Diastolic dysfunction	Postoperative BNP levels correlated with diastolic dysfunction grade	BNP post operatively predicts diastolic dysfunction
BNP	(Katz et al., 2012)	BNP and NTproBNP	Neurohormonal activation	Severe AS (n=64)	6 year all-cause mortality	BNP >135 pg/mL and NTproBNP > 1150pg/mL at baseline both associated with long term mortality (HR 3.2 and 4.3 respectively), even after adjustment	BNP and NTproBNP both independently predictive of mortality
BNP	(Iwahashi et al., 2011)	BNP	Neurohormonal activation	Severe AS considered for AVR (n=109)	Death, Heart failure, Stroke	In patients who underwent AVR, BNP >312 pg/mL predicted perioperative complications (OR 5.58) and post-operative death/hospitalisation /stroke (HR 8.8)	BNP predicts perioperative complications and long term mortality/heart failure/stroke

Class	Source	Biomarker	What it measures	Population	Outcomes	Findings	Comment
BNP	(Kefer et al., 2010)	BNP	Neurohormonal activation	Severe AS undergoing TAVI (n=58)	30 day mortality	Baseline BNP >428 mg/dL and increase of BNP by >170pg/mL at 24 hours after TAVI associated with higher risk of death at 30 days	High pre TAVI BNP and an acute rise in BNP post TAVI associated with highest risk of early death
BNP	(Lancellotti et al., 2010)	BNP	Neurohormonal activation	Asymptomatic moderate-severe AS (n=126)	Onset of symptoms, cardiovascular death and AVR	BNP >61pg/mL associated with a 10x higher risk of AVR/symptoms/death. Other markers were left atrial size and markers of diastolic dysfunction	BNP may reflect diastolic indices and associated with risk in asymptomatic moderate-severe AS. Exercise testing, AVA, Peak velocity and aortic MPG not independently associated with outcome
BNP	(Mizutani et al., 2017)	BNP	Neurohormonal activation	Patients undergoing TAVI (n=1094)	All-cause mortality	BNP >202pg/mL at discharge associated with higher risk of mortality at 2 years (HR 2.28)	High BNP levels at discharge associated with worse outcomes (BNP > 202 pg/mL similar risk to NTproBNP >4299 pg/mL)

Class	Source	Biomarker	What it measures	Population	Outcomes	Findings	Comment
NT-proBNP	(Kaneko et al., 2019)	NTproBNP	Neurohormonal activation	Severe AS and heart failure undergoing TAVI (n=717)	<30% reduction NTproBNP levels pre and post TAVI classed as non-response	NTproBNP non-reponse associated with lower survival rates. Determinants of non-response were female, diabetes, chronic kidney disease, atrial fibrillation, coronary revascularisation, permanent pacemaker after TAVI and baseline NTproBNP levels.	NTproBNP non-response associated with poorer survival after TAVI
NT-proBNP	(Mizutani et al., 2018)	NTproBNP	Neurohormonal activation	Severe AS with TAVI (n=500)	2 year prognostic impact (on all cause mortality and heart failure hospitalisation) of NTproBNP levels at discharge following TAVI	Higher NTproBNP levels at time of discharge associated with worse outcomes (adjusted hazard ratio 2.21 if discharge NTproBNP >4299pg/mL)	High NTproBNP levels following TAVI associated with worse outcomes

Class	Source	Biomarker	What it measures	Population	Outcomes	Findings	Comment
NT-proBNP	(Nguyen et al., 2017)	NTproBNP	Neurohormonal activation	Mild to severe AS (n=809)	AS related events within 2 years	NTproBNP associated with AS severity and symptom status. Determinants of levels also include coronary disease, rhythm and diastolic function. NTproBNP not associated with events after adjustment for AS severity	Negative study for NTproBNP in asymptomatic AS
NT-proBNP	(Farré et al., 2014)	NTproBNP and Monin score	Neurohormonal activation	Asymptomatic moderate/severe AS (n=237)	Aortic valve related events	NTproBNP adapted for the monin score risk stratifies patients into useful risk categories	Peak valve velocity, female sex and NTproBNP used in a risk score improves risk stratification in asymptomatic moderate-severe AS
NT-proBNP	(Boer et al., 2013)	NTproBNP	Neurohormonal activation	Severe aortic stenosis awaiting AVR (n=31)	Correlation of NTproBNP and diastolic indices	NTproBNP pre-AVR correlates with diastolic function before and after AVR	NTproBNP pre-operatively predicts diastolic dysfunction

Class	Source	Biomarker	What it measures	Population	Outcomes	Findings	Comment
NT-proBNP	(Mizutani et al., 2018)	NTproBNP	Neurohormonal activation	Severe AS with TAVI (n=500)	2 year prognostic impact (on all cause mortality and heart failure hospitalisation) of NTproBNP levels at discharge following TAVI	Higher NTproBNP levels at time of discharge associated with worse outcomes (adjusted hazard ratio 2.21 if discharge NTproBNP >4299pg/mL)	High NTproBNP levels following TAVI associated with worse outcomes
NT-proBNP	(Nguyen et al., 2017)	NTproBNP	Neurohormonal activation	Mild to severe AS (n=809)	AS related events within 2 years	NTproBNP associated with AS severity and symptom status. Determinants of levels also include coronary disease, rhythm and diastolic function. NTproBNP not associated with events after adjustment for AS severity	Negative study for NTproBNP in asymptomatic AS
NT-proBNP	(Farré et al., 2014)	NTproBNP and Monin score	Neurohormonal activation	Asymptomatic moderate/severe AS (n=237)	Aortic valve related events	NTproBNP adapted for the monin score risk stratifies patients into useful risk categories	Peak valve velocity, female sex and NTproBNP used in a risk score improves risk stratification in asymptomatic moderate-severe AS
NT-proBNP	(Boer et al., 2013)	NTproBNP	Neurohormonal activation	Severe aortic stenosis awaiting AVR (n=31)	Correlation of NTproBNP and diastolic indices	NTproBNP pre-AVR correlates with diastolic function before and after AVR	NTproBNP pre-operatively predicts diastolic dysfunction

Class	Source	Biomarker	What it measures	Population	Outcomes	Findings	Comment
NT-proBNP	(Elhmidi et al., 2013)	NTproBNP	Neurohormonal activation	Severe AS undergoing TAVI (n=373)	Mortality and heart failure hospitalisation	NTproBNP and atrial fibrillation were independent predictors of 1 year mortality after TAVI	
NT-proBNP	(Lopez-Otero et al., 2013)	NTproBNP	Neurohormonal activation	Severe AS undergoing TAVI (n=85)	Mortality after TAVI compared to Logistic Euroscore	Only log-NTproBNP was associated with short term (HR 11) and long term (HR 11) mortality, Euroscore was not.	NTproBNP better than Euroscore at predicting mortality following TAVI
NT-proBNP	(Weber et al., 2006)	NTproBNP	Neurohormonal activation	Conservatively treated or surgically treated AS (n=159)	Death, Heart failure	Baseline NTproBNP predicted outcome particularly in conservatively treated AS, but not predictive in patient who underwent AVR	Non-randomised study which may have replaced AVR in patients at lower risk of adverse events
NT-proBNP	(Bergler-Klein et al., 2004)	BNP, NTproBNP, NTproANP	Neurohormonal activation	Very Severe AS all-comers (n=130)	Symptom-free survival, postoperative survival	NTproBNP <80 pmol/L predicts symptom free survival in asymptomatic patients, independently predicts post-op death, NYHA class > II and EF <50% postoperatively	NTproBNP was the only predictor of poor outcome post AVR and low levels predict symptom free survival in asymptomatic aortic stenosis

Class	Source	Biomarker	What it measures	Population	Outcomes	Findings	Comment
Troponin	(Kohler et al., 2016)	HSTnT	Myocardial injury	Aortic stenosis undergoing TAVI (n=259)	Time to death	Highest quartile of preprocedural HsTnT independently predictive of mortality during follow-up, not in the 3 days post TAVI	Myocardial injury preTAVI is an independent predictor of death following TAVI
Troponin	(Koskinas et al., 2016)	cTnT	Myocardial injury	TAVI patients with severe AS (n=577)	All cause mortality at 30 days and 2 years	cTnT >15x ULN associated with higher risk of mortality at 30 days (HR 8.77) and still predicts mortality at 2 years (HR 1.98) and modified risk associated with complex coronary disease	Elevated troponin post-TAVI in patients with complex coronary disease associated with much higher risk of death
Troponin	(Chin et al., 2014)	HsTnI	Myocardial injury	Aortic stenosis (n=161) and controls (n=46) with MRI studies and aortic stenosis with follow-up (n=104)	Late gadolinium enhancement and all cause mortality	HsTnI associated with myocardial fibrosis, and increased risk of AVR and death (HR 1.77), even after adjustment	HsTnI also associated with death and AVR in patients with moderate-severe AS
Troponin	(Chorianopoulos et al., 2014)	Troponin T	Myocardial injury	Severe AS undergoing TAVI (n=198)	Mortality	Pre TAVI Troponin T and peak peri-TAVI Troponin T predicts 1 year mortality, but not short-term mortality.	Troponin T predicts mortality not NTproBNP

Class	Source	Biomarker	What it measures	Population	Outcomes	Findings	Comment
Troponin	(Frank et al., 2013)	HsTnT	Myocardial injury	Severe AS undergoing TAVI	mortality	Preprocedural HsTnT predicts survival post TAVI	
Troponin	(Saito et al., 2013)	HsTnT	myocardial injury	Aortic stenosis undergoing AVR (n=60)	Composite of heart failure, fatal arrhythmia, all cause mortality	HsTnT independently predicts composite outcome (HR 3.71) despite AVR	HsTnT associated with higher risk even after AVR
Troponin	(Rosjo et al., 2011)	HsTnT	Myocardial injury	Aortic stenosis with myocardial hypertrophy (n=57)	Correlation with left ventricular mass	HsTnT >27 ng/L and NTproBNP >3594 pg/mL associated with mortality during long term follow up	HsTnT and NTproBNP both predict mortality in patients with severe AS, and were of similar levels in patients who did and didn't have AVR



Class	Source	Biomarker	What it measures	Population	Outcomes	Findings	Comment
Multiple	(Ferrer-Sistach et al., 2019)	High sensitivity Troponin T, NTproBNP and ST2	Myocardial injury	Asymptomatic severe aortic stenosis (n=58)	Composite of cardiovascular death, new symptoms, cardiac hospitalisation, valve replacement	Hs-TNT independently associated with primary outcome, HR 9.62. ST2 not predictive even on univariate, NTproBNP predictive on univariate but not independent on multivariable analysis	Elevated high sensitivity troponin (>10ng/L) improved prediction of the primary outcome
Multiple	(Dahou et al., 2018)	BNP & HsTNT	Multimarker	Low flow low gradient aortic stenosis (n=98)	Two year mortality stratified by BNP >550pg/mL and hsTnT >15ng/L	The group with BNP >550pg/mL and HsTnT >15ng/L independently associated with highest risk of mortality at 2 years	Adding HsTnT to BNP provides additional information about long term mortality in LFLG aortic stenosis
Multiple	(Auensen et al., 2017)	BNP, Troponin T, HsCRP	Multimarker	Severe AS evaluated for possible valve replacement (n=442)	3 year all cause mortality and risk of MACE in 1 year	NTproBNP, HsTnT or hs-CRP not associated with 3 year all cause mortality following SAVR. HsTNT (HR 1.51) and LVEF (HR 0.97) associated with MACE for operated patients.	HsTNT associated with MACE not mortality, in SAVR. BNP not associated with mortality or MACE.

Class	Source	Biomarker	What it measures	Population	Outcomes	Findings	Comment
Multiple	(Kapelouzou et al., 2015)	MMP 2&9, TIMP1, TNFa, IL2, TGFb1, fetuin-A, Osteopontin, Osteoprotegerin, sclerostin, relaxin-2, MCP-1, MDA	collagen turnover, inflammatory factors, fibrosis regulation, calcification regulation, macrophagic migration/infiltration regulation, oxidation	Calcific aortic valves	Correlations between biomarkers and valvular calcification	Biomarkers associated with aortic valve stenosis, valvular calcification, remodelling and inflammation are increased both in the valve tissue and serum compared to healthy patients	hypothesis generating
Multiple	(Lindman et al., 2015)	GDF 15, ST2, NTproBNP, Galectin 3, HsTNT, Myeloperoxidase, HsCRP, MCP1	Cardiovascular stress, Neurohormonal activation, Myocardial injury	Patients referred for valve replacement (surgical and TAVI)	All-cause mortality	Only ST2, GDF 15 and NTproBNP retained in parsimonious model to predict mortality. Highest risk of death was associated with all three markers being elevated.	Multimarker approach to risk stratification may be better than single markers
Multiple	(Parenica et al., 2012)	Multiple markers	Multiple pathways	Severe AS undergoing TAVI/SAVR	Adverse clinical outcomes (death, hospitalisation and complications)	Malondialdehyde (marker of oxidative stress) predictive of adverse clinical outcomes (c-statistic = 0.77-0.87)	Malondialdehyde independently predicts adverse outcomes post TAVI

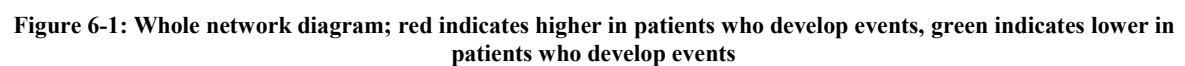
Class	Source	Biomarker	What it measures	Population	Outcomes	Findings	Comment
Multiple	(Solberg et al., 2012)	HsTnT and NTproBNP	Multimarker	Severe AS referred for AVR (n=136)	Mortality and AVR	NTproBNP correlated with aortic pressure gradient. Both HsTnT and NTproBNP correlated with LV function. HsTnT, NTproBNP and Diabetes associated with all cause mortality in symptomatic patients who underwent AVR	HsTnT and NTproBNP and Diabetes predicted death in patients who underwent AVR
5-adenosyl-homo-cysteine	(Elmariah et al., 2016)	Metabolite panel	Metabolomic profiling	TAVR patients (n=44)	Acute kidney injury after TAVR	5-adenosylhomocysteine at baseline predicted AKI after TAVR, independent of glomerular filtration rate, and also predictive of mortality during follow up.	Metabolite changes in TAVI patients at baseline predict acute kidney injury and mortality
Anaemia	(Arai et al., 2015)	Anaemia	Anaemia	French national TAVI registry (n=3472)	Acute kidney injury and 1 year mortality	Incremental Pre and post procedural anaemia associated with incremental risk of acute kidney injury and 1 year mortality.	Anaemia is an important risk factor for poor outcome post TAVI

Class	Source	Biomarker	What it measures	Population	Outcomes	Findings	Comment
cMyC	(Anand et al., 2018)	Cardiac myosin-binding protein C	Myocardial injury	Aortic stenosis (n=161) and controls (n=46) with MRI studies and aortic stenosis with follow-up (n=104)	Late gadolinium enhancement and all-cause mortality	cMyC associated with left ventricular mass, fibrosis and extracellular volume in aortic stenosis. cMyC higher if late gadolinium present, and is associated with all-cause mortality	cMyC similar to troponin
Cystatin C	(Johansson et al., 2014)	Cystatin C	Early kidney injury	Severe AS undergoing TAVI (n=68)	Acute kidney injury	Preoperative cystatin C is slightly better than eGFR with creatinine in predicting post-operative AKI.	Post-TAVI acute kidney injury is generally progressive and does not recover fully
Fib-1	(Dahl et al., 2012)	Fibulin-1	Remodelling processes	Severe aortic stenosis awaiting AVR (n=125)	LV diastolic function preoperatively	Fibulin-1 associated with restrictive filling of left ventricle	Fibulin-1, like natriuretic peptides is a marker of restrictive LV filling in patients with symptomatic AS
Galectin-3	(Arangalage et al., 2016)	galectin 3	myocardial fibrosis	mild to severe AS (n=583)	composite of AS related events (sudden death, heart failure, new onset of symptoms)	Galectin-3 was not associated with aortic valve related events	galectin-3 not associated with aortic valve related events
GDF15	(Krau et al., 2015)	GDF 15	Cardiac stress	Severe AS undergoing TAVI (n=217)	All cause mortality	GDF-15 superior to NTproBNP to predict mortality (HR 1.97) even after adjustment for other factors	High GDF-15 levels identifies patients undergoing TAVI at higher risk of death during follow up.

Class	Source	Biomarker	What it measures	Population	Outcomes	Findings	Comment
HMW-vWF	(Kellermair et al., 2018)	High-molecular-weight von willebrand factor Multimer Ratio	Marker of sheer flow	Low flow low gradient aortic stenosis	Differences in vWF HMW multimer ratios between true severe and pseudo severe aortic stenosis	HMW vWF multimer ratios are significantly higher in pseudo-severe AS	HMW vWF levels may help differentiate pseudo and true severe AS without other imaging modalities
LP(a)	(Ljungberg et al., 2017)	Lipoprotein(a) and Apolipoprotein B/A1 ratio	Adverse lipid risk factor	Population surveys of patients undergoing aortic valve replacements for AS	Lipoprotein(a) and Apolipoprotein B/A1 ratios differences between patients with or without concomittent coronary artery disease	High levels of Lp(a) and ApoB/A1 ratios associated with AVR for AS with concomittent CAD only (OR 1.29)	Adverse lipid profile identifies concomittent coronary artery disease, in patients with severe AS
Micro-particles	(Jung et al., 2017)	Microparticles	Mechanical shear stress	Severe AS undergoing TAVI (n=92)	Changes in levels of microparticles (endothelial and platelet microparticles) pre and post-TAVI	Endothelial microparticles (CD31+/CD42- did not change pre and post TAVI, but CD62E+/CD31+/CD 42- reduced significantly). Platelet microparticles (CD31+/CD42b+) increased significantly during follow-up.	TAVI may lead to improvement in shear stress and endothelial cell function
Micro-RNA	(Chen et al., 2014)	miR-378, miR-1, miR-133	Regulation of left ventricular hypertrophy	moderate severe AS (n=112)	left ventricular hypertrophy	miR-378 predicts LVH independent of pressure gradient (OR 4.11)	microRNA may play an important role in regulating LV adaptive remodelling
Micro-RNA	(Rosjo et al., 2014)	miR-210	Cardiovascular risk	Moderate-severe AS and matched healthy controls (n=57)	All-cause mortality	miR-210 higher in AS. Associated risk of mortality during follow up (HR 3.3)	miR-210 independently prognostic of death in patients with AS.

Class	Source	Biomarker	What it measures	Population	Outcomes	Findings	Comment
Micro-RNA	(Garcia et al., 2013)	miR-133a	Reverse remodelling	LV biopsies from AS patients who had AVR	Regression of LV hypertrophy	Preoperative circulating miR-133a associated with regression of LV mass 1-year after AVR, AUC (0.89)	Circulating miR-133a could identify highly likely responders to AVR
Mr-pro-ADM	(Csordas et al., 2015)	Midregional Proadrenomedullin	Left ventricular stretch/stress	Severe AS undergoing TAVI (n=153)	all-cause mortality	MRproADM > 1.3nmol/L independently associated with mortality (HR 9.9)	High MRproADM levels in TAVI patients predict mortality over and above Euroscore II
NGAL	(Kidher et al., 2014)	NGAL	kidney injury	Post-AVR for AS	Acute kidney injury (AKI)	Preoperative aortic pulse wave velocity does not predict AKI post operatively, but plasma NGAL predicts post OP AKI as well as need for early medical renal intervention	Preoperative NGAL is an important marker of immediate post-op renal injury
OPG	(Borowiec et al., 2015)	Osteoprotegerin	Calcification	Mild to moderate aortic stenosis (n=70)	Progression of aortic stenosis	Osteoprotegerin associated with degree of AS. Associated with age, valvular gradient, coronary artery disease. Only metabolic syndrome was independently predictive of progression of AS.	Osteoprotegerin associated with AS severity, not progression of disease

Class	Source	Biomarker	What it measures	Population	Outcomes	Findings	Comment
ST2	(Cai et al., 2019)	ST2	Cardiac stress	Comparing ST2 in stable severe left ventricular systolic dysfunction with severe aortic stenosis	Levels of ST2	ST2 was similar in HF and AS group with preserved ejection fraction. ST2 levels significantly higher in the heart failure group with reduced ejection fraction.	Raised ST2 may be marker for subclinical/clinical left ventricular dysfunction
SuPAR	(Hodges et al., 2016)	Soluble urokinase plasminogen activator receptor (SuPAR)	Inflammatory marker of subclinical cardiovascular damage	Wide range of aortic stenosis severity (SEAS population) n=1503	Ischaemic events, Aortic valve events, mortality	suPAR independently associated with ischaemic cardiovascular events (HR 1.5) and mortality (HR 2) but not significant for aortic valve events	suPAR may reflect presence of concomitant coronary disease and associated risk
ucMGP	(Ueland et al., 2010)	Undercarboxylated matrix Gla protein	Inhibition of (Valvular) Calcification	Symptomatic Severe AS (n=147) & Healthy controls (n=147)	All-cause mortality	Circulating uncarboxylated MGP levels (>950pmol/L) associated with LV function and mortality (HR 9) independent of NTproBNP and LV function	Uncarboxylated MGP levels provided additional prognostic information to NTproBNP and LV function in severe AS





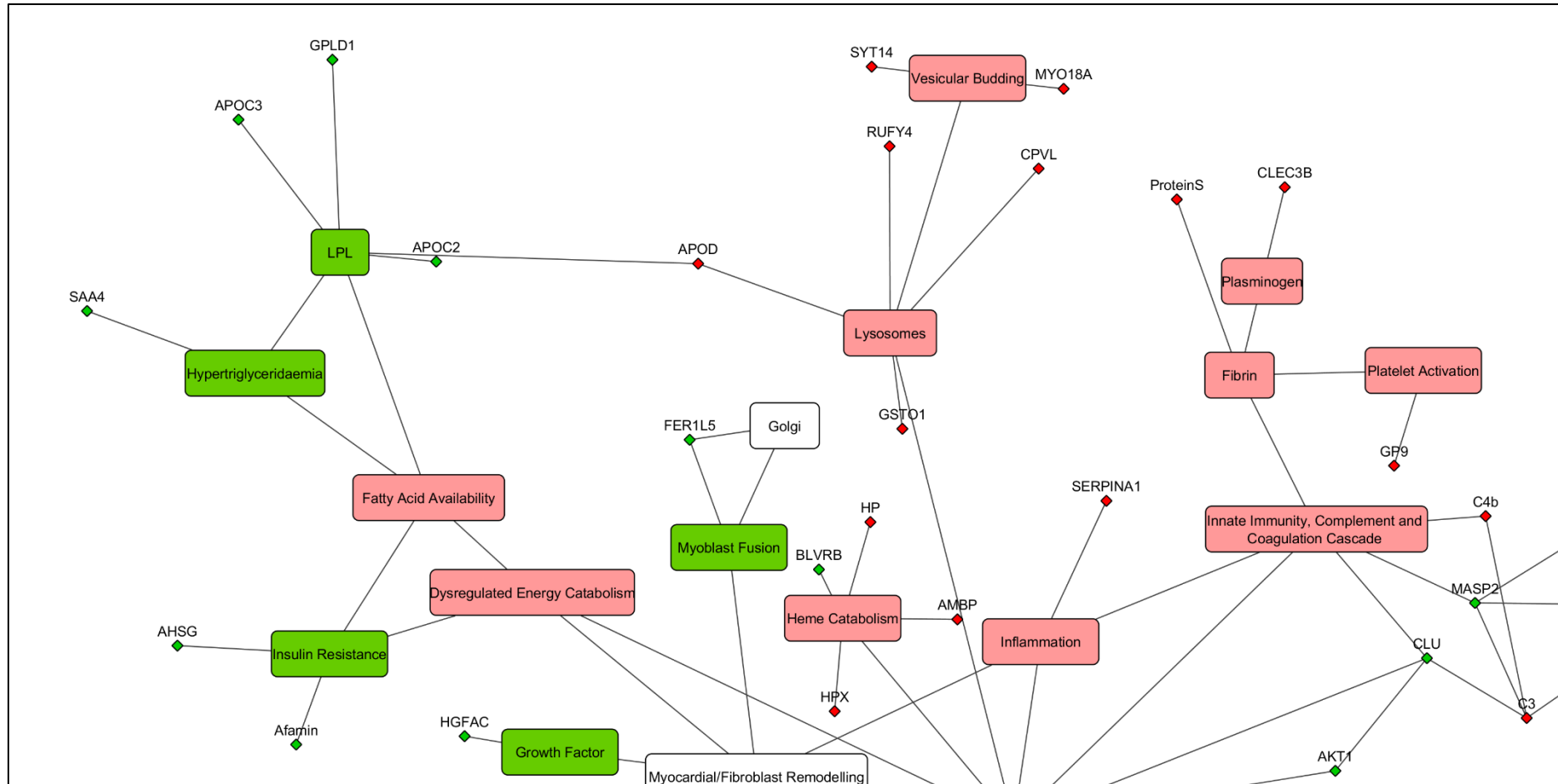
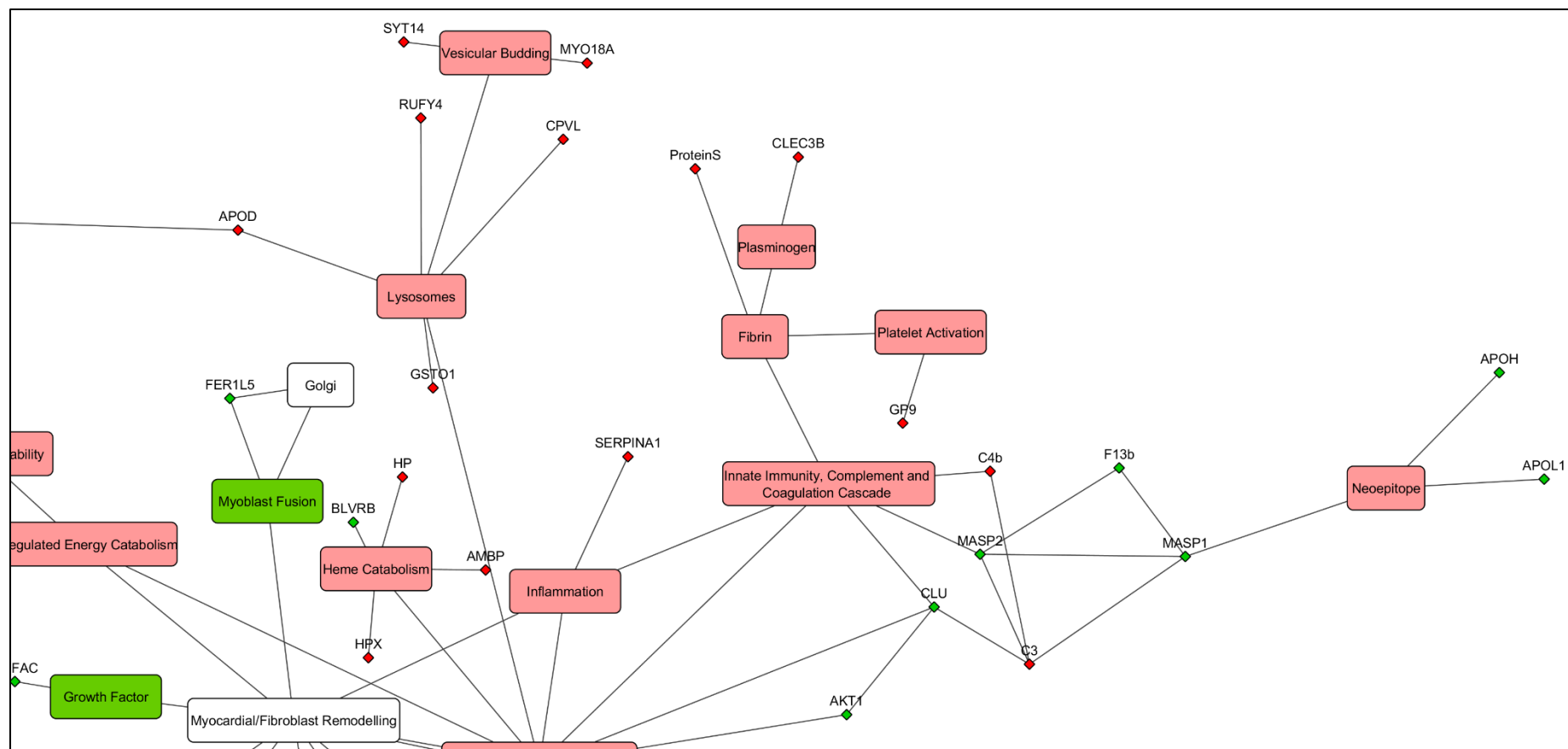


Figure 6-2: Top-left of network diagram in Figure 3-24; red indicates higher in patients who develop events, green indicates lower in patients who develop events



**Figure 6-3: Top-right of network diagram in Figure 3-24; red indicates higher in patients who develop events, green indicates lower in patients who develop events**

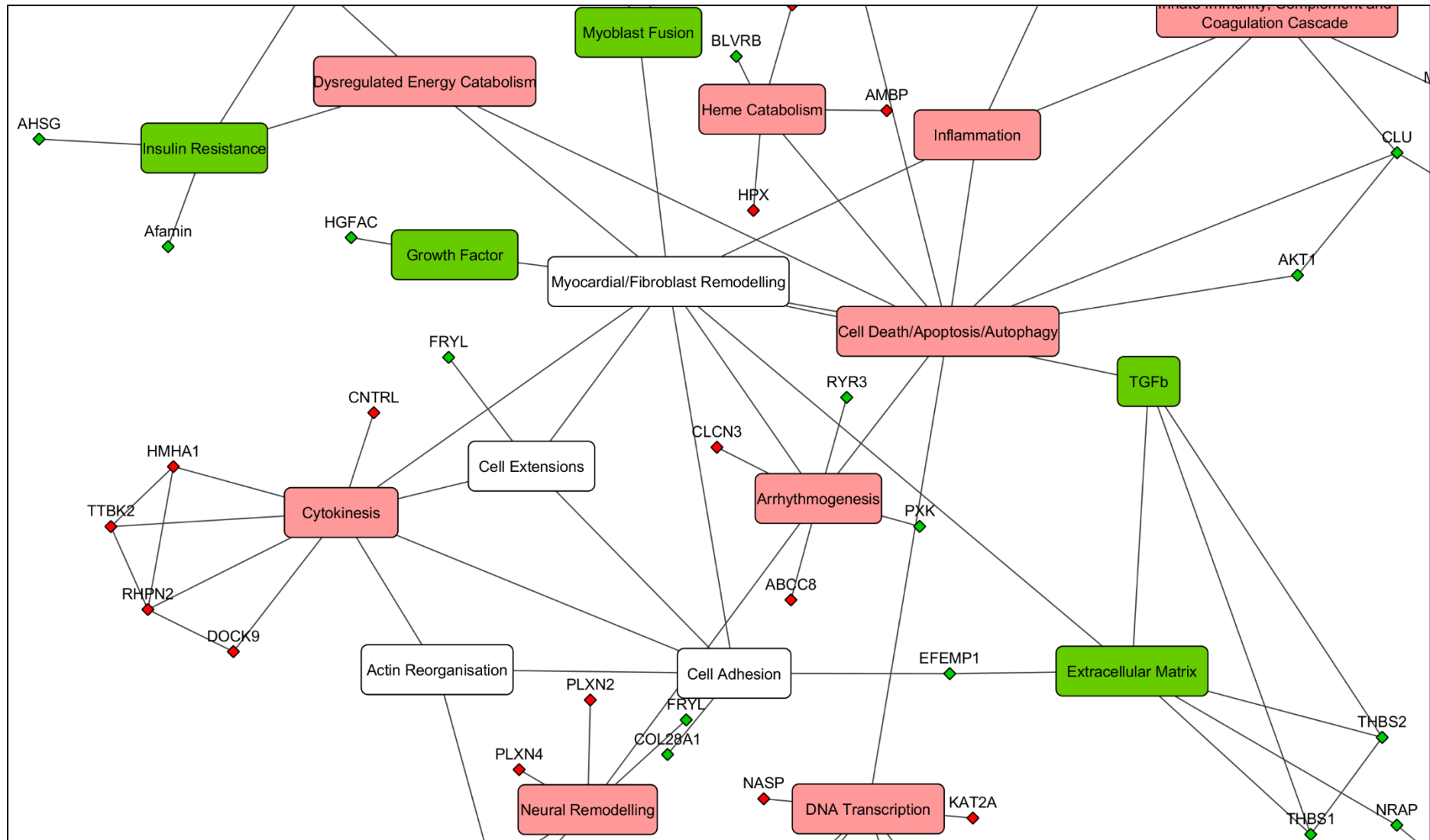


Figure 6-4: Middle of network diagram in Figure 3-24; red indicates higher in patients who develop events, green indicates lower in patients who develop events

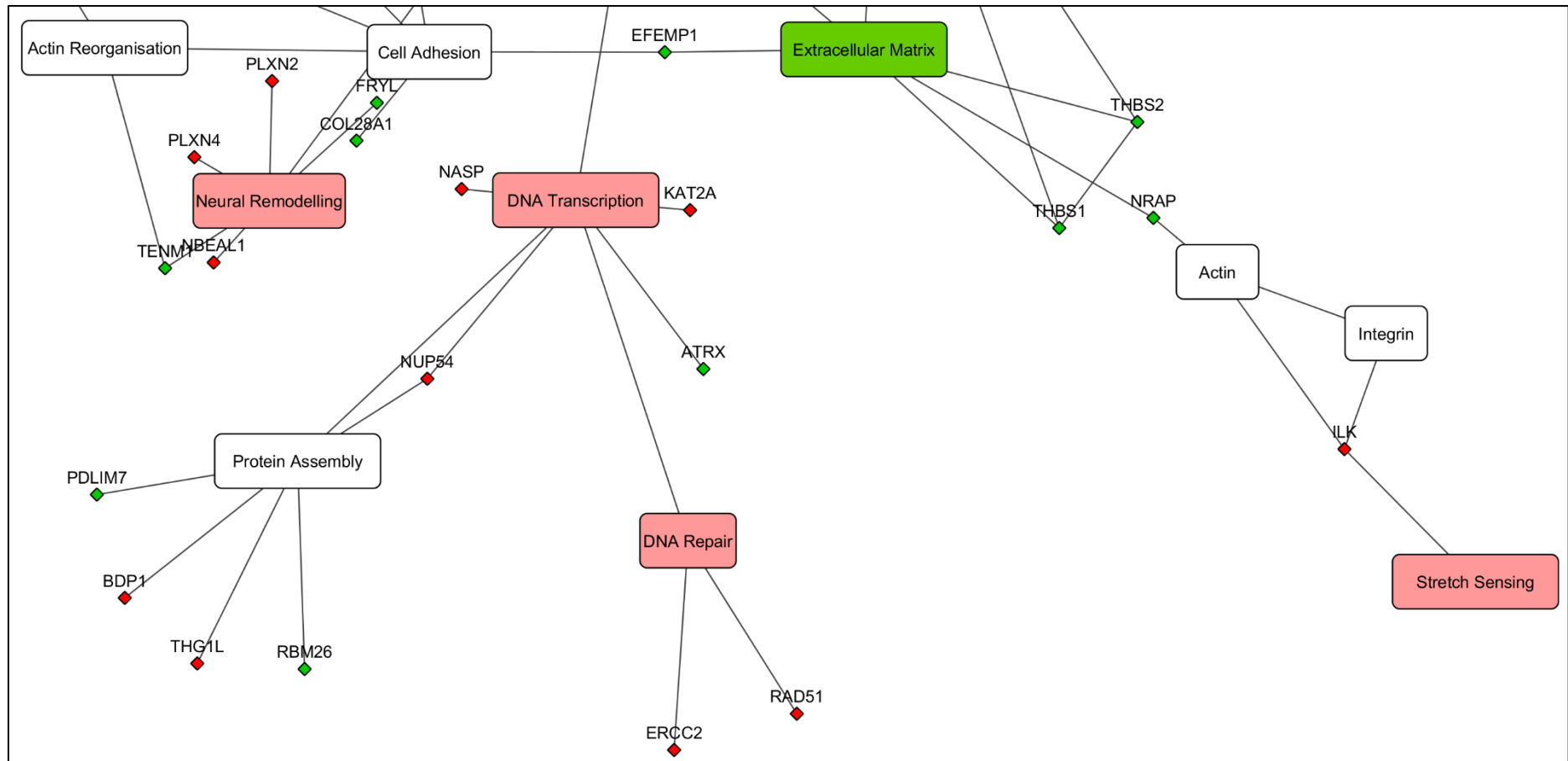


Figure 6-5: Bottom of network diagram in Figure 3-24; red indicates higher in patients who develop events, green indicates lower in patients who develop events

This Sheet contains a protein list from one run of 5 fractions using MARS14 Depletion -> Guanidine/DTT/IAA -> MRP-c18 -> Qexactive

Accession	Description	Coverage(%)	# Peptides	Fraction2	Fraction3	Fraction4	Fraction5	Fraction1+6
P35527	Keratin, type I cytoskeletal 9 OS=Homo sapiens GN=KRT9 PE=1 SV=3	15.24879615	7	X				
P62328	Thymosin beta-4 OS=Homo sapiens GN=TMSB4X PE=1 SV=2	43.18181818	2	X				
P01034	Cystatin-C OS=Homo sapiens GN=CST3 PE=1 SV=1	41.78082192	5		X			
P01608	Ig kappa chain V-I region Roy OS=Homo sapiens PE=1 SV=1	24.07407407	2		X			
P01609	Ig kappa chain V-I region Scw OS=Homo sapiens PE=1 SV=1	27.77777778	2		X			
P01624	Ig kappa chain V-III region POM OS=Homo sapiens PE=1 SV=1	24.7706422	2		X			
P04434	Ig kappa chain V-III region VH (Fragment) OS=Homo sapiens PE=4 SV=1	23.27586207	2		X			
P05019	Insulin-like growth factor I OS=Homo sapiens GN=IGF1 PE=1 SV=1	7.179487179	2		X			
P05362	Intercellular adhesion molecule 1 OS=Homo sapiens GN=ICAM1 PE=1 SV=2	5.263157895	2		X			
P07737	Profilin-1 OS=Homo sapiens GN=PFN1 PE=1 SV=2	37.14285714	4		X			
P08294	Extracellular superoxide dismutase [Cu-Zn] OS=Homo sapiens GN=SOD3 PE=1 SV=2	10	2		X			
P13598	Intercellular adhesion molecule 2 OS=Homo sapiens GN=ICAM2 PE=1 SV=2	9.090909091	2		X			
P14151	L-selectin OS=Homo sapiens GN=SELL PE=1 SV=2	7.795698925	2		X			
P22891	Vitamin K-dependent protein Z OS=Homo sapiens GN=PROZ PE=1 SV=2	30.5	9		X			
P33151	Cadherin-5 OS=Homo sapiens GN=CDH5 PE=1 SV=5	5.102040816	3		X			
P99999	Cytochrome c OS=Homo sapiens GN=CYCS PE=1 SV=2	22.85714286	2		X			
Q03591	Complement factor H-related protein 1 OS=Homo sapiens GN=CFHR1 PE=1 SV=2	42.12121212	8		X			
Q6UXB8	Peptidase inhibitor 16 OS=Homo sapiens GN=PI16 PE=1 SV=1	9.287257019	3		X			
Q99969	Retinoic acid receptor responder protein 2 OS=Homo sapiens GN=RARRES2 PE=1 SV=1	14.11042945	2		X			
Q9BXR6	Complement factor H-related protein 5 OS=Homo sapiens GN=CFHR5 PE=1 SV=1	12.30228471	6		X			
Q9Y5Y7	Lymphatic vessel endothelial hyaluronic acid receptor 1 OS=Homo sapiens GN=LYVE1 PE=1 SV=2	8.074534161	2		X			
P00746	Complement factor D OS=Homo sapiens GN=CFD PE=1 SV=5	22.52964427	4			X		
P03951	Coagulation factor XI OS=Homo sapiens GN=F11 PE=1 SV=1	10.88	4			X		
P0DJ19	Serum amyloid A-2 protein OS=Homo sapiens GN=SAA2 PE=1 SV=1	23.7704918	2			X		
P22105	Tenascin-X OS=Homo sapiens GN=TNXB PE=1 SV=3	0.512940079	2			X		
Q14520	Hyaluronan-binding protein 2 OS=Homo sapiens GN=HABP2 PE=1 SV=1	4.642857143	2			X		
P02042	Hemoglobin subunit delta OS=Homo sapiens GN=HBD PE=1 SV=2	48.29931973	7				X	
P06702	Protein S100-A9 OS=Homo sapiens GN=S100A9 PE=1 SV=1	35.96491228	3				X	
P0C0L4	Complement C4-A OS=Homo sapiens GN=C4A PE=1 SV=2	56.8233945	72				X	
P18206	Vinculin OS=Homo sapiens GN=VCL PE=1 SV=4	2.821869489	2				X	
P31151	Protein S100-A7 OS=Homo sapiens GN=S100A7 PE=1 SV=4	30.69306931	3				X	
P32119	Peroxiredoxin-2 OS=Homo sapiens GN=PRDX2 PE=1 SV=5	18.68686869	3				X	
P48740	Mannan-binding lectin serine protease 1 OS=Homo sapiens GN=MASP1 PE=1 SV=3	4.005722461	2				X	
Q6EMK4	Vasorin OS=Homo sapiens GN=VASN PE=1 SV=1	6.389301634	2				X	
Q8NBP7	Proprotein convertase subtilisin/kexin type 9 OS=Homo sapiens GN=PCSK9 PE=1 SV=3	3.757225434	2				X	
P02533	Keratin, type I cytoskeletal 14 OS=Homo sapiens GN=KRT14 PE=1 SV=4	4.449152542	2					X
P08779	Keratin, type I cytoskeletal 16 OS=Homo sapiens GN=KRT16 PE=1 SV=4	4.4397463	2					X
P19012	Keratin, type I cytoskeletal 15 OS=Homo sapiens GN=KRT15 PE=1 SV=3	4.605263158	2					X
P01344	Insulin-like growth factor II OS=Homo sapiens GN=IGF2 PE=1 SV=1	13.88888889	2	X	X			
P02775	Platelet basic protein OS=Homo sapiens GN=PPBP PE=1 SV=3	37.5	4	X	X			
P03950	Angiogenin OS=Homo sapiens GN=ANG PE=1 SV=1	24.48979592	2	X	X			
P17936	Insulin-like growth factor-binding protein 3 OS=Homo sapiens GN=IGFBP3 PE=1 SV=2	31.61512027	7	X	X			
P34096	Ribonuclease 4 OS=Homo sapiens GN=RNASE4 PE=1 SV=3	21.08843537	2	X	X			
P07996	Thrombospondin-1 OS=Homo sapiens GN=THBS1 PE=1 SV=2	2.564102564	2	X		X		
P04207	Ig kappa chain V-III region CLL OS=Homo sapiens PE=1 SV=2	19.37984496	2		X	X		
P49908	Selenoprotein P OS=Homo sapiens GN=SEPP1 PE=1 SV=3	15.4855643	5		X	X		
P61626	Lysozyme C OS=Homo sapiens GN=LYZ PE=1 SV=1	12.16216216	2		X	X		
P61769	Beta-2-microglobulin OS=Homo sapiens GN=B2M PE=1 SV=1	21.8487395	2		X	X		

P68104	Elongation factor 1-alpha 1 OS=Homo sapiens GN=EEF1A1 PE=1 SV=1	7.359307359	3		X	X		
Q04756	Hepatocyte growth factor activator OS=Homo sapiens GN=HGFA1 PE=1 SV=1	4.732824427	2		X	X		
Q05639	Elongation factor 1-alpha 2 OS=Homo sapiens GN=EEF1A2 PE=1 SV=1	7.343412527	3		X	X		
Q10588	ADP-ribosyl cyclase 2 OS=Homo sapiens GN=BST1 PE=1 SV=2	7.547169811	2		X	X		
Q5VTE0	Putative elongation factor 1-alpha-like 3 OS=Homo sapiens GN=EEF1A1P5 PE=5 SV=1	7.359307359	3		X	X		
P35908	Keratin, type II cytoskeletal 2 epidermal OS=Homo sapiens GN=KRT2 PE=1 SV=2	5.633802817	3		X			X
P01877	Ig alpha-2 chain C region OS=Homo sapiens GN=IGHA2 PE=1 SV=3	48.23529412	10			X	X	
P04070	Vitamin K-dependent protein C OS=Homo sapiens GN=PROC PE=1 SV=1	5.856832972	2			X	X	
P04406	Glyceraldehyde-3-phosphate dehydrogenase OS=Homo sapiens GN=GAPDH PE=1 SV=3	13.43283582	2			X	X	
P05109	Protein S100-A8 OS=Homo sapiens GN=S100A8 PE=1 SV=1	23.65591398	2			X	X	
P23142	Fibulin-1 OS=Homo sapiens GN=FBLN1 PE=1 SV=4	7.112375533	3			X	X	
P55056	Apolipoprotein C-IV OS=Homo sapiens GN=APOC4 PE=1 SV=1	18.11023622	3			X	X	
P98160	Basement membrane-specific heparan sulfate proteoglycan core protein OS=Homo sapiens GN=HSPG2 PE=1 SV=4	0.72876338	2			X	X	
O00391	Sulfhydryl oxidase 1 OS=Homo sapiens GN=QSOX1 PE=1 SV=3	8.701472557	4				X	X
O14791	Apolipoprotein L1 OS=Homo sapiens GN=APOL1 PE=1 SV=5	39.44723618	10				X	X
P02747	Complement C1q subcomponent subunit C OS=Homo sapiens GN=C1QC PE=1 SV=3	26.93877551	4				X	X
P02750	Leucine-rich alpha-2-glycoprotein OS=Homo sapiens GN=LRG1 PE=1 SV=2	38.04034582	9				X	X
P04180	Phosphatidylcholine-sterol acyltransferase OS=Homo sapiens GN=LCAT PE=1 SV=1	11.13636364	4				X	X
P04278	Sex hormone-binding globulin OS=Homo sapiens GN=SHBG PE=1 SV=2	21.14427861	5				X	X
P05154	Plasma serine protease inhibitor OS=Homo sapiens GN=SERPINA5 PE=1 SV=3	20.68965517	7				X	X
P05543	Thyroxine-binding globulin OS=Homo sapiens GN=SERPINA7 PE=1 SV=2	37.59036145	9				X	X
P06276	Cholinesterase OS=Homo sapiens GN=BCHPE=1 SV=1	5.315614618	2				X	X
P08185	Corticosteroid-binding globulin OS=Homo sapiens GN=SERPINA6 PE=1 SV=1	16.2962963	4				X	X
P08571	Monocyte differentiation antigen CD14 OS=Homo sapiens GN=CD14 PE=1 SV=2	13.6	3				X	X
P0C0L5	Complement C4-B OS=Homo sapiens GN=C4B PE=1 SV=2	59.11697248	75				X	X
P13796	Plastin-2 OS=Homo sapiens GN=LCP1 PE=1 SV=6	7.655502392	3				X	X
P18428	Lipopolysaccharide-binding protein OS=Homo sapiens GN=LBP PE=1 SV=3	17.04781705	6				X	X
P22792	Carboxypeptidase N subunit 2 OS=Homo sapiens GN=CPN2 PE=1 SV=3	17.98165138	6				X	X
P27348	14-3-3 protein theta OS=Homo sapiens GN=YWHAQ PE=1 SV=1	7.346938776	2				X	X
P29622	Kallistatin OS=Homo sapiens GN=SERPINA4 PE=1 SV=3	55.97189696	19				X	X
P31946	14-3-3 protein beta/alpha OS=Homo sapiens GN=YWHAB PE=1 SV=3	7.317073171	2				X	X
P31947	14-3-3 protein sigma OS=Homo sapiens GN=SFN PE=1 SV=1	7.258064516	2				X	X
P35858	Insulin-like growth factor-binding protein complex acid labile subunit OS=Homo sapiens GN=IGFALS PE=1 SV=1	37.19008264	17				X	X
P36955	Pigment epithelium-derived factor OS=Homo sapiens GN=SERPINF1 PE=1 SV=4	27.99043062	9				X	X
P43251	Biotinidase OS=Homo sapiens GN=BTDD PE=1 SV=2	7.550644567	2				X	X
P55058	Phospholipid transfer protein OS=Homo sapiens GN=PLTP PE=1 SV=1	7.505070994	2				X	X
P60709	Actin, cytoplasmic 1 OS=Homo sapiens GN=ACTB PE=1 SV=1	17.86666667	5				X	X
P61981	14-3-3 protein gamma OS=Homo sapiens GN=YWHAG PE=1 SV=2	7.287449393	2				X	X
P62258	14-3-3 protein epsilon OS=Homo sapiens GN=YWHAE PE=1 SV=1	7.058823529	2				X	X
P63104	14-3-3 protein zeta/delta OS=Homo sapiens GN=YWHAZ PE=1 SV=1	7.346938776	2				X	X
P63261	Actin, cytoplasmic 2 OS=Homo sapiens GN=ACTG1 PE=1 SV=1	17.86666667	5				X	X
P68032	Actin, alpha cardiac muscle 1 OS=Homo sapiens GN=ACTC1 PE=1 SV=1	17.24137931	5				X	X
P68133	Actin, alpha skeletal muscle OS=Homo sapiens GN=ACTA1 PE=1 SV=1	17.24137931	5				X	X
Q04917	14-3-3 protein eta OS=Homo sapiens GN=YWHAH PE=1 SV=4	7.317073171	2				X	X
Q13790	Apolipoprotein F OS=Homo sapiens GN=APOF PE=1 SV=2	15.03067485	2				X	X
Q15582	Transforming growth factor-beta-induced protein ig-h3 OS=Homo sapiens GN=TGFBI PE=1 SV=1	7.027818448	3				X	X
Q961Y4	Carboxypeptidase B2 OS=Homo sapiens GN=CPB2 PE=1 SV=2	21.27659574	6				X	X
Q96KN2	Beta-Ala-His dipeptidase OS=Homo sapiens GN=CNDP1 PE=1 SV=4	38.85601578	14				X	X
Q9UK55	Protein Z-dependent protease inhibitor OS=Homo sapiens GN=SERPINA10 PE=1 SV=1	16.89189189	6				X	X
Q9Y490	Talin-1 OS=Homo sapiens GN=TLN1 PE=1 SV=3	2.085792995	3				X	X
O43866	CD5 antigen-like OS=Homo sapiens GN=CD5L PE=1 SV=1	36.59942363	9	X	X	X		

P01591	Immunoglobulin J chain OS=Homo sapiens GN=IGJ PE=1 SV=4	20.75471698		3	X		X	X		
P01610	Ig kappa chain V-I region WEA OS=Homo sapiens PE=1 SV=1	36.11111111		3	X		X	X		
P0DJ18	Serum amyloid A-1 protein OS=Homo sapiens GN=SAA1 PE=1 SV=1	40.98360656		4	X		X	X		
P13645	Keratin, type I cytoskeletal 10 OS=Homo sapiens GN=KRT10 PE=1 SV=6	14.38356164		5	X		X		X	
P05090	Apolipoprotein D OS=Homo sapiens GN=APOD PE=1 SV=1	20.10582011		3	X				X	X
P07360	Complement component C8 gamma chain OS=Homo sapiens GN=C8G PE=1 SV=3	46.03960396		7	X				X	X
P16070	CD44 antigen OS=Homo sapiens GN=CD44 PE=1 SV=3	2.964959569		2			X	X	X	
P20851	C4b-binding protein beta chain OS=Homo sapiens GN=C4BPB PE=1 SV=1	20.63492063		4			X	X	X	
P36980	Complement factor H-related protein 2 OS=Homo sapiens GN=CFHR2 PE=1 SV=1	40		6			X	X	X	
Q15166	Serum paraoxonase/lactonase 3 OS=Homo sapiens GN=PON3 PE=1 SV=3	5.93220339		2			X	X	X	
Q92954	Proteoglycan 4 OS=Homo sapiens GN=PRG4 PE=1 SV=2	8.190883191		9			X	X	X	
P08519	Apolipoprotein(a) OS=Homo sapiens GN=LPA PE=1 SV=1	10.51011434		2			X	X		X
P00488	Coagulation factor XIII A chain OS=Homo sapiens GN=F13A1 PE=1 SV=4	14.48087432		8			X		X	X
O75882	Attractin OS=Homo sapiens GN=ATRN PE=1 SV=2	9.167249825		8				X	X	X
P00915	Carbonic anhydrase 1 OS=Homo sapiens GN=CA1 PE=1 SV=2	14.94252874		3				X	X	X
P01876	Ig alpha-1 chain C region OS=Homo sapiens GN=IGHA1 PE=1 SV=2	50.42492918		12				X	X	X
P01880	Ig delta chain C region OS=Homo sapiens GN=IGHD PE=1 SV=2	15.10416667		4				X	X	X
P04220	Ig mu heavy chain disease protein OS=Homo sapiens PE=1 SV=1	34.7826087		8				X	X	X
P07358	Complement component C8 beta chain OS=Homo sapiens GN=C8B PE=1 SV=3	51.77664975		20				X	X	X
P10643	Complement component C7 OS=Homo sapiens GN=C7 PE=1 SV=2	23.60616845		14				X	X	X
P15169	Carboxypeptidase N catalytic chain OS=Homo sapiens GN=CPN1 PE=1 SV=1	35.58951965		9				X	X	X
P22352	Glutathione peroxidase 3 OS=Homo sapiens GN=GPX3 PE=1 SV=2	22.56637168		4				X	X	X
P26927	Hepatocyte growth factor-like protein OS=Homo sapiens GN=MST1 PE=1 SV=2	22.22222222		11				X	X	X
P35542	Serum amyloid A-4 protein OS=Homo sapiens GN=SAA4 PE=1 SV=2	20		2				X	X	X
P51884	Lumican OS=Homo sapiens GN=LUM PE=1 SV=2	34.9112426		10				X	X	X
P80108	Phosphatidylinositol-glycan-specific phospholipase D OS=Homo sapiens GN=GPLD1 PE=1 SV=3	14.16666667		10				X	X	X
Q06033	Inter-alpha-trypsin inhibitor heavy chain H3 OS=Homo sapiens GN=ITH3 PE=1 SV=2	14.26966292		9				X	X	X
Q9NZP8	Complement C1r subcomponent-like protein OS=Homo sapiens GN=C1RL PE=1 SV=2	8.829568789		3				X	X	X
P01042	Kininogen-1 OS=Homo sapiens GN=KNG1 PE=1 SV=2	41.92546584		22	X		X	X	X	
P27918	Properdin OS=Homo sapiens GN=CFP PE=1 SV=2	17.48400853		6	X		X	X	X	
O95445	Apolipoprotein M OS=Homo sapiens GN=APOM PE=1 SV=2	22.87234043		3	X		X			X
P01008	Antithrombin-III OS=Homo sapiens GN=SERPINC1 PE=1 SV=1	57.75862069		26	X		X		X	X
P01019	Angiotensinogen OS=Homo sapiens GN=AGT PE=1 SV=1	36.28865979		14	X		X		X	X
P02649	Apolipoprotein E OS=Homo sapiens GN=APOE PE=1 SV=1	47.94952681		13	X		X		X	X
P04259	Keratin, type II cytoskeletal 6B OS=Homo sapiens GN=KRT6B PE=1 SV=5	3.90070922		2	X		X		X	X
P06727	Apolipoprotein A-IV OS=Homo sapiens GN=APOA4 PE=1 SV=3	62.62626263		24	X		X		X	X
P43652	Afamin OS=Homo sapiens GN=AFM PE=1 SV=1	44.74123539		19	X		X		X	X
P02655	Apolipoprotein C-II OS=Homo sapiens GN=APOC2 PE=1 SV=1	43.56435644		4	X			X	X	X
P02746	Complement C1q subcomponent subunit B OS=Homo sapiens GN=C1QB PE=1 SV=3	41.50197628		7	X			X	X	X
P68871	Hemoglobin subunit beta OS=Homo sapiens GN=HBB PE=1 SV=2	82.99319728		12	X			X	X	X
Q9UGM5	Fetuin-B OS=Homo sapiens GN=FETUB PE=1 SV=2	10.9947644		4	X			X	X	X
B9A064	Immunoglobulin lambda-like polypeptide 5 OS=Homo sapiens GN=IGLL5 PE=2 SV=2	32.24299065		4			X	X	X	X
O00187	Mannan-binding lectin serine protease 2 OS=Homo sapiens GN=MASP2 PE=1 SV=4	3.352769679		2			X	X	X	X
O75636	Ficolin-3 OS=Homo sapiens GN=FCN3 PE=1 SV=2	34.11371237		6			X	X	X	X
P00736	Complement C1r subcomponent OS=Homo sapiens GN=C1R PE=1 SV=2	35.88652482		14			X	X	X	X
P00740	Coagulation factor IX OS=Homo sapiens GN=F9 PE=1 SV=2	18.87201735		6			X	X	X	X
P00748	Coagulation factor XII OS=Homo sapiens GN=F12 PE=1 SV=3	17.39837398		8			X	X	X	X
P02745	Complement C1q subcomponent subunit A OS=Homo sapiens GN=C1QA PE=1 SV=2	20.40816327		3			X	X	X	X
P02753	Retinol-binding protein 4 OS=Homo sapiens GN=RBP4 PE=1 SV=3	56.21890547		8			X	X	X	X
P03952	Plasma kallikrein OS=Homo sapiens GN=KLKB1 PE=1 SV=1	20.37617555		10			X	X	X	X
P05160	Coagulation factor XIII B chain OS=Homo sapiens GN=F13B PE=1 SV=3	40.39334342		18			X	X	X	X

P06681	Complement C2 OS=Homo sapiens GN=C2 PE=1 SV=2	19.14893617	13		X	X	X	X
P07357	Complement component C8 alpha chain OS=Homo sapiens GN=C8A PE=1 SV=2	18.83561644	6		X	X	X	X
P0CG04	Ig lambda-1 chain C regions OS=Homo sapiens GN=IGLC1 PE=1 SV=1	65.09433962	4		X	X	X	X
P12259	Coagulation factor V OS=Homo sapiens GN=F5 PE=1 SV=4	5.575539568	10		X	X	X	X
P25311	Zinc-alpha-2-glycoprotein OS=Homo sapiens GN=AZGP1 PE=1 SV=2	57.38255034	18		X	X	X	X
Q96PD5	N-acetylmuramoyl-L-alanine amidase OS=Homo sapiens GN=PGLYRP2 PE=1 SV=1	39.58333333	14		X	X	X	X
A0M8Q6	Ig lambda-7 chain C region OS=Homo sapiens GN=IGLC7 PE=1 SV=2	50.94339623	3	X	X	X	X	X
P00450	Ceruloplasmin OS=Homo sapiens GN=CP PE=1 SV=1	66.1971831	51	X	X	X	X	X
P00734	Prothrombin OS=Homo sapiens GN=F2 PE=1 SV=2	52.25080386	30	X	X	X	X	X
P00738	Haptoglobin OS=Homo sapiens GN=HP PE=1 SV=1	64.28571429	27	X	X	X	X	X
P00739	Haptoglobin-related protein OS=Homo sapiens GN=HPR PE=1 SV=2	68.67816092	21	X	X	X	X	X
P00742	Coagulation factor X OS=Homo sapiens GN=F10 PE=1 SV=2	20.28688525	10	X	X	X	X	X
P00747	Plasminogen OS=Homo sapiens GN=PLG PE=1 SV=2	59.62962963	36	X	X	X	X	X
P00751	Complement factor B OS=Homo sapiens GN=CFB PE=1 SV=2	54.05759162	34	X	X	X	X	X
P01009	Alpha-1-antitrypsin OS=Homo sapiens GN=SERPINA1 PE=1 SV=3	66.50717703	30	X	X	X	X	X
P01011	Alpha-1-antichymotrypsin OS=Homo sapiens GN=SERPINA3 PE=1 SV=2	46.3356974	17	X	X	X	X	X
P01023	Alpha-2-macroglobulin OS=Homo sapiens GN=A2M PE=1 SV=3	62.21166893	66	X	X	X	X	X
P01024	Complement C3 OS=Homo sapiens GN=C3 PE=1 SV=2	37.34215274	42	X	X	X	X	X
P01031	Complement C5 OS=Homo sapiens GN=C5 PE=1 SV=4	20.82338902	23	X	X	X	X	X
P01613	Ig kappa chain V-I region Ni OS=Homo sapiens PE=1 SV=1	30.35714286	2	X	X	X	X	X
P01620	Ig kappa chain V-III region SIE OS=Homo sapiens PE=1 SV=1	31.19266055	2	X	X	X	X	X
P01622	Ig kappa chain V-III region Ti OS=Homo sapiens PE=1 SV=1	31.19266055	2	X	X	X	X	X
P01623	Ig kappa chain V-III region WOL OS=Homo sapiens PE=1 SV=1	31.19266055	2	X	X	X	X	X
P01701	Ig lambda chain V-I region NEW OS=Homo sapiens PE=1 SV=1	27.02702703	2	X	X	X	X	X
P01834	Ig kappa chain C region OS=Homo sapiens GN=IGKC PE=1 SV=1	82.0754717	7	X	X	X	X	X
P01857	Ig gamma-1 chain C region OS=Homo sapiens GN=IGHG1 PE=1 SV=1	50	13	X	X	X	X	X
P01859	Ig gamma-2 chain C region OS=Homo sapiens GN=IGHG2 PE=1 SV=2	46.3190184	10	X	X	X	X	X
P01860	Ig gamma-3 chain C region OS=Homo sapiens GN=IGHG3 PE=1 SV=2	45.0928382	13	X	X	X	X	X
P01861	Ig gamma-4 chain C region OS=Homo sapiens GN=IGHG4 PE=1 SV=1	32.72171254	8	X	X	X	X	X
P01871	Ig mu chain C region OS=Homo sapiens GN=IGHM PE=1 SV=3	38.27433628	14	X	X	X	X	X
P02647	Apolipoprotein A-I OS=Homo sapiens GN=APOA1 PE=1 SV=1	73.78277154	34	X	X	X	X	X
P02652	Apolipoprotein A-II OS=Homo sapiens GN=APOA2 PE=1 SV=1	72	10	X	X	X	X	X
P02654	Apolipoprotein C-I OS=Homo sapiens GN=APOC1 PE=1 SV=1	26.5060241	3	X	X	X	X	X
P02656	Apolipoprotein C-III OS=Homo sapiens GN=APOC3 PE=1 SV=1	55.55555556	6	X	X	X	X	X
P02671	Fibrinogen alpha chain OS=Homo sapiens GN=FGA PE=1 SV=2	25.05773672	18	X	X	X	X	X
P02675	Fibrinogen beta chain OS=Homo sapiens GN=FGB PE=1 SV=2	51.7311609	22	X	X	X	X	X
P02679	Fibrinogen gamma chain OS=Homo sapiens GN=FGG PE=1 SV=3	39.73509934	15	X	X	X	X	X
P02743	Serum amyloid P-component OS=Homo sapiens GN=APCS PE=1 SV=2	28.25112108	7	X	X	X	X	X
P02748	Complement component C9 OS=Homo sapiens GN=C9 PE=1 SV=2	33.81037567	14	X	X	X	X	X
P02749	Beta-2-glycoprotein 1 OS=Homo sapiens GN=APOH PE=1 SV=3	64.34782609	17	X	X	X	X	X
P02751	Fibronectin OS=Homo sapiens GN=FN1 PE=1 SV=4	35.37300922	46	X	X	X	X	X
P02760	Protein AMBP OS=Homo sapiens GN=AMBP PE=1 SV=1	37.21590909	10	X	X	X	X	X
P02763	Alpha-1-acid glycoprotein 1 OS=Homo sapiens GN=ORM1 PE=1 SV=1	40.7960199	10	X	X	X	X	X
P02765	Alpha-2-HS-glycoprotein OS=Homo sapiens GN=AHSG PE=1 SV=1	43.59673025	10	X	X	X	X	X
P02766	Transthyretin OS=Homo sapiens GN=TTR PE=1 SV=1	68.70748299	7	X	X	X	X	X
P02768	Serum albumin OS=Homo sapiens GN=ALB PE=1 SV=2	82.10180624	78	X	X	X	X	X
P02774	Vitamin D-binding protein OS=Homo sapiens GN=GC PE=1 SV=1	79.11392405	30	X	X	X	X	X
P02787	Serotransferrin OS=Homo sapiens GN=TF PE=1 SV=3	82.23495702	62	X	X	X	X	X
P02790	Hemopexin OS=Homo sapiens GN=HPX PE=1 SV=2	72.72727273	32	X	X	X	X	X
P04003	C4b-binding protein alpha chain OS=Homo sapiens GN=C4BPA PE=1 SV=2	45.05862647	20	X	X	X	X	X
P04004	Vitronectin OS=Homo sapiens GN=VTN PE=1 SV=1	21.12970711	8	X	X	X	X	X



P04114	Apolipoprotein B-100 OS=Homo sapiens GN=APOB PE=1 SV=2	47.16195485	171	X		X	X	X	X
P04196	Histidine-rich glycoprotein OS=Homo sapiens GN=HRG PE=1 SV=1	41.9047619	16	X		X	X	X	X
P04206	Ig kappa chain V-III region GOL OS=Homo sapiens PE=1 SV=1	31.19266055	2	X		X	X	X	X
P04208	Ig lambda chain V-I region WAH OS=Homo sapiens PE=1 SV=1	27.52293578	2	X		X	X	X	X
P04217	Alpha-1B-glycoprotein OS=Homo sapiens GN=A1BG PE=1 SV=4	56.76767677	16	X		X	X	X	X
P04264	Keratin, type II cytoskeletal 1 OS=Homo sapiens GN=KRT1 PE=1 SV=6	20.34161491	12	X		X	X	X	X
P05155	Plasma protease C1 inhibitor OS=Homo sapiens GN=SERPING1 PE=1 SV=2	31.8	13	X		X	X	X	X
P05156	Complement factor I OS=Homo sapiens GN=CFI PE=1 SV=2	29.67409949	16	X		X	X	X	X
P05452	Tetranectin OS=Homo sapiens GN=CLEC3B PE=1 SV=3	33.16831683	8	X		X	X	X	X
P05546	Heparin cofactor 2 OS=Homo sapiens GN=SERPIND1 PE=1 SV=3	30.46092184	13	X		X	X	X	X
P06396	Gelsolin OS=Homo sapiens GN=GSN PE=1 SV=1	35.42199488	16	X		X	X	X	X
P07225	Vitamin K-dependent protein S OS=Homo sapiens GN=PROS1 PE=1 SV=1	26.03550296	14	X		X	X	X	X
P08603	Complement factor H OS=Homo sapiens GN=CFH PE=1 SV=4	58.73273761	55	X		X	X	X	X
P08697	Alpha-2-antiplasmin OS=Homo sapiens GN=SERPINF2 PE=1 SV=3	44.60285132	13	X		X	X	X	X
P09871	Complement C1s subcomponent OS=Homo sapiens GN=C1S PE=1 SV=1	27.03488372	12	X		X	X	X	X
P0CG05	Ig lambda-2 chain C regions OS=Homo sapiens GN=IGLC2 PE=1 SV=1	65.09433962	4	X		X	X	X	X
P0CG06	Ig lambda-3 chain C regions OS=Homo sapiens GN=IGLC3 PE=1 SV=1	65.09433962	4	X		X	X	X	X
P10909	Clusterin OS=Homo sapiens GN=CLU PE=1 SV=1	35.63474388	17	X		X	X	X	X
P13671	Complement component C6 OS=Homo sapiens GN=C6 PE=1 SV=3	32.11991435	22	X		X	X	X	X
P19652	Alpha-1-acid glycoprotein 2 OS=Homo sapiens GN=ORM2 PE=1 SV=2	42.28855721	9	X		X	X	X	X
P19823	Inter-alpha-trypsin inhibitor heavy chain H2 OS=Homo sapiens GN=ITI2 PE=1 SV=2	40.06342495	27	X		X	X	X	X
P19827	Inter-alpha-trypsin inhibitor heavy chain H1 OS=Homo sapiens GN=ITI1 PE=1 SV=3	34.68715697	21	X		X	X	X	X
P27169	Serum paraoxonase/arylesterase 1 OS=Homo sapiens GN=PON1 PE=1 SV=3	43.09859155	9	X		X	X	X	X
P69905	Hemoglobin subunit alpha OS=Homo sapiens GN=HBA1 PE=1 SV=2	83.8028169	9	X		X	X	X	X
Q14624	Inter-alpha-trypsin inhibitor heavy chain H4 OS=Homo sapiens GN=ITI4 PE=1 SV=4	50.96774194	37	X		X	X	X	X
Q16610	Extracellular matrix protein 1 OS=Homo sapiens GN=ECM1 PE=1 SV=2	40.55555556	18	X		X	X	X	X

This list is representative of a no-acetate EV pulldown method on the Qexactive requiring 1 mL of plasma	
Accession	Description
P02768	Serum albumin OS=Homo sapiens GN=ALB PE=1 SV=2
P02647	Apolipoprotein A-I OS=Homo sapiens GN=APOA1 PE=1 SV=1
P07996	Thrombospondin-1 OS=Homo sapiens GN=THBS1 PE=1 SV=2
P01024	Complement C3 OS=Homo sapiens GN=C3 PE=1 SV=2
P08519	Apolipoprotein(a) OS=Homo sapiens GN=LPA PE=1 SV=1
P04275	von Willebrand factor OS=Homo sapiens GN=VWF PE=1 SV=4
Q9Y490	Talin-1 OS=Homo sapiens GN=TLN1 PE=1 SV=3
P35579	Myosin-9 OS=Homo sapiens GN=MYH9 PE=1 SV=4
P01023	Alpha-2-macroglobulin OS=Homo sapiens GN=A2M PE=1 SV=3
P00734	Prothrombin OS=Homo sapiens GN=F2 PE=1 SV=2
P02787	Serotransferrin OS=Homo sapiens GN=TF PE=1 SV=3
P04114	Apolipoprotein B-100 OS=Homo sapiens GN=APOB PE=1 SV=2
P02675	Fibrinogen beta chain OS=Homo sapiens GN=FGB PE=1 SV=2
P55072	Transitional endoplasmic reticulum ATPase OS=Homo sapiens GN=VCP PE=1 SV=4
P06576	ATP synthase subunit beta, mitochondrial OS=Homo sapiens GN=ATP5B PE=1 SV=3
Q9H4B7	Tubulin beta-1 chain OS=Homo sapiens GN=TUBB1 PE=1 SV=1
P11021	78 kDa glucose-regulated protein OS=Homo sapiens GN=HSPA5 PE=1 SV=2
P21333	Filamin-A OS=Homo sapiens GN=FLNA PE=1 SV=4
P19823	Inter-alpha-trypsin inhibitor heavy chain H2 OS=Homo sapiens GN=ITI2 PE=1 SV=2
P08603	Complement factor H OS=Homo sapiens GN=CFH PE=1 SV=4
P04264	Keratin, type II cytoskeletal 1 OS=Homo sapiens GN=KRT1 PE=1 SV=6
P02649	Apolipoprotein E OS=Homo sapiens GN=APOE PE=1 SV=1
P13645	Keratin, type I cytoskeletal 10 OS=Homo sapiens GN=KRT10 PE=1 SV=6
P35527	Keratin, type I cytoskeletal 9 OS=Homo sapiens GN=KRT9 PE=1 SV=3
P04003	C4b-binding protein alpha chain OS=Homo sapiens GN=C4BPA PE=1 SV=2
O00299	Chloride intracellular channel protein 1 OS=Homo sapiens GN=CLIC1 PE=1 SV=4
O00187	Mannan-binding lectin serine protease 2 OS=Homo sapiens GN=MASP2 PE=1 SV=4
P06727	Apolipoprotein A-IV OS=Homo sapiens GN=APOA4 PE=1 SV=3
P07737	Profilin-1 OS=Homo sapiens GN=PFN1 PE=1 SV=2
P02749	Beta-2-glycoprotein 1 OS=Homo sapiens GN=APOH PE=1 SV=3
P30101	Protein disulfide-isomerase A3 OS=Homo sapiens GN=PDIA3 PE=1 SV=4
P07225	Vitamin K-dependent protein S OS=Homo sapiens GN=PROS1 PE=1 SV=1
P01857	Ig gamma-1 chain C region OS=Homo sapiens GN=IGHG1 PE=1 SV=1
P00488	Coagulation factor XIII A chain OS=Homo sapiens GN=F13A1 PE=1 SV=4
P01834	Ig kappa chain C region OS=Homo sapiens GN=IGKC PE=1 SV=1
P00747	Plasminogen OS=Homo sapiens GN=PLG PE=1 SV=2
P01008	Antithrombin-III OS=Homo sapiens GN=SERPINC1 PE=1 SV=1
Q13201	Multimerin-1 OS=Homo sapiens GN=MMRN1 PE=1 SV=3
P02760	Protein AMBP OS=Homo sapiens GN=AMBP PE=1 SV=1
P00558	Phosphoglycerate kinase 1 OS=Homo sapiens GN=PGK1 PE=1 SV=3
P00736	Complement C1r subcomponent OS=Homo sapiens GN=C1R PE=1 SV=2
P61158	Actin-related protein 3 OS=Homo sapiens GN=ACTR3 PE=1 SV=3
P62937	Peptidyl-prolyl cis-trans isomerase A OS=Homo sapiens GN=PPIA PE=1 SV=2
P00751	Complement factor B OS=Homo sapiens GN=CFB PE=1 SV=2
P00738	Haptoglobin OS=Homo sapiens GN=HP PE=1 SV=1
P05090	Apolipoprotein D OS=Homo sapiens GN=APOD PE=1 SV=1
P02748	Complement component C9 OS=Homo sapiens GN=C9 PE=1 SV=2
P02766	Transthyretin OS=Homo sapiens GN=TTR PE=1 SV=1
P04004	Vitronectin OS=Homo sapiens GN=VTN PE=1 SV=1
Q13418	Integrin-linked protein kinase OS=Homo sapiens GN=ILK PE=1 SV=2
P51149	Ras-related protein Rab-7a OS=Homo sapiens GN=RAB7A PE=1 SV=1
P68366	Tubulin alpha-4A chain OS=Homo sapiens GN=TUBA4A PE=1 SV=1
O00151	PDZ and LIM domain protein 1 OS=Homo sapiens GN=PDLIM1 PE=1 SV=4
P02765	Alpha-2-HS-glycoprotein OS=Homo sapiens GN=AHSG PE=1 SV=1
O95810	Serum deprivation-response protein OS=Homo sapiens GN=SDPR PE=1 SV=3
P10809	60 kDa heat shock protein, mitochondrial OS=Homo sapiens GN=HSPD1 PE=1 SV=2
Q15365	Poly(rC)-binding protein 1 OS=Homo sapiens GN=PCBP1 PE=1 SV=2
Q9Y6C2	EMILIN-1 OS=Homo sapiens GN=EMILIN1 PE=1 SV=2
P02790	Hemopexin OS=Homo sapiens GN=HPX PE=1 SV=2
Q15942	Zyxin OS=Homo sapiens GN=ZYX PE=1 SV=1

P16671	Platelet glycoprotein 4 OS=Homo sapiens GN=CD36 PE=1 SV=2
P31948	Stress-induced-phosphoprotein 1 OS=Homo sapiens GN=STIP1 PE=1 SV=1
Q9Y624	Junctional adhesion molecule A OS=Homo sapiens GN=F11R PE=1 SV=1
P27169	Serum paraoxonase/arylesterase 1 OS=Homo sapiens GN=PON1 PE=1 SV=3
P04196	Histidine-rich glycoprotein OS=Homo sapiens GN=HRG PE=1 SV=1
P02775	Platelet basic protein OS=Homo sapiens GN=PPBP PE=1 SV=3
P14625	Endoplasmin OS=Homo sapiens GN=HSP90B1 PE=1 SV=1
P01859	Ig gamma-2 chain C region OS=Homo sapiens GN=IGHG2 PE=1 SV=2
P01876	Ig alpha-1 chain C region OS=Homo sapiens GN=IGHA1 PE=1 SV=2
P25311	Zinc-alpha-2-glycoprotein OS=Homo sapiens GN=AZGP1 PE=1 SV=2
P55209	Nucleosome assembly protein 1-like 1 OS=Homo sapiens GN=NAP1L1 PE=1 SV=1
P30041	Peroxiredoxin-6 OS=Homo sapiens GN=PRDX6 PE=1 SV=3
P52907	F-actin-capping protein subunit alpha-1 OS=Homo sapiens GN=CAPZA1 PE=1 SV=3
P18206	Vinculin OS=Homo sapiens GN=VCL PE=1 SV=4
P37802	Transgelin-2 OS=Homo sapiens GN=TAGLN2 PE=1 SV=3
P50552	Vasodilator-stimulated phosphoprotein OS=Homo sapiens GN=VASP PE=1 SV=3
P16109	P-selectin OS=Homo sapiens GN=SELP PE=1 SV=3
P14770	Platelet glycoprotein IX OS=Homo sapiens GN=GP9 PE=1 SV=3
O94919	Endonuclease domain-containing 1 protein OS=Homo sapiens GN=ENDOD1 PE=1 SV=2
P13489	Ribonuclease inhibitor OS=Homo sapiens GN=RNH1 PE=1 SV=2
P09871	Complement C1s subcomponent OS=Homo sapiens GN=C1S PE=1 SV=1
O75558	Syntaxin-11 OS=Homo sapiens GN=STX11 PE=2 SV=1
P26038	Moesin OS=Homo sapiens GN=MSN PE=1 SV=3
P12259	Coagulation factor V OS=Homo sapiens GN=F5 PE=1 SV=4
P68871	Hemoglobin subunit beta OS=Homo sapiens GN=HBB PE=1 SV=2
P00450	Ceruloplasmin OS=Homo sapiens GN=CP PE=1 SV=1
O43396	Thioredoxin-like protein 1 OS=Homo sapiens GN=TXNL1 PE=1 SV=3
P63104	14-3-3 protein zeta/delta OS=Homo sapiens GN=YWHAZ PE=1 SV=1
P07237	Protein disulfide-isomerase OS=Homo sapiens GN=P4HB PE=1 SV=3
P67936	Tropomyosin alpha-4 chain OS=Homo sapiens GN=TPM4 PE=1 SV=3
P04217	Alpha-1B-glycoprotein OS=Homo sapiens GN=A1BG PE=1 SV=4
P38646	Stress-70 protein, mitochondrial OS=Homo sapiens GN=HSPA9 PE=1 SV=2
P05106	Integrin beta-3 OS=Homo sapiens GN=ITGB3 PE=1 SV=2
P61224	Ras-related protein Rap-1b OS=Homo sapiens GN=RAP1B PE=1 SV=1
P01861	Ig gamma-4 chain C region OS=Homo sapiens GN=IGHG4 PE=1 SV=1
P01860	Ig gamma-3 chain C region OS=Homo sapiens GN=IGHG3 PE=1 SV=2
P61981	14-3-3 protein gamma OS=Homo sapiens GN=YWHAG PE=1 SV=2
P23528	Cofilin-1 OS=Homo sapiens GN=CFL1 PE=1 SV=3
Q13576	Ras GTPase-activating-like protein IQGAP2 OS=Homo sapiens GN=IQGAP2 PE=1 SV=4
P36955	Pigment epithelium-derived factor OS=Homo sapiens GN=SERPINF1 PE=1 SV=4
P08514	Integrin alpha-IIb OS=Homo sapiens GN=ITGA2B PE=1 SV=3
P19827	Inter-alpha-trypsin inhibitor heavy chain H1 OS=Homo sapiens GN=ITI1H PE=1 SV=3
P10643	Complement component C7 OS=Homo sapiens GN=C7 PE=1 SV=2
O43866	CD5 antigen-like OS=Homo sapiens GN=CD5L PE=1 SV=1
P04792	Heat shock protein beta-1 OS=Homo sapiens GN=HSPB1 PE=1 SV=2
P02730	Band 3 anion transport protein OS=Homo sapiens GN=SLC4A1 PE=1 SV=3
P07359	Platelet glycoprotein Ib alpha chain OS=Homo sapiens GN=GP1BA PE=1 SV=1
P24534	Elongation factor 1-beta OS=Homo sapiens GN=EEF1B2 PE=1 SV=3
P40197	Platelet glycoprotein V OS=Homo sapiens GN=GP5 PE=1 SV=1
P61225	Ras-related protein Rap-2b OS=Homo sapiens GN=RAP2B PE=1 SV=1
O95336	6-phosphogluconolactonase OS=Homo sapiens GN=PGLS PE=1 SV=2
P22792	Carboxypeptidase N subunit 2 OS=Homo sapiens GN=CPN2 PE=1 SV=3
Q15762	CD226 antigen OS=Homo sapiens GN=CD226 PE=1 SV=2
P07437	Tubulin beta chain OS=Homo sapiens GN=TUBB PE=1 SV=2
P50990	T-complex protein 1 subunit theta OS=Homo sapiens GN=CCT8 PE=1 SV=4
P40926	Malate dehydrogenase, mitochondrial OS=Homo sapiens GN=MDH2 PE=1 SV=3
Q96FZ7	Charged multivesicular body protein 6 OS=Homo sapiens GN=CHMP6 PE=1 SV=3
Q14974	Importin subunit beta-1 OS=Homo sapiens GN=KPNB1 PE=1 SV=2
P09486	SPARC OS=Homo sapiens GN=SPARC PE=1 SV=1
Q15691	Microtubule-associated protein RP/EB family member 1 OS=Homo sapiens GN=MAPRE1 PE=1 SV=3
P00491	Purine nucleoside phosphorylase OS=Homo sapiens GN=PNP PE=1 SV=2
Q9Y613	FH1/FH2 domain-containing protein 1 OS=Homo sapiens GN=FHOD1 PE=1 SV=3

P08758	Annexin A5 OS=Homo sapiens GN=ANXA5 PE=1 SV=2
P08567	Pleckstrin OS=Homo sapiens GN=PLEK PE=1 SV=3
O14672	Disintegrin and metalloproteinase domain-containing protein 10 OS=Homo sapiens GN=ADAM10 PE=1 SV=1
P18054	Arachidonate 12-lipoxygenase, 12S-type OS=Homo sapiens GN=ALOX12 PE=1 SV=4
P11142	Heat shock cognate 71 kDa protein OS=Homo sapiens GN=HSPA8 PE=1 SV=1
P07203	Glutathione peroxidase 1 OS=Homo sapiens GN=GPX1 PE=1 SV=4
P02671	Fibrinogen alpha chain OS=Homo sapiens GN=FGA PE=1 SV=2
P01011	Alpha-1-antichymotrypsin OS=Homo sapiens GN=SERPINA3 PE=1 SV=2
Q04917	14-3-3 protein eta OS=Homo sapiens GN=YWHAH PE=1 SV=4
P02655	Apolipoprotein C-II OS=Homo sapiens GN=APOC2 PE=1 SV=1
P46109	Crk-like protein OS=Homo sapiens GN=CRKL PE=1 SV=1
P62158	Calmodulin OS=Homo sapiens GN=CALM1 PE=1 SV=2
P43652	Afamin OS=Homo sapiens GN=AFM PE=1 SV=1
P60660-2	Isoform Smooth muscle of Myosin light polypeptide 6 OS=Homo sapiens GN=MYL6
O75636	Ficolin-3 OS=Homo sapiens GN=FCN3 PE=1 SV=2
P27105	Erythrocyte band 7 integral membrane protein OS=Homo sapiens GN=STOM PE=1 SV=3
O75116	Rho-associated protein kinase 2 OS=Homo sapiens GN=ROCK2 PE=1 SV=4
O75083	WD repeat-containing protein 1 OS=Homo sapiens GN=WDR1 PE=1 SV=4
O43707	Alpha-actinin-4 OS=Homo sapiens GN=ACTN4 PE=1 SV=2
P61160	Actin-related protein 2 OS=Homo sapiens GN=ACTR2 PE=1 SV=1
P06733	Alpha-enolase OS=Homo sapiens GN=ENO1 PE=1 SV=2
P25705	ATP synthase subunit alpha, mitochondrial OS=Homo sapiens GN=ATP5A1 PE=1 SV=1
P58546	Myotrophin OS=Homo sapiens GN=MTPN PE=1 SV=2
P01009	Alpha-1-antitrypsin OS=Homo sapiens GN=SERPINA1 PE=1 SV=3
P19971	Thymidine phosphorylase OS=Homo sapiens GN=TYMP PE=1 SV=2
Q12913	Receptor-type tyrosine-protein phosphatase eta OS=Homo sapiens GN=PTPRJ PE=1 SV=3
Q7L591	Docking protein 3 OS=Homo sapiens GN=DOK3 PE=1 SV=2
O15511	Actin-related protein 2/3 complex subunit 5 OS=Homo sapiens GN=ARPC5 PE=1 SV=3
P02763	Alpha-1-acid glycoprotein 1 OS=Homo sapiens GN=ORM1 PE=1 SV=1
P31146	Coronin-1A OS=Homo sapiens GN=CORO1A PE=1 SV=4
Q9NRW1	Ras-related protein Rab-6B OS=Homo sapiens GN=RAB6B PE=1 SV=1
P04350	Tubulin beta-4A chain OS=Homo sapiens GN=TUBB4A PE=1 SV=2
P02679	Fibrinogen gamma chain OS=Homo sapiens GN=FGG PE=1 SV=3
P61604	10 kDa heat shock protein, mitochondrial OS=Homo sapiens GN=HSPE1 PE=1 SV=2
P13667	Protein disulfide-isomerase A4 OS=Homo sapiens GN=PDIA4 PE=1 SV=2
P02656	Apolipoprotein C-III OS=Homo sapiens GN=APOC3 PE=1 SV=1
P62258	14-3-3 protein epsilon OS=Homo sapiens GN=YWHAE PE=1 SV=1
P48740	Mannan-binding lectin serine protease 1 OS=Homo sapiens GN=MASP1 PE=1 SV=3
Q99439	Calponin-2 OS=Homo sapiens GN=CNN2 PE=1 SV=4
Q9H4M9	EH domain-containing protein 1 OS=Homo sapiens GN=EHD1 PE=1 SV=2
P01877	Ig alpha-2 chain C region OS=Homo sapiens GN=IGHA2 PE=1 SV=3
P38606	V-type proton ATPase catalytic subunit A OS=Homo sapiens GN=ATP6V1A PE=1 SV=2
P08648	Integrin alpha-5 OS=Homo sapiens GN=ITGA5 PE=1 SV=2
O00194	Ras-related protein Rab-27B OS=Homo sapiens GN=RAB27B PE=1 SV=4
P01617	Ig kappa chain V-II region TEW OS=Homo sapiens PE=1 SV=1
P02042	Hemoglobin subunit delta OS=Homo sapiens GN=HBD PE=1 SV=2
P18669	Phosphoglycerate mutase 1 OS=Homo sapiens GN=PGAM1 PE=1 SV=2
P62879	Guanine nucleotide-binding protein G(I)/G(S)/G(T) subunit beta-2 OS=Homo sapiens GN=GNB2 PE=1 SV=3
P10720	Platelet factor 4 variant OS=Homo sapiens GN=PF4V1 PE=1 SV=1
O15144	Actin-related protein 2/3 complex subunit 2 OS=Homo sapiens GN=ARPC2 PE=1 SV=1
P47755	F-actin-capping protein subunit alpha-2 OS=Homo sapiens GN=CAPZA2 PE=1 SV=3
Q9NY65	Tubulin alpha-8 chain OS=Homo sapiens GN=TUBA8 PE=1 SV=1
P02776	Platelet factor 4 OS=Homo sapiens GN=PF4 PE=1 SV=2
P20339	Ras-related protein Rab-5A OS=Homo sapiens GN=RAB5A PE=1 SV=2
P62873	Guanine nucleotide-binding protein G(I)/G(S)/G(T) subunit beta-1 OS=Homo sapiens GN=GNB1 PE=1 SV=3
P01613	Ig kappa chain V-I region Ni OS=Homo sapiens PE=1 SV=1
P35908	Keratin, type II cytoskeletal 2 epidermal OS=Homo sapiens GN=KRT2 PE=1 SV=2
P14618	Pyruvate kinase PKM OS=Homo sapiens GN=PKM PE=1 SV=4
P01042	Kininogen-1 OS=Homo sapiens GN=KNG1 PE=1 SV=2
Q86UX7	Fermitin family homolog 3 OS=Homo sapiens GN=FERMT3 PE=1 SV=1
P60709	Actin, cytoplasmic 1 OS=Homo sapiens GN=ACTB PE=1 SV=1
P08238	Heat shock protein HSP 90-beta OS=Homo sapiens GN=HSP90AB1 PE=1 SV=4

P04075-2	Isoform 2 of Fructose-bisphosphate aldolase A OS=Homo sapiens GN=ALDOA
P01871-2	Isoform 2 of Ig mu chain C region OS=Homo sapiens GN=IGHM
P02774-3	Isoform 3 of Vitamin D-binding protein OS=Homo sapiens GN=GC
P12814-3	Isoform 3 of Alpha-actinin-1 OS=Homo sapiens GN=ACTN1
P0COL4	Complement C4-A OS=Homo sapiens GN=C4A PE=1 SV=2
P04406	Glyceraldehyde-3-phosphate dehydrogenase OS=Homo sapiens GN=GAPDH PE=1 SV=3
P00739-2	Isoform 2 of Haptoglobin-related protein OS=Homo sapiens GN=HPR
P06396	Gelsolin OS=Homo sapiens GN=GSN PE=1 SV=1
P47756	F-actin-capping protein subunit beta OS=Homo sapiens GN=CAPZB PE=1 SV=4
P48740-2	Isoform 2 of Mannan-binding lectin serine protease 1 OS=Homo sapiens GN=MASP1
P62820	Ras-related protein Rab-1A OS=Homo sapiens GN=RAB1A PE=1 SV=3
P13224-2	Isoform 2 of Platelet glycoprotein Ib beta chain OS=Homo sapiens GN=GP1BB
P60174	Triosephosphate isomerase OS=Homo sapiens GN=TPI1 PE=1 SV=3
Q14624	Inter-alpha-trypsin inhibitor heavy chain H4 OS=Homo sapiens GN=ITI4 PE=1 SV=4
P06753-2	Isoform 2 of Tropomyosin alpha-3 chain OS=Homo sapiens GN=TPM3
P09493-5	Isoform 5 of Tropomyosin alpha-1 chain OS=Homo sapiens GN=TPM1
O14791-2	Isoform 2 of Apolipoprotein L1 OS=Homo sapiens GN=APOL1
Q9HBI1-2	Isoform 2 of Beta-parvin OS=Homo sapiens GN=PARVB
Q71U36	Tubulin alpha-1A chain OS=Homo sapiens GN=TUBA1A PE=1 SV=1
P04899-4	Isoform sGi2 of Guanine nucleotide-binding protein G(i) subunit alpha-2 OS=Homo sapiens GN=GNAI2
P16284	Platelet endothelial cell adhesion molecule OS=Homo sapiens GN=PECAM1 PE=1 SV=1
P23229	Integrin alpha-6 OS=Homo sapiens GN=ITGA6 PE=1 SV=5
P62736	Actin, aortic smooth muscle OS=Homo sapiens GN=ACTA2 PE=1 SV=1
Q14766-4	Isoform 4 of Latent-transforming growth factor beta-binding protein 1 OS=Homo sapiens GN=LTBP1
P05556-3	Isoform Beta-1C of Integrin beta-1 OS=Homo sapiens GN=ITGB1
P15531-2	Isoform 2 of Nucleoside diphosphate kinase A OS=Homo sapiens GN=NME1
P10909-2	Isoform 2 of Clusterin OS=Homo sapiens GN=CLU
Q93084-5	Isoform SERCA3E of Sarcoplasmic/endoplasmic reticulum calcium ATPase 3 OS=Homo sapiens GN=ATP2A3
P48059-3	Isoform 3 of LIM and senescent cell antigen-like-containing domain protein 1 OS=Homo sapiens GN=LIMS1
P16190	HLA class I histocompatibility antigen, A-33 alpha chain OS=Homo sapiens GN=HLA-A PE=1 SV=3
Q9BWP8-1	Isoform 10 of Collectin-11 OS=Homo sapiens GN=COLEC11
P13746-2	Isoform 2 of HLA class I histocompatibility antigen, A-11 alpha chain OS=Homo sapiens GN=HLA-A
Q01433	AMP deaminase 2 OS=Homo sapiens GN=AMPD2 PE=1 SV=2
Q8IZP0	Abl interactor 1 OS=Homo sapiens GN=ABI1 PE=1 SV=4
P57721	Poly(rC)-binding protein 3 OS=Homo sapiens GN=PCBP3 PE=2 SV=2

This list is representative of an acetate-based EV pulldown method on the Qexactive requiring 200ul of plasma	
Accession	Description
P04275	von Willebrand factor OS=Homo sapiens GN=VWF PE=1 SV=4
P27169	Serum paraoxonase/arylesterase 1 OS=Homo sapiens GN=PON1 PE=1 SV=3
P07996	Thrombospondin-1 OS=Homo sapiens GN=THBS1 PE=1 SV=2
P02647	Apolipoprotein A-I OS=Homo sapiens GN=APOA1 PE=1 SV=1
P02768	Serum albumin OS=Homo sapiens GN=ALB PE=1 SV=2
P06727	Apolipoprotein A-IV OS=Homo sapiens GN=APOA4 PE=1 SV=3
P02787	Serotransferrin OS=Homo sapiens GN=TF PE=1 SV=3
P35579	Myosin-9 OS=Homo sapiens GN=MYH9 PE=1 SV=4
P10643	Complement component C7 OS=Homo sapiens GN=C7 PE=1 SV=2
P00734	Prothrombin OS=Homo sapiens GN=F2 PE=1 SV=2
P01031	Complement C5 OS=Homo sapiens GN=C5 PE=1 SV=4
P00747	Plasminogen OS=Homo sapiens GN=PLG PE=1 SV=2
P07358	Complement component C8 beta chain OS=Homo sapiens GN=C8B PE=1 SV=3
P09871	Complement C1s subcomponent OS=Homo sapiens GN=C1S PE=1 SV=1
P01023	Alpha-2-macroglobulin OS=Homo sapiens GN=A2M PE=1 SV=3
P02675	Fibrinogen beta chain OS=Homo sapiens GN=FGB PE=1 SV=2
P01008	Antithrombin-III OS=Homo sapiens GN=SERPINC1 PE=1 SV=1
Q9Y490	Talin-1 OS=Homo sapiens GN=TLN1 PE=1 SV=3
P05546	Heparin cofactor 2 OS=Homo sapiens GN=SERPIND1 PE=1 SV=3
P12259	Coagulation factor V OS=Homo sapiens GN=F5 PE=1 SV=4
P01024	Complement C3 OS=Homo sapiens GN=C3 PE=1 SV=2
Q9H4B7	Tubulin beta-1 chain OS=Homo sapiens GN=TUBB1 PE=1 SV=1
P02790	Hemopexin OS=Homo sapiens GN=HPX PE=1 SV=2
P00450	Ceruloplasmin OS=Homo sapiens GN=CP PE=1 SV=1
P00736	Complement C1r subcomponent OS=Homo sapiens GN=C1R PE=1 SV=2
P19823	Inter-alpha-trypsin inhibitor heavy chain H2 OS=Homo sapiens GN=ITI2 PE=1 SV=2
P02748	Complement component C9 OS=Homo sapiens GN=C9 PE=1 SV=2
P04114	Apolipoprotein B-100 OS=Homo sapiens GN=APOB PE=1 SV=2
P02766	Transthyretin OS=Homo sapiens GN=TTR PE=1 SV=1
P06576	ATP synthase subunit beta, mitochondrial OS=Homo sapiens GN=ATP5B PE=1 SV=3
P00488	Coagulation factor XIII A chain OS=Homo sapiens GN=F13A1 PE=1 SV=4
P02749	Beta-2-glycoprotein 1 OS=Homo sapiens GN=APOH PE=1 SV=3
P04196	Histidine-rich glycoprotein OS=Homo sapiens GN=HRG PE=1 SV=1
Q96KN2	Beta-Ala-His dipeptidase OS=Homo sapiens GN=CNDP1 PE=1 SV=4
P00742	Coagulation factor X OS=Homo sapiens GN=F10 PE=1 SV=2
P21333	Filamin-A OS=Homo sapiens GN=FLNA PE=1 SV=4
P04004	Vitronectin OS=Homo sapiens GN=VTN PE=1 SV=1
P02649	Apolipoprotein E OS=Homo sapiens GN=APOE PE=1 SV=1
P02671	Fibrinogen alpha chain OS=Homo sapiens GN=FGA PE=1 SV=2
P05160	Coagulation factor XIII B chain OS=Homo sapiens GN=F13B PE=1 SV=3
P00751	Complement factor B OS=Homo sapiens GN=CFB PE=1 SV=2
P04264	Keratin, type II cytoskeletal 1 OS=Homo sapiens GN=KRT1 PE=1 SV=6
P08603	Complement factor H OS=Homo sapiens GN=CFH PE=1 SV=4
Q13201	Multimerin-1 OS=Homo sapiens GN=MMRN1 PE=1 SV=3
P36955	Pigment epithelium-derived factor OS=Homo sapiens GN=SERPINF1 PE=1 SV=4
P55072	Transitional endoplasmic reticulum ATPase OS=Homo sapiens GN=VCP PE=1 SV=4
Q8NBP7	Proprotein convertase subtilisin/kexin type 9 OS=Homo sapiens GN=PCSK9 PE=1 SV=3
P29622	Kallistatin OS=Homo sapiens GN=SERPINA4 PE=1 SV=3
P80108	Phosphatidylinositol-glycan-specific phospholipase D OS=Homo sapiens GN=GPLD1 PE=1 SV=3
P02760	Protein AMBP OS=Homo sapiens GN=AMBP PE=1 SV=1
P35527	Keratin, type I cytoskeletal 9 OS=Homo sapiens GN=KRT9 PE=1 SV=3
Q13418	Integrin-linked protein kinase OS=Homo sapiens GN=ILK PE=1 SV=2
P07737	Profilin-1 OS=Homo sapiens GN=PFN1 PE=1 SV=2
P00738	Haptoglobin OS=Homo sapiens GN=HP PE=1 SV=1
P04003	C4b-binding protein alpha chain OS=Homo sapiens GN=C4BPA PE=1 SV=2
P01857	Ig gamma-1 chain C region OS=Homo sapiens GN=IGHG1 PE=1 SV=1
P16671	Platelet glycoprotein 4 OS=Homo sapiens GN=CD36 PE=1 SV=2
P02765	Alpha-2-HS-glycoprotein OS=Homo sapiens GN=AHSG PE=1 SV=1
P08519	Apolipoprotein(a) OS=Homo sapiens GN=LPA PE=1 SV=1
P07225	Vitamin K-dependent protein S OS=Homo sapiens GN=PROS1 PE=1 SV=1
P04070	Vitamin K-dependent protein C OS=Homo sapiens GN=PROC PE=1 SV=1
P08567	Pleckstrin OS=Homo sapiens GN=PLEK PE=1 SV=3

P30101	Protein disulfide-isomerase A3 OS=Homo sapiens GN=PDIA3 PE=1 SV=4
O00187	Mannan-binding lectin serine protease 2 OS=Homo sapiens GN=MASP2 PE=1 SV=4
P14625	Endoplasmin OS=Homo sapiens GN=HSP90B1 PE=1 SV=1
P05155	Plasma protease C1 inhibitor OS=Homo sapiens GN=SERPING1 PE=1 SV=2
P19827	Inter-alpha-trypsin inhibitor heavy chain H1 OS=Homo sapiens GN=ITIH1 PE=1 SV=3
Q14126	Desmoglein-2 OS=Homo sapiens GN=DSG2 PE=1 SV=2
P35443	Thrombospondin-4 OS=Homo sapiens GN=THBS4 PE=1 SV=2
P07384	Calpain-1 catalytic subunit OS=Homo sapiens GN=CAPN1 PE=1 SV=1
P0C0L5	Complement C4-B OS=Homo sapiens GN=C4B PE=1 SV=2
P01834	Ig kappa chain C region OS=Homo sapiens GN=IGKC PE=1 SV=1
P13645	Keratin, type I cytoskeletal 10 OS=Homo sapiens GN=KRT10 PE=1 SV=6
P04217	Alpha-1B-glycoprotein OS=Homo sapiens GN=A1BG PE=1 SV=4
Q9UBX5	Fibulin-5 OS=Homo sapiens GN=FBLN5 PE=1 SV=1
O00151	PDZ and LIM domain protein 1 OS=Homo sapiens GN=PDLIM1 PE=1 SV=4
O95810	Serum deprivation-response protein OS=Homo sapiens GN=SDPR PE=1 SV=3
O75083	WD repeat-containing protein 1 OS=Homo sapiens GN=WDR1 PE=1 SV=4
P02679	Fibrinogen gamma chain OS=Homo sapiens GN=FGG PE=1 SV=3
P07359	Platelet glycoprotein Ib alpha chain OS=Homo sapiens GN=GP1BA PE=1 SV=1
P02656	Apolipoprotein C-III OS=Homo sapiens GN=APOC3 PE=1 SV=1
P27824	Calnexin OS=Homo sapiens GN=CANX PE=1 SV=2
Q8NI99	Angiopoietin-related protein 6 OS=Homo sapiens GN=ANGPTL6 PE=1 SV=1
P68366	Tubulin alpha-4A chain OS=Homo sapiens GN=TUBA4A PE=1 SV=1
P27105	Erythrocyte band 7 integral membrane protein OS=Homo sapiens GN=STOM PE=1 SV=3
P23528	Cofilin-1 OS=Homo sapiens GN=CFL1 PE=1 SV=3
P01860	Ig gamma-3 chain C region OS=Homo sapiens GN=IGHG3 PE=1 SV=2
P14770	Platelet glycoprotein IX OS=Homo sapiens GN=GP9 PE=1 SV=3
P40926	Malate dehydrogenase, mitochondrial OS=Homo sapiens GN=MDH2 PE=1 SV=3
Q15762	CD226 antigen OS=Homo sapiens GN=CD226 PE=1 SV=2
P01019	Angiotensinogen OS=Homo sapiens GN=AGT PE=1 SV=1
P02652	Apolipoprotein A-II OS=Homo sapiens GN=APOA2 PE=1 SV=1
P02753	Retinol-binding protein 4 OS=Homo sapiens GN=RBP4 PE=1 SV=3
P07195	L-lactate dehydrogenase B chain OS=Homo sapiens GN=LDHB PE=1 SV=2
P61158	Actin-related protein 3 OS=Homo sapiens GN=ACTR3 PE=1 SV=3
P10809	60 kDa heat shock protein, mitochondrial OS=Homo sapiens GN=HSPD1 PE=1 SV=2
P55209	Nucleosome assembly protein 1-like 1 OS=Homo sapiens GN=NAP1L1 PE=1 SV=1
P22352	Glutathione peroxidase 3 OS=Homo sapiens GN=GPX3 PE=1 SV=2
P48735	Isocitrate dehydrogenase [NADP], mitochondrial OS=Homo sapiens GN=IDH2 PE=1 SV=2
Q08380	Galectin-3-binding protein OS=Homo sapiens GN=LGALS3BP PE=1 SV=1
Q86UX7	Fermitin family homolog 3 OS=Homo sapiens GN=FERMT3 PE=1 SV=1
P02776	Platelet factor 4 OS=Homo sapiens GN=PF4 PE=1 SV=2
P37802	Transgelin-2 OS=Homo sapiens GN=TAGLN2 PE=1 SV=3
P01876	Ig alpha-1 chain C region OS=Homo sapiens GN=IGHA1 PE=1 SV=2
P0C0L4	Complement C4-A OS=Homo sapiens GN=C4A PE=1 SV=2
P62873	Guanine nucleotide-binding protein G(I)/G(S)/G(T) subunit beta-1 OS=Homo sapiens GN=GNB1 PE=1 SV=3
P08514	Integrin alpha-IIb OS=Homo sapiens GN=ITGA2B PE=1 SV=3
P01011	Alpha-1-antichymotrypsin OS=Homo sapiens GN=SERPINA3 PE=1 SV=2
P07437	Tubulin beta chain OS=Homo sapiens GN=TUBB PE=1 SV=2
P01859	Ig gamma-2 chain C region OS=Homo sapiens GN=IGHG2 PE=1 SV=2
P01861	Ig gamma-4 chain C region OS=Homo sapiens GN=IGHG4 PE=1 SV=1
P52907	F-actin-capping protein subunit alpha-1 OS=Homo sapiens GN=CAPZA1 PE=1 SV=3
O00194	Ras-related protein Rab-27B OS=Homo sapiens GN=RAB27B PE=1 SV=4
Q9NZN3	EH domain-containing protein 3 OS=Homo sapiens GN=EHD3 PE=1 SV=2
P05106	Integrin beta-3 OS=Homo sapiens GN=ITGB3 PE=1 SV=2
P01009	Alpha-1-antitrypsin OS=Homo sapiens GN=SERPINA1 PE=1 SV=3
P18206	Vinculin OS=Homo sapiens GN=VCL PE=1 SV=4
P21291	Cysteine and glycine-rich protein 1 OS=Homo sapiens GN=CSRP1 PE=1 SV=3
P06681	Complement C2 OS=Homo sapiens GN=C2 PE=1 SV=2
O75915	PRA1 family protein 3 OS=Homo sapiens GN=ARL6IP5 PE=1 SV=1
Q13103	Secreted phosphoprotein 24 OS=Homo sapiens GN=SPP2 PE=1 SV=1
P21926	CD9 antigen OS=Homo sapiens GN=CD9 PE=1 SV=4
Q9Y6Z7	Collectin-10 OS=Homo sapiens GN=COLEC10 PE=2 SV=2
P02775	Platelet basic protein OS=Homo sapiens GN=PPBP PE=1 SV=3
P07203	Glutathione peroxidase 1 OS=Homo sapiens GN=GPX1 PE=1 SV=4
P30041	Peroxisomal protein 6 OS=Homo sapiens GN=PRDX6 PE=1 SV=3

P00740	Coagulation factor IX OS=Homo sapiens GN=F9 PE=1 SV=2
P49747	Cartilage oligomeric matrix protein OS=Homo sapiens GN=COMP PE=1 SV=2
O15145	Actin-related protein 2/3 complex subunit 3 OS=Homo sapiens GN=ARPC3 PE=1 SV=3
O94919	Endonuclease domain-containing 1 protein OS=Homo sapiens GN=ENDOD1 PE=1 SV=2
P02746	Complement C1q subcomponent subunit B OS=Homo sapiens GN=C1QB PE=1 SV=3
P12814	Alpha-actinin-1 OS=Homo sapiens GN=ACTN1 PE=1 SV=2
P62937	Peptidyl-prolyl cis-trans isomerase A OS=Homo sapiens GN=PPIA PE=1 SV=2
P06396	Gelsolin OS=Homo sapiens GN=GSN PE=1 SV=1
P18428	Lipopolysaccharide-binding protein OS=Homo sapiens GN=LBP PE=1 SV=3
P02730	Band 3 anion transport protein OS=Homo sapiens GN=SLC4A1 PE=1 SV=3
P23142	Fibulin-1 OS=Homo sapiens GN=FBLN1 PE=1 SV=4
P00748	Coagulation factor XII OS=Homo sapiens GN=F12 PE=1 SV=3
Q15485	Ficolin-2 OS=Homo sapiens GN=FCN2 PE=1 SV=2
P68871	Hemoglobin subunit beta OS=Homo sapiens GN=HBB PE=1 SV=2
P60660-2	Isoform Smooth muscle of Myosin light polypeptide 6 OS=Homo sapiens GN=MYL6
Q00610	Clathrin heavy chain 1 OS=Homo sapiens GN=CLTC PE=1 SV=5
P08697	Alpha-2-antiplasmin OS=Homo sapiens GN=SERPINF2 PE=1 SV=3
P61106	Ras-related protein Rab-14 OS=Homo sapiens GN=RAB14 PE=1 SV=4
P24844	Myosin regulatory light polypeptide 9 OS=Homo sapiens GN=MYL9 PE=1 SV=4
P25705	ATP synthase subunit alpha, mitochondrial OS=Homo sapiens GN=ATP5A1 PE=1 SV=1
P01877	Ig alpha-2 chain C region OS=Homo sapiens GN=IGHA2 PE=1 SV=3
P63104	14-3-3 protein zeta/delta OS=Homo sapiens GN=YWHAZ PE=1 SV=1
P11021	78 kDa glucose-regulated protein OS=Homo sapiens GN=HSPA5 PE=1 SV=2
P02654	Apolipoprotein C-I OS=Homo sapiens GN=APOC1 PE=1 SV=1
P48740	Mannan-binding lectin serine protease 1 OS=Homo sapiens GN=MASP1 PE=1 SV=3
P04220	Ig mu heavy chain disease protein OS=Homo sapiens PE=1 SV=1
P61224	Ras-related protein Rap-1b OS=Homo sapiens GN=RAP1B PE=1 SV=1
O43707	Alpha-actinin-4 OS=Homo sapiens GN=ACTN4 PE=1 SV=2
Q06830	Peroxiredoxin-1 OS=Homo sapiens GN=PRDX1 PE=1 SV=1
Q5SQ64	Lymphocyte antigen 6 complex locus protein G6f OS=Homo sapiens GN=LY6G6F PE=1 SV=2
Q13576	Ras GTPase-activating-like protein IQGAP2 OS=Homo sapiens GN=IQGAP2 PE=1 SV=4
P14618	Pyruvate kinase PKM OS=Homo sapiens GN=PKM PE=1 SV=4
O95445	Apolipoprotein M OS=Homo sapiens GN=APOM PE=1 SV=2
P12236	ADP/ATP translocase 3 OS=Homo sapiens GN=SLC25A6 PE=1 SV=4
P47755	F-actin-capping protein subunit alpha-2 OS=Homo sapiens GN=CAPZA2 PE=1 SV=3
Q15166	Serum paraoxonase/lactonase 3 OS=Homo sapiens GN=PON3 PE=1 SV=3
P07357	Complement component C8 alpha chain OS=Homo sapiens GN=C8A PE=1 SV=2
P60709	Actin, cytoplasmic 1 OS=Homo sapiens GN=ACTB PE=1 SV=1
P01625	Ig kappa chain V-IV region Len OS=Homo sapiens PE=1 SV=2
P02774-3	Isoform 3 of Vitamin D-binding protein OS=Homo sapiens GN=GC
P30740	Leukocyte elastase inhibitor OS=Homo sapiens GN=SERPINB1 PE=1 SV=1
P02751-11	Isoform 11 of Fibronectin OS=Homo sapiens GN=FN1
Q9UGM5	Fetuin-B OS=Homo sapiens GN=FETUB PE=1 SV=2
P16109	P-selectin OS=Homo sapiens GN=SELP PE=1 SV=3
P26038	Moesin OS=Homo sapiens GN=MSN PE=1 SV=3
P05141	ADP/ATP translocase 2 OS=Homo sapiens GN=SLC25A5 PE=1 SV=7
Q9NQC3-3	Isoform 3 of Reticulon-4 OS=Homo sapiens GN=RTN4
Q16610-4	Isoform 4 of Extracellular matrix protein 1 OS=Homo sapiens GN=ECM1
Q04917	14-3-3 protein eta OS=Homo sapiens GN=YWHAH PE=1 SV=4
P01042	Kininogen-1 OS=Homo sapiens GN=KNG1 PE=1 SV=2
P35858-2	Isoform 2 of Insulin-like growth factor-binding protein complex acid labile subunit OS=Homo sapiens GN=IGFALS
P01871-2	Isoform 2 of Ig mu chain C region OS=Homo sapiens GN=IGHM
P68371	Tubulin beta-4B chain OS=Homo sapiens GN=TUBB4B PE=1 SV=1
Q9Y277	Voltage-dependent anion-selective channel protein 3 OS=Homo sapiens GN=VDAC3 PE=1 SV=1
P04406	Glyceraldehyde-3-phosphate dehydrogenase OS=Homo sapiens GN=GAPDH PE=1 SV=3
Q06033	Inter-alpha-trypsin inhibitor heavy chain H3 OS=Homo sapiens GN=ITI3 PE=1 SV=2
P48740-2	Isoform 2 of Mannan-binding lectin serine protease 1 OS=Homo sapiens GN=MASP1
P00739-2	Isoform 2 of Haptoglobin-related protein OS=Homo sapiens GN=HPR
Q14520	Hyaluronan-binding protein 2 OS=Homo sapiens GN=HABP2 PE=1 SV=1
P14543	Nidogen-1 OS=Homo sapiens GN=NID1 PE=1 SV=3
P12931-2	Isoform 2 of Proto-oncogene tyrosine-protein kinase Src OS=Homo sapiens GN=SRC
Q15404	Ras suppressor protein 1 OS=Homo sapiens GN=RSU1 PE=1 SV=3
Q9HDC9	Adipocyte plasma membrane-associated protein OS=Homo sapiens GN=APMAP PE=1 SV=2
Q96PD5-2	Isoform 2 of N-acetylmuramoyl-L-alanine amidase OS=Homo sapiens GN=PGLYRP2



P13224-2	Isoform 2 of Platelet glycoprotein Ib beta chain OS=Homo sapiens GN=GP1BB
Q9HBI1-2	Isoform 2 of Beta-parvin OS=Homo sapiens GN=PARVB
P23219	Prostaglandin G/H synthase 1 OS=Homo sapiens GN=PTGS1 PE=1 SV=2
Q14624	Inter-alpha-trypsin inhibitor heavy chain H4 OS=Homo sapiens GN=ITIH4 PE=1 SV=4
P00387-3	Isoform 3 of NADH-cytochrome b5 reductase 3 OS=Homo sapiens GN=CYB5R3
P62258	14-3-3 protein epsilon OS=Homo sapiens GN=YWHAE PE=1 SV=1
P67936-2	Isoform 2 of Tropomyosin alpha-4 chain OS=Homo sapiens GN=TPM4
P10909-2	Isoform 2 of Clusterin OS=Homo sapiens GN=CLU
Q92928	Putative Ras-related protein Rab-1C OS=Homo sapiens GN=RAB1C PE=5 SV=2
O14791-2	Isoform 2 of Apolipoprotein L1 OS=Homo sapiens GN=APOL1
P22105	Tenascin-X OS=Homo sapiens GN=TNXB PE=1 SV=3
Q9NQ79	Cartilage acidic protein 1 OS=Homo sapiens GN=CRTAC1 PE=1 SV=2
P48059-3	Isoform 3 of LIM and senescent cell antigen-like-containing domain protein 1 OS=Homo sapiens GN=LIMS1
P04899-4	Isoform sGi2 of Guanine nucleotide-binding protein G(i) subunit alpha-2 OS=Homo sapiens GN=GNAI2
P68032	Actin, alpha cardiac muscle 1 OS=Homo sapiens GN=ACTC1 PE=1 SV=1
Q12805	EGF-containing fibulin-like extracellular matrix protein 1 OS=Homo sapiens GN=EFEMP1 PE=1 SV=2
Q9NQC3	Reticulon-4 OS=Homo sapiens GN=RTN4 PE=1 SV=2
P0CG05	Ig lambda-2 chain C regions OS=Homo sapiens GN=IGLC2 PE=1 SV=1
P56134	ATP synthase subunit f, mitochondrial OS=Homo sapiens GN=ATP5J2 PE=1 SV=3
P61204	ADP-ribosylation factor 3 OS=Homo sapiens GN=ARF3 PE=1 SV=2
Q14766-4	Isoform 4 of Latent-transforming growth factor beta-binding protein 1 OS=Homo sapiens GN=LTBP1
Q93084-5	Isoform SERCA3E of Sarcoplasmic/endoplasmic reticulum calcium ATPase 3 OS=Homo sapiens GN=ATP2A3
Q9BWP8-1	Isoform 10 of Collectin-11 OS=Homo sapiens GN=COLEC11
P06753-2	Isoform 2 of Tropomyosin alpha-3 chain OS=Homo sapiens GN=TPM3
O95866	Protein G6b OS=Homo sapiens GN=G6B PE=1 SV=1
P16284	Platelet endothelial cell adhesion molecule OS=Homo sapiens GN=PECAM1 PE=1 SV=1
P09493	Tropomyosin alpha-1 chain OS=Homo sapiens GN=TPM1 PE=1 SV=2
P23229	Integrin alpha-6 OS=Homo sapiens GN=ITGA6 PE=1 SV=5
P30508	HLA class I histocompatibility antigen, Cw-12 alpha chain OS=Homo sapiens GN=HLA-C PE=2 SV=2
P10319	HLA class I histocompatibility antigen, B-58 alpha chain OS=Homo sapiens GN=HLA-B PE=1 SV=1

This list demonstrates differences in types of proteins identified in CSH_Plasma, CSH_EV-free and EV_BigDiluteCold; there is minimal difference between CSH_Plasma and CSH_EV-free			
Description	CSH_Plasma	CSH_EV-free	EV_BigDiluteCold
Ig alpha-1 chain C region OS=Homo sapiens GN=IGHA1 PE=1 SV=2	X	X	X
Ig gamma-3 chain C region OS=Homo sapiens GN=IGHG3 PE=1 SV=2	X	X	X
Complement C4-A OS=Homo sapiens GN=C4A PE=1 SV=2	X	X	X
Apolipoprotein A-II OS=Homo sapiens GN=APOA2 PE=1 SV=1	X	X	X
Ig gamma-4 chain C region OS=Homo sapiens GN=IGHG4 PE=1 SV=1	X	X	X
Serum albumin OS=Homo sapiens GN=ALB PE=1 SV=2	X	X	X
Histidine-rich glycoprotein OS=Homo sapiens GN=HRG PE=1 SV=1	X	X	X
Fibrinogen gamma chain OS=Homo sapiens GN=FGG PE=1 SV=3	X	X	X
Haptoglobin OS=Homo sapiens GN=HP PE=1 SV=1	X	X	X
Serotransferrin OS=Homo sapiens GN=TF PE=1 SV=3	X	X	X
Complement factor B OS=Homo sapiens GN=CFB PE=1 SV=2	X	X	X
Apolipoprotein E OS=Homo sapiens GN=APOE PE=1 SV=1	X	X	X
Complement component C7 OS=Homo sapiens GN=C7 PE=1 SV=2	X	X	X
Isoform 2 of Clusterin OS=Homo sapiens GN=CLU	X	X	X
Complement component C9 OS=Homo sapiens GN=C9 PE=1 SV=2	X	X	X
Glutathione peroxidase 3 OS=Homo sapiens GN=GPX3 PE=1 SV=2	X	X	X
von Willebrand factor OS=Homo sapiens GN=VWF PE=1 SV=4	X	X	X
Fibulin-1 OS=Homo sapiens GN=FBLN1 PE=1 SV=4	X	X	X
Plasminogen OS=Homo sapiens GN=PLG PE=1 SV=2	X	X	X
Beta-2-glycoprotein 1 OS=Homo sapiens GN=APOH PE=1 SV=3	X	X	X
Ceruloplasmin OS=Homo sapiens GN=CP PE=1 SV=1	X	X	X
Ig gamma-2 chain C region OS=Homo sapiens GN=IGHG2 PE=1 SV=2	X	X	X
Serum paraoxonase/arylesterase 1 OS=Homo sapiens GN=PON1 PE=1 SV=3	X	X	X
Apolipoprotein A-IV OS=Homo sapiens GN=APOA4 PE=1 SV=3	X	X	X
Complement C1s subcomponent OS=Homo sapiens GN=C1S PE=1 SV=1	X	X	X
Vitamin K-dependent protein S OS=Homo sapiens GN=PROS1 PE=1 SV=1	X	X	X
Fibrinogen beta chain OS=Homo sapiens GN=FGB PE=1 SV=2	X	X	X
Apolipoprotein A-I OS=Homo sapiens GN=APOA1 PE=1 SV=1	X	X	X
CD5 antigen-like OS=Homo sapiens GN=CD5L PE=1 SV=1	X	X	X
Inter-alpha-trypsin inhibitor heavy chain H1 OS=Homo sapiens GN=ITI1 PE=1 SV=3	X	X	X
Prothrombin OS=Homo sapiens GN=F2 PE=1 SV=2	X	X	X
Ig gamma-1 chain C region OS=Homo sapiens GN=IGHG1 PE=1 SV=1	X	X	X
Plasma protease C1 inhibitor OS=Homo sapiens GN=SERPING1 PE=1 SV=2	X	X	X
Complement component C8 beta chain OS=Homo sapiens GN=C8B PE=1 SV=3	X	X	X
Talin-1 OS=Homo sapiens GN=TLN1 PE=1 SV=3	X	X	X
Alpha-1-antitrypsin OS=Homo sapiens GN=SERPINA1 PE=1 SV=3	X	X	X
Alpha-2-macroglobulin OS=Homo sapiens GN=A2M PE=1 SV=3	X	X	X
Hemopexin OS=Homo sapiens GN=HPX PE=1 SV=2	X	X	X
Ig kappa chain C region OS=Homo sapiens GN=IGKC PE=1 SV=1	X	X	X
Complement C3 OS=Homo sapiens GN=C3 PE=1 SV=2	X	X	X
Complement C2 OS=Homo sapiens GN=C2 PE=1 SV=2	X	X	X
Pigment epithelium-derived factor OS=Homo sapiens GN=SERPINF1 PE=1 SV=4	X	X	X
Heparin cofactor 2 OS=Homo sapiens GN=SERPIND1 PE=1 SV=3	X	X	X
Transthyretin OS=Homo sapiens GN=TTR PE=1 SV=1	X	X	X
Inter-alpha-trypsin inhibitor heavy chain H2 OS=Homo sapiens GN=ITI2 PE=1 SV=2	X	X	X
Fibrinogen alpha chain OS=Homo sapiens GN=FGA PE=1 SV=2	X	X	X
Isoform 2 of Insulin-like growth factor-binding protein complex acid labile subunit OS=Homo sapiens GN=IGFALS	X	X	X
Vitronectin OS=Homo sapiens GN=VTN PE=1 SV=1	X	X	X
Antithrombin-III OS=Homo sapiens GN=SERPINC1 PE=1 SV=1	X	X	X
Coagulation factor X OS=Homo sapiens GN=F10 PE=1 SV=2	X	X	X
Coagulation factor V OS=Homo sapiens GN=F5 PE=1 SV=4	X	X	X
Platelet basic protein OS=Homo sapiens GN=PPBP PE=1 SV=3	X	X	X
Alpha-2-HS-glycoprotein OS=Homo sapiens GN=AHSG PE=1 SV=1	X	X	X
Complement C5 OS=Homo sapiens GN=C5 PE=1 SV=4	X	X	X
Filamin-A OS=Homo sapiens GN=FLNA PE=1 SV=4	X	X	X
Inter-alpha-trypsin inhibitor heavy chain H4 OS=Homo sapiens GN=ITI4 PE=1 SV=4	X	X	X
Apolipoprotein B-100 OS=Homo sapiens GN=APOB PE=1 SV=2	X	X	X
C4b-binding protein alpha chain OS=Homo sapiens GN=C4BPA PE=1 SV=2	X	X	X
Complement C1r subcomponent OS=Homo sapiens GN=C1R PE=1 SV=2	X	X	X
Myosin-9 OS=Homo sapiens GN=MYH9 PE=1 SV=4	X	X	X
Protein AMBP OS=Homo sapiens GN=AMBP PE=1 SV=1	X	X	X
Apolipoprotein C-III OS=Homo sapiens GN=APOC3 PE=1 SV=1	X	X	X
Gelsolin OS=Homo sapiens GN=GSN PE=1 SV=1		X	X
Alpha-2-antiplasmin OS=Homo sapiens GN=SERPINF2 PE=1 SV=3		X	X
Apolipoprotein C-II OS=Homo sapiens GN=APOC2 PE=1 SV=1		X	X
Immunoglobulin J chain OS=Homo sapiens GN=IGJ PE=1 SV=4		X	X

Galectin-3-binding protein OS=Homo sapiens GN=LGALS3BP PE=1 SV=1	X		X
Cartilage oligomeric matrix protein OS=Homo sapiens GN=COMP PE=1 SV=2	X		X
Thrombospondin-1 OS=Homo sapiens GN=THBS1 PE=1 SV=2	X		X
Actin, cytoplasmic 1 OS=Homo sapiens GN=ACTB PE=1 SV=1			X
Apolipoprotein(a) OS=Homo sapiens GN=LPA PE=1 SV=1			X
Hyaluronan-binding protein 2 OS=Homo sapiens GN=HABP2 PE=1 SV=1			X
Ig alpha-2 chain C region OS=Homo sapiens GN=IGHA2 PE=1 SV=3			X
Ig lambda-2 chain C regions OS=Homo sapiens GN=IGLC2 PE=1 SV=1			X
Ig mu chain C region OS=Homo sapiens GN=IGHM PE=1 SV=3			X
Ig mu heavy chain disease protein OS=Homo sapiens PE=1 SV=1			X
Integrin alpha-IIb OS=Homo sapiens GN=ITGA2B PE=1 SV=3			X
Kininogen-1 OS=Homo sapiens GN=KNG1 PE=1 SV=2			X
Mannan-binding lectin serine protease 2 OS=Homo sapiens GN=MASP2 PE=1 SV=4			X
Tenascin-X OS=Homo sapiens GN=TNXB PE=1 SV=3			X
Isoform 2 of Mannan-binding lectin serine protease 1 OS=Homo sapiens GN=MASP1			X
Mannan-binding lectin serine protease 1 OS=Homo sapiens GN=MASP1 PE=1 SV=3			X
14-3-3 protein zeta/delta OS=Homo sapiens GN=YWHAZ PE=1 SV=1			X
A disintegrin and metalloproteinase with thrombospondin motifs 13 OS=Homo sapiens GN=ADAMTS13 PE=1 SV=1			X
Alpha-1B-glycoprotein OS=Homo sapiens GN=A1BG PE=1 SV=4			X
Angiopoietin-related protein 6 OS=Homo sapiens GN=ANGPTL6 PE=1 SV=1			X
Beta-Ala-His dipeptidase OS=Homo sapiens GN=CNDP1 PE=1 SV=4			X
Coagulation factor XIII A chain OS=Homo sapiens GN=F13A1 PE=1 SV=4			X
Cofilin-1 OS=Homo sapiens GN=CFL1 PE=1 SV=3			X
Cysteine and glycine-rich protein 1 OS=Homo sapiens GN=CSRP1 PE=1 SV=3			X
Desmoglein-2 OS=Homo sapiens GN=DSG2 PE=1 SV=2			X
Fibrillin-1 OS=Homo sapiens GN=FBN1 PE=1 SV=3			X
Fibulin-5 OS=Homo sapiens GN=FBLN5 PE=1 SV=1			X
Ficolin-2 OS=Homo sapiens GN=FCN2 PE=1 SV=2			X
Glyceraldehyde-3-phosphate dehydrogenase OS=Homo sapiens GN=GAPDH PE=1 SV=3			X
Hemoglobin subunit alpha OS=Homo sapiens GN=HBA1 PE=1 SV=2			X
Hemoglobin subunit beta OS=Homo sapiens GN=HBB PE=1 SV=2			X
Integrin-linked protein kinase OS=Homo sapiens GN=ILK PE=1 SV=2			X
Integrin beta-3 OS=Homo sapiens GN=ITGB3 PE=1 SV=2			X
Intelectin-1 OS=Homo sapiens GN=ITLN1 PE=1 SV=1			X
Isoform 10 of Collectin-11 OS=Homo sapiens GN=COLEC11			X
Isoform 2 of Tropomyosin alpha-3 chain OS=Homo sapiens GN=TPM3			X
Isoform 3 of Alpha-actinin-1 OS=Homo sapiens GN=ACTN1			X
Multimerin-1 OS=Homo sapiens GN=MMRN1 PE=1 SV=3			X
Nidogen-1 OS=Homo sapiens GN=NID1 PE=1 SV=3			X
Peptidyl-prolyl cis-trans isomerase A OS=Homo sapiens GN=PPIA PE=1 SV=2			X
Platelet factor 4 OS=Homo sapiens GN=PF4 PE=1 SV=2			X
Platelet glycoprotein Ib alpha chain OS=Homo sapiens GN=GP1BA PE=1 SV=1			X
Platelet glycoprotein IX OS=Homo sapiens GN=GP9 PE=1 SV=3			X
Platelet glycoprotein V OS=Homo sapiens GN=GP5 PE=1 SV=1			X
Pleckstrin OS=Homo sapiens GN=PLEK PE=1 SV=3			X
Profilin-1 OS=Homo sapiens GN=PFN1 PE=1 SV=2			X
Proprotein convertase subtilisin/kexin type 9 OS=Homo sapiens GN=PCSK9 PE=1 SV=3			X
Pyruvate kinase PKM OS=Homo sapiens GN=PKM PE=1 SV=4			X
Soluble scavenger receptor cysteine-rich domain-containing protein SSC5D OS=Homo sapiens GN=SSC5D PE=2 SV=3			X
Sushi, von Willebrand factor type A, EGF and pentraxin domain-containing protein 1 OS=Homo sapiens GN=SVEP1 PE=1 SV=3			X
Thrombospondin-4 OS=Homo sapiens GN=THBS4 PE=1 SV=2			X
Tropomyosin alpha-4 chain OS=Homo sapiens GN=TPM4 PE=1 SV=3			X
Tubulin alpha-1B chain OS=Homo sapiens GN=TUBA1B PE=1 SV=1			X
Tubulin beta-1 chain OS=Homo sapiens GN=TUBB1 PE=1 SV=1			X
Vinculin OS=Homo sapiens GN=VCL PE=1 SV=4			X
Complement component C8 alpha chain OS=Homo sapiens GN=C8A PE=1 SV=2	X	X	
Isoform 2 of Ig mu chain C region OS=Homo sapiens GN=IGHM	X	X	
Plasma kallikrein OS=Homo sapiens GN=KLKB1 PE=1 SV=1	X	X	
Retinol-binding protein 4 OS=Homo sapiens GN=RBP4 PE=1 SV=3	X	X	
Isoform 2 of N-acetylmuramoyl-L-alanine amidase OS=Homo sapiens GN=PGLYRP2	X	X	
Complement factor I OS=Homo sapiens GN=CFI PE=1 SV=2	X	X	
Isoform 2 of Haptoglobin-related protein OS=Homo sapiens GN=HPR	X	X	
Kallistatin OS=Homo sapiens GN=SERPINA4 PE=1 SV=3	X	X	
Lumican OS=Homo sapiens GN=LUM PE=1 SV=2	X	X	
Fetuin-B OS=Homo sapiens GN=FETUB PE=1 SV=2	X	X	
Afamin OS=Homo sapiens GN=AFM PE=1 SV=1	X	X	
Alpha-1-acid glycoprotein 2 OS=Homo sapiens GN=ORM2 PE=1 SV=2	X	X	

Phospholipid transfer protein OS=Homo sapiens GN=PLTP PE=1 SV=1	X	X	
Hepatocyte growth factor-like protein OS=Homo sapiens GN=MST1 PE=1 SV=2	X	X	
Isoform 4 of Extracellular matrix protein 1 OS=Homo sapiens GN=ECM1	X	X	
Complement component C8 gamma chain OS=Homo sapiens GN=C8G PE=1 SV=3	X	X	
Coagulation factor XII OS=Homo sapiens GN=F12 PE=1 SV=3	X	X	
Isoform 2 of Ig delta chain C region OS=Homo sapiens GN=IGHD	X	X	
Coagulation factor XIII B chain OS=Homo sapiens GN=F13B PE=1 SV=3	X	X	
Isoform 3 of Vitamin D-binding protein OS=Homo sapiens GN=GC	X	X	
Complement factor H OS=Homo sapiens GN=CFH PE=1 SV=4	X	X	
Phosphatidylinositol-glycan-specific phospholipase D OS=Homo sapiens GN=GPLD1 PE=1 SV=3	X	X	
Lipopolysaccharide-binding protein OS=Homo sapiens GN=LBP PE=1 SV=3	X	X	
Angiotensinogen OS=Homo sapiens GN=AGT PE=1 SV=1	X	X	
Complement component C6 OS=Homo sapiens GN=C6 PE=1 SV=3	X	X	
Plasma serine protease inhibitor OS=Homo sapiens GN=SERPINA5 PE=1 SV=3	X	X	
Apolipoprotein D OS=Homo sapiens GN=APOD PE=1 SV=1	X	X	
Alpha-1-antichymotrypsin OS=Homo sapiens GN=SERPINA3 PE=1 SV=2	X	X	
C4b-binding protein beta chain OS=Homo sapiens GN=C4BPB PE=1 SV=1		X	
Coagulation factor IX OS=Homo sapiens GN=F9 PE=1 SV=2		X	
Complement C4-B OS=Homo sapiens GN=C4B PE=1 SV=2		X	
Hepatocyte growth factor activator OS=Homo sapiens GN=HGFA PE=1 SV=1		X	
Isoform 10 of Fibronectin OS=Homo sapiens GN=FN1		X	
Apolipoprotein C-IV OS=Homo sapiens GN=APOC4 PE=1 SV=1		X	
Carboxypeptidase N subunit 2 OS=Homo sapiens GN=CPN2 PE=1 SV=3		X	
Complement C1q subcomponent subunit C OS=Homo sapiens GN=C1QC PE=1 SV=3		X	
Carboxypeptidase B2 OS=Homo sapiens GN=CPB2 PE=1 SV=2	X		
Isoform LMW of Kininogen-1 OS=Homo sapiens GN=KNG1	X		
Ig heavy chain V-III region GAL OS=Homo sapiens PE=1 SV=1	X		
Ig kappa chain V-I region Mev OS=Homo sapiens PE=1 SV=1	X		
Ig kappa chain V-I region Wes OS=Homo sapiens PE=1 SV=1	X		
Keratin, type II cytoskeletal 1 OS=Homo sapiens GN=KRT1 PE=1 SV=6	X		
Ig kappa chain V-I region Ni OS=Homo sapiens PE=1 SV=1	X		

## Chapter 7 References

- ABDURRACHIM, D., LUIKEN, J. J., NICOLAY, K., GLATZ, J. F., PROMPERS, J. J. & NABBEN, M. 2015. Good and bad consequences of altered fatty acid metabolism in heart failure: evidence from mouse models. *Cardiovasc Res*, 106, 194-205.
- ADACHI, J., KUMAR, C., ZHANG, Y., OLSEN, J. V. & MANN, M. 2006. The human urinary proteome contains more than 1500 proteins, including a large proportion of membrane proteins. *Genome Biol*, 7, R80.
- AGAH, A., KYRIAKIDES, T. R., LAWLER, J. & BORNSTEIN, P. 2002. The lack of thrombospondin-1 (TSP1) dictates the course of wound healing in double-TSP1/TSP2-null mice. *Am J Pathol*, 161, 831-9.
- AGAR, C., DE GROOT, P. G., MORGELIN, M., MONK, S. D., VAN OS, G., LEVELS, J. H., DE LAAT, B., URBANUS, R. T., HERWALD, H., VAN DER POLL, T. & MEIJERS, J. C. 2011. beta(2)-glycoprotein I: a novel component of innate immunity. *Blood*, 117, 6939-47.
- AGATSTON, A. S., JANOWITZ, W. R., HILDNER, F. J., ZUSMER, N. R., VIAMONTE, M. & DETRANO, R. 1990. Quantification of coronary artery calcium using ultrafast computed tomography. *J Am Coll Cardiol*, 15, 827-32.
- AHRNÉ, E., MOLZAHN, L., GLATTER, T. & SCHMIDT, A. 2013. Critical assessment of proteome-wide label-free absolute abundance estimation strategies. *Proteomics*, 13, 2567-78.
- AKAHORI, H., TSUJINO, T., NAITO, Y., MATSUMOTO, M., LEE-KAWABATA, M., OHYANAGI, M., MITSUNO, M., MIYAMOTO, Y., DAIMON, T., HAO, H., HIROTA, S. & MASUYAMA, T. 2011. Intraleaflet haemorrhage is associated with rapid progression of degenerative aortic valve stenosis. *Eur Heart J*, 32, 888-96.
- AKERSTROM, B. & GRAM, M. 2014. A1M, an extravascular tissue cleaning and housekeeping protein. *Free Radic Biol Med*, 74, 274-82.
- AKSOY, Y., YAGMUR, C., TEKIN, G. O., YAGMUR, J., TOPAL, E., KEKILLI, E., TURHAN, H., KOSAR, F. & YETKIN, E. 2005. Aortic valve calcification: association with bone mineral density and cardiovascular risk factors. *Coron Artery Dis*, 16, 379-83.

- ALLHORN, M., BERGGARD, T., NORDBERG, J., OLSSON, M. L. & AKERSTROM, B. 2002. Processing of the lipocalin alpha(1)-microglobulin by hemoglobin induces heme-binding and heme-degradation properties. *Blood*, 99, 1894-901.
- AMATO, M. C., MOFFA, P. J., WERNER, K. E. & RAMIRES, J. A. 2001. Treatment decision in asymptomatic aortic valve stenosis: role of exercise testing. *Heart*, 86, 381-6.
- ANAND, A., CHIN, C., SHAH, A. S. V., KWIECINSKI, J., VESEY, A., COWELL, J., WEBER, E., KAIER, T., NEWBY, D. E., DWECK, M., MARBER, M. S. & MILLS, N. L. 2018. Cardiac myosin-binding protein C is a novel marker of myocardial injury and fibrosis in aortic stenosis. *Heart*, 104, 1101-1108.
- ANDERSON, K. R., SUTTON, M. G. & LIE, J. T. 1979. Histopathological types of cardiac fibrosis in myocardial disease. *J Pathol*, 128, 79-85.
- ANDERSON, N. G. & ANDERSON, N. L. 1996. Twenty years of two-dimensional electrophoresis: past, present and future. *Electrophoresis*, 17, 443-53.
- ANDERSON, N. L. 2010. The clinical plasma proteome: a survey of clinical assays for proteins in plasma and serum. *Clin Chem*, 56, 177-85.
- ANDERSON, N. L. & ANDERSON, N. G. 2002. The human plasma proteome: history, character, and diagnostic prospects. *Mol Cell Proteomics*, 1, 845-67.
- ANDRESSOO, J. O., HOEIJMAKERS, J. H. & MITCHELL, J. R. 2006. Nucleotide excision repair disorders and the balance between cancer and aging. *Cell Cycle*, 5, 2886-8.
- ANTZELEVITCH, C. 2007. Ionic, molecular, and cellular bases of QT-interval prolongation and torsade de pointes. *Europace*, 9 Suppl 4, iv4-15.
- ANUMONWO, J. M. & PANDIT, S. V. 2015. Ionic mechanisms of arrhythmogenesis. *Trends Cardiovasc Med*, 25, 487-96.
- APPARI, M., WERNER, R., WÜNSCH, L., CARIO, G., DEMETER, J., HIORT, O., RIEPE, F., BROOKS, J. D. & HOLTERHUS, P. M. 2009. Apolipoprotein D (APOD) is a putative biomarker of androgen receptor function in androgen insensitivity syndrome. *J Mol Med (Berl)*, 87, 623-32.
- ARAI, T., MORICE, M. C., O'CONNOR, S. A., YAMAMOTO, M., ELTCHANINOFF, H., LEGUERRIER, A., LEPRINCE, P., LASKAR, M., IUNG, B., FAJADET, J., PRAT, A., LIEVRE, M., DONZEAU-GOUGE, P., CHEVREUL, K., TEIGER, E., LEFEVRE, T. & GILARD, M. 2015. Impact of pre- and post-procedural anemia on the incidence of acute kidney injury and 1-year mortality in patients undergoing

- transcatheter aortic valve implantation (from the French Aortic National CoreValve and Edwards 2 [FRANCE 2] Registry). *Catheter Cardiovasc Interv*, 85, 1231-9.
- ARAKEL, E. C., BRANDENBURG, S., UCHIDA, K., ZHANG, H., LIN, Y. W., KOHL, T., SCHRUL, B., SULKIN, M. S., EFIMOV, I. R., NICHOLS, C. G., LEHNART, S. E. & SCHWAPPACH, B. 2014. Tuning the electrical properties of the heart by differential trafficking of KATP ion channel complexes. *J Cell Sci*, 127, 2106-19.
- ARANGALAGE, D., NGUYEN, V., ROBERT, T., MELISSOPOULOU, M., MATHIEU, T., ESTELLAT, C., CODOGNO, I., HUART, V., DUVAL, X., CIMADEVILLA, C., VAHANIAN, A., DEHOUX, M. & MESSIKA-ZEITOUN, D. 2016. Determinants and prognostic value of Galectin-3 in patients with aortic valve stenosis. *Heart*, 102, 862-8.
- ASSOMULL, R. G., PRASAD, S. K., LYNE, J., SMITH, G., BURMAN, E. D., KHAN, M., SHEPPARD, M. N., POOLE-WILSON, P. A. & PENNELL, D. J. 2006. Cardiovascular magnetic resonance, fibrosis, and prognosis in dilated cardiomyopathy. *J Am Coll Cardiol*, 48, 1977-85.
- AUENSEN, A., HUSSAIN, A. I., FALK, R. S., WALLE-HANSEN, M. M., BYE, J., PETTERSEN, K. I., AUKRUST, P., UELAND, T. & GULLESTAD, L. L. 2017. Associations of brain-natriuretic peptide, high-sensitive troponin T, and high-sensitive C-reactive protein with outcomes in severe aortic stenosis. *PLoS One*, 12, e0179304.
- AVICE, M. N., RUBIO, M., SERGERIE, M., DELESPESE, G. & SARFATI, M. 2000. CD47 ligation selectively inhibits the development of human naive T cells into Th1 effectors. *J Immunol*, 165, 4624-31.
- BAENZIGER, N. L., BRODIE, G. N. & MAJERUS, P. W. 1971. A thrombin-sensitive protein of human platelet membranes. *Proc Natl Acad Sci U S A*, 68, 240-3.
- BAKER, W. A., HITMAN, G. A., HAWRAMI, K., MCCARTHY, M. I., RIIKONEN, A., TUOMILEHTO-WOLF, E., NISSINEN, A., TUOMILEHTO, J., MOHAN, V., VISWANATHAN, M. & ET AL. 1994. Apolipoprotein D gene polymorphism: a new genetic marker for type 2 diabetic subjects in Nauru and south India. *Diabet Med*, 11, 947-52.
- BANKS, R. & SELBY, P. 2003. Clinical proteomics--insights into pathologies and benefits for patients. *Lancet*, 362, 415-6.
- BANOVIC, M., IUNG, B., BARTUNEK, J., ASANIN, M., BELESLIN, B., BIOCINA, B., CASSELMAN, F., DA COSTA, M., DEJA, M., GASPAROVIC, H., KALA, P., LABROUSSE, L., LONCAR, Z., MARINKOVIC, J., NEDELJKOVIC, I.,

- NEDELJKOVIC, M., NEMEC, P., NIKOLIC, S. D., PENCINA, M., PENICKA, M., RISTIC, A., SHARIF, F., VAN CAMP, G., VANDERHEYDEN, M., WOJAKOWSKI, W. & PUTNIK, S. 2016. Rationale and design of the Aortic Valve replAcemenT versus conservative treatment in Asymptomatic severe aortic stenosis (AVATAR trial): A randomized multicenter controlled event-driven trial. *Am Heart J*, 174, 147-53.
- BAUMGARTNER, H., FALK, V., BAX, J. J., DE BONIS, M., HAMM, C., HOLM, P. J., IUNG, B., LANCELLOTTI, P., LANSAC, E. & RODRIGUEZ MUNOZ, D. 2017a. 2017 ESC/EACTS guidelines for the management of valvular heart disease. *European heart journal*, 38, 2739-2791.
- BAUMGARTNER, H., HUNG, J., BERMEJO, J., CHAMBERS, J. B., EDVARDBSEN, T., GOLDSTEIN, S., LANCELLOTTI, P., LEFEVRE, M., MILLER, F. & OTTO, C. M. 2017b. Recommendations on the Echocardiographic Assessment of Aortic Valve Stenosis: A Focused Update from the European Association of Cardiovascular Imaging and the American Society of Echocardiography. *J Am Soc Echocardiogr*, 30, 372-392.
- BECKMANN, J. S. & LEW, D. 2016. Reconciling evidence-based medicine and precision medicine in the era of big data: challenges and opportunities. *Genome Med*, 8, 134.
- BEER, L. A., KY, B., BARNHART, K. T. & SPEICHER, D. W. 2017. In-Depth, Reproducible Analysis of Human Plasma Using IgY 14 and SuperMix Immunodepletion. *Methods Mol Biol*, 1619, 81-101.
- BEER, L. A., TANG, H. Y., BARNHART, K. T. & SPEICHER, D. W. 2011. Plasma biomarker discovery using 3D protein profiling coupled with label-free quantitation. *Methods Mol Biol*, 728, 3-27.
- BEHNES, M., BRUECKMANN, M., LANG, S., ESPETER, F., WEISS, C., NEUMAIER, M., AHMAD-NEJAD, P., BORGGREFE, M. & HOFFMANN, U. 2013. Diagnostic and prognostic value of osteopontin in patients with acute congestive heart failure. *Eur J Heart Fail*, 15, 1390-400.
- BEN-DOR, I., MINHA, S., BARBASH, I. M., ALY, O., DVIR, D., DEKSISSA, T., OKUBAGZI, P., TORGUSON, R., LINDSAY, J., SATLER, L. F., PICHARD, A. D. & WAKSMAN, R. 2013. Correlation of brain natriuretic peptide levels in patients with severe aortic stenosis undergoing operative valve replacement or percutaneous transcatheter intervention with clinical, echocardiographic, and hemodynamic factors and prognosis. *Am J Cardiol*, 112, 574-9.



- BENDIG, G., GRIMMLER, M., HUTTNER, I. G., WESSELS, G., DAHME, T., JUST, S., TRANO, N., KATUS, H. A., FISHMAN, M. C. & ROTTBAUER, W. 2006. Integrin-linked kinase, a novel component of the cardiac mechanical stretch sensor, controls contractility in the zebrafish heart. *Genes Dev*, 20, 2361-72.
- BEREMAN, M. S., MACLEAN, B., TOMAZELA, D. M., LIEBLER, D. C. & MACCOSS, M. J. 2012. The development of selected reaction monitoring methods for targeted proteomics via empirical refinement. *Proteomics*, 12, 1134-41.
- BERGLER-KLEIN, J., KLAAR, U., HEGER, M., ROSENHEK, R., MUNDIGLER, G., GABRIEL, H., BINDER, T., PACHER, R., MAURER, G. & BAUMGARTNER, H. 2004. Natriuretic peptides predict symptom-free survival and postoperative outcome in severe aortic stenosis. *Circulation*, 109, 2302-8.
- BEUREL, E. & JOPE, R. S. 2006. The paradoxical pro- and anti-apoptotic actions of GSK3 in the intrinsic and extrinsic apoptosis signaling pathways. *Prog Neurobiol*, 79, 173-89.
- BHANDARI, S., GUPTA, P., QUINN, P., SANDHU, J., HAKIMI, A., JONES, D. & NG, L. 2015. Pleiotropic effects of statins in hypercholesterolaemia: a prospective observational study using a lipoproteomic based approach. *The Lancet*, 385, S21.
- BHOWMICK, P., MOHAMMED, Y. & BORCHERS, C. H. 2018. MRMAssayDB: an integrated resource for validated targeted proteomics assays. *Bioinformatics*, 34, 3566-3571.
- BINDEA, G., MLECNIK, B., HACKL, H., CHAROENTONG, P., TOSOLINI, M., KIRILOVSKY, A., FRIDMAN, W. H., PAGES, F., TRAJANOSKI, Z. & GALON, J. 2009. ClueGO: a Cytoscape plug-in to decipher functionally grouped gene ontology and pathway annotation networks. *Bioinformatics*, 25, 1091-3.
- BING, O. H., NGO, H. Q., HUMPHRIES, D. E., ROBINSON, K. G., LUCEY, E. C., CARVER, W., BROOKS, W. W., CONRAD, C. H., HAYES, J. A. & GOLDSTEIN, R. H. 1997. Localization of alpha1(I) collagen mRNA in myocardium from the spontaneously hypertensive rat during the transition from compensated hypertrophy to failure. *J Mol Cell Cardiol*, 29, 2335-44.
- BING, R. J., SIEGEL, A., UNGAR, I. & GILBERT, M. 1954. Metabolism of the human heart. II. Studies on fat, ketone and amino acid metabolism. *Am J Med*, 16, 504-15.
- BISHOPRIC, N. H., ANDREKA, P., SLEPAK, T. & WEBSTER, K. A. 2001. Molecular mechanisms of apoptosis in the cardiac myocyte. *Curr Opin Pharmacol*, 1, 141-50.

- BLANKLEY, R. T., FISHER, C., WESTWOOD, M., NORTH, R., BAKER, P. N., WALKER, M. J., WILLIAMSON, A., WHETTON, A. D., LIN, W., MCCOWAN, L., ROBERTS, C. T., COOPER, G. J., UNWIN, R. D. & MYERS, J. E. 2013. A label-free selected reaction monitoring workflow identifies a subset of pregnancy specific glycoproteins as potential predictive markers of early-onset pre-eclampsia. *Mol Cell Proteomics*, 12, 3148-59.
- BOER, B. P., VIEIRA, M. L., SAMPAIO, R. O., ABENSUR, H., OLIVEIRA, A. G., FERNANDES, J. R. & GRINBERG, M. 2013. Correlation to NT-ProBNP and remodeling after cardiac surgery. *Arq Bras Cardiol*, 100, 469-75.
- BONNEFOY, A., MOURA, R. & HOYLAERTS, M. F. 2008. The evolving role of thrombospondin-1 in hemostasis and vascular biology. *Cell Mol Life Sci*, 65, 713-27.
- BOROWIEC, A., DABROWSKI, R., KOWALIK, I., FIREK, B., CHWYCZKO, T., JANAS, J. & SZWED, H. 2015. Osteoprotegerin in patients with degenerative aortic stenosis and preserved left-ventricular ejection fraction. *J Cardiovasc Med (Hagerstown)*, 16, 444-50.
- BOUSKILA, M., ESOOF, N., GAY, L., FANG, E. H., DEAK, M., BEGLEY, M. J., CANTLEY, L. C., PRESCOTT, A., STOREY, K. G. & ALESSI, D. R. 2011. TTBK2 kinase substrate specificity and the impact of spinocerebellar-ataxia-causing mutations on expression, activity, localization and development. *Biochem J*, 437, 157-67.
- BOWNE, S. J., DAIGER, S. P., MALONE, K. A., HECKENLIVELY, J. R., KENNAN, A., HUMPHRIES, P., HUGHBANKS-WHEATON, D., BIRCH, D. G., LIU, Q., PIERCE, E. A., ZUO, J., HUANG, Q., DONOVAN, D. D. & SULLIVAN, L. S. 2003. Characterization of RP1L1, a highly polymorphic paralog of the retinitis pigmentosa 1 (RP1) gene. *Mol Vis*, 9, 129-37.
- BOZEAT, N. D., XIANG, S. Y., YE, L. L., YAO, T. Y., DUAN, M. L., BURKIN, D. J., LAMB, F. S. & DUAN, D. D. 2011. Activation of volume regulated chloride channels protects myocardium from ischemia/reperfusion damage in second-window ischemic preconditioning. *Cell Physiol Biochem*, 28, 1265-78.
- BRAHIMAJ, A., LIGTHART, S., IKRAM, M. A., HOFMAN, A., FRANCO, O. H., SIJBRANDS, E. J., KAVOUSHI, M. & DEHGHAN, A. 2017. Serum levels of apolipoproteins and incident type 2 diabetes: a prospective cohort study. *Diabetes Care*, 40, 346-351.

- BREISCH, E. A., WHITE, F. C. & BLOOR, C. M. 1984. Myocardial characteristics of pressure overload hypertrophy. A structural and functional study. *Lab Invest*, 51, 333-42.
- BRIAND, M., DUMESNIL, J. G., KADEM, L., TONGUE, A. G., RIEU, R., GARCIA, D. & PIBAROT, P. 2005. Reduced systemic arterial compliance impacts significantly on left ventricular afterload and function in aortic stenosis: implications for diagnosis and treatment. *J Am Coll Cardiol*, 46, 291-8.
- BROWNLEE, Z., LYNN, K. D., THORPE, P. E. & SCHROIT, A. J. 2014. A novel "salting-out" procedure for the isolation of tumor-derived exosomes. *J Immunol Methods*, 407, 120-6.
- BRUNO, J., POZZI, N., OLIVA, J. & EDWARDS, J. C. 2017. Apolipoprotein L1 confers pH-switchable ion permeability to phospholipid vesicles. *J Biol Chem*, 292, 18344-18353.
- BULL, S., LOUDON, M., FRANCIS, J. M., JOSEPH, J., GERRY, S., KARAMITSOS, T. D., PRENDERGAST, B. D., BANNING, A. P., NEUBAUER, S. & MYERSON, S. G. 2015. A prospective, double-blind, randomized controlled trial of the angiotensin-converting enzyme inhibitor Ramipril In Aortic Stenosis (RIAS trial). *Eur Heart J Cardiovasc Imaging*, 16, 834-41.
- BUSCHMAN, M. D. & FIELD, S. J. 2017. MYO18A: An unusual myosin. *Adv Biol Regul.*
- BUSS, F. & STEWART, M. 1995. Macromolecular interactions in the nucleoporin p62 complex of rat nuclear pores: binding of nucleoporin p54 to the rod domain of p62. *J Cell Biol*, 128, 251-61.
- CAI, A., MIYAZAWA, A., SUNDERLAND, N., PIPER, S. E., GIBBS, T. G. J., WANG, D., REDDING, S., AMIN-YOUSEFF, G., WENDLER, O., BYRNE, J., MACCARTHY, P. A., SHAH, A. M., MCDONAGH, T. A. & DWORAKOWSKI, R. 2019. ST2 in patients with severe aortic stenosis and heart failure. *Cardiol J*.
- CAIRA, F. C., STOCK, S. R., GLEASON, T. G., MCGEE, E. C., HUANG, J., BONOW, R. O., SPELSBERG, T. C., MCCARTHY, P. M., RAHIMTOOLA, S. H. & RAJAMANNAN, N. M. 2006. Human degenerative valve disease is associated with up-regulation of low-density lipoprotein receptor-related protein 5 receptor-mediated bone formation. *J Am Coll Cardiol*, 47, 1707-12.
- CAO, Z., TANG, H. Y., WANG, H., LIU, Q. & SPEICHER, D. W. 2012. Systematic comparison of fractionation methods for in-depth analysis of plasma proteomes. *J Proteome Res*, 11, 3090-100.

- CAPOULADE, R., YEANG, C., CHAN, K. L., PIBAROT, P. & TSIMIKAS, S. 2018. Association of Mild to Moderate Aortic Valve Stenosis Progression With Higher Lipoprotein(a) and Oxidized Phospholipid Levels: Secondary Analysis of a Randomized Clinical Trial. *JAMA Cardiol.*
- CARABELLO, B. A. 2013. Introduction to aortic stenosis. *Circ Res*, 113, 179-85.
- CARABELLO, B. A. & PAULUS, W. J. 2009. Aortic stenosis. *Lancet*, 373, 956-66.
- CARMELIET, E. 1999. Cardiac ionic currents and acute ischemia: from channels to arrhythmias. *Physiol Rev*, 79, 917-1017.
- CARR, S. A., ABBATIELLO, S. E., ACKERMANN, B. L., BORCHERS, C., DOMON, B., DEUTSCH, E. W., GRANT, R. P., HOOFNAGLE, A. N., HÜTTENHAIN, R., KOOMEN, J. M., LIEBLER, D. C., LIU, T., MACLEAN, B., MANI, D. R., MANSFIELD, E., NEUBERT, H., PAULOVICH, A. G., REITER, L., VITEK, O., AEBERSOLD, R., ANDERSON, L., BETHEM, R., BLONDER, J., BOJA, E., BOTELHO, J., BOYNE, M., BRADSHAW, R. A., BURLINGAME, A. L., CHAN, D., KESHISHIAN, H., KUHN, E., KINSINGER, C., LEE, J. S., LEE, S. W., MORITZ, R., OSES-PRIETO, J., RIFAI, N., RITCHIE, J., RODRIGUEZ, H., SRINIVAS, P. R., TOWNSEND, R. R., VAN EYK, J., WHITELEY, G., WIITA, A. & WEINTRAUB, S. 2014. Targeted peptide measurements in biology and medicine: best practices for mass spectrometry-based assay development using a fit-for-purpose approach. *Mol Cell Proteomics*, 13, 907-17.
- CHEN, H., HERNDON, M. E. & LAWLER, J. 2000. The cell biology of thrombospondin-1. *Matrix Biol*, 19, 597-614.
- CHEN, J., LU, Y., XU, J., HUANG, Y., CHENG, H., HU, G., LUO, C., LOU, M., CAO, G., XIE, Y. & YING, K. 2004. Identification and characterization of NBEAL1, a novel human neurobeachin-like 1 protein gene from fetal brain, which is up regulated in glioma. *Brain Res Mol Brain Res*, 125, 147-55.
- CHEN, L., MAO, S. J. & LARSEN, W. J. 1992. Identification of a factor in fetal bovine serum that stabilizes the cumulus extracellular matrix. A role for a member of the inter-alpha-trypsin inhibitor family. *J Biol Chem*, 267, 12380-6.
- CHEN, X., ZHANG, Y., CHEN, Q., LI, Q., LI, Y. & LING, W. 2017. Lower Plasma Fetuin-A Levels Are Associated With a Higher Mortality Risk in Patients With Coronary Artery Disease. *Arterioscler Thromb Vasc Biol*, 37, 2213-2219.

- CHEN, Y., HAN, H., YAN, X., DING, F., SU, X., WANG, H., CHEN, Q., LU, L., ZHANG, R. & JIN, W. 2015. Tetranectin as a Potential Biomarker for Stable Coronary Artery Disease. *Sci Rep*, 5, 17632.
- CHEN, Z., LI, C., XU, Y., LI, Y., YANG, H. & RAO, L. 2014. Circulating level of miR-378 predicts left ventricular hypertrophy in patients with aortic stenosis. *PLoS One*, 9, e105702.
- CHENG, W., LI, B., KAJSTURA, J., LI, P., WOLIN, M. S., SONNENBLICK, E. H., HINTZE, T. H., OLIVETTI, G. & ANVERSA, P. 1995. Stretch-induced programmed myocyte cell death. *J Clin Invest*, 96, 2247-59.
- CHIN, C. W., MESSIKA-ZEITOUN, D., SHAH, A. S., LEFEVRE, G., BAILLEUL, S., YEUNG, E. N., KOO, M., MIRSADRAEE, S., MATHIEU, T., SEMPLÉ, S. I., MILLS, N. L., VAHANIAN, A., NEWBY, D. E. & DWECK, M. R. 2016. A clinical risk score of myocardial fibrosis predicts adverse outcomes in aortic stenosis. *Eur Heart J*, 37, 713-23.
- CHIN, C. W., SHAH, A. S., MCALLISTER, D. A., JOANNA COWELL, S., ALAM, S., LANGRISH, J. P., STRACHAN, F. E., HUNTER, A. L., MARIA CHOY, A., LANG, C. C., WALKER, S., BOON, N. A., NEWBY, D. E., MILLS, N. L. & DWECK, M. R. 2014. High-sensitivity troponin I concentrations are a marker of an advanced hypertrophic response and adverse outcomes in patients with aortic stenosis. *Eur Heart J*, 35, 2312-21.
- CHIVA, C. & SABIDÓ, E. 2017. Peptide Selection for Targeted Protein Quantitation. *J Proteome Res*, 16, 1376-1380.
- CHO, H., THORVALDSEN, J. L., CHU, Q., FENG, F. & BIRNBAUM, M. J. 2001. Akt1/PKB $\alpha$  is required for normal growth but dispensable for maintenance of glucose homeostasis in mice. *J Biol Chem*, 276, 38349-52.
- CHORIANOPOULOS, E., KRUMSDORF, U., GEIS, N., PLEGER, S. T., GIANNITSIS, E., KATUS, H. A. & BEKEREDJIAN, R. 2014. Preserved prognostic value of preinterventional troponin T levels despite successful TAVI in patients with severe aortic stenosis. *Clin Res Cardiol*, 103, 65-72.
- CHRISTENSEN, L. & CLEMMENSEN, I. 1991. Differences in tetranectin immunoreactivity between benign and malignant breast tissue. *Histochemistry*, 95, 427-33.

- CIOFFI, G., FAGGIANO, P., VIZZARDI, E., TARANTINI, L., CRAMARIUC, D., GERDTS, E. & DE SIMONE, G. 2011. Prognostic effect of inappropriately high left ventricular mass in asymptomatic severe aortic stenosis. *Heart*, 97, 301-7.
- CLAASSEN, M., REITER, L., HENGARTNER, M. O., BUHMANN, J. M. & AEBERSOLD, R. 2012. Generic comparison of protein inference engines. *Mol Cell Proteomics*, 11, O110 007088.
- CLAVEL, M. A., MESSIKA-ZEITOUN, D., PIBAROT, P., AGGARWAL, S. R., MALOUF, J., ARAOZ, P. A., MICHELENA, H. I., CUEFF, C., LAROSE, E., CAPOULADE, R., VAHANIAN, A. & ENRIQUEZ-SARANO, M. 2013. The complex nature of discordant severe calcified aortic valve disease grading: new insights from combined Doppler echocardiographic and computed tomographic study. *J Am Coll Cardiol*, 62, 2329-38.
- CLAVEL, M. A., PIBAROT, P., MESSIKA-ZEITOUN, D., CAPOULADE, R., MALOUF, J., AGGARWAL, S., ARAOZ, P. A., MICHELENA, H. I., CUEFF, C., LAROSE, E., MILLER, J. D., VAHANIAN, A. & ENRIQUEZ-SARANO, M. 2014. Impact of aortic valve calcification, as measured by MDCT, on survival in patients with aortic stenosis: results of an international registry study. *J Am Coll Cardiol*, 64, 1202-13.
- CLEMMENSEN, I., PETERSEN, L. C. & KLUFT, C. 1986. Purification and characterization of a novel, oligomeric, plasminogen kringle 4 binding protein from human plasma: tetranectin. *Eur J Biochem*, 156, 327-33.
- COSMI, J. E., KORT, S., TUNICK, P. A., ROSENZWEIG, B. P., FREEDBERG, R. S., KATZ, E. S., APPLEBAUM, R. M. & KRONZON, I. 2002. The risk of the development of aortic stenosis in patients with "benign" aortic valve thickening. *Arch Intern Med*, 162, 2345-7.
- COWELL, S. J., NEWBY, D. E., BURTON, J., WHITE, A., NORTHRIDGE, D. B., BOON, N. A. & REID, J. 2003. Aortic valve calcification on computed tomography predicts the severity of aortic stenosis. *Clin Radiol*, 58, 712-6.
- CSORDAS, A., NIETLISPACH, F., SCHUETZ, P., HUBER, A., MULLER, B., MAISANO, F., TARAMASSO, M., MOAROF, I., OBEID, S., STAHLI, B. E., CAHENZLY, M., BINDER, R. K., LIEBETRAU, C., MOLLMANN, H., KIM, W. K., HAMM, C. & LUSCHER, T. F. 2015. Midregional Proadrenomedullin Improves Risk Stratification beyond Surgical Risk Scores in Patients Undergoing Transcatheter Aortic Valve Replacement. *PLoS One*, 10, e0143761.

- CUNNINGHAM, O., GORE, M. G. & MANTLE, T. J. 2000. Initial-rate kinetics of the flavin reductase reaction catalysed by human biliverdin-IXbeta reductase (BVR-B). *Biochem J*, 345 Pt 2, 393-9.
- CUYPERS, B., LECORDIER, L., MEEHAN, C. J., VAN DEN BROECK, F., IMAMURA, H., BUSCHER, P., DUJARDIN, J. C., LAUKENS, K., SCHNAUFER, A., DEWAR, C., LEWIS, M., BALMER, O., AZURAGO, T., KYEI-FARIED, S., OHENE, S. A., DUAH, B., HOMIAH, P., MENSAH, E. K., ANLEAH, F., FRANCO, J. R., PAYS, E. & DEBORGGRAEVE, S. 2016. Apolipoprotein L1 Variant Associated with Increased Susceptibility to Trypanosome Infection. *MBio*, 7, e02198-15.
- DAHL, J. S., MOLLER, J. E., VIDEBAEK, L., POULSEN, M. K., RUDBAEK, T. R., PELLIKKA, P. A., SCOTT ARGRAVES, W. & RASMUSSEN, L. M. 2012. Plasma fibulin-1 is linked to restrictive filling of the left ventricle and to mortality in patients with aortic valve stenosis. *J Am Heart Assoc*, 1, e003889.
- DAHOU, A., CLAVEL, M. A., CAPOULADE, R., O'CONNOR, K., RIBEIRO, H. B., COTE, N., LE VEN, F., RODES-CABAU, J., DUMESNIL, J. G., MATHIEU, P. & PIBAROT, P. 2018. B-Type Natriuretic Peptide and High-Sensitivity Cardiac Troponin for Risk Stratification in Low-Flow, Low-Gradient Aortic Stenosis: A Substudy of the TOPAS Study. *JACC Cardiovasc Imaging*, 11, 939-947.
- DAI, J., MATSUI, T., ABEL, E. D., DEDHAR, S., GERSZTEN, R. E., SEIDMAN, C. E., SEIDMAN, J. G. & ROSENZWEIG, A. 2014. Deep sequence analysis of gene expression identifies osteopontin as a downstream effector of integrin-linked kinase (ILK) in cardiac-specific ILK knockout mice. *Circ Heart Fail*, 7, 184-93.
- DANIELS, R. E., HAQ, K. T., MILLER, L. S., CHIA, E. W., MIURA, M., SORRENTINO, V., MCGUIRE, J. J. & STUYVERS, B. D. 2017. Cardiac expression of ryanodine receptor subtype 3; a strategic component in the intracellular Ca(2+) release system of Purkinje fibers in large mammalian heart. *J Mol Cell Cardiol*, 104, 31-42.
- DAS, P., RIMINGTON, H. & CHAMBERS, J. 2005. Exercise testing to stratify risk in aortic stenosis. *Eur Heart J*, 26, 1309-13.
- DAVIDSON, S. M., TAKOV, K. & YELLON, D. M. 2017. Exosomes and Cardiovascular Protection. *Cardiovasc Drugs Ther*, 31, 77-86.
- DAVIES, S. W., GERSHLICK, A. H. & BALCON, R. 1991. Progression of valvar aortic stenosis: a long-term retrospective study. *Eur Heart J*, 12, 10-4.

- DAWSON, D. W., PEARCE, S. F., ZHONG, R., SILVERSTEIN, R. L., FRAZIER, W. A. & BOUCK, N. P. 1997. CD36 mediates the In vitro inhibitory effects of thrombospondin-1 on endothelial cells. *J Cell Biol*, 138, 707-17.
- DE GROOT, P. G. & MEIJERS, J. C. 2011.  $\beta(2)$  -Glycoprotein I: evolution, structure and function. *J Thromb Haemost*, 9, 1275-84.
- DE KREUK, B. J., SCHAEFER, A., ANTHONY, E. C., TOL, S., FERNANDEZ-BORJA, M., GEERTS, D., POOL, J., HAMBACH, L., GOULMY, E. & HORDIJK, P. L. 2013. The human minor histocompatibility antigen 1 is a RhoGAP. *PLoS One*, 8, e73962.
- DE LAS FUENTES, L., HERRERO, P., PETERSON, L. R., KELLY, D. P., GROPLER, R. J. & DAVILA-ROMAN, V. G. 2003. Myocardial fatty acid metabolism: independent predictor of left ventricular mass in hypertensive heart disease. *Hypertension*, 41, 83-7.
- DE SERRES, F. & BLANCO, I. 2014. Role of alpha-1 antitrypsin in human health and disease. *J Intern Med*, 276, 311-35.
- DE VRIES, T. J., DE WIT, P. E., CLEMMENSEN, I., VERSPAGET, H. W., WEIDLE, U. H., BRÖCKER, E. B., RUITER, D. J. & VAN MUIJEN, G. N. 1996. Tetranectin and plasmin/plasminogen are similarly distributed at the invasive front of cutaneous melanoma lesions. *J Pathol*, 179, 260-5.
- DEBOSCH, B., TRESKOV, I., LUPU, T. S., WEINHEIMER, C., KOVACS, A., COURTOIS, M. & MUSLIN, A. J. 2006. Akt1 is required for physiological cardiac growth. *Circulation*, 113, 2097-104.
- DELCOMMENNE, M., TAN, C., GRAY, V., RUE, L., WOODGETT, J. & DEDHAR, S. 1998. Phosphoinositide-3-OH kinase-dependent regulation of glycogen synthase kinase 3 and protein kinase B/AKT by the integrin-linked kinase. *Proc Natl Acad Sci USA*, 95, 11211-6.
- DESAI, P. P., BUNKER, C. H., UKOLI, F. A. & KAMBOH, M. I. 2002. Genetic variation in the apolipoprotein D gene among African blacks and its significance in lipid metabolism. *Atherosclerosis*, 163, 329-38.
- DIEPLINGER, H. & DIEPLINGER, B. 2015. Afamin--A pleiotropic glycoprotein involved in various disease states. *Clin Chim Acta*, 446, 105-10.
- DISTLER, U., KUHAREV, J., NAVARRO, P., LEVIN, Y., SCHILD, H. & TENZER, S. 2014. Drift time-specific collision energies enable deep-coverage data-independent acquisition proteomics. *Nat Methods*, 11, 167-70.



- DO CARMO, S., FOREST, J. C., GIGUÈRE, Y., MASSE, A., LAFOND, J. & RASSART, E. 2009. Modulation of Apolipoprotein D levels in human pregnancy and association with gestational weight gain. *Reprod Biol Endocrinol*, 7, 92.
- DROVER, V. A., AJMAL, M., NASSIR, F., DAVIDSON, N. O., NAULI, A. M., SAHOO, D., TSO, P. & ABUMRAD, N. A. 2005. CD36 deficiency impairs intestinal lipid secretion and clearance of chylomicrons from the blood. *J Clin Invest*, 115, 1290-7.
- DWECK, M. R., JONES, C., JOSHI, N. V., FLETCHER, A. M., RICHARDSON, H., WHITE, A., MARSDEN, M., PESSOTTO, R., CLARK, J. C., WALLACE, W. A., SALTER, D. M., MCKILLOP, G., VAN BEEK, E. J., BOON, N. A., RUDD, J. H. & NEWBY, D. E. 2012a. Assessment of valvular calcification and inflammation by positron emission tomography in patients with aortic stenosis. *Circulation*, 125, 76-86.
- DWECK, M. R., JOSHI, S., MURIGU, T., ALPENDURADA, F., JABBOUR, A., MELINA, G., BANYA, W., GULATI, A., ROUSSIN, I., RAZA, S., PRASAD, N. A., WAGE, R., QUARTO, C., ANGELONI, E., REFICE, S., SHEPPARD, M., COOK, S. A., KILNER, P. J., PENNELL, D. J., NEWBY, D. E., MOHIADDIN, R. H., PEPPER, J. & PRASAD, S. K. 2011. Midwall fibrosis is an independent predictor of mortality in patients with aortic stenosis. *J Am Coll Cardiol*, 58, 1271-9.
- DWECK, M. R., JOSHI, S., MURIGU, T., GULATI, A., ALPENDURADA, F., JABBOUR, A., MACEIRA, A., ROUSSIN, I., NORTHRIDGE, D. B., KILNER, P. J., COOK, S. A., BOON, N. A., PEPPER, J., MOHIADDIN, R. H., NEWBY, D. E., PENNELL, D. J. & PRASAD, S. K. 2012b. Left ventricular remodeling and hypertrophy in patients with aortic stenosis: insights from cardiovascular magnetic resonance. *J Cardiovasc Magn Reson*, 14, 50.
- ECHAN, L. A., TANG, H. Y., ALI-KHAN, N., LEE, K. & SPEICHER, D. W. 2005. Depletion of multiple high-abundance proteins improves protein profiling capacities of human serum and plasma. *Proteomics*, 5, 3292-303.
- ELHMIDI, Y., BLEIZIFFER, S., PIAZZA, N., RUGE, H., KRANE, M., DEUTSCH, M. A., HETTICH, I., VOSS, B., MAZZITELLI, D. & LANGE, R. 2013. The evolution and prognostic value of N-terminal brain natriuretic peptide in predicting 1-year mortality in patients following transcatheter aortic valve implantation. *J Invasive Cardiol*, 25, 38-44.
- ELMARIAH, S., FARRELL, L. A., DAHER, M., SHI, X., KEYES, M. J., CAIN, C. H., POMERANTSEV, E., VLAHAKES, G. J., INGLESSIS, I., PASSERI, J. J.,

- PALACIOS, I. F., FOX, C. S., RHEE, E. P. & GERSZTEN, R. E. 2016. Metabolite Profiles Predict Acute Kidney Injury and Mortality in Patients Undergoing Transcatheter Aortic Valve Replacement. *J Am Heart Assoc*, 5, e002712.
- EMMENS, J. E., JONES, D. J. L., CAO, T. H., CHAN, D. C. S., ROMAINE, S. P. R., QUINN, P. A., ANKER, S. D., CLELAND, J. G., DICKSTEIN, K., FILIPPATOS, G., HILLEGE, H. L., LANG, C. C., PONIKOWSKI, P., SAMANI, N. J., VAN VELDHUISEN, D. J., ZANNAD, F., ZWINDERMAN, A. H., METRA, M., DE BOER, R. A., VOORS, A. A. & NG, L. L. 2018. Proteomic diversity of high-density lipoprotein explains its association with clinical outcome in patients with heart failure. *Eur J Heart Fail*, 20, 260-267.
- EPISKOPOU, H., DRASKOVIC, I., VAN BENEDEN, A., TILMAN, G., MATTIUSSI, M., GOBIN, M., ARNOULT, N., LONDOÑO-VALLEJO, A. & DECOTTIGNIES, A. 2014. Alternative Lengthening of Telomeres is characterized by reduced compaction of telomeric chromatin. *Nucleic Acids Res*, 42, 4391-405.
- ERIKSSON, J., HARING, R., GRARUP, N., VANDENPUT, L., WALLASCHOFSKI, H., LORENTZEN, E., HANSEN, T., MELLSTRÖM, D., PEDERSEN, O., NAUCK, M., LORENTZON, M., NYSTRUP HUSEMOEN, L. L., VÖLZKE, H., KARLSSON, M., BAUMEISTER, S. E., LINNEBERG, A. & OHLSSON, C. 2017. Causal relationship between obesity and serum testosterone status in men: A bi-directional mendelian randomization analysis. *PLoS One*, 12, e0176277.
- EVERETT, R. J., TASTET, L., CLAVEL, M. A., CHIN, C. W. L., CAPOULADE, R., VASSILIOU, V. S., KWIECINSKI, J., GOMEZ, M., VAN BEEK, E. J. R., WHITE, A. C., PRASAD, S. K., LAROSE, E., TUCK, C., SEMPLE, S., NEWBY, D. E., PIBAROT, P. & DWECK, M. R. 2018. Progression of Hypertrophy and Myocardial Fibrosis in Aortic Stenosis: A Multicenter Cardiac Magnetic Resonance Study. *Circ Cardiovasc Imaging*, 11, e007451.
- FARRÉ, N., GÓMEZ, M., MOLINA, L., CLADELLAS, M., BLÉ, M., ROQUETA, C., ASCOETA, M. S., COMIN-COLET, J., VILA, J. & BRUGUERA, J. 2014. Prognostic value of NT-proBNP and an adapted monin score in patients with asymptomatic aortic stenosis. *Rev Esp Cardiol (Engl Ed)*, 67, 52-7.
- FAYAD, Z. A., MANI, V., WOODWARD, M., KALLEND, D., ABT, M., BURGESS, T., FUSTER, V., BALLANTYNE, C. M., STEIN, E. A., TARDIF, J. C., RUDD, J. H., FARKOUH, M. E., TAWAKOL, A. & DAL, P. I. 2011. Safety and efficacy of

- dalcetrapib on atherosclerotic disease using novel non-invasive multimodality imaging (dal-PLAQUE): a randomised clinical trial. *Lancet*, 378, 1547-59.
- FEGHHI, S., MUNDAY, A. D., TOOLEY, W. W., RAJSEKAR, S., FURA, A. M., KULMAN, J. D., LOPEZ, J. A. & SNIADOCKI, N. J. 2016. Glycoprotein Ib-IX-V Complex Transmits Cytoskeletal Forces That Enhance Platelet Adhesion. *Biophys J*, 111, 601-608.
- FERRER-SISTACH, E., LUPON, J., CEDIEL, G., TEIS, A., GUAL, F., SERRANO, S., VALLEJO, N., JUNCA, G., LOPEZ-AYERBE, J. & BAYES-GENIS, A. 2019. High-sensitivity troponin T in asymptomatic severe aortic stenosis. *Biomarkers*, 24, 334-340.
- FLAGG, T. P., KURATA, H. T., MASIA, R., CAPUTA, G., MAGNUSON, M. A., LEFER, D. J., COETZEE, W. A. & NICHOLS, C. G. 2008. Differential structure of atrial and ventricular KATP: atrial KATP channels require SUR1. *Circ Res*, 103, 1458-65.
- FONG, L. G., YOUNG, S. G., BEIGNEUX, A. P., BENSADOUN, A., OBERER, M., JIANG, H. & PLOUG, M. 2016. GPIHBP1 and Plasma Triglyceride Metabolism. *Trends Endocrinol Metab*, 27, 455-69.
- FORREST, S. J., GEOERGER, B. & JANEWAY, K. A. 2018. Precision medicine in pediatric oncology. *Curr Opin Pediatr*, 30, 17-24.
- FRANK, D., STARK, S., LUTZ, M., WEISSBRODT, A., FREITAG-WOLF, S., PETZINA, R., ROSENBERG, M., LUTTER, G. & FREY, N. 2013. Preprocedural high-sensitive troponin predicts survival after transcatheter aortic valve implantation (TAVI). *Int J Cardiol*, 169, e38-9.
- GALANTE, A., PIETROIUSTI, A., VELLINI, M., PICCOLO, P., POSSATI, G., DE BONIS, M., GRILLO, R. L., FONTANA, C. & FAVALLI, C. 2001. C-reactive protein is increased in patients with degenerative aortic valvular stenosis. *J Am Coll Cardiol*, 38, 1078-82.
- GALIUTO, L., LOTRIONTE, M., CREA, F., ANSELMi, A., BIONDI-ZOCCAI, G. G., DE GIORGIO, F., BALDI, A., BALDI, F., POSSATI, G., GAUDINO, M., VETROVEC, G. W. & ABBATE, A. 2006. Impaired coronary and myocardial flow in severe aortic stenosis is associated with increased apoptosis: a transthoracic Doppler and myocardial contrast echocardiography study. *Heart*, 92, 208-12.
- GANFORNINA, M. D., DO CARMO, S., LORA, J. M., TORRES-SCHUMANN, S., VOGEL, M., ALLHORN, M., GONZALEZ, C., BASTIANI, M. J., RASSART, E. &

- SANCHEZ, D. 2008. Apolipoprotein D is involved in the mechanisms regulating protection from oxidative stress. *Aging Cell*, 7, 506-15.
- GARCIA, R., VILLAR, A. V., COBO, M., LLANO, M., MARTIN-DURAN, R., HURLE, M. A. & NISTAL, J. F. 2013. Circulating levels of miR-133a predict the regression potential of left ventricular hypertrophy after valve replacement surgery in patients with aortic stenosis. *J Am Heart Assoc*, 2, e000211.
- GARG, V., MUTH, A. N., RANSOM, J. F., SCHLUTERMAN, M. K., BARNES, R., KING, I. N., GROSSFELD, P. D. & SRIVASTAVA, D. 2005. Mutations in NOTCH1 cause aortic valve disease. *Nature*, 437, 270-4.
- GETZ, E. B., XIAO, M., CHAKRABARTY, T., COOKE, R. & SELVIN, P. R. 1999. A comparison between the sulfhydryl reductants tris(2-carboxyethyl)phosphine and dithiothreitol for use in protein biochemistry. *Anal Biochem*, 273, 73-80.
- GEYER, P. E., HOLDT, L. M., TEUPSER, D. & MANN, M. 2017. Revisiting biomarker discovery by plasma proteomics. *Mol Syst Biol*, 13, 942.
- GEYER, P. E., KULAK, N. A., PICHLER, G., HOLDT, L. M., TEUPSER, D. & MANN, M. 2016. Plasma Proteome Profiling to Assess Human Health and Disease. *Cell Syst*, 2, 185-95.
- GHAISAS, N. K., FOLEY, J. B., O'BRIAIN, D. S., CREAN, P., KELLEHER, D. & WALSH, M. 2000. Adhesion molecules in nonrheumatic aortic valve disease: endothelial expression, serum levels and effects of valve replacement. *J Am Coll Cardiol*, 36, 2257-62.
- GOETZ, S. C., LIEM, K. F., JR. & ANDERSON, K. V. 2012. The spinocerebellar ataxia-associated gene Tau tubulin kinase 2 controls the initiation of ciliogenesis. *Cell*, 151, 847-58.
- GOH, S. S., SIA, C. H., NGIAM, N. J., TAN, B. Y., LEE, P. S., TAY, E. L., KONG, W. K., YEO, T. C. & POH, K. K. 2017. Effect of Renin-Angiotensin Blockers on Left Ventricular Remodeling in Severe Aortic Stenosis. *Am J Cardiol*, 119, 1839-1845.
- GONZALEZ, A., FORTUNO, M. A., QUEREJETA, R., RAVASSA, S., LOPEZ, B., LOPEZ, N. & DIEZ, J. 2003. Cardiomyocyte apoptosis in hypertensive cardiomyopathy. *Cardiovasc Res*, 59, 549-62.
- GONZALEZ, A., LOPEZ, B., RAVASSA, S., QUEREJETA, R., LARMAN, M., DIEZ, J. & FORTUNO, M. A. 2002. Stimulation of cardiac apoptosis in essential hypertension: potential role of angiotensin II. *Hypertension*, 39, 75-80.

- GOODMAN, A., KUSUNOSE, K., POPOVIC, Z. B., PARIKH, R., BARR, T., SABIK, J. F., RODRIGUEZ, L. L., SVENSSON, L. G., GRIFFIN, B. P. & DESAI, M. Y. 2016. Synergistic Utility of Brain Natriuretic Peptide and Left Ventricular Strain in Patients With Significant Aortic Stenosis. *J Am Heart Assoc*, 5.
- GOODNO, C. C., SWAISGOOD, H. E. & CATIGNANI, G. L. 1981. A Fluorimetric Assay for Available Lysine in Proteins. *Analytical Biochemistry*, 115, 203-211.
- GORDON, S. M., DENG, J., LU, L. J. & DAVIDSON, W. S. 2010. Proteomic characterization of human plasma high density lipoprotein fractionated by gel filtration chromatography. *J Proteome Res*, 9, 5239-49.
- GRIMBERT, P., BOUGUERMOUH, S., BABA, N., NAKAJIMA, T., ALLAKHVERDI, Z., BRAUN, D., SAITO, H., RUBIO, M., DELESPESE, G. & SARFATI, M. 2006. Thrombospondin/CD47 interaction: a pathway to generate regulatory T cells from human CD4<sup>+</sup> CD25<sup>-</sup> T cells in response to inflammation. *J Immunol*, 177, 3534-41.
- GROMLEY, A., JURCZYK, A., SILLIBOURNE, J., HALILOVIC, E., MOGENSEN, M., GROISMAN, I., BLOMBERG, M. & DOXSEY, S. 2003. A novel human protein of the maternal centriole is required for the final stages of cytokinesis and entry into S phase. *J Cell Biol*, 161, 535-45.
- GROSSMAN, W., JONES, D. & MCLAURIN, L. P. 1975. Wall stress and patterns of hypertrophy in the human left ventricle. *J Clin Invest*, 56, 56-64.
- GU, C. & GIRAUDO, E. 2013. The role of semaphorins and their receptors in vascular development and cancer. *Exp Cell Res*, 319, 1306-16.
- GU, C., YOSHIDA, Y., LIVET, J., REIMERT, D. V., MANN, F., MERTE, J., HENDERSON, C. E., JESSELL, T. M., KOLODKIN, A. L. & GINTY, D. D. 2005. Semaphorin 3E and plexin-D1 control vascular pattern independently of neuropilins. *Science*, 307, 265-8.
- GUNDRY, R. L., FU, Q., JELINEK, C. A., VAN EYK, J. E. & COTTER, R. J. 2007. Investigation of an albumin-enriched fraction of human serum and its albuminome. *Proteomics Clin Appl*, 1, 73-88.
- GUNTHER, S. & GROSSMAN, W. 1979. Determinants of ventricular function in pressure-overload hypertrophy in man. *Circulation*, 59, 679-88.
- GUPTA, N. & PEVZNER, P. A. 2009. False discovery rates of protein identifications: a strike against the two-peptide rule. *J Proteome Res*, 8, 4173-81.
- GYÖRGY, B., MÓDOS, K., PÁLLINGER, E., PÁLÓCZI, K., PÁSZTÓI, M., MISJÁK, P., DELI, M. A., SIPOS, A., SZALAI, A., VOSZKA, I., POLGÁR, A., TÓTH, K.,

- CSETE, M., NAGY, G., GAY, S., FALUS, A., KITTEL, A. & BUZÁS, E. I. 2011. Detection and isolation of cell-derived microparticles are compromised by protein complexes resulting from shared biophysical parameters. *Blood*, 117, e39-48.
- HACHICHA, Z., DUMESNIL, J. G. & PIBAROT, P. 2009. Usefulness of the valvuloarterial impedance to predict adverse outcome in asymptomatic aortic stenosis. *J Am Coll Cardiol*, 54, 1003-11.
- HAKIMI, A., AULUCK, J., JONES, G. D., NG, L. L. & JONES, D. J. 2014. Assessment of reproducibility in depletion and enrichment workflows for plasma proteomics using label-free quantitative data-independent LC-MS. *Proteomics*, 14, 4-13.
- HAN, J. C. & HAN, G. Y. 1994. A procedure for quantitative determination of tris(2-carboxyethyl)phosphine, an odorless reducing agent more stable and effective than dithiothreitol. *Anal Biochem*, 220, 5-10.
- HANNIGAN, G. E., LEUNG-HAGESTEIJN, C., FITZ-GIBBON, L., COPPOLINO, M. G., RADEVA, G., FILMUS, J., BELL, J. C. & DEDHAR, S. 1996. Regulation of cell adhesion and anchorage-dependent growth by a new beta 1-integrin-linked protein kinase. *Nature*, 379, 91-6.
- HANSCOMBE, K. B., TRAYLOR, M., HYSI, P. G., BEVAN, S., DICHGANS, M., ROTHWELL, P. M., WORRALL, B. B., SESHADRI, S., SUDLOW, C., CONSORTIUM, M., WELLCOME TRUST CASE CONTROL, C., WILLIAMS, F. M., MARKUS, H. S. & LEWIS, C. M. 2015. Genetic Factors Influencing Coagulation Factor XIII B-Subunit Contribute to Risk of Ischemic Stroke. *Stroke*, 46, 2069-74.
- HARRIS, J., SCHWINN, N., MAHONEY, J. A., LIN, H. H., SHAW, M., HOWARD, C. J., DA SILVA, R. P. & GORDON, S. 2006. A vitellogenic-like carboxypeptidase expressed by human macrophages is localized in endoplasmic reticulum and membrane ruffles. *Int J Exp Pathol*, 87, 29-39.
- HASUNUMA, Y., MATSUURA, E., MAKITA, Z., KATAHIRA, T., NISHI, S. & KOIKE, T. 1997. Involvement of beta 2-glycoprotein I and anticardiolipin antibodies in oxidatively modified low-density lipoprotein uptake by macrophages. *Clin Exp Immunol*, 107, 569-73.
- HAYETTE, S., CORNILLET-LEFEBVRE, P., TIGAUD, I., STRUSKI, S., FORISSIER, S., BERCHET, A., DOLL, D., GILLOT, L., BRAHIM, W., DELABESSE, E., MAGAUD, J. P. & RIMOKH, R. 2005. AF4p12, a human homologue to the furry gene of Drosophila, as a novel MLL fusion partner. *Cancer Res*, 65, 6521-5.

- HEATHER, L. C., HOWELL, N. J., EMMANUEL, Y., COLE, M. A., FRENNEAUX, M. P., PAGANO, D. & CLARKE, K. 2011. Changes in cardiac substrate transporters and metabolic proteins mirror the metabolic shift in patients with aortic stenosis. *PLoS One*, 6, e26326.
- HEIN, S., ARNON, E., KOSTIN, S., SCHONBURG, M., ELSASSER, A., POLYAKOVA, V., BAUER, E. P., KLOVEKORN, W. P. & SCHAPER, J. 2003. Progression from compensated hypertrophy to failure in the pressure-overloaded human heart: structural deterioration and compensatory mechanisms. *Circulation*, 107, 984-91.
- HEINK, A., DAVIDSON, W. S., SWERTFEGER, D. K., LU, L. J. & SHAH, A. S. 2015. A Comparison of Methods To Enhance Protein Detection of Lipoproteins by Mass Spectrometry. *J Proteome Res*, 14, 2943-50.
- HEJA, D., KOCSIS, A., DOBO, J., SZILAGYI, K., SZASZ, R., ZAVODSZKY, P., PAL, G. & GAL, P. 2012. Revised mechanism of complement lectin-pathway activation revealing the role of serine protease MASP-1 as the exclusive activator of MASP-2. *Proc Natl Acad Sci U S A*, 109, 10498-503.
- HENNIGE, A. M., STAIGER, H., WICKE, C., MACHICAO, F., FRITSCHKE, A., HARING, H. U. & STEFAN, N. 2008. Fetuin-A induces cytokine expression and suppresses adiponectin production. *PLoS One*, 3, e1765.
- HENRI, C., DULGHERU, R., MAGNE, J., CABALLERO, L., LAARAIBI, S., DAVIN, L., KOU, S., VOILLIOT, D., NCHIMI, A., OURY, C., PIERARD, L. A. & LANCELLOTTI, P. 2016. Impact of Serial B-Type Natriuretic Peptide Changes for Predicting Outcome in Asymptomatic Patients With Aortic Stenosis. *Can J Cardiol*, 32, 183-9.
- HENRI, C., MAGNE, J., DULGHERU, R., DAVIN, L., LAARAIBI, S., VOILLIOT, D., KOU, S., NCHIMI, A., OURY, C., PIERARD, L. A. & LANCELLOTTI, P. 2014. Usefulness of serial B-type natriuretic peptide assessment in asymptomatic aortic stenosis. *Am J Cardiol*, 114, 441-8.
- HESS, K., AJJAN, R., PHOENIX, F., DOBO, J., GAL, P. & SCHROEDER, V. 2012. Effects of MASP-1 of the complement system on activation of coagulation factors and plasma clot formation. *PLoS One*, 7, e35690.
- HESS, O. M., RITTER, M., SCHNEIDER, J., GRIMM, J., TURINA, M. & KRAYENBUEHL, H. P. 1984. Diastolic stiffness and myocardial structure in aortic valve disease before and after valve replacement. *Circulation*, 69, 855-65.

- HO, D. E., IMAI, K., KING, G. & STUART, E. A. 2011. MatchIt: Nonparametric Preprocessing for Parametric Causal Inference. *Journal of Statistical Software*, 42.
- HODGES, G. W., BANG, C. N., EUGEN-OLSEN, J., OLSEN, M. H., BOMAN, K., RAY, S., GOHLKE-BARWOLF, C., KESANIEMI, Y. A., JEPPESEN, J. L. & WACHTELL, K. 2016. SuPAR Predicts Cardiovascular Events and Mortality in Patients With Asymptomatic Aortic Stenosis. *Can J Cardiol*, 32, 1462-1469.
- HOGDALL, C. K., CHRISTENSEN, I. J., STEPHENS, R. W., SORENSEN, S., NORGAARD-PEDERSEN, B. & NIELSEN, H. J. 2002. Serum tetranectin is an independent prognostic marker in colorectal cancer and weakly correlated with plasma suPAR, plasma PAI-1 and serum CEA. *APMIS*, 110, 630-8.
- HOLLANDER, Z., LAZÁROVÁ, M., LAM, K. K., IGNASZEWSKI, A., OUDIT, G. Y., DYCK, J. R., SCHREINER, G., PAUWELS, J., CHEN, V., COHEN FREUE, G. V., NG, R. T., WILSON-MCMANUS, J. E., BALSHAW, R., TEBBUTT, S. J., MCMASTER, R. W., KEOWN, P. A., MCMANUS, B. M. & EXCELLENCE, N. C. P. P. O. O. F. P. C. O. 2014. Proteomic biomarkers of recovered heart function. *Eur J Heart Fail*, 16, 551-9.
- HOLMAN, S. W., SIMS, P. F. & EYERS, C. E. 2012. The use of selected reaction monitoring in quantitative proteomics. *Bioanalysis*, 4, 1763-86.
- HOOD, B. L., ZHOU, M., CHAN, K. C., LUCAS, D. A., KIM, G. J., ISSAQ, H. J., VEENSTRA, T. D. & CONRADS, T. P. 2005. Investigation of the mouse serum proteome. *J Proteome Res*, 4, 1561-8.
- HU, B., THIRTAMARA-RAJAMANI, K. K., SIM, H. & VIAPIANO, M. S. 2009. Fibulin-3 is uniquely upregulated in malignant gliomas and promotes tumor cell motility and invasion. *Mol Cancer Res*, 7, 1756-70.
- HYDE, S. J., ECKENROTH, B. E., SMITH, B. A., EBERLEY, W. A., HEINTZ, N. H., JACKMAN, J. E. & DOUBLIE, S. 2010. tRNA(His) guanylyltransferase (THG1), a unique 3'-5' nucleotidyl transferase, shares unexpected structural homology with canonical 5'-3' DNA polymerases. *Proc Natl Acad Sci U S A*, 107, 20305-10.
- HÖGLUND, K., BOGSTEDT, A., FABRE, S., AZIZ, A., ANNAS, P., BASUN, H., MINTHON, L., LANNFELT, L., BLENNOW, K. & ANDREASEN, N. 2012. Longitudinal stability evaluation of biomarkers and their correlation in cerebrospinal fluid and plasma from patients with Alzheimer's disease. *J Alzheimers Dis*, 32, 939-47.



- IBA, K., ABE, Y., CHIKENJI, T., KANAYA, K., CHIBA, H., SASAKI, K., DOHKE, T., WADA, T. & YAMASHITA, T. 2013. Delayed fracture healing in tetranectin-deficient mice. *J Bone Miner Metab*, 31, 399-408.
- IBA, K., HATAKEYAMA, N., KOJIMA, T., MURATA, M., MATSUMURA, T., WEWER, U. M., WADA, T., SAWADA, N. & YAMASHITA, T. 2009. Impaired cutaneous wound healing in mice lacking tetranectin. *Wound Repair Regen*, 17, 108-12.
- INANO, S., SATO, K., KATSUKI, Y., KOBAYASHI, W., TANAKA, H., NAKAJIMA, K., NAKADA, S., MIYOSHI, H., KNIES, K., TAKAORI-KONDO, A., SCHINDLER, D., ISHIAI, M., KURUMIZAKA, H. & TAKATA, M. 2017. RFWD3-Mediated Ubiquitination Promotes Timely Removal of Both RPA and RAD51 from DNA Damage Sites to Facilitate Homologous Recombination. *Mol Cell*, 66, 622-634 e8.
- INGOGLIA, G., SAG, C. M., REX, N., DE FRANCESCHI, L., VINCHI, F., CIMINO, J., PETRILLO, S., WAGNER, S., KREITMEIER, K., SILENGO, L., ALTRUDA, F., MAIER, L. S., HIRSCH, E., GHIGO, A. & TOLOSANO, E. 2017. Hemopexin counteracts systolic dysfunction induced by heme-driven oxidative stress. *Free Radic Biol Med*, 108, 452-464.
- IUNG, B., BARON, G., BUTCHART, E. G., DELAHAYE, F., GOHLKE-BARWOLF, C., LEVANG, O. W., TORNOS, P., VANOVERSCHELDE, J. L., VERMEER, F., BOERSMA, E., RAVAUD, P. & VAHANIAN, A. 2003. A prospective survey of patients with valvular heart disease in Europe: The Euro Heart Survey on Valvular Heart Disease. *Eur Heart J*, 24, 1231-43.
- IWAHASHI, N., NAKATANI, S., UMEMURA, S., KIMURA, K. & KITAKAZE, M. 2011. Usefulness of plasma B-type natriuretic peptide in the assessment of disease severity and prediction of outcome after aortic valve replacement in patients with severe aortic stenosis. *J Am Soc Echocardiogr*, 24, 984-91.
- JACOBS, J. M., MOTTAZ, H. M., YU, L. R., ANDERSON, D. J., MOORE, R. J., CHEN, W. N., AUBERRY, K. J., STRITTMATTER, E. F., MONROE, M. E., THRALL, B. D., CAMP, D. G. & SMITH, R. D. 2004. Multidimensional proteome analysis of human mammary epithelial cells. *J Proteome Res*, 3, 68-75.
- JERKOVIC, L., VOEGELE, A. F., CHWATAL, S., KRONENBERG, F., RADCLIFFE, C. M., WORMALD, M. R., LOBENTANZ, E. M., EZEH, B., ELLER, P., DEJORI, N., DIEPLINGER, B., LOTTSPEICH, F., SATTLER, W., UHR, M., MECHTLER, K., DWEK, R. A., RUDD, P. M., BAIER, G. & DIEPLINGER, H. 2005. Afamin is a

- novel human vitamin E-binding glycoprotein characterization and in vitro expression. *J Proteome Res*, 4, 889-99.
- JIAN, B., NARULA, N., LI, Q. Y., MOHLER, E. R., 3RD & LEVY, R. J. 2003. Progression of aortic valve stenosis: TGF-beta1 is present in calcified aortic valve cusps and promotes aortic valve interstitial cell calcification via apoptosis. *Ann Thorac Surg*, 75, 457-65; discussion 465-6.
- JIMÉNEZ, B., VOLPERT, O. V., CRAWFORD, S. E., FEBBRAIO, M., SILVERSTEIN, R. L. & BOUCK, N. 2000. Signals leading to apoptosis-dependent inhibition of neovascularization by thrombospondin-1. *Nat Med*, 6, 41-8.
- JOHANSSON, M., NOZOHOO, S., BJURSTEN, H., KIMBLAD, P. O. & SJOGREN, J. 2014. Acute kidney injury assessed by cystatin C after transcatheter aortic valve implantation and late renal dysfunction. *J Cardiothorac Vasc Anesth*, 28, 960-5.
- JONES, J. A., SPINALE, F. G. & IKONOMIDIS, J. S. 2009. Transforming growth factor-beta signaling in thoracic aortic aneurysm development: a paradox in pathogenesis. *J Vasc Res*, 46, 119-37.
- JONG, M. C., HOFKER, M. H. & HAVEKES, L. M. 1999. Role of ApoCs in lipoprotein metabolism: functional differences between ApoC1, ApoC2, and ApoC3. *Arterioscler Thromb Vasc Biol*, 19, 472-84.
- JUHASZOVA, M., ZOROV, D. B., YANIV, Y., NUSS, H. B., WANG, S. & SOLLOTT, S. J. 2009. Role of glycogen synthase kinase-3beta in cardioprotection. *Circ Res*, 104, 1240-52.
- JUN, H. O., KIM, D. H., LEE, S. W., LEE, H. S., SEO, J. H., KIM, J. H., YU, Y. S., MIN, B. H. & KIM, K. W. 2011. Clusterin protects H9c2 cardiomyocytes from oxidative stress-induced apoptosis via Akt/GSK-3 $\beta$  signaling pathway. *Exp Mol Med*, 43, 53-61.
- JUNG, C., LICHTENAUER, M., FIGULLA, H. R., WERNLY, B., GOEBEL, B., FOERSTER, M., EDLINGER, C. & LAUTEN, A. 2017. Microparticles in patients undergoing transcatheter aortic valve implantation (TAVI). *Heart Vessels*, 32, 458-466.
- KADEN, J. J., BICKELHAUPT, S., GROBHOLZ, R., HAASE, K. K., SARIKOC, A., KILIC, R., BRUECKMANN, M., LANG, S., ZAHN, I., VAHL, C., HAGL, S., DEMPFLER, C. E. & BORGGREFE, M. 2004a. Receptor activator of nuclear factor kappaB ligand and osteoprotegerin regulate aortic valve calcification. *J Mol Cell Cardiol*, 36, 57-66.

- KADEN, J. J., BICKELHAUPT, S., GROBHOLZ, R., VAHL, C. F., HAGL, S.,  
BRUECKMANN, M., HAASE, K. K., DEMPFLER, C. E. & BORGGREFE, M.  
2004b. Expression of bone sialoprotein and bone morphogenetic protein-2 in calcific  
aortic stenosis. *J Heart Valve Dis*, 13, 560-6.
- KADEN, J. J., DEMPFLER, C. E., GROBHOLZ, R., TRAN, H. T., KILIC, R., SARIKOC, A.,  
BRUECKMANN, M., VAHL, C., HAGL, S., HAASE, K. K. & BORGGREFE, M.  
2003. Interleukin-1 beta promotes matrix metalloproteinase expression and cell  
proliferation in calcific aortic valve stenosis. *Atherosclerosis*, 170, 205-11.
- KALL, L., CANTERBURY, J. D., WESTON, J., NOBLE, W. S. & MACCOSS, M. J. 2007.  
Semi-supervised learning for peptide identification from shotgun proteomics datasets.  
*Nat Methods*, 4, 923-5.
- KANEKO, H., HOELSCHERMANN, F., TAMBOR, G., OKAMOTO, M., NEUSS, M. &  
BUTTER, C. 2019. Impact of N-terminal pro-B-type natriuretic peptide response on  
long-term prognosis after transcatheter aortic valve implantation for severe aortic  
stenosis and heart failure. *Heart Vessels*, 34, 777-783.
- KAPELOUZOU, A., TSOURELIS, L., KAKLAMANIS, L., DEGIANNIS, D.,  
KOGERAKIS, N. & COKKINOS, D. V. 2015. Serum and tissue biomarkers in aortic  
stenosis. *Glob Cardiol Sci Pract*, 2015, 49.
- KAPUSTA, P., WYPASEK, E., NATORSKA, J., GRUDZIEN, G., SOBCZYK, D.,  
SADOWSKI, J. & UNDAS, A. 2012. Factor XIII expression within aortic valves and  
its plasma activity in patients with aortic stenosis: association with severity of disease.  
*Thromb Haemost*, 108, 1172-9.
- KARAMPELA, I., KANDRI, E., ANTONAKOS, G., VOGIATZAKIS, E.,  
CHRISTODOULATOS, G. S., NIKOLAIDOU, A., DIMOPOULOS, G.,  
ARMAGANIDIS, A. & DALAMAGA, M. 2017. Kinetics of circulating fetuin-A  
may predict mortality independently from adiponectin, high molecular weight  
adiponectin and prognostic factors in critically ill patients with sepsis: A prospective  
study. *J Crit Care*, 41, 78-85.
- KATZ, A. M. 2002. Ernest Henry Starling, his predecessors, and the "Law of the Heart".  
*Circulation*, 106, 2986-92.
- KATZ, M., TARASOUTCHI, F., PESARO, A. E., LOPES, R. D., SPINA, G. S., VIEIRA,  
M. L. & GRINBERG, M. 2012. Natriuretic peptides and long-term mortality in  
patients with severe aortic stenosis. *J Heart Valve Dis*, 21, 331-6.

- KEFER, J., BEAULOYE, C., ASTARCI, P., RENKIN, J., GLINEUR, D.,  
DEKLEERMAEKER, A. & VANOVERSCHELDE, J. L. 2010. Usefulness of B-type  
natriuretic peptide to predict outcome of patients treated by transcatheter aortic valve  
implantation. *Am J Cardiol*, 106, 1782-6.
- KELLER, A., NESVIZHSKII, A. I., KOLKER, E. & AEBERSOLD, R. 2002. Empirical  
statistical model to estimate the accuracy of peptide identifications made by MS/MS  
and database search. *Anal Chem*, 74, 5383-92.
- KELLERMAIR, J., OTT, H. W., BAUMGARTNER, H., KIBLBOECK, D.,  
BLESSBERGER, H., KAMMLER, J., REITER, C., LAMBERT, T., GRUND, M. &  
STEINWENDER, C. 2018. High-Molecular-Weight von Willebrand Factor Multimer  
Ratio: A Novel Biomarker for Low-Flow, Low-Gradient Aortic Stenosis  
Subclassification. *J Am Coll Cardiol*, 72, 1982-1984.
- KHAN, S. Q., QUINN, P., DAVIES, J. E. & NG, L. L. 2008. N-terminal pro-B-type  
natriuretic peptide is better than TIMI risk score at predicting death after acute  
myocardial infarction. *Heart*, 94, 40-3.
- KIDHER, E., HARLING, L., ASHRAFIAN, H., NAASE, H., CHUKWUEMEKA, A.,  
ANDERSON, J., FRANCIS, D. P. & ATHANASIOU, T. 2014. Pulse wave velocity  
and neutrophil gelatinase-associated lipocalin as predictors of acute kidney injury  
following aortic valve replacement. *J Cardiothorac Surg*, 9, 89.
- KIGEL, B., RABINOWICZ, N., VARSHAVSKY, A., KESSLER, O. & NEUFELD, G.  
2011. Plexin-A4 promotes tumor progression and tumor angiogenesis by  
enhancement of VEGF and bFGF signaling. *Blood*, 118, 4285-96.
- KIM, H. L., KIM, M. A., CHOI, D. J., HAN, S., JEON, E. S., CHO, M. C., KIM, J. J., YOO,  
B. S., SHIN, M. S., SEONG, I. W., AHN, Y., KANG, S. M., KIM, Y. J., KIM, H. S.,  
CHAE, S. C., OH, B. H., LEE, M. M., RYU, K. H. & REGISTRY, K. H. F. 2017.  
Gender Difference in the Prognostic Value of N-Terminal Pro-B Type Natriuretic  
Peptide in Patients With Heart Failure - A Report From the Korean Heart Failure  
Registry (KorHF). *Circ J*, 81, 1329-1336.
- KIM, J. S., FILLMORE, T. L., LIU, T., ROBINSON, E., HOSSAIN, M., CHAMPION, B.  
L., MOORE, R. J., CAMP, D. G., SMITH, R. D. & QIAN, W. J. 2011. 18O-labeled  
proteome reference as global internal standards for targeted quantification by selected  
reaction monitoring-mass spectrometry. *Mol Cell Proteomics*, 10, M110.007302.
- KIMURA, Y., IZUMIYA, Y., HANATANI, S., YAMAMOTO, E., KUSAKA, H.,  
TOKITSU, T., TAKASHIO, S., SAKAMOTO, K., TSUJITA, K., TANAKA, T.,

- YAMAMURO, M., KOJIMA, S., TAYAMA, S., KAIKITA, K., HOKIMOTO, S. & OGAWA, H. 2016. High serum levels of thrombospondin-2 correlate with poor prognosis of patients with heart failure with preserved ejection fraction. *Heart Vessels*, 31, 52-9.
- KIRK, J. A. & CINGOLANI, O. H. 2016. Thrombospondins in the transition from myocardial infarction to heart failure. *J Mol Cell Cardiol*, 90, 102-10.
- KNOLL, R., POSTEL, R., WANG, J., KRATZNER, R., HENNECKE, G., VACARU, A. M., VAKEEL, P., SCHUBERT, C., MURTHY, K., RANA, B. K., KUBE, D., KNOLL, G., SCHAFER, K., HAYASHI, T., HOLM, T., KIMURA, A., SCHORK, N., TOLIAT, M. R., NURNBERG, P., SCHULTHEISS, H. P., SCHAPER, W., SCHAPER, J., BOS, E., DEN HERTOOG, J., VAN EEDEN, F. J., PETERS, P. J., HASENFUSS, G., CHIEN, K. R. & BAKKERS, J. 2007. Laminin- $\alpha$ 4 and integrin-linked kinase mutations cause human cardiomyopathy via simultaneous defects in cardiomyocytes and endothelial cells. *Circulation*, 116, 515-25.
- KOCHL, S., FRESSER, F., LOBENTANZ, E., BAIER, G. & UTERMANN, G. 1997. Novel interaction of apolipoprotein(a) with beta-2 glycoprotein I mediated by the kringle IV domain. *Blood*, 90, 1482-9.
- KOHLER, A. C., SAG, C. M. & MAIER, L. S. 2014. Reactive oxygen species and excitation-contraction coupling in the context of cardiac pathology. *J Mol Cell Cardiol*, 73, 92-102.
- KOHLER, W. M., FREITAG-WOLF, S., LAMBERS, M., LUTZ, M., NIEMANN, P. M., PETZINA, R., LUTTER, G., BRAMLAGE, P., FREY, N. & FRANK, D. 2016. Preprocedural but not periprocedural high-sensitive Troponin T levels predict outcome in patients undergoing transcatheter aortic valve implantation. *Cardiovasc Ther*, 34, 385-396.
- KOLLIPARA, L. & ZAHEDI, R. P. 2013. Protein carbamylation: in vivo modification or in vitro artefact? *Proteomics*, 13, 941-4.
- KOLODKIN, A. L., MATTHES, D. J. & GOODMAN, C. S. 1993. The semaphorin genes encode a family of transmembrane and secreted growth cone guidance molecules. *Cell*, 75, 1389-99.
- KOLTAI, T. 2014. Clusterin: a key player in cancer chemoresistance and its inhibition. *Oncotargets Ther*, 7, 447-56.
- KOSKINAS, K. C., STORTECKY, S., FRANZONE, A., O'SULLIVAN, C. J., PRAZ, F., ZUK, K., RABER, L., PILGRIM, T., MOSCHOVITIS, A., FIEDLER, G. M., JUNI,

- P., HEG, D., WENAWESER, P. & WINDECKER, S. 2016. Post-Procedural Troponin Elevation and Clinical Outcomes Following Transcatheter Aortic Valve Implantation. *J Am Heart Assoc*, 5.
- KOWAL, J., ARRAS, G., COLOMBO, M., JOUVE, M., MORATH, J. P., PRIMDAL-BENGTSON, B., DINGLI, F., LOEW, D., TKACH, M. & THÉRY, C. 2016. Proteomic comparison defines novel markers to characterize heterogeneous populations of extracellular vesicle subtypes. *Proc Natl Acad Sci U S A*, 113, E968-77.
- KOZARCANIN, H., LOOD, C., MUNTHE-FOG, L., SANDHOLM, K., HAMAD, O. A., BENGTSSON, A. A., SKJOEDT, M. O., HUBER-LANG, M., GARRED, P., EKDAHL, K. N. & NILSSON, B. 2016. The lectin complement pathway serine proteases (MASPs) represent a possible crossroad between the coagulation and complement systems in thromboinflammation. *J Thromb Haemost*, 14, 531-45.
- KRAU, N. C., LUNSTEDT, N. S., FREITAG-WOLF, S., BREHM, D., PETZINA, R., LUTTER, G., BRAMLAGE, P., DEMPFLER, A., FREY, N. & FRANK, D. 2015. Elevated growth differentiation factor 15 levels predict outcome in patients undergoing transcatheter aortic valve implantation. *Eur J Heart Fail*, 17, 945-55.
- KRAYENBUEHL, H. P., HESS, O. M., MONRAD, E. S., SCHNEIDER, J., MALL, G. & TURINA, M. 1989. Left ventricular myocardial structure in aortic valve disease before, intermediate, and late after aortic valve replacement. *Circulation*, 79, 744-55.
- KRIJNEN, P. A., CILLESSEN, S. A., MANOE, R., MULLER, A., VISSER, C. A., MEIJER, C. J., MUSTERS, R. J., HACK, C. E., AARDEN, L. A. & NIESSEN, H. W. 2005. Clusterin: a protective mediator for ischemic cardiomyocytes? *Am J Physiol Heart Circ Physiol*, 289, H2193-202.
- KRISHNA, S. M. & GOLLEDGE, J. 2013. The role of thrombospondin-1 in cardiovascular health and pathology. *Int J Cardiol*, 168, 692-706.
- KRONENBERG, F., KOLLERITS, B., KIECHL, S., LAMINA, C., KEDENKO, L., MEISINGER, C., WILLEIT, J., HUTH, C., WIETZORREK, G., ALTMANN, M. E., THORAND, B., MELMER, A., DAHNHARDT, D., SANTER, P., RATHMANN, W., PAULWEBER, B., KOENIG, W., PETERS, A., ADHAM, I. M. & DIEPLINGER, H. 2014. Plasma concentrations of afamin are associated with the prevalence and development of metabolic syndrome. *Circ Cardiovasc Genet*, 7, 822-9.

- KUMANOGOH, A. & KIKUTANI, H. 2013. Immunological functions of the neuropilins and plexins as receptors for semaphorins. *Nat Rev Immunol*, 13, 802-14.
- KUMON, Y., LOOSE, L. D., BIRBARA, C. A. & SIPE, J. D. 1997. Rheumatoid arthritis exhibits reduced acute phase and enhanced constitutive serum amyloid A protein in synovial fluid relative to serum. A comparison with C-reactive protein. *J Rheumatol*, 24, 14-9.
- KUNDU, S., AULCHENKO, Y. S., VAN DUIJN, C. M. & JANSSENS, A. C. 2011. PredictABEL: an R package for the assessment of risk prediction models. *Eur J Epidemiol*, 26, 261-4.
- KUSEBAUCH, U., CAMPBELL, D. S., DEUTSCH, E. W., CHU, C. S., SPICER, D. A., BRUSNIAK, M. Y., SLAGEL, J., SUN, Z., STEVENS, J., GRIMES, B., SHTEYNBERG, D., HOOPMANN, M. R., BLATTMANN, P., RATUSHNY, A. V., RINNER, O., PICOTTI, P., CARAPITO, C., HUANG, C. Y., KAPOUSOUZ, M., LAM, H., TRAN, T., DEMIR, E., AITCHISON, J. D., SANDER, C., HOOD, L., AEBERSOLD, R. & MORITZ, R. L. 2016. Human SRMATlas: A Resource of Targeted Assays to Quantify the Complete Human Proteome. *Cell*, 166, 766-778.
- LAI, C. J., CHENG, H. C., LIN, C. Y., HUANG, S. H., CHEN, T. H., CHUNG, C. J., CHANG, C. H., WANG, H. D. & CHUU, C. P. 2017. Activation of liver X receptor suppresses angiogenesis. *FASEB J*, 31, 5568-5576.
- LAM, C. S., CHENG, S., CHOONG, K., LARSON, M. G., MURABITO, J. M., NEWTON-CHEH, C., BHASIN, S., MCCABE, E. L., MILLER, K. K., REDFIELD, M. M., VASAN, R. S., COVIELLO, A. D. & WANG, T. J. 2011. Influence of sex and hormone status on circulating natriuretic peptides. *J Am Coll Cardiol*, 58, 618-26.
- LAMY, L., FOUSSAT, A., BROWN, E. J., BORNSTEIN, P., TICCHIONI, M. & BERNARD, A. 2007. Interactions between CD47 and thrombospondin reduce inflammation. *J Immunol*, 178, 5930-9.
- LANCELLOTTI, P., MOONEN, M., MAGNE, J., O'CONNOR, K., COSYNS, B., ATTENA, E., DONAL, E. & PIERARD, L. 2010. Prognostic effect of long-axis left ventricular dysfunction and B-type natriuretic peptide levels in asymptomatic aortic stenosis. *Am J Cardiol*, 105, 383-8.
- LARSSON, M., ALLAN, C. M., JUNG, R. S., HEIZER, P. J., BEIGNEUX, A. P., YOUNG, S. G. & FONG, L. G. 2017. Apolipoprotein C-III inhibits triglyceride hydrolysis by GPIHBP1-bound LPL. *J Lipid Res*, 58, 1893-1902.

- LAVIE, C. J., MILANI, R. V., PATEL, D., ARTHAM, S. M. & VENTURA, H. O. 2009. Disparate effects of obesity and left ventricular geometry on mortality in 8088 elderly patients with preserved systolic function. *Postgrad Med*, 121, 119-25.
- LEGATE, K. R., MONTANEZ, E., KUDLACEK, O. & FASSLER, R. 2006. ILK, PINCH and parvin: the tIPP of integrin signalling. *Nat Rev Mol Cell Biol*, 7, 20-31.
- LERI, A., CLAUDIO, P. P., LI, Q., WANG, X., REISS, K., WANG, S., MALHOTRA, A., KAJSTURA, J. & ANVERSA, P. 1998. Stretch-mediated release of angiotensin II induces myocyte apoptosis by activating p53 that enhances the local renin-angiotensin system and decreases the Bcl-2-to-Bax protein ratio in the cell. *J Clin Invest*, 101, 1326-42.
- LEUNG, W. C., LAWRIE, A., DEMARIES, S., MASSAELI, H., BURRY, A., YABLONSKY, S., SARJEANT, J. M., FERA, E., RASSART, E., PICKERING, J. G. & RABINOVITCH, M. 2004. Apolipoprotein D and platelet-derived growth factor-BB synergism mediates vascular smooth muscle cell migration. *Circ Res*, 95, 179-86.
- LEVY, D., WILSON, P. W., ANDERSON, K. M. & CASTELLI, W. P. 1990. Stratifying the patient at risk from coronary disease: new insights from the Framingham Heart Study. *Am Heart J*, 119, 712-7; discussion 717.
- LI, G. Z., VISSERS, J. P., SILVA, J. C., GOLICK, D., GORENSTEIN, M. V. & GEROMANOS, S. J. 2009. Database searching and accounting of multiplexed precursor and product ion spectra from the data independent analysis of simple and complex peptide mixtures. *Proteomics*, 9, 1696-719.
- LI, J., YOUSEFI, K., DING, W., SINGH, J. & SHEHADEH, L. A. 2017. Osteopontin RNA aptamer can prevent and reverse pressure overload-induced heart failure. *Cardiovasc Res*, 113, 633-643.
- LIEBERMAN, J. 1976. Elastase, collagenase, emphysema, and alpha1-antitrypsin deficiency. *Chest*, 70, 62-7.
- LIEBLER, D. C. & ZIMMERMAN, L. J. 2013. Targeted quantitation of proteins by mass spectrometry. *Biochemistry*, 52, 3797-806.
- LIN, C. C., TSAI, P., SUN, H. Y., HSU, M. C., LEE, J. C., WU, I. C., TSAO, C. W., CHANG, T. T. & YOUNG, K. C. 2014. Apolipoprotein J, a glucose-upregulated molecular chaperone, stabilizes core and NS5A to promote infectious hepatitis C virus virion production. *J Hepatol*, 61, 984-93.
- LIN, Y. S., CHANG, T. H., SHI, C. S., WANG, Y. Z., HO, W. C., HUANG, H. D., CHANG, S. T., PAN, K. L. & CHEN, M. C. 2019. Liver X Receptor/Retinoid X Receptor



- Pathway Plays a Regulatory Role in Pacing-Induced Cardiomyopathy. *J Am Heart Assoc*, 8, e009146.
- LINDMAN, B. R., BREYLEY, J. G., SCHILLING, J. D., VATTEROTT, A. M., ZAJARIAS, A., MANIAR, H. S., DAMIANO, R. J., JR., MOON, M. R., LAWTON, J. S., GAGE, B. F., SINTEK, M. A., AQUINO, A., HOLLEY, C. L., PATEL, N. M., LAWLER, C., LASALA, J. M. & NOVAK, E. 2015. Prognostic utility of novel biomarkers of cardiovascular stress in patients with aortic stenosis undergoing valve replacement. *Heart*, 101, 1382-8.
- LINDQUIST, C., BJORNDAAL, B., ROSSMANN, C. R., TUSUBIRA, D., SVARDAL, A., ROSLAND, G. V., TRONSTAD, K. J., HALLSTROM, S. & BERGE, R. K. 2017. Increased hepatic mitochondrial FA oxidation reduces plasma and liver TG levels and is associated with regulation of UCPs and APOC-III in rats. *J Lipid Res*, 58, 1362-1373.
- LIU, A. C., JOAG, V. R. & GOTLIEB, A. I. 2007. The emerging role of valve interstitial cell phenotypes in regulating heart valve pathobiology. *Am J Pathol*, 171, 1407-18.
- LIU, Y., HAIR, G. A., BODEN, S. D., VIGGESWARAPU, M. & TITUS, L. 2002. Overexpressed LIM mineralization proteins do not require LIM domains to induce bone. *J Bone Miner Res*, 17, 406-14.
- LJUNGBERG, J., HOLMGREN, A., BERGDAHL, I. A., HULTDIN, J., NORBERG, M., NASLUND, U., JOHANSSON, B. & SODERBERG, S. 2017. Lipoprotein(a) and the Apolipoprotein B/A1 Ratio Independently Associate With Surgery for Aortic Stenosis Only in Patients With Concomitant Coronary Artery Disease. *J Am Heart Assoc*, 6.
- LOGDBERG, L. & AKERSTROM, B. 1981. Immunosuppressive properties of alpha 1-microglobulin. *Scand J Immunol*, 13, 383-90.
- LOPEZ-OTERO, D., TRILLO-NOUCHE, R., GUDE, F., CID-ALVAREZ, B., OCARANZA-SANCHEZ, R., ALVAREZ, M. S., LEAR, P. V. & GONZALEZ-JUANATEY, J. R. 2013. Pro B-type natriuretic peptide plasma value: a new criterion for the prediction of short- and long-term outcomes after transcatheter aortic valve implantation. *Int J Cardiol*, 168, 1264-8.
- LOVEJOY, C. A., LI, W., REISENWEBER, S., THONGTHIP, S., BRUNO, J., DE LANGE, T., DE, S., PETRINI, J. H., SUNG, P. A., JASIN, M., ROSENBLUH, J., ZWANG, Y., WEIR, B. A., HATTON, C., IVANOVA, E., MACCONAILL, L., HANNA, M., HAHN, W. C., LUE, N. F., REDDEL, R. R., JIAO, Y., KINZLER, K., VOGELSTEIN, B., PAPADOPOULOS, N., MEEKER, A. K. & CONSORTIUM, A.

- S. C. 2012. Loss of ATRX, genome instability, and an altered DNA damage response are hallmarks of the alternative lengthening of telomeres pathway. *PLoS Genet*, 8, e1002772.
- LU, H., FEDAK, P. W., DAI, X., DU, C., ZHOU, Y. Q., HENKELMAN, M., MONGROO, P. S., LAU, A., YAMABI, H., HINEK, A., HUSAIN, M., HANNIGAN, G. & COLES, J. G. 2006. Integrin-linked kinase expression is elevated in human cardiac hypertrophy and induces hypertrophy in transgenic mice. *Circulation*, 114, 2271-9.
- LU, S., CRAWFORD, G. L., DORE, J., ANDERSON, S. A., DESPRES, D. & HOROWITS, R. 2011. Cardiac-specific NRAP overexpression causes right ventricular dysfunction in mice. *Exp Cell Res*, 317, 1226-37.
- LUND, O., NIELSEN, T. T., EMMERTSEN, K., FLO, C., RASMUSSEN, B., JENSEN, F. T., PILEGAARD, H. K., KRISTENSEN, L. H. & HANSEN, O. K. 1996. Mortality and worsening of prognostic profile during waiting time for valve replacement in aortic stenosis. *Thorac Cardiovasc Surg*, 44, 289-95.
- MA, Y., KONG, L., NAN, K., QI, S., RU, L., DING, C. & WANG, D. 2015. Apolipoprotein-J prevents angiotensin II-induced apoptosis in neonatal rat ventricular cells. *Lipids Health Dis*, 14, 114.
- MAKAROV, A. 2000. Electrostatic axially harmonic orbital trapping: a high-performance technique of mass analysis. *Anal Chem*, 72, 1156-62.
- MALEN, H., SOFTELAND, T. & WIKER, H. G. 2008. Antigen analysis of Mycobacterium tuberculosis H37Rv culture filtrate proteins. *Scand J Immunol*, 67, 245-52.
- MANI, D. R., ABBATIELLO, S. E. & CARR, S. A. 2012. Statistical characterization of multiple-reaction monitoring mass spectrometry (MRM-MS) assays for quantitative proteomics. *BMC Bioinformatics*, 13 Suppl 16, S9.
- MANNACIO, V., ANTIGNANO, A., DE AMICIS, V., DI TOMMASO, L., GIORDANO, R., IANNELLI, G. & VOSA, C. 2013. B-type natriuretic peptide as a biochemical marker of left ventricular diastolic function: assessment in asymptomatic patients 1 year after valve replacement for aortic stenosis. *Interact Cardiovasc Thorac Surg*, 17, 371-7.
- MANNING, W. J. 2013. Asymptomatic aortic stenosis in the elderly: a clinical review. *JAMA*, 310, 1490-7.
- MAO, H., FERGUSON, T. S., CIBULSKY, S. M., HOLMQVIST, M., DING, C., FEI, H. & LEVITAN, I. B. 2005. MONaKA, a novel modulator of the plasma membrane Na,K-ATPase. *J Neurosci*, 25, 7934-43.

- MARECHAUX, S., HACHICHA, Z., BELLOUIN, A., DUMESNIL, J. G., MEIMOUN, P., PASQUET, A., BERGERON, S., ARSENAULT, M., LE TOURNEAU, T., ENNEZAT, P. V. & PIBAROT, P. 2010. Usefulness of exercise-stress echocardiography for risk stratification of true asymptomatic patients with aortic valve stenosis. *Eur Heart J*, 31, 1390-7.
- MARTIN-ROJAS, T., GIL-DONES, F., LOPEZ-ALMODOVAR, L. F., PADIAL, L. R., VIVANCO, F. & BARDERAS, M. G. 2012. Proteomic profile of human aortic stenosis: insights into the degenerative process. *J Proteome Res*, 11, 1537-50.
- MARTOS, R., BAUGH, J., LEDWIDGE, M., O'LOUGHLIN, C., CONLON, C., PATLE, A., DONNELLY, S. C. & MCDONALD, K. 2007. Diastolic heart failure: evidence of increased myocardial collagen turnover linked to diastolic dysfunction. *Circulation*, 115, 888-95.
- MARTOSELLA, J., ZOLOTARJOVA, N., LIU, H., NICOL, G. & BOYES, B. E. 2005. Reversed-phase high-performance liquid chromatographic prefractionation of immunodepleted human serum proteins to enhance mass spectrometry identification of lower-abundant proteins. *J Proteome Res*, 4, 1522-37.
- MARY, A., ACHYUTHAN, K. E. & GREENBERG, C. S. 1988. b-chains prevent the proteolytic inactivation of the a-chains of plasma factor XIII. *Biochim Biophys Acta*, 966, 328-35.
- MELLER, N., IRANI-TEHRANI, M., KIOSSES, W. B., DEL POZO, M. A. & SCHWARTZ, M. A. 2002. Zizimin1, a novel Cdc42 activator, reveals a new GEF domain for Rho proteins. *Nat Cell Biol*, 4, 639-47.
- MELMER, A., FINEDER, L., LAMINA, C., KOLLERITS, B., DIEPLINGER, B., BRAICU, I., SEHOULI, J., CADRON, I., VERGOTE, I., MAHNER, S., ZEIMET, A. G., CASTILLO-TONG, D. C., EBENBICHLER, C. F., ZEILLINGER, R. & DIEPLINGER, H. 2013. Plasma concentrations of the vitamin E-binding protein afamin are associated with overall and progression-free survival and platinum sensitivity in serous ovarian cancer--a study by the OVCAD consortium. *Gynecol Oncol*, 128, 38-43.
- MEZEI, Z. A., BERECHKY, Z., KATONA, E., GINDELE, R., BALOGH, E., FIATAL, S., BALOGH, L., CZURIGA, I., ADANY, R., EDES, I. & MUSZBEK, L. 2015. Factor XIII B subunit polymorphisms and the risk of coronary artery disease. *Int J Mol Sci*, 16, 1143-59.

- MICHALSKI, A., COX, J. & MANN, M. 2011. More than 100,000 detectable peptide species elute in single shotgun proteomics runs but the majority is inaccessible to data-dependent LC-MS/MS. *J Proteome Res*, 10, 1785-93.
- MIZUTANI, K., HARA, M., IWATA, S., MURAKAMI, T., SHIBATA, T., YOSHIYAMA, M., NAGANUMA, T., YAMANAKA, F., HIGASHIMORI, A., TADA, N., TAKAGI, K., ARAKI, M., UENO, H., TABATA, M., SHIRAI, S., WATANABE, Y., YAMAMOTO, M. & HAYASHIDA, K. 2017. Elevation of B-Type Natriuretic Peptide at Discharge is Associated With 2-Year Mortality After Transcatheter Aortic Valve Replacement in Patients With Severe Aortic Stenosis: Insights From a Multicenter Prospective OCEAN-TAVI (Optimized Transcatheter Valvular Intervention-Transcatheter Aortic Valve Implantation) Registry. *J Am Heart Assoc*, 6.
- MIZUTANI, K., HARA, M., NAKAO, M., OKAI, T., KAJIO, K., MURAKAMI, T., SHIBATA, T., YOSHIYAMA, M., NAGANUMA, T., YAMANAKA, F., HIGASHIMORI, A., TADA, N., TAKAGI, K., ARAKI, M., UENO, H., TABATA, M., SHIRAI, S., WATANABE, Y., YAMAMOTO, M. & HAYASHIDA, K. 2018. Is elevation of N-terminal pro-B-type natriuretic peptide at discharge associated with 2-year composite endpoint of all-cause mortality and heart failure hospitalisation after transcatheter aortic valve implantation? Insights from a multicentre prospective OCEAN-TAVI registry in Japan. *BMJ Open*, 8, e021468.
- MOHAMED, B. A., ASIF, A. R., SCHNELLE, M., QASIM, M., KHADJEH, S., LBIK, D., SCHOTT, P., HASENFUSS, G. & TOISCHER, K. 2016. Proteomic analysis of short-term preload-induced eccentric cardiac hypertrophy. *J Transl Med*, 14, 149.
- MOHLER, E. R., 3RD, GANNON, F., REYNOLDS, C., ZIMMERMAN, R., KEANE, M. G. & KAPLAN, F. S. 2001. Bone formation and inflammation in cardiac valves. *Circulation*, 103, 1522-8.
- MOTEGI, K., HARADA, K., OHE, G., JONES, S. J., ELLIS, I. R., CROUCH, D. H., SCHOR, S. L. & SCHOR, A. M. 2008. Differential involvement of TGF-beta1 in mediating the motogenic effects of TSP-1 on endothelial cells, fibroblasts and oral tumour cells. *Exp Cell Res*, 314, 2323-33.
- MOURA, R., TJWA, M., VANDERVOORT, P., CLUDTS, K. & HOYLAERTS, M. F. 2007. Thrombospondin-1 activates medial smooth muscle cells and triggers neointima formation upon mouse carotid artery ligation. *Arterioscler Thromb Vasc Biol*, 27, 2163-9.

- MROZINSKI, P., ZOLOTARJOVA, N. & CHEN, H. 2008. Human Serum and Plasma Protein Depletion—Novel High-Capacity Affinity Column for the Removal of the “Top 14” Abundant Proteins Application. *Agilent Technologies*.
- MUFFAT, J. & WALKER, D. W. 2010. Apolipoprotein D: an overview of its role in aging and age-related diseases. *Cell Cycle*, 9, 269-73.
- MUFFAT, J., WALKER, D. W. & BENZER, S. 2008. Human ApoD, an apolipoprotein up-regulated in neurodegenerative diseases, extends lifespan and increases stress resistance in *Drosophila*. *Proc Natl Acad Sci U S A*, 105, 7088-93.
- MURPHY, C. L., WANG, S., KESTLER, D. P., STEVENS, F. A., WEISS, D. T. & SOLOMON, A. 2009. AA amyloidosis associated with a mutated serum amyloid A4 protein. *Amyloid*, 16, 84-8.
- NAKAYA, Y., SCHAEFER, E. J. & BREWER, H. B., JR. 1980. Activation of human post heparin lipoprotein lipase by apolipoprotein H (beta 2-glycoprotein I). *Biochem Biophys Res Commun*, 95, 1168-72.
- NATORSKA, J. & UNDAS, A. 2015. Blood coagulation and fibrinolysis in aortic valve stenosis: links with inflammation and calcification. *Thromb Haemost*, 114, 217-27.
- NAZARIAN, S. 2011. Is ventricular arrhythmia a possible mediator of the association between aortic stenosis-related midwall fibrosis and mortality? *J Am Coll Cardiol*, 58, 1280-2.
- NEGLIA, D., DE CATERINA, A., MARRACCINI, P., NATALI, A., CIARDETTI, M., VECOLI, C., GASTALDELLI, A., CIOCIARO, D., PELLEGRINI, P., TESTA, R., MENICHETTI, L., L'ABBATE, A., STANLEY, W. C. & RECCHIA, F. A. 2007. Impaired myocardial metabolic reserve and substrate selection flexibility during stress in patients with idiopathic dilated cardiomyopathy. *Am J Physiol Heart Circ Physiol*, 293, H3270-8.
- NESVIZHSKII, A. I. & AEBERSOLD, R. 2005. Interpretation of shotgun proteomic data: the protein inference problem. *Mol Cell Proteomics*, 4, 1419-40.
- NESVIZHSKII, A. I., KELLER, A., KOLKER, E. & AEBERSOLD, R. 2003. A statistical model for identifying proteins by tandem mass spectrometry. *Anal Chem*, 75, 4646-58.
- NGUYEN, V., CIMADEVILLA, C., ARANGALAGE, D., DEHOUX, M., CODOGNO, I., DUVAL, X., TUBIANA, S., VAHANIAN, A. & MESSIKA-ZEITOUN, D. 2017. Determinants and prognostic value of B-type natriuretic peptide in patients with aortic valve stenosis. *Int J Cardiol*, 230, 371-377.

- NICHOLS, C. G. 2006. KATP channels as molecular sensors of cellular metabolism. *Nature*, 440, 470-6.
- NICHOLSON, K. M. & ANDERSON, N. G. 2002. The protein kinase B/Akt signalling pathway in human malignancy. *Cell Signal*, 14, 381-95.
- NISHIMURA, R. A., OTTO, C. M., BONOW, R. O., CARABELLO, B. A., ERWIN, J. P., GUYTON, R. A., O'GARA, P. T., RUIZ, C. E., SKUBAS, N. J. & SORAJJA, P. 2014. 2014 AHA/ACC guideline for the management of patients with valvular heart disease: executive summary: a report of the American College of Cardiology/American Heart Association Task Force on Practice Guidelines. *Journal of the American College of Cardiology*, 63, 2438-2488.
- NKOMO, V. T., GARDIN, J. M., SKELTON, T. N., GOTTDIENER, J. S., SCOTT, C. G. & ENRIQUEZ-SARANO, M. 2006. Burden of valvular heart diseases: a population-based study. *Lancet*, 368, 1005-11.
- O'BRIEN, K. D., KUUSISTO, J., REICHENBACH, D. D., FERGUSON, M., GIACHELLI, C., ALPERS, C. E. & OTTO, C. M. 1995. Osteopontin is expressed in human aortic valvular lesions. *Circulation*, 92, 2163-8.
- O'BRIEN, K. D., REICHENBACH, D. D., MARCOVINA, S. M., KUUSISTO, J., ALPERS, C. E. & OTTO, C. M. 1996. Apolipoproteins B, (a), and E accumulate in the morphologically early lesion of 'degenerative' valvular aortic stenosis. *Arterioscler Thromb Vasc Biol*, 16, 523-32.
- O'BRIEN, K. D., SHAVELLE, D. M., CAULFIELD, M. T., MCDONALD, T. O., OLIN-LEWIS, K., OTTO, C. M. & PROBSTFIELD, J. L. 2002. Association of angiotensin-converting enzyme with low-density lipoprotein in aortic valvular lesions and in human plasma. *Circulation*, 106, 2224-30.
- OINUMA, I., ISHIKAWA, Y., KATOH, H. & NEGISHI, M. 2004. The Semaphorin 4D receptor Plexin-B1 is a GTPase activating protein for R-Ras. *Science*, 305, 862-5.
- OKA, T., AKAZAWA, H., NAITO, A. T. & KOMURO, I. 2014. Angiogenesis and cardiac hypertrophy: maintenance of cardiac function and causative roles in heart failure. *Circ Res*, 114, 565-71.
- OLSSON, M., THYBERG, J. & NILSSON, J. 1999. Presence of oxidized low density lipoprotein in nonrheumatic stenotic aortic valves. *Arterioscler Thromb Vasc Biol*, 19, 1218-22.
- ORLOWSKA-BARANOWSKA, E., PLACHA, G., GACIONG, Z., BARANOWSKI, R., ZAKRZEWSKI, D., MICHALEK, P., HOFFMAN, P. & RAWCZYNSKA-

- ENGLERT, I. 2004. Influence of ACE I/D genotypes on left ventricular hypertrophy in aortic stenosis: gender-related differences. *J Heart Valve Dis*, 13, 574-81.
- ORSINI, F., CHRYSANTHOU, E., DUDLER, T., CUMMINGS, W. J., TAKAHASHI, M., FUJITA, T., DEMOPULOS, G., DE SIMONI, M. G. & SCHWAEBLE, W. 2016. Mannan binding lectin-associated serine protease-2 (MASP-2) critically contributes to post-ischemic brain injury independent of MASP-1. *J Neuroinflammation*, 13, 213.
- ORTLEPP, J. R., HOFFMANN, R., OHME, F., LAUSCHER, J., BLECKMANN, F. & HANRATH, P. 2001. The vitamin D receptor genotype predisposes to the development of calcific aortic valve stenosis. *Heart*, 85, 635-8.
- OTSUKA, Y., NAKATANI, S., FUKUCHI, K., YASUMURA, Y., KOMAMURA, K., YAMAGISHI, M., SHIMOTSU, Y., MIYATAKE, K. & ISHIDA, Y. 2002. Clinical significance of iodine-123-15-(p-iodophenyl)-3-R, S-methylpentadecanoic acid myocardial scintigraphy in patients with aortic valve disease. *Circ J*, 66, 41-6.
- ØSTERGAARD, O., NIELSEN, C. T., IVERSEN, L. V., JACOBSEN, S., TANASSI, J. T. & HEEGAARD, N. H. 2012. Quantitative proteome profiling of normal human circulating microparticles. *J Proteome Res*, 11, 2154-63.
- OTTO, C. M. 2006. Valvular aortic stenosis: disease severity and timing of intervention. *J Am Coll Cardiol*, 47, 2141-51.
- OTTO, C. M. 2018. Aortic stenosis: treat the patient not the numbers. *Heart*, 104, 190-191.
- OTTO, C. M., BURWASH, I. G., LEGGET, M. E., MUNT, B. I., FUJIOKA, M., HEALY, N. L., KRAFT, C. D., MIYAKE-HULL, C. Y. & SCHWAEGLER, R. G. 1997. Prospective study of asymptomatic valvular aortic stenosis. Clinical, echocardiographic, and exercise predictors of outcome. *Circulation*, 95, 2262-70.
- OTTO, C. M., KUUSISTO, J., REICHENBACH, D. D., GOWN, A. M. & O'BRIEN, K. D. 1994. Characterization of the early lesion of 'degenerative' valvular aortic stenosis. Histological and immunohistochemical studies. *Circulation*, 90, 844-53.
- PACHULSKI, R. T. & CHAN, K. L. 1993. Progression of aortic valve dysfunction in 51 adult patients with congenital bicuspid aortic valve: assessment and follow up by Doppler echocardiography. *Br Heart J*, 69, 237-40.
- PAJANIAPPAN, M., GLOBER, N. K., KENNARD, S., LIU, H., ZHAO, N. & LILLY, B. 2011. Endothelial cells downregulate apolipoprotein D expression in mural cells through paracrine secretion and Notch signaling. *Am J Physiol Heart Circ Physiol*, 301, H784-93.

- PARENICA, J., NEMEC, P., TOMANDL, J., ONDRASEK, J., PAVKOVA-GOLDBERGOVA, M., TRETINA, M., JARKOVSKY, J., LITTNEROVA, S., POLOCZEK, M., POKORNY, P., SPINAR, J., CERMAKOVA, Z., MIKLIK, R., MALIK, P., PES, O., LIPKOVA, J., TOMANDLOVA, M. & KALA, P. 2012. Prognostic utility of biomarkers in predicting of one-year outcomes in patients with aortic stenosis treated with transcatheter or surgical aortic valve implantation. *PLoS One*, 7, e48851.
- PARHAMI, F., MORROW, A. D., BALUCAN, J., LEITINGER, N., WATSON, A. D., TINTUT, Y., BERLINER, J. A. & DEMER, L. L. 1997. Lipid oxidation products have opposite effects on calcifying vascular cell and bone cell differentiation. A possible explanation for the paradox of arterial calcification in osteoporotic patients. *Arterioscler Thromb Vasc Biol*, 17, 680-7.
- PARK, H. J., ZHANG, Y., GEORGESCU, S. P., JOHNSON, K. L., KONG, D. & GALPER, J. B. 2006. Human umbilical vein endothelial cells and human dermal microvascular endothelial cells offer new insights into the relationship between lipid metabolism and angiogenesis. *Stem Cell Rev*, 2, 93-102.
- PARKINSON, D. R. & MIER, J. W. 1983. T-lymphocyte malignancies: recent advances in the understanding of their biology, diagnosis and treatment. *Clin Immunol Rev*, 2, 59-121.
- PASCUA-MAESTRO, R., DIEZ-HERMANO, S., LILLO, C., GANFORNINA, M. D. & SANCHEZ, D. 2017. Protecting cells by protecting their vulnerable lysosomes: Identification of a new mechanism for preserving lysosomal functional integrity upon oxidative stress. *PLoS Genet*, 13, e1006603.
- PATWARDHAN, A. J., STRITTMATTER, E. F., CAMP, D. G., SMITH, R. D. & PALLAVICINI, M. G. 2006. Quantitative proteome analysis of breast cancer cell lines using 18O-labeling and an accurate mass and time tag strategy. *Proteomics*, 6, 2903-15.
- PAUL, S., JAKHAR, R., BHARDWAJ, M. & KANG, S. C. 2015. Glutathione-S-transferase omega 1 (GSTO1-1) acts as mediator of signaling pathways involved in aflatoxin B1-induced apoptosis-autophagy crosstalk in macrophages. *Free Radic Biol Med*, 89, 1218-30.
- PAWADE, T., CLAVEL, M. A., TRIBOUILLOY, C., DREYFUS, J., MATHIEU, T., TASTET, L., RENARD, C., GUN, M., JENKINS, W. S. A., MACRON, L., SECHRIST, J. W., LACOMIS, J. M., NGUYEN, V., GALIAN GAY, L., CUÉLLAR



- CALABRIA, H., NTALAS, I., CARTLIDGE, T. R. G., PRENDERGAST, B., RAJANI, R., EVANGELISTA, A., CAVALCANTE, J. L., NEWBY, D. E., PIBAROT, P., MESSIKA ZEITOUN, D. & DWECK, M. R. 2018. Computed Tomography Aortic Valve Calcium Scoring in Patients With Aortic Stenosis. *Circ Cardiovasc Imaging*, 11, e007146.
- PECK, J. W., OBERST, M., BOUKER, K. B., BOWDEN, E. & BURBELO, P. D. 2002. The RhoA-binding protein, rhophilin-2, regulates actin cytoskeleton organization. *J Biol Chem*, 277, 43924-32.
- PELLIKKA, P. A., SARANO, M. E., NISHIMURA, R. A., MALOUF, J. F., BAILEY, K. R., SCOTT, C. G., BARNES, M. E. & TAJIK, A. J. 2005. Outcome of 622 adults with asymptomatic, hemodynamically significant aortic stenosis during prolonged follow-up. *Circulation*, 111, 3290-5.
- PENCINA, M. J., D'AGOSTINO, R. B., SR., D'AGOSTINO, R. B., JR. & VASAN, R. S. 2008. Evaluating the added predictive ability of a new marker: from area under the ROC curve to reclassification and beyond. *Stat Med*, 27, 157-72; discussion 207-12.
- PENCINA, M. J., D'AGOSTINO, R. B. & STEYERBERG, E. W. 2011. Extensions of net reclassification improvement calculations to measure usefulness of new biomarkers. *Stat Med*, 30, 11-21.
- PERDOMO, G., KIM, D. H., ZHANG, T., QU, S., THOMAS, E. A., TOLEDO, F. G., SLUSHER, S., FAN, Y., KELLEY, D. E. & DONG, H. H. 2010. A role of apolipoprotein D in triglyceride metabolism. *J Lipid Res*, 51, 1298-311.
- PEREZ-MORGA, D., VANHOLLEBEKE, B., PATURIAUX-HANOCQ, F., NOLAN, D. P., LINS, L., HOMBLE, F., VANHAMME, L., TEBABI, P., PAYS, A., POELVOORDE, P., JACQUET, A., BRASSEUR, R. & PAYS, E. 2005. Apolipoprotein L-I promotes trypanosome lysis by forming pores in lysosomal membranes. *Science*, 309, 469-72.
- PERNEMALM, M. & LEHTIÖ, J. 2014. Mass spectrometry-based plasma proteomics: state of the art and future outlook. *Expert Rev Proteomics*, 11, 431-48.
- PETRITIS, B. O., QIAN, W. J., CAMP, D. G. & SMITH, R. D. 2009. A simple procedure for effective quenching of trypsin activity and prevention of 18O-labeling back-exchange. *J Proteome Res*, 8, 2157-63.
- PIEPER, R., SU, Q., GATLIN, C. L., HUANG, S. T., ANDERSON, N. L. & STEINER, S. 2003. Multi-component immunoaffinity subtraction chromatography: an innovative

- step towards a comprehensive survey of the human plasma proteome. *Proteomics*, 3, 422-32.
- PIÉRARD, S., DE MEESTER, C., SELDRUM, S., PASQUET, A., GERBER, B., VANCRAEYNES, D., ROBERT, A., EL KHOURY, G., NOIRHOMME, P. & VANOVERSCHELDE, J. L. 2014. Impact of preoperative symptoms on postoperative survival in severe aortic stenosis: implications for the timing of surgery. *Ann Thorac Surg*, 97, 803-9.
- POSEY, A. D., PYTEL, P., GARDIKIOTES, K., DEMONBREUN, A. R., RAINEY, M., GEORGE, M., BAND, H. & MCNALLY, E. M. 2011. Endocytic recycling proteins EHD1 and EHD2 interact with fer-1-like-5 (Fer1L5) and mediate myoblast fusion. *J Biol Chem*, 286, 7379-88.
- PROC, J. L., KUZYK, M. A., HARDIE, D. B., YANG, J., SMITH, D. S., JACKSON, A. M., PARKER, C. E. & BORCHERS, C. H. 2010. A quantitative study of the effects of chaotropic agents, surfactants, and solvents on the digestion efficiency of human plasma proteins by trypsin. *J Proteome Res*, 9, 5422-37.
- QIAN, W. J., KALETA, D. T., PETRITIS, B. O., JIANG, H., LIU, T., ZHANG, X., MOTTAZ, H. M., VARNUM, S. M., CAMP, D. G., HUANG, L., FANG, X., ZHANG, W. W. & SMITH, R. D. 2008. Enhanced detection of low abundance human plasma proteins using a tandem IgY12-SuperMix immunoaffinity separation strategy. *Mol Cell Proteomics*, 7, 1963-73.
- RACKIEWICZ, M., GROßE-HOVEST, L., ALPERT, A. J., ZAREI, M. & DENGJEL, J. 2017. Hydrophobic Interaction Chromatography for Bottom-Up Proteomics Analysis of Single Proteins and Protein Complexes. *J Proteome Res*, 16, 2318-2323.
- RAJAMANNAN, N. M., SUBRAMANIAM, M., RICKARD, D., STOCK, S. R., DONOVAN, J., SPRINGETT, M., ORSZULAK, T., FULLERTON, D. A., TAJIK, A. J., BONOW, R. O. & SPELSBERG, T. 2003. Human aortic valve calcification is associated with an osteoblast phenotype. *Circulation*, 107, 2181-4.
- RASSART, E., BEDIRIAN, A., DO CARMO, S., GUINARD, O., SIROIS, J., TERRISSE, L. & MILNE, R. 2000. Apolipoprotein D. *Biochim Biophys Acta*, 1482, 185-98.
- RAZAVI, M., ANDERSON, N. L., YIP, R., POPE, M. E. & PEARSON, T. W. 2016. Multiplexed longitudinal measurement of protein biomarkers in DBS using an automated SISCAPA workflow. *Bioanalysis*, 8, 1597-1609.
- REDPATH, G. M., SOPHOCLEOUS, R. A., TURNBULL, L., WHITCHURCH, C. B. & COOPER, S. T. 2016. Ferlins Show Tissue-Specific Expression and Segregate as

- Plasma Membrane/Late Endosomal or Trans-Golgi/Recycling Ferlins. *Traffic*, 17, 245-66.
- REITER, L., CLAASSEN, M., SCHRIMPF, S. P., JOVANOVIĆ, M., SCHMIDT, A., BUHMANN, J. M., HENGARTNER, M. O. & AEBERSOLD, R. 2009. Protein identification false discovery rates for very large proteomics data sets generated by tandem mass spectrometry. *Mol Cell Proteomics*, 8, 2405-17.
- RICHARDS, A. M., NICHOLLS, M. G., IKRAM, H., HAMILTON, E. J. & RICHARDS, R. D. 1984. Syncope in aortic valvular stenosis. *Lancet*, 2, 1113-6.
- RIECK, A. E., CRAMARIUC, D., STAAL, E. M., ROSSEBO, A. B., WACHTELL, K. & GERDTS, E. 2010. Impact of hypertension on left ventricular structure in patients with asymptomatic aortic valve stenosis (a SEAS substudy). *J Hypertens*, 28, 377-83.
- RIFAI, N., GILLETTE, M. A. & CARR, S. A. 2006. Protein biomarker discovery and validation: the long and uncertain path to clinical utility. *Nat Biotechnol*, 24, 971-83.
- ROBERTS, W. C. 1970. Anatomically isolated aortic valvular disease. The case against its being of rheumatic etiology. *Am J Med*, 49, 151-9.
- ROSENHEK, R., BINDER, T., PORENTA, G., LANG, I., CHRIST, G., SCHEMPER, M., MAURER, G. & BAUMGARTNER, H. 2000. Predictors of outcome in severe, asymptomatic aortic stenosis. *N Engl J Med*, 343, 611-7.
- ROSENHEK, R., ZILBERSZAC, R., SCHEMPER, M., CZERNY, M., MUNDIGLER, G., GRAF, S., BERGLER-KLEIN, J., GRIMM, M., GABRIEL, H. & MAURER, G. 2010. Natural history of very severe aortic stenosis. *Circulation*, 121, 151-6.
- ROSJO, H., ANDREASSEN, J., EDVARDSEN, T. & OMLAND, T. 2011. Prognostic usefulness of circulating high-sensitivity troponin T in aortic stenosis and relation to echocardiographic indexes of cardiac function and anatomy. *Am J Cardiol*, 108, 88-91.
- ROSJO, H., DAHL, M. B., BYE, A., ANDREASSEN, J., JORGENSEN, M., WISLOFF, U., CHRISTENSEN, G., EDVARDSEN, T. & OMLAND, T. 2014. Prognostic value of circulating microRNA-210 levels in patients with moderate to severe aortic stenosis. *PLoS One*, 9, e91812.
- ROSS, J., JR. & BRAUNWALD, E. 1968. Aortic stenosis. *Circulation*, 38, 61-7.
- ROTH, S. Y., DENU, J. M. & ALLIS, C. D. 2001. Histone acetyltransferases. *Annu Rev Biochem*, 70, 81-120.
- RU, Q. C., ZHU, L. A., KATENHUSEN, R. A., SILBERMAN, J., BRZESKI, H., LIEBMAN, M. & SHRIVER, C. D. 2006. Exploring human plasma proteome

- strategies: high efficiency in-solution digestion protocol for multi-dimensional protein identification technology. *J Chromatogr A*, 1111, 175-91.
- RÖST, H., MALMSTRÖM, L. & AEBERSOLD, R. 2012. A computational tool to detect and avoid redundancy in selected reaction monitoring. *Mol Cell Proteomics*, 11, 540-9.
- SAG, C. M., KOHLER, A. C., ANDERSON, M. E., BACKS, J. & MAIER, L. S. 2011. CaMKII-dependent SR Ca leak contributes to doxorubicin-induced impaired Ca handling in isolated cardiac myocytes. *J Mol Cell Cardiol*, 51, 749-59.
- SAITO, T., HOJO, Y., HIROSE, M., IKEMOTO, T., KATSUKI, T. & KARIO, K. 2013. High-sensitivity troponin T is a prognostic marker for patients with aortic stenosis after valve replacement surgery. *J Cardiol*, 61, 342-7.
- SAKURAI, A., DOCI, C. L. & GUTKIND, J. S. 2012. Semaphorin signaling in angiogenesis, lymphangiogenesis and cancer. *Cell Res*, 22, 23-32.
- SALCEDO, E. E., KORZICK, D. H., CURRIE, P. J., STEWART, W. J., LEVER, H. M. & GOORMASTIC, M. 1989. Determinants of left ventricular hypertrophy in patients with aortic stenosis. *Cleve Clin J Med*, 56, 590-6.
- SALIER, J. P., ROUET, P., RAGUENEZ, G. & DAVEAU, M. 1996. The inter-alpha-inhibitor family: from structure to regulation. *Biochem J*, 315 ( Pt 1), 1-9.
- SANSANWAL, P., LI, L. & SARWAL, M. M. 2015. Inhibition of intracellular clusterin attenuates cell death in nephropathic cystinosis. *J Am Soc Nephrol*, 26, 612-25.
- SARJEANT, J. M., LAWRIE, A., KINNEAR, C., YABLONSKY, S., LEUNG, W., MASSAELI, H., PRICHETT, W., VEINOT, J. P., RASSART, E. & RABINOVITCH, M. 2003. Apolipoprotein D inhibits platelet-derived growth factor-BB-induced vascular smooth muscle cell proliferation by preventing translocation of phosphorylated extracellular signal regulated kinase 1/2 to the nucleus. *Arterioscler Thromb Vasc Biol*, 23, 2172-7.
- SATO, K., KUMAR, A., KRISHNASWAMY, A., MICK, S., DESAI, M. Y., GRIFFIN, B. P., KAPADIA, S. R. & POPOVIC, Z. B. 2019. B-type natriuretic peptide is associated with remodeling and exercise capacity after transcatheter aortic valve replacement for aortic stenosis. *Clin Cardiol*, 42, 270-276.
- SCHAER, D. J., BUEHLER, P. W., ALAYASH, A. I., BELCHER, J. D. & VERCELLOTTI, G. M. 2013. Hemolysis and free hemoglobin revisited: exploring hemoglobin and heme scavengers as a novel class of therapeutic proteins. *Blood*, 121, 1276-84.

- SCHEERLINCK, E., DHAENENS, M., VAN SOOM, A., PEELMAN, L., DE SUTTER, P., VAN STEENDAM, K. & DEFORCE, D. 2015. Minimizing technical variation during sample preparation prior to label-free quantitative mass spectrometry. *Anal Biochem*, 490, 14-9.
- SCHILLACI, G., VERDECCHIA, P., PORCELLATI, C., CUCCURULLO, O., COSCO, C. & PERTICONE, F. 2000. Continuous relation between left ventricular mass and cardiovascular risk in essential hypertension. *Hypertension*, 35, 580-6.
- SCHLUTER, K. D. & WENZEL, S. 2008. Angiotensin II: a hormone involved in and contributing to pro-hypertrophic cardiac networks and target of anti-hypertrophic cross-talks. *Pharmacol Ther*, 119, 311-25.
- SCHRAMM, L., PENDERGRAST, P. S., SUN, Y. & HERNANDEZ, N. 2000. Different human TFIIB activities direct RNA polymerase III transcription from TATA-containing and TATA-less promoters. *Genes Dev*, 14, 2650-63.
- SCHROEN, B., HEYMANS, S., SHARMA, U., BLANKESTEIJN, W. M., POKHAREL, S., CLEUTJENS, J. P., PORTER, J. G., EVELO, C. T., DUISTERS, R., VAN LEEUWEN, R. E., JANSSEN, B. J., DEBETS, J. J., SMITS, J. F., DAEMEN, M. J., CRIJNS, H. J., BORNSTEIN, P. & PINTO, Y. M. 2004. Thrombospondin-2 is essential for myocardial matrix integrity: increased expression identifies failure-prone cardiac hypertrophy. *Circ Res*, 95, 515-22.
- SCHWARTZ, L. S., GOLDFISCHER, J., SPRAGUE, G. J. & SCHWARTZ, S. P. 1969. Syncope and sudden death in aortic stenosis. *Am J Cardiol*, 23, 647-58.
- SERANG, O. & NOBLE, W. 2012. A review of statistical methods for protein identification using tandem mass spectrometry. *Stat Interface*, 5, 3-20.
- SEVINSKY, J. R., BROWN, K. J., CARGILE, B. J., BUNDY, J. L. & STEPHENSON, J. L. 2007. Minimizing back exchange in  $^{18}\text{O}/^{16}\text{O}$  quantitative proteomics experiments by incorporation of immobilized trypsin into the initial digestion step. *Anal Chem*, 79, 2158-62.
- SHANNON, P., MARKIEL, A., OZIER, O., BALIGA, N. S., WANG, J. T., RAMAGE, D., AMIN, N., SCHWIKOWSKI, B. & IDEKER, T. 2003. Cytoscape: a software environment for integrated models of biomolecular interaction networks. *Genome Res*, 13, 2498-504.
- SHI, T., ZHOU, J. Y., GRITSENKO, M. A., HOSSAIN, M., CAMP, D. G., SMITH, R. D. & QIAN, W. J. 2012. IgY14 and SuperMix immunoaffinity separations coupled with

- liquid chromatography-mass spectrometry for human plasma proteomics biomarker discovery. *Methods*, 56, 246-53.
- SILKOFF, P. E., LAVIOLETTE, M., SINGH, D., FITZGERALD, J. M., KELSEN, S., BACKER, V., PORSEBJERG, C., GIRODET, P. O., BERGER, P., KLINE, J. N., KHATRI, S., CHANEZ, P., SUSULIC, V. S., BARNATHAN, E. S., BARIBAUD, F., LOZA, M. J. & INVESTIGATORS, A. 2016. Longitudinal stability of asthma characteristics and biomarkers from the Airways Disease Endotyping for Personalized Therapeutics (ADEPT) study. *Respir Res*, 17, 43.
- SILVA, J. C., GORENSTEIN, M. V., LI, G. Z., VISSERS, J. P. & GEROMANOS, S. J. 2006. Absolute quantification of proteins by LCMSE: a virtue of parallel MS acquisition. *Mol Cell Proteomics*, 5, 144-56.
- SIMARD, J., DAUVOIS, S., HAAGENSEN, D. E., LÉVESQUE, C., MÉRAND, Y. & LABRIE, F. 1990. Regulation of progesterone-binding breast cyst protein GCDP-24 secretion by estrogens and androgens in human breast cancer cells: a new marker of steroid action in breast cancer. *Endocrinology*, 126, 3223-31.
- SINGH, A., CHAN, D. C. S., GREENWOOD, J. P., DAWSON, D. K., SONECKI, P., HOGREFE, K., KELLY, D. J., DHAKSHINAMURTHY, V., LANG, C. C., KHOO, J. P., SPRIGINGS, D., STEEDS, R. P., ZHANG, R., FORD, I., JEROSCH-HEROLD, M., YANG, J., LI, Z., NG, L. L. & MCCANN, G. P. 2017a. Symptom Onset in Aortic Stenosis: Relation to Sex Differences in Left Ventricular Remodeling. *JACC Cardiovasc Imaging*.
- SINGH, A., FORD, I., GREENWOOD, J. P., KHAN, J. N., UDDIN, A., BERRY, C., NEUBAUER, S., PRENDERGAST, B., JEROSCH-HEROLD, M., WILLIAMS, B., SAMANI, N. J. & MCCANN, G. P. 2013. Rationale and design of the PRognostic Importance of Microvascular Dysfunction in asymptomatic patients with Aortic Stenosis (PRIMID-AS): a multicentre observational study with blinded investigations. *BMJ Open*, 3, e004348.
- SINGH, A., GREENWOOD, J. P., BERRY, C., DAWSON, D. K., HOGREFE, K., KELLY, D. J., DHAKSHINAMURTHY, V., LANG, C. C., KHOO, J. P., SPRIGINGS, D., STEEDS, R. P., JEROSCH-HEROLD, M., NEUBAUER, S., PRENDERGAST, B., WILLIAMS, B., ZHANG, R., HUDSON, I., SQUIRE, I. B., FORD, I., SAMANI, N. J. & MCCANN, G. P. 2017b. Comparison of exercise testing and CMR measured myocardial perfusion reserve for predicting outcome in asymptomatic aortic stenosis:

- the PRognostic Importance of Microvascular Dysfunction in Aortic Stenosis (PRIMID AS) Study. *Eur Heart J*, 38, 1222-1229.
- SMALLEY, D. M., ROOT, K. E., CHO, H., ROSS, M. M. & LEY, K. 2007. Proteomic discovery of 21 proteins expressed in human plasma-derived but not platelet-derived microparticles. *Thromb Haemost*, 97, 67-80.
- SMITH, M. P., WOOD, S. L., ZOUGMAN, A., HO, J. T., PENG, J., JACKSON, D., CAIRNS, D. A., LEWINGTON, A. J., SELBY, P. J. & BANKS, R. E. 2011. A systematic analysis of the effects of increasing degrees of serum immunodepletion in terms of depth of coverage and other key aspects in top-down and bottom-up proteomic analyses. *Proteomics*, 11, 2222-35.
- SMITH, P. K., KROHN, R. I., HERMANSON, G. T., MALLIA, A. K., GARTNER, F. H., PROVENZANO, M. D., FUJIMOTO, E. K., GOEKE, N. M., OLSON, B. J. & KLENK, D. C. 1985. Measurement of protein using bicinchoninic acid. *Anal Biochem*, 150, 76-85.
- SMYTHE, C. 1936. The reaction of iodoacetate and of iodoacetamide with various sulfhydryl groups, with urease, and with yeast preparations. *Journal of Biological Chemistry*, 114, 601-612.
- SOLBERG, O. G., UELAND, T., WERGELAND, R., DAHL, C. P., AAKHUS, S., AUKRUST, P. & GULLESTAD, L. 2012. High-sensitive troponin T and N-terminal-brain-natriuretic-peptide predict outcome in symptomatic aortic stenosis. *Scand Cardiovasc J*, 46, 278-85.
- SPIRITO, P., BELLONE, P., HARRIS, K. M., BERNABO, P., BRUZZI, P. & MARON, B. J. 2000. Magnitude of left ventricular hypertrophy and risk of sudden death in hypertrophic cardiomyopathy. *N Engl J Med*, 342, 1778-85.
- STEADMAN, C. D., JEROSCH-HEROLD, M., GRUNDY, B., RAFELT, S., NG, L. L., SQUIRE, I. B., SAMANI, N. J. & MCCANN, G. P. 2012. Determinants and functional significance of myocardial perfusion reserve in severe aortic stenosis. *JACC Cardiovasc Imaging*, 5, 182-9.
- STEEL, D. M., SELLAR, G. C., UHLAR, C. M., SIMON, S., DEBEER, F. C. & WHITEHEAD, A. S. 1993. A constitutively expressed serum amyloid A protein gene (SAA4) is closely linked to, and shares structural similarities with, an acute-phase serum amyloid A protein gene (SAA2). *Genomics*, 16, 447-54.

- SUGIMURA, D., FUKUE, H., ARAI, M., MATSUMOTO, K. & FUKUTAKE, K. 1996. [Changes of factor XIII a and b subunit in patients with disseminated intravascular coagulation syndrome]. *Rinsho Byori*, 44, 355-61.
- SUGIURA, T., OKUMIYA, T., KUBO, T., TAKEUCHI, H. & MATSUMURA, Y. 2016. Evaluation of Intravascular Hemolysis With Erythrocyte Creatine in Patients With Aortic Stenosis. *Int Heart J*, 57, 430-3.
- SUNG, M. M., BYRNE, N. J., KIM, T. T., LEVASSEUR, J., MASSON, G., BOISVENUE, J. J., FEBBRAIO, M. & DYCK, J. R. 2017. Cardiomyocyte-specific ablation of CD36 accelerates the progression from compensated cardiac hypertrophy to heart failure. *Am J Physiol Heart Circ Physiol*, 312, H552-H560.
- SUPINO, P. G., BORER, J. S., PREIBISZ, J. & BORNSTEIN, A. 2006. The epidemiology of valvular heart disease: a growing public health problem. *Heart Fail Clin*, 2, 379-93.
- SUTO, F., ITO, K., UEMURA, M., SHIMIZU, M., SHINKAWA, Y., SANBO, M., SHINODA, T., TSUBOI, M., TAKASHIMA, S., YAGI, T. & FUJISAWA, H. 2005. Plexin-a4 mediates axon-repulsive activities of both secreted and transmembrane semaphorins and plays roles in nerve fiber guidance. *J Neurosci*, 25, 3628-37.
- SUTO, F., MURAKAMI, Y., NAKAMURA, F., GOSHIMA, Y. & FUJISAWA, H. 2003. Identification and characterization of a novel mouse plexin, plexin-A4. *Mech Dev*, 120, 385-96.
- SWEETWYNE, M. T., PALLERO, M. A., LU, A., VAN DUYN GRAHAM, L. & MURPHY-ULLRICH, J. E. 2010. The calreticulin-binding sequence of thrombospondin 1 regulates collagen expression and organization during tissue remodeling. *Am J Pathol*, 177, 1710-24.
- SÓDAR, B. W., KITTEL, Á., PÁLÓCZI, K., VUKMAN, K. V., OSTEIKOETXEA, X., SZABÓ-TAYLOR, K., NÉMETH, A., SPERLÁGH, B., BARANYAI, T., GIRICZ, Z., WIENER, Z., TURIÁK, L., DRAHOS, L., PÁLLINGER, É., VÉKEY, K., FERDINANDY, P., FALUS, A. & BUZÁS, E. I. 2016. Low-density lipoprotein mimics blood plasma-derived exosomes and microvesicles during isolation and detection. *Sci Rep*, 6, 24316.
- TAKAHASHI, M., ISHIDA, Y., IWAKI, D., KANNO, K., SUZUKI, T., ENDO, Y., HOMMA, Y. & FUJITA, T. 2010. Essential role of mannose-binding lectin-associated serine protease-1 in activation of the complement factor D. *J Exp Med*, 207, 29-37.



- TAMAGNONE, L. 2012. Emerging role of semaphorins as major regulatory signals and potential therapeutic targets in cancer. *Cancer Cell*, 22, 145-52.
- TANASH, H. A., EKSTRÖM, M., WAGNER, P. & PIITULAINEN, E. 2016. Cause-specific mortality in individuals with severe alpha 1-antitrypsin deficiency in comparison with the general population in Sweden. *Int J Chron Obstruct Pulmon Dis*, 11, 1663-9.
- TANG, H. Y., BEER, L. A. & SPEICHER, D. W. 2011. In-depth analysis of a plasma or serum proteome using a 4D protein profiling method. *Methods Mol Biol*, 728, 47-67.
- TANIGUCHI, T., MORIMOTO, T., SHIOMI, H., ANDO, K., KANAMORI, N., MURATA, K., KITAI, T., KAWASE, Y., IZUMI, C., MIYAKE, M., MITSUOKA, H., KATO, M., HIRANO, Y., MATSUDA, S., NAGAO, K., INADA, T., MURAKAMI, T., TAKEUCHI, Y., YAMANE, K., TOYOFUKU, M., ISHII, M., MINAMINO-MUTA, E., KATO, T., INOKO, M., IKEDA, T., KOMASA, A., ISHII, K., HOTTA, K., HIGASHITANI, N., KATO, Y., INUZUKA, Y., MAEDA, C., JINNAI, T., MORIKAMI, Y., SAKATA, R., KIMURA, T. & INVESTIGATORS, C. A. R. 2015. Initial Surgical Versus Conservative Strategies in Patients With Asymptomatic Severe Aortic Stenosis. *J Am Coll Cardiol*, 66, 2827-38.
- TECKMAN, J. H. & LINDBLAD, D. 2006. Alpha-1-antitrypsin deficiency: diagnosis, pathophysiology, and management. *Curr Gastroenterol Rep*, 8, 14-20.
- TERAWAKI, S., CAMOSSETO, V., PRETE, F., WENGER, T., PAPADOPOULOS, A., RONDEAU, C., COMBES, A., RODRIGUEZ RODRIGUES, C., VU MANH, T. P., FALLET, M., ENGLISH, L., SANTAMARIA, R., SOARES, A. R., WEIL, T., HAMMAD, H., DESJARDINS, M., GORVEL, J. P., SANTOS, M. A., GATTI, E. & PIERRE, P. 2015. RUN and FYVE domain-containing protein 4 enhances autophagy and lysosome tethering in response to Interleukin-4. *J Cell Biol*, 210, 1133-52.
- THAI, H. M. & GORE, J. M. 2000. Prosthetic Heart Valves. In: ALPERT, J. S., DALEN, J. E. & RAHIMTOOLA, S. H. (eds.) *Valvular Heart Disease*. 3rd ed. Philadelphia: Lippincott Williams & Wilkins.
- THUBRIKAR, M. J., NOLAN, S. P., AOUAD, J. & DECK, J. D. 1986. Stress sharing between the sinus and leaflets of canine aortic valve. *Ann Thorac Surg*, 42, 434-40.
- THÉRY, C., WITWER, K. W., AIKAWA, E., ALCARAZ, M. J., ANDERSON, J. D., ANDRIANTSITOHAINA, R., ANTONIOU, A., ARAB, T., ARCHER, F., ATKINSMITH, G. K., AYRE, D. C., BACH, J. M., BACHURSKI, D., BAHARVAND, H., BALAJ, L., BALDACCHINO, S., BAUER, N. N., BAXTER, A. A., BEBAWY, M., BECKHAM, C., BEDINA ZAVEC, A., BENMOUSSA, A., BERARDI, A. C.,

- BERGESE, P., BIELSKA, E., BLENKIRON, C., BOBIS-WOZOWICZ, S., BOILARD, E., BOIREAU, W., BONGIOVANNI, A., BORRÀS, F. E., BOSCH, S., BOULANGER, C. M., BREAKFIELD, X., BREGGIO, A. M., BRENNAN, M., BRIGSTOCK, D. R., BRISSON, A., BROEKMAN, M. L., BROMBERG, J. F., BRYL-GÓRECKA, P., BUCH, S., BUCK, A. H., BURGER, D., BUSATTO, S., BUSCHMANN, D., BUSSOLATI, B., BUZÁS, E. I., BYRD, J. B., CAMUSSI, G., CARTER, D. R., CARUSO, S., CHAMLEY, L. W., CHANG, Y. T., CHEN, C., CHEN, S., CHENG, L., CHIN, A. R., CLAYTON, A., CLERICI, S. P., COCKS, A., COCUCCI, E., COFFEY, R. J., CORDEIRO-DA-SILVA, A., COUCH, Y., COUMANS, F. A., COYLE, B., CRESCITELLI, R., CRIADO, M. F., D'SOUZA-SCHOREY, C., DAS, S., DATTA CHAUDHURI, A., DE CANDIA, P., DE SANTANA, E. F., DE WEVER, O., DEL PORTILLO, H. A., DEMARET, T., DEVILLE, S., DEVITT, A., DHONDT, B., DI VIZIO, D., DIETERICH, L. C., DOLO, V., DOMINGUEZ RUBIO, A. P., DOMINICI, M., DOURADO, M. R., DRIEDONKS, T. A., DUARTE, F. V., DUNCAN, H. M., EICHENBERGER, R. M., EKSTRÖM, K., EL ANDALOUSSI, S., ELIE-CAILLE, C., ERDBRÜGGER, U., FALCÓN-PÉREZ, J. M., FATIMA, F., FISH, J. E., FLORES-BELLVER, M., FÖRSÖNITS, A., FRELET-BARRAND, A., et al. 2018. Minimal information for studies of extracellular vesicles 2018 (MISEV2018): a position statement of the International Society for Extracellular Vesicles and update of the MISEV2014 guidelines. *J Extracell Vesicles*, 7, 1535750.
- TOLOSANO, E., FAGOONEE, S., MORELLO, N., VINCHI, F. & FIORITO, V. 2010. Heme scavenging and the other facets of hemopexin. *Antioxid Redox Signal*, 12, 305-20.
- TOUTOUZAS, K., DRAKOPOULOU, M., SYNETOS, A., TSIAMIS, E., AGROGIANNIS, G., KAVANTZAS, N., PATSOURIS, E., ILIOPOULOS, D., THEODOROPOULOS, S., YACOUN, M. & STEFANADIS, C. 2008. In vivo aortic valve thermal heterogeneity in patients with nonrheumatic aortic valve stenosis the: first in vivo experience in humans. *J Am Coll Cardiol*, 52, 758-63.
- TRINDADE, F., FERREIRA, R., MAGALHAES, B., LEITE-MOREIRA, A., FALCAO-PIRES, I. & VITORINO, R. 2018. How to use and integrate bioinformatics tools to compare proteomic data from distinct conditions? A tutorial using the pathological similarities between Aortic Valve Stenosis and Coronary Artery Disease as a case-study. *J Proteomics*, 171, 37-52.

- TSUKAMOTO, K., MANI, D. R., SHI, J., ZHANG, S., HAAGENSEN, D. E., OTSUKA, F., GUAN, J., SMITH, J. D., WENG, W., LIAO, R., KOLODGIE, F. D., VIRMANI, R. & KRIEGER, M. 2013. Identification of apolipoprotein D as a cardioprotective gene using a mouse model of lethal atherosclerotic coronary artery disease. *Proc Natl Acad Sci U S A*, 110, 17023-8.
- TU, C., RUDNICK, P. A., MARTINEZ, M. Y., CHEEK, K. L., STEIN, S. E., SLEBOS, R. J. & LIEBLER, D. C. 2010. Depletion of abundant plasma proteins and limitations of plasma proteomics. *J Proteome Res*, 9, 4982-91.
- UELAND, T., GULLESTAD, L., DAHL, C. P., AUKRUST, P., AAKHUS, S., SOLBERG, O. G., VERMEER, C. & SCHURGERS, L. J. 2010. Undercarboxylated matrix Gla protein is associated with indices of heart failure and mortality in symptomatic aortic stenosis. *J Intern Med*, 268, 483-92.
- URENA, P., MALERGUE, M. C., GOLDFARB, B., PRIEUR, P., GUEDON-RAPOUD, C. & PETROVER, M. 1999. Evolutive aortic stenosis in hemodialysis patients: analysis of risk factors. *Nephrologie*, 20, 217-25.
- VAKEVA, A., LAURILA, P. & MERI, S. 1993. Co-deposition of clusterin with the complement membrane attack complex in myocardial infarction. *Immunology*, 80, 177-82.
- VAN DER VUSSE, G. J., GLATZ, J. F., STAM, H. C. & RENEMAN, R. S. 1992. Fatty acid homeostasis in the normoxic and ischemic heart. *Physiol Rev*, 72, 881-940.
- VIJAYARAGHAVAN, S., HITMAN, G. A. & KOPELMAN, P. G. 1994. Apolipoprotein-D polymorphism: a genetic marker for obesity and hyperinsulinemia. *J Clin Endocrinol Metab*, 79, 568-70.
- VOEGELE, A. F., JERKOVIC, L., WELLENZOHN, B., ELLER, P., KRONENBERG, F., LIEDL, K. R. & DIEPLINGER, H. 2002. Characterization of the vitamin E-binding properties of human plasma afamin. *Biochemistry*, 41, 14532-8.
- WANG, A. T., KIM, T., WAGNER, J. E., CONTI, B. A., LACH, F. P., HUANG, A. L., MOLINA, H., SANBORN, E. M., ZIERHUT, H., CORNES, B. K., ABHYANKAR, A., SOUGNEZ, C., GABRIEL, S. B., AUERBACH, A. D., KOWALCZYKOWSKI, S. C. & SMOGORZEWSKA, A. 2015. A Dominant Mutation in Human RAD51 Reveals Its Function in DNA Interstrand Crosslink Repair Independent of Homologous Recombination. *Mol Cell*, 59, 478-90.
- WANG, C., HSUEH, A. J. & ERICKSON, G. F. 1980. Prolactin inhibition of estrogen production by cultured rat granulosa cells. *Mol Cell Endocrinol*, 20, 135-44.

- WANG, J., FENG, M. J., ZHANG, R., YU, D. M., ZHOU, S. J., CHEN, R. & YU, P. 2016. Creactive protein/oxidized low density lipoprotein/beta2glycoprotein i complexes induce lipid accumulation and inflammatory reaction in macrophages via p38/mitogenactivated protein kinase and nuclear factorkappaB signaling pathways. *Mol Med Rep*, 14, 3490-8.
- WANG, J. J., GONG, J. B., LI, H. Q., NIU, D. M., HAN, A. Z., WU, J. & ZHANG, C. N. 2012. Lipoprotein(a) complexes with beta2-glycoprotein I in patients with coronary artery disease. *J Atheroscler Thromb*, 19, 81-9.
- WASHBURN, M. P., WOLTERS, D. & YATES, J. R. 2001. Large-scale analysis of the yeast proteome by multidimensional protein identification technology. *Nat Biotechnol*, 19, 242-7.
- WASINGER, V. C., CORDWELL, S. J., CERPA-POLJAK, A., YAN, J. X., GOOLEY, A. A., WILKINS, M. R., DUNCAN, M. W., HARRIS, R., WILLIAMS, K. L. & HUMPHERY-SMITH, I. 1995. Progress with gene-product mapping of the Mollicutes: Mycoplasma genitalium. *Electrophoresis*, 16, 1090-4.
- WASSERMAN, K., HANSEN, J. E., SUE, D. Y., WHIPP, B. J. & FROELICHER, V. F. 1987. Principles of exercise testing and interpretation. *Journal of Cardiopulmonary Rehabilitation and Prevention*, 7, 189.
- WEBER, K. T. 2004. Fibrosis in hypertensive heart disease: focus on cardiac fibroblasts. *J Hypertens*, 22, 47-50.
- WEBER, M., HAUSEN, M., ARNOLD, R., NEF, H., MOELLMAN, H., BERKOWITSCH, A., ELSAESSER, A., BRANDT, R., MITROVIC, V. & HAMM, C. 2006. Prognostic value of N-terminal pro-B-type natriuretic peptide for conservatively and surgically treated patients with aortic valve stenosis. *Heart*, 92, 1639-44.
- WEI, Y. J., HUANG, Y. X., ZHANG, X. L., LI, J., HUANG, J., ZHANG, H. & HU, S. S. 2008. Apolipoprotein D as a novel marker in human end-stage heart failure: a preliminary study. *Biomarkers*, 13, 535-48.
- WENDE, A. R., BRAHMA, M. K., MCGINNIS, G. R. & YOUNG, M. E. 2017. Metabolic Origins of Heart Failure. *JACC Basic Transl Sci*, 2, 297-310.
- WERNBOM, M., PAULSEN, G., NILSEN, T. S., HISDAL, J. & RAASTAD, T. 2012. Contractile function and sarcolemmal permeability after acute low-load resistance exercise with blood flow restriction. *Eur J Appl Physiol*, 112, 2051-63.
- WESTER-ROSENLOF, L., CASSLEN, V., AXELSSON, J., EDSTROM-HAGERWALL, A., GRAM, M., HOLMQVIST, M., JOHANSSON, M. E., LARSSON, I., LEY, D.,

- MARSAL, K., MORGELIN, M., RIPPE, B., RUTARDOTTIR, S., SHOHANI, B., AKERSTROM, B. & HANSSON, S. R. 2014. A1M/alpha1-microglobulin protects from heme-induced placental and renal damage in a pregnant sheep model of preeclampsia. *PLoS One*, 9, e86353.
- WEWER, U. M. & ALBRECHTSEN, R. 1992. Tetranectin, a plasminogen kringle 4-binding protein. Cloning and gene expression pattern in human colon cancer. *Lab Invest*, 67, 253-62.
- WEWER, U. M., IBA, K., DURKIN, M. E., NIELSEN, F. C., LOECHEL, F., GILPIN, B. J., KUANG, W., ENGVALL, E. & ALBRECHTSEN, R. 1998. Tetranectin is a novel marker for myogenesis during embryonic development, muscle regeneration, and muscle cell differentiation in vitro. *Dev Biol*, 200, 247-59.
- WHITE, D. E., COUTU, P., SHI, Y. F., TARDIF, J. C., NATTEL, S., ST ARNAUD, R., DEDHAR, S. & MULLER, W. J. 2006. Targeted ablation of ILK from the murine heart results in dilated cardiomyopathy and spontaneous heart failure. *Genes Dev*, 20, 2355-60.
- WHITEAKER, J. R., HALUSA, G. N., HOOFNAGLE, A. N., SHARMA, V., MACLEAN, B., YAN, P., WROBEL, J. A., KENNEDY, J., MANI, D. R., ZIMMERMAN, L. J., MEYER, M. R., MESRI, M., RODRIGUEZ, H., PAULOVICH, A. G. & (CPTAC), C. P. T. A. C. 2014. CPTAC Assay Portal: a repository of targeted proteomic assays. *Nat Methods*, 11, 703-4.
- WILLEMS, G. M., JANSSEN, M. P., PELSERS, M. M., COMFURIUS, P., GALLI, M., ZWAAL, R. F. & BEVERS, E. M. 1996. Role of divalency in the high-affinity binding of anticardiolipin antibody-beta 2-glycoprotein I complexes to lipid membranes. *Biochemistry*, 35, 13833-42.
- WU, S., YANG, K., LIANG, Z., ZHANG, L. & ZHANG, Y. 2011. Urea free and more efficient sample preparation method for mass spectrometry based protein identification via combining the formic acid-assisted chemical cleavage and trypsin digestion. *Talanta*, 86, 429-35.
- WURM, H., BEUBLER, E., POLZ, E., HOLASEK, A. & KOSTNER, G. 1982. Studies on the possible function of beta 2-glycoprotein-I: influence in the triglyceride metabolism in the rat. *Metabolism*, 31, 484-6.
- XIA, Y., DOBACZEWSKI, M., GONZALEZ-QUESADA, C., CHEN, W., BIERNACKA, A., LI, N., LEE, D. W. & FRANGOIANNIS, N. G. 2011. Endogenous

- thrombospondin 1 protects the pressure-overloaded myocardium by modulating fibroblast phenotype and matrix metabolism. *Hypertension*, 58, 902-11.
- XU, X., GILPIN, B., IBA, K., MAIER, A., ENGVALL, E., ALBRECHTSEN, R. & WEWER, U. M. 2001. Tetranectin in slow intra- and extrafusal chicken muscle fibers. *J Muscle Res Cell Motil*, 22, 121-32.
- YAMADA, T., KAKIHARA, T., KAMISHIMA, T., FUKUDA, T. & KAWAI, T. 1996a. Both acute phase and constitutive serum amyloid A are present in atherosclerotic lesions. *Pathol Int*, 46, 797-800.
- YAMADA, T., MIIDA, T., ITOH, Y., KAWAI, T. & BENSON, M. D. 1996b. Characterization of serum amyloid A4 as a plasma apolipoprotein. *Clin Chim Acta*, 251, 105-12.
- YAMADA, T., MIIDA, T., YAMAGUCHI, T. & ITOH, Y. 1997. Effect of serum amyloid A on cellular affinity of low density lipoprotein. *Eur J Clin Chem Clin Biochem*, 35, 421-6.
- YAMADA, T., MIYAKE, N., ITOH, K. & IGARI, J. 2001. Further characterization of serum amyloid A4 as a minor acute phase reactant and a possible nutritional marker. *Clin Chem Lab Med*, 39, 7-10.
- YAMAUCHI, Y., KUROKI, M., IMAKIIRE, T., ABE, H., UCHIDA, H., BEPPU, R., YAMASHITA, Y. & SHIRAKUSA, T. 2002. Thrombospondin-1 differentially regulates release of IL-6 and IL-10 by human monocytic cell line U937. *Biochem Biophys Res Commun*, 290, 1551-7.
- YAO, X., FREAS, A., RAMIREZ, J., DEMIREV, P. A. & FENSELAU, C. 2001. Proteolytic 18O labeling for comparative proteomics: model studies with two serotypes of adenovirus. *Anal Chem*, 73, 2836-42.
- YE, X. & LI, L. 2014. Macroporous reversed-phase separation of proteins combined with reversed-phase separation of phosphopeptides and tandem mass spectrometry for profiling the phosphoproteome of MDA-MB-231 cells. *Electrophoresis*, 35, 3479-86.
- YORIFUJI, H., ANDERSON, K., LYNCH, G. W., VAN DE WATER, L. & MCDONAGH, J. 1988. B protein of factor XIII: differentiation between free B and complexed B. *Blood*, 72, 1645-50.
- YOUNG, T. R. & LEAMEY, C. A. 2009. Teneurins: important regulators of neural circuitry. *Int J Biochem Cell Biol*, 41, 990-3.

- YU, Y., YE, L., LI, Y. G., BURKIN, D. J. & DUAN, D. D. 2016. Heart-specific overexpression of the human short CLC-3 chloride channel isoform limits myocardial ischemia-induced ERP and QT prolongation. *Int J Cardiol*, 214, 218-24.
- YUE, X. S. & HUMMON, A. B. 2013. Combination of multistep IMAC enrichment with high-pH reverse phase separation for in-depth phosphoproteomic profiling. *J Proteome Res*, 12, 4176-86.
- ZHANG, B., KALL, L. & ZUBAREV, R. A. 2016a. DeMix-Q: Quantification-centered Data Processing Workflow. *Mol Cell Proteomics*.
- ZHANG, J., XU, X., GAO, M., YANG, P. & ZHANG, X. 2007. Comparison of 2-D LC and 3-D LC with post- and pre-tryptic-digestion SEC fractionation for proteome analysis of normal human liver tissue. *Proteomics*, 7, 500-512.
- ZHANG, L., YAO, L., ZHANG, Y., XUE, T., DAI, G., CHEN, K., HU, X. & XU, L. X. 2012. Protein pre-fractionation with a mixed-bed ion exchange column in 3D LC-MS/MS proteome analysis. *J Chromatogr B Analyt Technol Biomed Life Sci*, 905, 96-104.
- ZHANG, N., AHSAN, M. H., PURCHIO, A. F. & WEST, D. B. 2005. Serum amyloid A-luciferase transgenic mice: response to sepsis, acute arthritis, and contact hypersensitivity and the effects of proteasome inhibition. *J Immunol*, 174, 8125-34.
- ZHANG, P., WEAVER, J. C., CHEN, G., BERETOV, J., ATSUMI, T., QI, M., BHINDI, R., QI, J. C., MADIGAN, M. C., GIANNAKOPOULOS, B. & KRILIS, S. A. 2016b. The Fifth Domain of Beta 2 Glycoprotein I Protects from Natural IgM Mediated Cardiac Ischaemia Reperfusion Injury. *PLoS One*, 11, e0152681.
- ZILBERSZAC, R., GABRIEL, H., SCHEMPER, M., LAUFER, G., MAURER, G. & ROSENHEK, R. 2017. Asymptomatic Severe Aortic Stenosis in the Elderly. *JACC Cardiovasc Imaging*, 10, 43-50.
- ZILE, M. R. & BRUTSAERT, D. L. 2002. New concepts in diastolic dysfunction and diastolic heart failure: Part II: causal mechanisms and treatment. *Circulation*, 105, 1503-8.
- ZINGMAN, L. V., HODGSON, D. M., BAST, P. H., KANE, G. C., PEREZ-TERZIC, C., GUMINA, R. J., PUCAR, D., BIENENGRAEBER, M., DZEJA, P. P., MIKI, T., SEINO, S., ALEKSEEV, A. E. & TERZIC, A. 2002. Kir6.2 is required for adaptation to stress. *Proc Natl Acad Sci U S A*, 99, 13278-83.
- ZOLOTARJOVA, N., MROZINSKI, P., CHEN, H. & MARTOSELLA, J. 2008. Combination of affinity depletion of abundant proteins and reversed-phase

fractionation in proteomic analysis of human plasma/serum. *J Chromatogr A*, 1189, 332-8.

ZWADLO, C., SCHMIDTMANN, E., SZAROSZYK, M., KATTIH, B., FROESE, N., HINZ, H., SCHMITTO, J. D., WIDDER, J., BATKAI, S., BÄHRE, H., KAEVER, V., THUM, T., BAUERSACHS, J. & HEINEKE, J. 2015. Antiandrogenic therapy with finasteride attenuates cardiac hypertrophy and left ventricular dysfunction. *Circulation*, 131, 1071-81.